



AGARD-CP-223

AGARD-CP-223

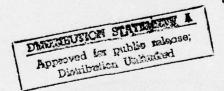
AD A 041795

ADVISORY GROUP FOR AEROSPACE RESEARCH & DEVELOPMENT

7 RUE ANCELLE 92200 NEUILLY SUR SEINE FRANCE

AGARD CONFERENCE PROCEEDINGS No. 223

Flight Test Techniques



Property of

NORTH ATLANTIC TREATY ORGANIZATION



DISTRIBUTION AND AVAILABILITY ON BACK COVER



# NORTH ATLANTIC TREATY ORGANIZATION ADVISORY GROUP FOR AEROSPACE RESEARCH AND DEVELOPMENT (ORGANISATION DU TRAITE DE L'ATLANTIQUE NORD)

AGARD Conference Proceedings No.223

FLIGHT TEST TECHNIQUES,

DISTRIBUTION STATEMENT A

Approved for public releases

Distribution Unlimited



Papers presented at the Flight Mechanics Panel Symposium held at DFVLR, Porz Wahn, Germany, 11-14 October 1976.

400043

Luce

### THE MISSION OF AGARD

The mission of AGARD is to bring together the leading personalities of the NATO nations in the fields of science and technology relating to aerospace for the following purposes:

- Exchanging of scientific and technical information;
- Continuously stimulating advances in the aerospace sciences relevant to strengthening the common defence posture;
- Improving the co-operation among member nations in aerospace research and development;
- Providing scientific and technical advice and assistance to the North Atlantic Military Committee in the field of aerospace research and development;
- Rendering scientific and technical assistance, as requested, to other NATO bodies and to member nations
  in connection with research and development problems in the aerospace field;
- Providing assistance to member nations for the purpose of increasing their scientific and technical potential;
- Recommending effective ways for the member nations to use their research and development capabilities for the common benefit of the NATO community.

The highest authority within AGARD is the National Delegates Board consisting of officially appointed senior representatives from each member nation. The mission of AGARD is carried out through the Panels which are composed of experts appointed by the National Delegates, the Consultant and Exchange Program and the Aerospace Applications Studies Program. The results of AGARD work are reported to the member nations and the NATO Authorities through the AGARD series of publications of which this is one.

Participation in AGARD activities is by invitation only and is normally limited to citizens of the NATO nations.

The content of this publication has been reproduced directly from material supplied by AGARD or the authors.

Published April 1977

Copyright © AGARD 1977 All Rights Reserved

ISBN 92-835-0194-2



Printed by Technical Editing and Reproduction Ltd Harford House, 7–9 Charlotte St, London, WIP 1HD

### PREFACE

Flight testing is the "proof of the pudding" — it is the culmination of the designer's efforts, simulation approaches, wind-tunnel tests, and ground tests of various components. Since technology is advancing at such a rapid rate and published material is so rapidly outdated, this Symposium was organized to disseminate information and exchange ideas on techniques to more safely, economically, and thoroughly evaluate aircraft in a timely fashion.

The Symposium was organized around three subject areas and concentrated on techniques rather than results:

- · Weapons System Clearance,
- Weapon System Development and Evaluation.
- Data Acquisition and Handling Techniques.

The first session was devoted to techniques used in flight clearance of the basic air vehicles, including flight control systems, engines, engine-inlet systems, etc., and the externally carried weapons. The major recurring theme was that efficient and effective flight testing depends on carefully planned and executed integration of ground testing with flight testing. It was also evident that digital flight control systems can benefit from testing and testing techniques not required of previous systems. While sophistication is a characteristic of many current flight test techniques, one author discussed a quite simple ground system that was effective in support of post stall spin testing.

Session II papers gave a broad but fairly coherent coverage of the techniques used in weapon system development. There were several examples of different techniques being used to meet the same basic objective. As a general rule, the techniques utilized seem to fit very naturally with the facilities available. The point was made that best accuracy is obtained by using more than one procedure and by combining results to obtain a weighted mean. There was wide recognition of outstanding problem areas and activity to fill these gaps was reported from widely separated organizations.

Papers in the third session covered advances in the state-of-the-art of instrumentation systems and components, data transmission, data processing, and airborne displays required for safe and efficient flight tests. Real-time flight test analysis and monitoring system presentations showed interesting approaches utilizing airborne and ground-based applications. The various systems all demonstrated versatility and a capability to permit reduction of flying and calendar time.

During the Round Table Discussion, a number of topics were raised both by the round table participants and members of the audience. The following is a brief review of the discussions:

- (a) There were many areas and/or techniques involving subsystems which were not covered during the Symposium primarily because of the lack of time. It was suggested that a specialists meeting on subsystem/system testing which would include adverse weather and climatic testing would be appropriate.
- (b) It was felt that the test pilot's role should be emphasized during test planning and conduct.
- (c) Modern data acquisition and processing systems are powerful, impressive, and often necessary. However, the flight test engineer and the instrumentation engineer should restrict their data gathering to what is really needed and use simpler methods when they are adequate.
- (d) A major problem of all the government flight test agencies is how to work with raw data from the contractors. It is regrettable that a standardization of the inputs and outputs of these systems has not been undertaken, as the ARINC committee did for equipment.
- (e) The importance of a well balanced man-machine relationship has long been recognized in many areas of technology. However, when considering the many complicated flight data acquisition and handling systems that are presently available, it appears doubtful whether the system designer has been well aware of this principle. The inclusion of a human interpretation link might result in a simpler and less expensive system with higher flexibility. The system designer, therefore, should always be aware of the potential of the human being and not be tempted to blindly apply advanced automatic handling techniques mainly for their technological or mathematical elegance!
- (f) Despite the abundance of off-the-shelf transducers for the majority of applications with well documented claims for high performance in manufacturers' brochures, it might nevertheless be useful to establish either a forum for exchange of users' experience or some central independent testing/assessment agency as already exists; for example, for domestic and household equipment, automobiles, hi-fi equipment, etc. What is required is not only the result of bench or environmental tests, but actual in-service experience with real, practical installations.

In general, the objectives of the Symposium were achieved; all areas intended to be covered were in fact covered. If time had permitted, additional coverage of subsystem flight testing would have been included.

K.H.DOETSCH Member Flight Mechanics Panel T. VAN OOSTEROM Member Flight Mechanics Panel F.N.STOLIKER Member Flight Mechanics Panel

### CONTENTS

	Page
PREFACE by K.H.Doetsch, T. Van Oosterom and F.N.Stoliker	iii
	Reference
SESSION I – WEAPONS SYSTEM CLEARANCE	
FLIGHT CONTROL SYSTEM STRUCTURAL RESONANCE AND LIMIT CYCLE RESULTS	
by P.W.Kirsten	1
HAWKER SIDDELEY HAWK SPINNING TRIALS by R.J.Poole	2
METHODES ET TECHNIQUES DE L'ESSAI DE VIBRATION EN VOL par G.Piazzoli	3
TORNADO FLIGHTS LOADS SURVEY by D.W.Altham, D.K.Potter, J.Nuscheler and W.Seidel	4
THE EFFECTS OF A COMMAND AND STABILITY AUGMENTATION SYSTEM ON FLIGHT TESTING by T.B.Saunders	5
DEVELOPMENT FLIGHT TEST TECHNIQUES FOR DIGITAL MULTIMODE FLIGHT CONTROL SYSTEMS	
by D.L.Carleton	6
FLIGHT ASSESSMENT AND DEVELOPMENT OF THE CONCORDE INTAKE SYSTEM by D.P.Morriss	7
WEAPONS TESTING TECHNIQUES by F.J.Bigg, N.Tait and D.W.Williams	8
COMMENTS ON SESSION I	C1
SESSION II – WEAPON SYSTEM DEVELOPMENT AND EVALUATION	
SUPERSONIC POWERPLANT TESTING FOR PREFLIGHT PERFORMANCE EVALUATION	
by G.G.Annear	9
PROCEDURES FOR THE MEASUREMENT OF ENGINE THRUST IN FLIGHT by J.C.Ascough	10
ESTIMATION OF DRAG AND THRUST OF JET-PROPELLED AIRCRAFT BY NON-STEADY FLIGHT TEST MANOEUVRES by J.A.Mulder and J.M. van Sliedregt	11
FLIGHT TESTING AND EVALUATION TECHNIQUES FOR THE DETERMINATION OF HANDLING QUALITIES by H.Wünnenberg and U. von Meier	12
A MISSION ORIENTED FLIGHT TEST TECHNIQUE FOR IDENTIFYING AIRCRAFT AND FLIGHT CONTROL SYSTEM TRANSFER FUNCTIONS	
by T.R.Twisdale, G.L.Jones and T.A.Ashurst  OVERALL AIRCRAFT SYSTEMS EVALUATION	13
by F.N.Lucero and C.E.Adolph	14

	Reference
DETERMINATION OF ANTENNA RADIATION PATTERNS, RADAR CROSS SECTIONS AND JAM-TO-SIGNAL RATIOS BY FLIGHT TESTS by O.B.M.Pietersen, G.J.Alders and R.B.A.Wasch	15
REAL TIME DATA TRANSMISSION AND PROCESSING FOR THE DETERMINATION OF AIRCRAFT ANTENNA RADIATION PATTERNS by H.Bothe	16
HYBRID REFERENCE SYSTEMS FOR FLIGHT TESTING by H.Winter and U.Brokof	17
FLIGHT TESTING OF DISPLAYS IN A HELICOPTER by R.Beyer	18
COMMENTS ON SESSION II	C2
SESSION III – DATA ACQUISITION AND HANDLING TECHNIQUES	
ANGULAR MOTION SENSING WITH GAS ROTORS by W.R.Macdonald	19
EXEMPLES D'UTILISATION DU LASER POUR LES ESSAIS DE CERTIFICATION D'AVIONS CIVILS par N.Lapchine	20
TELEMETRY AND DATA RELAY FOR MANNED SPACE PROGRAMS by K.W.Anson	21
RESORS – A SYSTEM FOR ON-LINE, ON-BOARD DATA REDUCTION AND PERFORMANCE ANALYSIS DEVELOPED ESPECIALLY FOR E-3A FLIGHT TESTS	
by H.A.Williams	22
AN ADVANCED AIRBORNE DATA ACQUISITION SYSTEM by F.Bartoli	23
USE OF ONBOARD REAL-TIME FLIGHT TEST ANALYSIS AND MONITOR SYSTEMS — A PROGRESS REPORT by W.S.Lieberman	24
THE AUTOMATED FLIGHT TEST DATA SYSTEM by C.O.Johnson and P.J.Sehnert	25
COMMENTS ON SESSION III	С3
SUMMARY OF ROUND TABLE DISCUSSION AND FLOOR COMMENTS	D

**SESSION I** 

WEAPONS SYSTEM CLEARANCE

## FLIGHT CONTROL SYSTEM STRUCTURAL RESONANCE AND LIMIT CYCLE RESULTS

by

Paul W. Kirsten Aerospace Research Engineer Air Force Flight Test Center/DOY Edwards AFB, California, USA

### SUMMARY

Theory, testing, and results pertaining to limit cycle and structural resonance characteristics of aircraft flight control systems are presented in this paper. Methods for insuring that limit cycling and structural resonance do not occur unexpectedly during flight are suggested. Ground tests and inflight envelope expansion tests have been used with success in the past to determine limit cycle and structural resonance characteristics. Data obtained from these tests will be presented for several aircraft. Also, control system modifications made on several aircraft to eliminate control system instabilities which were uncovered through ground testing will be included. Additional topics will be discussed which include digital sampling effects on limit cycle characteristics, large amplitude saturation limit cycles, and pilot-in-the-loop instabilities.

### LIST OF SYMBOLS

	LIST OF SYMBOLS
AFFTC	Air Force Flight Test Center
b	reference span
<del>c</del>	reference chord
CL	rolling moment coefficient
C <sub>m</sub>	pitching moment coefficient
c <sub>n</sub>	yawing moment coefficient
Hz	Hertz
ı,	rolling moment inertia
ı <sub>y</sub>	pitching moment inertia
ız	yawing moment inertia
K <sub>p</sub>	End-to-end roll axis flight control system gain
K <sub>q</sub>	End-to-end pitch axis flight control system gain
K <sub>r</sub>	End-to-end yaw axis flight control system gain
L <sub>δa</sub>	gsb c <sub>loa</sub>
<sup>M</sup> ôe	gsc c <sub>m</sub> e
N <sub>6</sub> r	Tz cn6r
p	roll rate
q	pitch rate
<u>ā</u>	dynamic pressure
r	yaw rate
S	reference area
SAS	Stability Augmentation System
V	True velocity

- a Angle of Attack
- β Angle of Sideslip
- δa Aileron position
- δe Elevator position
- δr Rudder position

### Subscripts:

 $\alpha$ ,  $\beta$ ,  $\delta$ a,  $\delta$ e,  $\delta$ r Denote partial derivatives with respect to subscripted variables

### INTRODUCTION

The advent of the modern, high gain flight control system in current aircraft has produced some new and complex interactions between the flight control system, the aircraft aerodynamics, the aircraft structure, and the pilot. Depending on your viewpoint, these interactions are considered to be either control system problems, flutter problems, unsteady aerodynamic problems, aeroelastic problems, or human factors problems according to the viewers past experience. Over the past few years, the AFFTC has witnessed the development of many new aircraft, each with its own peculiar set of developmental problems. This paper attempts to summarize some of these problems as they relate to the control system/structure/aerodynamic/pilot interface, and to suggest two simple ground test procedures which have been useful in helping to understand these interactions and, more importantly, in insuring flight safety during early test flights.

There are obviously many combinations of "instabilities" which can occur between the control system, the structure, the aerodynamics, and the pilot. Analytical math models are useful in predicting some of these interactions and instabilities, but are often limited by the validity of the input data. The flight test community has found that two simple ground tests performed on the flight hardware can significantly increase the confidence in the integrity of the total system.

The "limit cycle" test is aimed at quantifying the interaction between the control system (including nonlinearities) and the aerodynamic surface effectiveness. This test usually produces results in the 1 to 5 Hz frequency range and assumes a rigid structure (ignores structural modes, aeroelastic effects, and pilot interactions).

The "structural resonance" test is aimed at quantifying the interaction between the control system (including nonlinearities) and the actual aircraft structural modes. This test usually produces results in the frequency range above 5 Hz and assumes no aerodynamic effects (ignores aeroelastic effects, unsteady aerodynamics, and pilot interaction).

These two tests are obviously not all-inclusive. Any effort to expand the tests to increase the scope and/or the validity would destroy the simplicity of the technique and has therefore been avoided thus far.

### DEFINITION

A limit cycle oscillation is a sustained, closed-loop oscillation of a motion sensor and a control surface at relatively low frequencies which is created when the phase lag of the loop is 180 degrees and the loop gain is high. The "loop" involves the flight control system path from sensor to surface, and the aerodynamic path from surface back to sensor.

Structural resonance is a sustained, high frequency oscillation of a motion sensor and a control surface which is created when control system sensors sense small structural vibrations and send them back to the surface with 180 degrees of phase lag. The "loop" in this case involves the flight control system path from sensor to surface, and the structural path from surface back to sensor.

The data given in this paper will be concerned with "rigid body" limit cycle oscillations. Limit cycling can occur independent of structural deformation. A "rigid body" limit cycle therefore involves the aircraft's flight control system, control surface deflection, and aerodynamic response to control surface deflection. Structural deformation is not involved. Structural modes are not driven. The term "structural resonance" as used in this presentation will describe a structural vibration which is sustained by the aircraft's flight control system, and which is independent of aerodynamic feedback. Transmission of the control surface motion to the control system sensors is directly through the structure rather than through an aerodynamic response.

### PROCEDURE

Since control system instabilities can adversely affect flight safety, considerable time should be spent to insure that these characteristics are well known for all new aircraft. A reasonable approach to insure that limit cycling or structural resonance does not occur unexpectedly during flight is as follows. First, ground tests which use actual aircraft hardware should be conducted prior to first flight to predict limit cycle

and structural resonance characteristics. These tests should be used in conjunction with analytical prediction techniques. Second, large gain margins for flight control system instabilities should be applied for the first flight of a new aircraft to account for potential uncertainties. These uncertainties include inaccuracies in wind tunnel and theoretical predictions of stability derivatives, control system nonlinearities and anomalies, configuration variations, and inaccuracies in predicting sensor locations with regard to structural mode shapes. Third, carefully controlled inflight tests should be conducted early in the flight test program to establish the actual limit cycle and structural resonance characteristics of the aircraft. These tests will allow relaxation of the large gain margins applied to the initial flights.

If proper procedures and techniques are used, some of the uncertainties associated with predicting flight control system instabilities can be eliminated or reduced. The AFFTC feels that the best method of doing this is to conduct ground tests on the actual flight control system and structure of the aircraft. This eliminates all control system and structural uncertainties. Past experience has shown that nonlinearities and accurate control system and structural representation have a much more pronounced effect on limit cycle and structural resonance characteristics than approximations in aerodynamic effects.

To conduct limit cycle ground tests on actual aircraft, a small computer is connected to the control surface output and control system sensor input to simulate aerodynamic feedback. Since many aerodynamic terms have been found to have little effect on limit cycle characteristics, simplified aerodynamic equations may be used. Small and large inputs should then be inserted into the system at incrementally increasing values of total loop gain. Limit cycle amplitudes and frequencies are recorded at each gain setting until a divergent oscillation is obtained. These ground test results are used in conjunction with the limit cycle criteria which will be discussed later to establish the maximum allowable first flight control system gains.

Structural resonance ground tests are very simple to conduct on the actual aircraft. The tests simply involve inserting large, sharp inputs into each axis of the flight control system to excite structural vibrations. No aerodynamic computations are required. The frequency and amplitude of the resonance at control system gain values up to a factor of two above the maximum anticipated flight gains are recorded. From this data, gain margins for structural resonance are obtained.

A recommended procedure for obtaining inflight limit cycle and structural resonance characteristics of an aircraft is as follows. The ground tests just described should be conducted prior to first flight. Initial flights should then be performed using large gain margins for limit cycle and structural resonance. Before the flight envelope is expanded to higher airspeeds, carefully controlled inflight tests should be conducted to determine the actual limit cycle and structural resonance characteristics of the aircraft. The inflight tests are accomplished by inserting small inputs into each axis of the flight control system at incrementally increasing stabilized values of airspeed. An independent monitor should observe limit cycle tendencies at each stabilized airspeed. If no tendencies exist, the aircraft should be cleared by the flight controller to proceed to the next highest, predetermined airspeed until the tendency toward a large amplitude limit cycle occurs. At all times, the pilot should be ready to lower the flight control system gain should a large amplitude control system instability occur. The results obtained from inflight testing establish the actual aircraft characteristics and determine the maximum allowable flight control system gains based on limit cycle and structural resonance characteristics.

### CRITERIA

Based on experience gained from previous programs conducted at the Air Force Flight Test Center, criteria have been established which define acceptable gain margins for limit cycle and structural resonance. These criteria should be used for the initial flights of a new aircraft until the actual inflight characteristics are well known.

The limit cycle criterion is - With a gain margin of 6 db applied, no limit cycle shall exist with an amplitude greater than 0.5 degrees peak-to-peak in any axis.

The structural resonance criterion is - With a gain margin of 6 db applied, no structural resonance shall exist in any axis.

These seemingly conservative criteria were established to account for the many uncertainties discussed previously which exist in predicting limit cycle and structural resonance characteristics, and to insure safety of flight.

### SPECIAL TOPICS

Before presenting results, it is worthwhile to emphasize some special effects which have been experienced on previous programs. These effects should be considered in future system design and analysis. As will be shown later, large amplitude inputs have been found, through previous ground and flight testing, to saturate a system and cause divergent limit cycles to occur at a much lower gain value than they would have for an unsaturated system. Saturation limit cycles represent a severe hazard to flight safety, and every effort should be made to predict these characteristics as accurately as possible. Saturation limit cycles are highly nonlinear in nature and cannot be readily predicted by analytical methods. Ground tests should be used to predict these characteristics.

The next topic, digital sampling effects, have been seen to significantly degrade limit cycle characteristics by adding phase lag to a system. Thus sampling effects upon limit cycle characteristics should be considered in future system design. Additional gain margins should be designed into future digital systems to account for phase lag due to sampling.

### RESULTS

This section presents simulator, ground test, and flight test data for several different aircraft with which personnel at the AFFTC have been associated. It is hoped that this data can be used to more clearly understand and appreciate the phenomena of limit cycling and structural resonance. It is also hoped that the data can be used to show that rigid body limit cycles and structural resonance do indeed exist, and they must be thoroughly tested for and understood for all future aircraft.

Aircraft are identified symbolically only in this paper. Most of the aircraft discussed are relatively small and semi-rigid.

### AIRCRAFT A

Ground tests conducted on this aircraft (as described previously in this paper) prior to first flight showed that unacceptable limit cycle characteristics existed in the roll axis, and unacceptable structural resonance characteristics existed in the roll and yaw axis. Roll axis limit cycle amplitudes and frequencies obtained from ground tests are plotted versus total axis gain in Figure 1. For the original system, the limit cycle amplitude exceeded 0.5 degrees at a gain value well below the maximum anticipated first flight gain. The limit cycle characteristics did therefore not meet the criteria stated previously. Structural resonance oscillations in the roll and yaw axes obtained during ground test are shown in Figure 2. These oscillations occurred at gain values which were less than a factor of two greater than the maximum first flight gain, and therefore did not meet the structural resonance criteria.

A 17 radians per second lead and 40 radians per second lag network was added in the roll axis to improve the limit cycle characteristics. In addition, miscellaneous mechanical modifications were made to the flight control system. The resulting limit cycle characteristics are also shown in Figure 1. The electronic and mechanical modifications allowed the limit cycle criteria to easily be met.

A 13.5 Hz notch filter was added to the roll axis to eliminate structural resonance. The yaw servo actuator loop gain was reduced to eliminate structural resonance in the yaw axis. With these two modifications, no further resonance was encountered during ground tests up to a gain of twice the maximum expected in flight.

With the system modifications for limit cycle and structural resonance implemented, no control system instabilities of any nature were encountered on this aircraft during its flight test program. One additional problem which occurred midway through this aircraft's test program was discovered, through ground testing, when two 80 pound batteries were installed on the vehicle's center bay access door. The batteries altered the vehicle's structural characteristics and caused the pitch augmentation gyros, which were located near the access door, to pick up high frequency oscillations and sustain structural resonance in the pitch axis. Relocation of the gyros suppressed the resonance and gave acceptable structural resonance characteristics. This incident demonstrates the value of performing ground structural resonance and limit cycle tests after any significant structural or control system modification is made.

### AIRCRAFT B

This aircraft's flight control system was a derivative of aircraft A's flight control system, therefore most instability problems had been previously worked out. No limit cycling was predicted through ground test and none occurred during flight. The roll axis, which had been redesigned, did experience a structural resonance problem however. This resonance, shown in Figure 3, was discovered during ground tests. The resonance was not the normal type which is sustained through the control system feedback paths. It was a purely mechanical resonance sustained solely within the aileron surface actuator and its associated linkage. The resonance continued when the feedback paths were disengaged. If this would have occurred in flight, it may have caused a loss of aircraft. The resonance problem was eliminated by adding a mechanical damper within the aileron actuator. The damper decreased the sensitivity of the actuator to high frequencies, but did not significantly alter the response characteristics at the lower frequencies or reduce the maximum slew rate of the actuator.

### AIRCRAFT C

One of the most extensive series of limit cycle and structural resonance testing ever done on an aircraft was done of this aircraft. Thorough simulator, ground tests, and inflight tests were conducted. A primary purpose of running simulator limit cycle tests on this aircraft was to determine digital sampling effects upon limit cycle characteristics. To do this, the actual aircraft's flight control system digital computer was connected to an engineering simulation of the aerodynamics of the aircraft. The control system sensor outputs and stick commands, which were simulated on the aerodynamic simulator, were used as inputs to the digital computer. The digital computer outputs were the servo command

signals in each axis (pitch, roll, and yaw). These outputs were sent back to the simulator, where the servo and surface actuator response characteristics were simulated using an analog computer. Thus the aerodynamic effects and the servo and surface actuator response characteristics were the same for both the "analog" and "digital" results which will be shown in Figure 5. The only difference between the two sets of results were the control system effects from the sensor outputs to the servo inputs. In one case these effects were simulated on an analog computer (engineering simulator). In the other case the actual flight control system digital computer was used. The only digital effects which were not simulated on the analog computer were the digital sampling rates and the prefilters which were the input filters in the digital computer. The prefilters were first order filters with a break frequency of 100 radians in the pitch rate feedback path and 50 radians in the roll rate feedback path. (Limit cycle characteristics of the yaw axis were insignificant for this aircraft and will not be presented.) Digital sampling rates were 80 samples per second for the pitch rate feedback path and 40 samples per second for the roll rate feedback path. Resultant phase lag for various digital sampling rates are given in Figure 4. Note that there is no amplitude reduction associated with sampling effects as there is in the case of first order filters. Thus digital sampling effects should have a much more detrimental effect on limit cycle characteristics than the prefilters. Digital effects on limit cycle characteristics in the pitch and roll axes are shown in Figure 5. A degradation in limit cycle characteristics of 30 percent in the pitch axis and 18 percent in the roll axis is shown.

Large amplitude limit cycle data are also shown in Figure 5. These limit cycles were obtained by inserting large amplitude pulses into the system. Note that the large amplitude limit cycles occurred at much lower gain values than the small amplitude limit cycle data. The large amplitude pulses saturated the axis immediately, which resulted in some portion of the loop reaching a limit of some type (such as the rate limit of a surface actuator). When this limit was exceeded, additional phase lag was created in the loop. As is shown in the data, the additional phase lag caused the large amplitude limit cycles to occur at a much lower frequency than the unsaturated, small amplitude limit cycles. (The frequencies of the large amplitude data and the saturated small amplitude data were similar however.) Note that for this aircraft, large amplitude limit cycles were not the effect of digital saturation, since they occurred for both the analog and digital systems. They were therefore most likely caused by the rate limit of the surface actuators being exceeded.

Limit cycle characteristics obtained from ground test, inflight testing, and simulator results are shown in Figure 6. Limit cycle data is plotted versus dynamic pressure for the pitch axis data, and versus total axis gain for the roll axis data. Since the aircraft had flight control system gains which varied as a function of dynamic pressure in the roll axis, it was necessary to plot limit cycle data versus total axis gain. (The roll axis simulator data is for a different control system mode than the data which was shown previously, and therefore should not be compared to it.) Figure 6 shows that the only inflight data point obtained in the pitch axis (at the highest value of dynamic pressure attainable by the aircraft) compared fairly well with ground test results. It should also be noted that the first flight value of dynamic pressure was held to a value of 300 lbs/ft² to meet the limit cycle criteria. Inflight roll axis limit cycle data shown in Figure 6 also compares well with ground test results. Simulator results do not compare well to either flight or ground test results however. These particular simulator results were obtained with the actual digital flight control system computer connected to the simulator. Thus the only possible difference between the simulator results and ground test results was the servo and actuator response characteristics, and the deadband and hysteresis characteristics of the linkage in the actual control system. This is a good example of the importance of doing limit cycle ground tests on the actual aircraft.

Large amplitude limit cycle results obtained during ground tests on the actual aircraft are also shown in Figure 6. Again, the large amplitude saturation points occurred at a significantly lower gain value than the small amplitude divergent points. These large amplitude, saturation type instabilities must be taken into consideration when establishing flight boundaries. Although a large amplitude input is required to saturate the system at these lower gain values, the input size required to saturate the system gradually decreases as the gain increases, until only a small amplitude is required at the small amplitude divergent point. Thus, in the gain range between the large amplitude saturation point and the small amplitude divergent point, a moderate size input could be sufficient to saturate the system.

### AIRCRAFT D

This aircraft experienced three instances of unplanned inflight control system instabilities. This was an earlier aircraft, and ground testing techniques had not yet been fully developed. The experience gained from this aircraft hastened the development of these techniques at the AFFTC however.

Figure 7 is a time history of roll rate and aileron deflection during an inflight limit cycle oscillation on this aircraft. The motion was felt by the pilot and was considered to be objectionable. The amplitude of the oscillation was probably not constant due to the tendency of the control inputs to be fed back into the loop and cause a beating effect. The limit cycle was reduced to an acceptable level on subsequent flights by modifying an electronic filter in the control system.

Figure 8 in a time history of a 13 Hz structural resonance experienced during another flight of this aircraft. The oscillation was initiated at a relatively low value of dynamic pressure (130  $\rm lbs/ft^2$ ) and somewhat higher system gains, and continued through a large increase in dynamic pressure to a value of 1000  $\rm lbs/ft^2$ , at which point the control system gains were reduced slightly and the oscillation ceased. The pilot reported the oscillation to be the most severe that he had ever encountered. The structural resonance was eliminated on subsequent flights by installing a notch filter in the system.

A saturation limit cycle was also experienced during a different flight of this aircraft. A time history of this oscillation, which was primarily in the pitch axis, is shown in Figure 9. Due to the nature of the flight, dynamic pressure was rapidly increasing during the oscillation, and the instability was sustained and resulted in the loss of control and the eventual destruction of the aircraft from severe load-factor excursions experienced during the oscillation.

### AIRCRAFT E

Figure 10 presents limit cycle characteristics obtained from ground tests conducted on the actual aircraft, and compares these data with data obtained from limit cycle oscillations during flight. The data for the original configuration was obtained from a severe pitch limit cycle which occurred during the first flight of this aircraft. This was caused by the pitch control effectiveness (C ) being higher in flight than had  $^{\rm m}\delta {\rm e}$ 

been predicted from wind tunnel tests. A lead-lag filter was added to the original system, and all worn bearings and bushings were replaced. These modifications gave the improved characteristics shown in the figure.

### AIRCRAFT F

Ground test pitch axis limit cycle data for this aircraft is shown in Figure 11. Figure 12 is a time history of a pitch limit cycle which occurred during flight. Due to pilot inputs and inflight disturbances, the amplitude does not remain constant and cannot readily be compared with the ground data. However, the total loop gain was a value of 16 per second in the region which was considered objectionable by the pilot. This corresponds to an amplitude of about .65 degrees on the ground test data. It should be pointed out that the ground data represents steady state, constant amplitude, limit cycle oscillations. If the system is disturbed with a relatively large input which does not saturate the system, it will oscillate at an initial amplitude which is equal to the amplitude of the input, and then decay down to the steady state, constant amplitude value. Thus although the steady stated ground test value may only be .65 degrees, much larger amplitudes may be experienced in flight (as is shown in Figure 12) due to external or pilot-induced disturbances.

### AIRCRAFT G

Structural resonance was obtained in all three axes during ground tests conducted on this aircraft prior to first flight. Miscalculation of rate gyro sensor location with respect to structural mode shapes was the reason the resonance occurred. Resonant frequencies and modifications used to eliminate the resonances are given in Table II.

Table II
Structural Resonance Ground Test Results

Axis	Resonant Frequency (Hz)	Control System Gains	Modification Applied
Pitch	11.6	Nominal	11 Hz Notch Filter
	30.3	Nominal	53 percent Reduction in Servo Actuator Loop Gain
Roll	19.0	Nominal	20.3 Hz Notch Filter
	49.0	Nominal	<del></del>
Yaw	20.0	Nominal	20.5 Hz Notch Filter
	48.0	Nominal	

The modifications listed eliminated structural resonance in all three axes up to a gain value of twice the value expected during flight, which satisfied the structural resonance criteria and contributed to the flights being flown in a safe manner. The 49 Hz and 48 Hz oscillations shown in the original roll and yaw axes were of low amplitude and were evidently eliminated by amplitude reduction associated with the lower frequency notch filters.

This particular aircraft was predicted to have a flight control system aeroelastic instability of the type discussed previously in the roll axis. This instability was predicted through the use of an analytical program used primarily for flutter prediction,

and which contained a relatively good aerodynamic and flight control system model of the aircraft. Predicted curves for this roll instability are given as a function of airspeed in Figure 13. Carefully controlled inflight tests, which were conducted in a manner identical to that discussed previously, were performed to correlate inflight results with predicted data. A damped oscillation was obtained during these inflight tests. Data from this oscillation is also shown in Figure 13. Flight and predicted results agree well. A sophisticated notch-type filter was added to the roll axis, and the roll axis rate feedback gains were reduced to eliminate this oscillation.

### AIRCRAFT H

This aircraft experienced a flight control system/aeroelastic instability in flight which was very similar to the oscillation experienced by Aircraft G. The oscillation had not been predicted prior to flight however. The oscillation was eliminated during the flight by decreasing airspeed. The oscillation was eliminated on subsequent flights by applying similar modifications to the control system as those discussed for Aircraft G.

This aircraft also experienced a lower frequency (3.5 Hz), rigid body limit cycle oscillation in its roll axis during flight. The oscillation was damped, and was initiated several times by inflight disturbances. Since simulations had been done previously with the aircraft's actual flight control system electronic box connected to a six-degree-of-freedom aerodynamic simulation, it was wondered why this tendency to limit cycle had not been seen on the simulator. (Complete ground tests as described in this paper had not been performed on this aircraft.) Thus a short simulator study was conducted to try to obtain the limit cycle at the conditions it was observed in flight.

Three flight conditions were looked at on the simulator; Mach = 0.9, ALT = 15000 ft, Mach = 0.9 ALT = 10000 ft, and Mach = 0.95, ALT = 10000 ft. (The inflight damped limit cycle occurred at Mach = 0.90, ALT = 15000 ft.) All previous simulator studies had been conducted by simulating only the first order transfer function for the surface actuator  $(\frac{20}{5+20})$  and not simulating the higher frequency, second order transfer function of the

servo actuator  $(\frac{52^2}{S^2 + 72.8S + 52^2})$ . At Mach = 0.95, ALT = 10000 ft three cases were run.

In one case, the aircraft's flight control system was simulated on the computer. In another case, the aircraft's actual flight control system electronic box was connected to the computer. In both of these cases, only the first order surface actuator transfer function, and not the second order servo transfer function, was simulated on the computer. In the third case, the actual electronic box was connected to the computer and both the first order surface actuator and second order servo actuator transfer functions were simulated on the computer. The results are shown in Figure 14. Cases 1 and 2 compared well, indicating the actual flight control system electronics had been simulated accurately. A steady state limit cycle occurred for Case 3 which had not been present in Case 1 or 2, indicating that the second order transfer function made a significant difference for this condition. Data with and without the second order transfer function are also shown for Mach = 0.9, ALT = 15000 ft, and Mach = 0.9, ALT = 15000 ft. (the actual condition experienced in flight). The Mach = 0.9, ALT = 15000 ft condition shows a limit cycle of slightly over 3 Hz which has relatively low damping, which is very similar to what was experienced in flight.

This case indicates the importance of including an accurate representation of the aircraft's flight control system in all techniques which are used to predict limit cycle characteristics.

### CONCLUSIONS AND RECOMMENDATIONS

- 1. Significant time and effort should be devoted to predicting flight control system instabilities of a new aircraft prior to first flight.
- 2. A sufficient amount of data has been obtained from previous programs to show that "rigid body" limit cycles and structural resonance do indeed exist and can be predicted fairly accurately if ground test and analytical techniques which accurately describe the system are used.
- 3. Ground tests using actual vehicle flight control system hardware and software (or a duplication thereof) should be conducted prior to first flight to predict rigid body limit cycle characteristics. Structural resonance ground tests should be conducted on the actual vehicle prior to first flight. Actual vehicle hardware should be used in these tests to account for as much of the nonlinear nature of the problem as possible.
- 4. Large limit cycle and structural resonance gain margins should be applied until actual inflight characteristics are known. Large gain margins account for the many potential uncertainties which exist in predicting these phenomena.
- 5. Carefully controlled inflight limit cycle and structural resonance tests should be conducted early in the flight test program to establish the actual characteristics of the system.
- 6. Large amplitude inputs have been found to saturate flight control systems and cause lower frequency limit cycles to occur at significantly lower gains than limit cycles due to small amplitude inputs. Large amplitude limit cycles represent a severe hazard to



# DISTRIBUTION AND AVAILABILITY ON BACK COVER

1-8

flight safety, and every effort should be made to predict these highly nonlinear instabilities as accurately as possible.

7. Results obtained from one aircraft indicated a degradation in limit cycle characteristics of 30 percent in the pitch axis and 18 percent in the roll axis due to using the aircraft's actual digital flight control system computer as opposed to an anlog simulation of the flight control system. The degradation was felt to be primarily caused by digital sampling rate effects. Thus sampling effects upon limit cycle characteristics should be considered when designing digital flight control systems. Additional gain margins should be designed into future systems to account for phase lag due to sampling. Also, these effects should be included in the techniques used for predicting limit cycle characteristics.

### AIRCRAFT A

Original System
Modified System

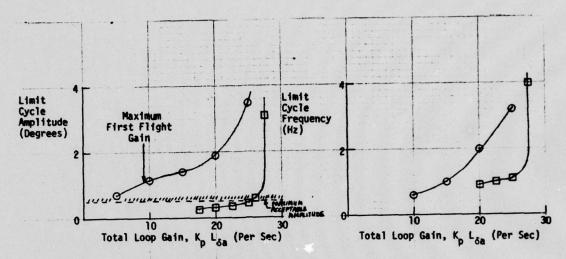
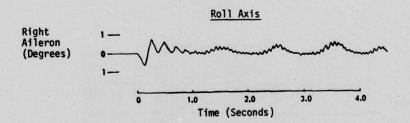


FIGURE 1 GROUND TEST LIMIT CYCLE PESINGS - ROLL AXIS



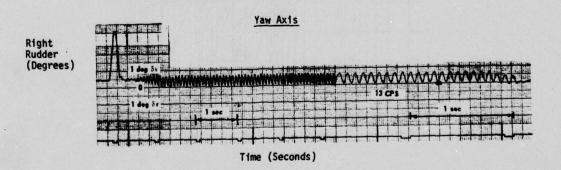


FIGURE 2 STRUCTURAL RESONANCE OBTAINED DURING GROUND TEST

Mechanical System Only -No Electronic Feedback

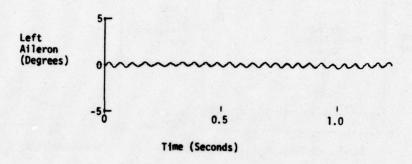


FIGURE 3 MECHANICAL RESONANCE OBTAINED DURING GROUND TEST

### AIRCRAFT C

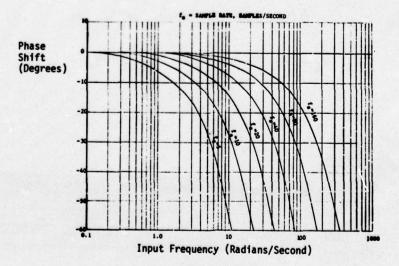


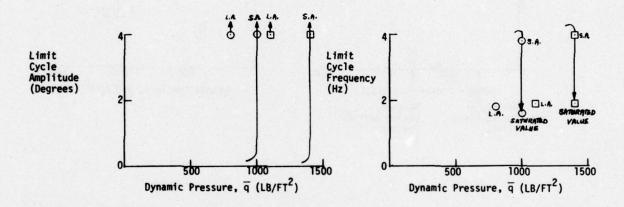
FIGURE 4 ZERO-ORDER-HOLD SAMPLING EFFECTS ON PHASE SHIFT

### AIRCRAFT C

NOTE: S.A.= Data obtained from small amplitude inputs

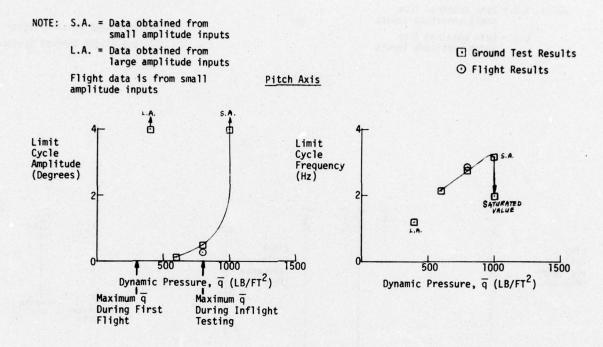
L.A.= Data obtained from large amplitude inputs ☐ Analog Flight Control System
○ Digital Flight Control System

### Pitch Axis



# Limit Cycle Amplitude (Degrees) 2 Dynamic Pressure, q (LB/FT²) Roll Axis Limit Cycle Frequency (Hz) Dynamic Pressure, q (LB/FT²) Dynamic Pressure, q (LB/FT²)

FIGURE 5 SIMULATOR LIMIT CYCLE RESULTS - DIGITAL EFFECTS



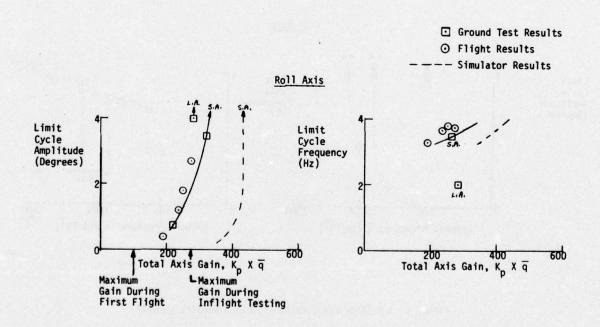
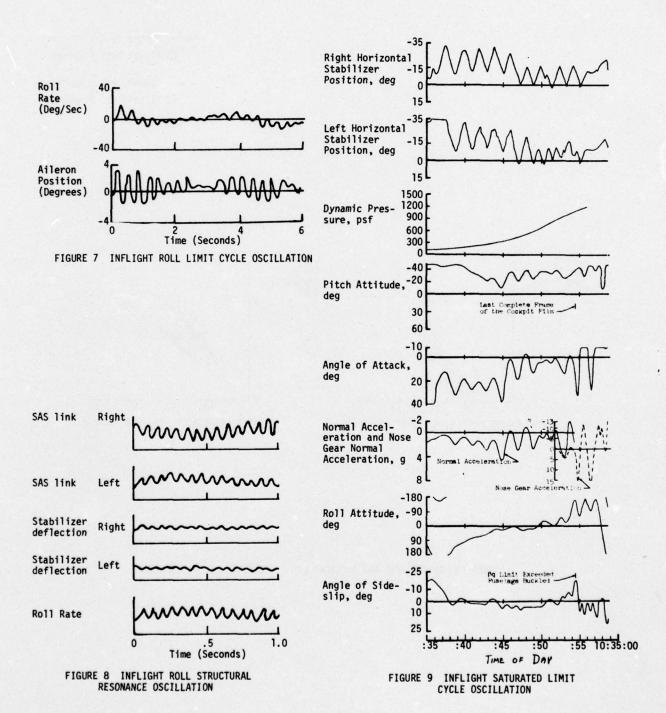
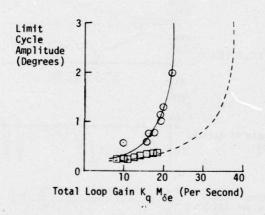


FIGURE 6 GROUND TEST, INFLIGHT, AND SIMULATOR LIMIT CYCLE RESULTS



Ground Test
O Flight Test
O Flight Test
O Flight Test
OFIGHT Test



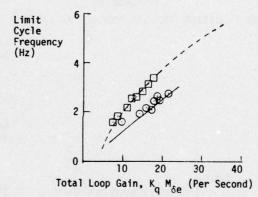


FIGURE 10 GROUND TEST AND INFLIGHT LIMIT CYCLE RESULTS - PITCH AXIS

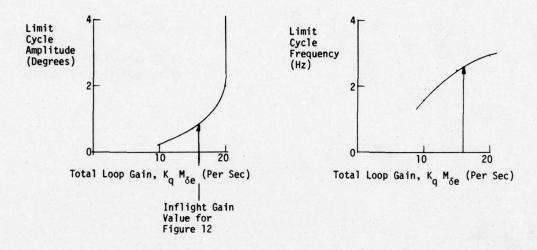


FIGURE 11 GROUND TEST LIMIT CYCLE RESULTS - PITCH AXIS

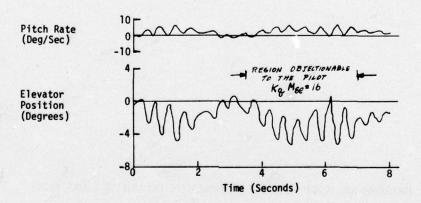


FIGURE 12 INFLIGHT PITCH AXIS LIMIT CYCLE

Predicted Results

O 30% Nominal Gain Flight

15% Nominal Gain Results

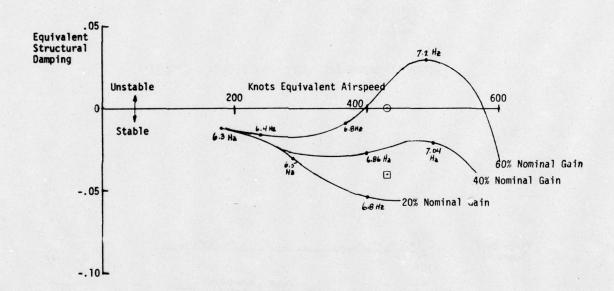
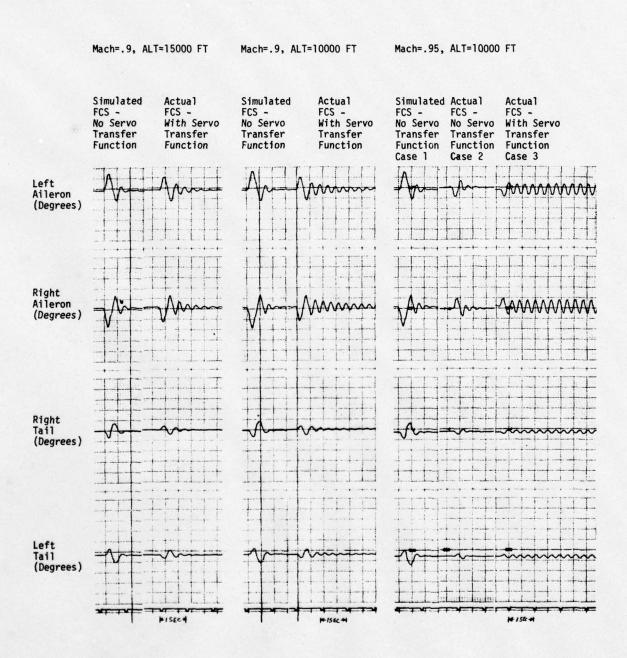


FIGURE 13 PREDICTED AND FLIGHT RESULTS FOR AEROELASTIC INSTABILITY - ROLL AXIS

FCS = Flight Control System



Time (Seconds)

FIGURE 14 SECOND ORDER TRANSFER FUNCTION EFFECTS ON LIMIT CYCLE CHARACTERISTICS

### AGARD FLIGHT MECHANICS PANEL SYMPOSIUM

### "FLIGHT TESTING TECHNIQUES" AUTUMN 1976

By: R.J. Poole, C.Eng., B.Sc. (Eng), M.R.Ae.S. Flight Test Engineer,
Hawker Siddeley Aviation Ltd.,
Dunsfold, England.

### SUMMARY

A test programme to demonstrate the aircraft's controllability in, and the recovery procedure from a spin was formulated with reference to spinning tunnel tests, and this paper describes its implementation.

Data presented here was gathered using the aircraft's PCM recording equipment and telemetered records observed by flight test engineers, together with the safety ground pilot, while the spins were being executed. This instrumentation together with the pilot displays and warnings in the cockpit are described herein.

Finally, the paper states the recovery procedures to be adopted and the pilots' qualitative assessment of their effectiveness.

### SYMBOLS

M	Inertia	moment	about pi	tching a	axis			
N	"	"	" yaı	wing	"			
L			" ro	lling	**			
A,Ix	Moment	of inert	ia about	rolling	g axis			
В		"		pitchin	ng "			
C,Iz		"	"	yawing				
p	Roll ra	te						
q	Pitch r	ate						
r	Yaw rat	е						
v	Sidesli	p veloci	ty					
1 <sub>r</sub>	Non dim	nensional	rolling	moment	due to	yawing		
1 <sub>p</sub>	"	"	"	"	**	rolling		
1 <sub>v</sub>	"	" .	**	"	"	sideslip		
19	"	"				rudder		
nr	"	"	yawing		**	yawing		
n <sub>p</sub>	"	"	•	•	"	rolling		
n <sub>v</sub>	"	"	"	"	"	sideslip		
n <sub>5</sub>	"	•		*	"	rudder		
n, B d	Sidesli	p angle						
d	Inciden	ce						
5	Rudder	angle						
T.G.T.	Turbine	gas tem	perature					
I.A.S.		ed air s						
CLO	Non dim	nensional	rolling	moment	due to	sideslip	(American	notation)
Cha	•	",	yawing	•	" '	. "		

### 1.0 INTRODUCTION

Intentional spinning of many modern combat aircraft is prohibited but nevertheless spins may result when these aircraft are manoeuvring near the extremes of their flight envelopes.

Departures from stable flight occasioned by wing rock, wing drop or excessive sideslip at high incidence can develop into wildly oscillatory or very fast flat spins from which recovery after a turn or so is not possible. Clearly, early identification of the type of spin an aircraft is entering will enable the pilot to apply correct control movement to return to controlled flight before the spin has developed to a point where recovery is unlikely.

One of the design aims for the Hawker Siddeley Hawk T Mk 1 was to produce a training aircraft with good spin entry and recovery characteristics in order that this disorientating environment could be demonstrated in safety. The airframe configuration was chosen to achieve this aim.

The Hawk is a tandem two seat intermediate flying and weapon training aircraft designed to fulfil roles currently covered by the H.S. Gnat and Hunter and the BAC Jet Provost within the Royal Air Force (See Figure 1). It is powered by a Rolls-Royce Turbomeca Adour turbofan engine operating behind a fixed geometry intake and is capable of supersonic flight in a dive. The fin is set well forward of the tailplane and consequently the fin and rudder remain unblanked by the tailplane wake at high incidence. With the exception of the rudder all the flying controls are power operated by dual hydraulic systems with spring feel units.

A flight test programme to demonstrate that the Hawk could be spun safely with and without underwing stores over the full centre of gravity range was formulated and its implementation is the subject of this paper.

### 2.0 FACTORS AFFECTING THE SPIN

A spin is a more or less steady motion which may result when an aircraft is disturbed in roll or yaw at incidences at or beyond the stall.

At incidences above that at which the stall occurs, some of the more important aerodynamic stability derivatives change sign or magnitude suddenly and enable the aircraft to enter a self-sustaining rotary motion or spin. The damping in roll derivative lp, which normally damps rolling disturbances, becomes positive and consequently accelerates the aircraft when it is disturbed in roll, i.e. the falling wing, although at a greater incidence than the rising wing, produces less lift and therefore carries on falling. Disturbances in yaw will also generate disturbances in roll, which can cause wing drop and entry into a spin.

Normally, an aircraft will enter a spin with the nose above the horizon and will take several turns before it attains a steady helical flight path about a vertical axis.

If the spin axis is above the aircraft, the spin is said to be erect and if below the spin is termed inverted.

The spinning motion is a complex one involving pitching, rolling, yawing and sideslipping, but if it is steady all the moments and forces acting on the aircraft must balance and the aircraft will be in a state of equilibrium.

Sometimes, a steady spin is not attained and the aircraft oscillates in pitch, roll and yaw, but more normally an aircraft with a conventional planform and inertia distribution, will orientate itself in such a way as to reach equilibrium.

In the spin, the resultant aerodynamic force normal to the plane of the wings acts through the axis of the spin. The aircraft drag is equal and opposite to the gravitational force and the lift force is reacted by the centrifugal force generated by the rotation of the aircraft about the spin axis. Sideforces are small since sideslip is usually small and sideforce balance plays little part in determination of the spin characteristics.

The type of spin and the aircraft's orientation are principally determined by the balance of the moments about the aircraft axes. For equilibrium, the inertia moments are exactly balanced by the aerodynamic moments, the balance being effected by the aircraft's adjustment of the rate of spin rotation and the sideslip angle.

Pitching moment balance :-

The inertia moment about the pitching axis is M = (C-A)pr

For the Hawk (C-A) is positive (See Figure 2) and in an erect spin, where p and r have the same sign, is a nose up pro-spin moment. This is balanced by the net aerodynamic nose down pitch moment of the wings and tailplane.

Rolling moment balance :-

The inertia moment about the rolling axis is L = (B-C) qr

L is negative (see Figure 2) and in an erect spin it is balanced by a net pro-spin aerodynamic rolling moment composed of  $l_p$ ,  $l_r$ ,  $l_v$  and  $l_v$  some of which are pro-spin and some anti-spin. For a standard spin  $l_p$ ,  $l_r$  and  $l_v$  are pro-spin and  $l_v$  is anti-spin.

Yawing moment balance :-

The inertia yawing moment about the yawing axis is N = (A-B) pq

N is -ve in an erect spin and is balanced by a net pro-spin aerodynamic moment composed of  $n_p$ ,  $n_r$ ,  $n_v$  and  $n_p$ .

In a standard spin  $n_p$  is anti-spin and  $n_v$ ,  $n_r$  and  $n_{\phi}$  are pro-spin.

Alterations in any of the flying control settings will change the balance of the moments and will result in a change in spin rate or sideslip angle or both.

Moving the stick forward will produce a nose down pitching moment and gyroscopic precession in yaw normally increases sideslip and spin rate. Increased spin rate increases the pro-spin nose up inertia moment and incidence will increase until balance is attained.

Application of aileron in the direction of the spin (in-spin aileron) will increase the roll rate and if the ailerons produce adverse yaw, will tilt the inner wing further below the horizon and slow the spin rate. If the ailerons produce proverse yaw, the wing tilt will be reduced and the spin rate will increase. See Figure 3 for aircraft orientation in a positive spin.

Application of aileron against the direction of spin (out-spin aileron) will produce the opposite effect, i.e. adverse yaw will decrease wing tilt and increase spin rate.

An increase in spin rate will usually result in an increase in incidence and will flatten the spin.

### 3.0 TEST PROGRAMME

The following programme was adopted to explore the spinning characteristics of the Hawk :-

- 1. Estimation of the aircraft's likely spinning behaviour and the effectiveness of various control inputs in inducing spin entry and recovery, from the results of wind tunnel tests.
- 2. Modification of the aircraft to provide additional spin recovery aids and the installation of telemetry equipment.
- 3. In flight testing of the anti-spin parachute deployment and release system.
- 4. In flight engine relighting checks to give confidence that the engine would relight satisfactorily if flame-out occurred or if it surged and had to be shut down.
- 5. In flight investigations of spin entry and recovery techniques and exploration of developed spins guided by the results of paragraph (1) above. These tests were made over the full aircraft centre of gravity (C.G.) range with and without underwing stores.

It was required to demonstrate that the aircraft would recover from four and two turn spins in the clean and with stores configurations respectively using a conventional simple technique.

6. Exploration of the effects of control mishandling on entry, during and on recovery from incipient and developed spins and also the tendency to spin from poorly executed aerobatic manoeuvres.

### 4.0 SPINNING BEHAVIOUR PREDICTIONS

Before embarking on a spinning clearance test programme, it is essential to examine results from wind tunnel tests in order to verify the computed values of the lateral and directional aerodynamic derivatives at high incidence. These tests should be conducted at the highest Reynolds Number possible and to incidences well beyond the stall. Typical derivative measurements for the Hawk are shown in Figure 4.

In the case of the Hawk, the spin and the effect of controls on spin entry and recovery were assessed in the vertical spinning wind tunnel at the Institut de Méchanique des Fluides de Lille, France using 1/18th scale models which had inertia distributions fully representative of the aircraft, at various centre of gravity positions.

The first model was scaled for a test altitude of 6,000 metres to achieve a light simple model and had adjustable control surfaces that were set for each chosen test condition. Model geometry could be varied by aft, forward and vertical movement of the fin and various nose and ventral strakes were added during the tests to change the aircraft's directional stability.

The second model was heavier than the first and was scaled for a test altitude of 9,000 metres. Any or all of the flying controls of this model could be actuated by radio control from pro-spin settings to neutral or anti-spin positions.

Effects of undercarriage, flaps, underwing pylons with and without Matra 155 rocket launchers, gun pod and airbrake extended could be evaluated on this model.

The scale factors applicable to the model motion inertias and dimensions are listed in Table 1.

Over three hundred spins, spin entries and recoveries were executed in the wind tunnel with the first model in its datum configuration and some interesting results were obtained.

Even with the controls set in a pro-spin sense a calm spin was rarely sustained beyond four turns. Usually the model became disturbed and the spin would stop and sometimes become inverted or develop into an unsteady auto roll at incidence below the stall.

Identical successive launchings were seen to produce motions of a different character.

In an attempt to obtain more consistent spin behaviour a further 600 launchings were made with the model modifications listed earlier and it was found that the nose strakes in particular made a steady spin more likely to occur.

The effects of nose strakes on the rolling and yawing moments due to sideslip  $(1_v$  and  $n_v$ ) as measured in the wind tunnel are shown in Figure 4.

The reduced fin effectiveness at about  $30^{\circ}$  incidence when the fin was immersed in the wing wake was improved by reducing the destabilizing effect of the nose with strakes as shown by the smoothing of the n and 1 curves.

A further 620 launches were made with the second model to determine the effects on the spin of flaps, undercarriage and airbrake in their extended positions and also fuel and store loadings. Further tests with the nose strakes were conducted with this model which confirmed the improvement conferred by these devices.

In the datum configuration, the second model exhibited the same characteristics in the spin as the first.

If the model was launched into a spin with anti-spin control settings rotation always stopped before some other motion started. The aircraft modifications investigated in the wind tunnel were not attractive to the design department. For example the nose strakes might upset the engine intake flow and reduce longitudinal stability, so it was decided to make some preliminary flight investigations to determine whether any modifications were in fact essential.

The justification for this philosophy was that the aircraft had shown itself to be very spin resistant during the wing stalling tests, and whenever recovery controls were set the tunnel model rotation always stopped before some other motion commenced. In addition, Reynolds Number effects were expected to be favourable at full scale.

By the time the full scale flight tests were commenced, however, it was decided to fit ventral strakes for reasons unconnected with spinning behaviour. In the event the percentage of successful spin entries was about 99%.

A criterion for judging whether an aircraft is prone to departure is the sign of the directional divergence parameter  $C_{n_{p,n}}$  (using American notation), i.e. if  $C_{n_{p,n}}$  is negative the aircraft will diverge into roll or yaw gyrations leading to possible spin entry.

Cagory (Cng) cos od - Iz (Cig) sin d

For the Hawk Common was always positive (See Figure 5) and the aircraft showed good spin resistance qualities requiring deliberate control input to enter a spin at the stall.

Free flight model spinning tests using models dropped from helicopters were not used for this programme. Some manufacturers use this technique but it has been shown to be very expensive and time consuming as the models are often damaged and weather conditions are often unsuitable. There is some doubt as to whether this form of testing will yield results that are not found in spinning tunnel tests although larger Reynolds Numbers can be covered. Hawker Siddeley have acquired considerable experience of spinning programmes with the Hunter and Gnat using drop models and the Harrier using the spinning tunnel.

### 5.0 SPINNING CHARACTERISTICS PREDICTED FROM SPINNING TUNNEL TEST RESULTS

Tunnel tests indicated that a spin could be maintained with pro-spin rudder and also the addition of out-spin aileron, although if the spin was at all agitated out-spin aileron was likely to increase the agitation. In some cases the spin could then be expected to degenerate into an auto roll, inverted spin or some other erratic motion. Application of in-spin aileron was less likely to produce agitation but it might actually stop the rotation with the rudder applied in the pro-spin direction.

Recovery was most likely to be achieved with the application of anti-spin rudder and in-spin aileron with the tailplane returned to the neutral position.

These tests indicated that tailplane setting would not have much influence on the spin but would influence the type of recovery obtained. Tailplane set to give a nose up pitching moment would produce a lateral recovery while a nose down pitching moment setting would generate a vertical recovery.

The recommended recovery procedure, should the spin become inverted, was rudder neutral or if necessary against inverted spin and the other controls to neutral.

### 6.0 THE TRIALS AIRCRAFT DESCRIPTION AND MODIFICATIONS

The aircraft allocated to the spinning trials was the fourth Hawk T Mk 1 fitted with the following modifications to provide an additional safety margin during the exploration of sustained and maybe oscillatory spins.

### a. Hydraulic System Accumulator Capacity Increase

The Hawk is fitted with a ram air turbine (R.A.T.) to supply emergency hydraulic power to the flying control circuit should the engine flame out or the hydraulic pumps fail. If the engine were to surge at high incidence and/or sideslip it would be necessary to shut it down to prevent turbine damage and make large recovery control demands on the hydraulic system before relighting the engine. In this case the RAT would deploy, but it could not be guaranteed to provide enough hydraulic power with the aircraft at low forward speed and high incidence. To guard against this possibility, two additional hydraulic accumulators were fitted to supply enough power for a number of attempts at recovery from a spin should the RAT stall.

### b. Additional U.H.F. Radio

A duplex UHF radio system was fitted to enable a ground safety pilot and the airborne pilot to converse freely should the latter become disorientated. The duplex system was attained by replacing the aircraft's standard VHF set by an additional UHF set and the UHF sets were tuned to different frequencies.

### c. Anti-spin Parachute Installation

A pre-requisite of any spinning programme is the provision of an emergency spin recovery device and a tail parachute was chosen for the Hawk. A 2.15 metre diameter anti-spin parachute attached to a 13 metre strop was mounted in a compartment in the rear fuselage behind the rudder and above the jet pipe. To deploy the parachute, the pilot would trigger a dual cartridge gun and fire a steel bolt beyond the wake of the aircraft dragging with it the drogue parachute. The drogue parachute would then deploy and stream the main parachute. A nose down pitching moment would result which would reduce incidence enabling the controls to stop rotation and allow recovery.

The parachute strop was attached to the aircraft with an electrically activated three claw clamp and could be jettisoned when level flight was registed.

A failure of the jettison system could be overcome by accelerating the aircraft to break a weak link fitted to the strop.

### 7.0 ADDITIONAL COCKPIT INSTRUMENTATION

The standard aircraft instrument display was adequate for spinning operationally but for spin exploration it was desirable to provide more orientation indications.

The following additional instrumentation was fitted above the centre of the instrument panel.

- 1. Incidence gauge
- 2. Sideslip gauge
- 3. Aileron position gauge
- Rudder position gauge
   Turn and slip gauge
- 6. Direction of roll lights
- 7. Optical and audio altitude warnings

Rudder and aileron position gauges were required to assist the pilot to apply less than full aileron or rudder consistently and also to enable the controls to be exactly centralized when required.

The altitude warnings were provided to warn the pilot that he had descended to the minimum height to initiate recovery (15,000 ft.) and also the height at which the pilot should eject (8,000 ft.).

At 15,000 ft. a 1.2 KHz tone sounded for  $1\frac{1}{2}$  secs. and at 8,000 ft. this tone was modulated at 3 KHz with two flashing lights prominently displayed at the top of the instrument panel.

When a rate of roll greater than 15°/sec. was sensed in either direction, a light was illuminated on the side of the instrument panel, to which the aircraft was rolling.

### 8.0 DATA RECORDING

Data recording for post flight analysis of the spins was made with the aircraft's pulse code modulated magnetic tape recording system. Analogue signals were multiplexed, fed through an analogue-to-digital converter and recorded serially on magnetic tape.

In addition, the quantities listed on the following page were telemetered to a ground station situated on Dunsfold Aerodrome, HSA Kingston's flight test centre, for observation by flight test engineers and a ground safety pilot.

Parameter	Range	Sampling Rates
Normal acceleration	-4 to +10g	16.63 samples/sec.
Roll rate	+220 /sec. to -220 /sec. +160 /sec. to -160 /sec. +60 to -60	
Yaw rate	+160°/sec. to -160°/sec.	
Incidence	+60° to -60°	"
Tailplane angle	+ 6° to -15° +12° to -12°	•
Aileron angle	+12° to -12°	
Rudder angle	+20° to -20°	•
Airspeed	0 to 600 km	
Altitude	0 to 60,000 ft.	
Turbine Gas Temp. (TGT)	0 to 800°C	
Sideslip	+30° to -30°	

After the initial few flights in the programme, normal acceleration was replaced with sideslip because relatively large sideslip angles were experienced.

Normal acceleration is the best indication as to whether a spin is inverted or erect but yaw and roll rates will provide a similar indication. When roll and yaw rate are of the same sign the spin is erect and when they are of opposite sign the spin is inverted.

The telemetered quantities were displayed on meters for observation by the ground safety pilot and on a multi-pen trace recorder for flight test engineers to monitor.

A magnetic tape recording was made of the telemetered data and radio communications, so that a spin could be replayed on the meters for discussion between spins if anything unexpected should occur. (See Figure 6.)

For some tests a 16mm cine camera with a 100 mm focal length lens was mounted in the rear cockpit facing forward above the pilot's head to record the pilot's eye view. Film from this camera assisted the interpretation of the time history traces of the manoeuvres obtained from the computer.

### 9.0 GROUND STATION

The ground station was a rustic but situated on the extremity of the airfield away from known sources of radio interference.

Situated within the hut was a UHF radio receiver fed by a steerable aerial mounted on top of a mast. A signal strength indicator enabled the mast to be orientated most favourably for reception, however, because the aerial was not particularly directional, it did not need much adjustment.

The signal received was demodulated, recorded on one channel of a stereophonic tape recorder and then displayed on the meters and the multi-pen trace recorder.

During the tests the telemetered parameters were observed on the meter display by a ground safety pilot whose function was to assist the airborne pilot should he become disorientated. The former would advise him if he was carrying any unintended control deflections or if the spin was becoming inverted and would monitor the engine TGT as a surge indication.

The ground and airborne pilots were in duplex radio contact and their conversations were recorded on the second channel of the stereophonic tape recorder.

Flight test engineers monitored the time histories on the pen recorder in order to spot any tendency of the aircraft to go inverted and to see if any oscillatory parameters were becoming divergent. If oscillatory spins occurred, the trace recorder would show whether recovery action was effective even if it was not apparent to the pilot.

### 10.0 ANTI-SPIN PARACHUTE TESTING

To ensure that the anti-spin parachute would deploy satisfactorily the system was tested in three stages :-

### 1. Ground Test

The aircraft tailcone containing the parachute and deployment gun was mounted on a ramp so that the jet pipe was inclined at 70° to the horizontal. The gun was fired and the trajectory of the bolt and parachute recorded with high speed cine cameras confirming that the charges would drag the parachute beyond the wake. Specimen strop weak links were tested in a tensile test machine and found to fail at the design load.

### 2. Runway Stream Test

The system as a whole was tested by streaming and jettisoning the parachute on landing at 100 km and 60 km respectively and the parachute deployment satisfactorily recorded on film.

### 3. Airborne Stream Test

Final testing to prove the reliability of the system consisted of three airborne stream tests at 150-160 km at 25,000 ft., which were filmed by a chase aircraft.

The final test was conducted after a 30 minute cold soak at 40,000 ft. On each test the parachute was fully inflated and was jettisoned after 30 seconds. The parachute was towed to a speed of 185 km without suffering any visible damage.

### 11.0 ENGINE RELIGHTING TESTS

It was considered possible that engine surge would occur if for any reason high sideslip and incidence were encountered together. If this happened it would be necessary to shutdown the engine and then carry out a cold relight. To gain confidence that the relight would be successful, the engine was shut down above the maximum permitted relight altitude (m.r.a.). The aircraft was then allowed to descend at the speed appropriate to the best engine windmilling speed for relighting and the relighting procedure initiated after 1 minute just below m.r.a.

### 12.0 SORTIE PROCEDURE

The following standard operating procedure was adhered to for each sortie during the trials.

- 1. On the airfield before taxiing.
  - a) Check of duplex radio communication.
  - b) Flying control full travel checks monitored on cockpit gauges and on telemetry and check calibration of control position meters.
- 2. During taxi.

### Check yaw rate by differential braking

- 3. On climb to test altitude.
  - a) Check of roll rate on telemetry and roll direction on the cockpit lights.
  - b) Cross check on TGT, sideslip and incidence.
  - c) Check on altitude warnings on the climb through 8,000 and 15,000 ft.
- 4. At the test altitude prior to spin entry.
  - a) Confirm intended test entry technique, control movements, number of turns and recovery procedure.
  - b) Check aircraft configuration as required, i.e. airbrake retracted, flaps up etc.
  - c) Check anti-spin parachute system integrity indications.
  - d) Close throttle to idle.
  - e) Count down for on board instrumentation event mark and ground station multi-pen recorder start.
- 5. On recovery.
  - a) Check engine for surge during throttle opening.
  - b) Check all systems normal.

### 13.0 FLIGHT TESTS

The flight test programme could be divided into three phases as follows :-

- a. Exploration of the incipient spin, the tendency to enter a spin with various control applications and early recovery.
- b. Development of a stable spin up to and beyond the specified four turns and recovery.
- c. Exploration of oscillatory spin modes and the effect of control mishandling at spin entry and recovery. This phase also included investigation of the tendency to enter a spin from mishandled aerobatics and entry with engine power other than idle.

Phase 1 was executed in the clean configuration with a mid CG at entry altitudes of 40,000 ft. and 30,000 ft., while other CG's and effect of underwing stores were examined in phase 2.

The standard operating procedure of section 12 was followed in all cases.

Table 2 shows the order of configurations investigated and the number of spin entries covered in each case.

### a. Exploration of the Incipient Spin

Exploration of the incipient spin commenced with the examination of the effect of pro-spin controls applied at the stall. It was expected that the rudder would be the most effective spin inducing control but as stalling tests had shown that the ailerons remained effective at the stall, entries with aileron alone were to be investigated.

Full rudder and aileron were applied progressively, separately and together at various rates when stick hard back was reached and the aircraft entered an incipient spin at between 110 and 120 km. At this entry speed an incipient spin was always obtained in the direction of the applied rudder, however, entry was somewhat hesitant with rudder alone and oscillatory with pro-spin aileron alone.

Recovery was made by centralizing the controls after 1 to 2 turns.

In an attempt to make entry less hesitant and more consistent, the effect of application of pro-spin rudder together with stick hard back at buffet onset was investigated. A more positive entry was obtained and the technique was modified further by the choice of 150 km.IAS for the application of pro-spin control.

These early investigations were made at entry heights of 30,000 and 40,000 ft., and the height lost in these incipient spins was typically 2,000 ft. in total including about 1,000 ft. during recovery.

### b. Development of a Stable Spin

Having established a predictable method of entering a spin, the pro-spin control settings were held for an increasing number of turns so that the aircraft could establish itself in a relatively stable spin. Initially developed spins were entered from wings level flight at 150 km. The speed dropped to about 115 km. during the first turn while the nose remained above the horizon and then began to rise as the axis of the spin became more vertical.

Recovery was normally initiated after a chosen number of turns, if the spin became very oscillatory, if excessive sideslip built up, or when the speed had reached 200 km.IAS.

The number of turns required for recovery rarely exceeded two and was normally about one when the controls were centralized.

The maximum number of turns reached before initiation of recovery was 11 and the spin did not flatten noticeably.

Spins entered as described above were relatively steep so techniques that would often increase spin rate and incidence such as application of out-spin aileron and pushing the stick forward (see section 2.) were investigated.

A faster flatter spin could be obtained consistently if the tailplane was returned to neutral after 1 turn and full out-spin aileron was applied after 2 turns.

This technique produced a spin that was a little oscillatory and aircraft speed usually remained below the entry speed.

Figure 7 shows a time history of a 6 turn spin to the right from a wings level entry at 150 km IAS. Sideslip is particularly oscillatory at first but it settles down to a relatively steady positive (inward) value and hence the inner wing is well below the horizon. Yaw rate and roll rate reach about  $30^{\circ}/\text{sec.}$  and  $70^{\circ}/\text{sec.}$  approximately at an airspeed of 190 km.

In contrast figure 8 shows a 7 turn spin to the left from a wings level entry at 150 km followed by stick to neutral after 1 turn and full out-spin aileron after 2 turns. All the parameters are oscillatory and when the speed stabilizes at 155 km after dropping to 115 km, yaw rate and mean roll rate are  $-75^{\circ}$ /sec. and  $-130^{\circ}$ /sec.

Yaw and roll rate increase on each control application but sideslip only shows a major change and becomes more oscillatory on aileron application.

Data presented here was obtained from a post flight read out of the onboard tape recording.

If the stick was pushed appreciably forward of neutral especially in the presence of full aileron, or if tailplane and aileron inputs occurred together, the spin would become very oscillatory. Recovery was almost immediate when the controls were centralized.

During the 99 spins executed in the mid CG position, the following control inputs were investigated:-

Rudder	<u>Aileron</u>	Tailplane
Full pro-spin	Neutral	SHB
	•	Relaxed to Neutral
	Up to Full out-spin	SHB
		Relaxed to Neutral
•		Relaxed to Neutral then fully forward
	In spin	SHB
Partial	Neutral	SHB

Using the standard entry technique, the aerodynamic and inertia effects of underwing stores were investigated on spins of up to 4 turns before initiation of recovery.

Stores had very little effect on the spinning characteristics but could be said to calm the oscillations in sideslip.

The final testing of phase 2 was to examine the effect of CG variation on the spinning characteristics using the two established techniques. Here again scatter of results in terms of incidence sideslip and spin rate was large but there were indications that for the clean aircraft spin rotation rate increased as CG moved forward. Spin rotation rate was judged to be independent of CG position with underwing stores over the range investigated.

During this phase of the programme, some spin entries were made from a  $40^{\circ}$  to  $60^{\circ}$  angle of bank level turn at 200 km IAS. The throttle was closed to idle and as the speed decayed to between 160 and 170 km, full rudder was applied in the direction of the turn, together with full aft stick movement keeping ailerons neutral.

A more consistent spin entry occurred using this technique than entry with wings level at 150 km so a turning entry became the recommended method. Both entry techniques were used during the remainder of the programme however.

### c. Effects of Control Mishandling

Two hundred and sixty-three spins of more than 2 turns were accomplished in phase 2 of the trials and from these experiences the following mishandlings of controls were chosen for further investigation.

### Mishandled controls on entry :

- a. SHB before rudder applied.
- b. Partial rudder.
- c. Out-spin aileron.
- d. Entry with take-off flap set.

### Control Mishandling during the spin :

a. Application of out-spin aileron following relaxation of stick forward to neutral.

### Mishandled Recovery

- a. Tailplane relaxed before rudder centralized.
- b. Tailplane relaxed well forward before rudder centralized.
- c. Full out-spin aileron held.
- Stick held hard back.
- e. Stick held hard back with full out-spin aileron.
- f. Part in-spin aileron held.
- g. Opposite rudder applied.
- h. Controls abandoned.

Recoveries were obtained when the rudder, the predominant control, was centralized.

The test programme was concluded with an assessment of the aircraft's tendency to enter a spin from mishandled aerobatic manoeuvres including slow rolls, rolls off the top of loops and recoveries from the vertical plane.

The aircraft would enter an incipient inverted spin from a roll at too low a speed with very coarse control movements but recovery was quick when controls were centralized. This inverted spin differed from an erect spin in that the rudder was blown on in the direction of the spin.

Recoveries from low speed in a vertical climb could be executed by pushing the stick forward or pulling it back on receipt of very light buffet warning at about 60 km. If the buffet warning was ignored and speed reduced further, the aircraft would enter either an erect or inverted spin. Centralizing the controls would stop the spin.

### 14.0 ENGINE BEHAVIOUR

The engine surged on only six occasions during the trials when very high incidence and sideslip were encountered together during oscillatory spins, deliberately provoked by coarse misuse of controls.

The relighting procedure established before the trials enabled successful relights to be accomplished.

### 15.0 CONCLUDING REMARKS

The Hawk was being built to a tight time schedule and hence it was required to complete these spinning trials as quickly as possible. They were in fact completed in five weeks in 25 flights consuming 30 hours flying time.

The 340 spins were executed without any incidents or surprises and this was attributed firstly to the careful design of the aircraft to have good recovery characteristics and secondly to the thorough tunnel testing and analysis made before the flying started.

The equipment used for the trials was simple and was never responsible for an abortive flight or one from which data could not be retrieved.

Since the completion of these trials, A & AEE Boscombe Down have carried out their own spinning trials on an identical Hawk with similar success.

The spinning behaviour of the Hawk is summed up in the following manner by Mr. A.P.S. Jones - Project Pilot Hawk - who did most of the flying.

The Hawk is extremely spin resistant and exhibits no "cliff-edge" departure characteristics even when grossly mishandled. However, as these tests have shown, intentional spins can be demonstrated with remarkable consistency of behaviour during entry, in the fully developed spin and recovery.

Such variables as CG and inevitable small differences in entry technique are not markedly critical, and the aircraft is tolerant of quite a considerable degree of mishandling, yet the effects of controls can be demonstrated with confidence.

The absence of any "special-to-Hawk" techniques allied with a wide variety of spin characteristics which are predictably control dependent, and a blanket recovery technique which is also applicable to the incipient stages of the spin in most modern aircraft, add up to a combination of characteristics ideally suiting the Hawk to its role.

TABLE 1	
SCALING FACTORS FOR MODEL TESTING	
Length	λ
Area	×2
Volume	*
Moment of Inertia	en*/e
Mass	en*/e en*/e
Time	X
Velocity	<b>I</b> >
Acceleration	1.0
Angular Velocity	VX
Angular Acceleration	i/x
Force	enx/e
Pressure	emz/e
Reynolds Number	en x/e en x /e en u x 2/e un
λ = Scale Factor	
e = Density	
u = Viscosity	
SUFFIX m = Model Values	

TABLE 2

PHASE	CONFIGURATION	NO. OF SPINS	C.G.	DATA REQUIRED FROM TESTS
1	Clean	31	MID	Development of suitable entry technique
2	Clean	99	MID	Exploration of developed spins
	Empty Matra 155 R/L's *	17	MID	Aerodynamic effect of stores
	Ballasted Matra 155 R/L's	13	MID	Inertia effect of stores
	Ballasted Matra 155 R/L's + ballasted gunpod	10	MID	Aerodynamic and inertia effect of complete store loading
	Clean	18	AFT	Effect of C.G.
	Ballasted Matra 155 R/L's + ballasted gunpod	30	AFT	Effect of C.G.
	Clean	50	FWD	Effect of C.G.
	Ballasted Matra 155 R/L's + ballasted gunpod	27	FWD	Effect of C.G.
3	Clean	35	MID	Effect of control mishandling

<sup>\*</sup> R/L = Rocket Launcher



H.S. HAWK T. MK.I.

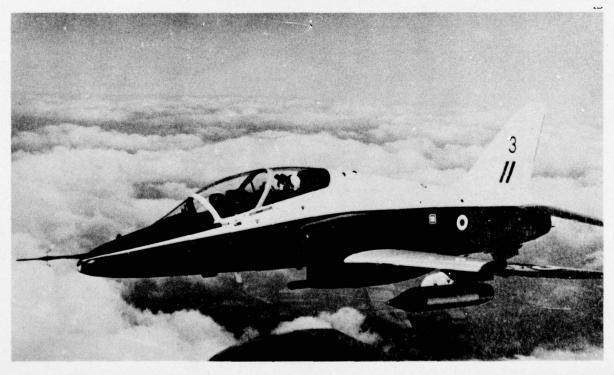


FIGURE 2

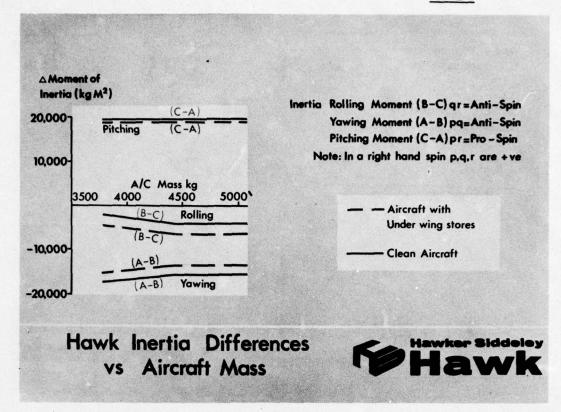
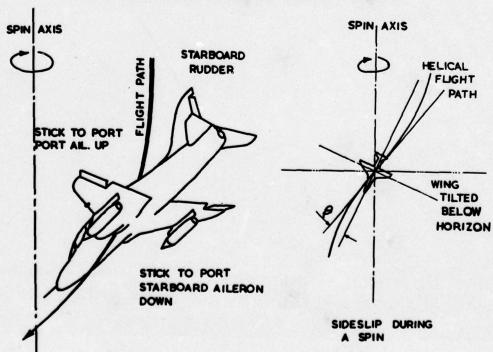


FIGURE 3

# ORIENTION OF AIRCRAFT IN A POSITIVE SPIN OUTSPIN AILERON AND PROSPIN RUDDER APPLIED



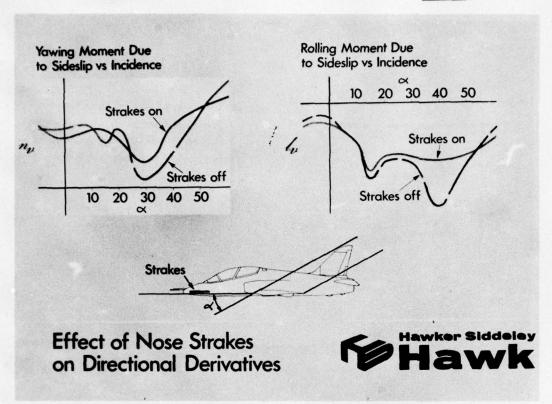
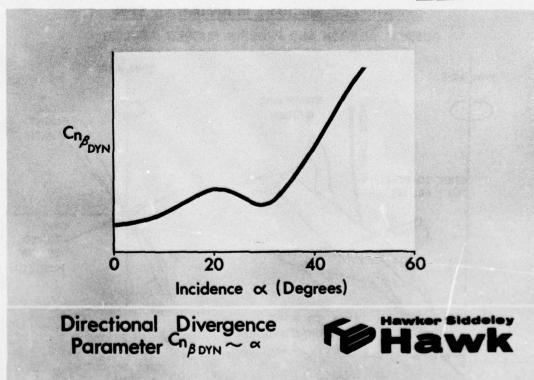
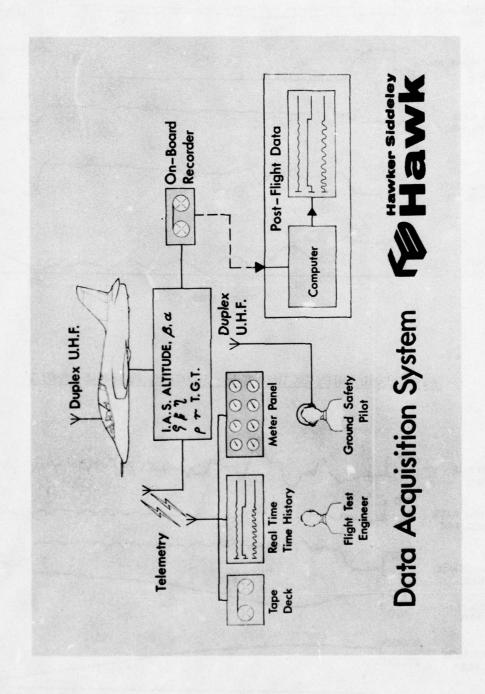
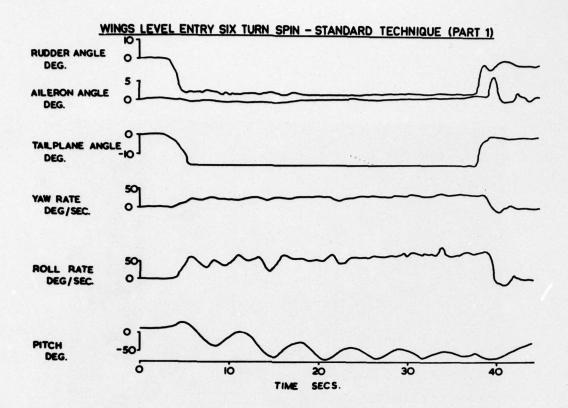


FIGURE 5

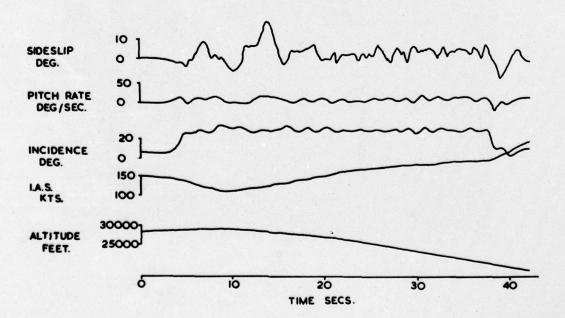




Carlotte Makes Colored

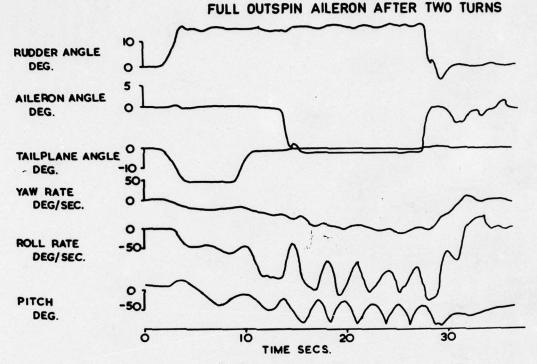


### WINGS LEVEL ENTRY SIX TURN SPIN - STANDARD TECHNIQUE (PART 2)

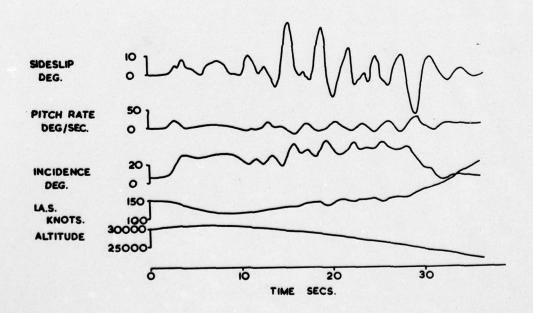


TO BE TO THE

# WINGS LEVEL ENTRY SEVEN TURN SPIN (PART 1) TECHNIQUE: STICK FORWARD TO NEUTRAL AFTER ONE TURN SINGLE CHARGE IN ALLERON AFTER TWO TURNS



# WINGS LEVEL ENTRY SEVEN TURN SPIN (PART 2) TECHNIQUE: - STICK FORWARD TO NEUTRAL AFTER ONE TURN FULL OUTSPIN AILERON AFTER TWO TURNS



#### MÉTHODES ET TECHNIQUES DE L'ESSAI DE VIBRATION EN VOL

par Gérard Piazzoli

Office National d'Etudes et de Recherches Aérospatiales (ONERA) 92320 Châtillon (France)

#### Résumé

Après un rappel du rôle joué par les essais de vibrations en vol vis-à-vis de l'ensemble de la recherche aéroélastique et des problèmes spécifiques posés par la représentation de la structure, on présente les trois méthodes mises en œuvre pour l'étude de la stabilité dynamique, dans le domaine subcritique : harmonique, impulsionnelle, aléatoire.

Le mémoire décrit : —les moyens technologiques, diversifiés, qui permettent de générer les forces d'excitation et leurs conditions d'application ; — les techniques de mesure et de conditionnement des signaux ; — les méthodes modernes d'exploitation fondées sur l'utilisation d'algorithmes de calcul en temps réel et la mise en œuvre de modèles de lissage.

Des exemples d'installations types sur des avions de divers types (avion léger, avion de transport subsonique, Concorde), illustrent l'exposé.

#### METHODS AND TECHNIQUES OF GROUND VIBRATION TESTING

#### Summary

Flight vibration tests are an important and sophisticated part of the aeroelastic research carried out for prototype clearance and certification of production aircraft. Three methods are used for dynamic investigations of the structure stability: harmonic, impluse, random, and, for each, are showed and illustrated:

— the different techniques for delivering excitation forces; — the special equipment of measurement and conditioning; — present methods of data processing and analysis, with the help of mathematical fitting models on computers.

Typical installations on aircraft of various types (light aircraft, subsonic transport, Concorde) are described.

#### 1 - GENERALITES

#### Rôle de l'essai en vol aéroélastique

La prévision et le contrôle expérimental du comportement aéroélastique des structures aéronautiques constituent pour les constructeurs l'une des démarches les plus complexes et les plus élaborées qui soient à accomplir lors de la réalisation d'un prototype. De nos jours, le domaine d'intérêt s'étend à toutes les catégories d'appareils, depuis le transport supersonique et les avions d'armes jusqu'aux avions de tourisme et aux planeurs, traduisant l'orientation générale de la construction aéronautique vers l'augmentation des performances par l'allègement des structures et l'affinement des formes.

En effet cette discipline , située à la charnière de deux domaines -le domaine structural et le domaine aérodynamique- prend en compte leurs difficultés propres et, dès le stade du projet, un vaste programme de recherches, théorique et expérimental, est généralement mis en oeuvre pour tout prototype important. Ainsi, avant réalisation du prototype :

- calculs dynamiques sur plans, à partir d'un devis de coefficients de masses et de raideurs,
- élaboration théorique des dérivées aérodynamiques instationnaires, en tridimensionnel,
- essais en soufflerie de maquettes dynamiquement semblables.

#### Après réalisation du prototype :

- essais de résonance au sol, pour déterminer les caractéristiques dynamiques de la structure, dans un schéma modal linéaire,
- calculs de stabilité aéroélastique.

Quelles que soient les précautions prises, au cours de ces différentes étapes, il subsiste toujours des incertitudes prévisionnelles, liées:

- sur le plan structural, à des effets non linéaires (raideurs d'ancrage de vérins en fonction de l'effort, frottements dans les timoneries, facteur de charge pour les surfaces portantes, contrainte thermique ...etc).
- sur le plan aérodynamique, au non respect simultané des paramètres de similitude aéroélastique, lors des essais sur maquette :

Fréquence réduite Nombre de Mach

L'essai de vibrations aéroélastiques constitue la dernière étape; son objectif est double :

- En premier lieu, étudier la stabilité dynamique de la structure prototype, afin de prévenir le dangereux phénomène de flottement lors de l'ouverture de domaine, en particulier dans le transsonique;
- 2) En second lieu, caractériser la réponse de la structure à des sollicitations quelconques, soit dans un concept "boucle ouverte" (action de l'environnement, turbulence atmosphérique par exemple), soit dans le concept d'asservissements type C.C.V. (action de volets spéciaux).

Si le point 1) ne nécessite que la mesure de l'évolution des paramètres dynamiques conditionnant la stabilité (fréquences, amortissements modaux), le point 2) requiert une connaissance complète des fonctions de transfert aboutissant à un véritable "étalonnage" de la structure soumise à l'écoulement aérodynamique. L'essai de vibrations en vol procure un apport d'informations globales, à échelle grandeur, dans les conditions réelles d'utilisation. Ces informations sanctionnent la qualité prévisionnelle des étapes antérieures (ou supplée à leur absence pour les projets plus modestes) et contribuent à assurer la sécurité et à fonder le dossier de certification.

#### 2 - MISE EN OEUVRE DE L'ESSAI AEROELASTIQUE -ASPECTS GENERAUX

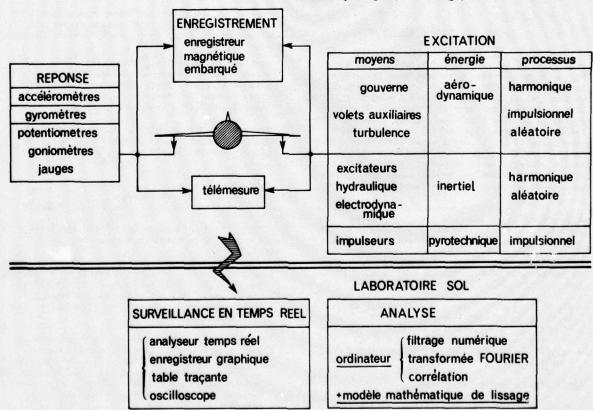
La mise en oeuvre de l'essai comporte, sur le plan des méthodes et de la technologie, plusieurs démarches dont les différents aspects sont schématisés figure 1.

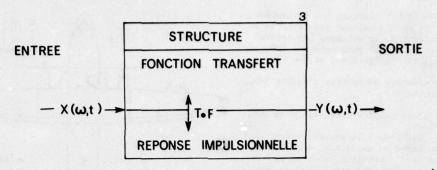
- l'Excitation constitue le problème le plus important, et il est souvent nécessaire de le prendre en compte dès le stade du projet. On peut distinguer trois aspects qui caractérisent l'excitation:
- la nature du processus, qui conditionne la méthode d'essai : Harmonique, Percussionnelle, Aléatoire ;
- le principe physique, ou la source d'énergie, auquel on fait appel pour engendrer les forces d'excitation : Aérodynamique, Inertiel, Pyrotechnique;
- les moyens technologiques d'application, très variés, que nous passerons en revue ultérieurement.
- La mesure comporte la détection de la réponse structurale par des capteurs spécialisés, leur conditionnement et le stockage des données, d'une part sur enregistreurs embarqués,

- d'autre part au laboratoire au sol, après transmission par télémesure .
- L'analyse comprend deux phases : la première est une surveillance de sécurité effectuée en temps réel ; la seconde assure l'exploitation complète en temps différé, par différents procédés.
  L'analyse utilise les méthodes générales d'identification des systèmes linéaires. La figure 2 présente les relations générales entrée-sortie d'un tel système. Quel que soit le processus d'excitation, le comportement de la structure peut être décrit soit dans le domaine fréquentiel (fonction de transfert), soit dans le domaine temporel (reponse impulsionnelle), les deux fonctions étant reliées par l'opérateur mathématique bi-univoque, transformée de Fourier, directe ou inverse.

## <u>Sur tous les plans les difficultés sont considérables</u>

- Les systèmes d'excitation doivent délivrer des forces importantes, dans des gammes de fréquences étendues, en l'absence de référentiel fixe alors que leur encombrement et leurs masses sont étroitement limités.
- Les systèmes de mesure doivent fonctionner en ambiance sévère, et la télétransmission des signaux pose des problèmes délicats à longue distance.
- Le temps imparti aux séquences d'essai est en général court, particulièrement en limite de domaine (piqués) où les paramètres aérodynamiques sont évolutifs.
- La structure de l'avion constitue toujours, en pratique, un système à entrées multiples (fig. 3), discrètes ou continues; les unes correspondent à des excitations appliquées dont on mesure les références d'entrée, les autres à des excitations parasites d'origine aérodynamique ("buffeting", tourbillons) dont





processus X (
$$\omega$$
,t)   

$$\begin{cases}
HARMONIQUE & Y(\omega)=A (j \omega) \cdot X(\omega) & - \begin{cases}
si x(\omega)=X_{\sigma}e^{-j\omega t} \\
et regime établi  $Y(\omega)=A(\omega) \\
si D(t) \rightarrow \delta(t), Y(t)=H(\sigma)
\end{cases}$ 

$$= si D(t) \rightarrow \delta(t), Y(t)=H(\sigma)$$

$$= si D(t) \rightarrow \delta(t), Y(t)=H(\sigma)$$

$$= si Spectre blanc \begin{cases}
\Phi_{XY}(s)=T(s) \\
R_{XY}(\sigma)=H(\sigma) \otimes R_{XX}(\sigma)
\end{cases}$$

$$= si Spectre blanc \begin{cases}
\Phi_{XY}(s)=T(s) \\
R_{XY}(z)=H(\sigma)
\end{cases}$$$$

Fig. 2 - Schéma bloc-relations entrée-sortie.

les références ne sont pas mesurées. Les fonctions de transfert sont multiples et le problème de la cohérence se pose. Lorsque ce coefficient est très inférieur à l'unité (bruits parasites importants), l'information est dégradée et les graphes des fonctions de transfert présentent de la dispersion.

- En outre la base de représentation modale est une base complexe où les modes structuraux sont couplés aérodynamiquement et souvent impossibles à isoler.

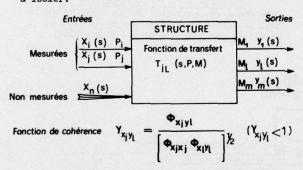


Fig. 3 - Entrées et sorties multiples en vol.

Pour résoudre ces difficultés, une technologie très spécialisée faisant appel à des solutions originales et des méthodes d'analyse très élaborées sont mises en oeuvre. Nous en illustrerons différents aspects.

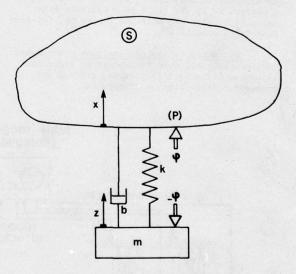
#### 3 - TECHNIQUES D'EXCITATION

#### 3.1 - Excitation inertielle

Principe - Le schéma de principe est donné figure 4. On fait appel à la force réactive engendrée par l'accélération d'une masse oscillante (M), dont les liaisons avec la structure comprenent des termes de raideurs (K) et des termes de viscosité (b).

La force f réellement appliquée à la structure est égale à la somme de la force développée par l'excitateur, des forces élastiques etdes forces de viscosité. Elle est aussi égale et opposée à celle produite par l'accélération absolue de la masse :

Dans tous les cas, le rapport  $\propto /_{M_3}$ " fournit la fonction de transfert au point P d'application de la force.



$$\begin{cases} f = \phi + k(z-x) + b(\dot{z} - \dot{x}) \\ f = -m\ddot{z} \end{cases}$$

Fig. 4 — Force d'excitation transmise à la structure par un excitateur de vibration.

Le processus pilote de l'excitation est en général un processus harmonique.

Excitateur électrodynamique - Il est constitué par deux blocs d'aimants permanents, en forme de U , de champ H , suspendus à la structure par ressorts, à très basse fréquence propre ( N ~ 1 Hz), ce qui constitue une plate-forme sismique.

Dans l'entrefer est placée une bobine plate de masse négligeable, liée rigidement à la structure, parcourue par un courant alternatif I. La force  $\,\Psi\,$  est alors proportionnelle au

courant  $[ \varphi = \lambda (H.I) ]$  suivant la loi de Laplace. Compte tenu de la faible raideur des ressorts et des faibles frottements de guidage, les termes de couplage avec les modes structuraux à fréquence plus élevée sont négligeables, et }~ 4

L'avantage de ce type d'excitation sismique est double :

- la structure n'est pas modifiée, en dynamique,

par l'excitateur, - la force f délivrée à la structure est contrôlée, en phase et amplitude, à partir du signal pilote de l'excitation, et l'on peut synchroniser et doser avec précision les forces appliquées par différents excitateurs répartis sur la structure.

Le schéma bloc de la chaîne électronique de commande est donné figure 5 et un exemple de l'installation d'essai du prototype de l'avion cargo franco-allemand Transall (fig. 6).

Un inconvénient réside dans la réversibilité de principe de l'excitateur sismique. Pour des structures très souples (voilures de gros appareils de transport), les mouvements induits à basse fréquence par des entrées parasites (turbulence par exemple) réduisent la course utile technologiquement limitée (environ 2 cm), donc les performances.

Un remède a été apporté en asservissant la plate-forme sismique à la structure aux basses fréquences, par l'apport d'un amortissement important de type visqueux. La fonction de transfert de la structure peut toujours être calculée localement, mais les forces ne sont plus dosables à volonté.

Excitateurs électromécaniques - Une autre amélioration peut être recherchée en augmentant la course utile de l'excitateur, grâce à une conception technologique différente.

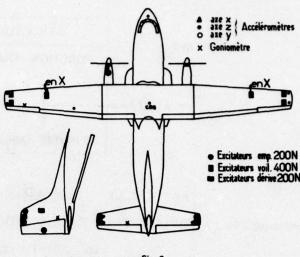


Fig. 6

Le schéma d'un tel dispositif est présenté figure 7. On utilise des moteurs couples qui sont accouplés à une crémaillère par l'intermédiaire de pignons, et constituent leur propre balourd.

La position moyenne de l'équipage est assurée par ressorts. Ce type d'excitateur peut être implanté aussi bien à la partie arrière d'un fuselage que dans un carénage d'extrémité de voilure d'un avion de transport, en ajustant à volonté la longueur de la crémaillère.

Excitateur électro-hydraulique - Cet excitateur est constitué par un vérin hydraulique, attaquant en général une masselotte en rotation, par l'intermédiaire d'un guignol.

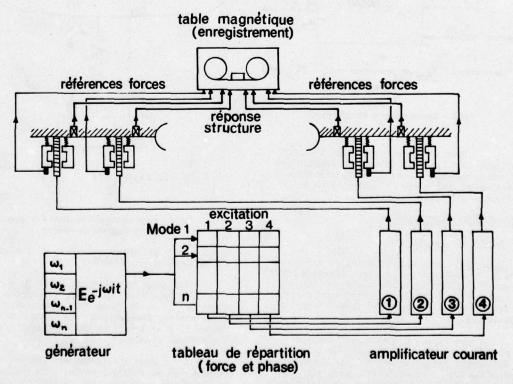


Fig. 5 - Schéma bloc chaîne d'excitation.

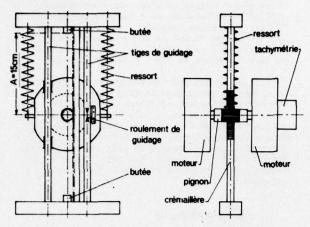


Fig. 7 - Schéma excitateur électromagnétique à grande course.

Le principal avantage de ce dispositif réside dans sa forme très aplatie qui permet de le loger dans des voilures ou des empennages d'avions d'armes, ainsi que dans son irréversibilité. Un inconvénient est que la masse ajoutée de l'excitateur modifie assez notablement la fonction de transfert locale de la structure.

#### 3.2 - Excitation percussionnelle [4] [5]

Principe - La structure est soumise à une fonction d'excitation très brève, ou percussion, et l'on étudie le régime de vibration libre de la structure (décrément ) jusqu'au retour à l'état d'équilibre.

Toutefois, la fonction d'entrée n'étant pas mesurée, cette technique n'e applicable que pour l'étude de la stabilité. n'est

Impulseurs - La mise en oeuvre est réalisée à l'aide de petits impulseurs à poudre. La poussée délivrée à la structure offre la forme générale d'un trapèze en fonction du temps et la . percussion présente un spectre de fréquence large, non sélectif.

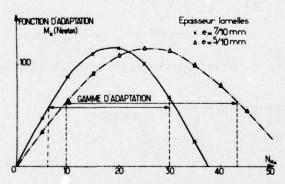


Fig. 8 - Impulseur plat (poussée max. 600 N).

tion d'adaptation fréquentielle. On recherche l'adaptation maximale correspondant au premier lobe, pour la gamme modale à étudier.

La figure 8 montre les lobes de la fonc-

La figure 9 donne un exemple d'impulseur de forme aplatie ( $e \simeq 10$  mm). Il est constitué par deux demi-coques métalliques sur lesquelles sont collées des lamelles de poudre. La tuyère perpendiculaire au plan des coques, est disposée à une extrémité et l'allumeur à l'extrémité opposée. L'épaisseur de la poudre est calibrée en fonction de la bande de fréquence à étudier ; quatre épaisseurs distinctes permettent de couvrir la bande 5-100 Hz. Le champ d'application de cette technique est vaste (planeurs, avions légers - intercepteurs ) et présente de nombreux avantages pour les constructeurs. En effet :

- la durée de l'essai est très courte, et il est possible d'effectuer des essais en piqué accentué en "gelant" les paramètres aérodynamiques :
- la masse et les dimensions de l'impulseur sont réduiteset il est possible de les loger à l'intérieur de plans très minces, ou de gouvernes, ou même à l'extérieur, carénés par des bulbes ;
- l'énergie électrique est minime (petite batterie) et l'installation d'essai très simple ;
- en outre moyennant certaines précautions dans la réalisation, (faible dispersion sur les délais d'allumage), des percussions quasi syn-chrones peuvent être délivrées en différents points de la structure.

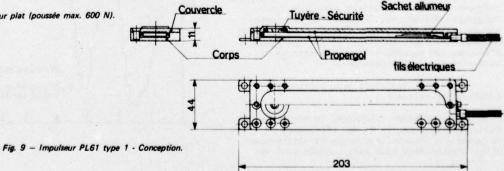
En contrepartie, les impulseurs sont soumis, pour des raisons de sécurité, à des normes de qualification aux ambiances (vibration, pression, humidité, électricité statique, température) extrêmement sévères, qui en rendent l'utilisation relativement coûteuse. La répétitivité des tirs est également limitée.

En France, plusieurs dizaines d'avions légers ont été étudiés en vol à partir de cette technique.

#### 3.3 - Excitation aérodynamique [6] [7]

L'écoulement aérodynamique autour de la cellule de l'avion constitue une source d'énergie "gratuite" qui peut être mise à profit pour l'excitation dynamique de la structure.

Gouvernes et volets spéciaux - La mobili-sation "artificielle" de gouvernes de vol servo-commandées, pilotées par des signaux instationnaires introduits au niveau de la servo-valve, procure un moyen simple et efficace d'excitation aéroélastique, en particulier pour les appareils de transport de grandes dimensions, doués de modes à très basse fréquence et de forte inertie. Sur "Concorde" par exemple, les



gouvernes de direction ont été mobilisées à l'aide de signaux de type harmonique, et les élevons de voilure l'ont été à l'aide de signaux impulsionnels, type "créneau", de durée convenable.

Une limitation vers les fréquences élevées résulte de la bande passante limitée des vérins (en général N 20 Hz) et de l'inadaptation de l'excitation pour certaines déformées modales. L'absence de mesure directe le la force d'excitation peut dans certains cas nuire à la précision d'analyse. Il faut également remarquer que, bien que les angles de braquages soient faibles (quelques degrés), ils induisent en haut transsonique une perturbation locale de l'écoulement non négligeable.

Sur certains appareils de transport (DC8 - B52), des profils oscillants spéciaux ont été implantés à l'extrémité de la voilure. Dans le cas d'avions d'armes, de petits volets mus par des vérins rapides permettent une excitation dynamique très étendue. [Exemple figure 10 -

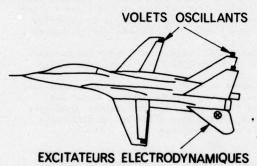


Fig. 10 - Equipement d'excitation par le Grumman F14 «Tomcat».

<u>Turbulence</u> - La turbulence atmosphérique est un processus aléatoire naturel qui affecte non seulement le domaine de la mécanique du vol mais également l'aéroélasticité.

Suivant la loi spectrale modélisée par von Karman, l'énergie du champ de turbulence, supposé localement stationnaire (hypotèse de Press), est décroissante avec les fréquences d'ondes suivant une loi exponentielle d'exposant - 5/3. Celles-ci sont corrélées à travers la vitesse de déplacement de l'avion, avec les fréquences structurales suivant l'hypothèse de Taylor. Plus la vitesse est élevée et plus la structure est souple, plus l'énergie délivrée à la structure est a priori importanté.

Lorsque l'on exploite les méthodes classiques décrites précédemment, la turbulence apparaît comme une entrée parasite augmentant la dispersion des mesures et rendant l'exploitation plus difficile. Mais lorsque l'influence de la turbulence devient, en moyenne, prépondérante pour certaines gammes de fréquences élastiques, la mesure de ses composantes instantanées permet d'établir la fonction de transfert correspondante, et par conséquent d'évaluer les caractéristiques dynamiques de stabilité des modes concernés.

Toutefois deux difficultés notables apparaissent :

- le processus étant aléatoire, la mesure est de nature statistique, et il est nécessaire de disposer d'un échantillon temporel suffisamment long. L'essai doit donc être conduit dans des zones géographiques où l'on rencontre fréquemment de la turbulence, et à basse altitude. A titre d'indication, signalons que sur une centaine d'heures de vol de Concorde effectuée à haute altitude (plus de 10 km), le temps passé en turbulence est de l'ordre de dix minutes.

- Le point choisi pour la mesure de la turbulence doit être un point significatif pour les modes concernés. En effet, en raison du caractère isotrope du phénomène, il existe une perte de cohérence rapide en envergure, dans la gamme de fréquences élastiques, entre les mesures effectuées ponctuellement au sein des différentes tranches de l'écoulement, qui peut rendre inexploitables certaines fonctions de transfert. (figures 11, 12).

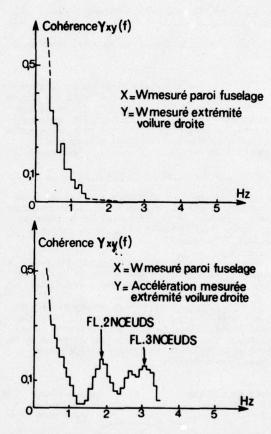


Fig. 11 - Vol Nord 2501 en turbulence,  $V_I = 120 \text{ kts}$ ,  $\sigma_W = 0.43 \text{ ms}^{-1}$ .

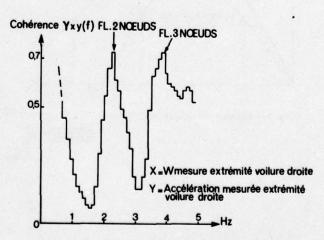


Fig. 12 - Vol Nord 2501 en turbulence,  $V_I = 120 \text{ kts, } \sigma_W = 0.43 \text{ ms}^{-1}$ .

#### 4 - TECHNIQUES DE MESURE

Nous illustrerons simplement un aspect particulier, qui est la mesure des composants de la turbulence.

La détermination des composantes verticale W; et transverse Wj s'effectue à partir de la mesure locale de :

i : angle d'incidence

θ: angle d'assiette

Z: vitesse verticale

3 : angle de dérapage

ψ: angle de cap

y: vitesse transverse

La figure 13 montre que :

id) étant mesurés par girouettes,

θ'Ψ' vitesses de tangage et lacet, étant mesurés par gyromètre,

Z",Y" étant mesurés par accéléromètres, les équations de la mécanique de vol permettent, par combinaison linéaire de ces paramètres et de leurs intégrales, de reconstituer W; et W;.

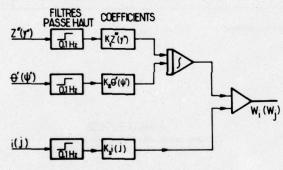


Fig. 13 - Restitution analogue de  $W_i(W_i)$ .

La figure 14 présente un montage à la paroi du fuselage. La girouette est un palet en delta, équilibré dynamiquement et couplé avec un potentiomètre continu. Son étalonnage est déterminé au préalable en soufflerie, et ajusté pour tenir compte de distorsions locales de l'écoulement, à l'aide de manoeuvres spéciales en air calme. La combinaison doit alors donner Wi, Wi = 0.

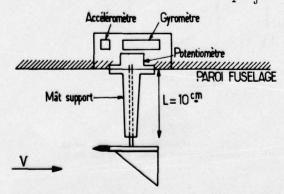


Fig. 14 - Installation de mesure de la turbulence (montage à la paroi).

5 - METHODES ET TECHNIQUES D'ANALYSES.

Compte tenu du contexte, les difficultés sont considérables pour exploiter les essais dans un délai très court et avec une bonne précision, et l'on fait appel aux méthodes et techniques les plus évoluées d'identification dynamique des systèmes.

L'exploitation comporte deux

phases :

- 1) l'obtention des fonctions caractéristiques de la structure, dans le domaine temporel ou fréquentiel, au moyen :
- ~ d'analyseurs spécialisés travaillant en temps réel par compression des données,
- d'ordinateurs sur lesquels sont programmés les algorithmes Transformée de Fourier rapide(Cooley-Tukey), convolution, filtrage digital, Méthode de Cole (applicable aux signaux aléatoires)[8].

Des problèmes mathématiques délicats se posent souvent (apodisation des fenêtres spectrales, fonctions de convergence temporelle) afin d'assurer une dégradation minimale de l'information[10, 11, 12].

2) L'analyse des fonctions caractéristiques (paramètres modaux). On utilise en général des méthodes de lissage à partir de modèles mathématiques convenablement dimensionnés, qui ont pour principal avantage de prendre en compte l'information brute sans lui apporter de distorsion préalable. La figure 15 présente un tableau résumant les principales méthodes et techniques d'identification et les paramètres dynamiques obtenus [13].

La méthode d'analyse de la fonction de transfert est fondée sur sa décomposition en fraction rationnelles : [14].

$$T(p) = \sum_{i=1}^{n} \frac{P_{i}(p)}{Q_{i}(p)}$$

Q et P étant des polynômes complexes liés respectivement aux poles ou valeurs propres du système et aux résidus, ou vecteurs propres.

Le lissage des points expérimentaux est effectué par un algorithme de moindres carrés. Les figures 16 et 17 en présentent un exemple.

La méthode d'analyse de la réponse impulsionnelle est fondée sur une extension de la méthode de Prony, permettant d'établir les coefficients d'une combinaison d'exponentielles amorties, passant par n points expérimentaux, à l'aide également d'un algorithme de moindres carrés.

Les figures 18 et 19 illustrent l'intérêt de la méthode dans le cas de non-convergence de la réponse impulsionnelle (bruit résiduel statistique).

PROCESSUS EX	CITATION	MÉTHODE	FONCTION	DOMAINE	TECHNIQUE	PARAMETRES POUVANT	
NATURE	MESURÉ	DE TRAITEMENT		D'EXPLOITATION	D'ANALYSE	ETRE OBTENUS	
HARMONIQUE OU ALÉATOIRE	MESURÉ	INTERSPECTRE	FONCTION TRANSFERT	FRÉQUENTIEL	LISSAGE MODELE MATHÉMATIQUE	VALEURS PROPRES : FRÉQUENCES, AMORTISSEMENTS VECTEURS PROPRES :	
		INTERCORRELATION	RÉPONSE IMPULSIONNELLE	TEMPOREL	LISSAGE MODELE MATHÉMATIQUE	FRÉQUENCES, AMOR- TISSEMENTS, AMPLI- TUDES, PHASE	
	NON MESURÉ	AUTO SPECTRE (RÉPONSE)	DENSITÉ SPECTRALE	FRÉQUENTIEL	SURTENSION DYNAMIQUE	FRÉQUENCES, AMORTISSEMENTS MODULE	
		AUTO-CORRÉLATION (RÉPONSE)	CORRELOGRAMME	TEMPOREL	LISSAGE MODELE MATHÉMATIQUE	FRÉQUENCES AMORTISSEMENTS	
		AUTO-CORRELATION +T.F DEMI-FONCTION	SPECTRE COMPLEXE	FRÉQUENTIEL	LISSAGE MODELE MATHÉMATIQUE	FREQUENCES AMORTISSEMENTS	
ALÉATOIRE	NON MESURÉ	COLE	RANDOMDEC	TEMPOREL	LISSAGE MODELE MATHÉMATIQUE	FREQUENCES AMORTISSEMENTS	
PERCUSSION	NON MESURÉ	CONVOLUTION [FILTRAGE DIGITAL]	RÉPONSE TRANSITOIRE	TEMPOREL	DÉCRÉMENT	FRÉQUENCES AMORTISSEMENTS	

Fig. 15 - Méthodes d'identification des systèmes.

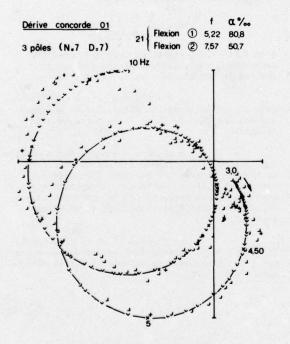
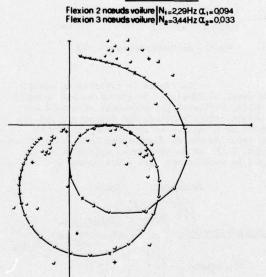


Fig. 16 - Excitation harmonique GD.



LISSAGE 3 PÔLES

Fig. 17 — Vol en turbulence Nord 2501 - Vol 63. Fontion de transfert - Voilure DR/W voil. DR.

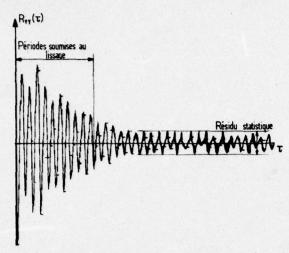


Fig. 18 – Lissage d'une fonction de corrélation non convergente (extension méthode de Pronv).

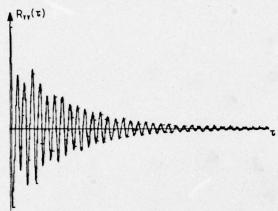


Fig. 19 - Fonction de corrélation lissée.

#### CONCLUSION

En dépit des progrès accomplis depuis quelques années par les méthodes et les moyens d'essais, l'expérimentation aéroélastique en vol reste une discipline difficile, qui allie les performances de la technique à l'art de l'interprétation.

Une préparation minutieuse est nécessaire et, chaque fois que la possibilité se présente, des techniques d'excitation et d'analyse redondantes sont à mettre en oeuvre en vue d'assurer des recoupements.

En ce qui concerne le rythme de conduite de l'essai, au cours de l'ouverture de domaine de vol, une grille de progression raisonnablement serrée doit être établie par avance et éventuellement modulée en fonction des résultats.

Enfin, si les méthodes actuelles d'analyse peuvent être considérées comme donnant des résultats suffisamment précis pour le calcul des pôles conditionnant la stabilité (prévention du flottement), il est nécessaire de les raffiner pour la détermination complète des fonctions de transfert, particulièrement lorsque la cohérence est faible.

En effet la connaissance précise des termes des matrices de transfert est indispensable pour l'étude des systèmes de contrôle actif du flottement et les dispositifs antiturbulent.

#### BIBLIOGRAPHIE

- G.DE VRIES- Quelques points particuliers de la technique d'excitation en vol par vibrations harmoniques. Rech. Aéron. Nº74 (1960).
- [2] J.BOISSEAU Les excitateurs à bobine plate pour les essais de vibration des structures. Rech. Aérosp. N° 94 (1963).
- [3] G.PIAZZOLI Appareillage d'essais de vibrations en vol de l'avion CONCORDE. Rech. Aérosp. N° 120 (1967).
- [4] G.COUPRY R. VALID G.PIAZZOLI Etude de l'amortissement des vibrations en vol par percussions sur les surfaces portantes. Rech. Aéron. N° 47 (1955).
- [5] P.LARUE M.MILLET G.PIAZZOLI Impulseurs pyrotechniques pour essais de structures en vol. Rech. Aérosp. N° 1974-3.
- [6] G.COUPRY G.PIAZZOLI Problèmes du vol en atmosphère turbulente. Rech. Aérosp. n°111 (1966)
- [7] G.COUPRY G.PIAZZOLI Utilisation de la turbulence comme source d'excitation lors d'essais en vol de flottement. Actes du Vème Congrès ICAS, LONDRES (1966)
- [8] H.A. COLE Méthods and instrumentation for measuring the damping characteristics of a structure. American patent N° 3.620.069 (1971)
- [9] <u>C.S CHANG</u> Study of dynamic characteristics of aeroel astic systems utilizing Randomdec signatures NASA.CR 132.563 (1975)
- [10] K.W.NEWMAN C.W.SKINGLE D.R.GAVKROGER!

  The development of rapid testing techniques for flutter experiment R.A.E. T.R. 73.067 (May 1973)
- [11] R.G.WHITE The resolution of close natural frequencies in the impulse response and severe truncature effects. I.S.V.R. T.R.N°17 (June 1969).
- [12] F.KANDIANIS Frequency response of structures excited by transient or random forces using cross-correlation and its Laplace transform. I.S.V.R. T.R. Nº 47 (August 1971).
- [13] ASTROM. K.J. EYKHOFF. P System identification - A. Survey. Automatica, Vol. 7 page 123-162 (1971).
- [14] R.DAT Determination des caractéristiques dynamiques d'une structure à partir d'un essai de vibration avec excitation pontuelle Rech.Aérosp. n° 1973-5.

#### TORNADO FLIGHT LOADS SURVEY

by

D.W. Altham D.K. Potter

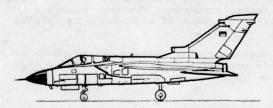
BRITISH AIRCRAFT CORPORATION Military Aircraft Division Warton Aerodrome Preston / U.K. J. Nuscheler W. Seidel

MESSERSCHMITT-BÖLKOW-BLOHM GMBH Military Aircraft Division 8 München 80, P.O.Box 801160 W-Germany

#### 1. INTRODUCTION

In the design of an aircraft the knowledge of the loads which act upon the aircraft during its operation is the basis for the development of an effective and economical structure.

The structural integrity to the design loads can be proven with no risk in a structural ground test. Uncertainty however exists in respect to design loads. Though prediction of loads is based on extensive wind tunnel testing and analytical methods have made great progress in recent years, it has to be realised that unconsidered or unknown effects may produce flight loads in excess of prediction. A flight loads survey as part of the flight test programme will help to overcome these uncertainties. More specifically, such a survey will establish critical loads resulting from quasi-static conditions and from truly dynamic manoeuvres, either confirming or redefining predictions - this is particularly necessary in the transonic regime, in which wind tunnel models and calculations cannot accurately represent the aircraft. It will also define the sub-critical loading characteristics, which in no way design the aircraft statically, but which may have a strong influence upon the determination of the aircraft's fatigue life. In consequence, a flight loads survey gives an early indication of both structural deficiencies and reserves that may be present in the design of the aircraft which may not otherwise be identified until late in the development phase and will yield data on high frequency (buffet) loads which it is virtually impossible to obtain otherwise.





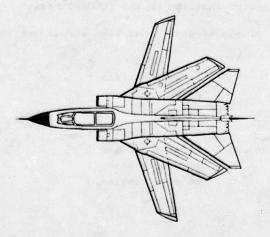


Fig. 1 TORNADO MRCA Three-Side View

For the TORNADO (Fig. 1), the European Multi Role Combat Aircraft, which is developed by PANAVIA (comprising AIT, BAC, MBB), a flight loads survey has therefore been planned from the outset as an integral part of the design and development of the aircraft. This survey will cover both the basic aircraft and the aircraft carrying external stores on its wing and fuselage pylons. The US MIL Spec, which gives detailed instructions for in-flight loads verification, was used as a guideline in the planning of TORNADO flight loads survey.

This paper gives a description of the flight loads survey instrumentation and its calibration; it will discuss the data acquisition and analysis techniques and give a description of the flight test programme.

Several examples of test results are given and will be discussed.

Since the flying for the production of loads data has not been started before mid of 1976 and only for the aircraft without external stores, this paper will only deal with the programme for the measurements of loads on the clean aircraft.

#### 2. INSTRUMENTATION

#### 2.1 General Description

In case of TORNADO the flight loads survey task is mainly put on one prototype, whereas other prototypes have limited loads instrumentation according to the particular task of each prototype.

The "loads survey" prototype carries essentially two blocks of test instrumentation, the first of which continuously measures the complete set of flight condition parameters and is also installed in the other prototypes.

In the following we will deal with the second block of test instrumentation which measures loads. General policy is to measure loads on both sides of the aircraft; in some cases, in order to save recording capacity of the data acquisition system, a few loads parameters are measured on one side only. This results in the need to perform some asymmetric manoeuvres in both directions in order to obtain the full loads picture.

#### 2.2 Instrumentation Techniques

The majority of loads is determined using well known strain gauge techniques. In complex structural areas, where useful results could not be expected from a limited number of strain gauge bridges, loads are being determined by means of pressure measurements.

As far as strain gauge technique is concerned emphasis was laid on temperature compensation and reliability. For reasons of temperature compensation, only full bridges are being used with inactive bridge arms placed in the same structural area. In cases where either reasonable linearity could not be expected or space for compensation gauges was scarce, compensation gauges were bonded to stress free pieces of sheet metal attached in temperature contact to the strain gauged structure. Wherever possible duplicate strain gauge bridges have been installed for sake of redundancy in case of bridge failure.

In order to derive loads from pressure measurements a large quantity of pressure tappings is sampled by use of scanivalves. These measurements are confined to static or quasi-static flight conditions. For pressure loads varying more rapidly single pressure pick-ups have to be installed.

#### 2.3 Type and Location of Loads Instrumentation

Fig. 2 shows a schematic sketch of the instrumentation of the TORNADO basic loads prototype.

In loose accordance with MIL Spec (Ref. 1) the structure has been strain gauged to measure sectional loads

#### on the movable wing:

left:	Bending	moment,	torque			at	wing	station	1	
	Bending	moment,	torque			at	wing	station	2	
	Bending	moment,	torque			at	wing	station	4	
right:	Bending	moment,	torque			at	wing	station	1	
	Bending	moment,	torque	and	shear	at	wing	station	2	
	Bending	moment,	torque			at	wing	station	3	
	Bending	moment.	torque			at	wing	station	4	

on the wing carry through structure:

Bending moment (Mx) and torque in A/Ccentreline

on the fuselage:

Vertical bending moment (My)

Lateral bending moment (Mz)

Shear and torque

at a fuselage station aft of the wing carry through structure

#### on the fin:

Bending moment, shear and torque with reference to the fin root

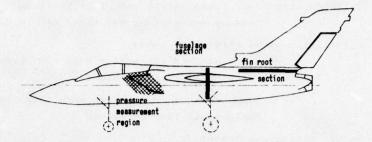
In addition to sectional loads, attachment loads can be determined by instrumentation for

Wing carry through box attachment loads (viz. Fig. 3)

x, y, z-loads in the forward and rear centre attachment lugs,

Endloads in the movable forward and rear attachment links,

Endloads in the forward and rear upper longerons and spine profiles.



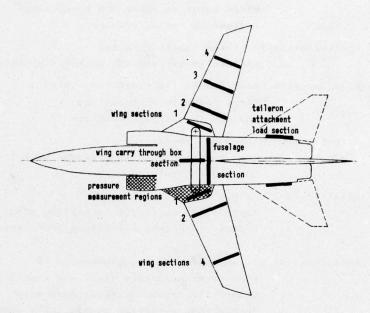


Fig. 2 Basic Structural Loads Instrumentation Locations

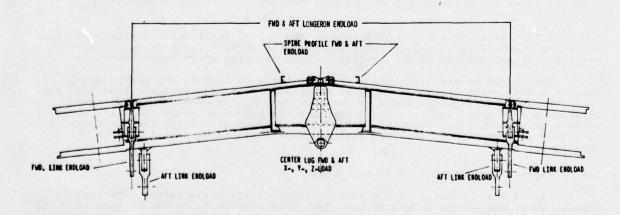


Fig. 3 Wing Carry-through Box Attachment Locations

Taileron attachment loads: (left and right taileron)

Bending moment (Mx, Mz) shear and torque (My)

High lift devices attachment loads

Hinge moments in leading edge slat tracks

Endloads in slat actuators ) right wing

Hinge moments in trailing edge flap tracks )

Endloads in flap actuators ) left wing

Rudder attachment loads:

Hinge loads in upper and lower hinge

Endload in rudder actuator

Spoiler actuation loads: (left wing only)

Endload in inboard and outboard spoiler actuator

Airbrake attachment loads: (left airbrake only)

Hinge loads in airbrake arm Endload in airbrake actuator

Arrestor hook attachment loads:

Drag and side load in arrestor hook trunnion

Endload in arrestor hook

Flight refuelling probe attachment loads:

Hinge loads in flight refuelling probe swinging link

Endload in flight refuelling probe actuator

Additional actuation loads are being measured in

Wing sweep actuators (left and right)

Krüger flap actuator (left side only)

Intake ramp actuation system (left intake only)

Main undercarriage actuators (left and right)

Nose undercarriage actuator

Main undercarriage door actuator (left side only)

Nose undercarriage door mechanism (right door only)

For determination of fixed wing nib and intake loads, the pressure distributions are being measured. The nib and fairing area has a total of 68 pressure tappings while in the intake area, including fuselage sidewall, 43 pressure tappings have been installed; these are connected to scanivalves. Additionally 10 dynamic pressure transducers have been installed for measurements of engine surge and hammershock pressures.

In deviation from MIL-A 8871, which asks for at least three fuselage sections to be instrumented for fuselage loads measurements TORNADO loads aircraft has only one instrumented section in the fuselage aft of the wing carry through box.

This could be accepted, since fuselage loads on TORNADO are predominantly inertia loads, which can confidently be calculated from accelerometer readings. The contribution of aerodynamic loads on the frontfuselage is comparably small and deviations from wind tunnel measured pressure distributions would only give small changes in overall front fuselage loads. The aft fuselage section was instrumented to give a confirmation of measured wing and tail loads as connected through the fuselage.

#### 2.4 Typical Installation of Strain Gauges

Fig. 4 shows, typically for wing sectional loads measurements, the bending moment, shear and torque gauges of the right wing section 3. As can be seen from the Figure 4, the bending moment is derived from one single bending bridge in the rear wing spar, whereas the instrumentation for torque and shear consists of a combination of bridges on the front and rear spars; at this section a shear measurement has been provisioned, in case of unserviceability of the measurement at section 2 or other possible need.

This combination is found in a Skopinski type calibration procedure (Ref. 2) which will be discussed in the next paragraph.

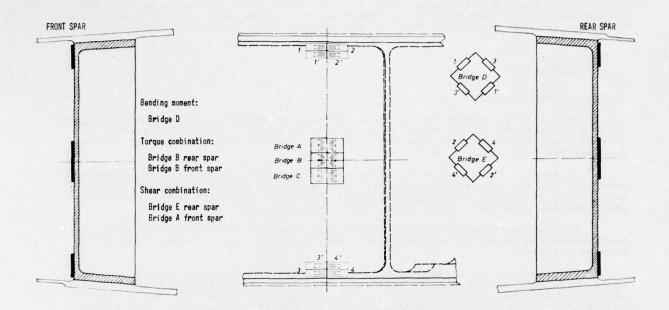


Fig. 4 Typical Wing Sectional Loads Instrumentation

For the measured load resulting from a combination of single bridge outputs, it is of no difference whether the bridge outputs are recorded separately and the combination is processed in the computer, or the bridges are combined electrically to give one single compensated output signal. Analytically, the computer combination procedure is preferable because bridge outputs could be used in more than one combination. However, since recording capacity of the data acquisition system is limited, electrical combination of bridges can be a necessity - this is especially so in the case of the moving wing for which there is a physical limit to the number of cables which can be carried around the wing pivot. In case of TORNADO flight loads survey instrumentation both procedures are being used as will be discussed in the calibration section of this paper.

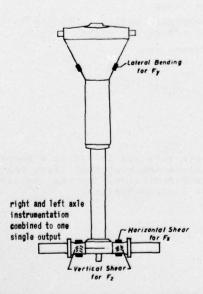


Fig. 5 Nose Undercarriage Strain Gauge Installation

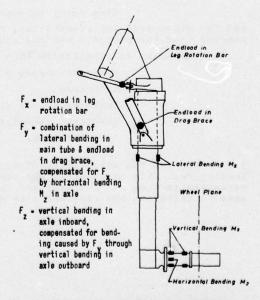


Fig. 6 Main Undercarriage Strain Gauge Installation

For landing and taxi loads trials, the undercarriage of one prototype is instrumented to determine longitudinal (Fx), lateral (Fy) and vertical (Fz) ground loads in all three legs of the undercarriage.

Figs. 5 and 6 are showing details of the loads instrumentation of nose and main undercarriage respectively. Instrumentation of shock absorber travel and other variables for determining the state of the undercarriage is omitted in the picture.

#### 3. CALIBRATION

#### 3.1 General Approach

Use of strain gauges in the loads carrying structure to measure applied loads makes a calibration of the strain gauge outputs in terms of load a necessity. A careful and deliberate approach to calibration is essential for a useful flight test and for trustworthy results.

If correct linearity in the instrumentation output would exist, the establishment of slope and intersection of a strain gauge bridge output versus load would be sufficient. This could be done (as is often done in strain gauge loads measurements calibrations) with load levels of up to 10... 15 % of limit load.

In structural areas, where load paths vary with applied load, i.e. where the instrumentation output is nonlinear with load, a calibration to higher load levels becomes necessary.

When calibration of TORNADO flight load survey instrumentation was planned, the general rule was accepted to calibrate up to 60 % of limit load. With this level of calibration load, it was believed to be high enough to detect all nonlinearities and to have sufficient safety margin for the not always representative local load introduction.

In retrospect, 10 % applied calibration load would have been sufficient in many areas. However, application of calibration loads up to 60 % or higher have proven necessary in several structural areas, (as for example taileron root rib shear) where the measured load is the key to structural modifications and is not backed up by different types of instrumentation.

#### 3.2 Off Aircraft and On Aircraft Calibration

Calibration of TORNADO flight load survey instrumentation can be divided into component calibration (off the aircraft) and in situ calibration with loading the structure of the assembled aircraft.

#### 3.2.1 Component calibration

was performed for all endload type bridges like

Actuator endloads (taileron, wingsweep, rudder, undercarriage etc.) Wing carry through box attachment loads

and for other load instrumentation, where the load carrying member could easily be removed from the aircraft and rig suspension did not affect the signal output.

Component calibration in this sense was performed for

Undercarriages,
Airbrakes,
Taileron (-root rib shear-)
In-flight refuelling probe
Arrestor hook.

3.2.2 For the "in situ" calibration the assembled aircraft was loaded in a complex loading rig. This calibration was performed to calibrate the sectional loads instrumentation in wing and fuselage and the fin loads instrumentation. The rig was also used to calibrate the flap and slat attachment loads instrumentation.

#### 3.3 Details of Calibrations

#### 3.3.1 Taileron Actuator Endload

On the taileron actuator, the only area where accessible load carrying structural materials have sufficient strain to guarantee a reasonable strain gauge output is the ram end lug. Since in lug areas the load paths for tension and compression are different, a scheme had to be found experimentally that gave similar tensile and compressive influence coefficients. Fig. 7 shows the resultant scheme, the temperature gauges being fitted to the collar. The installation on each actuator is accepted only if the positive and negative slopes differ by less than 10 % - the computer programme takes into account these two slopes.

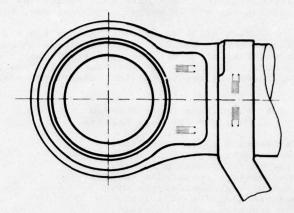


Fig. 7 Taileron Actuator Endload Strain Gauge Installation

#### 3.3.2 Undercarriage Calibration

During main undercarriage calibration, it was loaded in a loading rig by means of a dummy wheel. Outputs of all 19 installed bridges were recorded; x, y and z loads and combinations were applied in 10 loading steps up to 60 % of limit load for 4 shock absorber closures and 3 rolling radii of the wheel.

In a Skopinsky-combination calculation the minimum number of bridges was found to bring the probable error of the bridge combination within 5 % and the bridges were electrically combined. The check calibration showed that the bridge combinations give linear outputs with cross-axis effects less than five percent (typically 2.5 percent). The influence of shock absorber extension on lateral force instrumentation could not be compensated electrically; this has to be done in the computer.

Nose undercarriage instrumentation was calibrated in a similar manner. In contrast to main undercarriage, however, strain gauge locations could be found which gave responses in only one force direction; this made the combination of bridges unnecessary.

#### 3.3.3 Taileron Attachment

The calibration of the shear parameter at the taileron root rib was done off the aircraft in a rig on a representative spigot axle. Benefit of that procedure was that, at the same time when the taileron was calibrated, the aircraft could be loaded through the spigot axles for wing and fuselage calibration. Calibration was done for 4 different pitch angles and for a range of centre of pressure positions chordwise and spanwise. 4 different angles were selected, because the root rib shear output is not independent of the taileron torque loading, which is balanced through the taileron lever arm in the taileron actuator. There is no electrical combination to compensate that influence and the correction has to be done in the computer.

A considerable effort was spent in the investigation of thermal drift effects of the taileron root rib shear parameter, when it was learnt during flight testing that after flight this parameter was showing an output drift. Temperature measurements on the strain gauged structure during flight have shown that a temperature gradient develops across the structure which causes thermal stresses in the root rib material with associated strain gauge outputs simulating external loads.

After much laboratory investigation, compensation has been effected by using two temperature sensors and a calibration of bridge output versus thermal gradient.

Bending moments Mx and Mz in the taileron spigot root have been calibrated in reference to A/C axes with a dummy beam on the aircraft. These parameters will give the outer bearing shear forces of the tailplane in z and x direction. Shear forces for taileron angles other than zero have to be computed from the two shears and the taileron pitch angle.

#### 3.3.4 Fin

The calibration of the fin root sectional loads instrumentation was done on the aircraft. Point loads have been applied at three spanwise and two chordwise sections individually and in various combinations. Fig. 8 shows the loading points distribution.

With all 6 loads together the fin was loaded to about 20 % of its limit load. This is mainly because of difficulties in balancing the fin side loads without endangering other A/C components. Fin calibration was done with rudder removed, because rudder does not introduce stiffness into the fin. Combination of bridges for separation of bending moment, shear and torque is done in the computer analysis.

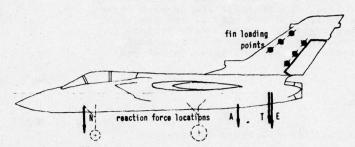
#### 3.3.5 Wing, Wing Carry Through Box, and Fuselage Section

Calibration of the sectional loads instrumentation at wing, wing carry through structure and fuselage required a complex loading rig. Loading the wing and reacting the wing loads in the front and rear fuselage gave calibration loads to the wing and fuselage instrumentation simultaneously.

Although the aircraft structure was standing on its landing gear, loads on wing and fuse-lage were balanced in such a way that no variation of undercarriage support forces did occur. This was done to preclude local influences of undercarriage support forces upon instrumentation of the rear fuselage section which is not far from the undercarriage support fittings (Fig. 2).

Fig. 8 is showing the loading points at the wing and the fuselage. For calibration of wing, wing carry through structure and fuselage instrumentation a number of loading cases was established with different loading combinations and for 3 different sweep angles which should have permitted to sort out the gauge responses to bending moment, shear and torque in the wing and fuselage structures.

It has to be noted that until now only full wing calibration was reached in the fully swept forward configuration and that loading cases for calibration of the fuselage section at the two additional wing sweep angles were deferred to a recalibration after the first set of loads flights.



- N Nose undercarriage attachment
- A Arrestor hook trunnion

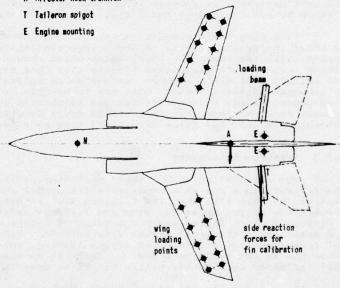


Fig. 8 Loading Points for Calibration

Owing to the simplicity of the wing structure with two main load carrying beams and the limited cable capacity from the wing, electrical strain gauge bridge combination technique was planned from the beginning to separate the responses to shear, bending moment and torque, whereas at the fuselage section computer combination technique of the single bridge outputs is applied. Therefore the wing calibration and combination had to be done before the first loads flight.

Loads were applied to the wings in the single loading points as given in Fig. 8. Using a computer program based upon the Skopinski technique (Ref. 2) the combinations were calculated and the combination resistors determined. Goal was to use as few bridges in the combination as possible.

After electrically combining the bridges, a check calibration was performed with repeating the single point loads application and then all other loads cases like pure torque, pure shear and bending and combinations of shear and bending up to loading all points simultaneously were performed; a negative load factor distribution was also applied.

As was shown in para 2.4 the bending instrumentation consists of single bridges, the torque instrumentation is a combination of two bridges where some of the sections need further compensation for bending in the computer, in order to achieve even better

accuracy.

The instrumentation for shear measurement is also a combination of two bridges; this is also further refined in the computer to remove the remaining cross effects.

The torque measurement at the wing root section 1 is not usable since the gauges suffer from local responses to the fairing fingers which are too close to the gauge locations.

Responses of wing carry through box and fuselage gauges were recorded during calibration. For accurate evaluation of flight loads results in that area more calibration cases with other wing sweep angles have to performed in the next calibration period.

#### 3.3.6 Flaps and Slats

Flaps and slats attachments could not be instrumented to determine completely the loading system.

In the case of slats the instrumentation is measuring the force exerted by the slat on the slat carriage rib and calibration forces were applied to this rib.

The flaps instrumentation is measuring the applied bending moment and was calibrated at four flap angles corresponding to the nominal retracted, manoeuvre, mid- and full flap positions, but at only a single centre of pressure position. Adjacent flaps were loaded simultaneously to provide a more representative track loading.

Results from these instrumentation schemes and from these calibrations are sufficient for confirmation of predicted loadings.

#### 4. FLIGHT LOADS PROGRAMME

#### 4.1 Overall Programme

The flight test programme was planned in two phases in conjunction with the loading programme on the static loads test airframe. The first phase comprises flying over the entire flight envelope and performing manoeuvres up to 80 % limit load. From the results of this phase any modifications to the loading distribution to be applied to the static test airframe are made before the tests to ultimate load. Following the ultimate test(s) comes the second phase of the flight programme, tests up to limit load in the most critical regions of the flight envelope, as defined in the first phase.

It goes almost without saying that the overall purpose of this programme is not only to perform sets of manoeuvres at flight conditions dictated by the prior-to-flight calculations, but also to identify critical conditions not indicated by these calculations, to con-sequently adapt the flight programme and to cover these conditions comprehensively. In order to achieve this the programme covers a grid of Mach numbers and altitudes in each configuration (Figure 9 shows the grid for the maximum wing sweep angle). Even in the case of the full flap configuration the effect of Mach number requires identification, owing to its effect upon the flow through the flap vane slots.

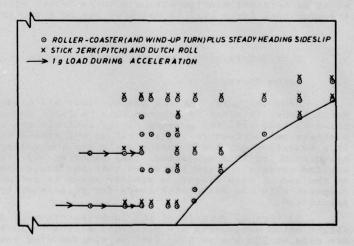


Fig. 9 Typical Distribution of Flight Loads Survey Manoeuvres

#### 4.2 Test Manoeuvres

Originally it was planned to test seven configurations, covering three wing sweep angles and the appropriate manoeuvre and hight lift devices extensions at the minimum and intermediate wing sweeps. The prime purpose of the programme was to cover symmetric quasi-static manoeuvres, but data is also required to allow matching of dynamic manoeuvres, both symmetric and asymmetric, so appropriate manoeuvres have been scheduled at a selection of conditions. At every test point a roller-coaster and a steady heading sideslip manoeuvre are performed. At selected points a pitch stickjerk and a dutch roll are also performed.

The limits of each manoeuvre are dictated by the flight conditions. Each roller-coaster reaches normal acceleration limits of lower than zero and the maximum dictated by either strength or angle of attack limitations; for test points permitting high accelerations, wind up turns are also performed in order to obtain more stabilised measurements at the peak. The duration of a typical roller-coaster is of the order of 15 to 20 seconds from steady level through zero up to the maximum and back to approximately unity. The steady heading sideslips are made in both directions and are of the same duration, the limits being dictated by either full rudder angle or angle of sideslip limitations. The dynamic manoeuvres are conventional doublets.

#### 4.3 Clearance to Service

Final clearance to service of the aircraft in respect of structural loads will be achieved in a composite manner, following the test(s) to ultimate load on the static test airframe. Quasi-static symmetric manoeuvres will be demonstrated in the most critical conditions by roller-coasters and wind up turns, based upon the results of the survey to 80 % limit load. Dynamic symmetric response manoeuvres will be demonstrated to, typically, 75 % limit load; these will be matched in the loads computer model and the abrupt full specification manoeuvres will be applied to this model to demonstrate clearance. This approach has been taken since experience has shown that an uneconomic proportion of flight time is taken in progressively working up to the 100 % response manoeuvres. Asymmetric manoeuvres will be cleared in the rapid rolling programme, the loads responses being matched in the relevant loads computer model alongside the aerodynamic model matching. The asymmetric quasi-static loads are less critical than the dynamic loads and will be cleared by these manoeuvres.

The flight loads programme to clear the clean aircraft has been scheduled to require 30 flights, 20 in the 80 % survey phase, the remainder being required for the symmetric demonstrations.

#### 4.4 Individual Components

The airbrake, flight refuelling probe, undercarriage and arrestor hook loads are being investigated separately. The airbrake loads are being measured during a specific programme covering all aspects. The flight refuelling probe loads are being measured during all refuelling trials; it is difficult to carry out controlleddeliberate misengagements of the drogue, so the programme is essentially of a monitoring type. This is partly true also of the undercarriage loads measurement programme; these loads are being monitored on a large number of take-offs and landings: however, there is also the necessary programme to specifically cover high sink rates, high weights and high crosswinds in critical configurations - these latter will be covered as conditions allow. Arrestor hook loads will be measured during a specific trials programme.

#### 5. DATA ACQUISITION, ANALYSIS AND EVALUATION TECHNIQUES

#### 5.1 Datum Checks

From the outset it was planned that all measurements would be presented as true total loads. In order to achieve this, a loads datum check is made on the runway just prior to take-off; the primary flying controls are centralised and the secondary controls are part-extended, so that no actuator-locking effects are experienced. In this condition all loads measurements are initialised, being put equal to the loads calculated for this condition, thus removing any random instrumentation shifts. The applied corrections are listed so that any instrumentation faults may be indicated. At the end of each flight, a similar check is performed and the measured loads are compared with the calculated loads for this condition and instrumentation drifts are identified.

In further pursuit of the identification of instrumentation problems, two inflight datum manoeuvres are performed at the beginning and end of each flight. These are made at 250 kts at 5000 feet at minimum wing sweep angle and are used to indicate any in-flight instrumentation problems that may not be revealed by the ground datum checks. These manoeuvres are not specifically used to derive any corrections, only to indicate potential problems; when considered appropriate, the data may be modified based upon these indications.

#### 5.2 Analysis

Four stages of analysis of in-flight manoeuvres were initially planned:

- 1) During manoeuvre
- 2) Inter-manoeuvre
- 3) Immediate post-flight
- 4) In-depth post-flight

These stages are depicted in Figure 10, which deals with wing root bending moment response; for this particular measurement, no fourth stage analysis has been made yet the third stage results being sufficient to support the flying programme.

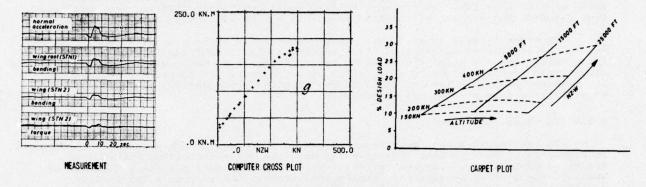


Fig. 10 Stages of Analysis

#### 5.2.1 During Manoeuvre

The first stage of analysis, during manoeuvre, presents the time history of a selection of loads to the engineer during the flight, so that he can judge whether the manoeuvre has been performed satisfactorily (covering sufficient range of normal acceleration, without too high a rate of application), whether the resultant total loads are of the expected order and whether any loads have been critically high. It was planned originally that the engineer could choose between a presentation of total loads or of loads expressed as a percentage of the limit loads at those conditions. However, it has proved to be uneconomic to continuously calculate the limit load combinations, for example, for bending/torque/shear at each wing station, so the percentage loads presentation is not used. The display ranges of the total loads reflect the order of the limit loads.

#### 5.2.2 Inter-Manoeuvre

It was planned that, between manoeuvres, it would be possible to obtain crossplots of a limited number of loads against the primary variable for the last manoeuvre, but this facility has not been pursued for in-flight monitoring - it is incorporated, of course, in the next stage.

#### 5.2.3 Immediate Post-Flight

The third stage of analysis is the key to all further analysis. Immediately after flight, the airborne tape is processed and transcribed onto a set of secondary computer-compatible tapes. A special loads secondary tape is made which comprises both pre- and post-flight datum "manoeuvres" and the broad time-slices containing the inflight lodas manoeuvres.

The large number of input/output parameters - there are 322 required loads and pressures plus almost 100 flight conditions parameters - dictates that the data processing be divided into a number of parallel processing modules. These modules comprise respectively the wings, empennage (taileron/fin/rudder), fuselage, pressures and flight conditions parameters.

After initialisation, using the pre-flight datum check data, each programme module performs the following calculations on each manoeuvre time-slice. At each sampling instant is derived the measured total load and the related limit load (in cases for which this is a function of the combination of loads at the station);

the inertia load is also calculated using the measured rates and accelerations. The limit load is used only on the "MAXMIN" monitor - two tables are produced of maximum and minimum loads experienced in each manoeuvre, one of total loads and one of percentage loads. The total and inertia loads are written to the permanent database store; this contains all the data processed by all the modules, including the flight conditions.

This database store is copied onto magnetic tapes and copies are sent to each of the participating companies for the detailed fourth stage analysis. It is also the source for the further third stage analysis, which is performed essentially within the flight test environment in order to obtain the basic behaviour within assumptions of quasi-static manoeuvres. This concentrates upon the total and aerodynamic (total minus inertia) loads and comparisons between these and pre-flight calculations, involving mainly presentation of cross-plots of, typically, total load versus nW (normal acceleration times mass) or aerodynamic load normalised by dynamic pressure versus angle of attack or lift coefficient. Multi-dimensional carpet plotting routines have been planned, but are not yet commissioned - this work is done by hand at present.

In order to make detailed and direct comparisons between measured and predicted loads, the structural specialists have prepared a significant quantity of predicted loads variations for quasi-static manoeuvres for selected measurement stations. These allow rapid comparisons to be made, which do not require the complete breakdown of the measured data into loading derivatives. From these comparisons the development of deviations from predictions can be seen.

#### 5.2.4 In-Depth Post-Flight

In the fourth stage, more detailed analysis is made by the structural specialists, as appropriate, each company concentrating upon the structural items within their design responsibility. This concentrates not only on the more precise definition of quasi-static loading derivatives, taking into account the secondary controlling variables, but also on the analysis of the dynamic manoeuvres since these cannot be analysed by the quasi-static techniques. In the case of the dynamic manoeuvres, predictions have been made for standard control inputs, to provide flight clearances and a guide to upper bounds for monitoring purposes, but these predictions are of little help in making a quick analysis of measured loads because the aircraft response and resultant loads depend upon the individual control inputs. This can be illustrated by considering a pitch stick jerk; the taileron load is not a unique function of normal acceleration, as it is in a roller-coaster or wind up turn (to the first order), since it is the forcing function and analysis must be in terms of the direct loading derivatives due to aircraft angle of attack, taileron angle and pitch acceleration inertia loads.

For detailed analysis one technique used is to predict loads from the representation:

LOAD (L) = 
$$\frac{\partial L}{\partial \eta}$$
  $\eta$  +  $\frac{\partial L}{\partial p}$   $p$  + ......

- by (1) interpolating loading derivatives such as \(\frac{\partial L}{\partial n}\) to the measured flight condition the loading derivatives being represented at a discrete set of sweeps, Mach numbers, speeds, incidences, control angles and aircraft configurations interpolation is by splined hypercubes,
  - (2) scaling these interpolated loading derivatives by the measured aircraft control input and response parameters such as taileron angle (n) and roll rate (p), etc., extracted from the database
- and (3) summing the scaled contributions.

Because of the volume of data to be handled the scheme is computerised but with a large involvement of the engineer. The predicted and measured loads and their difference can be machine plotted in a variety of forms; and if the engineer considers the comparison inadequate he can instruct the computer to 'match' the difference by a range of functions which he selects. The results of such analyses over the flown flight envelope are assessed as a whole and are used to refine the computer stored representation of the predicted loading derivatives. In parallel, analyses are made of measured prototype responses to refine the predicted aircraft stability derivatives and the characteristics of the control and stability augmentation system (CSAS). This data, with extrapolations if necessary, is then used to predict aircraft responses and loads for standard control inputs and these form the basis for:

- clearance for future high load level flights and
- structural re-assessment at design conditions.

#### 6. FLIGHT LOADS SURVEY RESULTS

#### 6.1 General

At the present time flight testing is continuing, the 80 % design load survey for the clean aircraft being almost complete. It must be noted that, in addition to this flying, additional loads information is obtained from flight tests on other prototypes, particularly in respect of actuator loads on the aircraft engaged in flight envelope expansion. As described earlier, the undercarriage, airbrake, flight refuelling probe and arrestor hook loads have been measured in separate programmes.

Regarding the 80 % survey, which identifies the loading distributions over the aircraft, the performance of the manoeuvres and of the programme for each configuration has been monitored by creating "worm" plots. An example is shown in Fig. 11. This shows, for each manoeuvre, the variation of load factor with Mach number superposed on a presentation of altitude. Thus accuracy of manoeuvres and coverage of flight envelope are easily seen by the engineer. Real-time monitoring of the more important loads has proved its worth throughout the programme.

Some results of the flight loads survey are presented below.

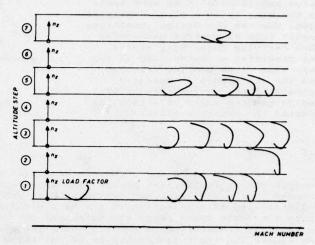


Fig. 11 'Worm' Plots from Three Consecutive Test Flights

#### 6.2 Airbrake

Fig. 12 shows the airbrake hinge moment characteristics up to high transonic Mach numbers at an intermediate setting to be slightly lower than the mean predictions, thus indicating that the jack capacity was more than sufficient to meet target opening angles to satisfy drag performance.

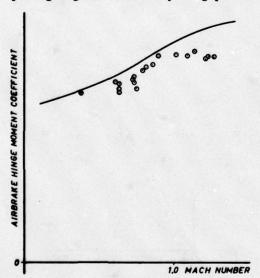


Fig. 12 Comparison of Measured and Predicted Airbrake Loads

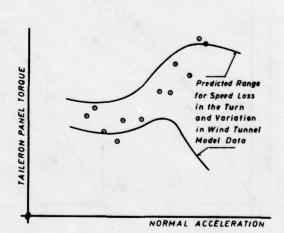


Fig. 13 Comparison of Measured and Predicted Taileron Torques in a Wind-up Turn

#### 6.3 Taileron

Taileron torques are difficult to measure on wind tunnel models and for an aircraft with large aeroelastic effects these compounded to warrant a prototype with a facility to optimize the torque characteristic by changes to the aerofoil section. Flight data has shown no reason to utilize this facility yet as a typical example in Fig. 13 demonstrates.

#### 6.4 Wing Sweep Actuator

Fig. 14 shows a comparison of measured and predicted wing sweep actuator holding forces at low wing sweep/low Mach number during a roller-coaster manoeuvre.

The actuator force is presented as a percentage of the design value and is seen to be very small as the wing is in a clean configuration, whereas the design conditions result from asymmetric manoeuvres when carrying under wing stores. The predicted actuator load is for zero wing pivot bearing friction and the difference in measured actuator force during increasing and decreasing angle of attack indicates the friction effects.

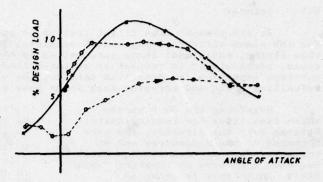


Fig. 14 Wing Sweep Actuator Holding Force

#### 6.5 Wing

For a mid sweep and 25 000 ft condition Fig. 15 plots predicted aerodynamic bending moment coefficient at the wing inboard strain gauged station versus aircraft trimmed lift coefficient for transonic Mach numbers. Data measured in early flights and presented at a selection of the Mach numbers in the figure shows that over the whole transonic speed range the agreement over the linear region of the predictions is good. At transonic Mach numbers above the predicted linear region, measurements show the linear loading relationship to be sustained to higher lift coefficients.

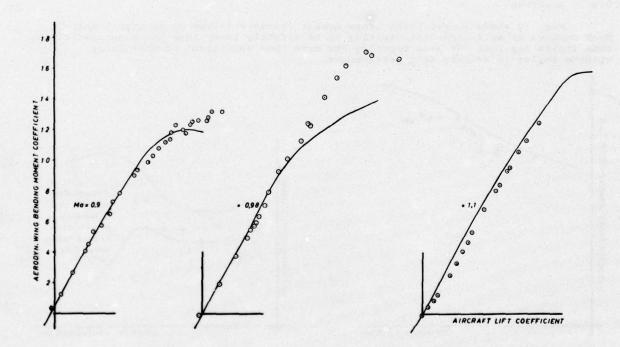


Fig. 15 Comparison of Measured and Predicted Aerodynamic Wing Bending Moment (at Stn. 1) in the Transonic Region

This effect at near-sonic Mach numbers can only be explained by a combination of full scale Reynolds number and Mach effects resulting in "supersonic" type flow being established at high incidence at a slightly lower Mach number in flight than in the tunnel. This has given better high incidence handling and manoeuvrability, at the expense of slightly higher wing and rear fuselage loads in this small transonic region. To investigate this characteristic the flight programmes were changed to include trials at additional sweeps and this resulted in similar levels of loading but at slightly different Mach numbers.

#### 6.6 Undercarriage

Fig. 16 shows loads time histories measured on the right main undercarriage during an almost symmetrical two point landing with sink rate slightly above half design sink rate. For comparison the figure also contains the results of a recalculation (same initial conditions as the actual landing) performed by means of a computer model (dashed lines). The comparison shows that extremal values of loads are quite well predicted by the computer model, whereas the strong fluctuations of the vertical load are not. The reason for this is being investigated.

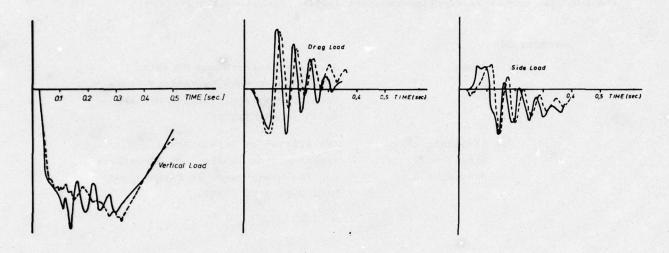


Fig. 16 Comparison of Measured and Calculated Time Histories of Undercarriage Loads

#### 7. CONCLUSIONS

Considerable effort is required for setting up, performing and evaluating a complete flight loads survey. Chronologically, one must consider -

- a) choice of how much to measure and at which sections;
- design of the strain gauge installations, including some laboratory assessments and development of some schemes;
- c) calibration of the main structure and components application of loads and distributions;
- d) assessment of the calibration, yielding calibration coefficients;
- e) flight tests, including safety monitoring;
- f) quasi-static (stage 3) analysis to quickly indicate correlation with predictions and any problem areas;
- g) further (stage 4), more detailed analysis to define the aircraft loading characteristics.

These succeeding stages are qualified by the number of parameters, or associated strain gauges. Consequently, the size of the task is of the same order as any of the more established flight test and development disciplines.

As was stated earlier, the flight loads survey for the TORNADO without externally-carried stores is not yet completed, as a result it is too early to draw overall conclusions on the value of this programme. The examples shown in the preceding chapter are only a small cross-section of the results obtained. Taking into account the entirety of the results, it can be stated that

- a) the design predictions are accurate to a substantial degree;
- b) a flight loads survey is very useful for unveiling potential structural advantages as well as problems;
- c) some discrepancies have appeared in the high incidence transonic area, where they might be expected;
- d) vibratory loads have been surveyed also it would have been virtually impossible to do this otherwise.

Consequently, it is possible to draw interim conclusions which do provide a quite favourable indication. It is considered that the TORNADO flight loads survey programme is resulting in much greater confidence in the knowledge of the structural loads, in the earlier identification and easier rectification of structural problems than would otherwise be possible, and that the case for a flight loads survey within the European combat aircraft procurement system is thus well justified.

#### REFERENCES

1 Anon.

Airplane Strength and Rigidity
Flight and Ground Operations Tests
US Military Specification MIL-A8871A (USAF) (1971)

2 Skopinski, T.H. Calibration of Strain Gauge
Aiken, W.S., jr. Installations in Aircraft Structures
Huston, W.B. for the Measurement of Flight Loads
NACA Rep. 1178 (1954)

THE EFFECT OF A COMMAND AND STABILITY AUGMENTATION SYSTEM ON FLIGHT TESTING

by

T.B. Saunders

British Aircraft Corporation Limited Military Aircraft Division Warton Aerodrome ENGLAND

#### Summary

The flight clearance programme for an aircraft with CSAS requires extra ground and flight tests to assess the operation of the system itself including the transient and long term effects of system failures.

However the presence of such a system also requires a different approach to several related aspects of flight testing. The influence of a CSAS on flight test procedures, analysis techniques and instrumentation requirements is discussed and is shown to be a significant factor in promoting developments in these three areas.

Current handling qualities criteria are considered in relation to the CSAS. Some handling qualities requirements are written in terms that cover the introduction of major new concepts like the CSAS. However requirements must be reviewed continually if meeting the specification is to remain synonymous with satisfactory handling in flight.

#### 1. Introduction

For many years now it has been common practice to provide high performance civil and military aircraft with some degree of stability augmentation. The systems employed have varied from simple, limited authority yaw dampers to full authority three axis multiplexed systems which could be used to implement the concept of the control configured vehicle (CCV). However there is a general tendency for their power and authority to increase with successive generations of aircraft of any type.

The flight development and assessment of primary flying control systems is consequently assuming an increasingly important part in flight test programmes. But the influence of the control system on flight testing techniques is certainly not confined to its own development. Many other aspects of the flight development programme require new techniques or philosophies to take account of the influence of the control system. This paper will consider some of the other areas in which the influence of the control system on flight test techniques and philosophy can be seen.

These other areas will be seen to comprise:

Pre-flight ground testing
The planning of a flight test programme
Flight test instrumentation
Individual test techniques
Analysis methods
Handling qualities specifications
Formulation of service clearances

Before going on to discuss each of these in detail it will be useful to consider briefly what is meant by a command and stability augmentation system (CSAS).

### 2. Definition of a Command and Stability Augmentation System (CSAS)

The fundamental property of a stability augmentation system (SAS) is angular rate feedback in at least one axis, and, even if it has only limited control authority, this is all that is needed to have some influence on the flight test techniques available. However modern systems stabilise all three axes and have large control authority. The SEPECAT Jaguar system (Fig. 1) is an example of a three axis limited authority SAS. Here the control surfaces are operated directly by the control column and the simplex damper system shown commands additional inputs from limited authority first stage actuators. The term command and stability augmentation system (CSAS) implies some significant shaping of the command input either by simple scheduling of the gain with flight condition or by low frequency filtering which can itself be a function of flight condition.

Such a system is the one fitted to the PANAVIA Tornado aircraft (Fig. 2). The whole system depends on electrical signalling and has full authority over the control surfaces so multiplexing is used for safety reasons. There is a facility which allows parts of the system to be switched off to simulate the effects of multiple failures for training purposes.

The properties of these systems which are interesting from the present point of view are as follows:

- a) They interact with the aerodynamics and structural characteristics of the airframe in a variety of ways, some of which are desirable but some of which are merely unavoidable by-products of the main design aims.
- b) They alter the response characteristics of the basic aircraft to a very marked extent. They can disguise handling problems and, in some cases, can produce characteristics unlike any that have been achieved hitherto by purely aerodynamic means.
- c) When operating, they deprive the pilot of direct control over the positions of the control surfaces. In particular there is no means, save by switching off the system, of maintaining the control surfaces stationary while the aircraft is responding to turbulence or to previous control inputs.
- d) They are not completely immune from failure but are designed so that the consequences of each possible mode of failure shall be acceptable bearing in mind the probability of its occurrence.

The effects of the first of these properties need to be allowed for in ground testing before the aircraft even embarks on its initial flight trials.

#### 3. Ground Testing

Normal flight safety regulations demand thorough checks of any primary flight control system before the aircraft is cleared for flight and these become more complex and time consuming when stability augmentation is involved. It is important, when these checks are done initially or after modification, to take the opportunity to establish the control laws actually achieved in a given set of equipment.

In the case of large authority multiplex systems failure detection logic must be checked regularly since it is not always possible to do this by simple end-to-end checks on the flight line. Built-in test equipment (BITE) can cater for this need only if it has been fully developed before first flight and can then be modified quickly enough to keep up with modifications to CSAS standard. In the case of the Tornado a separate computer controlled automatic test equipment (ATE) has been provided by MBB for routine first line checks and diagnosis of faults. (Fig. 3). This has prevented unnecessary delays in development of the CSAS which might otherwise have been caused by the need to keep the BITE up to date. It is now evident that recourse to entirely manual testing would not have been practicable. A typical routine check, carried out every 30 CSAS operating hours at BAC consists of about 2800 separate checks. These can be carried out and the quantitative results recorded in approximately 4 hours using the ATE.

One important function of the ATE in these 30 hour checks is the measurement of filter frequency response characteristics up to frequencies approaching 20 Hz. This is important because in order to have adequately fast response at rigid aircraft mode frequencies there must be a risk of instability due to coupling of the system with aircraft structural modes. This risk is eliminated by the incorporation of filters, usually notch filters, which can be designed once the structural characteristics and control system and actuator responses are known accurately.

It is necessary to check the effectiveness of the structural filters in a series of CSAS/structure coupling tests before the CSAS is switched on in closed loop modes. The open loop frequency response can be measured and the closed loop stability confirmed by standard analysis methods (e.g. Nichols charts) before closing the loop and measuring the closed loop response.

Power control actuator response is strongly amplitude dependent and it is necessary to confirm the stability at the highest amplitudes that the structure will stand. Thorough monitoring of structural loads and a certain amount of repeat testing at different amplitudes is needed. The effects of significant external store loads must be checked during these tests. Clearly a considerable length of time on the aircraft must be allocated for this purpose before first flight. On Tornado 9 days were spent on structural coupling tests to give a clearance for full use of the CSAS in the first flight of the first prototype. Subsequently 20 days of testing were carried out on various prototypes to check the effects of external stores and relevant aircraft modifications.

Examples of the results are shown in Figs. 4 and 5. The policy was to ensure adequate gain margins in the zero speed case regardless of phase. This is because the combination of reduced CSAS gearings and aerodynamic damping can be assumed to reduce overall loop gain in flight at moderate airspeeds but changes in the phasing of the response are not as predictable and may be destabilising in some modes.

Fig. 4 shows a composite plot of open loop pitch amplitude responses with no notch filter included for a wide variety of test cases including some with external stores. Two of the modes in the middle of the frequency range would be potentially unstable in most cases and the high frequency taileron mode could have neutral stability in some cases. The inverse amplitude response of the chosen notch filter is plotted above the results, showing that ample gain margin is achieved in all cases. The open loop responses measured with this notch included confirms this (Fig. 5).

The subject of testing to ensure electromagnetic compatibility (EMC) of all aircraft systems with each other is a specialised one which has taken on a new significance since the introduction of electrical signalling into the primary flying control systems of aircraft. It is sufficent to note here that EMC testing is another area of ground testing for which time must be allowed in the programme before first flight and whenever significant modifications are made involving the use of electrical power in the aircraft.

Once the flying programme has started decisions must be taken regarding the amount of routine testing between flights that is necessary and desirable. A built-in test equipment (BITE) designed for use in service is not necessarily ideal for routine diagnostic checks in the early stages of a development programme.

On Tornado at Warton the special ATE mentioned above was used instead, initially for a check before each day's flying. Confidence in the system was built up quickly and the daily check was reduced to a simple end to end functioning check of the system with ATE being used every 30 hours of CSAS running time. With strict control of CSAS running time on the ground this gave a much better ratio of flying hours to testing hours. There was no evidence of any increase in faults experienced in flight due to this change of philosophy and the number of unit changes demanded by the routine checks remained very low. With a fully developed system in service this testing will be taken over by BITE with a consequent reduction in the testing time required.

To summarise, the presence of the CSAS introduces new aspects of ground testing before and during the flying programme and planning must take account of the extra ground testing time required. New features also have to be introduced with the flying programme itself.

#### 4. The Flight Test Programme

In most stability augmentation systems there is a finite probability of a failure causing a significant change in the state of the system and the aircraft must be shown to behave in an acceptable manner in these reversionary states. For instance in a simplex artificial damper system a single gyro failure can eliminate the damper in one axis or even cause a limited authority hardover in one control.

In multiplex systems such as that fitted to the Tornado the possibility of a hardover is effectively eliminated but loss of stability augmentation is possible, and must be checked. In fact the service pilot will be provided with the ability to select reversionary modes to gain experience of the effect on aircraft handling during training.

Therefore some part of the flight test programme must be devoted to the checking of the effects of failures even though the normal state of the aircraft with CSAS fully operative must receive most attention. Effects of system failures must be assessed from the following points of view:

Transient effects at the time of failure Long term effects on handling Effects on flutter

This is done by deliberately inducing failure at flight conditions throughout the flight envelope, and by repeating a proportion of handling and flutter tests in reversionary CSAS states. This has been allowed for in the Tornado programmes for normal handling assessment and flutter testing. The probability of a critical failure occurring during large amplitude manoeuvres such as rapid rolls or maximum rate terms is very remote and this will not be demonstrated in flight. These cases have been studied by theory and simulation.

The programme cannot allow for inadvertant failures of the system which are likely to occur in the development phase. These are of great value in learning about the system and its response to component failures and instrumentation must be included in early prototypes to gain the maximum information from them should they occur.

#### 5. Instrumentation

Instrumentation of signals at several stages in all axes is quite feasible with a simplex autostabiliser. With a multiplex system the number of signals to be recorded can become very large and the state of the failure detection logic needs to be monitored. In such cases a compromise on the amount of instrumentation is needed.

On Tornado the areas where more than a single channel is instrumented are limited to the air data signals to the CSAS where disparities are inevitable and their magnitude is of interest.

Buffered test outputs of certain other signals are available in all lanes and could be recorded at fairly short notice to investigate a specific problem. This data is backed up by extensive instrumentation of events in the failure logic.

The existence of such a system with high quality control position feedbacks, angular rates etc recorded on flight test instrumentation leads to the suggestion that independent measurements of these quantities could be omitted. This is undesirable in the early stages of development when the effect of CSAS faults on aircraft response must be monitored independently. Later on, in aircraft for which handling considerations are less important there may be a stronger case for saving transducers by utilising those already existing in the CSAS. If the signals are to be used for precise analysis care must be taken to determine their characteristics. For instance significant phase lags can be introduced if gyro signals are picked off downstream of noise or structural filters.

In the next section we shall consider the effects of the CSAS on flight test techniques.

#### 6. Test Techniques

The aircraft can usually be flown in a number of different CSAS states. The state on which it will be flown in service is with the CSAS operating fully and this should give the best handling qualities and the greatest precision in carrying out the scheduled tests. Therefore tests should be carried out in full CSAS except where there is a good reason for doing otherwise. Some of the reasons for testing with the CSAS switched off partially or fully will be examined below:

a) Clearance of Handling Qualities in CSAS Failure States.

As stated above, it is necessary to examine in flight the aircraft characteristics in failure states and the transient effects of CSAS failures. Some indication of the former could be obtained from tests in full CSAS by relating the response of the aircraft to the control surface movements and hence obtaining the characteristics of the unaugmented aircraft but qualitative handling and failure transients must be assessed by direct flight experiment.

Fig. 6 shows a typical record of the result of failure of a pitch damper at a fairly severe flight condition. The pilot is not expecting the failure and for a few seconds he goes on flying the aircraft as if it were a highly damped vehicle while he cancels the attention getters, scans the centralised warning panel and diagnoses the failure. During this time his gain is too high for the altered pitch response characteristics of the aircraft and the pilot -aircraft system becomes mildly oscillatory in behaviour. Then he adapts to the new situation and the oscillations are damped out.

A deliberate test will always lack the element of surprise and the pilot will anticipate the change in aircraft damping and adapt to it very quickly. A deliberate test to simulate the failure shown in Fig. 6 is shown in Fig. 7. The transient oscillatory tendency seen in Fig. 6 is almost non-existent.

b) To simplify analysis of dynamic tests.

Dynamic test manoeuvres such as dutch rolls, or longitudinal stick jerks in full CSAS are invariably very well damped. This fact and the movement of control surfaces associated with any continuing response after the end of the pilot's input makes such manoeuvres quite difficult to analyse.

Fig. 8 compares dutch roll responses with and without roll and yaw dampers at the same flight conditions. It is clear that, whatever analysis method is used, the augmented response will be more difficult to analyse accurately because it contains less information about the dutch roll mode.

Therefore, if the basic aerodynamic characteristics of the aircraft are to be measured, it is preferable to carry out such dynamic tests with dampers switched off whenever the unaugmented handling of the aircraft is known to be acceptable for this purpose.

Where the test has to be done in full CSAS special analysis methods must be used to determine the response characteristics with the necessary accuracy. These will be discussed later. c) To improve the pilot's cues signalling the onset of handling problems.

One of the features of a high gain CSAS is that it disguises handling problems. Where a progressive work-up is being made to a limiting condition eg. maximum incidence this is not necessarily conducive to the safety and effectiveness of the test. It would certainly be better to make the initial investigation of the approach to stall or departure conditions with dampers switched off.

Following departure there is certainly a possibility of the CSAS impeding recovery, for instance by applying out-spin roll control in a spin. On Tornado any such tendency can be overcome by a pilot lateral control input and predictions suggest that the aircraft will be more spin resistant and equally recoverable with the CSAS. However provision has been made for an instinctive cut-out to switch the CSAS to a direct control mode during recovery should this prove necessary.

Fig. 9 shows on the left an example of wing rocking at high incidence being controlled, and hence disguised, by the CSAS.

At the top of the figure the aircraft responses and required control inputs of which the pilot would be aware are showing little activity. Only the actual control surface angles at the bottom are showing that the CSAS is having to work hard to control the aircraft.

At the right of the figure with dampers off the pilot is having to supply all the controlling inputs through the controls and even so the response of the aircraft is less tightly controlled.

d) To clear the worst case in some respects.

Other aspects than handling may turn out to be worse with the CSAS off and at least some of the related testing must then be done with the CSAS off.

One example is Tornado flutter testing. Most of this is done with dampers off because the predicted flutter speeds are lower in this case. Checks are made in full CSAS to confirm that this is so.

The converse is true in the field of flight load measurement where it is expected that the more rapid control onset available with full CSAS will lead to higher loads. In this case brief checks are done with dampers off.

#### 7. Stability and Control Analysis

As stated above the need to carry out some dynamic manoeuvres in full CSAS places greater demands on the analysis methods to be used.

In the past BAC has used various methods for extracting stability derivatives from the records of dynamic manoeuvres. One of the earliest to be used was the time vector method presented by Prof Doetsch in Refs. 1 and 2 in the 1950's. This method still has advantages where it can be used successfully. It gives a good physical picture of the forces and moments affecting the response. This is particularly useful in explaining unpredicted handling problems.

The method has been adopted for use on Tornado even with yaw damper on. The necessary frequency, damping and relative phases and amplitudes are derived from a least squares curve fit and the vector equations are solved on the computer in a single operation. Very fast turn round of results is possible and these can include plots of the vector diagrams for a better physical understanding of the response. Figs. 10 and 11 show typical outputs from the dampers off dutch roll illustrated in Fig. 8.

Because of the high degree of automation these results can be available within an hour of the flight. Input data can be restricted to the time slice to be analysed, and initial estimates of period and damping to act as starting values for the curve fitting process. However there are disadvantages in such automation. If autostabiliser inputs are to be included in the analysis the number of unknowns is increased and this is overcome by specifying the relevant control powers. If these are wrong misleading results for the stability derivatives can be obtained.

The strategy for solving the vector equations is fixed in the interests of simplicity of the input. If the program is used to analyse dutch rolls of a particularly unusual form an ill-conditioned problem can result. This can be avoided if necessary by manual analysis adopting different terms as unknowns say.

The program is small enough to run on the flight test groundstation computer and in spite of its limitations its simplicity and fast turn round make it very useful. Where more rigorous results are required or more complex control inputs are used an automatic matching program is available. This runs on the large central IBM computer at Warton and the transfer of data by magnetic tape inevitably lengthens the turn round time.

The program was developed specifically to deal with the problem of analysis of responses of augmented aircraft. A number of programs were tried before the one in current use. This minimises the cost function:

$$J = \frac{nt}{2} \frac{nz}{2} \frac{nz}{2}$$

$$i=1 \quad j=1$$

$$\frac{Zij - Zij}{0j}^{2} + K \quad nt \quad \frac{nc}{2}$$

$$i=1$$

$$u_{i}$$

by modifying the nc coefficients  $c_i$  starting from the a priori values  $C_{0i}$ . nz responses  $Z_{ij}$  sampled at nt instants are matched,  $Z_{ij}$  being the value at the ith instant calculated using the measured control input and the current set of coefficients  $c_i$ .  $C_{ij}$  and  $C_{ij}$  are measures of the uncertainty of the instrumentation data  $Z_{ij}$  and the a priori values of the coefficients respectively.  $C_{ij}$  is a scaling factor which affects the relative weightings between the fit error part of the cost function and the a priori coefficient part. The cost function is minimised using a subroutine based on Powell's method for minimising a sum of squares without calculating derivatives. (Ref. 3).

An example of the match produced by the program is shown in Figs. 12 and 13. Fig. 12 shows the initial match and Fig. 13 the final one after optimisation.

In spite of the rather longer turn-round time this program has now become the standard method at BAC for extraction of derivatives from dynamic test manoeuvres of all kinds with other methods such as time vector analysis being used mainly in quick look or back-up roles. It can give accurate results with little scatter in the important derivatives even when analysing heavily damped full CSAS manoeuvres.

In handling trials it is usually the pilot's opinion that is important, the stability derivatives being merely a means to obtain characteristics which lead to a good qualitative assessment. In the next section we shall examine how a CSAS affects the interpretation of pilot opinion and the degree to which current specifications allow for the characteristics of heavily augmented aircraft.

#### 8. Handling Quality Assessment

This section is based on a small number of cases in which handling has been criticised but it has not been immediately obvious that the aircraft fails to meet any particular paragraph of the specified requirement. This does not make it any less important to remedy the problem but it is interesting to consider in such cases whether the specification is entirely relevant to the current design of aircraft.

In most of these cases there is an applicable paragraph in the specification although it may not initially appear to be directly related to the problem encountered.

The first case to be considered is of low directional stability in the basic aircraft. This occurred at a particular flight condition and configuration on an early Tornado prototype. The applicable specification was based on MIL F 8785 B.

The pilots complained of "untidiness" in lateral control and difficulty in trimming the aircraft directionally at high speed. The handling with yaw damper out at the worst flight condition was rated unacceptable and with full CSAS was far from satisfactory. Analysis of augmented dutch rolls (Fig. 14) showed a very low level of directional stability, barely 20% of that predicted for this condition. There was a clear need for modification and later prototypes have modified rear fuselage lines which have restored the predicted level of directional stability.

In this case one would expect that the dutch roll period, which first indicated the problem to engineers, would not meet the requirements of para 3.3.1.1 of MIL F 8785 B. But it does because we are looking at a high speed case with a low value of the unit of aerodynmic time t = Town The minimum frequency observed was 1.4 rad/second and this was associated with a more than adequate level of damping.

The problem here is directly one of low stability and there were many reasons, on this particular aircraft why this could not be tolerated. The flight condition was one at which a clearance for rapid rolling would be needed and at which destabilising external stores would be carried. But if this had in fact been a "worst case" the situation would have been less clear. The level of directional stability is clearly inadequate but to find areas of the MIL SPEC that are not met we have to look at rather vague statements such as:

"Directional stability and control characteristics shall enable the pilot to balance yawing moments and control yaw and sideslip" (para 3.3.5).

The situation is better defined in the longitudinal axis where specific requirements for positive static stability and minimum levels of flight path stability are supplemented by a requirement for minimum short period frequency defined as a function of nz i.e. effectively as a function of speed or t.

The second example concerns the unusually abrupt roll response produced by the high gain roll CSAS on early Tornado prototypes. The harshness of roll response was criticised initially in small amplitude tracking control inputs where the high CSAS gain was effectively increased by non-linear spoiler rolling moment characteristic. A similar response characteristic was also found in large amplitude rolling manoeuvres at some flight conditions. In extreme cases very high roll acceleration could lead to the involuntary reduction of the control input thus producing a jerky roll response. (Fig. 15).

These problems have now been completely cured by changes in gearing and filter characteristics on one of the prototypes and these changes will be incorporated in production aircraft.

There is no doubt that an unaugmented aircraft would not exhibit these types of response and there is a slight temptation to consider them as "unusual" rather than "unacceptable". However the pilots were quite definite in their requirement for some modification.

In the small amplitude case para 3.3.2.1 could be relevant. This states that:

"Lateral-directional response to atmospheric disturbances" should be such that the aircraft will have "acceptable response and controllability characteristics in atmospheric disturbances". The harsh spoiler inputs could sometimes be detected in turbulence although generally the ride and handling of this aircraft are assessed as exceptionally good even in severe turbulence.

"Linearity of roll response" is also required in para 3.3.4.3 but the spoiler non-linearity referred to above is apparent only when magnified by the effect of the CSAS and in that case is not readily identifiable as a non-linearity since there is no obvious non-linearity in roll rate response and the effect is confined to very small control deflections.

The harshness of the larger amplitude response does not seem to be covered by any MIL SPEC requirement and this may be an area which would justify inclusion in future requirements.

#### 9. Service Clearance

Finally we should mention the effect of the CSAS on the end product of the flight trials programme - the recommendation for a service clearance. Here it is important to define flight envelope and manoeuvre clearances appropriate to various failure states of the CSAS. These clearances must take into account the consequences and probability of further failures. It should be possible to assume that the probability of a failure occurring during a specific short duration manoeuvre is negligibly small. However this cannot be assumed if there is any possibility of the manoeuvre itself provoking failures eg. by sideslip induced in a rapid roll aggravating air data disparities.

The resulting clearances should be a compromise between maximum available envelopes in failure states and simplicity. Given the reliability of modern electronic systems it is unlikely that the failure state envelopes will have to be applied very often and the bias should probably be in favour of simplicity.

#### 10. Conclusions

The introduction of command and stability augmentation systems has had a major impact on flight testing techniques in the following areas:

The amount of ground testing before flight and between flights has been increased and special equipment is sometimes needed to carry out this testing efficiently.

Programmes of handling, flutter, or structural load testing must be extended to include testing in various failure states as well as the fully operational state of the CSAS.

The CSAS creates a large requirement for flight test instrumentation on early prototypes when the behaviour of the system must be monitored carefully. Later it is possible to consider the use of CSAS sensors for measuring aircraft response in selected trials.

In the areas of handling, flutter and structural load measurement careful consideration must be given to determine the correct CSAS state for testing at each stage.

The increasing reliance on stability augmentation systems has been a prime motivation for the development of new analysis techniques particularly in the field of derivative extraction.

Some amendment of specification requirements may be called for because of the unconventional types of response possible with a high gain CSAS.

Recommendations for service clearance must include envelopes which can be flown following various levels of failure in the CSAS.

#### REFERENCES

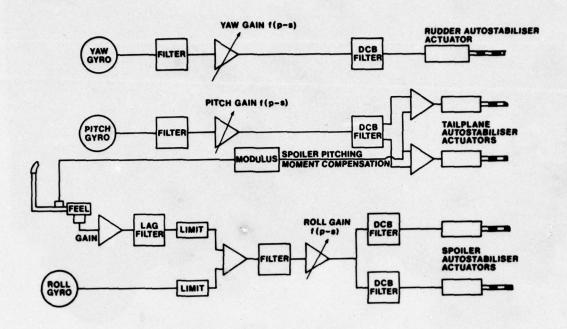
1.	K.H. Doetsch	"The time vector method for stability investigation" RAE Technical Report Aero 2495 (ARC 16275)
		R & M 2945
2.	K.H. Doetsch	"The time vector method for lateral stability investigations" RAE Technical Report 67200 August 1967
3.	M.J.D. Powell	"A method for minimising a sum of squares of non-linear functions without calculating derivatives"  Computer Journal Vol 7 No. 4 p. 303

#### ACKNOWLEDGEMENT

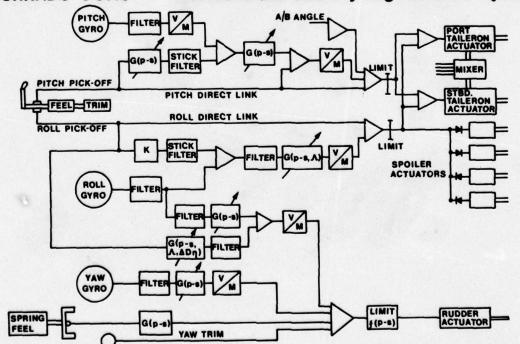
The author wishes to acknowledge the contribution of his colleagues at BAC to the preparation of this paper. The views experienced in it are his own and not those of BAC itself.

SEPECAT JAGUAR

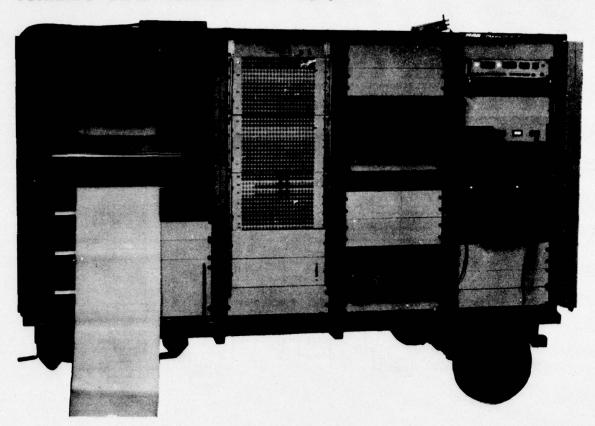
FIG. 1
Three Axis Autostabilisation System



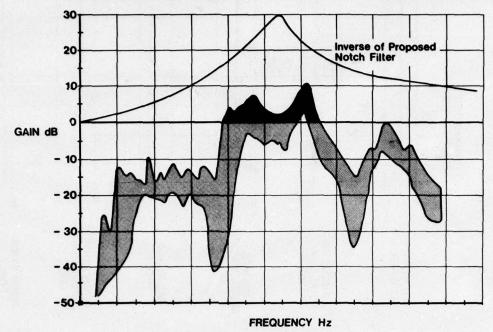
TORNADO CSAS Command and Stability Augmentation System



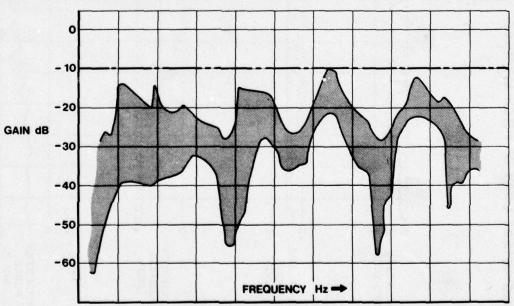
THE RESERVE THE PROPERTY OF THE PARTY OF THE



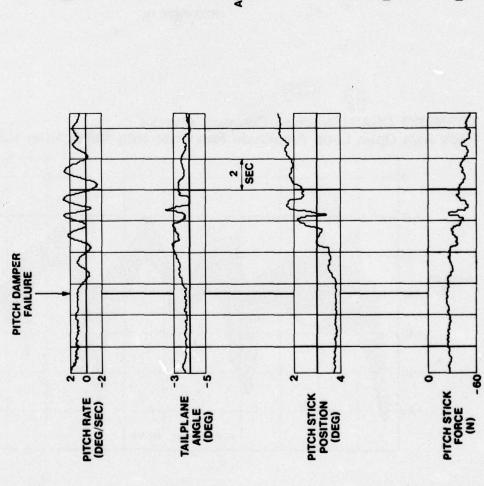
TORNADO CSAS/Structure Coupling Checks FIG. 4
Pitch Axis Open Loop Amplitude Response with No Notch Filter



TORNADO CSAS/Structure Coupling Checks
Pitch Axis Open Loop Amplitude Response with Notch Filter Included

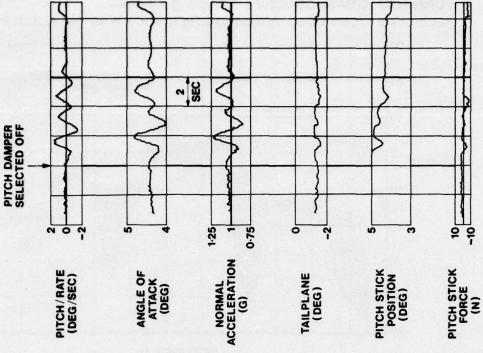


Inadvertant Loss of Pitch Damper FIG. 6

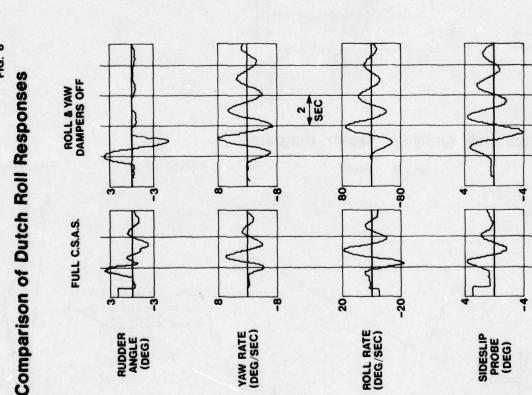


Selection of Pitch Damper Off

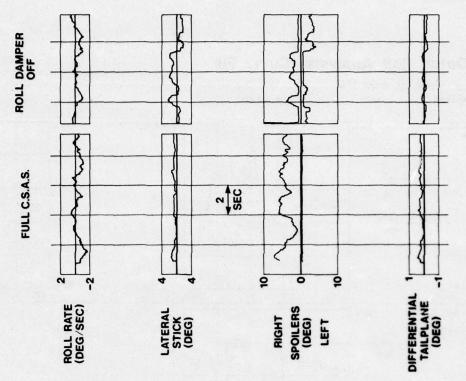
FIG. 7



Comparison of Dutch Roll Responses

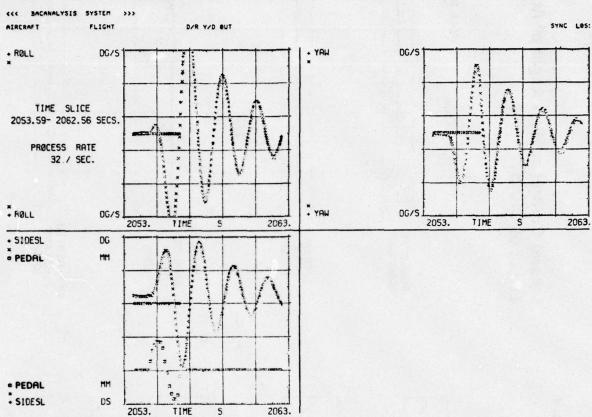


Lateral Control at High Angle of Attack **Effect of CSAS** 



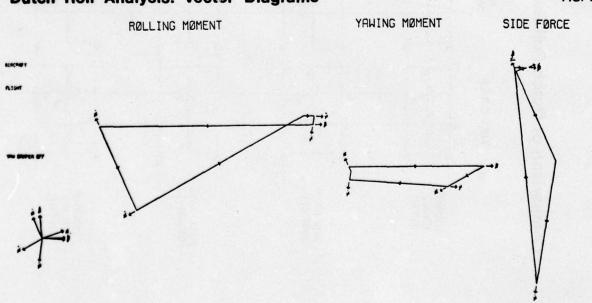
### **Dutch Roll Analysis. Curve Fit**

FIG. 10



## **Dutch Roll Analysis. Vector Diagrams**

FIG. 11

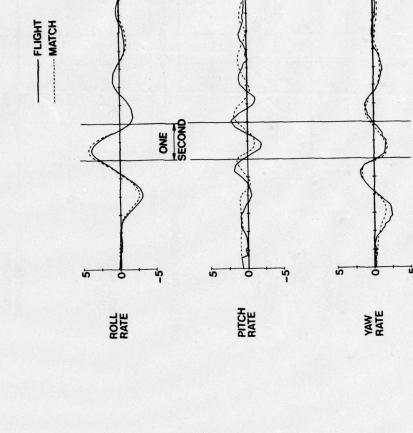


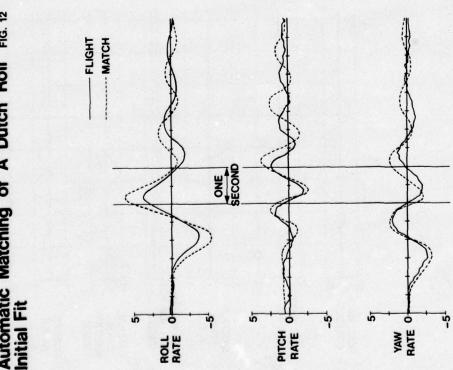
10

Automatic Matching of A Dutch Roll FIG. 12 Initial Fit

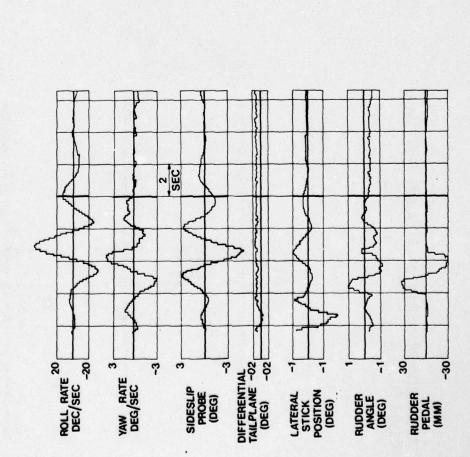
FIG. 13

Automatic Matching of a Dutch Roll Final Fit





Dutch Roll Time History Low Cng Case



0

LATERAL STICK (DEG)

0

5

DIFFERENTIAL TAILPLANE (DEG)

SEC SEC

S

SIDESLIP PROBE (DEG)

5

YAW RATE (DEG/SEC)

0

LATERAL ACCELERATION (G)

-0.2

6

ROLL RATE DEG/SEC

0

Example of Harsh Roll Response

FIG. 15

#### DEVELOPMENT FLIGHT TEST TECHNIQUES FOR DIGITAL MULTIMODE FLIGHT CONTROL SYSTEMS

DAVID L. CARLETON
HQ AERONAUTICAL SYSTEMS DIVISION
WRIGHT-PATTERSON AFB, OHIO 45433

#### SUMMARY:

Several attempts have been made to quantify aircraft flying qualities in mission related tasks. One currently used criteria are those set forth in MIL-F-8785B, "Flying Qualities of Piloted Aircraft". A technique that has been recently developed is to assess the aircrafts' ability to allow the pilot to perform precision tracking tasks, such as air-to-air gunnery and air-to-ground weapon delivery. The technique assesses the Handling Qualities During Tracking (HQDT) and is referred to as such. The technique allows for a closed pilot-in-the loop evaluation of multi-axis stability and control of the aircraft. Data outputs include real time tracking data and pilot qualitative assessment. This paper will present a brief history and technical description of the technique and data requirements. Several applications where the HQDT methods were used to develop and evaluate systems will be discussed. Finally, conclusions concerning relative merits and shortcomings of the HQDT techniques will be discussed.

#### INTRODUCTION:

The importance of assessing the ability of an aircraft to successfully perform the task for which it was designed has been a major objective of the flight test effort. The primary role of the fighter/attack aircraft is to deliver ordnance. Delivery of non-guided ordnance requires that the aircraft be precisely pointed at the target prior to and during delivery. Using Commands have historically conducted operational type tests that are geared toward assessing the ability of the weapon system to deliver ordnance. The output of these tests are bomb scores and holes in the aerial or ground targets and pilot qualitative comments. These tests do evaluate the system after it is developed but are not structured to illuminate problems in a particular subsystem. System development evaluation criteria, i.e., handling qualities specification evaluations do not necessarily quantify the aiming capabilities required to successfully deliver non-guided ordnance. The reason for this is that these specifications are directed toward open loop, single axis evaluation test techniques, whereas precision tracking is a closed-loop multiple axis task. In an attempt to quantify the tracking capabilities and identify handling qualities deficiencies in the tracking task, the Handling Qualities During Tracking (HQDT) techniques were developed. These techniques were developed to (1) gather and correlate quantitative and qualitative data during the development and evaluation process and (2) develop a technique to develop and evaluate modern flight control systems. The requirement for the later capability has been driven by non-linear systems whose characteristics can be considerably altered via simple avionics changes on the ground or in flight.

The potential for quantifying air-to-air tracking capabilities and illuminating deficiencies was first identified by Mr. Thomas Sisk of the National Aeronautics and Space Administration Flight Research Center, Edwards AFB, California, (References 1 and 2). This potential was also recognized by the Air Force Flight Test Center (AFFTC) at Edwards AFB, California, (Reference 3). This paper will present the test techniques data requirements, and evaluation criteria, several examples of how the HQDT technique was used in flight test programs, and conclude with a discussion of merits and limitations of the technique.

#### THE HANDLING QUALITIES DURING TRACKING (HQDT) TECHNIQUE:

The objectives of the techniques are to rapidly illuminate closed, pilot-in-theloop tracking problems over a large portion of the flight envelope while performing mission oriented tasks, such as air-to-air and air-to-ground tracking. The paper will be confined to the air-to-air tracking techniques only.

The tests are conducted by actually tracking a target aircraft with the test airelected points in the envelope. The tracking can be done by flying the target
mach number, constant load factor, and constant angle-of-attack, or by
target angle-of-attack (normal load factor) at a constant Mach (windmach are conducted by using a gunsight pipper and tracking a point on

displacement), aircraft rates and accelerations, and pilot

the basic maneuvers outlined above are conducted for the purpose

the basic maneuvers outlined above are conducted for the purpose

the basic maneuvers outlined above are conducted for the purpose

the basic maneuvers outlined above are conducted for the purpose

the basic maneuvers outlined above are conducted for the purpose

the basic maneuvers outlined above are conducted for the purpose

the basic maneuvers outlined above are conducted for the purpose

the basic maneuvers outlined above are conducted for the purpose

the basic maneuvers outlined above are conducted for the purpose

the basic maneuvers outlined above are conducted for the purpose

the basic maneuvers outlined above are conducted for the purpose

the basic maneuvers outlined above are conducted for the purpose

the basic maneuvers outlined above are conducted for the purpose

the basic maneuvers outlined above are conducted for the purpose

the basic maneuvers outlined above are conducted for the purpose

the basic maneuvers outlined above are conducted for the purpose

the basic maneuvers outlined above are conducted for the purpose

the basic maneuvers outlined above are conducted for the purpose

the basic maneuvers outlined above are conducted for the purpose

the basic maneuvers outlined above are conducted for the purpose

the basic maneuvers outlined above are conducted for the purpose

the basic maneuvers outlined above are conducted for the purpose

the basic maneuvers outlined above are conducted for the purpose

the basic maneuvers outlined above are conducted for the purpose

the basic maneuvers outlined above are conducted for the purpose

the basic maneuvers outlined above are conducted for the purpose

the basic maneuvers outlined above are conducted for the purpose

the basic maneuvers outlined above are conducted for the purpose

the basic maneuvers outlined above are conducted for the purpose

the basic maneuvers outlined above are conducted for the purpose

the ba

defined by the Harper-Cooper Scale (Table 1) and specific comments regarding any favorable or detrimental observations made by the pilot. Reference 3 contains an extensive discussion of the development of the technique and detailed procedures for conducting the flight tests and gathering and reducing the data. One should thoroughly review the information in Reference 3 prior to actually conducting flight tests. The remainder of the paper will discuss examples of programs that have relied heavily on the technique to develop and evaluate fighter aircraft handling characteristics in the tracking tasks.

#### THE TACTICAL WEAPON DELIVERY (TWeaD PROGRAM):

The TWeaD Program was an exploratory development program whose objective was to demonstrate the enhancement in weapon delivery capability that could be realized via improved handling qualities. This objective was achieved by installation of a high-gain, large authority flight Control Augmentation System (CAS) in a F-4C aircraft. Two development phases (References 4 and 5) and a weapon delivery evaluation were conducted. A 27 percent increase in weapon delivery accuracy was demonstrated. The two phase development program was conducted to optimize the longitudinal and lateral directional portions of the flight control systems.

The system was developed and optimized by utilizing tracking techniques. The first phase attempted to optimize the system for weapon delivery by performing close formation flying type tracking. Performing air-to-air and air-to-ground tracking tasks revealed that the system could be further refined. Changes were made to the lateral directional system, and a second evaluation phase was conducted.

The system was configured with cockpit adjustable gains so that twenty system parameters could be varied in flight. The gains could be varied in ten discrete steps. Although this represented a large number of configuration possibilities, the actual optimization was completed by two pilots in a total of twenty-two flights. The system tracking capabilities are presented in Figures 4 and 5. Shown are the tracking capabilities with the systems optimized, the gains in an off-optimum configuration, and that of the unaugmented, basic test aircraft. The qualitative conclusions of the program were that the optimized control harmony, dead beat response in pitch and roll, and a certain amount of adverse yaw where the optimum handling characteristics to minimize tracking error. It was also concluded that the capabilities provided by in flight gain changing greatly expedited the optimization process.

#### SURVIVABLE FLIGHT CONTROL SYSTEM (SFCS) FLY-BY-WIRE FLIGHT CONTROL SYSTEM:

The SFCS Program was undertaken to develop and demonstrate the enhanced survivability and performance capabilities that could be realized from a Fly-By-Wire (FBW) flight control system in a fighter aircraft. The system was a three-axis, four channel analog FBW system installed in a F-4 aircraft. A complete description of the system and test and evaluation data are contained in Reference 6. The system contained a conventional center stick and a side stick controller. No provisions were made for in flight system reconfiguration for development purposes. The tracking data were obtained for evaluation purposes only.

Data shown in Figures 6 and 7 for a constant angle-of-attack for the center and side stick controls. No specific conclusions were drawn as to the benefit of the side stick, as only two pilots participated in the evaluation. One pilot favored the side stick to the center stick and the other did not.

#### YF-16 DEVELOPMENT AND EVALUATION TESTS:

The technique was used as a development and evaluation method during the Lightweight Fighter Prototype Program. The HQDT was used to expeditiously illuminate and solve problems while conducting mission oriented tests. Unique flight control and stability concepts, such as the side stick, fly-by-wire, and negative static stability combined with the reclined seat required unique test techniques to evaluate handling qualities. The program consisted of twenty-six flights for HQDT data collection. Six pilots provided the bulk of the data on seventy-six tracking runs. A detailed discussion of the data collection, data, and conclusions are presented in Reference 7. Several flight control system modifications were investigated to improve tracking capability. These included varying the pitch rate washout time constant, roll command gains, roll and pitch prefiller time constants, pitch rate to normal acceleration blend ratios, rudder force gradients and breakouts, and stick displacement characteristics. The flight control system configuration was defined in a ground based simulation, but the above changes were investigated in the flight test phase.

Data that were gathered included a tracking error time history and various cross plots. A typical data plot with qualitative comments is shown in Figure 8. A summary of HQDT results during the program is shown in Figures 9 and 10. These plots show mean, median, and RMS tracking error in azimuth and elevation and total as the program progressed. Several flight control system modifications are noted in Figure 9. As shown in the plots, the tracking performance did improve as changes were made that altered the handling characteristics. The final configuration appeared to represent an improvement over the TWeaD system, which was discussed previously. The program concluded that the HQDT was indeed useful for rapid illumination of problems and correction of deficiencies.

#### DIGITAL MULTIMODE FLIGHT CONTROL SYSTEM PROGRAM;

The Digital Multimode Flight Control System Program was undertaken to investigate the feasibility of using digital computers in an automatic flight control system and develop multimode control logic. The test aircraft was an A-7D Corsair II, with the production control augmentation system analog computers replaced with digital computers. Because of the increased computational capability of the digital hardware, several control laws were programmed into the computer, each designed to aid the pilot in completing a specific task. In addition to the standard control logic, specific modes were designed to aid in (1) gross maneuvering, (2) terminal tracking and (3) actual gun firing. A complete description of the system control logic, hardware, and test results are contained in Reference 8.

Flight development of the system was accomplished in thirty flights using four pitches. Approximately two hundred data runs were flown. The system had the capability to vary seven parameters in flight, which were established via ground software changes.

Results of the tracking capabilities of the test aircraft are shown in Figure 11. The plot also contains TWeaD and YF-16 data at comparable flight conditions. As shown, the tracking capabilities with a fixed depressed reticle are nearly the same. A weapon delivery evaluation was also conducted, and a twenty-seven percent increase in hits was demonstrated in air-to-ground gunnery.

#### CONCLUSIONS:

As shown by the examples, the Handling Qualities During Tracking Technique does provide a method of quantifying handling qualities in the mission oriented task. The advantages are that large portions of the flight envelope can be examined very quickly and deficiencies can be corrected early in the development cycle. The technique becomes even more attractive as the number of flight control configurations or mission task evaluations increase, such as the multimode scheme. Because the technique allows for rapid evaluation in flight, flight control system reconfiguration capabilities should be included for development purposes.

Some current shortcomings of the technique are that there are no criteria to quantify pilot workload, and that the technique has currently used a fixed depressed reticle gunsight. Pilot comments are currently used to identify and reconfigure the flight control system to correct deficiencies. This would suggest that workload criteria data needs to be developed so that criteria can be established to aid and expedite the flight control design process. The use of a fixed depressed reticle gunsight excludes the dynamics of a lead computing sight, so that the qualitative measure of merit pertaining to tracking capability may change with sight dynamics introduced. One should then use on board instrumentation to compute the fire line with respect to the aim point to determine tracking capability and hit probabilities with the fire control system dynamics included.

#### REFERENCES:

- 1. Sisk, Thomas R., Factors Affecting Tracking Precision of Fighter Aircraft, AIAA Fighter Airplane Conference, St Louis, Missouri, March 5-7, 1970.
- 2. Sisk, Thomas R., Kier, David A., and Carr, Peter C., Factors Affecting Tracking Precision of Fighter Aircraft, NASA-TM-2248, November 1970.
- 3. Twisdale, Thomas R., Franklin, David L., Capt, USAF, Tracking Test Techniques for Handling Qualities Evaluation, AFFTC-TD-75-1, Air Force Flight Test Center, Edwards AFB, California, May 1975.
- 4. Rickard, Richard R., Major, USAF, and Powell, Cecil W., Major, USAF, Stability and Control Evaluation of an F-4C Aircraft with a High Gain Adaptive Control Augmentation System, FTC-TR-71-17, Air Force Flight Test Center, Edwards AFB, California, June 1971.
- 5. Carleton, David L., Captain, USAF, Lawyer, Richard E., Lieutenant Colonel, USAF, and Powell, Cecil W., Major, USAF, Development and Evaluation of the TweaD II Flight Control Augmentation System, FTC-TD-72-1, Air Force Flight Test Center, Edwards AFB, California, November 1972.
- 6. Ettinger, Robert C., Major, USAF, Majoros, Robert L., Capt, USAF, Powell, Cecil W., Lieutenant Colonel, USAF, Air Force Evaluation of the Fly-By-Wire Portion of the Survivable Flight Control System Advanced Development Program, FTC-TR-73-32, Air Force Flight Test Center, Edwards AFB, California, August 1973.
- 7. Eggers, James A., Major, USAF, Bryant, William F., Jr., Major, USAF, Flying Qualities Evaluation of the YF-16 Prototype Lightweight Fighter, AFFTC-TR-75-15, Air Force Flight Test Center, Edwards AFB, California, July 1975.
- 8. Damon, Lawerence, Captain, USAF, Flight Test Development and Evaluation of a Multimode Digital Flight Control System Implemented in an A-7D Aircraft, FTC-TR-76- Air Force Flight Test Center, Edwards AFB, California, (to be published).

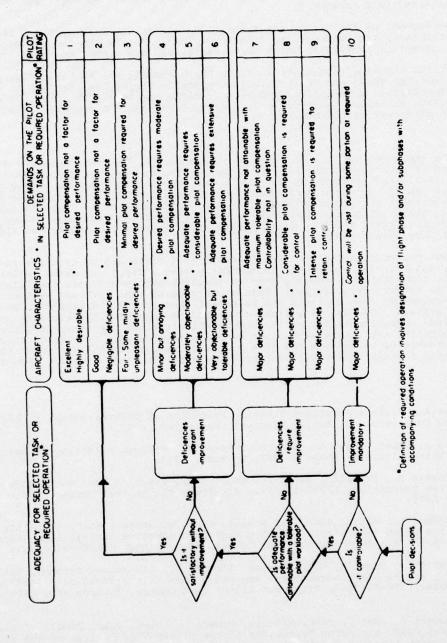
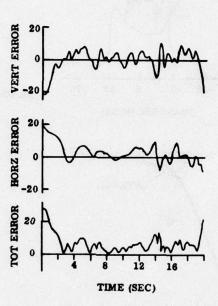


TABLE 1 (1.5) PILOT RATING SCALE

27



ERROR TIME HISTORY

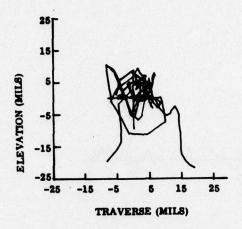


FIGURE 2

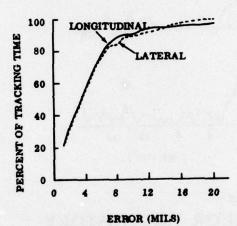
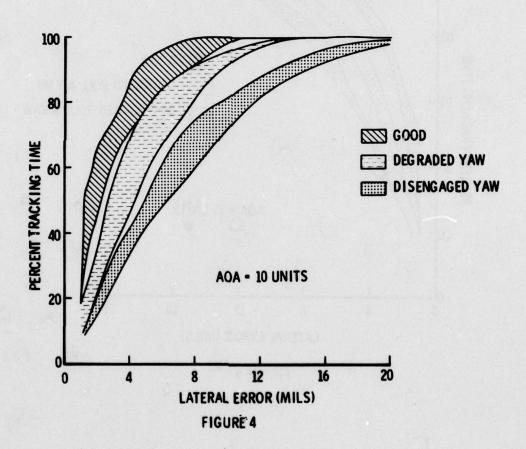


FIGURE 3

# PERCENTAGE TRACKING TIME WITHIN GIVEN ERROR RANGE



# PERCENTAGE TRACKING TIME WITHIN GIVEN ERROR RANGE

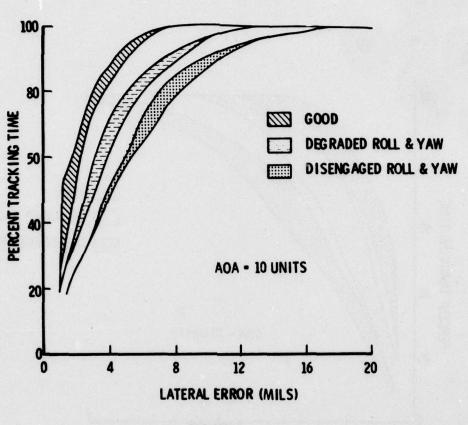
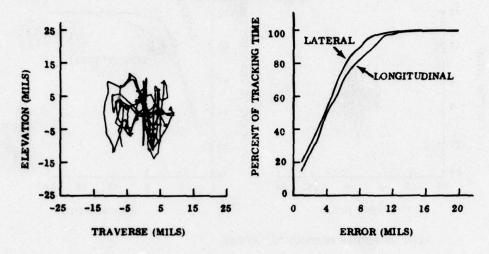
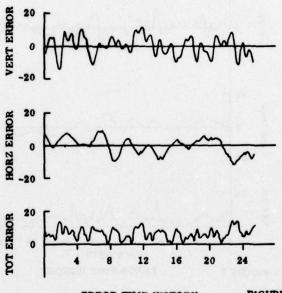


FIGURE 5

# AIR-TO-AIR TRACKING, CENTER STICK, PILOT 1 22,000 FEET, 0.94 MN, 14 UNITS AOA



PLOT OF PIPPER POSITION VS TARGET

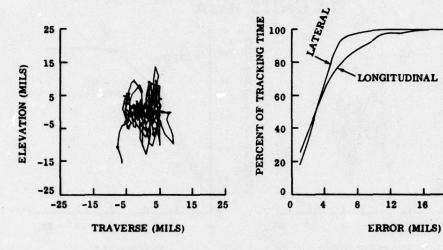


ERROR TIME HISTORY

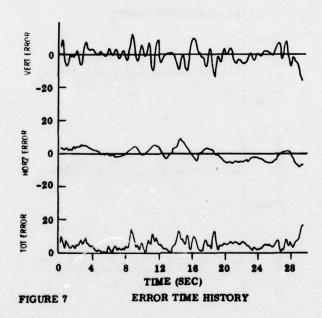
FIGURE 6

8

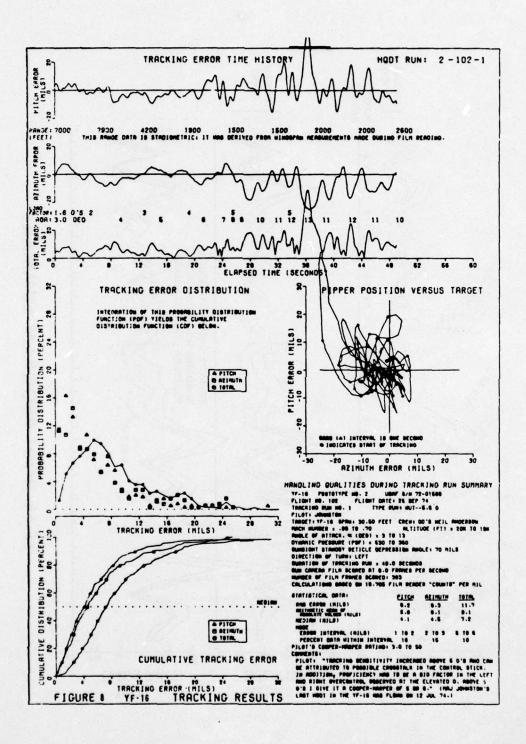
## AIR-TO-AIR TRACKING, SIDE STICK, , PILOT 1 23,000 FEET, 0.87 MN, 14 UNITS AOA

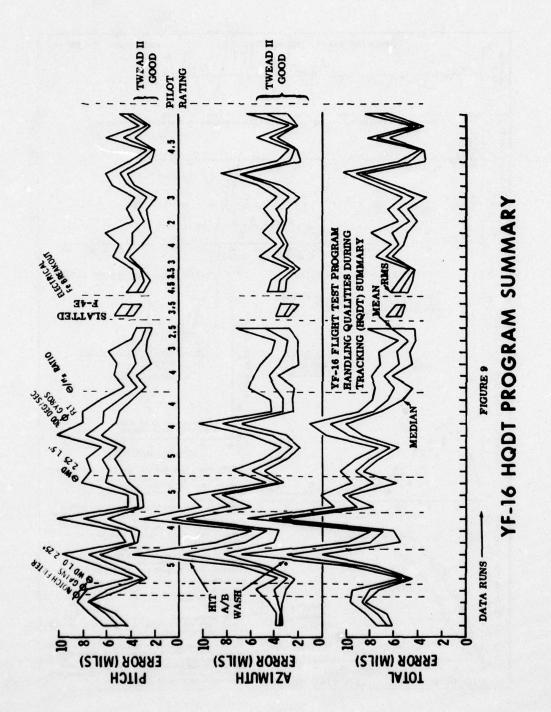


PLOT OF PIPPER POSITION VS TARGET

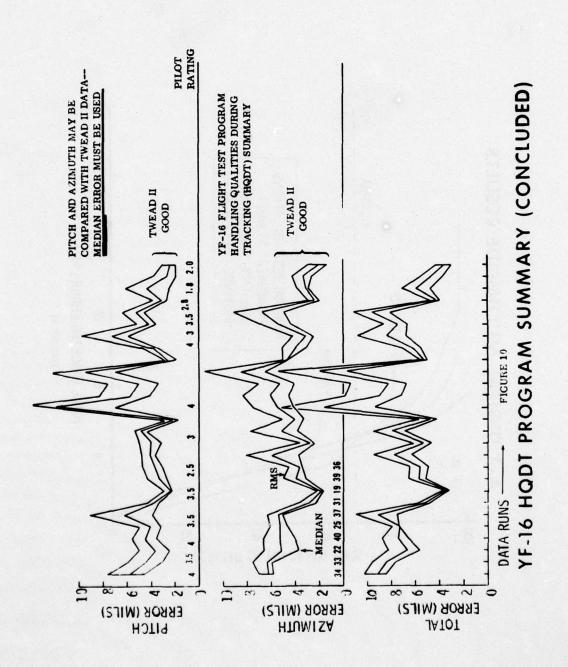


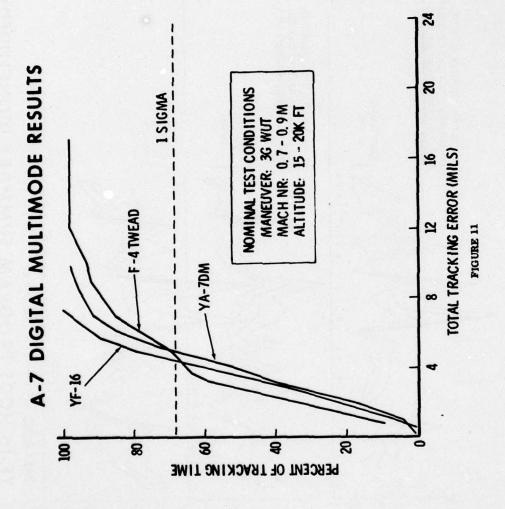
16

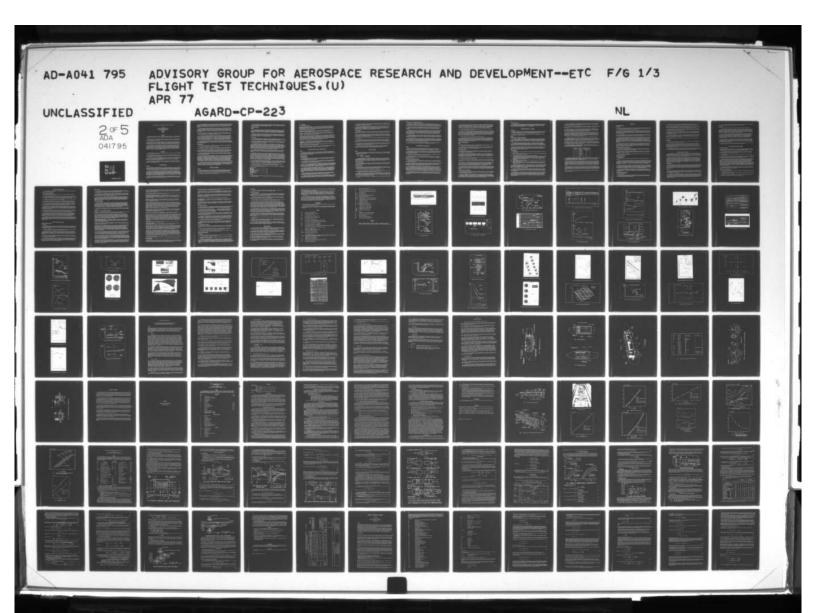




¥į







#### FLIGHT ASSESSMENT AND DEVELOPMENT OF THE CONCORDE INTAKE SYSTEM

bv

D.P. Morriss
Head of Propulsion Development
British Aircraft Corporation Limited
Commercial Aircraft Division
Filton House
Bristol
BS99 7AR
England

#### ABSTRACT

The rapid exposure and resolution of problems represented prime objectives of the flight investigation programme, devised to exploit fully the advantage of pre-flight prediction of potential problem areas.

An account of the flight investigation, including a description of the test techniques employed, is placed in perspective by a brief recapitulation of the design of the engine air inlet system and the associated fundamental control concepts.

The impact of flight investigation on the evolution of the certification standard aircraft is apparent e.g. modification of the prototype standard wing leading edge to improve surge free negative incremental normal acceleration capability; suppression of local reference pressure sensing for automatic air inlet control in favour of computed reference signals derived from central air data sources.

In similar context the clear emergence of the necessity to place reliance on flight test data as the basis of formulation of the production standard air inlet control system functional laws, is of paramount significance. Flight determination of the sensitivity of engine surge thresholds and hence the effective manoeuvre, Mach Number and throttling limits, to systematic variation of inlet geometry proved to be essential. The delicate balance between the requirements of performance, inlet/engine compatibility and simplicity of crew management, dictated by considerations of commercial viability, was achieved by the air inlet control system laws so derived.

#### INTRODUCTION

Novelty equates to risk is a maxim which adequately reflects the cautious approach of airworthiness authorities to acceptance of innovation.

The Concorde establishes a precedent in this context, from the fundamental basic concept of supersonic flight applied to civilian transportation to the associated multiplicity of complex sophisticated systems incorporated at the dictates of viability.

The clearly obvious formidable nature and magnitude of the certification task needs little emphasis and directs attention to the flight development/validation phase of the project. This represents the major factor in the promotion of the requisite confidence level on the part of the airworthiness authorities and indeed the design teams concerned.

This paper is devoted to consideration of the flight assessment and development, to certification standard, of the Concorde intake system which merits particular attention by virtue of its advanced concept in the civil transport field.

#### THE CONCORDE POWERPLANT

#### ARRANGENENT

The four powerplants are housed in pairs in a single nacelle mounted beneath each wing. Complete independence of powerplant functioning is achieved in normal operating conditions, aerodynamic independence of the paired intakes being realised even in supersonic operation, by extension of the leading edge of the centre wall separating engines and intakes to project forward of the swept intake entry plane.

In plan view the intakes are 'toed in' relative to the aircraft centre line to approximately match the underwing side wash field at supersonic cruise incidence. Choice of vertical displacement of the intakes relative to the wing represents a compromise between the requirements of performance and intake/engine compatibility. The intakes ingest approximately 40% of the wing boundary layer depth in supersonic cruise conditions with consequent beneficial effects on the drag of the diverter system. This, occupying the gap between intakes and the wing, deflects the remaining underwing surface boundary layer around the nacelle sides by virtue of the faired wedge planform.

It should be noted that the underwing compression field at cruise reduces the intake entry approach Mach Number from the free stream value e.g. at M=2.0 cruise, approach Mach Number to outer intake is approximately M=1.89 and that of the inner intakes M=1.92.

Fig. 1 shows a diagram of the production standard powerplant arrangement. At supersonic and transonic speeds the intake supplies primary air to the engine and the cabin air heat exchanger system for cooling purposes. Secondary air from the throat bleed slot between front and rear ramps, which represents the major source of secondary flow to the dual stream nozzle, functions as cooling/ventilating flow for the engine bay.

At low speeds, the intake provides primary air to the engine only, the throat bleed system being isolated from the secondary system by closure of the four actuated secondary air control valves. A blow in door in the bottom of the nacelle provides nacelle bay cooling/ventilating and secondary nozzle flow. Heat exchanger cooling flow is provided from a separate source at the nacelle side. The secondary air flaps double as fire flaps; initiation of this mode of operation involves actuated closure of the ground running flaps.

The production standard evolved essentially through two preceeding development standards - the prototype and pre-production. The more significant differences of these, aside from engine differences, related to the intake (prototype) and propelling nozzle designs (both).

The prototype intakes were of reduced entry area with less sophisticated main and auxiliary entry designs. The main entry featured straight swept sidewalls which were cut back for the later aircraft, and a straight lower cowl lip leading edge in plan view, in place of the later designs featuring local cut back, or sweep, adjacent to the centre wall. The auxiliary inlet was of the actuated scoop type (see later) in place of the subsequent 'blow in' door design. Vertical displacement of the intake relative to the wing was increased, compared with the pre-production and production standard, to avoid intake ingestion of underwing surface boundary layer; also the diverter system plan form was less refined.

Propelling nozzle designs for both prototype and pre-production aircraft were based on the blow in door throat bleed ejector principle, with freely floating petals forming the secondary nozzle divergence which differed from the actuated variable 'bucket' design of the production standard with integral secondary nozzle and thrust reverser.

#### THE INTAKE SYSTEM

For the purpose of this paper, the intake system is defined as comprising the variable geometry intake and the directly associated control and actuation system.

Although purists may venture to disagree, the intake is essentially a refined multi-shock external compression design which incorporates isentropic partial compression and relatively low drag cowl.

The 7° angle front wedge is of fixed geometry; variable geometry comprises linked front and rear ramps with screw jack/hydraulic motor actuation via longitudinal torque tubes and suitable linkage, and an aft spill (dump) door in the lower subsonic diffuser wall which incorporates a freely floating 'blow in' auxiliary flap or vane to supplement the main intake air supply at low speeds (dump closed).

The dump door complements the ramp (primary) spill system in matching the variable air demand of the engine and secondary system over the wide spectrum of supersonic Mach Number ambient temperature and engine operating conditions required.

The Air Inlet Control System (AICS) automatically slaves the variable inlet geometry to the appropriate functioning laws of which more detailed consideration is deferred to later sections. The principle of intake control is illustrated by the data presentation of Fig. 2 which relates intake supply and engine demand airflows. Superimposed on the intake characteristics for varied ramp angle, expressed in the traditional terms of compressor inlet pressure recovery (7,1) and main duct airflow (ratioed to theoretical maximum capture flow) the engine demanded airflow relationships define potential intake/engine airflow matching points for varied ambient temperature. The additional data presented relates the pressure recovery (7,8) in the space above the ramps (ramp void), and the throat bleed mass flow ratio (5), with main duct airflow ratio, and hence defines corresponding secondary system airflow matching conditions.

By judicious choice of the control level of ramp void pressure recovery, which governs intake/engine and secondary system matching, near optimum powerplant performance can be realised over a range of ambient temperature conditions. In the simplest terms, the scheduling of \$\sigma\$s as a function of Mach Number represents the fundamental control principle of the Concorde inlet system. Accurate closed loop control of matching is affected by nulling excursions from the scheduled value.

#### APPROACH TO FLIGHT TESTING

#### PHILOSOPHY

Despite the impressive volume of pre-flight design/development testing applied in the powerplant area, problems were anticipated, particularly in the field of intake/engine compatibility, because of obvious difficulties associated with achieving adequate simulation of the Concorde installation.

The approach to the flight assessment of the intake system therefore emphasised the vital necessity for rapid exposure of problems to permit timely remedial action.

Potential problem areas could be identified from pre-flight design development investigations and detailed test schedules were formulated accordingly. Inevitably, however, technological and political pressures precipitated deflection from this course at times.

#### FLIGHT DATA ACQUISITION

#### General

The flight data acquisition system was designed to satisfy the primary test objective of rapid exposure and understanding of problems. Data measurement recording and processing systems were geared in terms of capacity, accuracy, resolution and rapidity of data production to facilitate and ensure expedient tactical decisions relating to remedial action or redirection of the flight programme as required.

Furthermore, capability and facility of comparison of the data acquired with relevant pre-flight development test information was an important factor contributory to formulation of the system. This ensured advanced warning of problem thresholds signalled by adverse discrepancies between flight data and the relevant interpretations of, for example, model data.

#### Instrumentation

Fig. 3 presents a diagram of the standard intake pressure instrumentation, indicating the more significant transient measurement point locations. Typical of development standard aircraft, this diagram in fact relates to the prototype which established the pattern followed by later aircraft.

Absolute transducers were utilised for primary and secondary duct transient pressure measurement, whereas differential transducers were applied to quasi-steady measurement, confined to compressor face pitot rakes and associated wall static tappings.

The compressor face total pressure measurement chain (quasi-steady) is illustrated in Fig. 4. Pressure distribution was measured by 36 pitots in the case of prototype aircraft, mounted at selected points on the engine LP compressor inlet guide vanes. On later aircraft with more advanced standard of engine, this was reduced to 25 in number because of the revised design with reduced number of guide vanes. Local compressor face pitot pressure was measured, using a Scanivalve, relative to that at a selected position which itself was measured relative to the aircraft rear plenum chamber pressure. A further differential transducer defined the level of the latter relative to the aircraft nose probe static. Scanivalve functioning was checked by measurement of the reference against itself.

In addition to pressure instrumentation, the intake carried strain gauging of selected components, notably intake/wing attachment links, ramp torque shaft drive links, spill door actuator etc., for monitoring of flight loads. Furthermore, adequate intake variable geometry position pick offs were featured.

Comprehensive monitoring of air inlet control system functioning was provided in its own right, more particularly in the case of the later production development systems based on the hybrid digital/analogue design concept. Appropriate facilities were included to record the outputs from integral components of the system, effectively utilising these as instrumentation - e.g. control pressures, function limits generated within the system, intake variable geometry position pick-offs, switch/selector functions, monitors etc. These included outputs from the system serial digital data highway. Conditioning of the AICS signals to be compatible with the aircraft recording systems was achieved by a specially designed interface unit, known as the Flight Test Acquisition Unit (FTAU), which also performed a buffer function to protect the AICS. Although an item of flight test equipment, the FTAU was rack mounted as an integral module of the AICS and designed and built to similar standards.

It should be noted that the foregoing brief description of the intake instrumentation system relates to port intakes (apart from the AICS). The nominal standard for starboard intakes comprised considerably less items - e.g. compressor face instrumentation was suppressed, for example, so too the majority of the duct transient pressures - flight investigation being concentrated on the port intake pair.

For special test purposes, i.e. resolution of particular problems, for example, the standard instrumentation was augmented as described in the appropriate sections of the paper.

In one such special test series it is interesting to note the total complement of instrumentation as follows, relating to the port inner intake.

Position Indicators			 	 	7
Pressures			 	 	69
Strain Gauges			 	 	1
Temperatures			 	 	7
AICS limits/intake g	-	try	 	 	20
AICS Pressures			 	 	4
AICS Switches/Select	ors		 	 	12
AICS Monitors			 	 	34
Data Highway Outputs			 	 	30

#### Recording

Aside from on board monitoring and accident recording, three types of system were used to record flight data, as follows:-

- (a) Digital tape
- (b) Analogue tape
- (c) Oscillograph (Photographic)

Digital Tape - Quasi-Steady (QS) System - Application of this multiplexed system was limited to those parameters which vary slowly or, if oscillatory, with frequency less than 5 cycles/sec. Data sampling rates available were 1, 5 or 25 points/sec. Compressor face total pressure distribution represented a typical application in the case of the intake system, with sampling rate 1 point/sec., together with for example, intake variable geometry positions etc.

Analogue Tape - Frequency Modulated (FM) System - Analogue magnetic recorders (Frequency Modulation) were used for wide band pass parameters, the analysis of which required complex processing.

Two types of recorder were employed for aircraft applications viz. with 0-50 cycles and 0-6000 cycles band pass. A third special type was supplied by the engine manufacturer to deal with internal engine parameters - notably, compressor blade vibration stresses.

Recording of structural vibration stresses and accelerations, transient surge pressures, acoustic pressures etc., represented typical applications of this recording system in the intake context. In addition, however, selected intake transient pressures, normally recorded on the oscillograph system (see following section), were duplicated on the FM system to facilitate data analysis. In the case, for example, of unexpected engine surge, in which oscillograph recorders would be operating at low speed with accompanying difficulties in trace resolution, the FM system provided invaluable supporting data.

FM data processing provided analogue or digital output as required.

Oscillograph - The oscillograph (photographic) recording system was used to record wide band pass parameters (0-150 cycles/sec) which did not demand complex processing, and also for duplicating selected parameters recorded on the QS system, to facilitate analysis.

Typically, recording of all intake transient pressures and variable geometry positions, together with a number of AICS outputs utilised the Oscillograph system.

Winding rates of recorders delegated to the intake system were 40 and 400 MM/sec approximately. Naturally, to conserve film, the higher speed was selected during the test phases of flight only.

#### PREPARATION FOR INITIAL FLIGHT - CLEARANCE FOR FLIGHT

#### GENERAL

To facilitate crew familiarisation with the aircraft, the intake variable ramp system was fixed in the subsonic/transonic configuration. Moreover, the variable dump door/auxiliary intake system was suppressed in favour of a fixed geometry inlet devised essentially to perform the auxiliary inlet function only, and limited to subsonic operation.

#### CLEARANCE FOR FLIGHT

#### Installed Surge Margin

Domonstration of adequacy of installed surge margin at low speed and aerodynamic independence of the paired intakes dominated the approach to acceptance of the intake system for flight. Ground static operation was demonstrated to be the critical case.

It was considered essential to define the actual surge margin in terms of high pressure compressor relative speed  $N_2\sqrt{6}$ . The engine manufacturers advised a minimum of  $2\frac{1}{2}$ , in these terms below the 'cold rating point' to cope with control system accuracy.

Fig. 5 shows the results of tests carried out on British prototype 002 and the Vulcan flying test bed (Ref. 1.0.). The test technique exploited the advantage of the flexibility of the two spool Olympus 593 engine in terms of datum surge margin. By the introduction of false signals into the engine control system the engine was induced to operate at sequential functioning points approaching the surge line (to the left of the normal operating line, or E<sub>2</sub> schedule at low speeds).

Surge points for particular engines are shown (Fig. 5) relative to the control lines expressed in terms of LP and HP relative spool speeds,  $N_1/N_2$  and  $N_2/N_3$  respectively. These are compared with relevant engine test bed data for the same engines with bias gauze simulation of quasi-steady compressor entry flow quality (DC(O)  $\stackrel{\text{def}}{=}$  DC(60) = 0.50). Deterioration of surge margin was indicated between the aircraft installation and the engine bed assessment from comparison of surge points particularly when related to the relevant quasi-steady distortion levels, which were less severe in the case of the aeroplane.

These results encouraged revision of the low speed engine control line  $E_2$  as shown in Fig. 5. Henceforward, demonstration of operating capability without surge at  $2\frac{1}{16}$  HP rpm below the revised cold rating point was accepted as adequate clearance for flight of newly installed engines.

It should be noted that the  $E_1$  and  $E_2$  schedules represent the limiting control lines of the earlier standard engines. Actual engine control lines translated as a function of stagnation temperature,  $T_1$ , from  $E_2$  at low values typical of take-off to  $E_1$  at the higher values appropriate to supersonic cruise.

The variation of compressor inlet flow distortion with engine mass flow, showed a gratifying agreement between full scale aircraft and model test results. This excellent correlation extended to forward speed conditions as indicated by taxying trials.

The confidence thus generated in model prediction techniques at low speed eased potential anxieties in relation to full scale confirmation of acceptable operation in cross winds, which could not be investigated to order. Credence was placed in the model data with respect to sideslip (cross wind) and incidence effects (e.g. rotation before lift-off) on compressor inlet flow quality, which in fact were shown to be of little significance with the fixed geometry auxiliary inlet.

#### Intake Independence

Aerodynamic independence at low speeds of the paired intakes was demonstrated by provoking surge of an engine operating at maximum dry rating at ground static conditions with the adjacent engine at similar rating.

Fig. 6 illustrates results typical of this category of testing from French prototype Aircraft 001; the time history of transient pressure measured in the subsonic diffuser, just forward of the compressor face, is shown for all intakes during a surge induced on No. 3 engine (starboard inner) by the introduction of false signals into the engine control system.

The main surge pulse is shown to achieve a peak duct pressure significantly greater than the initial steady state level.

There is little evidence of genuine interaction effects in the adjacent intake No. 4 (starboard outer), the apparent slight transient reduction of pressure shown being due to the shock experienced by the recording system, as evidenced by the sympathetic behaviour of the port intakes with engines inoperative.

This evidence of low speed aerodynamic independence of paired intakes was sufficient to convince the airworthiness authorities that the 'paired' powerplant concept achieved safety standards equivalent to four independent engines at low speeds and altitude.

Accordingly on the 2nd March 1969, the French prototype Aircraft 001 took off from Toulouse initiating a flight test investigation which was to occupy six years to complete to certification standard. On the 9th April 1969 it was joined by the British prototype Aircraft 002.

#### INITIAL FLIGHT PHASES

#### GENERAL

Initial flight investigation, prior to development of aircraft and engines to a standard appropriate to the achievement of Mach 2.0 and beyond, was sub-divided into three phases with successively extended flight envelope limits as follows:-

Phase	Limits	
1	M = 0.80	V = 350 Kt. CAS
2	M = 0.90	V = 380 Kt. CAS
3	W - 1.50	V = 500 Kt. CAS

Interphase groundings were occupied with embodiment of equipment, systems etc., relevant to the subsequent phase test objectives. As might be anticipated, critical path to achievement of supersonic speed was essentially represented by flutter and aircraft flying qualities clearance, and these together with aircraft systems clearance represented primary objectives of the initial flight phases.

#### POWERPLANT INVESTIGATION

Powerplant investigation in Phases 1 and 2 concentrated on engine handling, relighting, afterburner light up, fuel system investigation, assessment of accuracy of scheduled engine control and adequacy of engine bay cooling flow.

#### INTAKE INVESTIGATION

Specific investigation directed towards the intake system included transient pressure and internal performance measurement. The effects of sideslip and landing gear configuration were included. Flight techniques were quite straight forward and require no specific description.

Typical results from these initial investigations are presented in Figs. 7 to 9.

The reducing amplitude pressure fluctuations with increasing speed during take-off, Fig. 7, provide tangible evidence of the suppression of flow separations within the intake.

Comparable data, Fig. 8, indicates a loss of pressure recovery for both inboard and outboard inlets at rotation to lift off and moreover, a deterioration of inboard inlet flow quality. The source of the latter is identified and quantified at 205 Kt. CAS in Fig. 9, i.e. nose landing gear interference effects; equality between inlets is achieved with gear retracted.

The limited sideslip investigations of flight Phases 1 and 2, i.e. ±5° sideslip angle, indicated no problems.

#### PREPARATION FOR INITIAL SUPERSONIC INVESTIGATION

During the later stages of Phase 2 investigation, the British prototype 002 was diverted to commissioning and flight clearance of the initial type of variable geometry auxiliary inlet to be featured on Concorde aircraft. A trial installation for initial ground running/taxying investigations was undertaken on the port intake pair, the fixed geometry auxiliary inlets being retained on the starboard side.

Based on the design concept of a dual hinged, dual function single door and colloquially known as the 'barn door' this type of inlet promoted anxieties in relation to the undesirably high levels of quasi-steady flow distortion shown at small scale, more particularly in sideslip and high incidence conditions.

Clearance for flight of the trial installation followed closely the initial pre-flight investigation of the fixed geometry type with the addition of high speed taxy tests with stabilised nose wheel raised attitude. Technique adopted involved aircraft acceleration along the runway at full power raising the nose to achieve lift off attitude at speeds approaching rotation speed with an allowed safe margin to avoid inadvertant take-off. Attitude and speed were held constant by throttling outer engines for as long as safely permitted.

Although a disappointingly high level of quasi-steady flow distortion was shown at incidence, this was less than the maximum at ground static conditions under which equivalent surge margin was demonstrated to that with the fixed intake. This gave rise to the conclusion that the surge margin at lift-off would be adequate if not impressive.

When commissioned, the trial installation doors were limited to manual operation so too the hinge changeover mechanism. The limited flight clearance programme confirmed the adequacy of the proposed manual drill, e.g. closure of barn doors after take-off at M = 0.40, re-open at 0.50 Mach Number in deceleration and descent towards approach. During engine handling and similar limited sideslip investigation to that with fixed geometry intakes, powerplant behaviour was satisfactory.

On the basis of this evidence both prototypes were equipped with barn door intakes with manual control only, in preparation for initial excursions into the supersonic speed regime.

#### INITIAL SUPERSONIC FLIGHT INVESTIGATION

#### GENERAL

Apart from the auxiliary inlet/spill door system, fixed intake geometry was perpetuated as being adequate for initial supersonic flight investigation embracing envelope extension to M=1.50, the proposed limit of Phase 3, and beyond which automatic control of air inlet geometry was essential.

In the intake system context, therefore, attention in the initial supersonic excursions was focussed on flight confirmation of the behaviour of the proposed pressure signal sources for the air inlet control system in the Mach range approaching M=1.50 and of the need for automatic control down to M=1.30, the proposed switching threshold.

Intense interest in the forthcoming Phase 3 investigation also centred on extension of barn door assessment in order to formulate the applicable automatic control laws.

To facilitate appreciation of the intent and results of flight investigation it is opportune to present a brief description of the essential features and functional characteristics of the prototype air inlet control system.

#### PROTOTYPE AIR INLET CONTROL SYSTEM (AICS)

The prototype AICS was a totally analogue closed loop system, Fig. 10. Each intake was equipped with identical completely independent duplicated control lanes, each comprising intake and engine condition sensing and signal processing.

Closure of the control loop was achieved through the intake aerodynamics, the discriminant of correct intake functioning being the ramp void pressure recovery, 7,8, as a function of intake entry approach Mach Number, i.e. local mean underwing Mach Number, Mo. Error from scheduled pressures fed to an integrating loop controlled the variable ramp and spill door actuators.

This was accomplished in practice by control of the ramp void static pressure, pv, to the scheduled ratio of the reference pressure, pc, provided by a 15° semi-angle cone (one per control lane) sited at the rear of the fixed geometry front wedge of the intake. The control pressure ratio,  $\mathcal{N}_{V}$ , hence defined, was thought to be equivalent to  $\mathcal{N}_{B}$  from relevant pre-flight investigation. Reference and control pressures were fed to duplicated balanced beam sensors mounted in the intake ramp void (Fig. 11). Beam fulcrum position, hence control pressure ratio, was programmed as a function of Mach No. The output from a differential transformer (E - core output) which sensed beam deflection, controlled the integrating loop.

Bias of scheduled control pressure ratio from the normal Mach variable function was provided to minimise intake sideslip sensitivity (sideslip input from ADC) in the supersonic regime, a known problem of the prototype intake geometry. Provision for trimming the scheduled law was also included for flight experimentation.

The ramp was free to respond to sensor error signals within angular limits  $\partial_{2 \text{ MIN}}$  and  $\partial_{2 \text{ MAX}}$  determined by intake/engine compatibility considerations. The former represented a 'hard' limit avoiding surge provoking front ramp shock ingestion by the intake; the latter a 'soft' limit which was permitted to increase with increased dump door angle. At ramp deflection beyond  $\partial_{2 \text{ MAX}}$ , the maximum permissible ramp angle with zero dump door angle, ramp and dump door were effectively geared to minimise growth of compressor inlet flow distortion as spill flow requirement increased (e.g. engine throttling).

A sideslip input provided for reduction of 2 MAX, again shown from pre-flight investigation to be effective in avoiding sideslip induced surge.

A further limit to intake functioning was defined by the minimum permissible value of control pressure ratio;  $N_{V \, M \, IN}$ . At low ambient temperature conditions or extreme Mach Number, excessive engine mass flow demand could drive the intake supercritical, even at maximum capture area (ramp angle  $O_{2 \, M \, IN}$ ), sufficiently to provoke engine surge due to deterioration of compressor inlet flow quality. Increased E - core output level in a given sense indicated the approach towards these conditions. Achievement of a selected level ( $O_{V \, M \, IN}$ ) was therefore arranged to illuminate an  $N_1$  warning light directing the crew to throttle the engines, hence reducing engine mass flow demand.

The static control laws for the prototype system are summarised in Fig. 12.

To ensure adequate dynamic response in rapid engine induced transients (e.g. engine failure) the system accepted LP spool speed  $N_1$  input signals from the engine. Transientised open loop demand of ramp and dump door opening rate based on the derivative of this signal were utilised to 'phase advance' system response. System interface with the engine also included 'E-line dip' as a function of sideslip, or achievement of extreme Mach Number by which means the engine control line was depressed away from surge to increase engine tolerance to distorted inlet flow.

#### PHASE 3 - FLIGHT INVESTIGATION

#### General

French prototype Aircraft 001 was the first to achieve supersonic speed, exceeding Mach 1.0 on the 1st October 1969, during flight envelope extension towards M = 1.50.

Following further successful comprehensive investigation of barn doors, initial transonic handling qualities investigation etc., attention was directed towards supersonic intake behaviour and more particularly the behaviour of AICS control reference pressure.

#### AICS Reference Pressure

Investigation of cone reference pressure concentrated on two aspects (1) effect of variation of engine operation between maximum rating and idling and (2) the effect of Mach Number variation in the range of interest at constant engine power.

Accordingly, at selected constant Mach Number in the range M = 1.20 to 1.50, port engines were individually throttled in stages between maximum dry rating and idle conditions to establish effects on intake parameters. Subsequently, at constant maximum dry rating and idling throttle settings, the effect of Mach Number variation was determined by accelerating and decelerating the aircraft with appropriate power adjustments on the other engines.

Finally, the port engines were individually cut at M = 1.50 approximately, to assess the effect of manually inching the dump door on intake/engine behaviour.

The results were illustrative of potential problems. Cone reference pressure increased with engine throttling due to cone envelopment by the expelled intake normal shock in conditions of large fore spillage so induced.

The need for control system functioning down to well below Mach Number of 1.50 was confirmed by the engine cut tests (Fig. 13). Transient intake pressure behaviour indicated substantial penetration of the intake 'buzz' threshold under conditions of engine windmilling at M = 1.50. Buzz was suppressed by opening the dump door. An additional point of particular concern was the obvious reference pressure response to intake instability. Similar data were obtained at M = 1.35 approximately.

Taken in conjunction with similar data appropriate to high subsonic speeds with a windmilling engine this information confirmed the need for spill door scheduling to suppress intake oscillations at very low engine rpm even through the transonic speed range. Inclusion of such additional scheduling was not possible within the prototype aircraft AICS but was incorporated in the later design of AICS for the production aircraft.

#### Manoeuvring Flight - Intake Behaviour

Intake behaviour in limited manoeuvres only was investigated during Phase 3. These included pushover manoeuvres to approximately 0.80g and sideslip manoeuvres up to  $\pm 2^{\circ}$  sideslip angle using flying controls. No problems were indicated in sideslip.

However, crew complaints of intake roughness induced in pushovers were supported by oscillograph recorder traces of inboard intake transient pressure (Fig. 14) showing significant intake disturbance at 1.50 Mach Number for example. This was attributed to shock induced separation of the front ramp boundary layer, the intake matching engine demanded airflow at transonic geometry (ramps fully retracted) with large subsonic forespillage. This represented advanced warning of a low incidence problem.

#### Validation of Barn Door

Comprehensive systematic exploration of the barn door showed it to be adequate to the task, confirming the acceptability of the proposed simplistic scheduling incorporated within the air inlet control system i.e. ramped closure/opening between M=0.38 to 0.55 during aircraft acceleration/deceleration with appropriate automatic hinge changeover at M=0.70 approximately.

#### APPROACH TO MACH NUMBER M = 2.0 (PHASE 4)

#### PREPARATION

Completion of Phase 3 of the flight investigation by the French prototype signalled major grounding of both aircraft to update to Mach 2.0 standard in preparation for Phase 4 of the flight investigation concluding with the achievement of Mach 2.0. This included commissioning of the AICS.

Resumption of flying was initiated by the British prototype 002, to assess the behaviour of the intake functioning under automatic control.

#### TESTING

#### Automatic Control - Preliminary Investigation

Assessment of intake automatic functioning initially comprised limited restrained engine handling and gentle aircraft manoeuvres. This followed sequential introduction of AUTO mode on all intakes at M=1.40. Subsequent deceleration of the aircraft to M=1.20 through the auto-switching threshold was carried out successfully with all intakes retracting ramps to transonic geometry smoothly and without problems.

The subsequent flight confirmed acceptable behaviour of the system in aircraft acceleration to M=1.40 through arming Mach Number with AUTO mode selected. Further engine throttling assessment involving increasing rate throttle applications between max. dry rating and idle, up to slam acceleration and deceleration engine transients, was successfully completed at M=1.40 with no problem evident to the crew.

Analysis of the records confirmed fears concerning sensitivity of cone reference pressure to engine throttling, previously found on Aircraft 001 (Fig. 15) with fixed intake geometry. Increased ramp angle gave rise to shock interference with reference pressure, conditioning the intake to subcritical operation approaching buzz with engine throttled.

#### Envelope Extension

A standard pattern of testing was adopted in the envelope extension investigation directed towards increased Mach Number.

In general successive flight Mach Number increments of  $\Delta M = 0.10$  were made at the achievement of each of which the following programme was carried out.

- (1) Crew familiarisation with aircraft characteristics gentle handling etc.
- (2) Slow individual handling of port engines between maximum dry power and idling operation progressing to slam acceleration and deceleration repeated together. This was preceded by progressive throttling of individual engines in stages to idle operation to study development of compressor inlet flow distortion with increasing intake spill.
- flow distortion with increasing intake spill.

  (3) Steady state sideslip up to ±2° angle each held for ten seconds to stabilise compressor face flow measurements.
- (4) Pushover manoeuvre to approximately 0.50g.
- (5) Single (critical) engine failure simulation by slam throttling outboard engine to idle and closing high pressure fuel cocks.
- (6) Reduction of Mach Number by AM = 0.10 (previously cleared Mach Number) and double engine failure simulation by cutting outboard engine as in (5) above immediately followed by adjacent engine slam throttling to idle.

The range of exploration undertaken, more particularly in terms of sideslip and negative incremental normal acceleration was somewhat limited. The need to demonstrate Mach 2.0 capability, and the associated performance level, predominated at this time. The aim therefore up to initial achivement of Mach 2.0, was to clear minimum margins to give crew confidence using normal flight techniques, in excursions to Mach 2.0 for the purpose of performance assessment.

Based on the pattern of testing outlined above, Mach Number 1.60 was achieved and cleared without event. However, as test Mach Number increased, the predictable shrinking margins to buzz in conjunction with ramp shock interference effects (Fig. 15) heralded buzz penetration in engine throttled conditions at high Mach Number.

Subsequent flight confirmed the worst fears; intake buzz was provoked in slam throttling an imboard engine to idling at M=1.67, precipitating an immediate decision to relocate the cones to a forward position. A precedent was set by this decision. No pre-flight test experience existed in relation to the revised cone positions and reliance was placed on flight development of the system henceforward. The cone sensitivity to throttling was shown to be eliminated with the cones positioned just aft of the wedge leading edge.

Limited cross comparison of cone pressure between intakes was introduced into the AICS monitoring system in efforts to compensate and permit development flying to proceed. However, the achieved comparator levels were unsuitable for service application.

Flight envelope extension was resumed with the revised cone sensing system, both aircraft achieving Mach 2.0 in November 1970. Manoeuvring excursions, however, within the extended flight envelope were very limited.

The first excursion to Mach 2.0 by the British prototype exposed problems. Two separate engine surge events were encountered. In both cases interactive effects provoked surge of the adjacent engine; both events were associated with partial throttling and flight conditions below lg (e.g. 0.80 - 0.90g). Recovery from surge automatically followed re-establishment of level flight.

Suspicions of intake/engine compatibility problems induced by low incidence and exacerbated by increasing flight Mach Number had been generated by pre-flight small scale test evidence. (This is discussed later). The subsequent programme of systematic tests, directed towards isolating throttling and incidence effects, involved stepped, slow and slam engine throttling in nominally level flight, and mild pushover manoeuvres at constant throttle. Both aircraft contributed to this investigation in the Mach Number range M = 1.8 to 2.04 with the greater emphasis on 002.

The conclusions arising from the testing and analysis of Phase 4 can be summarised as follows:

(a) AICS Reference Pressure - Repeatibility of cone reference pressure signals, intake to intake, was poor and comparison with predicted Mach Number relationship disappointing. This is illustrated in Fig. 17 showing meaned data applicable to Aircraft 002. Each installation required unique trimming to achieve the desired intake matching points, a completely unacceptable feature for service aircraft.

An unacceptable sensitivity to incidence variation was also shown - the cone pressure overcompensating for the underwing Mach Number changes on the outboard intake, and providing the opposite sign of correction to that required in the case of the inboard (Fig. 16). The inherent compensation for incidence expected of a local sensing system had not therefore been realised.

(b) Intake/Engine Compatibility - Throttling Effects - Severley restricted throttling drills were required to avoid surge in the higher Mach Number range. Throttling restrictions as follows were formulated and observed in the subsequent prototype flying.

MACH NO. ENGINE		THROTTLING LIMI	
1.80	Outboard Inboard	No throttling 92%	
1.80 - 1.70	Outboard) Inboard )	92%	
1.70 - 1.60	Outboard) Inboard )	88%	
1.60	Outboard) Inboard )	Idling	

(c) <u>Intake/Engine Compatibility - Low Incidence</u> - Outboard engines were shown to be extremely sensitive to flight below lg at high Mach Number - particularly when throttled, both throttling and reducing incidence having similar adverse effects on compressor inlet flow quality in relation to generation of flow separations from the upper walls of the subsonic diffuser.

Fig 18 shows the growth of compressor inlet flow distortion with reducing incidence for engine throttled conditions consistent with fairly large dump door deflection. Local pressure recovery reduces markedly in the upper and sidewall sectors of the compressor face associated with respectively outboard intake capture of the thickening lower wing surface boundary layer, and flow separation from the intake sidewall leading edge; the latter was due to the induced sideslip effect of reduced sidewash in the underwing flow field at the intake entry plane, the intakes being toed in to match the cruise incidence sidewash field.

It should be noted that even at the highest incidence for which data are shown, flow separation in the centre wall/ramp sector of the subsonic diffuser is evident due to the effective overexpansion introduced by the dump door spill flow. At the same time, the dump door 'bleeds off' poor flow on the cowl side of the subsonic diffuser hence providing the lower sector of the compressor inlet with high pressure recovery flow.

Clearly, had the prototype system permitted, control law revision was required to improve flow quality with engines throttled.

#### RECOVERY ACTION

#### AIR INLET CONTROL SYSTEM

#### Local Sensing

By this stage the problems exposed by the prototype flight experience emphasised the high risk nature of an inlet control system completely dependent on the eventual development of an adequate system of local sensing. Indeed as described later our worst fears were realised.

The single cone reference pressure sensing system, which had permitted limited exploration only of the prototype aircraft at high Mach Number, was quite unacceptable for service application. The loss of system reliability and integrity attending relaxation to a single reference pressure source was acceptable only to gain flight experience of the prototype aircraft to confirm performance at high Mach Number and expose potential problems.

The system envisaged for the pre-production aircraft, a logical development of the prototype, was based on four wedge mounted flush static tappings per intake to provide control and monitoring reference pressures and did not merit a high confidence level in the light of this experience.

In systematic investigations to identify the source of cone sensitivity to incidence, and inconsistencies between comparable intake signals, attempts were made to study the approach flow to the intake wedge leading edge and wing boundary layer diverter system. A suitable pigmented oil was used, defined on the basis of wind tunnel experience to flow freely at skin temperatures associated with Mach 2.0. Although no precision could be claimed for such techniques photographs taken of Aircraft 002, on return from flight, proved interesting (Fig. 19), and supported small scale evidence that the prototype diverter system remained unstarted up to at least Mach 2.0, with implied adverse effects on cone signal and intake behaviour.

The problem was further studied by assessment of the effects of modifying the diverter system on French prototype Aircraft 001 to the later design defined for pre-production and production aircraft. In fact this showed little improvement in terms of consistency and incidence sensitivity of the cone pressures, although however, later flow investigation on pre-production Aircraft 101 showed the modified diverter to have overcome the unstart problem (Fig. 19).

#### Intake/Engine Compatibility Considerations

The problems of intake/engine compatibility, dominated by intake sensitivity to throttling and reducing incidence at high Mach Number signalled potential requirements for increased control system flexibility in terms of additional functional relationships.

Equally importantly, a protracted development programme was foreshadowed in view of the apparent inadequacy of the pre-flight development programme. This emphasised the need for systematic flight investigation of control law variation.

Both these aspects of additional system flexibility were beyond the capability of the prototype/pre-production air inlet control system.

#### INTAKE/ENGINE COMPATIBILITY

#### Low Incidence Problem

The low incidence problem afflicting outboard intakes was predictable from small scale model experience.

Source of the problem with the prototype aircraft wing leading edge, designated BA1, was an underwing leading edge vortex type flow separation generated at low incidence by the inboard wing section forward camber (Fig. 20). Spanwise washout of forward camber precipitated detachment of the vortex from the wing undersurface to pass downstream just outboard of the outboard intake with significant adverse effects on the boundary layer ingested. The 'unstarted' wing boundary layer diverter system exacerbated the situation.

The modified diverter system assessed on Aircraft 001 effected no improvement in this problem area, as indicated in further 'pushover' manoeuvre investigations at high Mach No. These included exploration of the effects on underwing surface boundary layer of reducing incidence using the array of wing mounted pitot rakes forward of the intakes as shown in Fig. 21. These showed an alarming growth of the boundary layer ingested by the outboard intake, as incidence reduced in the higher Mach Number range.

Further similar investigations with a modified wing leading edge validated at small scale and designated BA18 (Fig. 20) showed the desired improvement. Fig. 21 illustrates the boundary layer growth with reducing incidence for the modified leading edge indicating an approaching limit of approximately zero incidence.

#### PRODUCTION AIRCRAFT REDEFINITION

#### Air Inlet Control System

Prototype flight experience had clearly demonstrated that the then current AICS and projected developments did not provide adequate control or monitoring. For these reasons the system could not achieve compliance with certification requirements.

In addition the system did not permit the radical modification necessary to meet envisaged service requirements in terms of improved accuracy dictated by control and performance considerations.

Hence the clear requirement emerged for a new system design, centred on provision of accuracy, integrity and reliability compatible with airworthiness and performance objectives. Moreover, inherent flexibility to facilitate ongoing flight development represented a further essential feature.

A prime consideration in redefinition of the AICS was the apparent weakness of a system design philosophy based on local sensing data inputs. An inability to select a sensor location which provided a satisfactory data source had been clearly demonstrated.

A comprehensive requirement specification, devised in the light of the experience gained with the prototype aircraft, formed the basis of the new system design. Moreover, the fundamental requirement invoked computation of control reference signal as a function of local Mach Number to be derived from aircraft mainstream manometrics.

It should be noted, however, that despite the prototype experience accumulated to date, a body of technical opinion still cherished the view that a system dependent on local sensing data input from a 'magic hole' remained feasible. The very nature of the new system design provided the capability of acceptance of such data inputs with no problem.

Onward planning provided for installation of the redesigned system in British pre-production Aircraft 101.

#### Wing Geometry

Following the encouraging flight investigation with the modified prototype, leading edge BA18 was accepted in principle as the defined production standard.

Residual potential problems associated with sideslip induced at intake entry at low incidence (Fig. 18) were anticipated to be resolved by the modified lower cowl and sidewall leading edges of the already defined pre-production/production standard intake, which incorporated cut-back on the basis of the associated benefits in terms of sideslip sensitivity, demonstrated at small scale. To provide advanced warning of potential problems in this context, modification of Aircraft 001 intakes to simulated production geometry was initiated.

Remaining doubts were associated with the increased immersion of pre-production/production intakes in the wing boundary layer. However, it was anticipated that the design philosophy and inherent flexibility of the new control system would provide adequate means of dealing with any problems arising.

# SYSTEMATIC SURGE LOAD INVESTIGATION

With design/manufacture of airframe modifications in progress flight investigations continued on both prototype aircraft in Phases 5 and 6 of the flight programme. These concentrated on high Mach Number performance measurement, handling qualities, flutter clearance and flight envelope consolidation, within the limits set by the intake system. For performance measurement, AICS control pressure ratio was adjusted individually for each intake to compensate for reference pressure errors.

During the course of this investigation the French prototype Aircraft 001 suffered damage to the starboard outer intake following interactive surge precipitated by the inboard engine surging as a result of transient overspeed associated with cancellation of afterburning. This was a common cause of surge, accepted on the basis of pending afterburner control system modification. The forward ramp broke away from the intake on this occasion, the major piece escaping forward around the lower lip, causing damage to the lip; a minor piece was ingested causing severe engine damage. Both aircraft were immediately grounded for modifications to strengthen the intakes. Subsequently, Aircraft 002 was diverted to flight investigation of surge loads as hereunder.

### INSTRUMENTATION

Standard instrumentation was augmented on port intakes for this test series; upper and lower front and rear ramp surface pressure transducers were fitted to measure time variant load distribution in surge (Fig. 22). Ramp torque tube links were strain gauged in association with other selected components with the objective of correlating time variant load and strain to determine dynamic overswing factors. On line monitoring of link strain and compressor face pressure was provided by brush recorder at the flight engineers position.

## TESTING

The flight test programme involved a progressive step by step clearance of increasing flight speed, engine power and Mach Number, culminating in deliberate surges at maximum dry power at Vc (530 Knots) at Mach 2.0, repeating the conditions for ramp failure. Mach range explored was M = 1.70 to 2.0 with associated speed range 460 to 530 Knots CAS.

Test technique to provoke deliberate surge utilised a specially devised 'surge switch' accessible to pilot or flight crew by which means a preselected level of false  $T_1$  signal was injected into the engine control system. This induced engine overspeed and surge following the consequent intake excursion into the supercritical regime. In cases in which the engine proved reluctant to surge, the dump door was opened by manual control. The successful surge provoking means was cancelled following two seconds surge duration approximately.

Tests were discontinued following achievement of critical levels of link strain or subsonic diffuser pressure, as indicated by the brush recorder, pending analysis of the results.

#### TEST RESULTS

The testing adequately explained the exceedance of design loads leading to ramp failure.

Fig. 23 illustrates the commonly accepted form of the relationship between peak surge pulse duct pressure and stabilised compressor pressure ratio just before surge. Values achieved in the case of primary surge were shown to agree with design assumptions; those for interactive surges to be somewhat scattered and in general of lower level. The latter are explicable in terms of the prior transient duct depression, the fundamental cause of interactive surge, due to disruption of the intake shock system in sympathy with the shock expulsion of the adjacent (primary surge) intake.

Fig. 24 compares the relationship between front ramp incremented load (derived from measured link strain) and ramp void incremental pressure for primary and interactive surges. Whereas, primary surge data exhibits a reasonable correlation, the interactive surge data is scattered with considerably greater envelope values consistent with no incremental pressure relief on the ramp undersurface. The typical examples of upper and lower surface time variant pressure, Fig. 25, clearly demonstrate the random nature of differential loading in the interactive case supporting the scattered nature and severity of the loads.

It was concluded that interactive surge is a highly complex process defying prediction in terms of loadings involved. The phasing and magnitude, within limits, of upper and lower surface front ramp incremental loading is by nature random due to the random phasing and relative magnitude of interactive and primary surge pulse pressures. This is illustrated in Fig. 26 which shows three typical examples of time variant compressor face pressure.

Intake design loads were revised to cater for interactive surge loads defined on the basis of this investigation; the appropriate intake structural modifications were defined.

# PROTOTYPE SIMULATION OF PRODUCTION STANDARD

#### INTAKE/ENGINE COMPATIBILITY

A high confidence level was established in the resolution of fundamental problems by the flight investigation of French prototype Aircraft 001 with intakes suitably modified to simulate the production standard installation, and of course fitted with the modified wing leading edge, BA18.

Flight assessment concentrated on the definition of surge free low 'g' and sideslip capability, together with the effects of intake cowl bleed (subsequently defined for production inboard intakes only), and suppression of 'E line dip' within the AICS.

In broad summary the aircraft achieved a maximum of M=2.14 approximately in level flight with nominally zero sideslip.

Excursions in sideslip up to  $\pm 2^{\circ}$  and  $\pm 4^{\circ}$  at flight Mach Numbers of M = 2.08 and M = 2.02 respectively were successfully achieved without surge provocation. Moreover excursions to near zero 'g' in pushover manoeuvres were successfully accomplished up to flight Mach Numbers of M = 2.08.

It should be noted, in placing these achievements in perspective, that the limiting Mach Number of the aircraft was anticipated to be dictated by the onset of engine surge due to approaching the limit of supercritical intake functioning tolerable to the engine. (This is discussed in more detail later). However, during the course of this investigation engines were throttled in response to warning of the approach of this condition given by the inlet control system (% v Min threshold). Therefore, the apparent surge free Mach Number capability could not be interpreted as that available with engines operating at cruise power in coping with rapid adverse. Mach Number transients from cruise conditions ~ i.e. the consideration which essentially dominates Mach capability requirements. However, these demonstrations represented confirmation of the effectiveness of the modified wing leading edge and wing boundary layer diverter system in dealing with the low incidence problem and the modified intake entry geometry in the context of sideslip capability.

Although not wholly representative therefore, in terms of severity of the standard of achievement required for certification, this flying by the modified French prototype was regarded as a positive contribution in the development of the intake system.

## ALTERNATIVE AICS REFERENCE SOURCES

In parallel with the intake/engine compatibility investigation the quest proceeded for alternative control reference pressure sources.

The characteristics of various potential reference pressure locations were assessed, the details of which are beyond the scope of this paper.

Suffice it to state that of the many variants investigated, no satisfactory local sensing source was identified as an alternative to a computed control reference signal.

#### PRODUCTION STANDARD INTAKE SYSTEM

Before proceeding to the evolution of the final certification standard system the revised design of the AICS deserves brief description.

### PRODUCTION AIR INLET CONTROL SYSTEM

The production standard Air Inlet Control System is a hybrid digital analogue system based on a special purpose digital processor (Fig. 27).

The system, comprising Sensor Units (four) and Control Units (eight), computes the required control laws and monitoring functions determining the appropriate intake geometry by complex non linear relationships in terms of ramp void pressure, incidence, free stream static and stagnation pressures.

Free stream air data is derived from three pitot static probes, i.e. the aircraft central air data sources, shared with but derived upstream from, the air data computers.

The sensor units digitise the probe static and pitot pressure and incidence data which are transmitted along serial data highways to the control units. The control units, comprising the digital processor and dynamic control loops, effect computation of the control laws and monitoring functions.

The digital computation uses hard wired routines with programme and data storage by Programmable Read Only Memories (PROMs). Development standard equipment featured plug in PROMs facilitating rapid changes to the digital control programme for flight development of the control laws.

Fundamental control and failure philosophy of the earlier systems is in general followed, i.e. closed loop control of ramp void pressure, as a function of local Mach Number utilising duplicated self-monitored control lanes. Accurate computation of control reference signal, however, replaced the locally sensed pressure of previous systems and, furthermore, complete independence from the aircraft air data computation system is achieved.

Although for initial flight investigation the revised system control laws followed in principle those of previous system standards, except in relation to the interface with the engine, (see later), the additional computing capacity available provided for significantly increased sophistication.

In addition to the traditional low pressure spool speed input to the AICS to increase system response the engine interface included control of maximum LP spool speed at extreme Mach Number, which became the prerogative of the inlet system by the inclusion of an open loop schedule of  $(\Lambda_{1/6})_{MAX}$  as a function of local Mach Number, Mo, fed to the engine control system. The consequent permitted  $(N/6)_{MAX}$  of the engines is illustrated in Fig. 28 which explains the underlying philosophy.

The  $(N_1//)$   $)_{LIMIT}$  function, by restricting maximum LP rpm in the higher Mach Number range preserves a margin to the predicted surge threshold which is governed by supercritical intake operating limits. Margin requirements are dependent upon the permitted probability in service of surge provoked by atmospheric transient disturbances with rate of onset beyond the response capability of the engine to follow the  $(N_1//)$  ) limiter.

### EVOLUTION OF CERTIFICATION STANDARD

### AIRWORTHINESS DESIGN OBJECTIVES

### Flight Envelope

Fig. 29 defines the normal or authorised flight envelope for which certification was sought. Also illustrated is the associated circumscribing or peripheral flight envelope up to which limits the aircraft must be demonstrated to function safely in recovery to the authorised envelope without excessive skill on the part of the flight crew.

The margins, so defined, are required to provide assurance of safety during inadvertent excursions of the aeroplane beyond the limits of the authorised envelope from any cause.

Singularly significant in the powerplant certification context is the required Mach Number margin  $M_{DF} - M_{MO}$  anticipated to be limited by the onset of engine surge. This was defined on the basis of a rationalised approach in negotiation with the airworthiness authorities, to cope with transiently increased Mach Number associated with atmospheric or pilot induced disturbances as well as those due to upset manoeuvres.

Survey of world wide extreme atmospheric induced transients specified in statutory requirements justifies a Mach Number margin requirement of approximately  $\Delta$  M = 0.10 to cope with the worst predictable ambient temperature and wind shear effects.

Presuming  $M_{MO} = 2.05$ , and accounting for .02M accuracy of air data computer Mach display, the aircraft could achieve a true Mach Number of M = 2.11 before the crew is warned of Mach overshoot (nominally  $M_{MO} + .04$ ). The authorities agreed, however, that compounding this relatively improbable event with the remote encounter of world wide extreme atmospheric transients, was too stringent. On the basis of the associated probabilities a value of  $M_{DF} = 2.18$  was agreed.

#### Manoeuvre Envelopes

In the case of pitching manoeuvres potential negative incremental normal acceleration cases, as representing the more critical, were scrutinised together with statutory requirements. Fig. 30 illustrates the cases considered and the consequently derived pitching manoeuvre envelope.

Similarly, survey of factors contributory to involuntary excursions in sideslip e.g. engine failure cases, atmospheric gusts, autostabiliser hard over failure etc., in conjunction with initial adverse 20 sideslip angle miss-trim served as the basis of formulation of the sideslip/normal acceleration envelopes of Fig. 30 which account for relevant sympathetic response in pitch.

The objective of the forthcoming intake system flight evaluation and evolution to certification standard could therefore be simply stated - to assess and develop the intake system to accommodate normal engine functioning at and within the authorised flight envelope boundaries and associated manoeuvre boundaries with remote probability of surge occurrence. Furthermore, to realise acceptably low surge probability at and within the circumscribing flight envelope boundaries together with the associated manoeuvre limits specified.

#### Flight Testing Philosophy

The first flight development standard of the production AICS design was installed in the British pre-production Aircraft 101. Powerplant standard differed from the defined production standard mainly in respect of the propelling nozzle geometry. The predicted similar secondary mass flow acceptance characteristics and hence anticipated intake/engine, secondary system matching, however, prompted the decision to develop laws etc. to certification standard using Aircraft 101 with subsequent assessment by the airworthiness authorities as a 'dummy run'. Potentially contentious aspects could then be resolved with the authorities, prior to their final formal assessment of production aircraft.

In parallel, the French pre-production Aircraft 102, featuring the production nozzle, was delegated to similar activities in the context of performance, development of flight control systems, and handling qualities.

#### FLIGHT TESTING - INITIAL DEVELOPMENT STANDARD AICS

AICS Laws - As previously stated, these, in principle followed previous standards of control system with the exception of the interface with the engine and the addition of transonic schedules.

Fig. 31 illustrates the more significant law revisions from the previous standard. Aside from the transonic schedules the most notable deviation relates to the generation of the control pressure ratio,  $N_{\rm V}$ , which incorporated a ramp angle function  $f(\hat{\mathbf{d}}_{2})$  modifying the Mach scheduled relationship in the moderate to high ramp angle range. This was based on flight measurement of discrepancies between  $N_{\rm V}$  and  $N_{\rm B}$  (the true criterion of intake/engine and secondary system matching) indicated in the higher ramp angle range. Performance requirements dictated compensation of scheduled control pressure ratio to preserve the near optimum required  $N_{\rm B}$  relationship with Mach Number.

Surge Margin at Higher Mach Number - It was considered essential to determine the surge threshold in terms of (N/O) and Mach Number to demonstrate that the selected limiter schedule, essentially chosen on the basis of performance optimisation, was permissible from the viewpoint of surge probability in transient adverse Mach Number excursions.

The basic technique adopted for surge threshold determination was to accelerate the aircraft to the point of surge provocation of the selected subject powerplants. In general, port engines were selected with subsequent Checks on starboard units.

Attention was focussed on inboard powerplants which suffered the higher local underwing Mach Numbers in level flight. Aircraft acceleration was undertaken with  $(N_1/\sqrt{6})$  limiters inoperative with the subject engines adjusted to the selected LP spool speed. Remaining engines were throttled relatively by approximately  $1\frac{1}{4}\%$   $N_1$  to ensure surge occurrence initially on the subject engines. Varying ambient temperature conditions were simulated by throttling the subject engines to selected levels dependent on prevailing air temperature. To ensure adequate coverage of ambient temperature range Aircraft 101 was based in Tangier Morocco for this test series, taking full advantage of the low prevailing ambient temperature at high altitude.

Fig. 32 shows the initially determined surge threshold applicable to the port inboard powerplant, together with the relevant surge provoking compressor face distortion patterns. The surge threshold achieved was disappointing in the higher N/O range compared with anticipation from altitude facility experience, due to relatively exaggerated low pressure zones in the upper sector of the compressor face, at the low levels of throat bleed pressure and mass flows associated with supercritical intake operation.

Plausible argument encouraged reduction of the scheduled minimum ramp angles, permitting intake operation with the front ramp compression system inside the lip. The degree of ingestion permissible from intake stability considerations was unknown but the relief of engine mass flow demand afforded by the associated reduction of intake pressure recovery was seen as a potential solution providing increased surge Mach Number by virtue of the consequent increased throat bleed mass flow and hence improved balance of upper and lower sector pressures at the compressor inlet.

This conceptual solution was proved by flight investigation. At selected Mach Numbers and inboard engine power settings the ramp was inched under manual control to lower angles then previously permitted by the AICS schedules. Fig. 33 illustrates typical results. The improved balance of compressor inlet flow is clearly shown as ramp angle is reduced from the scheduled minimum values. Equally inportant, no intake instability problem was encountered.

From the performance investigation proceeding in parallel on Aircraft 102 refinement of intake management techniques for optimum performance evolved. This indicated a potential conflict between intake/engine compatibility and performance requirements, confirming that revision of the minimum ramp angle function could prove injurious to performance.

Flight investigation continued on Aircraft 101 with a revised minimum ramp angle schedule. Further surge probes showed the improvement of surge threshold shown in Fig. 34.

Intake/Engine Compatibility at Low Power - It was considered important in terms of crew work load to achieve, as far as possible, orthodox powerplant management techniques, with as little as possible restriction of crew freedom in terms of engine handling. However, the initial engine throttling investigations at high Mach Number showed intake/engine compatibility problems on the inboard engines, surges occurring at flight idle.

Once again, recourse was had to flight evaluation of compressor inlet flow quality by systematic manual adjustment of intake variable geometry. The ramp and dump doors were varied according to a selected pattern in the Mach Number range M=2.0 to 2.08 at flight idle engine setting, also at M=2.05 at a selected intermediate throttle setting.

Fig. 35 typifies the results. To minimise flow distortion the need to match the intake to an idling engine at elevated throat bleed pressure levels, subcritical of typical cruise values, was clearly shown. Furthermore, at intermediate throatle setting a unique level within close limits was shown to be desirable. These requirements, in combination with those emerging in the cruise performance context from Aircraft 102 dictated the compromise law relating incremental control pressure ratio and ramp angle shown in Fig. 36. To avoid control into intake buzz in throatled conditions at low Mach Number a further law governing maximum permissible control pressure ratio, as a function of Mach Number, was introduced ~ denoted \( \bar{\cappa}\_{\text{VMAX}} \). The essential nature of this law is clarified in Fig. 36 wherein control pressure ratio is shown as a function of local Mach Number for selected ramp angles.

Application of similar law standards to outboard intakes proved inadequate in terms of surge freedom at idling. Supersonic deceleration, fully throttled, commonly provoked surge of the starboard outer engine in the approximate flight Mach Number range M = 1.7 to 1.8. Although of a mild nature the potential disturbing influence on passengers dictated avoidance.

Further manual inching investigation of the outboard intake yielded the compressor inlet flow distortion data of Fig. 37 and the revised law shown for  $\eta_{VMAX}$  which differed from that of the inboard.

Evenso, although introduction of this revised law reduced the frequency of outboard engine surge in aircraft deceleration, particular engines in the starboard outer position proved to be surge prone to an unacceptable degree for a service aircraft. As these apparently sensitive engines could not be identified in the normal acceptance procedures carried out by the engine manufacturers, coping with such engines in service had to be accepted. The need to invoke throttling restrictions in the higher Mach Number range was recognised as the only positive solution. Accordingly a "propped idle" technique was adopted which called upon the crew to observe normal throttling limits, in terms of lever angle position, in the Mach Number range above M = 1,60. These, indicated by appropriate throttle quadrant markings dependent upon ambient air temperature, increased minimum engine mass flow demand above normal idle to levels compatible with surge avoidance.

Emergency deceleration and descent procedures retained throttling to idle on the basis that the mild surges possibly invoked were acceptable in this case.

<u>Pitching Manoeuvre Capability</u> - The surge free capability in terms of negative incremental aircraft normal acceleration was investigated in pushover manoeuvres at selected power settings.

Target minimum normal acceleration was nominally zero 'g', except in the case of statutory upset manoeuvres to 0.50g, achieved either by pushovers from level flight or from positive incremental normal acceleration conditions achieved in preceding gentle 'pull ups', Manoeuvres were executed with the subject engines (port) at selected power settings with all (N/D) limiters inoperative. Fig. 38 shows cases in which surge was encountered on the inboard engine shown to be the more critical. Comparison of the achieved surge points with the mean surge line established in level flight showed good correlation.

It is important to differentiate between the negative incremental 'g' margin to cope with transient disturbances of rate of application beyond the capability of the engine, (e.g. remote gust cases) and alternative cases which involve engine response to the (N/6) limiter. The foregoing testing, Fig. 38, covers the former case and for this purpose tests were conducted with limiters inoperative; the latter were covered by additional tests with the limiter operative. Similar pushover techniques were utilised with surge encountered on the outboard engines as shown in Fig. 39, these proving the more critical in these effectively partially throttled cases. Tests were repeated with engines approaching idling conditions providing similar acceptable normal acceleration capability.

These data were considered to demonstrate achievement of the design airworthiness objectives with respect to pitching manoeuvre capability.

Sideslip Capability - Investigation of surge free sideslip capability involved both steady state and dynamic techniques.

At selected Mach Number in level flight, in the approximate range M = 1.90 to 2.16 up to 3.5° sideslip angle was applied in both directions using flight controls. Peak angles achieved in dynamic cases covered, with adequate margin, the most severe engine failure cases and lateral gusts specified.

Investigation concentrated on port engines which functioned at selected rating with starboard engines relatively throttled by  $1\frac{1}{2}$ %  $N_1$ , all  $(N/\sqrt{6}^*)$  limiters were inoperative.

The results, as illustrated in Fig. 40 were extremely gratifying demonstrating sideslip up to 3° angle to be achievable without surge at flight conditions closely approaching the level flight surge threshold: moreover, similar levels were achievable up to within close proximity to the intended value of MDF e.g. M = 2.16.

Additional sideslip investigations were directed towards determining effects on low 'g' capability. Pushover manoguves to nominally zero 'g' were carried out with an initial  $\pm 2^{\circ}$  sideslip angle initially applied and held. No difference of minimum normal acceleration capability was detected in comparison with nominally zero sideslip cases.

This represented conclusive evidence of compliance with the design airworthiness objectives.

<u>Mach Number Capability</u> - A prime objective of the Moroccan campaigns with the pre-production aircraft was to demonstrate the acceptability of the aircraft at the intended  $M_{DF} = 2.18$  associated with the scheduled  $M_{DC} = 2.05$ .

This represented in fact, a by-product of the surge probes as indicated by Fig. 32 showing the maximum equivalent flight Mach Number reached to be approximately M = 2.20. Advantage was taken in the approach to such extreme Mach Numbers to confirm the acceptability of aircraft handling qualities in gentle manoeuvres.

#### Impact on AICS Control Laws

Apart from the detailed law revisions already discussed a major impact of the pre-production aircraft investigation resulted from the clear demonstration of the need to invoke low ramp angles to provide adequacy of surge margin in the higher Mach Number range, at the risk of compromising performance.

Refinement of the performance requirement in the control pressure 7V and the ramp angle (Fig. 36), partly resolved this conflict by permitting themse ramp angle schedules appropriate to compatibility requirements. The residual problem convened the rapid establishment of minimum ramp angle required to cope with high rate adverse disturbance

The switching logic introduced into the control system a achieve this is illustrated in Fig. 41. A compatibility mode was introduced defined in terms of control pressure ratio as  $1 \text{N}_{V \text{ COMP}}$ . This mode catered for rapid transient excursions beyond the normal (N/O) limit, invoking ramp angle less than a selected threshold value  $2 \text{ MIN} + X^{\circ}$ .

Provided that the associated rate of Mach Number increase exceeded a selected level, signalled by rate of change of pitot pressure to the system, the activation of this mode signalled ramp deflection towards minimum angle at maximum rate due to the large subcritical control pressure error seem by the system. Recovery to the normal operating situation was effected through response of the N/O limiter.

It should be noted that activation of the compatibility mode triggered visual crew warning to throttle the engines to supplement the action of the  $(N_1/\sqrt{3})$  limiter.

These modes of functioning were introduced into the AICS during the Moroccan campaign utilising the pre-production aircraft. The later phase of flight investigation explored the adequacy of the compatibility mode and the associated laws prior to submission of the aircraft to the airworthiness authorities.

### Certification Process - Evolution

Following their own flight evaluation of powerplant characteristics the Civil Aviation Authority accepted the aircraft as having achieved an adequate standard for certification in the intake system context.

Quoting from the relevant CAA Flight Test Report - "the datum established in (pre-production aircraft) 101 is acceptable provided that it is repeated on production aircraft."

The objective was therefore set for the subsequent and final phase of flight evaluation - i.e. to validate a production aircraft as having achieved a similar standard.

### PRODUCTION AIRCRAFT EVALUATION

### AICS Standard

French production Aircraft 201 was selected for the final phase of evolution of the intake system to achieve the agreed standard in a production installation.

Development standard AICS equipment was installed i.e. featuring 'plug in' PROMs in anticipation of requirements for further law trimming.

Functioning laws were modified from the final standard of Aircraft 101 with respect to parameter values, notably minimum ramp angle 0.2 MIN, in the higher Mach regime. These changes were devised essentially to offset predictably differing secondary system matching of the production standard, due to improved nacelle scaling generally, invoking reduced intake throat bleed mass flow hence possibly provoking premature surge in supercritical intake operation. Law structure remained unchanged from the previous standard.

The state of the s

## Flight Testing

The aircraft once again operated out of Morocco (Casablanca) and flight techniques followed the pattern evolved in the previous investigations on the pre-production aircraft.

#### Surge Margin Determination

The suspected problem of low throat bleed mass flow associated with the improved nacelle sealing was immediately exposed by the initial exploration of the higher Mach Number range, which demonstrated considerable loss of surge threshold Mach Number compared with the pre-production aircraft achievement, illustrated in Fig. 40 curve 1 compared with 2 (inboard engine).

Adjustment of minimum control pressure ratio successfully overcame the problem by driving the intake onto the minimum scheduled ramp angle. This represented the first of many detailed law changes required to achieve the standard set by the pre-production aircraft.

Detailed discussion of all further difficulties exposed, and their resolution, is beyond the scope of this paper. However, a particular problem relating to inboard intakes merits attention.

This concerned the onset of an intake 'unstart' induced surge threshold, curve 3B of Fig. 42. As previously stated, the surge threshold at high NAO is normally governed by achievement of the limiting degree of supercritical functioning of the intake tolerable to the engine. Hence the emphasis on reduced minimum ramp angle, 2 MIN, in order to delay the onset of such intake conditions as Mach number increased. The revised minimum ramp angle schedule, invoking further reduced angles compared with the pre-production standard, in fact improved the surge threshold at high levels of (NAO) - as anticipated - curve 3A. However, further exploration at simulated increased ambient temperature (reduced (NAO)) indicated 'premature' surge occurrence preceded by quite violent intake pressure oscillation, suggesting a different surge provocation mechanism from that at the higher (N/AO) levels.

Careful examination of the records indicated that the reduced scheduled minimum ramp angles promoted mixed compression functioning of the intake and moreover that the matching value of control pressure ratio was sufficiently large to invoke intake unstart over the particular M, (N/6) range of the problem. Further revision of the minimum ramp angle schedule together with further adjustment of minimum scheduled control pressure ratio avoided the intake unstart surge threshold. As shown in Fig. 42, curve 4, this was gained at the expense of surge margin in the higher (N/6) range.

Outboard powerplants also suffered problems of premature surge, largely confined to functioning zones beyond the achievement of the pre-production aircraft equipped with earlier development standard engines of lower power. Fig. 43 effectively summarises the gains of surge margin achieved by judiciously chosen law revision; notably concerning  $\sum_{N} 10^{10} \, N_{N}$  and  $\sum_{N} 10^{10} \, N_{N}$  with the introduction of Mach and incidence functions respectively.

Figs. 42 and 43 present the finally achieved surge thresholds relating to inboard and outboard intakes respectively.

Validation of the final law standard was undertaken using the established pattern of testing in the assessment of sideslip and normal acceleration capability. Fig. 44 demonstrates compliance with the airworthiness objectives in relation to manoeuvre capability.

The airworthiness authorities actively participated in the final phases of development flying in addition to their ultimate formal acceptance tests. On the basis of these, together with the data of Figs. 42, 43 and 44, they agreed that production Aircraft 201 had achieved parity with the datum standard set by the pre-production aircraft in the intake system context.

### CONCLUDING REMARKS

A number of salutory lessons were learned from the development and certification of the overall intake system for Concorde. In many respects these must be applicable to other supersonic vehicles, to a greater or lesser extent, dependent on the stringency of the relevant requirements.

In all, intake system development occupied some 500 flying hours of which some 50% involved supersonic investigation. Moreover, some 500 surge events were encountered, the vast majority intentionally. This represents an impressive volume of flight testing, by any standards, emphasising the formidable nature of the task but also underlining the dominant lessons emerging, viz:

- 1. More particularly in the case of an aerodynamically integrated powerplant concept, the importance for flight evaluation purposes of definitive standards of the major components, e.g. engine, air inlet, propelling nozzle, systems and the vehicle must be emphasised.
- 2. Profound repercussions attend apparently minor changes and moreover this relates to the total integrated concept including the vehicle. It is quite erroneous, in this context, to consider major components, e.g. the engine air inlet, independently.
- 3. It should be accepted that integration should be undertaken by the prime airframe constructors. This viewpoint is reinforced by the experience of the Concorde inlet system, the success of which is solely attributable to:

(a) the bold but prudent decision to redesign the control system at a relatively advanced stage of the

(b) the innovative nature - i.e. digital control - the first application in the civil aviation context,

proved acceptable to the appropriate authorities

(c) most importantly, the control system in entirety was designed and developed 'in house' by BAC with all the inherent advantages of absolute control of the design. Equally, cross fertilisation of specialist skills within the design team engaged proved invaluable - e.g. aerodynamicists acquired considerable expertise in the field of the systems engineer and vice versa. The logical projection of this concept in relation to future advanced applications almost certainly involving integrated control is clearly obvious.

The ultimate dependence upon flight test investigation in the formulation of intake management techniques, to satisfy the requirements of performance and intake/engine compatibility has profound implications. Concorde does not represent a precedent in this context among aircraft of advanced concept, except in relation to the relatively more rigorous standards required for certification in the passenger carrying context. The Concorde experience in particular, however, serves to emphasise the inherent flexibility required of automatic control systems in these circumstances, an aspect which must be firmly borne in mind in system designs for similar future applications.

### ACKNOWLEDGEMENTS

The author acknowledges with gratitude, the permission of BAC to publish this paper, at the same time emphasising that opinions expressed are his own.

He also wishes to express his gratitude for the advice given by members of BAC Design and Flight Test staff, as follows. T.W. Brown, J.M. Legg and I.L.K. Rye of Design and B.V. Gammon and G. Skillen of Flight Test.

## SYMBOLS

Mac	flight or free stream Mach Number
<b>*</b> o	local approach Mach Number to the intakes
Pes	free stream stagnation pressure
P <sub>1</sub>	mean stagnation pressure at compressor face
P <sub>T11</sub>	local stagnation pressure at compressor face
٦,	air inlet pressure recovery P <sub>1/Pe0</sub>
P <sub>B</sub>	air inlet throat bleed stagnation pressure (ramp void rear)
P <sub>v</sub>	static (control) pressure sensed in ramp void above forward ramp
NB	air inlet throat bleed pressure recovery PB/PB
٧v	air inlet control pressure ratio p <sub>v/Peo</sub> 1 B
Pc	static pressure sensed by cone - air inlet control system reference pressure (prototype)
rb	air inlet control system control ratio (prototype) = p
	$1.0.7_{b} = r_b \times p_{cd}(r_b = f(Mo))$
Pc	aircraft rear plenum chamber static pressure
Pr	aircraft nose probe static pressure
DC (😉)	compressor inlet flow distortion index
	$= (P_1 - P_{T1i_{MIN}} (\Phi)) / q$
P <sub>Tli</sub> MIN	minimum mean stagnation pressure over sector surrounding the region of lowest pressure at the compressor inlet (relevant = 0 and 600).
q	mean dynamic head at compressor inlet
W <sub>1</sub>	compressor inlet (engine) mass flow
¥ eo	maximum equivalent free stream capture mass flow of the air inlet
w <sub>B</sub>	air inlet throat bleed mass flow

```
= W<sub>1/W ∞</sub>
= W<sub>B/W ∞</sub>
            compressor inlet mass flow ratio
٤,
EB
            air inlet throat bleed mass flow ratio
            air inlet throat bleed exhaust sonic area ratio
92
            forward ramp angle
            spill (dump) door angle
a MAX
            maximum permissible ramp angle with \Theta_{DD} = 0^{\circ}
9 T MIN
            minimum permissible ramp angle
T V MAX
            maximum permissible air inlet control pressure ratio
TV MIN
            minimum permissible air inlet control pressure ratio
N<sub>1</sub>
            LP compressor rotor speed
            HP compressor rotor speed
N<sub>2</sub>
N<sub>LD</sub> or N<sub>1D</sub> LP compressor rotor 'design' speed
            HP compressor rotor 'design' speed
N<sub>2D</sub>
            LP compressor delivery static pressure
P2
            HP compressor delivery static pressure
P3
            LP compressor rotor relative speed
N1/10
N2/10
            HP compressor rotor relative speed
            T<sub>1/288</sub>
 0
            LP compressor inlet flow stagnation temperature
T,
d
            aircraft incidence angle (angle of attack)
            aircraft sideslip angle
            sustained operating Mach Number limit
            flight demonstrated maximum Mach Number
```

# REFERENCE

 Johnson P.J. Olympus in Concorde. The Tools of Development. AIAA/RAeS/CASI 10th Anglo-American Aeronautical Conference, Los Angeles, California, 18th - 20th October 1967 (AIAA 67-753).

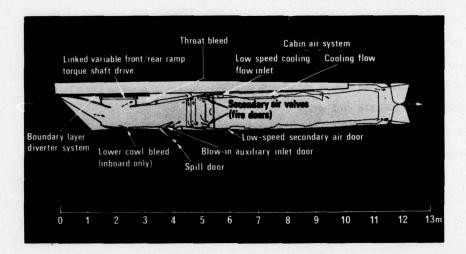


Fig.1 Powerplant arrangement

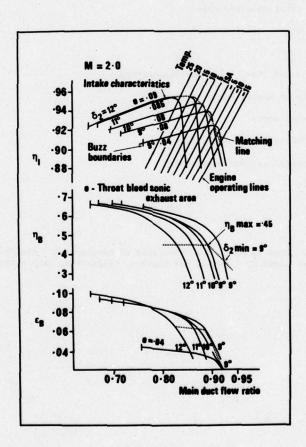


Fig.2 Intake/engine matching

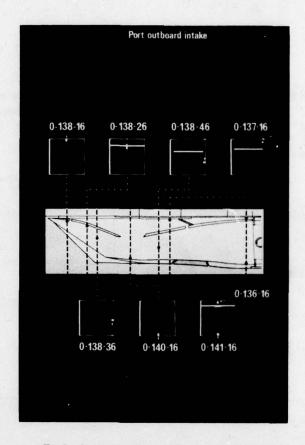
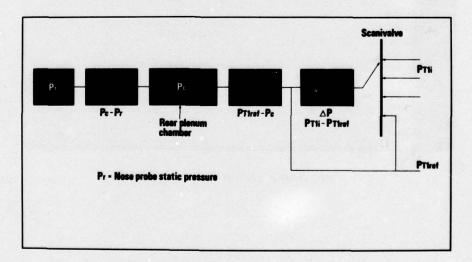


Fig.3 Intake transient pressure measurement



 $Fig. 4 \quad Pressure\ measurement-compressor\ face$ 

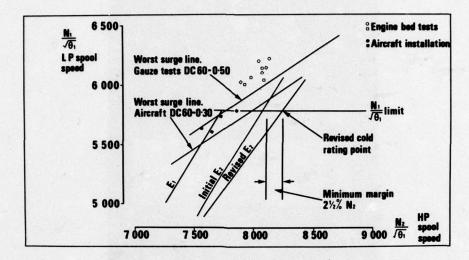


Fig.5 Surge margin prototype static ground running

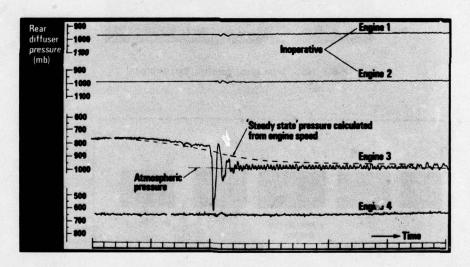


Fig.6 Surge interaction tests - prototype

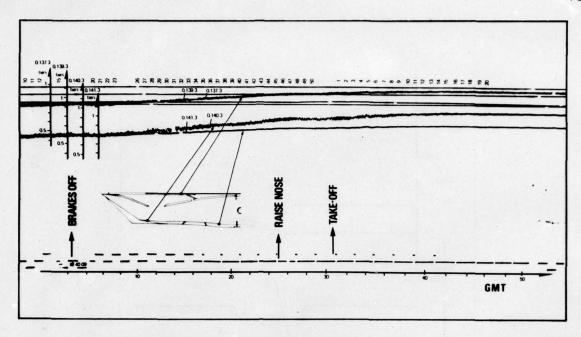


Fig.7 Intake transient pressures at take off - starboard inboard

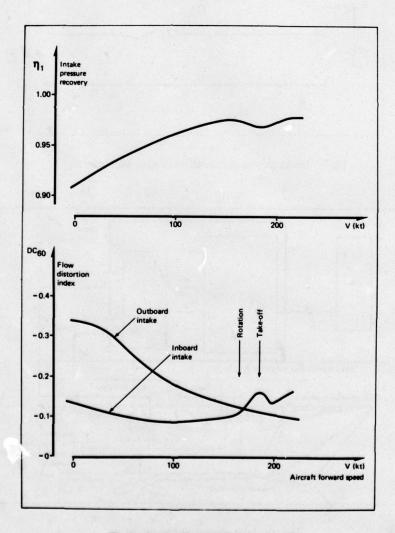


Fig.8 Intake flow quality at take off

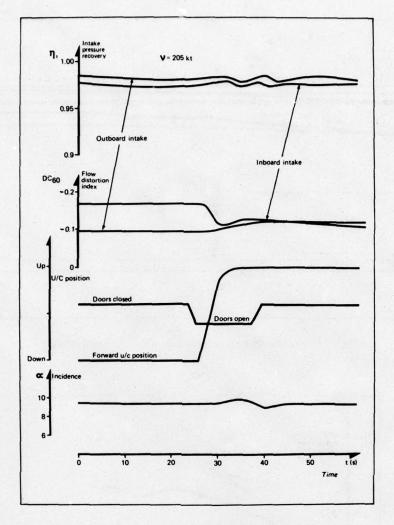


Fig.9 Intake flow quality - effect of nose undercarriage

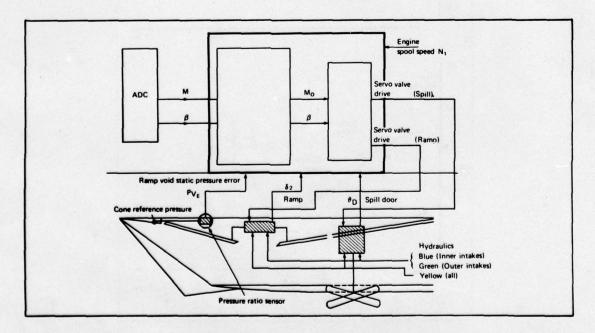


Fig.10 Inlet control system prototype

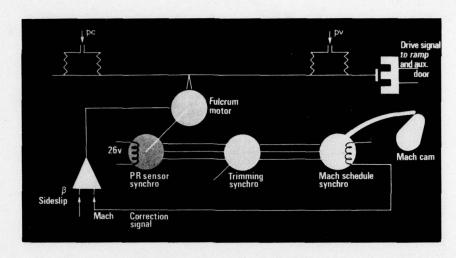


Fig.11 Pressure ratio sensor - prototype

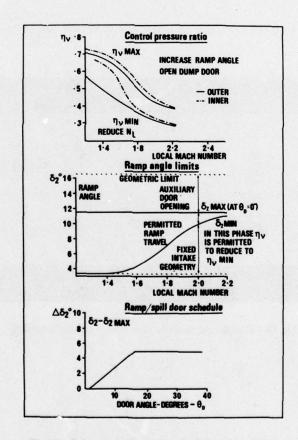


Fig.12 Inlet control system schedules - prototype

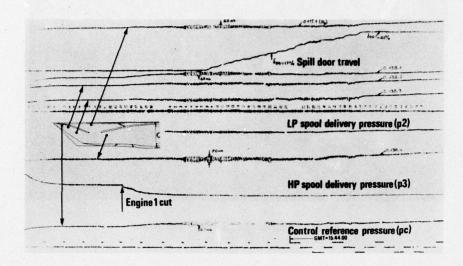


Fig.13 Port outer engine cut - M = 1.50 intake transient pressures

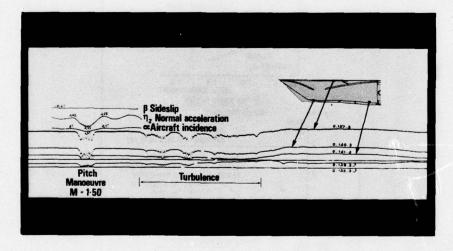


Fig.14 Pitching manoeuvre M = 1.50 - intake instability

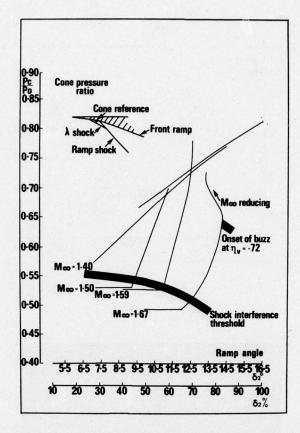


Fig.15 Cone reference pressure - aft cones - effect of throttling

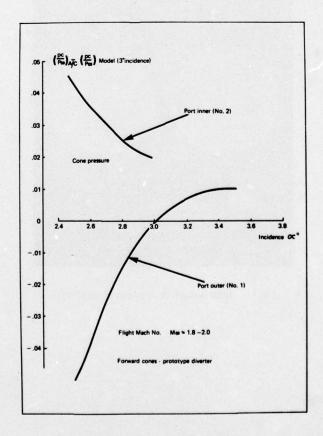


Fig.16 Cone pressure - effect of incidence

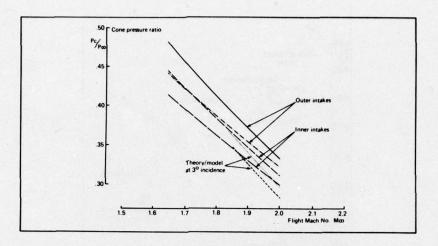


Fig.17 Cone pressures - forward cones

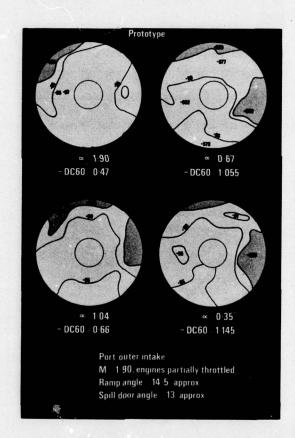


Fig.18 Inlet distortion - effect of incidence

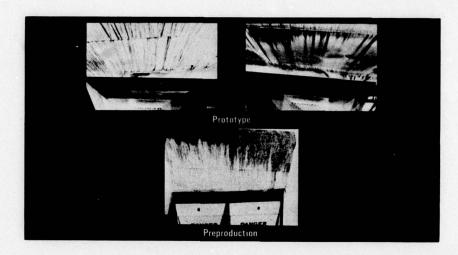


Fig.19 Diverter system flow visualisation

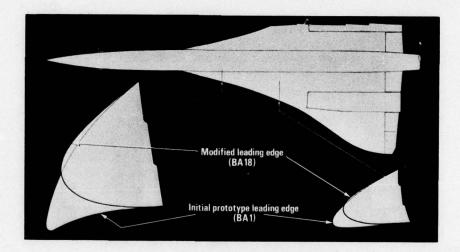


Fig.20 Suppression of vortex at leading edge at low incidence

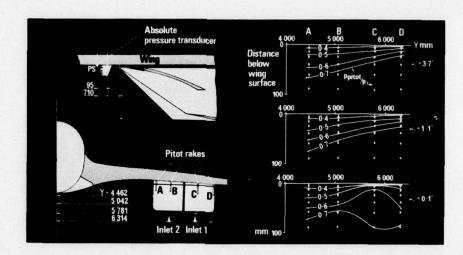


Fig.21 Measurement of boundary layer forward of intakes

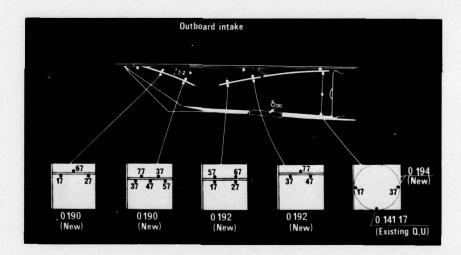


Fig.22 Augmented instrumentation - surge pressure measurement

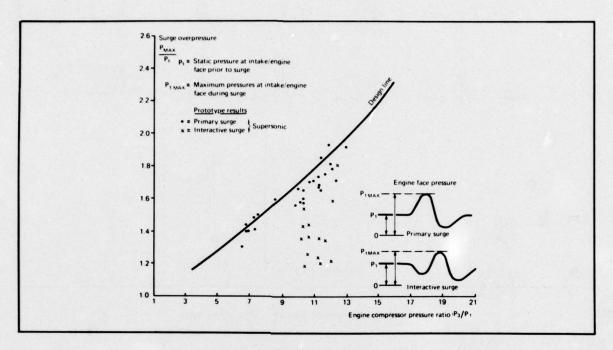


Fig.23 Engine surge pressures

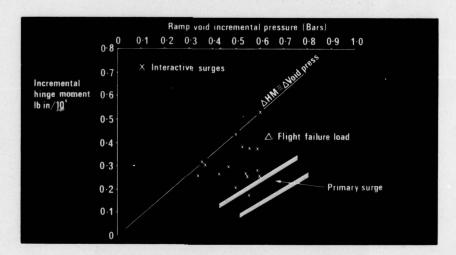


Fig.24 Front ramp loads

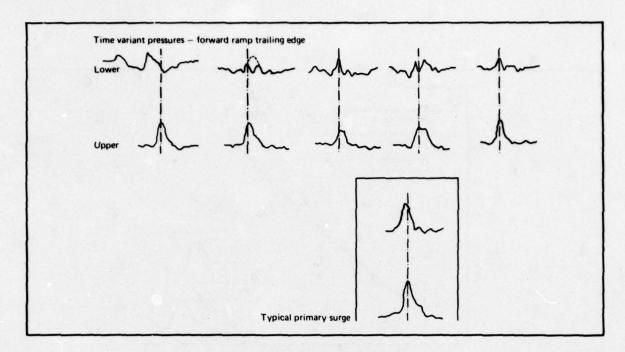


Fig.25 Ramp differential loading - interactive surge

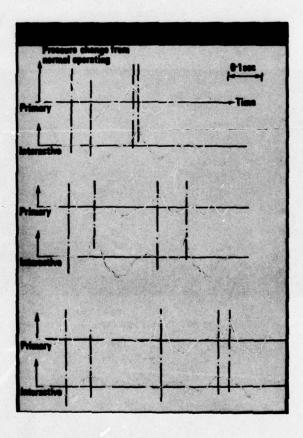


Fig.26 Engine face surge pressures

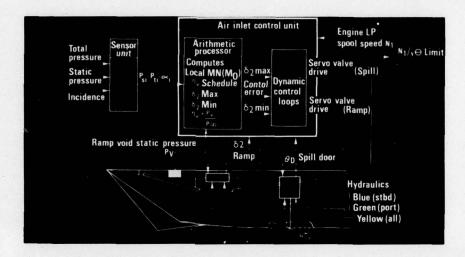


Fig.27 Production standard air inlet control system

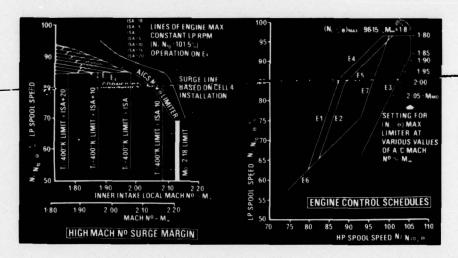


Fig.28 Air inlet control system limits

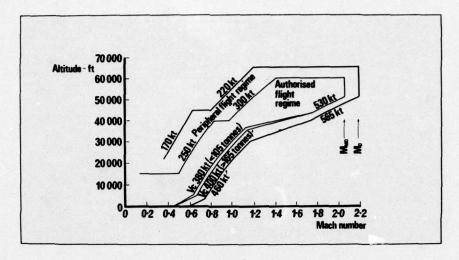


Fig.29 Powerplant certification flight envelope for surge free operation

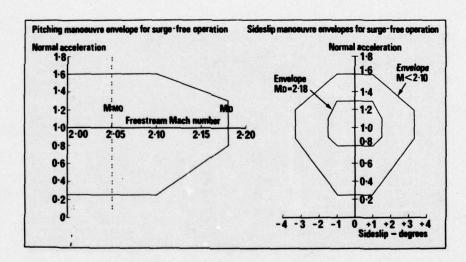


Fig.30A Surge free manoeuvre envelopes

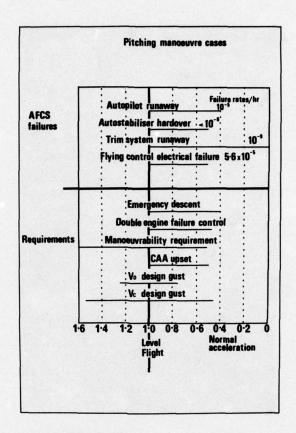


Fig.30B Surge free manoeuvre envelopes

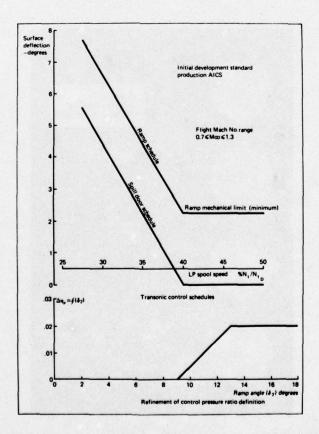


Fig.31 Additional control schedules production development AICS

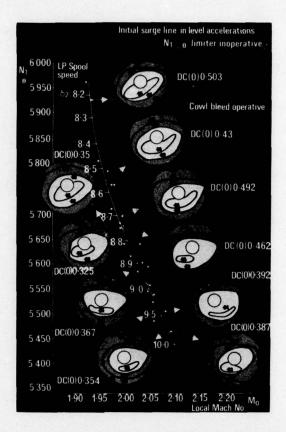


Fig.32 Inboard intake - initial surge line in level accelerations

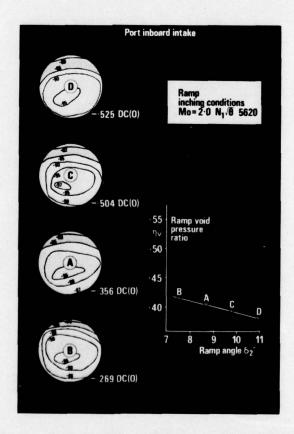


Fig.33 Manual variation of intake geometry preproduction aircraft 101

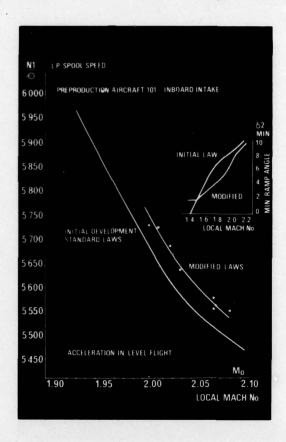


Fig.34 Surge line improvement with reduced minimum ramp angle

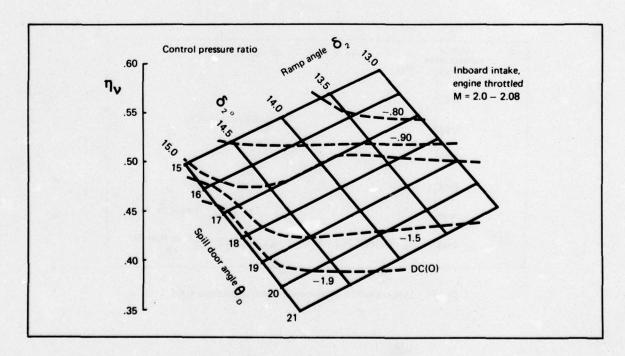


Fig.35 Manual ramp and spill door variation

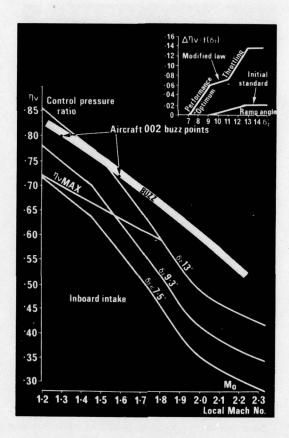


Fig.36 Revised control pressure ratio schedules

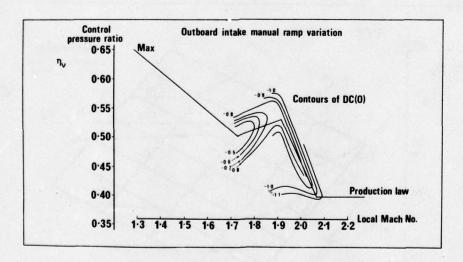


Fig.37 Determination of maximum control pressure ratio

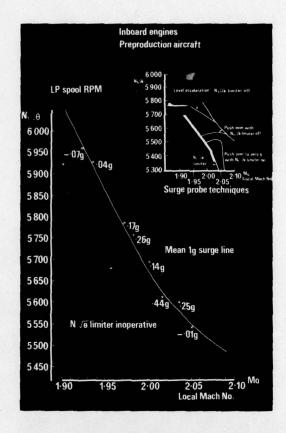


Fig.38 Surge threshold at low 'g' - inboard engines

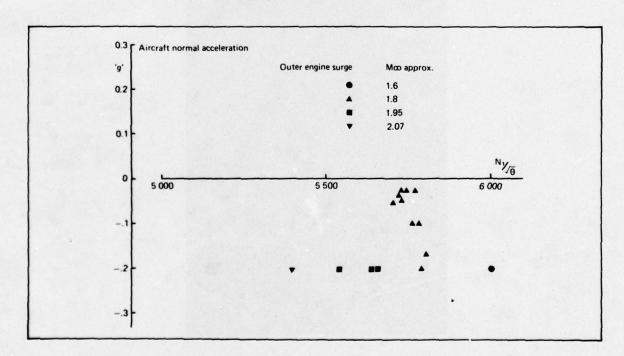


Fig.39 Low 'g' - Nï limiters operative

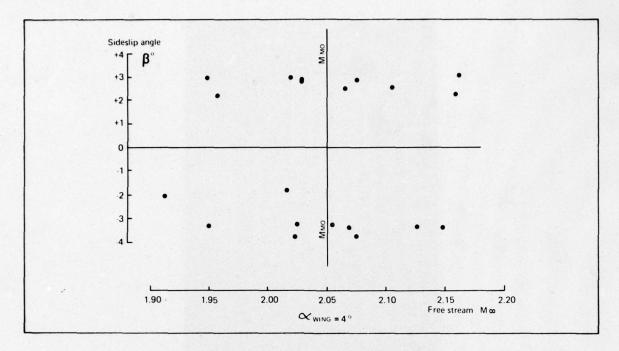


Fig.40 Surge free sideslip excursions

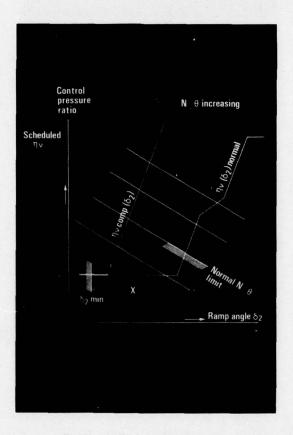


Fig.41 AICS functioning modes

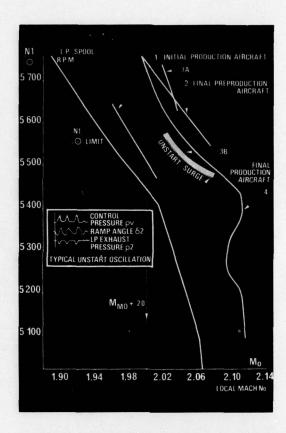


Fig.42 Surge threshold comparison - inboard intake

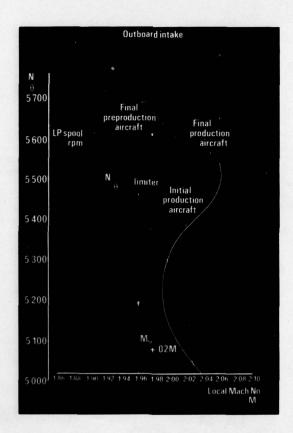


Fig.43 Surge threshold comparison - outboard intake

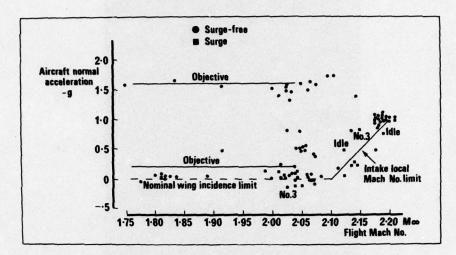


Fig.44A Production aircraft normal acceleration capability

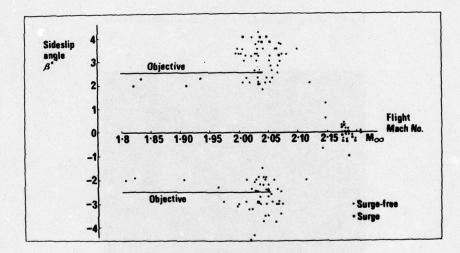


Fig.44B Production aircraft sideslip capability

#### WEAPONS TESTING TECHNIQUES

hy

F J Bigg, Royal Aircraft Establishment Farnborough, UK N Tait, Cape Engineering Limited, Warwick, UK D A Williams, Cranfield Institute of Technology, UK

#### SUMMARY

This paper describes the philosophy adopted by the Directorate of Air Armaments MOD (PE) United Kingdom and the Air Armaments Department, Royal Aircraft Establishment, Farnborough in obtaining experimental information relevant to the design and clearance of free fall weapons and associated carriage equipment. A number of instrumented stores which have been developed as a result are described in some detail, and certain of the conclusions which have been drawn from those trials which have been executed to date are presented.

#### 1. INTRODUCTION

- 1.1 Improvements in aircraft performance and changes in the methods of transport and delivery of weapons which occurred in the past two decades have placed increasing emphasis on optimising the design of weapons and the carriage equipment which supports and delivers them. Prior to this period, ballistic weapons were generally transported in an enclosed bomb bay and the release units which supported them fulfilled a limited function of support and gravity release. In general, the release unit was designed to react only the vertical component of applied load at a single point, other components of load arising from manoeuvres being reacted at widely separated points on the weapon carrier or bomb bay structure. Problems encountered in attempting to release weapons from bomb bays at increasingly higher speeds, followed by the trend towards multi-role aircraft, have resulted in the almost universal adoption of external weapon carriage. The constraints on the design of carriage equipment and weapons thus became more severe: the need to minimise frontal area resulted in moments imposed by the store on the carriage equipment being reacted at points closer to the suspension lug than previously, thus increasing the forces to be reacted by sway braces; in addition, aerodynamically induced forces became much more important.
- 1.2 For some time, weapons and carriage equipment have been designed by using the data gathered during previous development trials of similar devices, and by extrapolating this information in order to predict operating conditions for the new design. Because weapons and, to a lesser extent, carriage equipments, are frequently subjected to a vast range of operating conditions, some of which cannot be defined at the design stage of the weapon, this state of affairs was regarded as unsatisfactory. It was recognised that a much more detailed understanding of the various factors which determine the total efficacy of the weapon system in the carriage phase was required.
- 1.3 The course of action decided upon was to construct a number of general purpose instrumented weapons capable of measuring steady state aerodynamic loads, the forces imposed by the weapon on its carriage equipment during manoeuvres, and vibration experienced by the weapon throughout the captive phase. As well as providing a broad spectrum of data to the designer, the instrumented weapons could be utilised at the early prototype stage of future aircraft to assist in establishing clearance criteria for weapons still under development, and possible operating constraints for existing weapons.

### 2. AREAS OF INTEREST

- 2.1 Flight testing of externally carried stores may be divided into two categories. The first category comprises those trials which are designed to further an understanding of the environment to which a store may be subjected during flight carriage and to determine the effect of environmental parameters on store and/or store-aircraft performance. The second category comprises trials which are intended to validate assumptions made during the design and ground testing of a particular store and/or suspension equipment and to verify that the equipment is capable of operating satisfactorily throughout the intended flight envelope. In both cases, the areas of interest may be divided into quasi-steady state loads acting upon a store, loads induced by non-steady forces and weapon system performance characteristics.
- 2.2 Loads to which a store responds as a rigid body are quasi-steady state aerodynamic and inertia loads arising out of forward motion and manoeuvring of the aircraft, but may also include the effects of aircraft structural response and loads induced by atmospheric turbulence. Knowledge of these loads is required for the design of suspension equipment, strongback areas of stores and certain other areas such as store tail fins and sectional joints and fittings.

The usefulness of trials in which store loads are measured is enhanced considerably if the motion of the store is also measured. This allows the aerodynamic components of measured loads to be separated from inertial components.

Measurements of rigid body store loads, separated into aerodynamic and interial components, form the basis for validating theoretical aerodynamic load estimation procedures, wind tunnel testing techniques and for comparing actual inertia loads imposed during a manoeuvre with the simplified models used for design purposes, although the last must be interpreted with caution because measurements are rarely made under circumstances of pilot stress, and therefore may not constitute representative design cases.

2.3 The vibration levels experienced within a store are a function of store design, kinetic pressure, Mach number, and the location and configuration of a store on an aircraft. For this reason, but also because the spectral shape of the vibration varies from one location to another in a store, specifications for ground clearance testing of stores call for "envelope" acceleration response spectra to be generated at a specified reference point. For various reasons the acceleration responses are normally generated by exciting stores mechanically via the suspension points. Stores cleared according to such specifications have occasionally suffered unexpected service failures (Refs 1 and 2) which have raised questions as to the validity of the procedures. It is now generally believed that ground tests performed in this way have serious shortcomings in that, whilst the major part of the structure is severely overtested, representative levels may not be generated at particular frequencies in some components. The current area of interest is therefore to devise a more realistic method for ground clearance testing of stores and, incidentally, to isolate the various parameters affecting store vibration levels so that guidelines for developing more efficient designs may be formulated.

Aspects of the design of a store which may be affected by increased vibration levels as operating kinetic pressures increase are:

- 2.3.1 Strength of structural components, where the loads induced by vibration are added to the manoeuvre loads (this is not normally critical as it should be covered by fatigue calculations).
- 2.3.2 Fatigue of structural components, usually in combination with manoeuvre loads.
- 2.3.3 Deterioration of the store structure caused by fretting of joints and fittings. This is not strictly a fatigue phenomenon, but non-linear behaviour of the structure introduced by the fretting action may ultimately result in a fatigue failure.
- 2.3.4 Store malfunction which may be caused directly (eg bounce of relay contacts) or indirectly as a result of fretting and wear (eg intermittent connector contact caused by dilation of the socket contacts).

The effects described above, if they are identified during ground testing, would be prevented from occurring in service either by modifying the store or by placing a conservative operational life on the components affected. If either course of action is taken unnecessarily, due to unrepresentative ground testing, then the cost of modifications or replacements, accumulated over the service life of the store, could be considerable.

Finally, it should be noted that the majority of the effects described are not amenable to accelerated testing, when increased vibration levels are used to effect a reduction of test time.

2.4 The estimation of store/aircraft performance is important to the designer because of the vital effect it can have on the effectiveness of the total system. For example, if the location of stores on an aircraft is not optimised, the result can be a marked increase in drag, particularly at high Mach numbers, with an associated decrease in operating height, speed, and range. Further, the interference field between a store and the aircraft can critically affect the trajectory of the store after release with important implications on the accuracy and/or operational flexibility of the total system.

Theoretical estimation of store/aircraft performance, particularly drag, is extremely complicated and the problems will probably not be solved for a number of years. For the present, therefore, the development of model testing techniques appears to be the only practical solution to the estimation problem.

As has been noted previously, the aerodynamic forces acting upon a store in the near field of an aircraft are often highly dependent upon Reynold's number. Estimation of the effects of this dependence, and compensating for them, depends heavily upon reliable measurements of aerodynamic loads at full scale, both on the store and on the store/aircraft combination.

#### DESIGN CONSIDERATIONS

- 3.1 A recent change in the design of carriage equipment which affected the instrumented weapon design was the introduction of MACE (Minimum Area Crutchless Equipment). The purpose of this approach to ERU (Ejector Release Unit) and EMRU (Electro-Magnetic Release Unit) design was to eliminate the high-drag sway braces and thus improve performance and range. In order to use the MACE principle in conjunction with existing weapons, it was necessary to devise saddle lugs to fit on to the external casing of different bombs, using the existing lug pockets to secure the saddle-lugs, by means of a special bolt. The instrumented weapons were designed for use with conventional and MACE systems. A brief description of the two types of suspension is presented in Appendix A.
- 3.2 The procurement of instrumented weapons was initiated by the Directorate of Air Armaments (D A Arm) A Arm 12 Division; the design and construction was the responsibility of the Royal Aircraft Establishment (RAE). It was agreed that the standard 1000 lb bomb should form the basis of the instrumented weapons and, where necessary, different versions would be produced to ensure compatibility with both MACE and conventional release units.
- 3.3 The instrumented weapons were to be independent of aircraft power supplies. Weapon fuzing switches in the cockpit of every aircraft capable of carrying the weapons were to be used to initiate the magnetic tape recorders used to store the data, thus maximising utilisation of the recording time available.
- 3.4 The tape recorders were of a type specially developed to operate in the rigorous conditions likely to be encountered in the wide range of environments for which the weapons were required. Recording eight tracks of information onto half inch wide tape, the recorders conformed to the electrical standard of IRIG FM intermediate band, with 45 minutes of recording time available at  $7\frac{1}{2}$  inches per second.
- 3.5 The decision to construct separate stores to measure vibration levels, manoeuvre induced forces and steady state aerodynamic loads was a practical one, based on the volume of equipment necessary to record a given number of data channels which could be accommodated within the store envelope, and the space required to house the necessary force measuring elements. The loads likely to be encountered can be broadly classified as:
  - a) crutching preloads
  - b) inertial
  - c) aerodynamic

It was considered necessary to monitor the sway brace loads to determine their effect on store carriage. This information was to be measured by the manoeuvre load measuring weapons (force stores) which would also monitor those components of load which affect the design of carriage equipment. The method of application of crutching loads for MACE and conventional release units is described in Appendix A. The fluctuating component of inertial and aerodynamically induced loads was to be measured by the vibration measuring weapons (vibration stores). The third group of instrumented weapons was designed to measure steady state aerodynamically induced loads (aero stores).

### 4. THE VIBRATION STORES (VO1, VO2 & VO3)

- 4.1 Each of the three stores can be carried on both MACE and conventional release units, the build standards being virtually identical. The design uses a 1000 1b bomb body, modified to provide a removable nose section for access to the instrumentation. Ballast weights are fitted to provide the correct weight and C of G (Fig 1).
- 4.2 The two sites chosen for vibration measurement were immediately below the centre lug pocket (C of G) and in the centre of the aft face of the body (tail). Three Endevco 223C piezo-electric accelerometers were used to measure vertical, lateral and axial acceleration at each site, mounted on a suitably shaped block of steel securely attached to the weapon.
- 4.3 Accelerometer outputs were conditioned by high impedence voltage amplifiers in the case of VO1 and VO2 and by charge amplifiers in the case of VO3. Precision switched gain amplifiers/attenuators were used to match amplifier outputs to recorder input requirements. The weapon did not require to be calibrated as a vehicle, the transducers and associated signal conditioning equipment being calibrated prior to installation. A reference signal was recorded on a separate track to permit both time and amplitude compensation during analysis. The bandwidth of the measurement system was 3 Hz to 3 KHz in standard configuration; a wideband version of the recorder was later produced to permit an extension to 10 KHz with no loss of recording time.

#### THE FORCE STORES (FO1, FO3)

- 5.1 Fig 2 shows a sectional view of FOl which was designed to be used with a special release unit, having strain gauges mounted on each sway brace arm. The strain gauge bridge outputs of the four sway brace arms were fed into the weapon body for recording via an umbilical cord and a plug and socket on the upper surface of the bomb. The all up weight was made up to 1040 lbs by adding lead to the removable nose and to the rear bulkhead of the centre body as on the vibration store.
- 5.2 The twin lugs were screwed into the top of the measuring columns. Each column contained a flexible joint retained in a vertical axis by pistons moving in the outer sleeves. The axial load in the column was taken by the lower strain gauged link which connected the column to the bottom shell surface.

The fore and aft loads on the bomb lugs were reacted by a pair of strain gauged beams bearing against each column and situated above the flexible joint (Fig 2). Side loads at the bomb lugs were reacted by a similar pair of strain gauged beams situated in the same horizontal plane.

To record the lug vertical, fore and aft, side and sway brace loads required two eight track magnetic tape recorders and associated conditioning equipment. Correlation between records was obtained by recording lug vertical loads on both recorders.

- 5.3 Each lug assembly was calibrated for vertical, side and fore and aft loads before fitting into the store. Each sway brace arm was calibrated separately against known loads. The complete assembly of the bomb and ERU 119 was suspended in a loading frame and recalibrated by loading in all three major axes. All the calibrations were compared to give confidence in the accuracy of the complete system.
- 5.4 FO3 was designed for use with MACE release units (Fig 3). The measurement of the loads and moments acting on the saddle lug was by means of four load cells arranged in a symmetrical diamond formation around the central securing bolt which fits into the lug pocket.

The load cell outputs were summed to obtain vertical load, pitching moment, and rolling moment at each lug. The store was ballasted to the weight and C of G of a 1000 lb bomb.

5.5 A DC energised measurement system was employed in both weapons. Each strain gauge signal was conditioned by a strain gauge amplifier followed by a second order low pass filter, the cut-off frequency of which could be adjusted between 10 Hz and 3 KHz. A further stage of amplification followed the filter; this arrangement was designed to minimise the risk of inadvertent overload. The possibility of errors introduced by bridge supply voltage variations and amplifier drift was reduced by an automatic sequencing circuit which switched the bridge supply: off, to bridges with known imbalances, and finally to the measurement bridges whenever the recorder was activated.

# 6. AERODYNAMIC STORES (AO1, AO2)

- 6.1 A01 was designed for carriage on a conventional (ERU119) release unit (Fig 4). The shape was based on a 1000 1b bomb but the structure was purpose built with the exception of the tail unit. The basis of the design is two parallel horizontal plates coupled together by six pivoted links each having a strain gauged load measuring element interposed between it and the upper plate. The upper (suspension) plate is coupled to the ERU, the lower (balance) plate being coupled to the store body.
- 6.2 The links and load measuring elements are designed to react the loads and moments acting upon the store body. Three links are arranged to transmit vertical load, rolling moment and pitching moment to the measuring elements; a further two links transmit side load and yawing moment, and the remaining link transmits drag load.

Care was taken to ensure that the balance was fully temperature compensated.

6.3 To obtain the high accuracy required, it was necessary to minimise the inertial forces, hence the live weight of the store was kept as low as possible. All the internal equipment, batteries, recorder, electronic pack etc were supported by the suspension plate. To the balance plate was attached two support rings on which the nose, tail and the centre body skins were fitted. These items were made as light as possible.

The top half of the centre body outer skin was shaped to allow clearance around the lug pocket and the sway brace pad supports which were integral with the suspension plate; these clearances were sealed by flexible rubber gaskets.

6.4 Calibrations were performed prior to flight by suspending the weapon in a space frame in known attitudes and using dead weights to apply a range of loading combinations. The results of these calibrations were compared with the theoretical values based on the geometry of the balance and the angle of loading.

- 6.5 The design of AO2 incorporates a new lug pocket fitment which can accommodate both conventional and MACE ERU's without modification.
- 6.6 The measurement system employed in the aerodynamic stores is similar to that used in the force measuring stores.

# 7. AIRCRAFT MOTION RECORDING STORE (DO1)

- 7.1 A requirement to measure aircraft motion arises when inertia forces acting on a store are of interest, and when a knowledge of the aircraft flight path is necessary. When the latter is required for a short period of time only starting from a known (usually steady) condition, then the flight path can be reconstructed using a knowledge of the aircraft characteristics and measurements of the inertial motion of a known point on the aircraft. This concept has the effect of dispensing with the necessity for measuring sideslip, incidence, and aircraft total and static pressure during a manoeuvre, it being noted that accurate measurements of these quantities are difficult to obtain without expensive aircraft modifications. The DOI instrumented store was designed to fulfil both aspects of the requirement to measure aircraft motion.
- 7.2 The design consisted of a self-contained pack installed in the shell of a 1000 lb bomb which was modified to provide a removable nose section in a similar manner to the vibration stores. The pack was conceived as a modular design to provide system flexibility and to facilitate maintenance.
- 7.3 Three force balance accelerometers and three rate gyroscopes were aligned accurately to provide measurements of linear acceleration along, and angular rates about, each store axis. The rate gyroscopes selected were of conventional design with inductive sensing elements energised by a precision AC supply. Carrier amplifiers and phase sensitive demodulators were installed to recover voltages proportional to angular rate. Precision switched gain amplifiers were inserted to permit the sensitivities of all channels to be optimised prior to recording. A magnetic tape recorder, rate gyroscope drive units, stabilised DC supplies and a 28 volt battery completed the pack.
- 7.4 Each transducer and its associated signal conditioning equipment was calibrated individually to establish accurate static and dynamic characteristics for each measurement channel. In-flight system calibration was provided by recording automatically a sequence of reference voltages on each recorder track whenever the recorder was activated.

# 8. FLIGHT TRIALS

- 8.1 Several series of flight trials, each involving one or more of the instrumented stores, have been, or are in the process of being executed. Amongst those which have been completed are a systematic investigation of vibration encountered by a store during flight carriage on Phantom and Mirage aircraft, and the measurement of suspension equipment loads in level flight and during a variety of manoeuvres.
- 8.2 A detailed discussion of the results of these trials cannot be included here, but certain of the conclusions are presented in the following section. A list of those flights which have been executed, or are planned for the near future, is presented in Fig  $^5$ .

# 9. CONCLUSIONS DRAWN FROM SOME RESULTS

- 9.1 An appraisal of the acceleration power spectra obtained from a number of trials revealed that the measured responses of the store were characteristic of a resonant structure excited by broad band random vibration, at least above a frequency of 200 Hz. A mathematical model of the bomb body was used to confirm that the shell modes corresponded to the resonant peaks. Below 200 Hz, the responses were peaky but the frequencies and relative amplitudes varied with store location and configuration. It was thus induced that vibration transmitted to the weapon from the suspension equipment, pylon and wing or fuselage occurs mainly at low frequencies. Since the majority of power in the measured spectra occurred in the region above 200 Hz, concern was raised regarding the validity of ground vibration trials which attempt to transmit wideband power to a weapon through the suspension equipment.
- 9.2 Confirmation that the use of MACE suspension equipment resulted in a significant reduction in vibration was achieved in a special trial during which two separate tail units were employed, one of which had no tail fins. The results indicated that the mechanism by which the turbulent airflow generated by excrescences in the airstream excites the weapon is via the tail fins. The reduction in vibration achieved by substituting the MACE unit for a conventional release unit could not significantly be improved by the removal of tail fins.
- 9.3 Ground trials using the vibration store VO2 in the efflux of a blow-down wind tunnel and in a reverberant acoustic chamber have been carried out to demonstrate whether distributed excitation of the weapon can produce acceleration responses in the laboratory corresponding to those measured in the air. The results of this work are as yet unpublished but the results assessed to date confirm the view that a distributed input is required to produce realistic vibration responses.

- 9.4 The relatively small number of flights carried out to date using the force store F01 has shown clearly that the distribution of forces in the system by which crutching pre-loads are applied to a store/suspension unit combination is indeterminate. In constant flight conditions, the distribution of load varies with time in a random manner, the general trend being that the mean values of pre-load measured were lower than expected.
- 9.5 The few flights performed to date using the aerodynamic store A01 have served to confirm that the balance provides a repeatable measuring system. Insufficient results are available to establish trends in behaviour.

#### 10. CONCLUSION

10.1 The measurement stores described in this paper were constructed at relatively modest cost. In the short time that they have been operational, insights gained into the behaviour of weapons in the captive phase have clarified, to a considerable degree, understanding of the environment and its effects. The decision to proceed with this work has been more than vindicated: as well as fulfilling the original objectives, the instrumented stores have proved their value as an aid to investigating problems occurring at the development stage. The likely cost savings which may occur in the future as a result are inestimable.

#### **ACKNOWLEDGMENTS**

Preparation of this paper and the work described herein would not have been possible without the help and cooperation of a number of individuals operating at different levels within the Authorities responsible for the work, and in other associated establishments and companies.

The authors feel that special mention must be made of the contribution to the overall programme of work by the late Squadron Leader S R Hathaway, RAF (retd), whose enthusiasm and perseverance guided the project from its initial concept in 1968 through development, manufacture and deployment, and who encouraged the authors to produce this paper.

#### REFERENCES

- Dreher J F Aircraft Stores Dynamics Safety Criteria, USAF Science & Engineering Symposium, October 1969.
- Epstein C S Aircraft/Stores Compatibility Analysis and Flight Testing, AGARDo graph No 219 on Range Instrumentation, Weapons Systems Testing & Related Techniques, February 1976.

#### APPENDIX A

#### RELEASE UNIT DESIGNS

#### 'CONVENTIONAL' EJECTOR AND ELECTRO-MAGNETIC RELEASE UNITS

1.1 A typical unit utilises four crutch pads each  $1\frac{1}{2}$ " diameter which incorporate a spherical socket in contact with the ball end of adjustment screws located at the outer ends of the two sway braces (Fig 6).

The centres of the pads are approximately 6" apart spanwise and typically 17" apart longitudinally. They are situated symmetrically, two on each side of the ERU hooks which engage with bail lugs located at 14" centres.

- 1.2 In order to distribute the crutch load as evenly as possible, the preferred method is to screw all four pads down "finger tight" then to apply increasing increments intorque load to each screw in turn up to the desired value. Where two pads are inaccessible, as when the store is loaded on to the ERU of the shoulder station on a triple carrier, the two non adjustable pads are preset and locked before the store is fitted; the outer crutch pads are then screwed down to obtain the desired pre-load which ideally produces identical pre-loads in the fixed pads on the opposite crutch arms.
- 1.3 Flight tests have indicated that crutch loads are not maintained in flight; even during taxiing and take off a reduction in pre-load can occur as the store is subjected to vibration and the system 'settles down'.
- 1.4 Ideally, the pre-load applied should be just sufficient to keep the pads in contact with the weapon under all conditions of use, thus providing a restraint to minimise vibration and movement due to normal flight manoeuvres; over-crutching increases stress levels but gives no benefits. As a general rule the load applied to each crutch pad is equivalent to  $1\frac{1}{2}$  times the weight of the store which corresponds to an initial load in each lug equivalent to  $3\frac{1}{2}$  g<sub>n</sub>.
- 1.5 Tests using strain gauged sway braces have shown that it is not possible to devise a torque loading procedure which will consistently produce equal pre-loads in each sway brace in a given set of hardware. Variations in screw thread friction and manufacturing tolerances combine to provide a very wide variance in the value of pre-load generated for a given torque load on the adjustment screws.
- 1.6 A typical release unit would be designed to react vertical downloads via the suspension hooks, and uploads through the sway braces; pitching moments by a combination of both. Side force and rolling moments would be reacted by sway braces and would vary the vertical hook load. Drag loads would be reacted through friction between crutch pads and the store body and also would appear as an aft load on the hooks through friction. Depending on the coincidence of tolerances and possible movement of the store, drag loads may also be reacted through the vertical face of the forward hook. Yawing moments would be reacted through the sway braces, as lateral forces applied to the hooks through friction and, depending on tolerances and possible movement, through the yaw restraints built into the unit.

The design of conventional release equipment and measurement of loads which occur in service is thus complicated by the indeterminate nature of load distribution in any given set of circumstances.

# 2. MACE RELEASE UNITS

- 2.1 The MACE system was designed to speed up and simplify the process of loading stores on an aircraft, to render the distribution and reaction of applied loads more deterministic for a given set of conditions, to maintain coherence between store and release unit in all flight conditions, and to reduce overall drag by dispensing with sway braces.
- 2.2 The bail lug/hook combination of conventional systems is replaced by a dual nib hook saddle/lug arrangement using wedges which automatically take up clearances as the store is loaded (Fig 7).

The wedge angle and spring rate are arranged so that a side or rolling motion of the store results in movement of the wedge to take up any play which develops. Preloads between store and release unit are small compared to the weight of the store; the wedge acts simply to take up any play which might otherwise develop during flight.

CONTRACTOR OF STATE

- The second sec

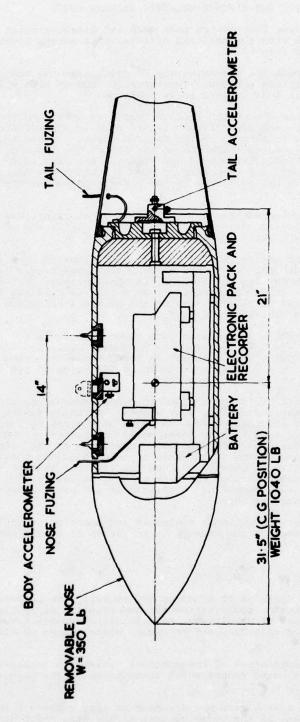


FIG. I VIBRATION STORE VO2

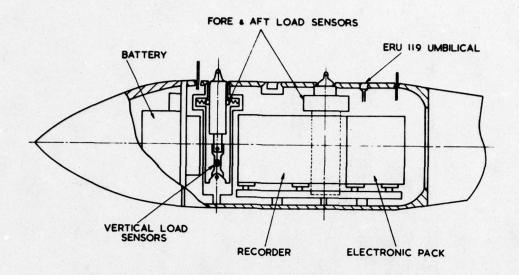


FIG. 2 FORCE STORE FO I

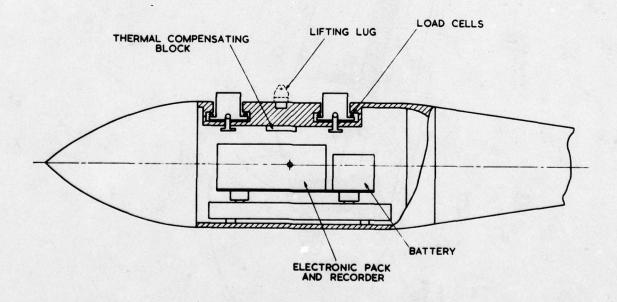


FIG. 3 FORCE STORE FO 3

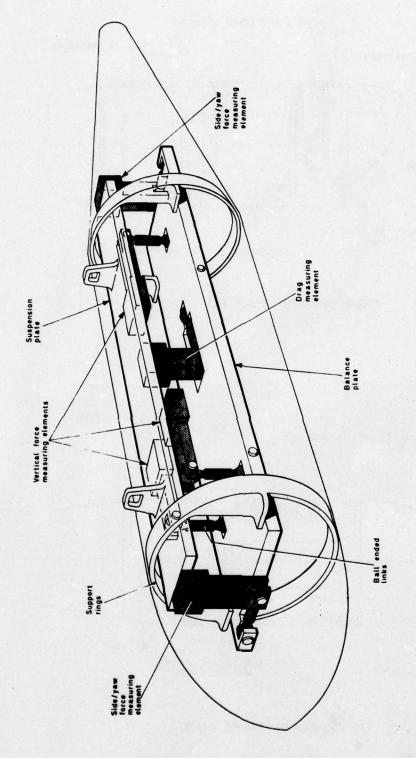


Fig.4 Aerodynamic stores A01 for ERU 119 A02 for L/DERU

Store	Aircraft	Test Authority	No of Flights
	٠		
V01	Phantom	AAEE	2
VOl	Mirage	ARDU Melbourne Australia	6
VO2	Phantom	AAEE	18
	Jaguar	AAEE	1
	Buccaneer	RAE	4
VO3	Phantom	AAEE	1
FO1	Phantom	AAEE	8
FO3	Buccaneer	RAE	6 planned Oct 19
A01	Phantom	AAEE	8
	Phantom	NATC (USA)	4
A02	Buccaneer	RAE	6 planned Mar 19
DO1	Buccaneer	RAE	6 planned Oct 19

Fig 5 Flight trials planned or executed to date

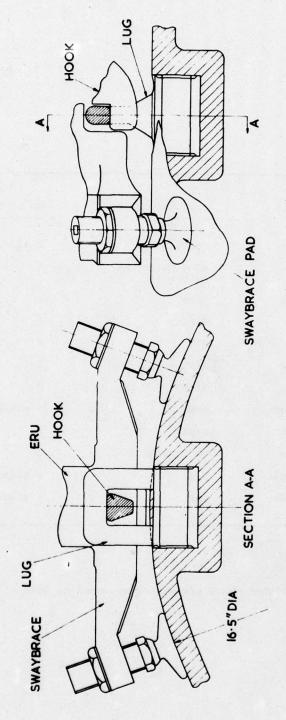


FIG. 6 CONVENTIONAL ERU/BAIL LUG CONFIGURATION

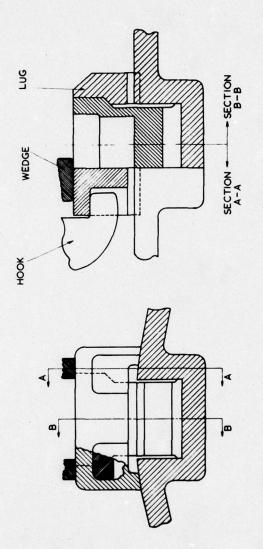


FIG. 7 MACE-ERU / SADDLE LUG CONFIGURATION

#### COMMENTS ON SESSION I

The initial eight papers were devoted to techniques used in achieving flight clearance of the basic air vehicle and its externally carried weapons. The basic air vehicle includes those airframe systems essential for flight, such as flight control systems and engine inlet systems; and with the great strides in technology being made in these two particular areas, it's not surprising that half the session papers were associated with these areas. Structural loads and characteristics, both as regards the basic airframe and the external carriage of weapons, also received major attention, with the remaining author addressing the ever vexing area of post stall/spin testing.

The major theme of this session was that efficient and effective flight testing today depends on carefully planned and executed integration of ground tests and ground facilities with flight testing. This is not a new theme, but it is given new emphasis and application in the current environment of air vehicle development. The new and more complex systems introduce a need for more precise measurement of pertinent parameters to insure operating effectiveness as well as safety of flight. The ever increasing cost of development work, both ground and flight, makes it essential to achieve the optimum balance between facilities and tests on the ground and those in the air. Decisions as to which ones to use and how to use them will have a significant effect on the cost/effectiveness of the overall weapon system clearance process — as well as the cost/effectiveness of the weapon system itself.

New systems, such as digital flight control systems, either require or can benefit from testing and testing techniques not previously needed as pointed out in three of the papers in the session. In two of these and in the discussion following them, the use of flight simulators in ground simulation prior to and in support of flight tests received considerable attention. Specific examples of such use were given by the authors, and they and other discussors generally agreed that further use should be exploited.

While sophistication is a major characteristic of current flight test techniques, one author pointed out that quite simple ground systems can be fully effective in support of the post stall spin testing of a current trainer/tactical aircraft. The fact that alternative techniques are available from which to select the most cost effective was addressed in the structural dynamics area — illustrative of the situation in many areas.

Maximum effectiveness of ground testing requires that the pertinent flight environment and conditions be adequately simulated. This was pointed out with regard to engine inlets, but is of course generally true. Unique flight testing, flight research in the true sense, may be necessary to provide this information; the last paper of the session dealt with the external weapons flight environment in this respect.

Flight clearance for weapons systems which are used throughout their maximum possible flight envelope will always be done in flight — just as it always has been. The papers in this session clearly pointed to the increasingly complex role played by new techniques and ground testing and facilities in performing this vital job in the most cost-effective manner possible.

# **SESSION II**

WEAPON SYSTEM DEVELOPMENT
AND EVALUATION

# SUPERSONIC POWERPLANT TESTING FOR PREFLIGHT PERFORMANCE EVALUATION

by
G. G. Annear
National Gas Turbine Establishment
Pyestock, Farnborough, Hampshire, England, GU13 OLS

# SUMMARY

The paper describes the facilities used at NGTE to evaluate the performance at supersonic speeds of complete propulsion units, (inlet, engine and exhaust system). A description is given of the way in which ground level test bed data are used to predict flight performance, and how the prediction may be refined by the use of altitude Cell data.

	LIST OF SYMBOLS	
Symbol .	<u>Item</u>	Units
٨	area	sq m
C <sub>D</sub>	area coefficient = A <sub>isen</sub> /A	
c <sub>x</sub>	thrust coefficient = X <sub>G</sub> /X <sub>Gisen</sub>	
HP	high pressure	
IRF	inlet recovery factor	
LP	low pressure	
Mn	Mach number	
N	speed	rev/min
P	total pressure	kPa
P	static pressure	kPa
sfc	specific fuel consumption	gm/s/kN
T	total temperature	K
W	airflow	kg/s
	fuel flow	gm/s
x	thrust	kN
θ	temperature ratio $\frac{288}{T}$	
μ	$\left(\frac{\text{Secondary airflow}}{\text{Engine gas flow}}\right) = \frac{W_{SA}\sqrt{T_{SA}}}{W_{S}\sqrt{T_{S}}}$	
	Powerplant Stations	
0	upstream infinity	
1	inlet lip	
2	engine face	
2.2	HP compressor entry	
3	HP compressor outlet	
4	HP turbine inlet	
5	LP turbine exit	
7	primary nozzle entry	
8	primary nozzle exit	
8a	divergent secondary nozzle entry	
9	divergent secondary nozzle exit	
00	ambient infinity	
	Suffices	
con-di	convergent-divergent	
Fe	engine fuel flow	
Fr	reheat fuel flow	
G	gross thrust	
Н	high pressure	
isen	isentropic compression/expansion	
L	low pressure	
N	net thrust	

# Definitions

# Convergent nozzle

a. choked conditions

X<sub>Gisen</sub> - isentropic choked velocity thrust + pressure thrust

unchoked conditions

X<sub>Gisen</sub> = isentropic velocity thrust for complete expansion

Convergent-divergent nozzle

XGisen = isentropic velocity thrust for complete expansion

ISA SLS  $T_2 = 288.13 \text{ K}$   $P_2 = 101.\text{k kPa}$ 

#### 1.0 INTRODUCTION

Concern to assess the in-flight performance of a propulsion system for a supersonic aircraft at the earliest possible stage of development leads to the use of performance data on the major components of the propulsion unit, which is inevitably meagre. Performance predictions have therefore to be synthesised using data from many sources, including model-scale tests on the inlet and exhaust systems, and full scale tests on engines run on ground level test beds and in altitude test cells.

The prediction of steady state performance is only one aspect of the evaluation process; it is also necessary to assess the behaviour of the propulsion unit under transient conditions such as those resulting from rapid changes in the engine power settings, changes in aircraft attitude, or from unscheduled events such as control system or engine malfunctions. Information under steady state and transient conditions can only be satisfactorily explored by full scale trials in altitude test facilities, where the interaction and response of the components of the propulsion system can be determined over the flight envelope under closely controlled conditions.

This paper describes some of the facilities used at the National Gas Turbine Establishment (NGTE) for testing supersonic propulsion systems. Test techniques used to determine the steady state performance are described, using the prototype Concorde propulsion unit by way of example. The method of synthesising altitude and ground level test bed data to predict the in-flight performance of specific engines for use in the aircraft flight test programme is also outlined.

#### 2.0 ALTITUDE TEST FACILITIES AT NGTE

The NGTE altitude facility enables engines to be tested at conditions precisely simulating those encountered in flight. It provides a way of proving new designs in the early stages of development without recourse to flight testing, a technique which is limited in scope and which may involve serious risk, particularly when investigating off-design cases. Facility testing enables a much more comprehensive range of test measurements to be made than is possible in flight, and a far greater precision in the measurement of the performance of the propulsion unit.

The NGTE facility consists of a centralised pressure air supply/exhaust extraction plant, five test cells each with its control room, and a data processing centre. In addition there is a ground level test bed which can be used for calibrating engines before installation in the altitude cells and for research testing.

Two main types of test arrangement, "free-jet" and "connected", are employed. In a free-jet test a stream of air moving at the aircraft flight speed is produced in a manner similar to that used in a conventional wind tunnel; the inlet with an engine coupled behind can thus be tested together under conditions encountered in free flight. In a connected test, air is piped directly to the engine at the pressure and temperature provided in flight by the inlet.

Both types of test require large quantities of air. Compressors are used to supply this air to the engine and exhausters to extract the engine exhaust gases from the low pressure required in the test cell to simulate the altitude condition. These requirements are met by multi-stage machines, having a total installed power in excess of 300 MW.

Air is taken from atmosphere through driers and is compressed by the compressor/exhauster units to a pressure depending on the test requirements. It is then heated or cooled to achieve the required temperature before being passed into the test cell. Temperatures between -80°C and 600°C can be achieved. The exhaust leaving the engine is cooled, pumped from the cell and discharged to atmosphere. The air supply system is thus capable of simulating flight conditions by providing the correct total pressure and temperature at the front of the inlet and engine for free-jet and connected tests. The exhauster can provide the correct flight ambient pressure for the inlet for free-jet tests, and for the engine for connected jet tests.

Each of the NGTE test cells was designed to perform a specific task. This paper is concerned with two of them, Cell 3 a 6.0 m diameter connected test cell and Cell 4 a free-jet supersonic test cell with a working section 1.55 m  $\times$  1.55 m in which the Mach number can be varied and the pitch and yaw angles of flow into the inlet changed whilst a test is in progress.

Steady-state data from the cells are acquired and processed on-line by a central computer; transient data are recorded either as analogue signals on magnetic tape for subsequent off-line processing or displayed on U/V chart recorders to provide a "quick look" capability. A detailed description of the methods employed for the acquisition and processing of data is given in Reference 1.

# 2.1 Test capabilities of Cells 3 and 4

The flight envelope that can be covered in Cell 3 is determined by the exhauster capacity as well as by the inlet pressure and temperature limitations imposed by the air supply and the cell structural limits. The test capability is thus a complex function of flow, pressure and temperature in which the pressure recovery of the exhaust diffuser is an important item. Broadly speaking the cell can test the Concorde engine/exhaust system over a range of altitudes and forward speeds under steady-state and transient conditions, from a minimum altitude of about 5000 ft to a maximum of at least 70,000 ft and from zero

forward speed to a value in excess of Mach 2.3. Aircraft accelerations can be simulated as can slam engine accelerations and decelerations.

Cell 4 is capable of testing the Concorde propulsion unit at cruise conditions (Mach 2.0; 60,000 ft altitude) with an inlet temperature of 127°C corresponding to (ISA + 5°C) conditions. The full test capabilities of the cell and an account of its design and development are given in Reference 2. A description of tests on the inlet/engine combination of the prototype Concorde propulsion system is given in Reference 3.

# 3.0 DESCRIPTION OF THE PROTOTYPE CONCORDE PROPULSION UNIT

Although the main design features of the Concorde powerplant have been presented many times, it is thought worth recapitulating them briefly. The aircraft has four propulsion units mounted in pairs under the wing on either side of the fuselage, each pair sharing a single nacelle divided by a longitudinal bulkhead. The main components of the propulsion unit are:

- A variable geometry inlet. An Olympus 593 twin spool turbojet. ъ.
- A dual stream exhaust system comprising:
  - the jet pipe, reheat system and variable convergent primary nozzle,
  - the secondary system in which air from the inlet throat bleed flows rearward through the space between the engine and the inner walls of the nacelle to surround the exhaust flow from the primary nozzle. The two flows expand through a fixed throat convergent-divergent nozzle and continue expansion through a variable secondary nozzle. Under the action of aerodynamic forces the petals of the secondary nozzle assume the position required to expand the exhaust gas stream to ambient pressure.

Figure 1 shows the configuration of the propulsion unit in supersonic flight.

#### 4.0 DETAILS OF TESTS

The most direct method for arriving at the thrust developed by the propulsion units in flight would be to calibrate each engine in an altitude test cell over a range of flight conditions using its flight instrumentation. However this would be a costly and time-consuming exercise and an alternative procedure was therefore adopted in which the basic performance from the calibration of the engine on the manufacturer's GLTB was compared with the performance measured in the cell for several prototype engines. The altitude performance of any particular flight engine could then be predicted from the results of a ground level test on that engine. It is worth noting that this procedure concedes some loss of precision when compared with the direct altitude cell test method.

# Tests on the ground level test bed

The engine and its primary nozzle were calibrated on the engine manufacturer's GLTB over the full speed range at selected settings of low pressure compressor shaft speed, whilst varying the high pressure compressor shaft speed by changing the area of the primary nozzle. The data obtained from this test, after the usual test bed corrections had been applied, were processed to derive the total pressure, temperature and flow at the inlet and outlet stations of the main engine components. These variables were then expressed in the conventional non-dimensional form and assembled as carpet plots for constant values of NL/ $\sqrt{\theta_2}$  and NH/ $\sqrt{\theta_2}$ . As no pressure or temperature measurements were taken downstream of the LP turbine exit it was necessary to calculate the gas flow conditions at the entry and exit of the primary nozzle (Stations 7 and 8).

The effective gas flow at Station 8 was established by tests on an engine fitted in turn with

- a flight-type jet pipe and variable primary nozzle, and
- a slave jet pipe and a series of fixed geometry convergent nozzles.

The gas leakage through the petals of the primary nozzle was deduced by comparing the thrust coefficients of the two systems for equal nozzle areas and convergence angles.

The reheat cold loss was calculated by an iterative process which initially found an 'ideal' value for the mean total pressure at entry to the primary nozzle (P7) using primary nozzle characteristics obtained from model tests, i.e. the variation of CD and CX with P7/P00 for constant values of nozzle semiangle. The 'ideal' value of  $P_7$  had then to be corrected to allow for the leakage through the primary nozzle petals, since this was not included in the model characteristics. The reheat cold loss was expressed in the non-dimensional form,  $(P_3 - P_7)/P_5$ , and plotted against  $N_H/\sqrt{\theta_2}$  for constant values of  $N_L/\sqrt{\theta_2}$ .

For the reheat OFF case the above corrections are sufficient but for reheat ON further iterative processes are required to determine the effects of reheat combustion. This paper does not cover the reheat condition 'n detail, but these processes yield the calculated values for the reheat temperature and pressure of the gas flow at entry to the primary nozzle.

Having established conditions at the primary nozzle exit, calculations were made to derive the isentropic convergent thrust of the engine and primary nozzle system. The GLTB measured thrust is divided by this isentropic convergent thrust to derive the primary nozzle thrust coefficient.

# Tests in Cell 3

The engine was installed in a simulated aircraft nacelle (SAN) which represented as closely as possible the environment existing on the aircraft. Great care was taken to simulate the blockages in the flow path of the secondary air to the nozzle caused by the engine accessories and such items as the cabin air heat exchanger. A detailed description of the SAN is given in Reference 4 from which Figure 2 is produced. Figure 3 shows a photograph of the installation in Cell 3.

# 4.2.1 Tests for comparison with GLTB data

The engine and primary mozzle were calibrated at engine inlet conditions of P2 = 73 kPa and T2 = 288 K, for direct comparison with data from the GLTB, and the results are plotted in Figures 4 to 7.

The relationship between fuel flow and thrust, expressed as ratios of the values obtaining at the cruise value of LP compressor shaft speed and referred to ISA SLS conditions, is shown in Figure 4. Data from the GLTB and from Cell 3 lie on a unique line but this agreement is achieved at different settings of engine speeds. Further investigations were made, the non-dimensional air and fuel flows were plotted against LP spool speed and expressed in relative form; the comparisons are shown in Figures 5 and 6. It is seen in both cases that the air and fuel flows are greater in the cell for a given  $N_L/\sqrt{T_2}$ . The LP compressor pressure ratio showed the same effect; and Figure 5 shows the LP compressor operating line. It can be seen that the LP compressor operates on the same pressure ratio/flow characteristic on the GLTB as in the cell, but it runs at different shaft speeds.

Additional data were available from the calibration of the engine and the exhaust system without the secondary air supply, as this is a situation occurring during flight operation. The engine was operated at take-off ratings on different speed schedules; only two points are available from the calibration for direct comparison with GLTB data, and they too are included in Figures 4 to 7.

The effect can be graphically summarised by stating that the engine appears to be "larger" in the cell than on the GLTB. For a given LP speed it passes more air, uses more fuel and develops more thrust. The sfc remains unchanged. This phenomenon, for which a convincing and comprehensive explanation has not yet been found, is commonly referred to as 'Cell effect'. When first observed it was thought that it might be due to differences in the total pressure profile at inlet to the LP compressor - the cell installation has a long length of ducting upstream of the engine whereas the GLTB uses a relatively short inlet flare. However measurements of the respective boundary layer profiles revealed only small differences and compressor rig tests showed they did not noticeably influence the compressor characteristics, certainly not to the extent observed on the engine.

'Cell effect' has been observed to apply equally for the engine running behind the inlet in Cell 4 and has since been found to be similar to the 'Installed Effect' noted in the comparison of GLTB and aircraft data. It has also been noticed on other types of engine, although to a varying extent.

# 4.2.2 Performance of the exhaust system and the primary nozzle

The exhaust system was extensively instrumented for a further series of tests in Cell 3. The secondary airflow was carefully metered and adjusted to match the correct percentage split in flows required between the port and starboard and the upper and lower portions of the nacelle. Tests to evaluate the performance of the exhaust system were conducted with the engine bleed and power off-take services off. The first series of tests yielded an overall nozzle thrust coefficient for the exhaust system at supersonic cruise conditions.

A second series of tests was conducted on the engine and primary nozzle with the secondary nozzle removed and the secondary air off. These tests were run at the same engine inlet conditions and speeds as the tests with the secondary system fitted, but with the cell ambient pressure set to the static pressure that was measured between the exit of the primary nozzle and the entry to the fixed throat convergent-divergent nozzle.

The performances of the primary nozzle and the exhaust system are shown in Figures 8a and b. The apportionment of the absolute levels for each system is dependent upon the following assumptions:

- a. The flow leakage loss at the jet pipe manacle clamp and through the petals of the primary nozzle.
- b. The flow leakage loss through the nacelle walls and through the petals of the secondary nozzle.
- c. The pressure loss in the secondary flow system between the engine inlet face and the fixed throat convergent-divergent nozzle.

# 4.2.3 Tests to establish altitude correction factors

As altitude increases the aerodynamic performance of the components of the propulsion unit deteriorates due to the changes in Reynolds numbers. This causes an increase in fuel flow for a given specific thrust. The losses in the engine and primary nozzle can be determined by individual tests on the compressors, the combustion chamber, the turbines and the reheat system, but full scale engine tests are required to assess the overall loss due to the influence of interaction effects. As an example, tests were made to establish correction factors for engine inlet pressure and temperature effects.

The inlet pressure tests were conducted at a constant inlet temperature  $T_2=288$  K for values of  $P_2=83.0$ , 73.0, 55.2, 41.4 and 27.6 kPa. The inlet temperature tests were conducted at a constant inlet pressure of  $P_2=73.0$  kPa for values of  $T_2=288$ , 340, 370 and 400 K. The ' $P_2$ ' and ' $T_2$ ' tests had therefore a common datum calibration over the speed range of  $P_2=73.0$  kPa,  $T_2=288$  K. These values were close to the basic calibration of the engine in Cell 3 for comparison with GLTB data. The test at  $P_2=73.0$  kPa and  $T_2=400$  K was close to the engine inlet conditions at the commencement of sustained supersonic cruise. At the end of cruise, the values of  $P_2$  and  $T_2$  are 52.4 kPa and 400 K respectively. The ' $P_2$ ' and ' $T_2$ ' tests therefore covered the full range of supersonic cruise and subsonic flight conditions at a fixed schedule of engine speeds and constant primary nozzle area.

Figure 9 shows the relationship between the relative static specific thrust and fuel flow, for constant values of  $N_L/\sqrt{T_2}$  and  $N_H/\sqrt{T_2}$ . The 'P<sub>2</sub>' results show that the performance of the engine and primary nozzle are virtually unaffected above an engine inlet pressure of P<sub>2</sub> = 27.6 kFa. At engine inlet pressures below this value, a degradation in performance appears and Figure 10 shows the increase in relative specific fuel flow (WF<sub>e</sub>/W<sub>2</sub>) as engine inlet pressure is reduced at a constant inlet temperature of 288 K. The 'T<sub>2</sub>' results show that the performance of the engine is sensitive to changes in the engine inlet temperature. The increases in specific thrust were largely due to the temperature effect on the engine airflow, which for a given non-dimensional value reduced as T<sub>2</sub> increased. The non-dimensional thrust function was unaffected by T<sub>2</sub>, so the thrust remained the same, whilst the airflow reduced; thus the specific thrust increased as T<sub>2</sub> increased. The same effect occurred on the dimensional values of  $N_L$  and  $N_H$  which increased as  $\sqrt{T_2}$  increased, for constant values of  $N_L/\sqrt{T_2}$  and  $N_H/\sqrt{T_2}$ .

Figure 11 shows the effect of various combinations of  $P_2$  and  $T_2$ , for constant values of  $N_L/\sqrt{T_2}$  on the operation of the LP compressor. Figures 9 and 11 can be used in conjunction with each other to predict an aero-thermodynamically matched performance of the engine for any combination of  $P_2$  and  $T_2$ . The derived variables for the datum and other conditions are compared to establish correction factors. To check

whether the engine variables were affected by changes in flight speed above choking primary nozzle pressure ratios, a series of subsidiary tests was undertaken at constant settings of  $P_2$  and  $T_2$  while varying the cell pressure. This had the effect of creating simulated flight speeds, and the results showed that the engine non-dimensional variables remained constant; hence the ' $P_2$ ' and ' $T_2$ ' correction factors are suitable for application over a wide spectrum of flight speed.

#### 4.3 Tests in Cell 4

# 4.3.1 Brief description of tests

An engine to the same build standard as the engine tested in Cell 3 was tested over a range of Mach number from 1.7 to 1.9 at the same inlet temperature as the tests in Cell 3. A direct comparison can therefore be made of the inlet/engine combination with the engine/exhaust combination.

# 4.3.2 Comparison of Cell 3 and Cell 4 data

Measurements of  $P_5$ ,  $p_5$ ,  $T_5$  were used to derive the airflow through the engine in Cell 4 using the unique correlation between  $P_5/p_5$  and  $W_5/T_5/p_5$  obtained from the calibration of the engine on the GLTB. In Cell 4 the engine was tested at different combinations of  $N_L/\sqrt{\theta_2}$  and  $N_H/\sqrt{\theta_2}$  from those in Cell 3, and it therefore operated with different nozzle throat areas. This difference in engine operation caused differences in the LP spool matching and the comparison of data was therefore based on the operation of the HP spool. The comparison is shown in Figure 12 where  $W_Fe/P_2$ ,  $V_F$ , and  $V_F$ ,  $V_F$ , are plotted against  $V_F$ ,  $V_F$ ,  $V_F$ , and  $V_F$ , and  $V_F$ ,  $V_F$ , and  $V_F$ ,  $V_F$ , and  $V_F$ , are constant and  $V_F$ , are constant and  $V_F$ .

#### 5.0 THE PREDICTION OF MISSION PERFORMANCE

The characteristics of the aircraft systems are applied to a computer programme which can calculate in small increments of time, from engine 'lit' to engine 'out', the performance requirements of the propulsion unit over a flight mission. The requirements are annalysed and optimum control laws established for the propulsion system. The flight mission is then broken down into equivalent steady-state stages for application to the prediction of performance of individual flight engines.

The sources of information required for the prediction are listed below:

- An aero-thermodynamically matched calibration of the sign on the GLTB including the nozzle gas flow conditions, the reheat system cold loss and performance characteristics.
- The 'Cell effect' correction factors obtained from the calibration of an engine in the cell so that GLTB data can be corrected to match cell data.
- The aerodynamic performance of the inlet in terms of inlet recovery factor and Mach number obtained from cell data.
- The combined flight performances of the reheat and overall exhaust systems when operating with reheat ON and OFF obtained from cell data.
- 5. The effects on engine performance obtained from cell data due to:
  - a. Engine bleed from the HP compressor
  - b. Power off-takes from the HP spool shaft
  - c. Changes in engine inlet total pressure and temperature 'P2' and 'T2' tests
- 6. The flight characteristics of the secondary system in terms of airflow and pressure loss
- 7. The external drag losses obtained from wind-tunnel model data.

All Olympus 593 flight engines and primary nozzles are tested on the engine manufacturer's GLTB. The test data are corrected for test bed calibrations, and the carpet plots of the engine variables assembled to form an engine individual brochure. For the prediction of flight performance the flight freestream conditions modified by the inlet pressure recovery factor are used to obtain the engine inlet values of P<sub>2</sub> and T<sub>2</sub>. A value of N<sub>L</sub>/ $\sqrt{\theta_2}$  is chosen to give an entry into the individual brochure for the extraction of N<sub>H</sub>/ $\sqrt{\theta_2}$  from the relationship of N<sub>L</sub>/ $\sqrt{\theta_2}$  v N<sub>H</sub>/ $\sqrt{\theta_2}$ . The two speed values are corrected for 'Cell effect'. The engine non-dimensional variables are extracted from the brochure for the corrected speeds. Correction factors for 'P2' and 'T2', engine bleed and power off-takes are extracted and applied by algebraic addition to the non-dimensional variables to give the flight non-dimensional variables. These are converted to dimensional values and checked to ensure dimensional limitations have not been exceeded, together with the reheat characteristics if required. The gas flow conditions at exit from the primary nozzle are expanded to ambient pressure to derive the gross isentropic convergent-divergent thrust (XGisen con-di primary nozzle). The secondary airflow is expanded from its effective pressure to ambient pressure to derive  $X_G$  (isen con-di SA). The two isentropic thrusts are added to give the total isentropic thrust of the propulsion unit, which is then factored by the exhaust system overall thrust coefficient to give the total thrust  $X_G$  (con-di propulsion unit). The external losses obtained from model wind-tunnel data are subtracted from the total thrust to give  $X_G$  (effective con-di propulsion unit). The inlet entry air freestream momentum force is subtracted from XG effective to give the flight net thrust of the propulsion unit XN (flight). If the resultant value of XN does not match the equivalent steady-state mission requirement, the process is repeated iterating on  $N_L/\sqrt{\theta_2}$  until a balance is achieved. The specific fuel consumption (WFe + WFr)/XN is then calculated. The fuel-time increments for the steady state stages of the flight mission are then added to give the total fuel consumption. This value will decide whether the propulsion system is capable of meeting the aircraft requirement.

# 6.0 CONCLUSIONS

The in-flight performance of a supersonic propulsion system has to be synthesised using data from many sources, including model-scale tests on inlet and exhaust systems and full scale tests on engines run on ground level beds and in altitude cells.

To achieve the highest level of precision each engine fitted to a performance evaluation aircraft should be separately calibrated in an altitude cell using the same instrumentation as would be used in flight.

An alternative, but less precise, procedure first establishes the relationships between ground level and altitude performance by tests on several engines and then applies these factors to GLTB calibrations of the flight engines.

The paper has presented the results of tests on the Concorde powerplant as an example of this latter method. The tests showed:

- At steady-state supersonic cruise conditions the inlet and exhaust system did not influence the thermodynamic performance of the engine and primary nozzle.
- 2. For standard sea level conditions the non-dimensional performance of the engine measured in the altitude cell was in close agreement with that obtained on the ground level test bed, but it was achieved at different settings of engine speeds. This difference has become known as 'Cell effect'; it occurs in a similar manner on engines installed in the aircraft as well as in the cell.
- 3. Altitude facility data can be used in conjunction with ground level static calibrations to refine predictions for the flight performance of the propulsion unit by taking into account those effects of inlet pressure and temperature which are not non-dimensional.
- 4. The precise control of the simulated flight conditions possible in an altitude facility and the ability to investigate off-design situations and even failure cases in a controlled manner and without hazard to aircraft or personnel make its contribution vital to the successful development of a supersonic powerplant.

# ACKNOWLEDGEMENTS

The author has drawn heavily on information supplied by colleagues at NGTE and thanks are due to them. The views expressed are his own.

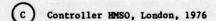
#### REFERENCES

Dean, G. W., White, S. W., American Society of Mechanical Engineers, Data acquisition and processing in the NGTE Altitude Test Facility. 1975, 75-GT-124

Ashwood, P. F., Royal Aeronautical Society Symposium on Altitude Testing, The design and development of a large free jet test cell. 1970, Vol. 74, pp.205-212

Ashwood, P. F., AGARD Conference Proceedings No. 91. Inlets and nozzle for aerospace engines. Free jet tests of a full scale supersonic inlet/engine combination. 1971, CP-91-71 Section 19, pp.1-11

Ascough, J. C., AGARD Conference Proceedings No. 91. Inlets and nozzles for aerospace engines. Measurement full-scale of propelling nozzle performance in an altitude test facility. 1971, CP-91-71 Section 6, pp.1-2



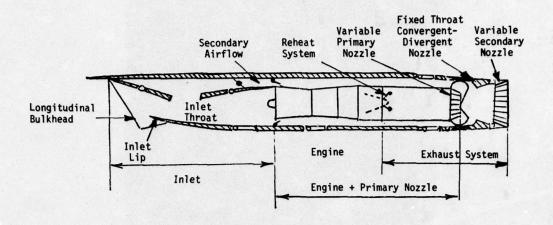


FIGURE 1 PROTOTYPE CONCORDE PROPULSION UNIT

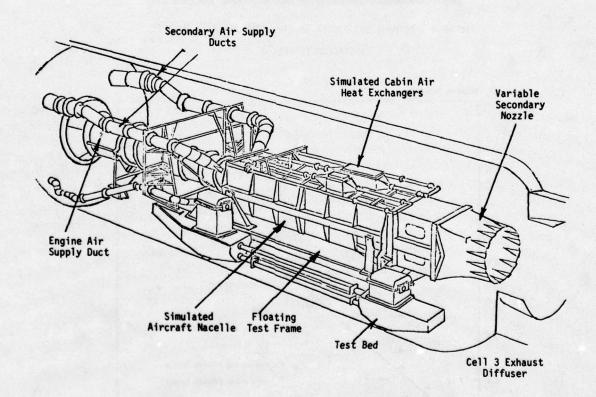


FIGURE 2 PORTSIDE VIEW OF THE ENGINE AND NACELLE INSTALLATION IN CELL 3

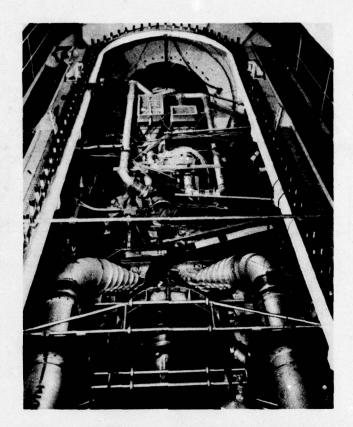


FIGURE 3 OLYMPUS 593 ENGINE IN SIMULATED AIRCRAFT NACELLE
INSTALLED IN CELL 3

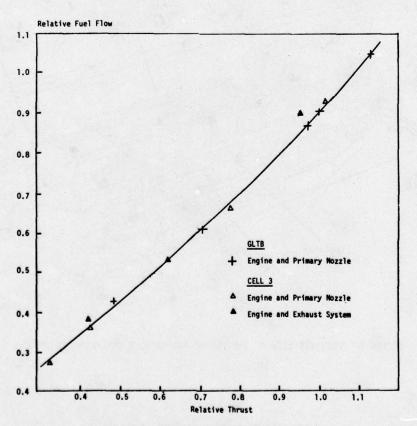


FIGURE 4 COMPARISON OF PERFORMANCE GLTB V CELL 3

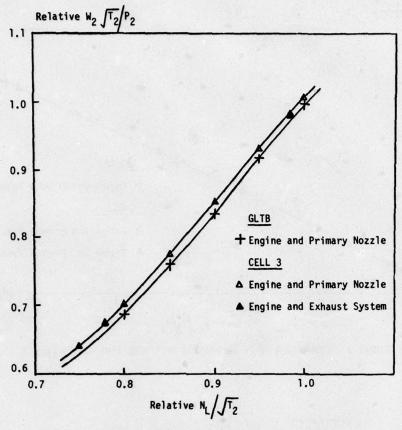


FIGURE 5 COMPARISON OF AIRFLOW GLTB V CELL 3

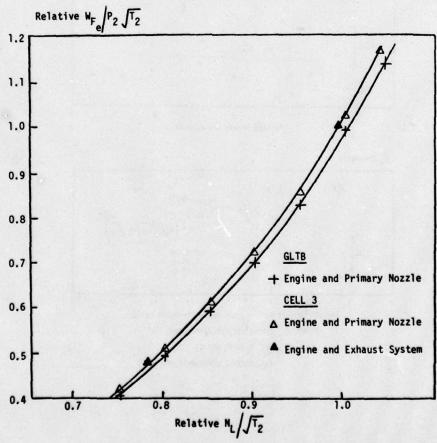


FIGURE 6 COMPARISON OF FUEL FLOW GLTB V CELL 3

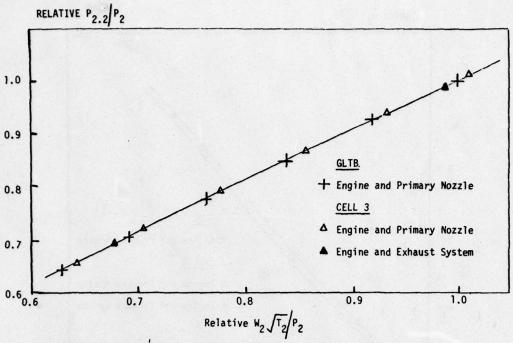
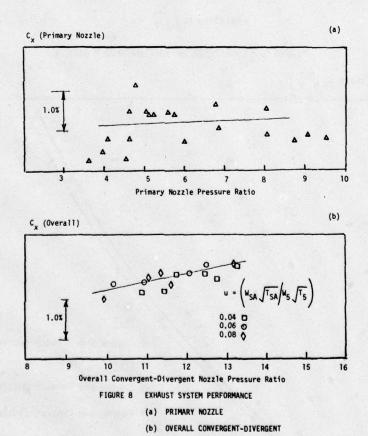


FIGURE 7 COMPARISON OF LP COMPRESSOR OPERATING LINE GLTB V CELL 3



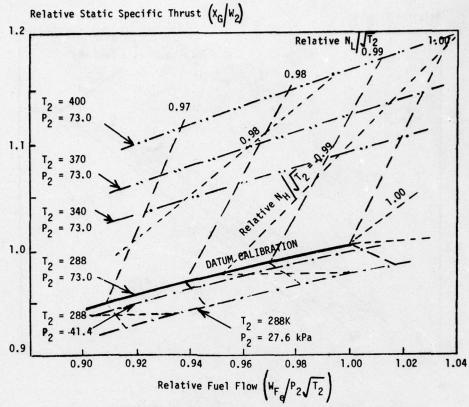


FIGURE 9 VARIATION IN SPECIFIC THRUST AND FUEL FLOW DUE TO CHANGES IN ENGINE INLET CONDITIONS

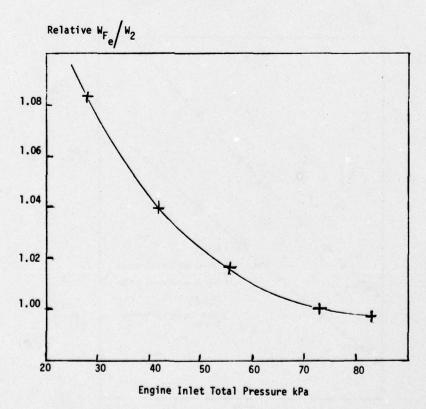


FIGURE 10 INCREASE IN SPECIFIC FUEL FLOW DUE TO CHANGES IN ENGINE INLET PRESSURE AT A CONSTANT ENGINE INLET TEMPERATURE

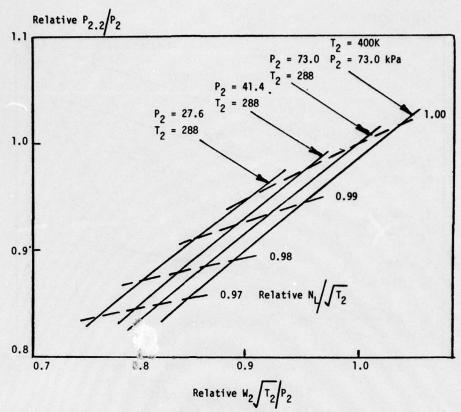


FIGURE 11 VARIATION IN THE LP COMPRESSOR OPERATING LINE DUE TO CHANGES IN ENGINE INLET CONDITIONS

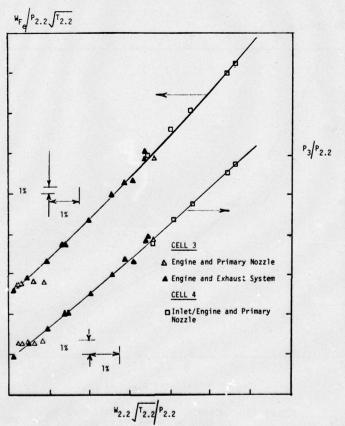


FIGURE 12 COMPARISON OF HP SPOOL PERFORMANCE CTLL 3 V CELL 4

# PROCEDURES FOR THE MEASUREMENT OF ENGINE THRUST IN FLIGHT

J. C. Ascough National Gas Turbine Establishment Pyestock, Farnborough, Hampshire, England, GU13 OLS

# SUMMARY

This paper summarizes the problem of measuring thrust in flight. All aspects have been considered from basic principles to the practical procedures which have evolved as the result of experiences on several types of powerplant. General principles of thrust and drag accounting are discussed, the essential fluid flow relationships on which measurements are based are presented, and the necessary testing of model components and full scale engine is indicated. A strong emphasis is placed upon error estimation and thrust option management.

		NOTA	TION		
Symbol	Description	Units	Symbol	Description	Units
A	either (a) flow area	m <sup>2</sup>	M	Mach number	non-D
	or (b) IC (F <sub>N</sub> : C <sub>G</sub> )	non-D	m	number of tests in Class II	non-D
ATF	Altitude Test Facility		N	shaft speed	Hz
В	IC (F <sub>N</sub> : C <sub>D8</sub> )	non-D	n	number of items in Class I	non-D
C <sub>D</sub>	Drag Coefficient = D/100 V0	non-D	NPF	Net Propulsive Force	kN
CDi	Discharge Coeff at plane "i"	non-D	NPR	Nozzle Pressure Ratio = $\frac{r_{t7}}{r}$	non-D
CG, con	Gross Thrust Coeff "AP" method	non-D	P	probability Pso	non-D
C <sub>G,con-di</sub>	Gross Thrust Coeff "AP" method	non-D	Ps	static pressure	k Pa
C <sub>T</sub>	In-flight Net Thrust Coeff		P <sub>t</sub>	total pressure	k Pa
	$= \frac{F_{N1} + F_{N2}}{\frac{1}{2}\rho V^2} $ for a twin-engined aircraft		s	surface area	m <sup>2</sup>
	aircraft		SLSTB	Sea Level Static Test Bed	
c <sub>v</sub> .	Gross Thrust Coeff "W √T" method		Ts	static temperature	K
CX	Gross Thrust Coeff "W $\sqrt{T}$ " method		T <sub>t</sub>	total temperature	ĸ
D	Drag, by fundamental definition	kN	v	velocity	m/s
EL()	2σ Error Limit of ( )	as ()	W	mass flow rate	kg/s
FGi	Gauge Stream Thrust at plane "i"	kN	×i	general input parameter	as approp.
F <sub>N</sub>	Net Thrust	kN	y	general output result	as approp.
$IC(y:x_i)$	Influence Coefficient	non-D	Y	specific heat ratio	non-D
IRF	Intake Recovery Factor	non-D	ρ	density	kg/m <sup>3</sup>
LCV	Lower Calorific Value of fuel	J/kg	σ()	standard deviation of ( )	as ()
L	number of engines	non-D	•	rearward acting force	kN
MFR	Mass Flow Ratio = Ao/A1	non-D			

# 1. INTRODUCTION

# 1.1 THE NEED FOR IN-FLIGHT THRUST MEASUREMENT

It might at first sight seem unnecessary to measure thrust in flight. An operator's main interest is in the effectiveness of the aircraft in terms of load carried, distance travelled, speeds achieved, fuel used, acceleration climb and manoeuvre capability - none of those things necessarily require the measurement of thrust. However, this passive attitude would only be valid if the aircraft had reached its final standard and no possible future development were contemplated.

Thrust measurement in flight is certainly required during aircraft development for many reasons which may be summarized as follows:

- 1. Demonstration of compliance with contractual requirements.
- 2. Problem identification and rectification in the event of performance shortfall.
- Extrapolation of measured performance to a wide range of flight conditions which may not have been tested.
- Identification of components which can be modified to give performance gains for later developments of the aircraft.
- Validation and development of the analytical model used in performance prediction during the design stage.

# 1.2 THE PROCESS OF IN-FLIGHT THRUST AND DRAG MEASUREMENT

Direct measurement of drag in flight is not feasible - it can only be determined in practice by equating it to the thrust, with allowances for acceleration and changes in height. Even thrust cannot be measured directly in flight with the available technology. Instead, it is evaluated from correlations against combinations of various parameters such as pressure, temperature, area, shaft speed, fuel flow, etc. which can be measured in flight. These correlations of thrust against the measured parameters should be calibrated by full scale testing of the engines on the ground (where measurements of thrust and airflow are available) either in a Sea Level Static Test Bed (SLSTB) or, preferably, in an Altitude Test Facility (ATF).

It is also necessary to carry out wind-tunnel tests at model scale to establish Intake Spillage Drag and the Exit Nozzle Jet Interference Drag. These latter tests cannot be done at full scale with external flow because of the prohibitive cost of providing the necessary facilities.

It is essential for all parties to agree upon a consistant "bookkeeping" system to account for the interfaces between thrust and drag. The basic principles behind this are described in Section 2.0.

#### 1.3 SELECTION FROM A MULTIPLICITY OF METHODS

There are a large number of possible thrust and mass flow correlations available to suit different types of engine and aircraft installations. Even with a given aircraft installation there are many possible methods to consider. The most unpromising options can be weeded out at an early stage with the help of a Sensitivity Survey as explained in Section 5.2. At this early stage the Instrumentation Specification should be agreed so that the "accuracy" requirements are fully understood in good time to allow any problems to be sorted out.

A fair number of different options (perhaps 8 or 10) should be carried through into the flight-testing phase. The traditional procedure in the past has been to choose a preferred method with one, or perhaps two, backup methods as insurance in case of failure of the preferred one. A more efficient procedure is to take the "weighted mean value" of all the methods as explained in Section 5.7.

# 1.4 ERROR ESTIMATION AND CONTROL

The estimation of the uncertainty of a flight test result is, in the opinion of the writer, almost as important as the result itself. But because the subject is specialised and time consuming, most workers can only give it limited attention while they get on with their main jobs. An attempt is made in Section 5 to draw attention to some important ideas from statistical theory, viz: the relationship of Error Limits to Probability Distributions, the different classes of error, the use of Influence Coefficients in error combination, the crucial importance of whether errors are "Independent" or "Common", the advantages of "linked methodology" and error combinations in multi-engined aircraft.

The propagation of uncertainty of engine test calibration to the in-flight test results is illustrated by extracts from a recently-published paper 1. This shows how a commonly misapplied assumption of independence of calibration errors can lead to large over-estimation of in-flight thrust uncertainty.

#### 1.5 POWERPLANT STATION DESIGNATION

It is a tremendous advantage to make use of a universally common notation. For example, if T<sub>4</sub> always denotes turbine inlet temperature, no matter what the engine, this greatly simplifies comparisons and discussion. The system adopted by this paper is well on the way to being universally accepted, based on ARP 755A (Reference 2).

Figure 1 illustrates the scheme, using as example a 3-shaft by-pass engine with separate nozzle for fan flow.

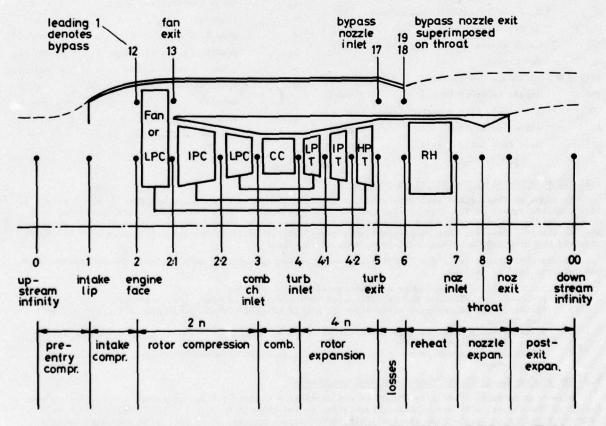


FIG. 1 EXAMPLE OF UNIVERSAL ENGINE STATION DESIGNATION

Of particular note for thrust purposes is the fact that the propelling nozzle exit can always be denoted by the digit "9" ("19" for by-pass nozzle exit) while the nozzle throat is always denoted by the digit "8" ("18" for by-pass nozzle throat). If the nozzle has no divergent part, i.e. is convergent only, then "9" superimposes upon "8" (in Figure 201 we have "19" superimposed upon "18").

# 2. THRUST AND DRAG ACCOUNTING

# 2.1 BASIC REQUIREMENTS

A practical bookkeeping system must conform to the following requirements:

- 1. It must be consistent and free from ambiguity, so that no component is overlooked and non is counted twice.
- It must, so far as possible, provide for the separate study of engine and airframe performance by the respective manufacturers, both in preliminary paper projects and in any subsequent model and/ or flight testing.
- 3. It must include clear definition of the interfaces where engine and airframe responsibilities meet, and facilitate a proper understanding of any zones where responsibilities overlap.

# 2.2 NET PROPULSION FORCE AND NET THRUST

The simplest expression for net propulsion force is:

$$NPF = F_{N,int} - \phi_{nac}$$
 (1)

as shown in Figure 2.

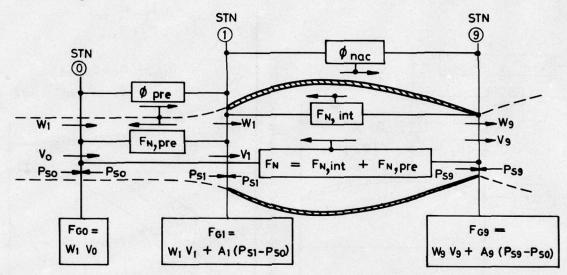


# FIG. 2 NET PROPULSIVE FORCE AND NET THRUST

FN. int is the Intrinsic Net Thrust:

$$F_{N,int} = F_{G_9} - F_{G_1}$$
 (2)

i.e. the difference in Gauge Stream Thrust between stations 9 and 1, and  $\phi_{\text{nac}}$  is the force on the outer surface of the nacelle (defined as positive rearwards) between stations 1 and 9.

Unfortunately,  $F_{G1}$  would neither be easy to measure in flight, nor would it be easy to reproduce in the engine test cell. Being influenced both by the engine and the 'airframe', the use of station 1 contravenes Requirement 2 of Section 2.1. Hence, in practice most bookkeeping systems use instead the Standard Net Thrust, FN:

$$F_N = F_{G_9} - F_{G_0}$$
 (3)

where FGo is the freestream momentum:

$$F_{C_0} = W_1 V_0 \tag{4}$$

Now .

$$F_{G_0} = W_1 V_0$$
 (4)  
 $F_N = (F_{G_0} - F_{G_1}) + (F_{G_1} - F_{G_0})$  (5)

 $F_{N,pre}$  is the Pre Entry Force (defined as positive forwards) acting from the internal stream to the outside region as shown in Figure 2. There is an equal opposing force.

$$\phi_{\text{pre}} = F_{\text{N,pre}}$$
 (7)

acting from the outside region to the internal stream (defined as positive rearwards).

Substituting for FN, int in Equation (1) from (6) and (7) the Net Propulsive Force becomes:

$$NPF = F_{N} - \left[\phi_{nac} + \phi_{pre}\right]$$
 (8)

# 2.3 DISTINCTION BETWEEN FUNDAMENTAL DRAG AND REARWARD-ACTING FORCE

The previous Section 2.2 introduced the concept of the force \$\phi\$ (defined as positive rearwards) acting \( \frac{\text{from}}{\text{to}} \) the external flow \( \frac{\text{to}}{\text{to}} \) the internal flow, (or \( \frac{\text{to}}{\text{a}} \) an internal boundary). There is a practical book-keeping system which deals in terms of these forces and the name 'Drag' is loosely applied to them.

In this paper, however, the word 'Drag' and symbol D is restricted to a more fundamental definition. Drag is the name given to the departure of the force from what would occur in potential flow i.e. the contribution to the momentum defect at downstream infinity. Thus:

Drag, D = 
$$\phi - \phi_{\text{pot}}$$
 (9)

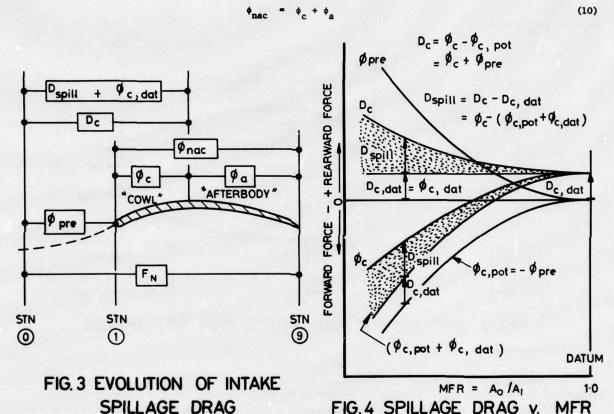
The term \$\phi\_{pot}\$ is the "Potential Flow Buoyancy".

By this definition, the Drag on part of a body always acts rearwards (the positive direction) whereas the force  $\phi$  may act either rearwards or forwards (+ or - senses).

Bookkeeping in terms of Drag, D reveals the losses on isolated parts of a body which may not be obvious in terms of the force,  $\phi$ .

#### 2.4 INTAKE SPILLAGE DRAG

It is convenient to split the force,  $\phi_{\text{nac}}$ , acting over the whole of the nacelle outer surface in Figure 2, into two parts as shown in Figure 3:



The front part  $\phi_{\rm C}$  acts over the "cowl" from intake lip to mid nacelle, while the rear part  $\phi_{\rm A}$  acts over the "afterbody" from mid nacelle to trailing edge. It is assumed that interaction from the preentry force  $\phi_{\rm pre}$  will only apply to the "cowl" part of the nacelle. Thus the second term of Equation (8) becomes:

$$\left[\phi_{\text{nac}} + \phi_{\text{pre}}\right] = \left[\phi_{\text{c}} + \phi_{\text{pre}}\right] + \phi_{\text{a}} \tag{11}$$

The present Section will deal with  $[\phi_c + \phi_{pre}]$  leaving the behaviour of  $\phi_a$  to Section 2.5.

In potential flow, there is no drag on a semi-infinite body, (the Prandtl/d'Alembert paradox). For a ducted body, the pre-entry streamtube and cowl together form a "semi-infinite body" so that

$$\phi_{c,pot} + \phi_{pre} = 0 \tag{12}$$

where  $\phi_{c,pot}$  is the force on the cowl in potential flow. If there are no strong shocks, the real preentry flow approximates very closely to potential flow: hence applying Equation (9) to the cowl:

$$D_{c} = \phi_{c} - \phi_{c,pot} \tag{13}$$

$$= \phi_{\rm c} + \phi_{\rm pre} \tag{14}$$

For the particular condition when the free streamtube area  $A_0$  is equal to the inlet entry area  $A_1$ , the preentry streamtube is parallel and so  $\phi_{\text{pre}} = 0$ .

This condition is normally considered as a datum, with

Intake Mass Flow Ratio (MFR) = 
$$\frac{A_0}{A_1}$$
 = 1.0

and thus Equation (14) becomes

$$D_{c,dat} = \phi_{c,dat}$$
 (15)

"Spillage Drag" is defined as the increase in cowl drag as MFR decreases from 1.0 (i.e. as spillage occurs), thus

$$D_{\text{spill}} = D_{\text{c}} - D_{\text{c,dat}}$$
 (16)

Substituting from Equation (14) and (15) we have

$$D_{\text{spill}} = (\phi_{c} + \phi_{\text{pre}}) - \phi_{c,\text{dat}}$$

$$= \phi_{\text{pre}} - (\phi_{c,\text{dat}} - \phi_{c})$$
(17)

The quantity  $\left(\phi_{\text{C,dat}} - \phi_{\text{C}}\right)$  represents a forward acting force resulting from reduced pressures around the cowl. Hence it is commonly termed the "Cowl Suction Force". Equation (17) thus represents an alternative view of  $D_{\text{Spill}}$  as the amount by which the "Cowl Suction Force" fails to balance the "Pre-entry Force". In potential flow the two would exactly cancel each other.

From Equations (15) and (16)

$$D_{c} = D_{spill} + \phi_{c,dat}$$
 (18)

We can now substitute into Equation (8) from (11), (14) and (18) giving

$$NPF = F_N - \left(\phi_C + \phi_{DPE}\right) - \phi_a \tag{19}$$

$$= F_{N} - D_{C} - \phi_{a}$$
 (20)

$$= F_{N} - D_{spill} - \phi_{c,dat} - \phi_{a}$$
 (21)

Note that by introducing  $D_{spill}$ , the term  $\phi_{pre}$  has been eliminated from the thrust/drag account. In effect Equation (20) avoids the necessity for separating  $D_C$  into its component parts  $\phi_C$  and  $\phi_{pre}$  (which would be equivalent to a determination of  $F_{G1}$  and subject to all the difficulties previously explained). Equation (21) provides the means of relating  $D_C$  to quantities which can be directly measured in a wind tunnel.

The possible variation of these "Drags" and "Forces" associated with the Intake Cowl is shown in Figure 4 plotted against Mass Flow Ratio.

# 2.5 EXIT JET INTERFERENCE DRAG

There is a school of thought which applies a similar "Drag" treatment to the afterbody as is applied to the cowl in Section 2.4. This theory postulates an isentropic jet expansion producing the post-exit thrust  $F_{N,post}$  and its equal and opposite force  $\phi_{post}$  as indicated in Figure 5.

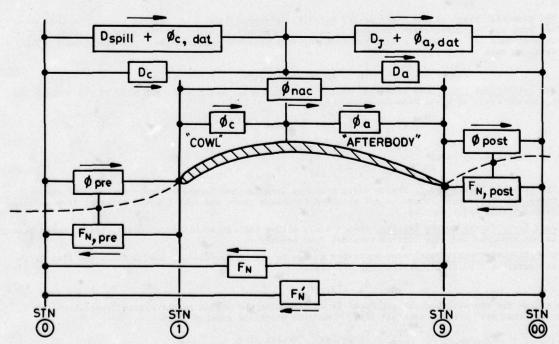


FIG. 5 POSSIBLE SYMMETRICAL TREATMENT OF AFTERBODY DRAG

The Jet Interference Drag,  $D_J$  is the counterpart to Spillage Drag,  $D_{spill}$ . With the notation of Figure 5 the Afterbody Force can be expressed:

$$\phi_{\mathbf{a}} = D_{\mathbf{a}} - \phi_{\mathbf{post}} \tag{22}$$

$$= D_J + \phi_{a,dat} - \phi_{post}$$
 (23)

where  $\phi_{a,dat}$  is the afterbody force at the datum condition of Nozzle Pressure Ratio, NPR<sub>dat</sub> which is taken to be the isentropic PR for the particular nozzle geometry.

Substituting into Equations (20) and (21) the Net Propulsive Force becomes:

$$NPF = F_{N} - D_{C} - D_{A} + \phi_{post}$$
 (24)

$$= F_N - D_{spill} - \phi_{c,dat} - D_J - \phi_{a,dat} + \phi_{post}$$
 (25)

$$= F_N - D_{spill} - D_{c,dat} - D_J - D_{a,dat} + \phi_{post}$$
 (26)

$$F_N' - D_{spill} - D_{c,dat} - D_J - D_{a,dat}$$
 (27)

where  $F'_N = F_N + \phi_{DOST}$  (28)

Thus, with this pure Drag treatment  $\phi_{\text{pre}}$  is eliminated, but  $\phi_{\text{post}}$  is not. ( $\phi_{\text{post}}$  may be hidden in FN but it would still need to be evaluated, unlike  $\phi_{\text{pre}}$ . Also,  $\phi_{\text{post}}$  cannot be evaluated by testing, but can only be calculated from various assumptions.) This is a consequence of the use of Station 9 as the practical exit station for standard Net Thrust, FN.

It is however possible to eliminate  $\phi_{\text{post}}$  by accounting for afterbody/jet interference in terms of "Forces", rather than "Drags" Thus defining a Jet Interference Force,  $\phi_J$ :

$$\phi_{J} = \phi_{a} - \phi_{a,dat} \tag{29}$$

and substituting in Equation (21):

$$NPF = F_N - D_{spill} - \phi_{c,dat} - \phi_{a,dat} - \phi_{J}$$
 (30)

Equation (30) represents a practical treatment which can be conveniently applied to reference model tests, as explained in Section 2.6. It is a hybrid in which "Drag" concepts are applied to the cowl, but "Force" concepts applied to the afterbody.

# 2.6 REFERENCE MODEL AND FULL SCALE TESTING (LEADING TO COMPLETE EXPRESSION FOR NPF)

The Spillage Drag and Jet Interference Drag of the previous Sections 2.4 and 2.5 are defined in relation to Datum MFR and Datum MFR. It simplifies matters if these Datum conditions can be set up on the Airframe Reference Model, but this is usually impossible, especially to get both intake and nozzle datums set up simultaneously. Indeed, it is sometimes arranged that the airframe reference model has no internal flow at all! Furthermore, it is rarely possible to test the full scale engine/nozzle combination with correctly simulated external flow: the Reference thrust of the engine is therefore normally established in quiescent air. The Net Propulsive Force for the complete aircraft is then synthesized by testing a series of models relating the actual operating conditions to the various Reference conditions as indicated in Figure 6.

The measured 'Drag' of the <u>Airframe</u> (or <u>Nacelle</u>) <u>Reference Model</u> 6(a) will in general include some Spillage Drag and Jet Interference Force. It is also necessary to allow for the negative thrust of the flow-through duct (if provided) calculated from internal pressure measurements. Applying Equation (21) to this test, we have

NPF = 
$$F_N - D_{\text{spill,ref}} - \phi_{c,\text{dat}} - \phi_{a,\text{ref}}$$
 (31)

The Intake/Cowl Model must be tested at the Reference MFR, sketch 6(b), and also at the correct MFR values, sketch 6(c), to yield from Equation (18)

$$D_{c,ref} = D_{spill,ref} + \phi_{c,dat}$$
 (32)

and

$$D_{c} = D_{spill} + \phi_{c,dat}$$
 (33)

Hence by difference we have:

$$\Delta D_{\text{spill}} = D_{\text{c}} - D_{\text{c,ref}} = D_{\text{spill}} - D_{\text{spill,ref}}$$
 (34)

The <u>Internal Intake Model</u>, Sketch 6(d), produces data for the Intake Recovery Factor, IRF and <u>Distortion Profiles</u>. Force measurement is not required for these tests and only limited external flow is necessary with suitable spill ducting.

Full Scale Intake/Engine Testing, sketch 6(e), allows for compatibility studies. Again, force measurement is not required and only limited external flow needed.

The Afterbody/Nozzle Model must be tested at the Reference conditions, sketch 6(f), and also at the correct operating conditions, sketch 6(g), to yield:

$$\Delta \phi_{\mathbf{a}} = \phi_{\mathbf{a}} - \phi_{\mathbf{a}, \text{ref}} \tag{35}$$

Another task for the Afterbody/Nozzle Model is to determine the change in the nozzle Gross Thrust  $\Delta F$  by operating first with correct external flow, then with quiescent external flow:

$$\Delta F = F_{G9,quies} - F_{G9,ext.flow}$$
 (36)

Note that  $\Delta F$  and  $\Delta \phi_{\bf a}$  cannot be separated unless a duplex internal balance is provided, but their sum will be correctly measured by a single balance.

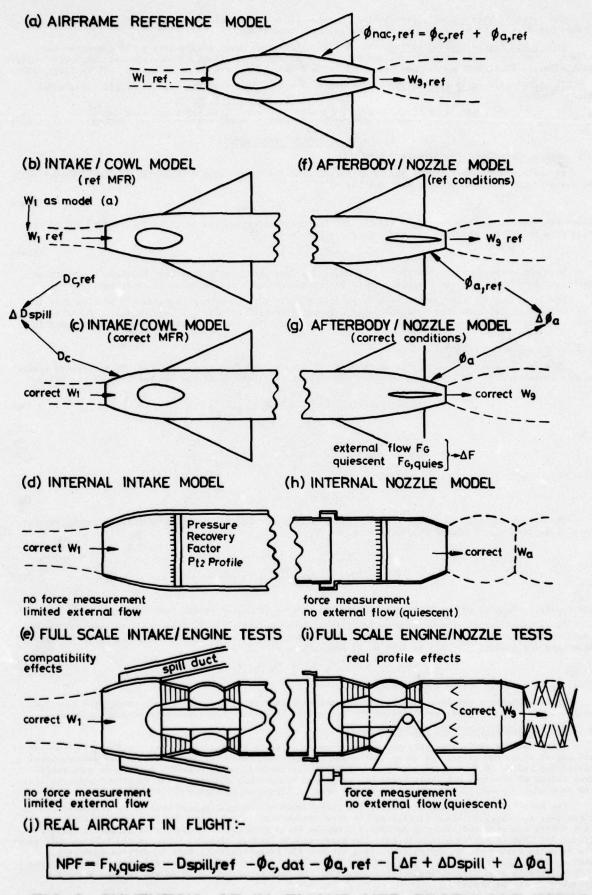


FIG. 6 SYNTHESIS OF IN-FLIGHT NET PROPULSIVE FORCE

The Internal Nozzle Model, sketch 6(h), permits study of internal performance at economical model scale, but with uniform and usually cold nozzle inlet conditions.

<u>Full Scale Engine/Nozzle Testing</u>, sketch 6(i), allows the model nozzle data to be corrected for effects of scale, of gas temperature, and with the real engine profiles. These tests are done with quiescent external flow, both in the Sea Level Static Test Bed, SLSTB, and in the Altitude Test Facility, ATF.

The final expression for Net Propulsive Force is synthesised from the results of all these model tests, thus:

NPF = 
$$F_{N,quies} - D_{spill,ref} - \phi_{c,dat} - \phi_{a,ref} - \left[ \Delta F + \Delta \phi_a + \Delta D_{spill} \right]$$
 (37)

# 3. THRUST EXPRESSIONS

# 3.1 GENERAL OUTLINE OF THRUST MEASUREMENT

As explained in Section 2.2, the usual arrangement for Thrust/Drag Bookkeeping is that "Thrust" shall be evaluated in the form of "Standard Net Thrust"

$$F_{N} = F_{G_9} - F_{G_0}$$
 (3) bis

There are several general methods available for in-flight determination of Gross Thrust  $F_{G^9}$ , and of the Mass Flow needed for the Free Stream Gauge Force  $F_{G^0}$ , where:

$$F_{Co} = W_1 V_0 \tag{4} bis$$

With all methods, a calibration of the engine is required in an Engine Test Facility to establish correlations of both  $F_{C_9}$  and W against suitable parameters which can be measured in flight.

The remainder of this Section will first deal briefly with "Brochure" methods (in Section 3.2) but the main effort is devoted to "Gas Generator/Calibrated Nozzle" methods (in Section 3.3). Other methods, such as "Jet Traverse" and "Trunnion Thrust" which have not yet become established are not included in this present paper.

# 3.2 BROCHURE THRUST METHODS

This is the simplest method, in which a set of curves, usually non-dimensional, is correlated against simple measurements in flight such as shaft non-dimensional speed N/ $\sqrt{\theta}$  and Ram Ratio  $P_{t_1}/P_{s_0}$ . Thus:

Thrust Function = 
$$\left(\frac{F_{G9}}{A_9} + 1\right) \frac{P_{S0}}{P_{t2}} = f\left(\frac{N}{\sqrt{\theta}}, \frac{P_{t2}}{P_{S0}}\right)$$
 (38)

Mass Flow Function = 
$$\frac{W_2}{P_{t2}} = f\left(\frac{N}{\sqrt{\theta}}, \frac{P_{t2}}{P_{s0}}\right)$$
 (39)

from which Net Thrust may be found from:

$$F_N = F_{G_9} - W_1 V_0$$
 (40)

The reason why this ND Thrust Function can be correlated against N/ $\sqrt{T}$  is because it can be shown to be a disguised form of Engine Pressure Ratio,  $P_{t_7}/P_{t_2}$ :

$$\frac{1}{2} \left( \frac{\gamma + 1}{2} \right)^{\frac{1}{\gamma - 1}} \left\{ \frac{F_{G_9}}{C_G A_9 P_{S0}} + 1 \right\} \frac{P_{S_0}}{P_{t_2}} = \frac{P_{t_7}}{P_{t_2}}$$
(41)

and  $P_{t7}/P_{t2} = P_{ts}/P_{t2}$  can be correlated versus shaft speed N/ $\sqrt{T}$ , or versus fuel flow  $W_F/P_{t2}/T_2$ .

It is usual to omit the  $\gamma$  group on the left of Equation (41). It is also usual to omit the Thrust Coefficient  $C_G$  on the assumption that it will be the same in flight as it is during engine calibration. Sometimes the product  $(C_{D_9}$   $A_9$ ) is used as an approximation:

$$C_{G} A_{9} = C_{X} C_{D_{9}} A_{9} \simeq C_{D_{9}} A_{9}$$
 (42)

where Cx is a "W JT" method Thrust Coefficient.

Brochure methods are long established and are satisfactory if the engines are calibrated over the whole of the flight regime, and provided the Pt profile at engine face remains reasonably uniform.

# 3.3 GAS GENERATOR/CALIBRATED NOZZLE METHODS

These methods avoid the problems of distorted profiles at the engine face by dealing with the rear of the engine where the effects of inlet distortion are smaller. Nevertheless, there may be some residual distortion and so it is advisable to put in as much instrumentation as possible to measure good radial mean values of pressure and temperature at the chosen measurement stations. (An important point is that the same instrumentation arrangement should be used in flight as in engine calibration.)

The main feature of these methods is the performance of the exit nozzle related to its inlet conditions  $(W_7, P_{t7}, T_{t7})$  to its area  $(A_8)$  and to free stream static  $(P_{80})$ , and possibly base pressure  $(P_{8b})$ . In a simple non-reheated turbojet  $P_{t7}$  and  $T_{t7}$  may be found from direct measurements at nozzle entrance (plane 7). But it may be better to take the measurements further upstream -  $P_{t5}$  in the turbine exit annulus is often used - and to derive  $P_{t7}$ . With reheat, the temperature  $T_{t7}$  must be derived from other measurements. There might be a good case for determining mass flow  $W_7$  from nozzle characteristics even with a variable area nozzle, but other stations of the "gas generator" such as the turbine stators (Station 4) can be used.

The full scale Gas Generator/Nozzle combination should be calibrated in an Altitude Test Facility (Figure 6(i)) over the range of altitude and Mach number expected in flight. These calibrations will

yield curves of Gross Thrust Coefficients and Discharge Coefficients. Calibrations in a Sea Level Static Test Bed are not so good - it is not possible there to achieve the flight nozzle pressure ratios, nor the flight engine inlet temperatures. Extrapolation of the SLSTB calibrations to flight conditions might be guided to some extent by model nozzle test curves, (Figure 6(h)), but this leaves an uncertainty greater than that of an ATF calibration. It should be noted that even the ATF does not calibrate with external flow around the nozzle, hence a correction ΔF is needed as found from model nozzle tests, (Figure 6(g)).

There are two broad types of correlation in use for nozzle calibrations, the "W  $\sqrt{T}$ " type and the "AP" type. It is possible to produce curves of  $F_G/W$   $\sqrt{T}$  and  $F_G/AP$  plotted against nozzle pressure ratio and nozzle half angle, but these are rather steep and therefore a source of error. A better scheme is to express these correlations in the form of coefficients, i.e. as ratios of "actual" values to "ideal" values. Thus:

$$C_{X} = \left[\frac{F_{G9}}{W_{9} \sqrt{T_{9}}}\right]_{act} \cdot \sqrt{\left[\frac{F_{G}}{W \sqrt{T}}\right]_{id,con}}$$
(43)

$$C_{V} = \left[\frac{F_{G9}}{W_{9}\sqrt{T_{9}}}\right]_{act} / \left[\frac{F_{G}}{W\sqrt{T}}\right]_{id,con-di}$$
(44)

or

$$C_{G,con} = \left[\frac{F_{G9}}{A_9 P_{S0}}\right] / \left[\frac{F_G}{A P_{S0}}\right]_{id,con}$$
(45)

$$C_{G,con-di} = \left[\frac{F_{G9}}{A_9 P_{so}}\right] / \left[\frac{F_G}{A P_{so}}\right]_{id,con-di}$$
(46)

In Equations (43), (45) the ideal groups are evaluated for ideal flow in a <u>convergent</u> nozzle, while in Equations (44), (46) the ideal groups are evaluated for ideal flow in a 'flexible' <u>con-di</u> nozzle in which the flow expands exactly to P<sub>80</sub>.

Mass flow may be expressed by a nozzle correlation in the form of a Discharge Coefficient

$$c_{D_8} = \left[\frac{W_8 \sqrt{T_8}}{A_8 P_{t8}}\right] / \left[\frac{W \sqrt{T}}{A P_t}\right]_{id,con}$$
(47)

This is always related to the throat area  $A_8$  no matter whether the nozzle is convergent, or con-di. For convergent nozzles the exit plane 9 coincides with plane 8 and the two types of Thrust Coefficient Cx and  $C_{G,con}$  are related through  $C_{D8}$ :

$$C_{G,con} = C_{X} \times C_{D8}$$
 (48)

Formulae for evaluating the Ideal groups in Equations (43) through (47) are given in Table A.

TABLE A - IDEAL THRUST EXPRESSIONS (SINGLE STREAM NOZZLES)

Ideal Thrust Group	P <sub>t7</sub>	Convergent nozzle (Note: Station 8 = Station 9)	Variable con-di nozzle		
r- 7	sub crit	$\left[\frac{2RY}{Y-1}\left\{1\right.\right.\right]$	$\left(\frac{P_{S_0}}{P_{t7}}\right)^{\frac{y-1}{y}}\right\}^{\frac{1}{2}}$		
$\left[\frac{\mathbf{F}_{\mathbf{G}}}{\mathbf{W}\sqrt{\mathbf{T}_{\mathbf{t}}}}\right]_{9,\mathbf{id}}$	crit	$\left[\frac{2R}{Y+1}\right]^{\frac{1}{2}}$			
L U,,id	super crit	$\left\{\frac{2R(\gamma+1)}{\gamma}\right\}^{\frac{1}{2}} - \frac{P_{so}}{P_{t_{\gamma}}} \left\{\frac{R}{\gamma} \left(\frac{\gamma+1}{2}\right)^{\frac{\gamma+1}{\gamma-1}}\right\}^{\frac{1}{2}}$	as sub-crit		
F <sub>G</sub> AP <sub>so</sub> , id	sub crit	$\frac{2\gamma}{\gamma-1}\left\{\begin{pmatrix} 1\\ i\end{pmatrix}\right\}$	$\left(\frac{P_{t7}}{P_{s_0}}\right)^{\frac{\gamma-1}{\gamma}} - 1$		
	crit	de la constante architecto de	Y the state of the		
	super crit	$\left\{2\left(\frac{2}{\gamma+1}\right)^{\frac{1}{\gamma-1}}\right\}\frac{P_{t7}}{P_{80}}-1$	as sub-crit		
F <sub>G9</sub> As P <sub>so</sub> ld	super crit		$\frac{2\gamma}{\sqrt{\gamma^2 - 1}} \left(\frac{2}{\gamma + 1}\right)^{\frac{1}{\gamma - 1}} \cdot \frac{P_{t7}}{P_{s0}} \left\{ 1 - \left(\frac{P_{s0}}{P_{t7}}\right)^{\frac{\gamma - 1}{\gamma}}\right\}^{\frac{1}{2}}$		

The formulae in Table A can be evaluated most simply by assuming constant Y - convenient values might be:-

γ = 1.40 for model nozzle tests γ = 1.33 for non-reheat engine nozzles γ = 1.27 for reheated engine nozzles.

There is a practice of using ideal gas enthalpy relationships instead of the  $\gamma$ - expressions of Table A. A somewhat different practice, followed for ATF tests at NGTE, is to calculate the expressions with variable  $\gamma$ . These differing practices can cause variations of the order of 1 per cent in the nozzle coefficients and so it is important for all parties concerned with a project to follow consistent procedures.

Typical curves of  $C_X$ ,  $C_G$  and  $C_{D8}$  obtained by calibrating an engine with a convergent nozzle in an ATF are shown in Figure 7.

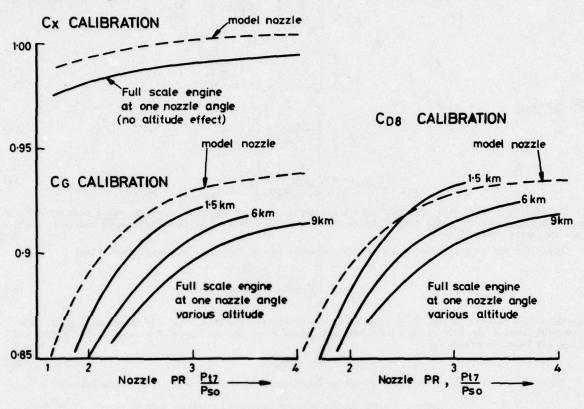


# FIG. 7 EXAMPLE OF ENGINE / NOZZLE CALIBRATION IN ATF

The "AP" method for thrust in flight

Gross Thrust is given by:

$$F_{G} = C_{G,con} A_{0} P_{00} \begin{bmatrix} F_{G} \\ \overline{AP} \\ id,con \end{bmatrix}$$
(49)

perhaps with a "linked methodology" mass flow:

$$W_{\theta} = C_{De} \frac{A_{\theta} P_{te}}{\sqrt{T_{ts}}} \left[ \frac{W \sqrt{T}}{A P_{t}} \right]_{id,con}$$
 (50)

or with "unlinked methodology" mass flow from the compressor characteristics:

$$W_2 = \frac{P_{t2}}{\sqrt{T_2}} \left[ \frac{W_2 \sqrt{T_2}}{P_{t2}} \right]_{fan chic}$$
 (51)

or with "unlinked methodology" mass flow from the turbine stators:

$$W_{4} = C_{D4} \frac{A_{4} P_{t4}}{\sqrt{T_{t4}}} \left[ \frac{W \sqrt{T}}{A P_{t}} \right]_{id,4}$$
 (52)

or with "unlinked methodology" mass flow from turbine

$$W_{6} = C_{D6} \frac{A_{6} P_{t6}}{\sqrt{T_{t6}}} \left[ \frac{W \sqrt{T}}{A P_{t}} \right]_{id,6}$$
 (53)

From any of these methods the mass flow  $W_1$  at intake lip is found by accounting for the various bleed flows and fuel flows. Thence the Net Thrust in flight is:

$$F_{N} = F_{G} - W_{1} V_{0}$$
 (40)bis

In this example there would be four different values obtained for  $F_N$ , each with a different value of  $W_1$ . The procedure for selecting the best value for  $F_N$  is discussed in Sections 5.2 and 5.7.

# The "W √T" method for thrust in flight

First, the mass flow would be calculated from any of Equations (50) through (53) above. The flow W<sub>7</sub> at nozzle entrance is then found after accounting for bleeds and fuel flows. Gross Thrust is given by:

$$F_G = C_X W_7 \sqrt{T_7} \left[ \frac{F_G}{W \sqrt{T}} \right]_{id,con}$$
 (54)

Dealing with the mass flow again, the value at intake lip  $W_1$  is found from any of Equations (50) through (53) with allowances for bleeds and fuel flows. Thence the Net Thrust is

$$F_{N} = F_{G} - W_{1} V_{0}$$
 (40)bis

The beauty of the "W  $\sqrt{T}$ " method is that every option for mass flow is automatically a "linked method-ology" with its valuable properties of self-cancelling errors (see Section 5.3).

From this "W  $\sqrt{T}$ " example there would come another four values of  $F_N$  which, added to the four from the "AP" method, gives eight values of  $F_N$  in all. The procedure for selecting the best value is given in Sections 5.2 and 5.7.

As was noted in Section 2.6, these values of  $F_N$  only apply in the absence of external flow around the nozzle. The correction  $\Delta F$ , as required for NPF in Equation (37) for example, must be obtained by model nozzle tests in a wind tunnel (Figure 6(g)).

# 4. POWERPLANT CALIBRATION

# 4.1 INTAKE TESTING

Full scale Intake/Engine testing (Part (e) of Figure 6) has been done for many years at NGTE<sup>3</sup>, first for the Concorde/OL593, and more recently for the Tornado/RB199. The sensitivity of the engine (surge margin, turbomachinery component performance, control system behaviour etc) to the effects of pitch and yaw are studied over a wide range of altitude and flight Mach number. Intake performance (Recovery Factor, distortion coefficients for both steady-state and transient conditions etc) is also observed at full scale, 6(e). Such tests are also made at model scale, 6(d).

One important feature, however, is not tested at full scale and that is Intake Spillage Drag - it would be prohibitively expensive to provide such a facility at full scale. However, adequate data on Spillage Drag  $\Delta D_{spill}$  are obtained from model tests (b) and (c) of Figure 6.

Some allowance should be made for the Uncertainty of  $\Delta D_{spill}$  due to the fact that it is not tested at full scale.

# 4.2 ENGINE TEST FACILITIES

These facilities fall into two main classes: the Sea Level Static Test Bed (SLSTB) and the Altitude Test Facility (ATF), (Part (i) of Figure 6) both of which are capable of measuring thrust and mass flow so that the correlations required for in-flight thrust measurement may be established.

In the SLSTB the engine itself induces an airflow through the acoustic splitters as shown in Figure 8. The pressure, temperature and humidity are those of the outside ambient air.

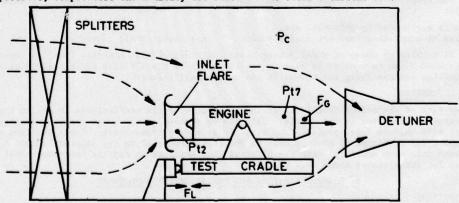


# FIG. 8 SEA LEVEL STATIC TEST BED

Part of the splitter flow passes through the engine while the rest passes around it to rejoin the engine exhaust in the detuner. The bellmouth inlet flare serves two purposes: it is an airflow measuring device, and it also balances the inlet Stream Force by tension in the duct walls due to 'suction' force on the flare which is approximately equal to the absolute Stream Force,  $F_2$ . Hence the net reaction  $F_L$  at the load cell is approximately equal (within 2 or 3 per cent, say) to  $F_G$ . It is usual to correct the load cell readings by means of comparisons with a reference engine run on an open-air test bed.

It is only possible to test the engine over a limited range of conditions in the SLSTB. Nozzle Pressure Ratio,  $P_{t7}/P_C$  usually varies from about 1.4 to 2.8, with a turbojet at sea level. This will only

cover a small part of the nozzle coefficient graphs shown in Figure 7 so a large extrapolation is required to flight conditions. This extrapolation may be guided by model nozzle test results but an uncertainty is introduced because of differences between real engine/nozzle flow and the more uniform model nozzle conditions.

A better calibration of the engine/nozzle can be obtained by testing in an ATF. Figure 9 shows a typical arrangement. Air, possibly dried to a low humidity is supplied to the Plenum Chamber at the appropriate value of  $P_t$  and  $T_t$  for the flight altitude and Mach number being simulated. Mass flow is measured in the Air Meter in the fixed ducting upstream of the engine.

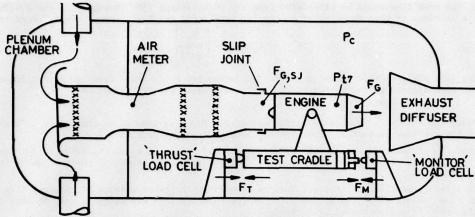


# FIG 9 ALTITUDE TEST CELL

A slip joint just in front of the engine separates the fixed ducting from the 'free' engine, and the Stream Force at this plane,  $F_{G,SJ}$  is derived from measurements using a 60-point pitot rake together with the known air mass flow. As the value of  $F_{G,SJ}$  can sometimes exceed the Gross Thrust, it is necessary to apply a Preload as shown to prevent a rearward-acting net force and to ensure that the 'Thrust' load cell always gives a positive reading,  $F_T$ . The preload  $F_M$  is measured by the 'monitor' load cell so that the net force on the Test Cradle would be

$$F_{L} = F_{T} - F_{M} \tag{55}$$

which might be a positive or negative quantity. A simplified equation for Gross Thrust would be:

$$F_{G} \simeq F_{L} + F_{G,SJ} \tag{56}$$

The full scale engine nozzle coefficients can be obtained over the full range of flight altitude and Mach number in the ATF, and plotted as shown in Figure 7.

A significant altitude effect is sometimes observed in the  $C_G$  and  $C_{D8}$  graphs. This would not be revealed by tests on the SLSTB, nor by model nozzle tests. It should be stressed that a particular set of coefficients is associated with a particular scheme of the gas generator instrumentation. The same scheme must be used in flight as in the ATF, otherwise the calibration is invalid. Indeed, the ATF test is a calibration of the gas generator instrumentation just as much as a calibration of the nozzle.

There are two respects in which the ATF engine thrust calibration does not faithfully simulate the flight situation:

- 1. The nozzle is surrounded by quiescent air.
- 2. The profiles at compressor face are nearly uniform (unless deliberately distorted).

Problem 1 is tackled by means of model nozzle tests, with and without external flow, as explained in Section 4.3. Problem 2 can be tackled by running special tests in the ATF with artifically-distorted engine inlet profiles and observing the change in the nozzle coefficients.

# 4.3 MODEL NOZZLE TESTING

The greater part of the defect from ideal of the full scale nozzle coefficients is due to the 3-dimensional nature of the flow in the nozzle. This can be studied on the model nozzle test rigs (Part (h) of Figure 6) with uniform inlet profiles and with air at modest temperature. Tests with and without external flow (Part (g) of Figure 6) produce data on the interference  $\Delta F$  to the internal thrust  $F_G$ . Comparison between this same model (g) with the external flow switched on and the reference model (f) produces data on Jet Interference Force  $\Delta \phi_a$ .

# 5. ERROR ESTIMATION AND THRUST OPTION MANAGEMENT

# 5.1 BASIC DEFINITIONS

Several attempts have been made in recent years to define the words "Accuracy" and "Precision".

Abernethy<sup>4</sup> and a British Standard<sup>5</sup> both propose that "Accuracy" be associated with absence of "Bias" or "Systematic Error", while "Precision" be associated with absence of "Random Error". However, it is very difficult to apply these words consistently because they are already in such common use in many other senses. To ensure a better discipline and to prevent a false impression of 'accuracy' from improper mean values, the following numerical Error Classes are introduced:

Class I : short term random error (Precision) during a single test period

Class II : short term fixed error during a single test period, but liable to random shift in

the longer term between tests

Class III : long term systematic error.

The spread of errors around a mean value can be described in terms of the standard deviation:

$$\sigma(x) = \sum_{i} \frac{(x_i - \bar{x})^2}{n-1}$$
 (57)

If the distribution is Gaussian, then about 95 per cent of  $x_i$  values lie within  $\pm 2\sigma(x)$ . If the distribution is Rectangular, then 100 per cent of  $x_i$  values lie within  $\pm 2\sigma(x)$ . The present text will deal with such "2 $\sigma$ " Error Limits of x, the notation for which is  $\pm EL$  (x).

The effect of an error xi upon a result y is given by the Influence Coefficient:

IC 
$$(y : x_i) = \frac{dy}{dx} \cdot \frac{x_i}{y}$$
 (58)

An alternative definition is the percentage change in y for 1 per cent change in  $x_i$ , which can be found by running a computer calculation with successive numerical perturbations in the  $x_i$  inputs.

If the errors in xi are independent then it is proper to combine them by Root-Sum-Squares, RSS:

$$\frac{\text{EL } (y, \text{ due to all } x_i)}{y} = \sqrt{\sum_{i} \left[ \text{IC } (y : x_i) \times \frac{\text{EL } (x_i)}{x_i} \right]^2}$$
 (59)

If, however, the errors are linked by some definite relationship, then RSS combination is invalid. Such non-independent errors are combined algebraically:

$$\frac{\text{EL } (y, \text{ due to all } x_i)}{y} = \sum_{i} \left[ \text{IC } (y : x_i) \times \frac{\text{EL } (x_i)}{x_i} \right]$$
 (60)

It is much more important to get the question of independence right than to worry about whether the distribution is Gaussian or Rectangular.

# 5.2 EARLY SENSITIVITY STUDY

A number of distinctly different options should always be provided for in-flight thrust measurement. Everyone accepts the wisdom of planning a certain amount of redundancy so that if a measurement vital to one method were to fail, then another option could take its place.

During the earlier stages of a new project a large number of different combinations of possible methods (20 say) should be considered. This number would be reduced to manageable size (10 say) by eliminating the least attractive methods with the aid of a Sensitivity Study. Table B illustrates the principle by comparing Option 1 against Option 5, but in practice all the possible options should be shown on the same table. There is no attempt at this stage to introduce Error Classes into the table, but the "instrumentation" is separated from the "Calibrated Coefficients".

Option 1 uses "AP" for  $F_G$ , but Option 5 uses "W  $\sqrt{T}$ ", while both obtain mass flow from fan characteristics. The Error Limits,  $EL(x_1)$  are multiplied by the appropriate Influence Coefficients,  $IC(y:x_1)$  and combined by RSS as in Equation (59).

TABLE B - EXAMPLE OF SIMPLE SENSITIVITY SURVEY (SINGLE ENGINED FIGHTER AIRCRAFT)

Flight condition: supersonic cruise with reheat on

Type of output:  $y = F_N$ 

ratio = 1.6		Option 1 "AP" method		Option 5 "W √T" method		
Input paramet	ter xi	Error Limit EL (xi)	IC(y:xi)	EL × IC	IC(y:x;)	EL × IC
Calibrations						
Full scale nozzle		1.5%	-		1.6	2.4
Full scale nozzle		1.5%	1.6	2.4	-	-
Full scale nozzle	CDs carpet	1.5%	-	-	-	-
Fan chic		1.5%	-0.6	-0.9	-0.6	-0.9
Turbine stator CD		2.0%	-	-	-	-
BP duct CD13		2.0%	- 0	-	-	- 1
Fuel cal. val. LCV	1	1.0%	0	0	0.5	0.5
Z EL (y) - √Ε [ ;	EL × IC 12	+	-	2.6%	-	2.6%
Instrumental	ion	Residence of the second				The state of
Eng. face	Pta	1.0%	-0.6	-0.6	0.3	0.3
Eng. face	Tt2	1.0%	0.4	0.4	-0.2	-0.2
Free stream	Pso	0.5%	0.2	0.1	0.2	0.1
By-pass duct	ΔP13	1.0%	-	-	5 PM -	-
By-pass duct	P813	1.0%	0.9	0.9	-0.5	0.5
Nozzle inlet	P 87	2.0%	1.8	3.6	0.4	0.8
CC fuel flow	WFC	2.0%	-	-	0.1	0.2
RH fuel flow	WFR	4.0%	-	-	0.5	2.0
LP spool	NL	0.5%	-1.1	-0.55	0.5	0.25
Nozzle area	As	2.0%	0.9	1.8	0.1	0.1
Power offtake	Q	0.5%	-	-	0	0
Services bleed	WR	1.0%	-		-0.4	-0.4
$z \in L(y) = \sqrt{\sum [z \in L \times IC]^2} \rightarrow$		-	4.2%		2.3%	

If one of these options had to be thrown out, the axe would fall on Option 1 with its per cent EL  $(F_N)$  = 4.2 per cent due to instrumentation, compared with 2.3 per cent for Option 5.

Another use of the Sensitivity Analysis table is to direct early attention to the critical items of measurement. In the case of Option 1 the most critical item is nozzle inlet pressure  $P_{87}$  - a modest 2 per cent EL in  $P_{87}$  produces 3.6 per cent EL in  $F_N$  due to the large influence coefficient of 1.8. In the case of Option 5 the most critical item is reheat fuel flow - the influence coefficient is only 0.5, but the large EL in  $W_{FR}$  of 4 per cent produces 2 per cent EL in  $F_N$ . Thus effort can be directed to improve these critical items of instrumentation at an early stage of a new project.

## 5.3 ADVANTAGE OF LINKED METHODOLOGY

For purposes of explanation, suppose preliminary calculations had been made of  $F_G$  and  $W_1$   $V_0$ . These could be regarded as inputs  $x_1$  to a calculation of a result y, thus:

$$F_N = F_G - W_1 V_0$$
 (61)

i.e. 
$$y = x_1 - x_1$$
 (62)

Providing the errors in  $F_G$  and  $W_1$   $V_0$  are <u>completely independent</u>, such as might occur in the so-called "AP" method of Reference 6 (an alternative name is "unlinked methodology") then we can apply Equation (59)

$$\frac{EL(y)}{y} = \sqrt{\left[IC(y : x_a) \times \frac{EL(x_a)}{x_a}\right]^2 + \left[IC(y : x_b) \times \frac{EL(x_b)}{x_b}\right]^2}$$
 (63)

Typical values of the Influence Coefficients might be

Suppose for argument's sake that the Error Limit in F<sub>G</sub>, due for example to nozzle area measurement were:

$$\frac{EL(F_G)}{F_G} = 1 \text{ per cent}$$

and suppose the Error Limit in  $W_1$  (and hence  $W_1$   $V_0$ ) due, for example, to shaft speed measurement were also:

$$\frac{EL(W_1 \ V_0)}{W_1 \ V_0} = 1 \text{ per cent}$$

then from Equation (63)

$$\frac{\text{EL}(F_{\text{N}})}{F_{\text{N}}} = \sqrt{\left[2 \times 1\right]^2 + \left[-1 \times 1\right]^2} = 2.4 \text{ per cent}$$
 (64)

Hence the Uncertainty of  $F_N$  has increased from the 1 per cent of either  $F_G$  or  $W_1$   $V_0$ . This is an undesirable feature of "unlinked methodology" with independent errors.

If, on the other hand, errors in  $F_G$  and  $W_1$   $V_0$  were of <u>completely common origin</u> then the root-sum-square combination of Error Limits does not apply. Instead, we have from Equation (60)

$$\frac{\text{EL}(F_{N})}{F_{N}} = \left[ \text{IC}(F_{N} : F_{G}) \times \frac{\text{EL}(F_{G})}{F_{G}} \right] + \left[ \text{IC}(F_{N} : W_{1} \mid V_{0}) \times \frac{\text{EL}(W_{1} \mid V_{0})}{V_{0}} \right]$$
(65)

Perhaps the "TTW" method of Reference 6 is being used. This is a "linked methodology" in which the same mass flow used for  $W_1$   $V_0$  is also used to calculate  $F_G$ . Suppose as before that the only relevant error is 1 per cent in W (1 per cent error in nozzle area is now irrelevant), then

$$\frac{EL(F_G)}{F_G} = \frac{EL(W_1 \ V_0)}{V_0} = 1 \text{ per cent}$$

With the same Influence Coefficients as before, we have from Equation (65):

$$\frac{\mathrm{EL}(\mathrm{F}_{\mathrm{N}})}{\mathrm{F}_{\mathrm{N}}} = \left[2 \times 17\right] + \left[(-1) \times 17\right] = 1 \text{ per cent}$$
 (66)

which is a vast improvement on the 2.4 per cent Uncertainty of Equation (64) caused by "unlinked methodology".

The beneficial effects of Non-Independent errors are here due to the minus sign in the Net Thrust Equation (61). In other cases this may not apply, for example in the case of a multi-engined aircraft the least Uncertainty comes with independent engines by root-sum-squares combination.

# 5.4 ERROR COMBINATIONS IN MULTI-ENGINED AIRCRAFT

It has been noted experimentally that the uncertainty of the total thrust of a multi-engined aircraft, expressed as a percentage, is less than that of a single engine. Reference 7 illustrates this phenomenon for the 6-engined XB-70 airplane.

In general, for an aircraft with & engines, suppose:

EL (one engine 
$$F_N$$
) = 10 per cent, say  $\equiv \frac{1}{\ell} \times 10\%$  of total  $F_N$  (67)

If the engines are independent then:

EL(total F<sub>N</sub> from & engines) = 
$$\int_{1}^{\frac{R}{L}} \left[ \frac{1}{k} \times 10 \right]^{2} Z = \frac{1}{\sqrt{k}} \times 10Z$$
 (68)

If the errors were common to all engines then:

EL(total F<sub>N</sub> from £ engines) = £ × 
$$\left[\frac{1}{2} \times 102\right]$$
 = 10% (69)

i.e. just the same as for one engine.

In practice some errors are independent, e.g. nozzle areas, while other errors are common, e.g. fuel calorific value. In such cases of mixed independent and common errors the Error Limit of  $F_N$  for the multi-engined aircraft would be:

ZEL (total 
$$F_N$$
 from  $\ell$  engines) = 
$$\left\{ \left[ \frac{1}{\sqrt{\ell}} \times \text{ZEL (each engine } F_N \text{ due to independent errors)} \right]^2 + \left[ \text{ZEL (each engine } F_N \text{ due to common errors)} \right]^2 \right\}^{\frac{1}{2}}$$
(70)

## 5.5 PROPAGATION OF ENGINE TEST CALIBRATION UNCERTAINTY TO FLIGHT (SINGLE-ENGINED AIRCRAFT)

An important concept in the transfer of Uncertainty from one stage to another is the 'fossilisation' into Class III which occurs before such transfer.

When an engine is calibrated in an ATF, the output\_is a set of curves of Thrust Coefficient  $C_G$  (related to the 'AP' method) or  $C_X$  (related to the 'W $\sqrt{T}$ ' method) and Nozzle Discharge Coefficient  $C_{D_8}$  etc. The Uncertainty of the best  $C_G$  curve is:

$$EL(\text{overall best } C_G \text{ curve}) = \left\{ \frac{1}{mn} \left[ EL_I(\text{spot point } C_G]^2 + \frac{1}{m} \left[ EL_{II}(\text{different } C_G \text{ tests}) \right]^2 + \left[ EL_{III}(C_G) \right]^2 \right\}_{(71)}^{\frac{1}{2}}$$

Three classes of error are involved here: Class I is very much alive during each calibration test, Class II shows variations from test-to-test, and Class III is present at constant level all the time. But once the Overall Best CG curve is selected, all this Uncertainty is frozen exclusively into a new, fixed, Class III. This 'fossilised' Uncertainty of the Thrust Coefficient is transferred to the in-flight thrust calculation. (The original Class I and II errors are now dead, but they have left their mark.)

When these curves are transferred from the ATF for use in flight their Uncertainties are also transferred, as 'fossilised' Class III Error Limits, but the situation is more complicated for two main reasons:

- (i) There may be implied methodology linking between the coefficients (indeed this is desirable)
- (ii) The aircraft may be multi-engined.

Item (i) is treated in the present Section 5.5, the added complication of (ii) in the next Section 5.6.

A full discussion is given in Reference 1 of an example of the propagation of Engine Calibration Uncertainty from ATF to flight, for a linked 'AP' method, using  $C_G$  and  $C_{D8}$  curves for a twin-engined aircraft. The salient features of that example are now summarised in the remainder of this present Section.

Treating  $C_G$  and  $C_{D8}$  separately to begin with, their uncertainty is transferred to flight according to the following equations:

$$\frac{\text{EL }(F_{N})}{F_{N}} = \text{IC }(F_{N}: C_{G}) \times \frac{\text{EL }(C_{G})}{C_{G}} = A \times \frac{\text{EL }(C_{G})}{C_{G}}$$
(72)

$$\frac{\text{EL }(F_{N})}{F_{N}} = \text{IC }(F_{N} : C_{D_{0}}) \times \frac{\text{EL }(C_{D_{0}})}{C_{D_{0}}} = B \times \frac{\text{EL }(C_{D_{0}})}{C_{D_{0}}}$$
(73)

However some of the test bed errors causing EL ( $C_G$ ) are the same ones that cause EL ( $C_{D_8}$ ) so some partial cancellation is to be expected.  $C_G$  and  $C_{D_8}$  are not independent and so a root-sum-squares combination is not valid.

Reference 1 shows that the non-independent part of the error relationship between  $C_0$  and  $C_{08}$  can be allowed for by including the error of  $C_{18}$ , thus:

$$\frac{\text{EL } (F_{\text{N}})}{F_{\text{N}}} = \sqrt{(A^2 + AB) \left[\frac{\text{EL } (C_{\text{G}})}{C_{\text{G}}}\right]^2 + (B^2 + AB) \left[\frac{\text{EL } (C_{\text{D}_{\text{R}}})}{C_{\text{De}}}\right]^2 - AB \left[\frac{\text{EL } (C_{\text{X}})}{C_{\text{X}}}\right]^2}$$
(74)

To use a numerical example taken from Reference 1, for a single-engine aircraft, the Error Classes of the ATF engine calibration could be combined, by root-sum-squares to yield the 'fossilised' Class III Error Limits as shown in Table C:

TABLE C - FOSSILISED ERROR LIMITS TRANSFERRED FROM ATF TO FLIGHT FOR SINGLE-ENGINED AIRCRAFT

	D	uring ATF tes	Fossilised Class III	
	Class I	Class II	Class III	RSS all classes
ZEL (CG curve)	0.21	0.49	1.15	1.5
ZEL (CDs curve)	0.22	0.50	1.14	1.4
ZEL (Cx curve)	0.08	0.13	0.26	0,3

Then using typical values of the Influence Coefficients A and B defined in Equations (72) and (73), viz: A = 2.18, B = -1.53 the resulting Error Limit of  $F_N$  from Equation (74) is:

$$\frac{\text{EL } (F_{\text{N}})}{F_{\text{N}}} = \int (4.75 - 3.34) \left[1.5\right]^2 + (2.34 - 3.34) \left[1.4\right]^2 + (3.34) \left[0.3\right]^2 = 1.27 \tag{75}$$

Now, the well-known but misused 'Old Theory' would have assumed complete independence between  $C_G$  and  $C_{D8}$  leading to a simple combination by root-sum-squares:

$$\frac{\text{EL } (F_{N})}{F_{N}} = \sqrt{A^{2} \left[ \frac{\text{EL } (C_{G})}{C_{G}} \right]^{2} + B^{2} \left[ \frac{\text{EL } (C_{D8})}{C_{D8}} \right]^{2}} = \sqrt{4.75 \left[ 1.5 \right]^{2} + 2.34 \left[ 1.4 \right]^{2}} = 3.9\%$$
 (76)

This value for the Uncertainty of  $F_N$  due to ATF calibration of  $C_G$  and  $C_{De}$  by the 'Old Theory' is an enormous over-estimation!

It must be pointed out that the beneficial error-cancelling effects only apply with 'Linked Methodology'. In the case discussed above  $F_G$  in flight would be derived from the calibration of  $C_G$  while Mass Flow would be derived from  $C_{D8}$ , hence common errors in the calibration of  $C_G$  and  $C_{D8}$  tend to be self-cancelling in flight. Other forms of 'Linked Methodology' can be used, e.g. Burcham's 'TTW' for which a rigorous Uncertainty-propagation theory could be devised for the calibration coefficients of that method.

# 5.6 IN-FLIGHT THRUST UNCERTAINTY OF A MULTI-ENGINED AIRCRAFT

Continuing the example of a "Linked AP" method using  $C_G$  for  $F_G$  and  $C_{D8}$  for mass flow, the complication of a multi-engined aircraft (in fact twin-engined) is introduced. The rigorous Equation (74) is applied separately to

i. errors independent of the other engine; ii. errors common to both engines.

A full explanation is given in Reference 1, in which the theory of Section 5.4 for the combination of independent and common errors in multi-engined aircraft is applied to the following cases:

- a. both engines calibrated in the ATF
- b. No. 1 engine calibrated in the ATF
- c. No. 2 engine calibrated in the SLSTB
- d. both engines calibrated in the SLSTB
- e. both engines calibrated in the ATF (Old Theory).

The complete prediction of in-flight thrust Uncertainty is shown in Table III taken from Reference 1. The end products are the Error Limits of twin-engined  $C_{\mathrm{T}}$  where:

$$C_{T} = \frac{F_{N_1} + F_{N_2}}{\frac{1}{2}\rho \ V_0^2 \ S} \tag{77}$$

For the case of both engines calibrated in the ATF, the "Old Theory" EL  $(C_T)$  of 2.7% remains a big overestimate compared with the EL  $(C_T)$  of 1.6% by the rigorous theory. Also, case (b+c) with EL  $(C_T)$  of 2.0% remains much nearer to case a. than to case d., i.e. there is a surprisingly good return to be had from calibrating just one of the two engines in the ATF, although the best scheme is to calibrate both engines there.

## 5.7 THE WEIGHTED MEAN RESULT OF SEVERAL OPTIONS

When flight testing begins, a modest number of options should remain available for use, and the problem is how to choose between them. Traditionally a single preferred method has been selected (perhaps with the aid of the Sensitivity Survey Table) and the results from this one method only are published. Often, however, there is controversy over the rival result of an alternative method. This situation can be avoided by the use of the weighted mean value, which combines the results of all the different options in the most efficient way, and none of the data are wasted (i.e. not used).

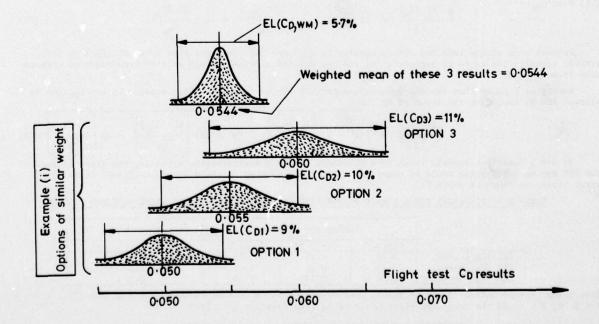
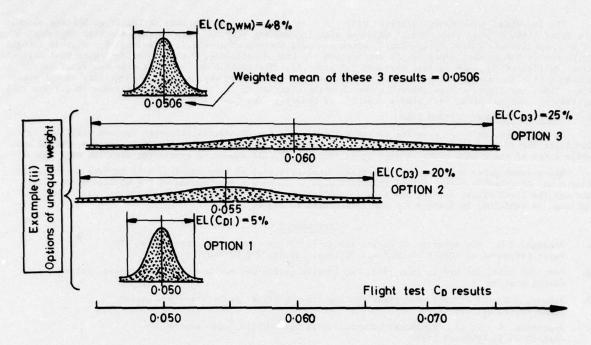


FIG. 10 (i) WEIGHTED MEAN FLIGHT TEST RESULT



# FIG. 10 (ii) WEIGHTED MEAN FLIGHT TEST RESULT

Figure 10 illustrates an example where the results are Drag Coefficients given by 3 different options of thrust measurement in flight. In example (i) the 3  $\rm C_D$  results of 0.050, 0.055 and 0.060 have similar Uncertainties or Error Limits of  $\pm 9$  per cent,  $\pm 10$  per cent and  $\pm 11$  per cent. The Weighted Mean Drag Coefficient is 0.0554 and its Uncertainty is 5.7 per cent. Thus, in this example (i) the Uncertainty of the Weighted Mean is much less than that of any of the single options and this is always the case when separate options have similar Uncertainty.

In example (ii), the three  $C_D$  results are the same as in example (i) viz: 0.050, 0.055 and 0.060, but this time Option 1 is supposed to have a much smaller Uncertainty of  $\pm 5$  per cent, than the other two,  $\pm 20$  per cent and  $\pm 25$  per cent. The Weighted Mean Drag Coefficient is 0.0506 and its Uncertainty is 4.8 per cent. Thus, in this example (ii) the Uncertainty is only a little better than that of the best option (Option 1), while the Weighted Mean Drag Coefficient is very close to that of the best option.

The lesson from example (ii) is that if any one option clearly has a much smaller Uncertainty than the rival options, then this one good option can be accepted straight away as the definitive result (although it would do no harm to calculate the weighted mean). But the situation is more likely to be as example (i) in which no single option is clearly the best. In this general case the Weighted Mean will produce a valuable reduction in the Uncertainty of the Drag Coefficient from the flight tests.

## 6. CONCLUDING REMARKS

## 6.1 THEME A: THRUST AND DRAG ACCOUNTING

The paper emphasises the distinction between a "Rearward-acting Force",  $\phi$  and a "Fundamental Drag", D. If all are aware of this, then the risk of misunderstanding will be reduced.

It should be recognised that the allocation of "Standard Net Thrust",  $F_N$  for separate study and engine testing, unhindered by "Intake Spillage Drag"  $D_{\rm Spill}$  and "Jet Interference Force",  $\phi_J$  is a convenient division of responsibilities. To arrive at the Net Propulsive Force:

NPF = 
$$F_{N,quies}$$
 -  $D_{spill,ref}$  -  $\phi_{c,dat}$  -  $\phi_{a,ref}$  -  $[\Delta F + \Delta \phi_a + \Delta D_{spill}]$  (37)bis

it is necessary to take account of several different but interrelated test facilities, both full scale and model scale, as summarised in Figure 6. The paper gives a modest description (Section 4.2) of the full scale engine test facilities, as the writer is on familiar ground here. Although no descriptions are offered for the other facilities indicated in Figure 6, these are just as necessary as the engine testing

# 6.2 THEME B: THE QUESTION OF ERROR INDEPENDENCE

To put the problem most simply, suppose a result y were the sum (or difference) of two items  $x_a$  and  $x_b$  then it is usually assumed that the Error Limit of y is given by "Root Sum of Squares":

$$EL(y) = \sqrt{\left[EL(x_a)\right]^2 + \left[EL(x_b)\right]^2}$$
 (78)

However, this is only valid if the errors of  $x_a$  and  $x_b$  are Independent of each other. It is much more important to get this right than to worry about whether a probability distribution is Gaussian or Rectangular or any other shape.

If the errors in  $x_a$  and  $x_b$  in the simple example were Common to each other, then the Error Limit of y is found by arithmetic addition or subtraction:

$$EL(y) = EL(x_a) + EL(x_b)$$
 (79)

or 
$$EL(y) = EL(x_a) - EL(x_b)$$
 (80)

The important point about Equation (80) is that common errors here tend to cancel each other so that the Error Limit of y is less than it would be with Independent errors. This is the essential explanation of the benefits of "Linked Methodology", which are well documented (see e.g. Reference 6). What is thought to be new in the present paper is the application of "Linked Methodology" theory to the Engine Test calibration coefficients  $C_{\rm G8}$  and  $C_{\rm D}$  (see Sections 5.5 and 5.6). The problem is complicated by the simultaneous presence of both Independent and Common errors, but the benfits are well worth the complexity of the analysis. Thus, the rigorous 'new theory' gives an Error Limit of  $F_{\rm N}$  of 1.6 per cent compared with 2.7 per cent by the 'old theory' which uses simple Root Sum of Squares, (see Table III).

## 6.3 THEME C: THE MANY-OPTIONS PLAN

It has always been the practice to start a new project with several different options available for In-Flight Thrust measurement. But the usual plan has been to select one method as the main preferred one, while a few of the others might be kept on as reserves in case something went wrong with the main method.

The present paper would regard this traditional treatment as very wasteful - it amounts to throwing away a lot of valuable data. A more efficient plan is to keep a good number of the options going right through the final flight testing and then to publish the "Weighted Mean Value" of the results of all the options, as explained in Section 5.7 and illustrated in Figure 10.

### REFERENCES

- Ascough, J C, The accuracy of engine thrust in flight from calibrations in an ATF. Paper presented to 10th ICAS Congress, Ottawa, Canada, 4-8 October 1976
- SAE, ARP 755A, 3rd draft, June 1973, Gas turbine engine performance nomenclature and station identification
- Annear, G G, Supersonic powerplant testing for pre-flight performance evaluation AGARD Paper, October 1976
- Abernethy, R B et al, Handbook: Uncertainty in Gas Turbine Measurements AEDC-TR-73-5, February 1973
- 5. BSS 1042, Part 1, 1964 Methods for the measurement of fluid flow in pipes, Section 4
- Burcham, F W, An investigation of two variations of the gas generator method to calculate the thrust
  of the afterburning turbofan engines installed in an F-lll airplane
  NASA TN D-6297, April 1971
- Arnaiz, H H, Techniques for determining propulsion system forces for accurate high speed vehicle drag measurements in flight AIAA 75-964, August 1975

## ACKNOWLEDGEMENTS

The paper has drawn upon the extensive expertise of colleagues in many branches of the UK aero industry. The author is particularly grateful for the help and criticism received from Mr. C. M. Milford of Hawker Siddeley Aviation on the subject of Thrust and Drag accounting.

## DISCLAIMER

Any views expressed are those of the author and do not necessarily represent those of the UK Ministry of Defence (PE).



Controller, HMSO, London, 1976

TABLE III CONPLETE PREDICTION OF IN-FLIGHT THRUST UNCERTAINTY FOR TWIN ENGINE AIRCRAFT

Extract from Reference 1

Flight condition: 0.9 M at low altitude, "high-power", dry

	II SIGN WOOD	10119	If both engines calibrated in ATF  If only this engine calibrated in SLATE  If noly this engine calibrated in SLATE  If both engines calibrated in SLATE  Both engines calibrated in ATF (Old Theory)	RSS all classes √∑[C × KL]* = MKL(Single engine spot point Cp)	Common to Combined both engines	1.46 1.70 ATF 1.17 3.26 SISTB 2.89 3.26 SISTB 1.17 3.65 ATF		
						RSS all c = %EL(Single	Independent of other engine	0.87 1.24 3.04 1.52 3.46
			וֹוֹוֹוֹוֹ					֓֓֓֓֓֓֓֓֓֓֓֓֓֓֓֓֓֓֓֓֓֓֓֓֓֓֓֓֓֓֓֓֓֓֓֓֓
		IC × EL Common	0.88 5 × 0.88	0.03	0.13	0.65	0.18	1.14 0.72 0.72 2.74 0.72
	Class III	IC * EL Independent	0.44 0.98 3 × 0.98 3 × 0.44 3 × 3.38	$\times$		$\times$		0.44 0.98 2.94 1.32 3.38
1		XET.	$\times$	0.1	0.25	201	0.5	$\times$
		IC × EL Common		-0.16	0.26/12	0.65/12	° -0.06/VZ	0.77 0.77 0.77 0.77
P. Sp	Class II	IC * EL Independent		X	0.26/42 - -	0.65//2	° 0.06/√2	0.56 0.56 0.56 0.56 0.56
5		WII.		0.5	0.5	÷ ; ,	0 0.5	$\times$
igle engine		IC × EL Common		-0.16		><	/	0.50 0.50 0.50 0.50 0.50
Part 1 Single engine Or	Class I	IC * EL Independent		X	0.26	0.26	90.0-	0.51 0.51 0.51 0.51
				0.5	0.5	1.0	0.5	$\times$
		1C (OT: x <sub>1</sub> )	X	-0.33 -0.18 -0.95	0.52	0.65	0.35	சேசபவக
		Input parameter	Linked calibration curves of $C_G$ , $C_{D\bullet}$ , $C_K$	Aircraft instrumentation (Pto - Pso)	Ps, - Pto Pto Fto	Engine Ae instrumentation WFCC	ren LCV TP	ASS separate classes $= \sqrt{\frac{1}{1}} \mathbb{C} \times \mathbb{E} \mathbb{J}^{8}$ $= \frac{\mathbb{E} \mathbb{E} (1 \text{ engine spot point } \mathcal{Q}_{2})}{\mathbb{E} \mathbb{E} (1 \text{ engine spot point } \mathcal{Q}_{2})}$

Part 2: Twin engined pircraft $C_{\rm T}$ = $\frac{F_{\rm NA}$ + $F_{\rm Me}}{qS}$	MEL (Twin engine spot point Cr.)
engines calibration in ATF	a + a [[0.87/25] + 1.46   44 = 1.58%
ngine calibration in ATF + 1 engine in SLSTB	b + c - [[1.24/2] + [3.04/2] + 1.178 4 = 2.038
gines calibration in SLSTB	d + d → {[1.52/√2] * + 2.892   41° = 3.08%
Each engine calibration in different ATF	
Each engine calibration in different SLSTB	0+0 [\$-04/J2] * +1.17°   18 = 2.45%
engines calibration in ATF (Old Theory)	· · · ·   [5.46/2] 2 + 1.172 118 = 2.718

# ESTIMATION OF LRAG AND THRUST OF JET-PROPELLED AIRCRAFT BY NON-STEADY FLIGHT TEST MANOEUVRES

by

J.A. Mulder

J.M. van Sliedregt

Department of Aerospace Engineering
Delft University of Technology
Delft
The Netherlands

## SUMMARY

When measuring aircraft performance or lift-drag characteristics in steady or non-steady flight numerical apriori information is required from engine (altitude) test facilities for an accurate determination of engine thrust. It is shown in the paper that this need for apriori information may be eliminated by an inflight calibration of the measuring probes for engines gross thrust and mass flow simultaneously with the measurement of the aircraft lift-drag characteristics.

Results are presented of 9 non-steady flight test manoeuvres with a Hawker Hunter mk VII jet aircraft at 10.000, 20.000 and 30.000 ft nominal flight altitude. Besides lift-drag characteristics and engine gross thrust and mass flow calibration factors several alternative performance characteristics as excess thrust in horizontal flight and also stability and control characteristics may be deduced from the measurements. The validity of the flight test results, in particular with respect to the inflight calibration of the gross thrust and mass flow measuring probes is, because of te particular aircraft exploited for the flight tests, restricted to the case of a socalled straight jet engine configuration and a non-flexible aircraft.

#### 1. INTRODUCTION

Aircraft lift and drag characteristics can be measured in flight by subtracting the components . engine net thrust along and perpendicular to airspeed from the corresponding components of the total aerodynamic force.

In steady-flight conditions the components of the total aerodynamic force follow directly from the condition of steady straight flight when only the flight path angle is known. Measurements in steady-straight conditions however are time consuming and furthermore the resulting accuracies limited due to unavoidable deviations from the nominal steady-straight flight condition.

For the measurement of the components of the total aerodynamic force in non-steady flight conditions additional instrumentation is required in the form of accelerometers. Furthermore the angle of attack must accurately be known. Usually the angle of attack is measured by means of a vane positioned on a boom some distance ahead of the aircraft in order to minimize aircraft induced position errors. Still an inflight calibration in a series of steady-straight measuring runs is necessary. The question then remains to what extent this calibration applies to the non-steady flight conditions for the measurement of lift and drag.

An alternative constitutes the technique of calculating rather than measuring the angle of attack. The reliability of this technique has by now been proven in the course of several flight test programs, Ref. 7, 13 and 18.

In order to obtain accurate lift-drag data engine net thrust must accurately be known in flight. In the case of jet propulsion net thrust is indirectly derived from gross thrust and mass flow. Gross thrust and mass flow can in principle be measured by means of total pressure and temperature probes positioned in the jet pipe exit. For reliable results these measuring probes must be calibrated on an engine (altitude) test facility. The result is usually expressed in terms of gross thrust and mass flow calibration factors. The implication is that for the measurement of aircraft lift and drag characteristics numerical apriori information is required from tests on an engine (altitude) test facility.

In the present flight test technique the need for numerical apriori information is eliminated by performing an inflight rather than a static calibration of the measuring probes simultaneously with the estimation of lift and drag characteristics.

The main features of the flight test method may be summarized as:

- 1) inflight calibration of the gross thrust and mass flow measuring probes;
- 2) calculation rather than the measurement of the angle of attack;
- 3) measurements are made in non-steady flight;
- besides lift and drag characteristics the calculation of several important performance and stability and control characteristics;
- 5) application of accurate instrumentation techniques.

Many aspects of the flight test technique have been develloped earlier, e.g. Ref. 7, where results are reported of a flight test program with a low speed piston engined aircraft.

In the present paper preliminary results are presented of a flight test program with a high subsonic jet aircraft, Fig. 1. Some data on the aircraft are given in Table 1.

Because of the particular aircraft exploited in the flight test program the validity of the results, in particular with respect to the inflight calibration of the gross thrust and mass flow measuring probes is restricted to the case of a socalled straight jet configuration and a non-flexible aircraft.

The paper has been organized as follows. In Section 3 the principles underlying the technique of calculating the angle of attack in non-steady flight are described. Section 4 provides an introduction to the

measurement of gross thrust and mass flow in flight. Furthermore the aerodynamic model and the engine model are presented. In Section 5 preliminary experimental results are described of 9 non-steady flight test manoeuvres at different nominal flight altitudes. From the 9 flight test manoeuvres 3 independent estimates of the gross thrust calibration factor could be obtained which were within 0.5% of the corresponding value of a static calibration. Concluding remarks are made in Section 6. In the appendix a brief introduction to regression analysis is presented.

## 2. NOTATION

•	aspect ratio, specific force (quantity sensed by an accelerometer)
<b>%</b>	exhaust area
A	effective exhaust area
•	scalar or vector of parameters
C	dimensionless coefficient, rate of climb
CDo	minimum drag coefficient
C <sub>L1</sub>	lift coefficient at minimum drag
C <sub>Lo</sub>	lift coefficient at zero angle of attack
D	aircraft drag
B	expectation operator
•	Oswald factor, residual of a regression analysis
g	acceleration due to gravity
h	nominal flight altitude
i <sub>p</sub>	angle between gross and thrust and X-axis
Ke	externally acting propulsive force
K <sub>1</sub>	internally acting propulsive force
k <sub>o</sub> , k <sub>1</sub>	constants in the expression of critical Mach number
L	aircraft lift
M	flight Mach number, aerodynamic moment about Y-axis
M <sub>c</sub>	critical Mach number
	aircraft mass
N	number of measurements
	engine rpm, normal load factor
,•	"dimensionless" engine rpm $n/\sqrt{\theta}$
npr	(2018년 12월 12일 - 12일
	nozzle pressure ratio pte/po
P	static pressure
Pt	total pressure mass flow
δ. δ.	
	"dimensionless" mass flow Q √θ/δ
q	rate of pitch
R R	total aerodynamic force
	resultant of lift and drag
Re	Reynolds number
Re	total correlation coefficient
r	angular speed about Z-axis
S	wing surface area
T	thrust, static temperature
7	"dimensionless" thrust T/6
To	static temperature at sea level S.A.
T <sub>t</sub>	total temperature
٧	airspeed, variance matrix
٧	aircraft weight
	speed of exhaust gases
x, xw	aerodynamic force along X, resp. X <sub>w</sub> -axis
x	vector or matrix of independent variables
x	state vector, element of X
×cg	location of aircraft centre of gravity
×mp	location of manoeuvre point
×np	location of neutral point

Y	scalar or vector of dependent variable
У	element of Y
z, z <sub>w</sub>	aerodynamic force along Z, resp. Zw-axis
$\Delta z_{T}$	change of altitude
α	angle of attack
Υ	flight path angle, ratio of specific heats
ε	equation error
δ	ratio p/p (sea level standard atmosphere)
$\delta_{\mathbf{e}}$	elevator angle
φ	roll angle
θ	pitch angle, ratio T <sub>+</sub> /T <sub>O</sub>
ρ	air density, simple correlation coefficient
σ	standard deviation

### Superscript

•	time derivative
* A REPUBLIC	estimated quantity
-	mean quantity
T	vector or matrix transpose
-1	matrix inverse

## Subscript

е	jet pipe exit
GT	gross thrust
i	engine inlet
m ENGLANDS	measured quantity
MF	mass flow
N	net thrust
pre	pre-entry
post	post-exit
0, ∞	undisturbed air flow at infinity
x, z	
$x_w, z_w$	refering to the resp. reference frames
x <sub>T</sub> , z <sub>T</sub>	

# Reference frames

All reference frames are vehicle carried, rectangular and right handed with the origin in the aircraft centre of gravity, Fig. 2.

X, Y, Z	body fixed reference frame, X, Z in the aircraft's plane of symmetry
Xw, Yw, Zw	air-trajectory reference frame
X <sub>T</sub> , Y <sub>T</sub> , Z <sub>T</sub>	vertical reference

## 3. CALCULATION OF FLIGHT PATH AND ANGLE OF ATTACK IN NON-STEADY FLIGHT

As stated in Section 1 the calculation of the aircraft trajectory and in particular of the time history of the angle of attack in non-steady flight constitutes an essential aspect of the present flight test technique.

The underlying principles are briefly described in this Section. The following set of differential equations represent the kinematical relations of an aircraft in symmetrical flight in a with respect to a flat earth horizontally and uniformly moving airmass:

$$\dot{\mathbf{v}}_{\mathbf{x_T}} = \mathbf{A_x} \cos \theta + \mathbf{A_z} \sin \theta$$

$$\dot{\mathbf{v}}_{\mathbf{z_T}} = -\mathbf{A_x} \cos \theta + \mathbf{A_z} \cos \theta + \mathbf{g}$$

$$\dot{\mathbf{\Delta z_T}} = \mathbf{v_{z_T}}$$

$$\dot{\theta} = \mathbf{q}$$
(3-1)

In the present flight test technique high accuracy instrumentation techniques result in very accurate measurements of the independent variables in (3-1) i.e.  $A_{x}$ ,  $A_{z}$  and q.

This means that an estimate of the time history of the state vector  $\mathbf{\hat{x}} \triangleq \operatorname{col} \left[ \hat{\mathbf{v}}_{\mathbf{Z_T}}, \hat{\mathbf{v}}_{\mathbf{Z_T}}, \hat{\Delta}_{\mathbf{Z_T}}^2, \hat{\theta} \right]$  could be calculated by numerical integration of (3-1) if the initial value of  $\mathbf{x}$  at the start of the flight test manoeuvre were exactly known.

Then also the time history of airspeed and angle of attack would follow immediately:

$$\hat{\mathbf{v}} = \left\{ \hat{\mathbf{v}}_{\mathbf{x_T}}^2 + \hat{\mathbf{v}}_{\mathbf{z_T}}^2 \right\}^{\mathbf{L}}$$

$$\hat{\mathbf{a}} = \hat{\theta} - \hat{\mathbf{\gamma}}, \ \hat{\mathbf{\gamma}} = - \operatorname{arctg} \frac{\hat{\mathbf{v}}_{\mathbf{z_T}}}{\hat{\mathbf{v}}_{\mathbf{x_T}}}$$
(3-2)

In practice the initial value of x is not exactly known.

It can be shown however that the initial value of x may be very accurately obtained by selecting that value which results in the smallest deviations between  $V_m$  and  $\hat{V}$ ,  $\Delta z_{T_m}$  and  $\Delta \hat{z}_T$  where  $V_m$  and  $z_{T_m}$  are directly measured with barometric transducers. This has been illustrated in Fig. 3 where different time histories result, when starting the numerical integration from different initial values. When the initial value of x is accurately known it may be expected that the corresponding time history of  $\alpha$  will also be very accurate.

The technique described above of calculating the time history of the angle of attack by selecting the "best" initial value of x has been successfully applied in different flight test programs as reported in Ref. 7 and 18.

In Ref. 11 a more advanced method for the calculation of the time history of  $\alpha$  is introduced. Two methods were compared in Ref. 13 yielding almost identical results.

4. THE ESTIMATION OF LIFT-DRAG CHARACTERISTICS AND INFLIGHT CALIBRATION OF GROSS THRUST AND MASS FLOW MEASURING PROBES

In symmetrical flight conditions the total aerodynamic force R is in the plane of symmetry of the aircraft. Per definition R is the resultant of engine net thrust  $T_N$  and the resultant of lift and drag,  $R^{\Xi}$ , Fig. 4.

The components of R along and perpendicular to the airspeed vector V can be written as, e.g. Ref. 14:

$$X_{W} = T_{GT} \cos (\alpha + i_{p}) - QV - D$$

$$Z_{W} = -T_{GT} \sin (\alpha + i_{p}) - L$$
(4-1)

in which QV represents engine ram drag.

 $X_W$  and  $Z_W$  can be determined in flight from the specific forces  $A_X$ ,  $A_Z$  and the angle of attack  $\alpha$  according to:

$$X_{W} = m (A_{X} \cos \alpha + A_{Z} \sin \alpha)$$

$$Z_{W} = m (-A_{X} \sin \alpha + A_{Z} \cos \alpha)$$
(4-2)

The specific forces  $A_{\chi}$  and  $A_{Z}$  are measured with accelerometers while the angle of attack  $\alpha$  may be calculated by applying the flight path reconstruction technique as described in Section 3.

When gross thrust  $T_{GT}$  and mass flow Q can sufficiently accurate be measured in flight, lift and drag follows directly from:

$$D = T_{GT} \cos (\alpha + i_{p}) - QV - X_{w}$$

$$L = -T_{GT} \sin (\alpha + i_{p}) - Z_{w}$$
(4-3)

(4-3) is used in classical techniques for the measurement of lift and drag characteristics in steady and non-steady flight. In steady flight  $X_W$  and  $Z_W$  may be readily obtained from the flight path angle and the condition of steady flight while in non-steady flight accelerometers and an estimate of the angle of attack must be used, e.g. Ref. 10 and 14.

Gross thrust and mass flow may be determined in flight from total pressure and temperature measurements in the jet pipe exit. This however requires the calibration of the total pressure and temperature measuring equipment on an engine (altitude) test facility. The result of such a calibration is usually expressed in terms of gross thrust and mass flow calibration factors as described in Section 4.1.

In the present flight test method it is proposed to derive these calibration factors from measurements in flight simultaneously with aircraft drag. The method is based upon an aerodynamic model, which is described in Section 4.2.

#### 4.1. THE MEASUREMENT OF GROSS THRUST AND MASS FLOW

Engine gross thrust can be defined in terms of net thrust and ram drag according to:

$$T_{GT} = T_N + QV \tag{4-4}$$

Engine net thrust is defined in Fig. 6 for the case of a straight jet configuration and idealized one dimensional flow. In Fig. 6  $X_{\rm pre}$  denotes the pre-entry thrust i.e. the thrust resulting from the compression of the airflow before entering the air intake,  $X_{\rm i}$  is called the internal thrust and  $X_{\rm post}$  denotes the post-exit thrust i.e. the thrust resulting from the expansion of the exhaust gases to the static pressure of the undisturbed external airflow.

Net thrust may now be written as, Ref. 2 and 19:

$$T_{N} = X_{pre} + K_{i} + X_{post}$$
 (4-5)

In the ideal case aerodynamic mechanism's convert the pre-entry and post-exit propulsive forces into  $K_e$  acting on the outside of the engine nacelle:

$$K_{e} = X_{pre} + X_{post}$$
 (4-6)

With (4-5) this results in the socalled Jones net thrust:

$$T_{N} = K_{i} + K_{e} \tag{4-7}$$

 $x_{\mathrm{post}}$  can be converted into a propulsive force acting on the outside of the engine nacelle only when the exhaust gases expand isentropically to the static pressure of the undisturbed external flow. In the one-dimensional flow model post-exit expansion will occur at supersonic speeds. In practice this implies adiabatic rather than isentropic expansion and  $x_{\mathrm{post}}$  reaches only a fraction of its theoretical value. In the socalled Pearson or Standard definition of net thrust the propulsive effect of the post-exit expansion is neglected all together resulting in a slightly less optimistic estimate of net thrust.

The two definitions of net thrust of Jones and Pearson have been compared in Fig. 7.

Because of the more realistic assumption concerning the post-exit expansion of the exhaust gases and furthermore the relatively minor differences up to moderate nozzle pressure ratio's the Pearson net thrust has been selected as the most appropriate in the present case.

Pearson gross thrust and engine mass flow can be calculated from total pressure and temperature measurements according to the following well-known formula's:

$$T_{GT} = A_{e} p_{t_{e}} \left\{ (\gamma + 1) \left( \frac{2}{\gamma + 1} \right) \exp \left( \frac{\gamma}{\gamma - 1} \right) - \frac{1}{npr} \right\}$$

$$Q = \frac{A_{e} p_{t_{e}}}{T_{t_{e}}} \left\{ \frac{\gamma}{R} \left( \frac{2}{\gamma + 1} \right) \exp \left( \frac{\gamma + 1}{\gamma - 1} \right) \right\}^{\frac{1}{2}}$$
(4-8)

which hold for supercritical nozzle pressure ratio's (i.e. npr > 1.85) and when the mass flow entering the engine equals the mass flow leaving the jet pipe exit.

Fig. 5 presents a view of the quipment for the measurement of total pressure and total temperature in the jet pipe as exploited in the present flight test program.

In (4-8)  $A_e$  denotes the geometrical jet pipe exhaust area. When applying these relations in practive, a so called effective exhaust area  $A_e^{\pm}$  must be substituted instead. The effective exhaust area is smaller compared to the geometrical exhaust area due to the following deviations from the idealized one dimensional model of jet flow, Ref. 17.

1) In Fig. 9 a more realistic two dimensional model is presented of jet exhaust flow, e.g. Ref. 4. In the one dimensional case static pressure would have a constant value of  $p_e$  (1). Because  $p_e(r) > p_e(1)$  there will be a <u>subsonic</u> post-exit expansion resulting in an effective exhaust area, Fig. 8.

In the sequence  $T_{GT}$  and Q indicate gross thrust and mass flow as calculated according (4-8) in contrast to (4-1) and (4-3) were these symbols indicated actual gross thrust and mass flow.

$$A_e^{\pm} = \iint \cos \phi \cdot dA < A_e$$
 (4-9)

surface of sonic flow

Gross thrust and mass flow calculated according to (4-8) must be multiplied by the ratio  $A_e^{\frac{\pi}{6}}/A_e$  to correct for this effect of subsonic post-exit expansion.  $A_e^{\frac{\pi}{6}}/A_e$  may be interpreted as a gross thrust and mass flow calibration factor:

$$C_{GT} = C_{MF} = \frac{A_e^{\frac{\pi}{4}}}{A_e} \tag{4-10}$$

In fig. 10  $\frac{A_e^{\frac{\pi}{4}}}{A_e}$  has been calculated for different values of nozzle pressure ratio and the parameter  $\frac{\Delta p_e(o)}{p_{t_e}}$ .

2) In practive a boundary layer will develope in the jet pipe which will affect gross thrust as well as mass flow. This may also be expressed in terms of a further reduction of effective exhaust area as well as in terms of a decrease of gross thrust and mass flow calibration factors.

The elliptical distribution of static pressure  $p_e$  results in identical gross thrust and mass flow calibration factors. Actual gross thrust and mass flow calibration factors may not be expected to be equal due to a different effect of the boundary layer on gross thrust and mass flow.

Prior to the present flight test program the gross thrust calibration factor was determined as a function of npr by comparing actually produced thrust  $T_{\overline{GT_m}}$  with the corresponding value resulting from (4-8) during a static test of the complete aircraft:

$$C_{GT} = \frac{T_{GT_m}}{T_{GT}} \tag{4-11}$$

resulting in the measured curve of Fig. 11.

The calculated curve is made with the help of Fig. 10 and shows the effect of the subsonic post-exit expansion. The difference between these curves, representing the effect of the boundary layer, reaches a constant value of approximately 0.03 as the npr increases. At the supercritical npr's of the flight test manoeuvres the parameter  $\Delta p_{\rm e}({\rm o})/p_{\rm te}$  proved to be almost constant resulting in a constant calibration factor of 0.99 for the effect of subsonic post-exit expansion as shown in Fig. 10. It may thus be concluded that in flight the gross thrust calibration factor will have an approximately constant value of 0.96.

The mass flow calibration factor cannot be determined without an engine (altitude) test facility. From Fig. 10 it follows that the mass flow calibration factor will be smaller than 0.99 because of the effect of the boundary layer. Experience from altitude test facilities has shown that, in contrast to the gross thrust calibration factor, the mass flow calibration factor may vary as a function of flight altitude, e.g. Ref. 3.

## 4.2. THE AERODYNAMIC AND ENGINE MODEL

A polar drag curve may be postulated according to:

$$c_{D} = c_{D_{O}} + \frac{(c_{L} - c_{L_{1}})^{2}}{\pi Ae}$$
 (4-12)

Substitution of (4-12) into (4-1) results in:

$$X_W = C_{GT} T_{GT} \cos (\alpha + i_p) - C_{MF}(h) QV - (C_{D_Q} + \frac{(C_L - C_{L_1})^2}{\pi Ae}) \frac{1}{2} \rho V^2 S$$

This may be written in dimensionless form with  $i_p = 0$ :

$$C_{X_{W}} = C_{X_{W_{O}}} + C_{GT} \frac{T_{GT}}{I_{1}\rho V^{2}S} \cos \alpha - C_{MF}(h) \frac{QV}{I_{1}\rho V^{2}S} +$$

$$+ C_{X_{WC_{L}}} C_{L} + C_{X_{WC_{L}^{2}}} C_{L}^{2}$$
(4-13)

In (4-13) the lift coefficient  $C_{\underline{L}}$  may be obtained from (4-1) in dimensionless from:

$$C_{L} = -C_{Z_{W}} - C_{GT} \frac{T_{GT}}{I_{P}V^{2}S} \cdot \sin (\alpha + i_{p}) \approx -C_{Z_{W}} - \frac{T_{GT}}{I_{P}V^{2}S} \sin \alpha$$
 (4-14)

because  $\frac{T_{GT}}{k_P v^2 s} \sin \alpha$  is small compared to  $c_{Z_W}.$ 

No supercritical drag rise is modeled, therefore (4-13) applies only to the subcritical flight region. The subcritical flight region is defined by:

$$M < M_C$$
 with  $M_C = \frac{1}{k_O + k_1 |C_L|}$  (4-15)

Approximate values of the constants in (4-15) for the present case follow from Ref. 8;  $k_0$  = 1.2, k = 0.4. The resulting critical Mach number is presented in Fig. 12.

The lift coefficient  $C_L$  may be written as:

$$C_L = C_{L_{\Omega}} + C_{L_{\Omega}}(M) (\alpha - \alpha_0)$$

A quadratic model is postulated for the variation of  $C_{\mathbf{L}_{\mathbf{Y}}}$  as a function of Mach number:

$$C_{\mathbf{L}_{\Omega}} = C_{\mathbf{L}_{\Omega}} + C_{\mathbf{L}_{\Omega M}} M + C_{\mathbf{L}_{\Omega M}^2} M^2$$

resulting in the following expression for  $C_T$ :

$$\begin{aligned} \mathbf{C_L} &= \mathbf{C_{L_O}} + \mathbf{C_{L_{CL}}} \, \alpha_O + \mathbf{C_{L_{CLM}}} \, \alpha_O \, \, \mathbf{M} + \mathbf{C_{L_{CLM}}}^2 \, \alpha_O \, \, \mathbf{M}^2 + \mathbf{C_{L_{CL}}} \, . \, \, \alpha + \mathbf{C_{L_{CLM}}} \, \, \alpha \mathbf{M} \\ &+ \mathbf{C_{L_{CLM}}}^2 \, \, \alpha \mathbf{M}^2 \, \approx \\ &\qquad \qquad \mathbf{C_{L_O}} + \mathbf{C_{L_O}} \, \, \alpha + \mathbf{C_{L_{CLM}}} \, \, \mathbf{M} + \mathbf{C_{L_{CLM}}}^2 \, \, \mathbf{M}^2 \end{aligned} \tag{4-16}$$

because  $\alpha$  is very small. (4-13) and (4-16) represent approximate models of dimensionless excess thrust  $C_{X_w}$  and lift coefficient  $C_{L}$ . Additional terms might be added to account for the effects of Reynolds number variations, elevator angle, non-steadiness of the airflow etc. The significance of these additional terms may be examined when analyzing actual flight test data. In the present case the effect of adding one or more of these terms to the models of excess thrust and lift coefficient proved to be very small. The pitch moment coefficient is written in the usual form:

$$c_{m} = c_{m_{0}} + c_{m_{\alpha}} \cdot \alpha + c_{m_{q}} \cdot \frac{q\bar{c}}{V} + c_{m_{\delta}} \cdot \delta_{e}$$
 (4-17)

in which the derivatives  $C_{m_Q}$ ,  $C_{m_Q}$ ,  $C_{m_Q}$  and  $C_{m_Q}$  for a given location of the aircraft centre of gravity may be expected to vary as a function of Mach number.

The aerodynamic model of the pitch moment does play a role in the correction methods described in Section 5.2. in particular with respect to the calculation of various stability and control characteristics. Most of these results will be left to a future report.

From Ref. 1 it follows finally that dimensionless gross thrust  $T_{GT}^{\sharp}$  and mass flow  $\varrho^{\sharp}$  may be written as a function of two dimensionless parameters  $n^{\sharp}$  and M:

$$T_{GT}^{\sharp} = T_{GT}^{\sharp} (n^{\sharp}, M)$$

$$Q^{\sharp} = Q^{\sharp} (n^{\sharp}, M)$$
(4-18)

In (4-18) the effect of viscosity has been neglected. Furthermore these relations do hold only when the compressor inlet guide vanes are fixed in one position. In the present series of flight test measurements these guide vanes have always been in the fully open position.

The engine model (4-18) may be identified simultaneously with the parameters in the aerodynamic model of  $C_{X_n}$ ,  $C_L$  and  $C_m$ . The resulting models are used in the above mentioned correction methods for the calculation of various performance and stability and control characteristics as described in Section 5.2.

## 5. EXPERIMENTAL RESULTS

The flight test program consisted out of 19 flight during which 45 non-steady flight test manoeuvres were executed and recorded. All measurements were made in nominally symmetrical flight conditions. In this Section the results are presented of 9 manoeuvres at three different nominal flight altitudes of 10.000, 20.000 and 30.000 ft.

For a proper interpretation of the results the shape of the non-steady flight test manoeuvre must first be described. Each manoeuvre is commenced at low speed and approximately steady symmetrical horizontal flight. The engine thrust is increased to a preselected level resulting in a longitudinal acceleration at nominally constant flight altitude.

Because the normal load factor remains close to 1 and rate of pitch (or aerodynamic pitch moment) small this would result in a quasi-steady increase of airspeed until a steady horizontal flight condition is reached. However at various instants regulary spaced in time the quasi-steady motion is interrupted and a non-steady pull-up-push-down type of manoeuvre is executed by means of the elevator control. In Fig. 13 time histories of the specific force along the vertical axis and the flight Mach number may illustrate the verbal description of the flight test manoeuvre.

From the measurements made of the flight test manoeuvre, performance as well as stability and control characteristics may be derived. In those cases, for instance during the initial phase of a flight test program, when performance characteristics are of a major concern compared to quantitative assessment of stability and control characteristics the non-steady pull-up-push-down manoeuvres need not to be executed.

A description of the flight test instrumentation system is presented in Ref. 9. In flight 20 variables are sampled and recorded in digital form at a rate of 20 per second. The resolution of the measurement system equals 0.01%. The accuracy of the inertical transducers is of the order of 0.01%, the accuracy of the barometric transducers is of the order of 0.1%.

## 5.1. IDENTIFICATION OF THE AERODYNAMIC AND ENGINE MODEL

The relations (4-13), (4-16), (4-17) constitute the aerodynamic and (4-18) the engine model. These relations may all be written symbolically as:

$$y(i) = a_0 x_0(i) + a_1 x_1(i) + ... + a_r x_r(i)$$
 (5-1)

in which i refers to a particular time instant  $t_i$  during the flight test manoeuvre. As described in the previous Sections y(i),  $x_0(i)$ ,  $x_1(i)$ , ...,  $x_r(i)$  are measured in flight. The residual e(i) is defined as:

$$e(i) = y(i) - \hat{a}_0 x_0(i) - \hat{a}_1 x_1(i) \dots - \hat{a}_r x_r(i)$$
 (5-2)

which will in general not be zero because of modelling and measurement errors. Least squares or regression estimates of the parameters in (5-1) can be calculated by minimizing  $\sum_{i=1}^{N} e^{2}(i)$  with respect to  $\hat{a}_{0}$ ,  $\hat{a}_{1}$ , ...,  $\hat{a}_{r}$ . The parameter estimation accuracies may be expressed in terms of a variance matrix which can be derived from the measurements simultaneously with the least squares estimates of the parameters.

A basic problem constitutes the selection of the "optimum" number of parameters in the model (5-1). It is shown in the Appendix that too many parameters result in unacceptably low estimation accuracies while a model which is to simple (i.e. a model in which one or more important parameters are missing) generates large equation errors or residuals.

A case in which the model did contain to many parameters has been encountered in the present flight test program with respect to the estimation of the parameters in the aerodynamic model of  $C_{X_W}$  (4-13). Because some of these parameters represent gross thrust and mass flow calibration factors as discussed in Section 4 the solution of this estimation problem is of particular importance.

It is well known that the mass flow calibration factor does vary as a function of flight altitude. Taking the mass flow calibration factor at 10.000 ft nominal flight altitude as a reference the following incremental mass flow calibration factors may be defined as:

$$\Delta C_{MF}(20) = C_{MF}(10) - C_{MF}(20)$$

$$\Delta C_{MF}(30) = C_{MF}(10) - C_{MF}(30)$$

in which the numbers 10, 20 and 30 refer to the nominal flight test manoeuvre altitudes of 10.000, 20.000 and 30.000 ft.

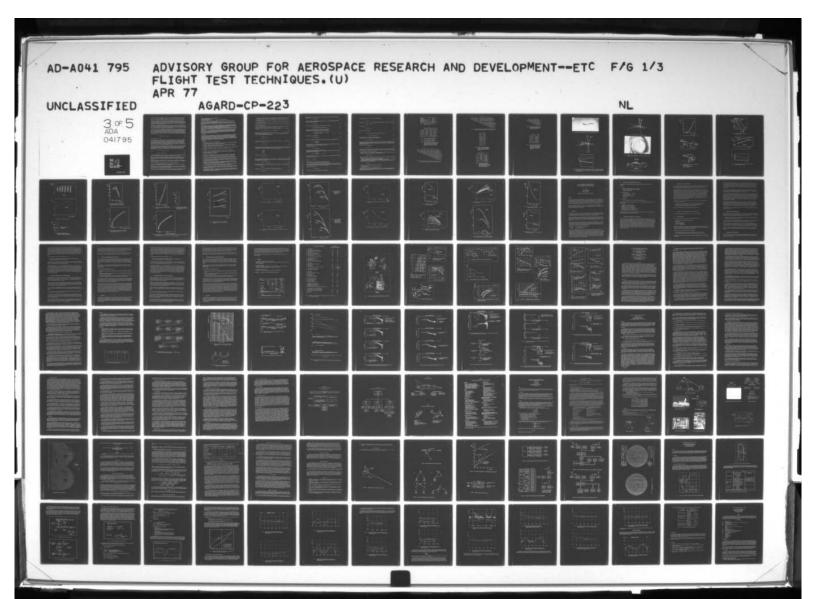
(4-13) may now be written as:

$$C_{X_{W}} = C_{X_{W_{O}}} + C_{GT} \frac{T_{GT}}{I_{1}\rho V^{2}S} \cos \alpha - C_{MF} (10) \frac{QV}{I_{2}\rho V^{2}S}$$

$$+ \Delta C_{MF} (20) \frac{Q(20) V}{I_{2}\rho V^{2}S} + \Delta C_{MF} (30) \frac{Q(30) V}{I_{2}\rho V^{2}S}$$

$$+ C_{X_{W_{C_{T}}}} \cdot C_{L} + C_{X_{W_{C_{L}^{2}}}} \cdot C_{L}^{2}$$
(5-3)

In (5-3) the variable  $\frac{Q(20)}{4\rho V^2 S}$  is identical to  $\frac{QV}{4\rho V^2 S}$  at 20.000 ft but vanishes at the other nominal flight



altitudes. The same holds for  $\frac{Q(30)}{4pV^2S}$  with respect to 30.000 ft nominal flight altitude. In contrast to (4-13), (5-3) contains only constant parameters while valid all the same for different nominal flight altitudes. An attempt can now be made to estimate these parameters by means of a regression analysis.

Because (5-3) does hold only in the subcritical flight regime (supercritical drag rise has not been modelled) only the subcritical data points of the flight test manoeuvres must be selected for the regression analysis. Therefore for the present, supercritical data points will be neglected. The next step is to also neglect the data points in the strongly non-steady parts of the flight test manoeuvres. This still leaves an ample amount of measurements and does eliminate beforehand the problemen of aerodynamic model inaccuracies in non-steady flight conditions.

The results of a regression analysis taking the remaining data points of a flight test manoeuvre at 10.000, 20.000 and 30.000 ft nominal flight altitude together, are presented in Table 2 and 3. It follows from Table 3 that the estimation errors of the gross thrust and mass flow calibration factors and the constant part of  $C_{X_W}$  are very highly correlated. This results in very high estimation errors and does indicate the model must be simplified in order to improve the accuracy of the results.

In Table 2 and 4 the results are presented of a simplified model resulting when substotuting  $C_{MF}(10) = C_{GT}$  in (5-3). It follows that the simplified model does equally well fit to the measurements while the correlation between the parameter estimation errors has considerably been reduced. This usually goes hand in hand with a significant improvement of parameter estimation accuracies as shown in Table 5. Results of 9 flight test manoeuvres are given in Fig. 14 and 15. It follows that the estimated gross thrust calibration factors are within 0.5% from the corresponding value of the static calibration discussed in Section 4. It follows from (5-3) that a parabolic polar drag curve can be calculated by substituting the estimated parameter values into:

$$c_D = -c_{X_{W_O}} - c_{X_{W_{C_L}}} \cdot c_L - c_{X_{W_{C_L}^2}} \cdot c_L^2$$
 (5-4)

The results are given in Fig. 16.

Fig. 19 shows mean and  $\frac{1}{2}$  10 region of 9 polar drag curves resulting when, as in the classical technique for the measurement of  $\frac{1}{2}$  11 ift-drag characteristics, (4-3) is applied using one set of values of the gross thrust and mass flow calibration factors. The range of subcritical  $C_L$  values traversed in the quasisteady portions of the flight test manoeuvres is approximately from 0.1 to 0.35. It follows that the corresponding maximum dispersion in terms of standard deviation of  $C_D$  amounts up to 4 to 5 drag counts. The dispersion of the individual curves however did not appear to be fully random in the statistical sense: curves from different nominal flight altitudes were mutually slightly "rotated". This effect might be ascribed to a minor, but yet unidentified aerodynamic model error.

Results of a regression analysis with the model of  $C_L$  (4-16) are given in Tabel 6 and 7. Only subcritical, quasi-steady data points were selected as described above and also three flight test manoeuvres at different nominal flight altitudes were taken together. The relatively high correlations between estimation errors of  $C_{L_{\rm CM}}$  and  $C_{L_{\rm CMM}}$  and the corresponding limited estimation accuracies need not be of much concern now because the interest is usually restricted to the resulting estimate of  $C_{L_{\rm CM}}$  (M) and  $C_{\rm L}$  according to:

$$C_{\mathbf{L}_{\Omega}}(\mathbf{M}) = C_{\mathbf{L}_{\Omega}} + C_{\mathbf{L}_{\Omega \mathbf{M}}} \cdot \mathbf{M} + C_{\mathbf{L}_{\Omega \mathbf{M}}^2} \cdot \mathbf{M}^2$$
 (5-5)

and:

$$C_{L} = C_{L_{O}} + C_{L_{\Omega}}(M) (\alpha - \alpha_{O})$$
 (5-6)

in which the individual parameter estimation errors do to a certain extent cancel out. Estimates of  $C_{L_Q}(M)$ ,  $C_{L_Q}$  and  $C_L$  as obtained from 9 flight test manoeuvres are presented in Fig. 17, 18 and 20.

Results of the estimation of the aerodynamic moment derivatives in (4-17) will be presented in a future report. In contrast to the estimation of the parameters in the model of  $C_{X_W}$  and  $C_L$ , here data points in the non-steady parts of the flight test manoeuvres are essential for the accuracy of the resulting estimates.

Finally the results of regression analyses with the engine model are given in Table 8. In this case also the accuracy of  $T_g^{\pm}$  and  $Q^{\pm}$  calculated from (4-18) is more important than the accuracies of the individual parameters in the model.

## 5.2. THE CALCULATION OF VARIOUS PERFORMANCE AND STABILITY AND CONTROL CHARACTERISTICS

In Section 4 an aerodynamic model was postulated for the aerodynamic forces  $X_w$  and  $Z_w$ , the aerodynamic moment M and also an engine model for gross thrust and mass flow.

The parameters in these models can be estimated from measurements in quasi-steady or non-steady flight as described in Section 5.1. After these models have been identified they may be exploited for the calculation of various performance, stability and control characteristics.

The principle is to correct the measurements for deviations from a given set of nominal standard conditions (like c.g., W, rpm, flight altitude, T), and to a set of different symmetrical flight conditions:

- 1) Steady straight flight with prescribed engine rpm.
- 2) Steady horizontal flight.
- 3) Accelerating horizontal flight.
- 4) Horizontal manoeuvring flight (i.e. C. = 0, normal load factor differs from 1).

The data points to which these corrections are applied are selected such that the magnitudes of these corrections can be expected to be relatively small.

For instance, data points during quasi-steady flight are used when correcting to flight condition 1), 2) and 3) while data points in the non-steady parts of the manoeuvre are exploited when correcting to flight condition 4).

13

The corrections are calculated using the aerodynamic and engine model which were identified earlier. When the corrections are small, model errors will have a neglectable effect on the results and thus any scatter must be attributed to measurement errors, atmospheric disturbances and inexact knowledge of aircraft-weight and c.g. location. For a more detailed discussion reference can be made to Ref. 15.

Fig.'s 21 to 27 present results of correcting the data point in quasi-steady flight, while Fig.'s 28 to 32 present results of correcting data points in non-steady flight to the specific symmetrical flight conditions defined above.

In Fig.'s 21, 22, 25, 26, 28 and 29 indivial corrected data points of one flight test manoeuvre are shown while in Fig.'s 23, 24 and 25 different flight test manoeuvres have been compared. From these figures it may be deduced that aircraft performance characteristics as rate of climb in steady straight flight and excess thrust in horizontal straight as well as in horizontal manoeuvering flight could be determined accurately in quasi-steady and non-steady flight.

#### 6. CONCLUSIONS

In the case of straight jet propulsion and a rigid aircraft it is shown that measurements of lift and drag characteristics can be made without the need for numerical apriori information in the form of gross thrust and mass flow calibration factors from tests on an engine (altitude) test facility. These calibration factors may be estimated in flight simultaneously with aircraft lift and drag. Three independent flight estimated values of the gross thrust calibration factor proved to be within 0.5% of the corresponding value of a static thrust calibration. It has further been shown that various performance and stability and control characteristics may simultaneously be obtained from the measurements.

## 7. REFERENCES

- 1. AGARD, Flight test manual, Volume 1, Performance, 1959.
- An., "Definitions of the thrust of a jet engine and of the internal drag of a ducted body", The Journal
  of the Royal Aeronautical Society, Volume 59, No. 536, August 1955.
- J.C. Ascough, "Procedures for the measurement of engine thrust in flight", AGARD Flight Mechanics Symposium on "Flight Test Techniques", Cologne, October 1976.
- 4. T.W. Davidson, "Measurement of net thrust in flight", Journal of Aircraft, Vol. 1, No. 3, May-June 1964.
- H. Mc.Donald, P.F. Hughes, "Righ subsonic after body drag", Journal of Aircraft, Vol. 2, No. 3, June 1965.
- 6. N.R. Draper, H. Smith, "Applied Regression Analysis", John Wiley & Sons, Inc., March 1968.
- O.H. Gerlach, "Determination of performance and stability parameters from non-steady flight test manoeuvres", SAE paper no. 700236, March 1970.
- 8. S.F. Hoerner, "Fluid-dynamic drag", 1958.
- R.J.A.W. Hosman, "Advanced flight test instrumentation: design and calibration", AGARD Conference proceedings no. 172 on "Methods for Aircraft State and Parameter Identification", November 1974.
- 10. K.W. Lliff, "Maximum likelihood estimates of lift and drag characteristics obtained from dynamic aircraft maneuvers", AIAA 3rd Atmospheric Flight Mechanics Conference, Arlington, Texas, June 1976.
- H.L. Jonkers, "Application of the Kalman filter to flight path reconstruction from flight test data
  including estimation of instrumental bias errors", Report VTH-162, Department of Aerospace Engineering,
  Delft University of Technology, February 1976.
- 12. H.W. Kleingeld, "Design and evaluation of a symmetric flight test manoeuvre for the estimation of performance, stability and control characteristics", AGARD Conference Proceedings no. 172 on "Methods for Aircraft State and Parameter Identification", November 1974.
- 13. J.A. Mulder, "Estimation of the aircraft state in non-steady flight", AGARD Conference Proceedings no. 172 on "Methods for Aircraft State and Parameter Identification", November 1974.
- 14. E.C. Rooney, "Development of techniques to measure in-flight drag of a U.S. Navy fighter airplane and correlation of flight measured drag with wind tunnel data", AGARD Conference Proceedings No. 124 on "Aerodynamic Drag", April 1973.
- 15. J.M. van Sliedregt, J.A. Mulder, "Procedures for the calculation of performance, stability and control characteristics from non-steady flight data", Memorandum M-256, Department of Aerospace Engineering, Delft University of Technology, to be published.

- 16. J. Stephenson, R.T. Shields, D.W. Bottle, "An investigation into the pitot rate method of measuring turbo jet engine thrust in flight", A.R.C. Technical Report, C.P. No. 143 (15, 509), 1954.
- J.P.K. Vleghert, "Bepaling van de stuwkracht van straalmotoren", Report TM1922, National Aerospace Laboratory, March 1964.
- R.C. Wingrove, "Applications of a technique for estimating aircraft states from recorded flight test data", AIAA paper 72-965, 1972.
- 19. H. Wittenberg, "The propulsion of supersonic airplanes", De Ingenieur, Vol. 74, No. 6, February 1962.
- 8. APPENDIX. REGRESSION ANALYSIS

For the sake of completeness a brief introduction to regression analysis is presented in this Section. For a more detailed treatment reference can be made to the literature, e.g. Ref. 6.

In regression analysis the following problem is posed. Estimate the parameters  $a_0$ ,  $a_1$ , ...,  $a_r$  of the linear model:

$$y(i) = a_0 x_0(i) + a_1 x_1(i) + ... + a_r x_r(i) + \varepsilon(i)$$
 (a-1)

when N sets of values are given of the independent variables  $x_0(i)$ ,  $x_1(i)$ , ...,  $x_r(i)$  and the dependent variable y(i), while  $\varepsilon(i)$  is unknown. In (a-1)  $\varepsilon(i)$  results from model or measurement errors.  $\varepsilon(i)$  is usually assumed to be adequately represented by an independent random sequence with:

$$E\{\varepsilon(i)\} = 0$$

$$E\{\varepsilon(i)\ \varepsilon(j)\} = \sigma^2\ \delta_{ij}$$

$$i = 1, \dots, N$$

(a-1) can be written more compactly by defining the row vector  $X(i) = [x_0(i), x_1(i), ..., x_r(i)]$  and the column vector  $a = col[a_0, a_1, ..., a_r]$ :

$$y(i) = X(i) a + \varepsilon(i)$$
  
 $i = 1, ..., N$ 
(a-2)

In regression analysis it will be convenient to manipulate with all N equations (a-2) simultaneously. To achieve this, the N dimensional column vectors Y and  $\varepsilon$  are defined as Y = col[y(o), y(1), ..., y(N)] and  $\varepsilon$  = col[ $\varepsilon$ (1),  $\varepsilon$ (2), ...,  $\varepsilon$ (N)]. Furthermore the N x r matrix X is defined as:

$$x = \begin{bmatrix} x(1) \\ x(2) \\ \vdots \\ x(N) \end{bmatrix}$$

after which (a-2) can be written as:

$$Y = Xa + \varepsilon$$
 (a-3)

When  $\hat{a}$  is an estimate of the parameter vector a the residual e(i) is defined as  $e(i) = y(i) - X(i)\hat{a}$ . Defining the N dimensional vector e in the usual way by e = col[e(i), e(2), ..., e(N)] the sum of the squares of the residuals e(i) can be written as:

$$\mathbf{e}^{\mathbf{T}}\mathbf{e} = (\mathbf{Y} - \mathbf{x}\hat{\mathbf{a}})^{\mathbf{T}} (\mathbf{Y} - \mathbf{x}\hat{\mathbf{a}}) \tag{a-4}$$

The least squares estimate of a is obtained by minimizing (a-4) with respect to  $\hat{a}$ . A necessary condition for  $\hat{a}$  to minimize (a-4) is:

$$\frac{\partial e^{T}e}{\partial z} = 0 \tag{a-5}$$

Substitution of (a-4) in (a-5) leads directly to the socalled normal equations:

$$[x^Tx] \hat{a} = x^Ty \tag{a-6}$$

when the matrix  $[x^Tx]$  is positive definite (i.e. its inverse exists) the least squares estimate of a follows from:

$$\hat{\mathbf{a}} = [\mathbf{x}^{\mathrm{T}}\mathbf{x}]^{-1} \mathbf{x}^{\mathrm{T}}\mathbf{y}$$
 (a-7)

Besides the numerical value an important characteristic of the least squates estimate constitutes the accuracy of â which is expressed by:

$$\Delta a = \hat{a} - E(\hat{a}) \tag{a-8}$$

E(a) can be calculated by substituting (a-3) into (a-7) which then yields:

$$E(\hat{a}) = E\{[x^Tx]^{-1} x^Tx \ a + [x^Tx]^{-1} x^T \ \epsilon\} = a$$
 (a-9)

because  $E(\epsilon)=0$ . This means that  $\hat{a}$  is a socalled inbiased estimate of a. The variance matrix of the estimation errors  $\Delta a$  may now be written as:

$$V(\hat{\mathbf{a}}) = \mathbf{E} \left\{ \Delta \mathbf{a} \Delta \mathbf{a}^{T} \right\} = \mathbf{E} \left\{ [\hat{\mathbf{a}} - \mathbf{E}(\hat{\mathbf{a}})] [\hat{\mathbf{a}} - \mathbf{E}(\hat{\mathbf{a}})]^{T} \right\} =$$

$$= \mathbf{E} \left\{ [\hat{\mathbf{a}} - \mathbf{a}] [\hat{\mathbf{a}} - \mathbf{a}]^{T} \right\}$$
(a-10)

Substitution of (a-7) then results in:

$$V(\hat{a}) = \sigma^2 [x^T x]^{-1}$$
 (a-11)

From (a-11) the matrix of simple estimation error correlation coefficients may be obtained from:

$$[\rho_{ij}] = \frac{v_{ij}}{\{v_{ii} \ v_{jj}\}^{l_i}}$$

In many applications  $\sigma^2$  is not precisely known. This will be the case in particular when  $\epsilon(i)$  must be attributed to model errors rather than measurement errors of  $\gamma(i)$ .

Then  $\sigma^2$  may be estimated by:

$$\hat{\sigma}^2 = \frac{1}{n-r-1} e^{\mathrm{T}} e^{\mathrm{T}}$$

which can be calculated posterior to the calculation of  $\hat{a}$ . The goodness of fit of the mathematical model to the measurements is expressed by the so called total correlation coefficient  $R_t$  defined as:

$$R_{t} = \left\{1 - \frac{e^{T}e}{y^{T}y}\right\}^{l_{2}}, \qquad 0 \leq R_{t} \leq 1$$

In case of perfect fit  $e^{T}e=0$  and thus  $R_{t}=1$ . When the model (a-3) is completely invalid the parameter estimate will be identical zero:

â = 0

hecause of.

$$x^T y = 0$$

Then it follows that e=Y and  $R_{r}$  reaches its minimum value of zero. (a-7), (a-11) and (a-12) are well known results in regression analysis.

In flight testing problems, when accurate instrumentation systems are exploited errors measurement errors can be relatively small. It is therefore important to further evaluate the effect of modelling errors on the accuracy and the numerical value of the least square estumate â.

Assume the actual model to be:

$$Y = X_1 a_1 + X_2 a_2 + \varepsilon$$
 (a-13)

The state of the second second

in which a, and a, are r and s dimensional vectors of parameters.

A least squares estimate of a is made by using a simplified model

$$Y = X_1 a_1 \tag{a-14}$$

Minimization of  $e_1^T e_1$  with  $e_1 = Y - X_1 \hat{a}_1$  leads via the necessary conditions to the set of normal equations:

$$[x_1^T x_1] \hat{a}_1 = x_1^T y$$
 (a-15)

and the estimate of a,:

$$\hat{\mathbf{a}}_{1} = [\mathbf{x}_{1}^{T}\mathbf{x}_{1}]^{-1} \mathbf{x}_{1}^{T}\mathbf{y}$$
 (a-16)

when  $[X_1^T X_1]$  is positive definite.

From:

$$E(\hat{a}_1) = [x_1^T x_1]^{-1} x_1^T E(y) = [x_1^T x_1]^{-1} x_1^T [x_1 a_1 + x_2 a_2] =$$

$$= a_1 + [x_1^T x_1]^{-1} [x_1^T x_2] a_2$$
(a-17)

follows that now  $\hat{a}_1$  will in general be a biased estimate of  $a_1$ . The estimate variance of the residuals may now be obtained from:

$$\hat{\sigma}_{1}^{2} = \frac{1}{N-r-1} e_{1}^{T} e_{1}$$
 (a-18)

In practical applications a major problem is the selection of the "optimum" number of parameters in the mathematical model of the physical proces. In general a trade off must be made between reduced extimation accuracies after an additional parameter is added and a better fit of the model to the measurements. This may be clarified as follows.

The matrix X2 can always be written as:

$$x_2 = x_1C + \Delta x_2 \tag{a-19}$$

in which C denotes a constant r x s matrix. It follows from (a-19) that each column of the matrix  $X_2$  may be constituted out of a linear combination of the column of the matrix  $X_1$  and one column of the matrix  $\Delta X_2$ .

The following important results may now be derived.

1) When  $\Delta x_2$  is very small, i.e. the columns of  $x_2$  depend linearly on the columns of  $x_1$ , the estimate of the parameter  $a_1$  using the simplified model will be biased according to:

When attempting however to eliminate this bias by adding the parameters  $a_2$  to the model it can be shown that:

that: a)  $\hat{\sigma}_1^2 = \hat{\sigma}^2$ , the variance of the residuals has not been decreased,

b) parameter estimation errors tend to infinity due to singularity of the matrix X<sup>T</sup>X, one or more simple correlation coefficients in the estimation error correlation matrix will approach 1.

2) In case all elements of C are identical zero  $(x_2 = \Delta x_2)$ , the estimate of the parameter  $a_1$  using the simplified model will be unbiased because of:

$$x_1^T \Delta x_2 = 0$$

When adding now the parameters a2 to the model it follows that:

a)  $\hat{\sigma}_1^2$  decreases to  $\hat{\sigma}^2$ ,

b) parameter estimation errors of a1 will remain unchanged.

It may be deduced that in case 1) extra parameters should not, while in case 2) extra parameters may be added to the model. In practical situations the decision whether or not to add an extra parameter to the model might be more difficult to make.

Length	14.90 m
Wing span	10.26 m
Wing surface	33.30 m <sup>2</sup>
a chord wing sweep angle	40°
Max. take of weight	9752 kgf
Engine type	Rolls Royce Avon 122
Max. thrust at sea level	3450 kgf

Table 1. Some data on the Hawker Hunter mk VII laboratory aircraft.

	flight altitude (ft)	Model 1	Model 2
ē (drag	10.000	+0.12	+0.12
counts	20.000	-0.01	-0.02
	30.000	-0.09	-0.09
σ <sub>e</sub> (drag	10.000	4.29	4.15
counts	20.000	3.52	3.63
	30.000	2.08	2.13
Rt		0.999398	0.999402

- Model 1. Three thrust calibration parameters:  $C_{MF}(10) = C_{GT}$ ,  $\Delta C_{MF}(20)$ ,  $\Delta C_{MF}(30)$ .
- Model 2. Four thrust calibration parameters:  $C_{GT}$ ,  $C_{MF}$ (10),  $\Delta C_{MF}$ (20),  $\Delta C_{MF}$ (30).
- Table 2. Total correlation coefficients and residuals of regression analysis with different models of C<sub>Xw</sub>. Three flight test manoeuvres at different flight altitudes. Subcritical, quasi-steady data points (1 drag count 0.0001).

	CXWCL2	CXWCL	ΔC <sub>MF</sub> (30)	ΔC <sub>MF</sub> (20)	C <sub>MF</sub> (10)	CGT	c <sub>xwo</sub>
CXwo	+0.485	+0.328	-0.998	-0.998	-0.998	+0.989	+1.000
CGT	+0.485	+0.360	-0.991	-0.993	-0.993	+1.000	
C <sub>MF</sub> (10)	-0.457	-0.310	+0.999	+0.999	+1.000		
ΔC <sub>MF</sub> (20)	-0.454	-0.305	+0.999	+1.000			
ΔC <sub>MF</sub> (30)	-0.455	-0.298	+1.000				
CXWCL	+0.863	+1.000					
CXWCL2	+1.000						

Table 3. Correlation coefficients of parameter estimation errors resulting from a regression analysis with model 2 of  $C_{X_{\mathbf{W}}}$  (Ref. Table 2).

CXWO	CGT		ΔC <sub>MF</sub> (20)	ΔC <sub>MF</sub> (30)	$c^{X^{M}C^{\Gamma}}$	$C_{X_{\mathbf{W}_{\mathbf{C_L}^2}}}$	
+1.000	-0.555	-	-0.087	-0.288	+0.388	+0.670	CXwo
	+1.000	- T	+0.248	+0.692	+0.488	+0.032	CGT
		-	-	-	-	-	
			+1.000	+0.565	+0.369	+0.214	ΔC <sub>MF</sub> (20)
				+1.000	+0.525	+0.111	ΔC <sub>MF</sub> (30)
					+1.000	+0.854	CXWCL
						+1.000	CXWCL2

Table 4. Correlation coefficients of parameter estimation errors resulting from a regression analysis with model 1 of  $C_{X_W}$  (Ref. Table 2).

c <sub>Xwo</sub>	24
C <sub>GT</sub>	10
C <sub>MF</sub> (10)	64
ΔC <sub>MF</sub> (20)	73
ΔC <sub>MF</sub> (30)	46
CXWCT	1
CXWCL2	1

Table 5. Comparison of estimation accuracies of model 2 with model 1 expressed as the ratio of normalized parameter estimation error standard deviations (Ref. Table 2).

	flight altitude (ft)	
ē	10.000	-0.0031
	20.000	+0.0074
	30.000	-0.0029
σ <sub>e</sub>	10.000	0.0036
	20.000	0.0045
	30.000	0.0019
Rt		0.997855

Table 6. Total correlation coefficient and residuals of regression analysis with model of  $C_L$ . Three flight test manoeuvres at different flight altitudes. Subcritical, quasi-steady data points.

	CLOM2	CLOM	$c_{L_{\alpha}}$	Cro
CLo	-0.322	+0.282	-0.283	+1.000
CLa	+0.981	-0.995	+1.000	
CLam	-0.995	+1.000		
CLOM	+1.000	148E		

Table 7. Correlation coefficients of parameter estimation errors resulting from a regression analysis with model of  $\mathrm{C_L}$  (Ref. Table 5).

	T <sub>CG</sub>	δ <sub>æ</sub>
ē	-0.11	-0.0014
	+0.51	+0.0072
	-0.40	-0.0059
σ <sub>e</sub>	16	0.021
	11	0.019
	22	0.045
Rt	0.999817	0.999159

Table 8. Total correlation coefficient and residuals of regression analysis with model of "dimensionless" thrust  $T_{CG}^{\bullet}$  and "dimensionless" mass flow  $Q^{\bullet}$ . Three flight test manoeuvres at different flight altitudes.

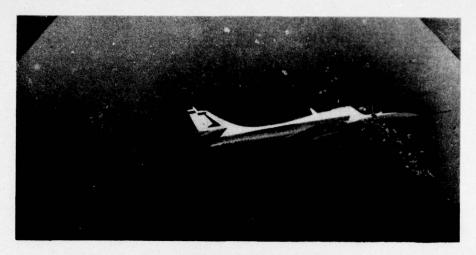


Fig. 1. Hawker Hunter laboratory aircraft with static pressure trailing cone.

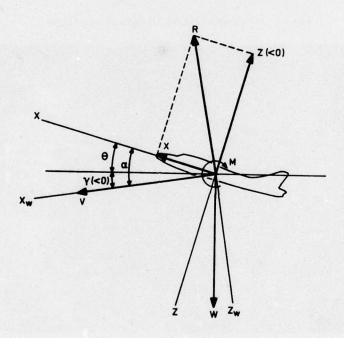


Fig. 2. Body and wind axes in symmetrical flight.

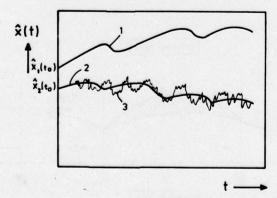


Fig. 3. Principle of aircraft trajectory estimation. Trajectory 1 from intertial information and initial State vector  $\hat{\mathbf{x}}_1$  (t<sub>0</sub>), trajectory 2 from inertial information and "optimal" initial State vector  $\hat{\mathbf{x}}_2$ (t<sub>0</sub>), resulting in a "best" fit to trajectory 3 from barometric measurements.

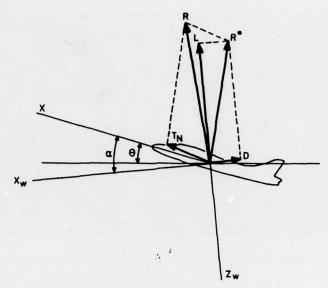


Fig. 4. Aerodynamic forces in symmetrical flight.

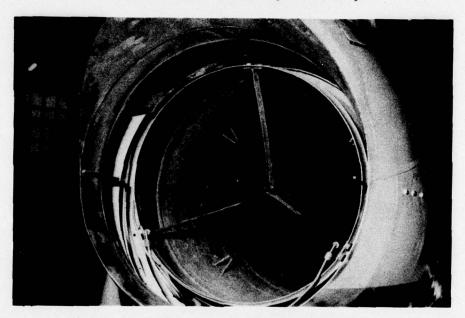


Fig. 5. Measurement of mean total pressure, central static pressure and total temperature in the jet pipe.

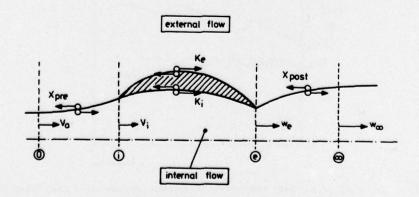


Fig. 6. Definition of engine net thrust.

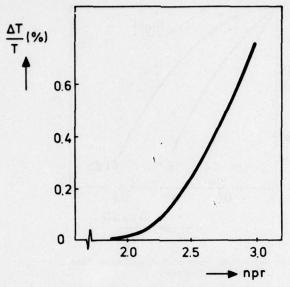


Fig. 7. Difference between Jones and Pearson net thrust.

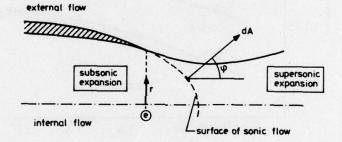


Fig. 8. Effect of Subsonic post exit expansion.

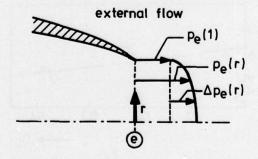


Fig. 9. Two-dimensional model for gross thrust and mass flow measurement,  $p_{\text{te}}(r) \text{ and } T_{\text{te}}(r) \text{ constant.}$  If npr > 1.85 then  $p_{\text{e}}(1)$  >  $p_{\infty}$ .  $\Delta p_{\text{e}}(r)$  is ellipsoid.

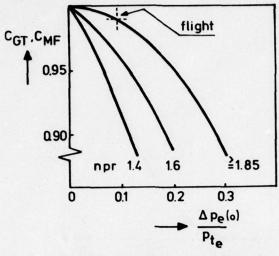


Fig. 10. Calulated gross thrust and mass flow calibration factors.

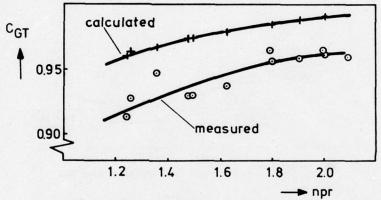


Fig. 11. Results static gross thrust calibration.

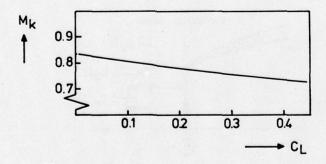


Fig. 12. Critical Mach number as a function of lift coefficient (Hoerner, Fluid dynamic Drag).

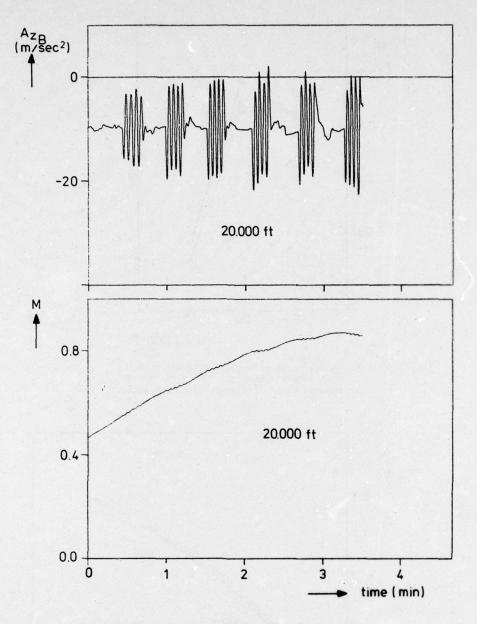


Fig. 13. Shape of non-steady flighttest manoeuvre.

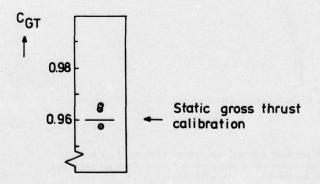


Fig. 14. Gross thrust calibration factor.
Each estimate obtained from 3 flighttest
manoeuvres at different flight altitudes.

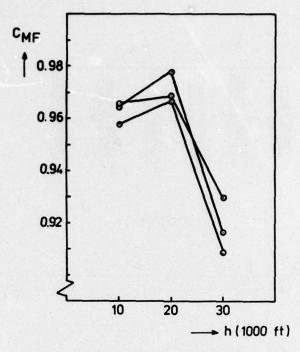


Fig. 15. Variation of mass flow calibration factor.

Each estimate obtained from 3 flighttest manoeuvres at different flight altitudes.

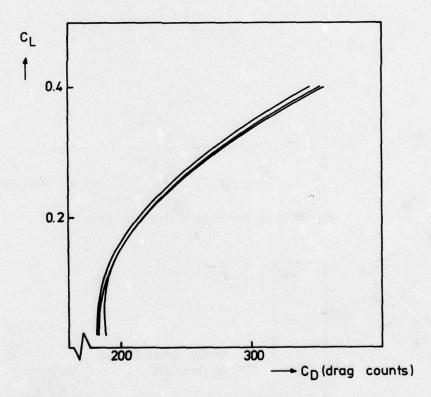


Fig. 16. Polar drag curves, no engine testbed data used. Each curve obtained from 3 flighttests manoeuvres at different flight altitudes.

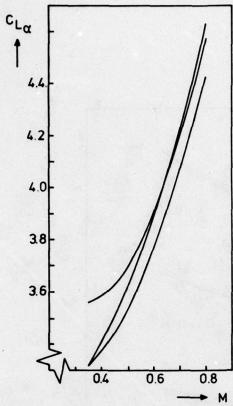


Fig. 17.  $C_{L_{Q}}$  versus M curves. Each curve obtained from 3 flighttest manoeuvres at different flight altitudes.

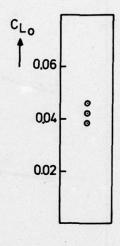


Fig. 18. Lift coefficient at zero angle of attack. Each estimate obtained from 3 flighttest manoeuvres at different flight altitudes.

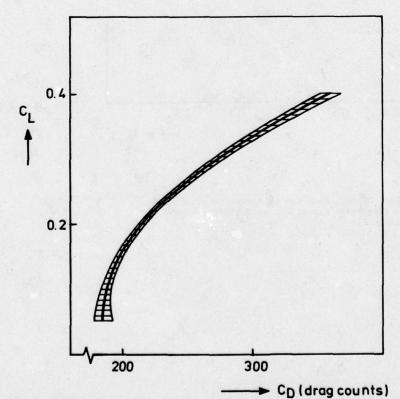


Fig. 19. Polar drag curve, mean and standard deviation obtained from 9 flighttest manoeuvres at different flight altitudes.

One set of values used for gross thrust and mass flow calibration factors.

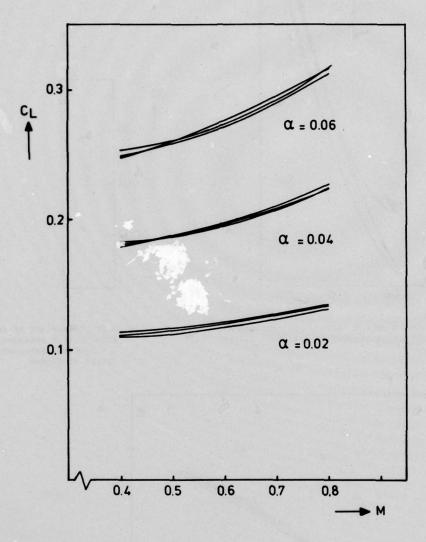


Fig. 20. Lift carpet. Each set of curves obtained from 3 flighttest manoeuvres at different flight altitudes.

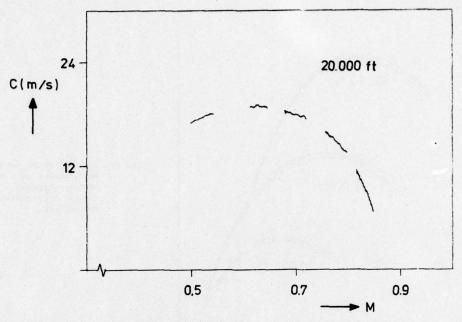


Fig. 21. Rate of climb versus Mach number in steady straight flight.

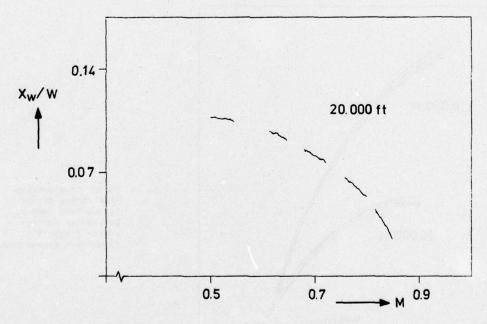


Fig. 22. Dimensionless excess thrust versus Mach number in horizontal accelerating flight.

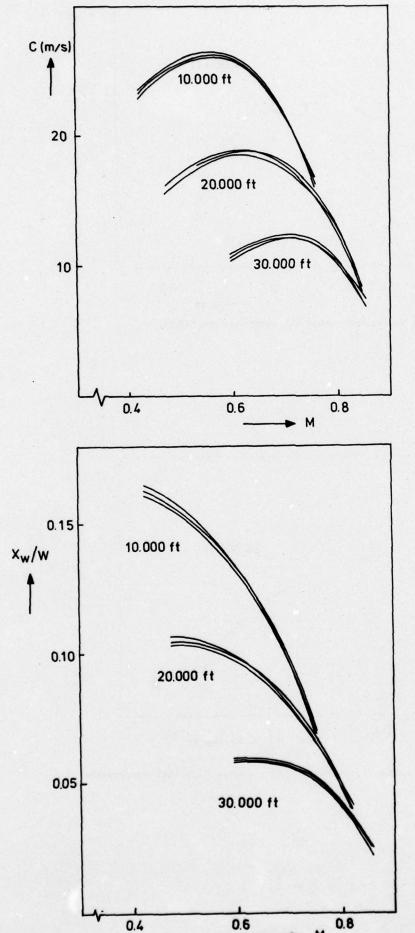


Fig. 23. Rate of climb versus
Mach number curves,
steady straight
flight 9 flighttest
manoeuvres.

Fig. 24. Curves of dimensionless excess thrust versus Mach number, horizontal accelerating flight 9 flighttest manoeuvres.

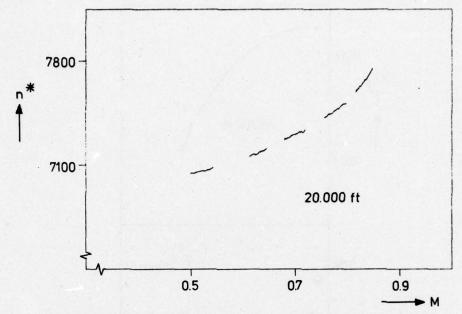


Fig. 25. Dimensionless engine rpm versus Mach number in steady horizontal flight.

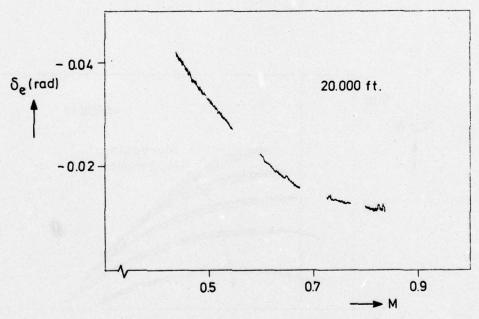


Fig. 26. Elevator angle versus Mach number in steady straight flight.

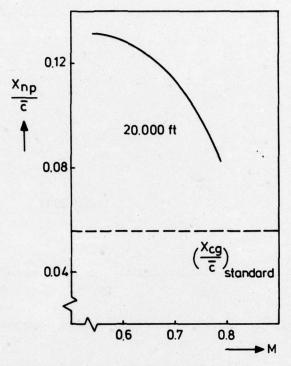


Fig. 27. Neutral point versus Mach number. Steady straight flight.

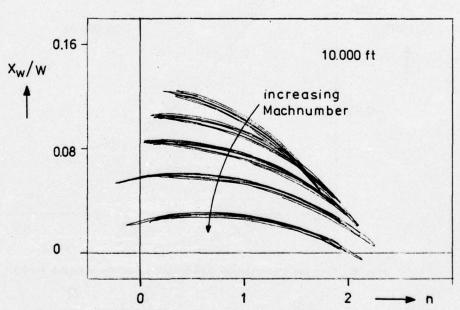


Fig. 28. Dimensionless excess thrust versus normal load factor in horizontal manoeuvring flight.

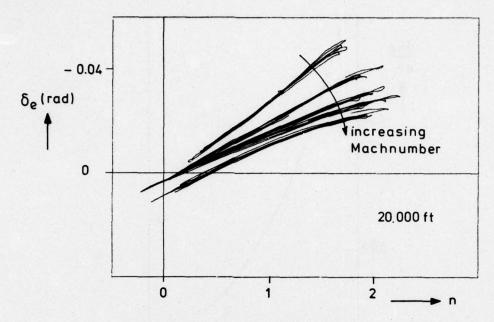


Fig. 29. Elevator angle versus normal load factor in horizontal manoeuvring flight.

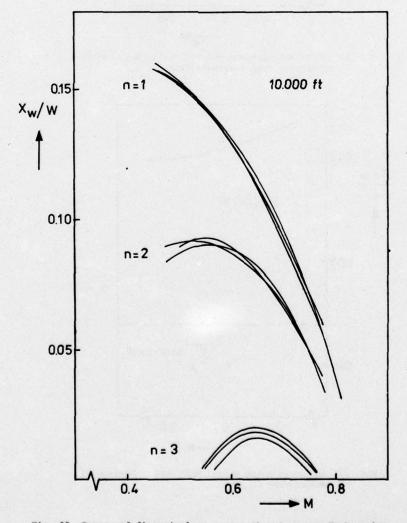


Fig. 30. Curves of dimensionless excess thrust versus Mach number, horizontal manoeuvering flight, 3 flight test manoeuvres.

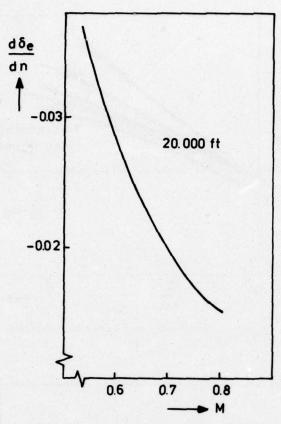


Fig. 31. Stick displacement per "g" versus Mach number horizontal manoeuvring flight.

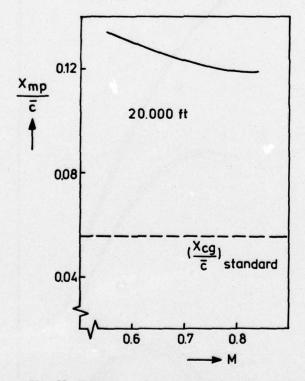


Fig. 32. Manoeuvre point versus Mach number horizontal manoeuvring flight.

# FLIGHT TESTING AND EVALUATION TECHNIQUES FOR THE DETERMINATION OF HANDLING QUALITIES

BY

HORST WÜNNENBERG ULRICH VON MEIER

DORNIER GMBH, D-799 FRIEDRICHSHAFEN, POSTFACH 1420

## SUMMARY

The techniques of Handling Qualities Determination in Flight Testing tends from mere pilot comments up to the accomplishment of detailed specifications by comprehensive documentation. After a definition of the main targets for the H.Q. flight testing, which lead to the necessary requirements for the instrumentation system and the flight test program, examples from the Alpha Jet flight testing are presented in correlation to the requirements given by the contract, by certification purposes and by the manufacturer.

Especially a proposal of the necessary information for flight manual and certification documentation is made by a detailed table, which can be satisfied only by reasonable combination of pilot comments, flight test evaluations and theoretical calculations.

## INTRODUCTION

The intention of this paper is not to give a complete summary of all existing flight testing and evaluation techniques, but to discuss the main headlines of this task in correlation to the possible and necessary requirements given by the contract, by certification purposes and by the manufacturer.

Contrary to the performance where the requirements are well defined and specified already as a main and most important part of the contract, the requirements for the Handling Qualities are normally not as well defined in detail, perhaps with the exception of several important points depending on the mission of the aircraft.

As there is no general concept of Handling Qualities Flight Testing for all AGARD-countries for instance, different opinions of the way "how to do the job" can be found depending on the country and on the type of the program. The extreme points of scale of possibilities can be provocatively characterized by the cartoons of fig. 1 and 2, which can be interpreted shortly as:

- Method 1: Trust the well experienced test pilot

Method 2: Trust the specification.

Of course these two extreme versions are not to be found in reality. Nobody will be satisfied if the Handling Qualities Flight Testing consists only of pilot comments, and on the other hand it surely is not reasonable to meet the whole specification MIL-F-8785 B. But from our personal feeling there is a tendency to the method 1 within national programs and a tendency to the method 2 within multinational programs. Therefore we think it is reasonable to discuss the Handling Qualities Flight Testing from a more general point of view. This should lead to the opinion, that it is necessary and possible to find a reasonable compromise of the above mentioned two methods individually for each type of aircraft in order to reduce the necessary amount of time and efforts to a minimum.

## 2. MAIN TARGETS OF THE HANDLING QUALITIES FLIGHT TESTING

The importance of the Handling Qualities can be characterized by three main topics in the order of importance:

## a. SAFETY

- Limits of the flight envelope (e.g. c.g. range)
- Manoeuvre limits (stall, spin, transonic phenomena)
- Effects of system failures

## b. MISSION EFFECTIVENESS

- Control effectiveness and coordination
- Stability behaviour
- Control forces and displacements
- Trim changes

## c. PILOT WORKLOAD

- No unusual attention or skill to fly the aircraft (fatigue, stress).

Corresponding to these topics the main targets of the H.Q. Flight Testing can be defined again in the order of importance:

- Determination of flight safety limits
- Demonstration of contract requirements
- Optimization of H.Q. due to pilot comments
- Basic information for the Flight Manual
- Documentation of the H.Q. for certification purposes
- Estimation of aerodynamic data and derivatives.

The above mentioned topics are simultaneously the headlines of this paper and will be discussed later-on in detail with examples from the Alpha Jet Flight Testing.

# 3. INSTRUMENTATION REQUIREMENTS FOR H.Q. DETERMINATION

In addition to the normal test equipment for flight control and performance measurements table 1 gives a list of the additional instrumentation, which as a minimum is necessary for H.Q. flight testing. The table gives also information of the necessary range and accuracy of the sensors. The important parameters should be measured by sensors of different range to improve the accuracy. It is obvious that in addition to these values the angle of attack, static and dynamic pressures, Mach-number, thrust, c.g. position, weights and moments of inertia have to be known. Furthermore the scanning frequency must be about two orders faster than the highest frequency to be examined in order to keep the phase errors low. Nevertheless even these remaining small scanning errors have to be compensated during the data reduction phase. Very good calibration of the main sensors are essentially necessary, if possible, before each flight and during the evaluation phase as a check.

## 4. REQUIREMENTS FOR THE FLIGHT TEST PROGRAM

As it is neither necessary nor reasonable to demonstrate all Handling Qualities characteristics within the total flight envelope by individual flight tests, a selection of the representative configurations, altitude and speed combinations, control inputs, weights and c.g. positions have to be chosen.

Representative configurations means the influence of flap settings, sweep-back angles for variable geometry configurations, thrust levels, external stores at critical and reference flight conditions. Critical speeds will be near to the stall speed and at the manoeuvre limits. An example for reference flight conditions according to combinations of altitudes and speed is given by fig. 2. If the reference conditions are chosen for example in this way there is the advantage that the effects of Mach number (at constant VC), of the angle of attack (at constant Mach number by different load factors) and of the dynamic pressure (at constant Mach by different VC) can be found individually with a minimum of flying time and by a relative simple set of reference altitude/speed combinations. These different influence factors are necessary for the determination of the stability derivatives, which can be used to compute the missing H.Q. characteristics or the unimportant effects.

In order to get all necessary informations different types of control inputs at the reference flight conditions have to be carried out:

- Stabilisation and very slow manoeuvres for polar curve and pitching moment characteristics
- Slow manoeuvres to get forces, moments and the effects of configuration changes
- Rapid manoeuvres for stability derivatives, forces and moments.

Within ref. 2 a detailed description and explanation of this subject is given.

# 5. EXAMPLES OF THE H.Q. EVALUATION FROM THE ALPHA JET FLIGHT TESTING

The following chapters give examples according to the list of targets of chapter 2.

## 5.1 Flight safety limits

The results of this subject are of course nearly all defined by pilot opinions:

- Departure limits in low and transonic flight regimes
- Spin recovery
- Center of gravity range
- Failures of system components
- H.Q. in the overspeed region.

Though the stall behaviour of the Alpha Jet was not bad from the very beginning of the flight testing an optimization was carried out by modifications of the nose drop and a shift of the saw tooth, which leads to a good stall behaviour with a sufficient warning buffeting, fig. 3.

The manoeuvre limits of the aircraft are given by two boundaries:

- Active manoeuvre boundary (a tracking manoeuvre with weapon aiming is still possible)
- Passive manoeuvre boundary (weapon aiming is not possible but escape manoeuvre is possible).

As shown by fig. 4 both boundaries are far beyond the buffet-onset boundary in the lift coefficient/Mach number diagram.

As the spin behaviour should be demonstrative due to the training purposes of the french version a lot of flight testing was done to improve the spin and spin recovery characteristics. Two small modifications are provided for the french version: a rounding of the fuselage nose and the additional installation of strips on the nose. For more details of the spin testing see ref. 3. The results of these tests are clear descriptions of the phenomena and the recovery procedures depending on speed, initial altitude and configuration.

The c.g. range has to be demonstrated in flight test, too. It usually is given by nose wheel lift-off in take-off and the static stability margin. But other possibilities as trim capability at low speeds or at go-around manoeuvres can be found as limitations of the c.g. range, too.

The effects of a system or a system component failure is of course an important aspect of the safety limits flight testing. As an example a failure of the stick force simulation device was investigated during the Alpha Jet flight testing. Fig. 5 shows the pitch control system with the variable gearing bellcrank, called "Arthur", which is controlled by the dynamic pressure and increases the pitch control forces with increasing dynamic pressure q. If this device failes at high speeds it automatically is reduced to small forces which leads to small trim changes and a high sensitivity of the pitch control, and has to be known and described within the flight manual.

Another important aspect is the evaluation of the H.Q. characteristics in the over speed region. The Alpha Jet can be flown at speeds far above the required max. Mach number up to Mach 1. Of course there are some typical phenomena, which have to be described in the flight manual, too. Fig. 6 shows the longitudinal transonic effects: small trim changes and a small pitch-up tendency at Mach 0.9 combined with a local reduction of static stability expressed by the slope of elevator angle per lift change.

The lateral behaviour is characterized by a reduction of the aileron efficiency though the total efficiency remains sufficient, fig. 7.

# 5.2 Demonstration of contract requirements

Even the shortest contract will require more special H.Q. characteristics than the general headline "simple and easy to fly within the permissible flight envelope". It is obvious that these special requirements have to be demonstrated in flight. Two examples of the Alpha Jet contract are shown here:

- Increase of thrust and the extension of the speed brakes should produce no nose down pitching moment
- A minimum roll rate is required at a given speed.

Fig. 8 shows the effects of thrust and speed brake extension on the trim curves. It can be seen that both the increase of the RPM and the speed brake extension give a pitch-up tendency as required.

Fig. 9 gives a comparison of the maximum attainable roll rates in level flight and with different load factors in comparison to the requirement. The decrease of the max. roll rate with increasing load factor is caused by induced side slip angles which are produced mainly by the yawing moment due to roll rate  $c_{np}$ .

There are of course other requirements concerning different attainable load factors at given speeds and altitudes, a cross wind landing requirement, manoeuvre limits etc., which have to be demonstrated respectively.

# 5.3 Optimization of the Handling Qualities

This task can only be done with the aid of pilot comments. Though the MIL-Spec. can be used as a guideline for the first approach it is the experienced test pilot, who finally qualifies the flight control characteristics as "acceptable". As an example the optimization of the pitch control system will be explained in more detail. The control system, fig. 5, consists of a mechanical connection from the dual control sticks to the elevator servo through the kinematic operating mechanism called "Heini", which provides a non-linear gearing between stick deplacement and stabilizer angle to reduce the control sensitivity for little stick movements near the stick neutral position, which corresponds to the high speed trim position. A parallel connected artificial stick force system with a variable gearing named "Arthur", which is operated by the dynamic pressure, followed by a triple-gradient bungee, the attachment point of which is electrically shifted by the trim actuator.

The variable gearing bellcrank "Arthur" has two effects, fig. 10:

- Increase of the stick force per stick displacement as a function of the dynamic pressure
- Auto trim capability depending on the initial trim position.

The optimization of this autotrim facility and the coordination of the stick forces for longitudinal and lateral control for both the training and the close air support version with all the possible loads takes a lot of effort and needs highly skilled and experienced pilots.

Another example is given by fig. 11. The Dutch Roll damping of the aircraft is slightly below Level 1 of MIL-F-8785 B DR-damping specification at medium altitudes. Though the pilots reported a certain sensitivity of the aircraft due to turbulence, this criticism was not so strong as to provide the installation of a yaw damper. Finally the simulation of real ground attack approaches at severe turbulence conditions where the amplitudes of the lateral displacement could be read in mrad on the gun sight led to the decision of providing a simple yaw damper. The effect of this yaw damper with an authority of 10 % and a fixed-gain operating order can be seen in the fig. 11. By this device a significant improvement of the D.R. damping could be realized.

# 5.4 Basic data for Flight Manual and certification documentation

Within the Flight Manual all necessary information about the main H.Q. characteristics should be available helping a new pilot to get quickly familiar with the aircraft, including normal and emergency procedures and the operational limitations. For certification purposes a more detailed description of all essential H.Q. characteristics should be documented.

A proposal of the different items to be considered either for Flight Manual or for the certification was developed in cooperation with the German Aeronautical Qualification Center (ML) and is listed in table 2. The list presents an extension of the German GAF-TO Requirements (according to MIL-M-7700 A), as the latter was judged to be unsufficient for modern aircraft.

To fulfill all points of this recommendation a summary of pilot comments, flight test results and calculated results based on aerodynamic coefficients and derivatives evaluated from flight tests will be necessary.

As it is not possible to show all results within this short paper and as the job is not yet finished, two examples of possible presentations will be shown.

Fig. 12 presents the different possibilities of the static longitudinal stability definition. The most familiar version is a plot of the trim angle versus speed as shown in the upper part of the fig., where a positive slope means positive static stability. The interpretation of this plot however is a little bit difficult for the higher speeds.

A better definition and much easier to interpret is shown by the medium presentation of the figure: The slope of elevator angle per lift coefficient, which can be easily computed into the static margin if the elevator effectiveness and the actual c.g. position are well-known.

The classical presentation is the neutral point position, shown in the lower part of the fig. 12, which can be derived either from short period oscillation results or from the manoeuvre point which can be determined by extrapolations of trim curves at different c.g. positions. This presentation has the advantage of showing directly the static margin in comparison with the actual c.g. position.

Static lateral stability as expressed by the weather cock stability and the dihedral effect can be presented easily by the slopes of rudder and aileron angle per degree side slip angle as shown in fig. 13.

## 5.5 Evaluation of aerodynamic coefficients and derivatives

This part of the H.Q. Evaluation from Flight Tests is mainly interesting for the manufacturer. The comparison of the theoretical, wind tunnel and flight test results is necessary for the improvement of the methods as a base for further developments. In addition to that these values are necessary to explain special effects (e.g. due to modifications) and to optimize the characteristics of stability augmentation systems.

The methods to be used in finding these values can be found in the Conference Proceedings of a special AGARD-FMP-Meeting on this subject in Fall 1974 at NASA-Langley see ref. 4, so I don't go into detail within this paper.

On principle three types of methods are existing:

- Simple methods as examination of special manoeuvres by manual evaluation techniques or time vector analysis
- Half automatic methods as matching programs, which try to fit simulation and flight test results by manual or half automatic procedures
- Full automatic statistical methods where the fit is done automatically by mean square root criteria with different optimization procedures using complicated optimal input procedures, too.

The latter are well suitable for high sophisticated aircraft with a comfortable instrumentation equipment and data reduction facilities. For more simpler aircraft with reduced equipment the simpler methods seem to be more effective. Within the Alpha Jet program manual evaluation techniques are used in combination with time vector analysis and digital matching programs, ref. 2.

Examples of the results of this evaluation efforts are given by the next figures in comparison with wind tunnel results. There are some values, which can be found easily as the influence on the analysed manoeuvre is important. But there are other, especially some of the coupling derivatives, which are difficult to evaluate. Fig. 14 shows the yawing and rolling moment due to side slip compared with wind tunnel test results, the scattering of the evaluated data is small and the accommodation with the wind tunnel results is good. The contrary can be seen on fig. 15 especially for the rolling moment due to yaw rate, on the upper part of the figure. The scattering is high and there is a remarkable difference between wind tunnel and flight test results. The expression "estimation" on fig. 15 means that the Mach number effect has been estimated and added to the low speed wind tunnel results.

# 6. CONCLUSION

The determination of the Handling Qualities is an important part of the flight testing of a new aircraft, even then, if no serious problems have to be solved. It has been pointed out by this paper that all important aspects and requirements of a Handling Qualities determination by flight testing can only be satisfied by a reasonable combination of pilot comments, flight test evaluations and additional theoretical calculations.

As an example the optimization of the pitch control system will be explained in more detail. The control system, fig. 5, consists of a mechanical connection from the dual control sticks to the elevator servo through the kinematic operating mechanism called "Heini", which provides a non-linear gearing between stick deplacement and stabilizer angle to reduce the control sensitivity for little stick movements near the stick neutral position, which corresponds to the high speed trim position. A parallel connected artificial stick force system with a variable gearing named "Arthur", which is operated by the dynamic pressure, followed by a triple-gradient bungee, the attachment point of which is electrically shifted by the trim actuator.

The variable gearing bellcrank "Arthur" has two effects, fig. 10:

- Increase of the stick force per stick displacement as a function of the dynamic pressure
- Auto trim capability depending on the initial trim position.

The optimization of this autotrim facility and the coordination of the stick forces for longitudinal and lateral control for both the training and the close air support version with all the possible loads takes a lot of effort and needs highly skilled and experienced pilots.

Another example is given by fig. 11. The Dutch Roll damping of the aircraft is slightly below Level 1 of MIL-F-8785 B DR-damping specification at medium altitudes. Though the pilots reported a certain sensitivity of the aircraft due to turbulence, this criticism was not so strong as to provide the installation of a yaw damper. Finally the simulation of real ground attack approaches at severe turbulence conditions where the amplitudes of the lateral displacement could be read in mrad on the gun sight led to the decision of providing a simple yaw damper. The effect of this yaw damper with an authority of 10 % and a fixed-gain operating order can be seen in the fig. 11. By this device a significant improvement of the D.R. damping could be realized.

## 5.4 Basic data for Flight Manual and certification documentation

Within the Flight Manual all necessary information about the main H.Q. characteristics should be available helping a new pilot to get quickly familiar with the aircraft, including normal and emergency procedures and the operational limitations. For certification purposes a more detailed description of all essential H.Q. characteristics should be documented.

A proposal of the different items to be considered either for Flight Manual or for the certification was developed in cooperation with the German Aeronautical Qualification Center (ML) and is listed in table 2. The list presents an extension of the German GAF-TO Requirements (according to MIL-M-7700 A), as the latter was judged to be unsufficient for modern aircraft.

To fulfill all points of this recommendation a summary of pilot comments, flight test results and calculated results based on aerodynamic coefficients and derivatives evaluated from flight tests will be necessary.

As it is not possible to show all results within this short paper and as the job is not yet finished, two examples of possible presentations will be shown.

Fig. 12 presents the different possibilities of the static longitudinal stability definition. The most familiar version is a plot of the trim angle versus speed as shown in the upper part of the fig., where a positive slope means positive static stability. The interpretation of this plot however is a little bit difficult for the higher speeds.

A better definition and much easier to interpret is shown by the medium presentation of the figure: The slope of elevator angle per lift coefficient, which can be easily computed into the static margin if the elevator effectiveness and the actual c.g. position are well-known.

The classical presentation is the neutral point position, shown in the lower part of the fig. 12, which can be derived either from short period oscillation results or from the manoeuvre point which can be determined by extrapolations of trim curves at different c.g. positions. This presentation has the advantage of showing directly the static margin in comparison with the actual c.g. position.

Static lateral stability as expressed by the weather cock stability and the dihedral effect can be presented easily by the slopes of rudder and aileron angle per degree side slip angle as shown in fig. 13.

# 5.5 Evaluation of aerodynamic coefficients and derivatives

This part of the H.Q. Evaluation from Flight Tests is mainly interesting for the manufacturer. The comparison of the theoretical, wind tunnel and flight test results is necessary for the improvement of the methods as a base for further developments. In addition to that these values are necessary to explain special effects (e.g. due to modifications) and to optimize the characteristics of stability augmentation systems.

The methods to be used in finding these values can be found in the Conference Proceedings of a special AGARD-FMP-Meeting on this subject in Fall 1974 at NASA-Langley see ref. 4, so I don't go into detail within this paper.

On principle three types of methods are existing:

- Simple methods as examination of special manoeuvres by manual evaluation techniques or time vector analysis
- Half automatic methods as matching programs, which try to fit simulation and flight test results by manual or half automatic procedures
- Full automatic statistical methods where the fit is done automatically by mean square root criteria with different optimization procedures using complicated optimal input procedures, too.

The latter are well suitable for high sophisticated aircraft with a comfortable instrumentation equipment and data reduction facilities. For more simpler aircraft with reduced equipment the simpler methods seem to be more effective. Within the Alpha Jet program manual evaluation techniques are used in combination with time vector analysis and digital matching programs, ref. 2.

Examples of the results of this evaluation efforts are given by the next figures in comparison with wind tunnel results. There are some values, which can be found easily as the influence on the analysed manoeuvre is important. But there are other, especially some of the coupling derivatives, which are difficult to evaluate. Fig. 14 shows the yawing and rolling moment due to side slip compared with wind tunnel test results, the scattering of the evaluated data is small and the accommodation with the wind tunnel results is good. The contrary can be seen on fig. 15 especially for the rolling moment due to yaw rate, on the upper part of the figure. The scattering is high and there is a remarkable difference between wind tunnel and flight test results. The expression "estimation" on fig. 15 means that the Mach number effect has been estimated and added to the low speed wind tunnel results.

## CONCLUSION

The determination of the Handling Qualities is an important part of the flight testing of a new aircraft, even then, if no serious problems have to be solved. It has been pointed out by this paper that all important aspects and requirements of a Handling Qualities determination by flight testing can only be satisfied by a reasonable combination of pilot comments, flight test evaluations and additional theoretical calculations.

The H.Q. flight testing can be done in parallel to the performance and system tests. Due to this reason it is difficult to specify the necessary amount of time of flying hours for this task. For the Alpha Jet aircraft an estimation can be given of about 200 hrs for the clean configuration which has been performed within 1,5 years by two prototype-aircraft and two industry-test pilots. After this time the geometry and the characteristics of the control system have been frozen for the production stage.

Meanwhile the Alpha Jet has been flown by 60 pilots, who all judged the Handling Qualities of the aircraft as excellent.

## 7. REFERENCES

- [1] H. Wünnenberg, H. Friedrich, U.v. Meier, H.J. Munser Determination of stability derivatives from flight test results. Comparison of five analytical techniques; in AGARD-CP 172
- [2] R. Guiot, H. Wünnenberg Comparison des coefficients aerodynamiques issus des calculs theoriques, essais en soufflerie et depouillements d'essais en vol effectues sur l'Alpha Jet; in AGARD-CP 187
- [3] J. Differ, J.P. Duval, J. Plessy
  Essais de vrilles du Jaguar, du Mirage F1 et de l'Alpha Jet; in AGARD-CP 199
- [4] AGARD-CP 172: Methods for aircraft state and parameter identification;

Sensor		Dim.	Range	Accuracy
linear accelerations	x - Axis	9	Ŧ 1,5	∓ 0.3 %
	y - Axis	9	Ŧ 1,5	Ŧ 0.3 %
	z · Axis	9	¥ 1,5, +10 -4	Ŧ 0,3 %
angular velocities	x - Axis	deg/sec	Ŧ 60, 300	Ŧ 0,4 %
	y - Axis	deg/sec	Ŧ 20	Ŧ 0,4 %
	z - Axis	deg/sec	Ŧ 20	Ŧ 0,4 %
angle of attack		deg	- 10 ÷ 30	< 0,15 deg
angle of sideslip		deg	₹ 20	< 0,15 deg
positions of the control		deg	according to	< 0,2 deg
surfaces			possible deflection	
attitude platform		deg	0 ÷ 360	0,25 deg
(if available, necessary f	or spin tests)			

Table 1
INSTRUMENTATION REQUIREMENTS FOR THE H.Q. DETERMINATION

1.	PITCH CONTROL		
1.1	Description of the control system	yes	yes
1.2	Trim positions, influence of configuration	yes	yes
1.3	Control forces	yes	yes
1.4	Pitch control at "g"-manoeuvres	yes	yes
1.5	Effects of system components failures	yes	yes
1.6	Static stability	yes	no
1.7	c.g. ranges, influence of external stores	yes	yes
2.	DYNAMIC LONGITUDINAL STABILITY		
2.1	Phugoid damping	yes	no
2.2	Short period characteristics	yes	no
2.3	Dynamic effects at configuration changes	yes	yes
•	DOLL CONTROL		
3.	ROLL CONTROL	Vac	VAS
3.1	Description of the control system	yes	yes
3.2	Roll performance Control forces	yes	yes
3.3		yes	yes yes, if restric-
3.4	Roll coupling effects, influence of load factor	yes	tions necessary
3.5	Dynamic response characteristics	yes	no
3.6	Trim range and trim failure	yes	yes
4.	YAW CONTROL		
4.1	Description of the control system	yes	yes
4.2	Cross wind effects	yes	yes
4.3	Control forces	yes	yes
4.4	Lateral static stability	yes	yes
4.5	Trim range and trim failure	yes	yes
5.	LATERAL DYNAMIC STABILITY		
5.1	Dutch roll characteristics	yes	no
5.2	Roll time constants	yes	no
5.3	Yaw damper characteristics	yes	partly
6.	UNSYMMETRICAL FLIGHT CONDITIONS		
		was	wo c
6.1	그리고 생물하다 하는 사람들은 사람들이 살아보고 있다면 살아보고 있다면 하는 것이 없는 것이 없는 것이 없는 것이 없는 것이 없는 것이다.	yes	yes
6.3		yes	yes
0.3	by mainte response effects of weapon defivery and gun fiffing	yes	yes
7.	HANDLING QUALITIES AT THE OPERATIONAL LIMITS		
7.1		yes	yes
7.2	Characteristics within the over speed region	yes	yes
7.3	Spin behaviour	yes	yes
7.4	Dives	no	yes

Table 2 Summary of necessary Handling Qualities Characteristics for flight manual and certification documentation



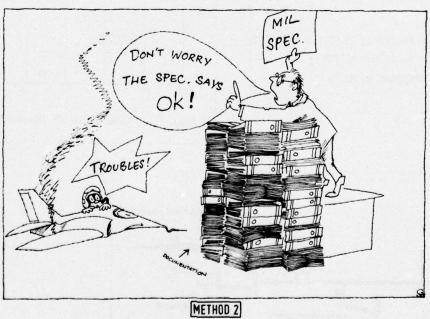
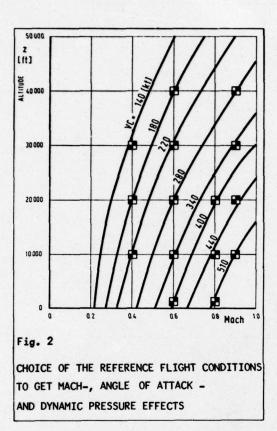
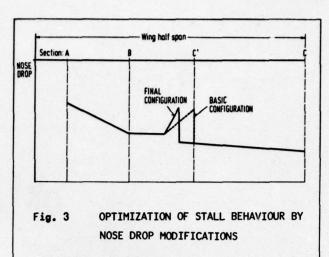
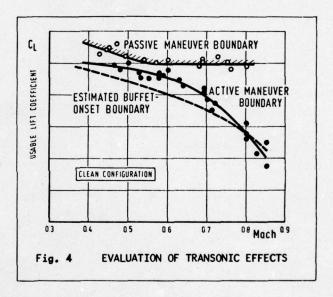
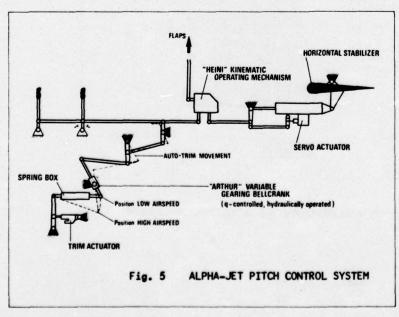


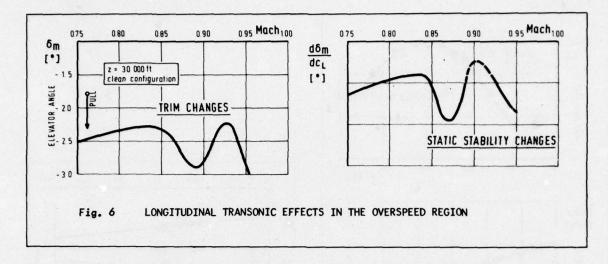
Fig. 1 METHODS OF HANDLING QUALITIES DETERMINATION IN FLIGHT TEST

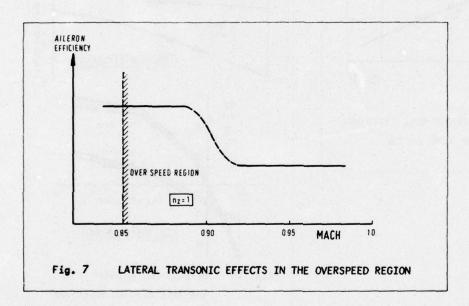


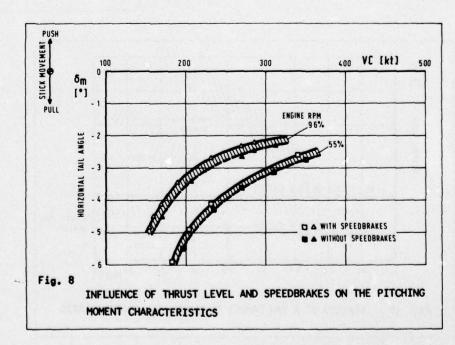


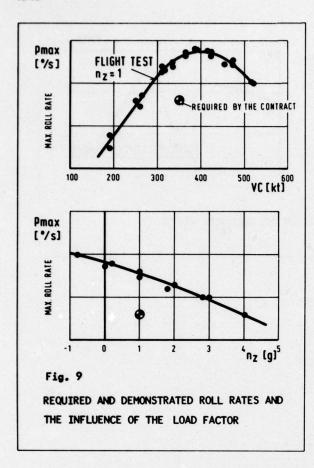


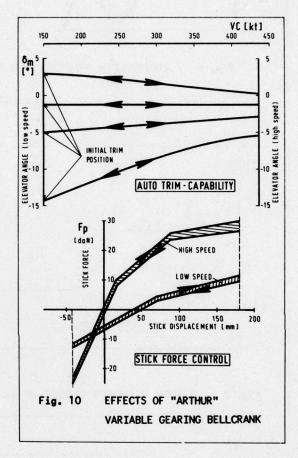


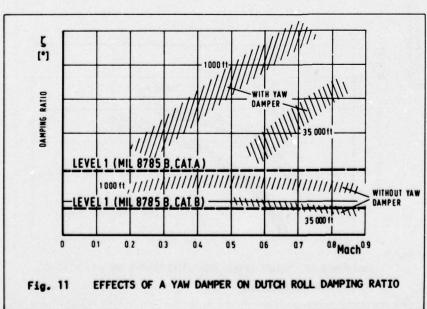












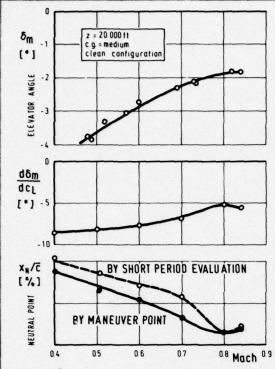
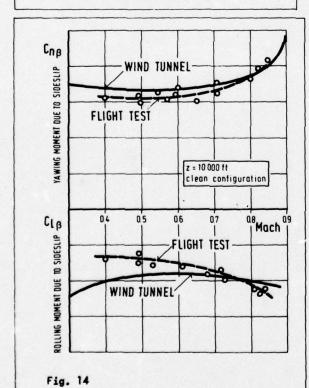


Fig. 12
STATIC LONGITUDINAL STABILITY, EXAMPLES OF DIFFERENT POSSIBLE PRESENTATIONS



COMPARISON OF WIND TUNNEL AND FLIGHT TEST
RESULTS FOR LATERAL STATIC DERIVATIVES

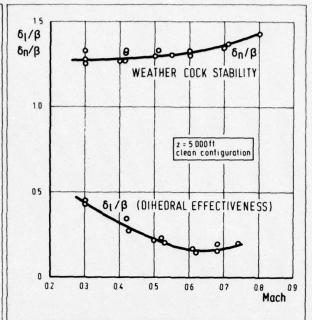


Fig. 13 STATIC LATERAL STABILITY,
EXAMPLES OF POSSIBLE PRESENTATION

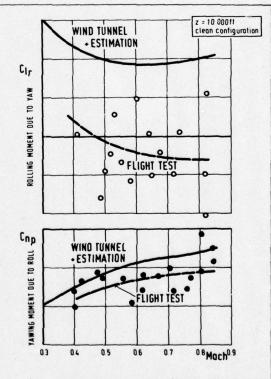


Fig. 15 COMPARISON OF WIND TUNNEL AND FLIGHT TEST RESULTS FOR LATERAL DYNAMIC CROSSCOUPLING DERIVATIVES

A MISSION ORIENTED FLIGHT TEST TECHNIQUE FOR IDENTIFYING AIRCRAFT AND FLIGHT CONTROL SYSTEM TRANSFER FUNCTIONS

by
Thomas R. Twisdale, Aerospace Engineer
Flight Test Technology Branch
AFFTC/DOEST
Edwards AFD, California 93523

Gerald L. Jones, Aerospace Engineer Performance and Flying Qualities Branch AFFTC/DOEEP Edwards AFB, California 93523

Tice A. Ashurst, Mathematician/Programmer
Software Management Branch
AFFTC/DOEDM
Edwards AFB, California 93523

#### ABSTRACT

New data analysis techniques have been developed at the Air Force Flight Test Center (AFFTC) which offer unique and quantitative insights into pilot-in-the-loop handling qualities. These new data analysis techniques, called System Identification From Tracking (SIFT), are based on time series analysis procedures. These procedures are used to perform a frequency domain evaluation of data obtained during closed-loop, mission oriented precision tracking maneuvers. Normal stability and control test parameters are measured and recorded in the time domain during the maneuver. As many as four of these parameters are selected as multiple inputs to the system being evaluated and one parameter is selected as the system response. These time domain data are Fourier transformed into the frequency domain, where spectral content, multiple frequency response transfer functions, and coherence functions are estimated and plotted. Depending on the parameters selected for analysis, either the flight control system (or its components), or the airframe aerodynamics, or the total system characteristics (control system plus aerodynamics) may be identified. It should be pointed out that handling qualities are a function of the total system characteristics.

Interim results of an analysis of flight test data obtained during a precision airto-air tracking maneuver and during a pilot induced oscillation are discussed. These interim results show that, for the aircraft being analyzed, lateral-directional coupling into the pitch axis has an unexpected and apparently significant impact on longitudinal handling qualities, even for small angles of attack and sideslip.

## INTRODUCTION

The advent of sophisticated flight control systems has introduced new problems for the flight test engineer. Three of these are: (1) the problem of optimizing the flight control system to satisfy the operational requirements of the aircraft; (2) the problem of gaining quantitative insights into closed-loop handling qualities; and (3) the problem of identifying the in-flight characteristics of the flight control system (which may differ from the characteristics identified by ground testing).

The first problem, that of optimizing the flight control system to the operational requirements of the aircraft, has been largely resolved at AFFTC for fighter and ground support type aircraft with the help of tracking test techniques (also referred to as HQDT, or Handling Qualities During Tracking). These techniques, which were developed and introduced for this purpose by the AFFTC in 1971-72 have been formally documented (reference 1).

A potential solution to the second and third problems - of quantitatively evaluating closed-loop handling qualities and of identifying the in-flight characteristics of the flight control system - is being developed and tested at AFFTC. This solution is based on a frequency domain analysis of tracking data, using time series analysis techniques. Time series analysis, which was developed largely by the communications industry, is widely used in other engineering disciplines, particularly since the advent of the Fast Fourier Transform in 1965. As far as we know however, time series analysis techniques have never been successfully applied to handling qualities flight testing.

There are several advantages to the test techniques which are being developed, called System Identification From Tracking (SIFT). Two of these are that closed-loop handling qualities may be evaluated in a mission oriented context, and that the in-flight characteristics of the flight control system may be identified. Traditionally, open-loop tests have been performed to evaluate handling qualities. While open-loop tests provide some insight into closed-loop characteristics, they do not provide an opportunity to assign useful pilot ratings. A third important advantage is that the data for this analysis is already routinely acquired during flight test programs, so that a minimum of additional dedicated flight time is required.

This approach to flight control system and closed-loop handling qualities testing is a potentially powerful new approach to flight testing today's new aircraft.

#### TEST MANEUVERS

Time series analysis is central to the new SIFT frequency domain handling qualities analysis techniques which are being developed by AFFTC. Several characteristics of time series analysis influence the test maneuvers which are being used to obtain data and the quantity of data being obtained. First, time series analysis techniques are least square linear estimation techniques. This means that the system transfer function being analyzed should be as nearly linear as possible in order to improve the likelihood of an accurate identification. Second, a good identification requires that the system input signals should have frequency content throughout the frequency range of interest. In other words, the system must be excited across the frequency resolution are functions, respectively, of the rate at which the measured flight parameters are sampled and the length of the time histories of these parameters. Higher sample rates yield higher identifiable frequencies and longer time histories (data record lengths) yield finer frequency resolution. Fourth, the statistical stability of the frequency domain results is a function of the degrees of freedom and the coherence of the data. Uncorrelated noise (such as aerodynamic buffet, turbulence, and wake encounters) and system non-linearities adversely influence coherence so that more data becomes necessary in order to obtain reasonably stable estimates. Considerations of this nature are widely discussed in the literature (e.g. references 2 and 3).

The precision air-to-air tracking maneuver which was used to obtain part of the data presented in this paper was, nominally, a constant angle of attack, constant Mach number "tail chase" turning maneuver. A complete discussion of the maneuver and special piloting techniques is presented in reference 1. Briefly, the tracking pilot's task was to precisely and assiduously track the target aircraft, using a fixed (non-computing) gunsight. Floating or drifting the pipper was not permitted. For the frequency domain analysis the pilot was allowed to use the rudder pedals if he so desired. In order to prevent uncorrelated trends in the stick force data, retrimming the airplane during the maneuver was not permitted.

This precision air-to-air tracking maneuver has the multiple advantages of reducing non-linear effects, eliciting good frequency content, and giving the pilot a mission oriented task to perform and evaluate. This latter aspect is important since it provides an opportunity to associate Cooper-Harper ratings and pilot comments with the closed-loop data being analyzed. The non-linear effect of stability derivative variation with angle of attack and Mach number (dependent on the particular airframe and the area of the envelope being investigated) is reduced by attempting to maintain constant angle of attack and Mach number during the raneuver. However, it is often necessary to sacrifice altitude in order to maintain Mach number, resulting in an increase in dynamic pressure and inducing a non-linear effect through its influence on airframe response to surface deflection (i.e. an uncorrelated change in airframe response for the same input). Flight control system non-linearities are reduced since, for nominally unchanging flight conditions and trim, an assumption of piecewise linearity is not too unrealistic within the range of system excursions encountered during the maneuver. The special piloting technique (precise and assiduous tracking of the target; immediate and positive corrective action for even a one mil error) does a good job of exciting the system across the frequency range of interest.

Of course, constant angle of attack and Mach number precision tracking turns are not the only maneuvers suited to a frequency domain analysis of handling qualities, although our experience has shown (reference 1) that these maneuvers do provide an excellent and reliable indication of overall handling qualities. It is likely that air-to-air refueling, station keeping (formation flying), and glide slope tracking would serve as satisfactory maneuvers for a frequency domain evaluation of the handling qualities associated with these tasks. We plan to evaluate the suitability of these maneuvers in the near future.

Results of a frequency domain analysis of a pilot induced oscillation (PIO) are also presented in this paper. This condition was encountered during an attempt to acquire -lg on the cockpit accelerometer following a 2g pull-up.

DATA REDUCTION: FREQUENCY RESPONSE ANALYSIS COMPUTER PROGRAM (FRA)

The new SIFT analysis techniques are embodied in a Frequency Response Analysis computer program (FRA), which was written at AFFTC. Data for the program are acquired in the form of digitized time histories of various parameters of interest, such as stick forces, normal acceleration, pitch rate, flight control system signals, pipper error, etc. For any one analysis, as many as four of these parameters are selected as inputs to the system and one additional parameter is selected as the system response.

An abbreviated schematic outline of the computations performed by FRA is presented in figure 1. The program is being modified and improved as our experience with these new frequency domain handling qualities analysis techniques expands.

In the time domain, the selected parameter time histories are digitally filtered if desired; the mean is computed and subtracted out; and the covariance coefficient function is computed. After computing the covariance coefficient function, the time histories are passed through a Hann window in the time domain by multiplying the data record by a cosine bell function. The modified time histories are then Fast Fourier Transformed into the frequency domain where the ensemble and frequency averaged power spectral density and cross-spectral density functions are estimated. The ordinary, multiple, and partial coherence functions and the frequency response transfer functions (Bode amplitude and phase angle) with confidence limits are then estimated. The matrix formulation and various large and small details of these computations are not elaborated here since they are discussed in the literature.

The accuracy of the computational techniques implemented in FRA has been verified by modeling time histories of system response to doublet inputs to known transfer functions. These modeled time histories were then analyzed to obtain frequency response transfer functions, which were compared to the known frequency response transfer functions. An example comparison is presented in figure 2. The imperfect phase angle match results from the inaccuracy of the imaginary part of the discreet Fourier transform (figure 3).

Nyquist theory says that the highest identifiable frequency is equal to  $1/(2\Delta t)$ , where  $\Delta t$  is the time interval between samples. However, it has been our experience at AFFTC that the highest accurately identifiable frequency is at least  $1/(4\Delta t)$ . Figure 2 illustrates the effect on the phase match of increasing the sample rate and figure 3 shows why a higher sample rate is desirable. If the highest frequency of interest in the analysis were one half the Nyquist frequency, a smaller inaccuracy in the imaginary part of the discreet Fourier transform would be incurred, resulting in better phase angle identification. Thus a sample rate of four times the highest desired frequency (in Hertz), instead of two times, is preferable. The data discussed in this paper were sampled at about six times (20 samples/second) the highest frequency of interest (10 radians/second).

A digital filtering capability was implemented in FRA when it appeared that PCM resolution error "noise" (due to digitizing the data into an eight bit word) might be contributing unwanted power to the time histories being analyzed. Figure 4 shows a time history of angle of attack which clearly displays this resolution noise, and the same time history with the noise filtered out (using a four pole Butterworth filter). Figure 5 presents a plot of the power spectral density of the filtered resolution noise. When the frequency range of interest is below about one half the Nyquist frequency it is clear that power contributed by the resolution error noise will not be troublesome.

## DISCUSSION OF DATA

PRECISION AIR-TO-AIR TRACKING DATA. These data were obtained during five nominally constant angle of attack, constant Mach number turning maneuvers. The flight conditions during the five maneuvers are summarized in figure 6. Cooper-Harper ratings and other data are summarized in table I.

FRA was used to ensemble and frequency average these data and to identify the aerodynamic transfer function of pitch rate to stabilator position  $(0/\delta_e)$ . The results of this analysis are presented in figure 7 (Bode amplitude plots) and figure 8 (phase angle plots).

Stabilator deflection and lateral stick force were used as input signals for the first plot in figure 7. Lateral stick force was selected as the second input because it was presumably uncorrelated with stabilator deflection. This transfer function of pitch aerodynamics is particularly interesting because it clearly exhibits two distinct resonances, or oscillatory modes, where only one was expected. The three radians/second resonance is the longitudinal short period of the aircraft. A review of these results led to a suspicion that the second resonance, at about five radians/second, might be caused by lateral-directional coupling into the pitch axis. Further analysis confirmed this suspicion in an interesting sequence of steps.

When rudder deflection was substituted for lateral stick force as an input signal, the second amplitude plot in figure 7 was identified. This plot shows that for this airplane, rudder deflection does couple into the pitch axis since the prominence of the second resonance is somewhat reduced when the contribution due to rudder deflection is accounted for.

The third plot in figure 7 shows that when rolling tail deflection is added to stabilator and rudder deflection as inputs to the system, the prominence of the second resonance is still further attenuated, although the change is not as large as that due to rudder deflection. This result demonstrates that rolling tail effectiveness is not symmetrical for this airplane, so that a small pitching moment is inadvertently introduced when pure roll is commanded.

The fourth plot in figure 7 shows that when the pitch axis contributions of sideslip angle, as well as of rolling tail and rudder deflection, are accounted for, the amplitude plot that remains is the usual one expected for an uncoupled, linear approximation of the longitudinal aerodynamic transfer function of pitch rate to stabilator deflection.

These results are especially interesting for their impact on handling qualities design and assessment. It appears that the usual assumption of decoupled lateral-directional and pitch axes is not always a good one, even for small angles of attack and sideslip. (Reference 4 analyzes and discusses lateral-directional and pitch coupling for high angle of attack flight conditions.) Clearly, for this airplane there is a very significant and previously unsuspected coupling at small angles of attack and sideslip. Judging by the first plot in figure 7 (which is the effective transfer function that the pilot sees and must deal with) the effect of the coupling resonance on longitudinal handling qualities is only slightly less significant than the effect of the short period (a difference of about 3 db), which is a surprising discovery. This suggests that attempts to improve longitudinal handling qualities by modifying apparent short period dynamics, either by airframe or flight control system changes, may sometimes be entirely misdirected. It also suggests that, for modern aircraft, the phenomenon of aerodynamic coupling between the lateral-directional and pitch axes deserved additional attention with respect to its impact on the design and integration of the airframe and flight control system and on handling qualities optimization.

FRA has also been used to identify lateral-directional frequency response transfer functions. For example, the amplitude and phase curves of the yaw rate to rudder deflection transfer function are presented in figure 9.

Generally, the lateral-directional aerodynamic transfer functions are more difficult to accurately identify. This is because more than one flight control surface contributes to each lateral and directional response. For example, for the data being discussed the rudder, aileron, and rolling tail each generate a yawing as well as a rolling response. Because these surface deflections are correlated by an aileron-to-rudder interconnect and an aileron-to-rolling tail schedule, it is difficult for FRA to determine what part of the total aerodynamic response is caused by each control surface. We are still in the early stages of analysis of lateral-directional transfer functions.

Investigation of these and similar data is continuing at AFFTC.

PILOT INDUCED OSCILLATION (PIO) DATA. Data were obtained during a condition described by the pilot as a PIO. The pilot reported that he encountered this condition during an attempt to acquire -lg on the cockpit accelerometer following a 2g pull-up.

FRA was used in an effort to determine whether the condition encountered by the pilot actually was a PIO. Since the pilot was attempting to acquire a specific value of normal acceleration, we directed our attention to identifying the total system transfer function of normal acceleration to pitch stick position  $({\rm N_z/\delta_e})$ , the aerodynamic transfer function of normal acceleration to stabilator position  $({\rm N_z/\delta_e})$ , and the pitch axis flight control system transfer function of stabilator deflection to pitch stick deflection  $(\delta_e/\delta_s)$ . Only ten seconds of data were available for analysis.

Time history plots of the normal acceleration, pitch stick position, and stabilator position are presented in figure 10. Power spectral density plots of normal acceleration, stick position, and stabilator position are presented in figure 11. The frequency response transfer function plots are presented in figures 12, 13, and 14.

Figure 11 shows that both the pilot and the airplane response exhibited a significant amount of relatively narrow band power at about seven radians/second, which is the frequency of the oscillation being investigated. At seven radians/second the phase angle of the normal acceleration to stick position transfer function is about -235 degrees. Figure 13 shows that aerodynamics account for about -180 degrees of the total system phase angle of -235 degrees. Figure 14 shows that the pitch axis flight control system accounts for the remaining 55 degrees of phase angle at the PIO frequency.

These results support the pilot report that a PIO condition had indeed been encountered. They also show that the apparent source of the PIO problem is the airframe aerodynamics, which at best are only marginally stable for the conditions being investigated. When the mechanical flight control system characteristics are added to the aerodynamics, the instability becomes too extensive for the pilot to compensate.

Other flight test data are available which indicate that for the configuration and flight condition under investigation, the short period frequency is 5.6 radians/second and the damping ratio is 0.09. The  $\rm N_{\rm Z}/\delta_{\rm e}$  amplitude plot (figure 13) is ambiguous with respect to identification of the short period resonance. However, the phase angle transitions from zero degrees to -180 degrees at about 5.6 radians/second, indicating that the short period probably is located at this frequency. The ambiguous nature of the amplitude plot may be the result of insufficient data for a good analysis (a single ten second record), or it may be that lateral-directional coupling is showing up in this case also, in such a way as to obscure the short period. We are continuing to investigate these data.

It is clear from the power spectral density plots that the pilot's usable frequency range is limited to about ten radians/second. This observation is substantiated by other flight test data that we have analyzed and generally agrees with the literature. It is also interesting to note the frequency content centered at about fourteen radians/second. Evidently this is a neuromuscular contribution.

## SUMMARY

New frequency domain test and analysis techniques developed at AFFTC have proven to be a valuable tool for evaluating pilot-in-the-loop handling qualities in a mission oriented environment. This new approach to handling qualities testing and evaluation is based on time series analysis techniques.

Results of an analysis of precision air-to-air tracking data and of a pilot induced oscillation have offered valuable insights into the aircraft's closed-loop response and the pilot's in-flight power spectral density characteristics. Of especial interest is the discovery that, for the airplane being analyzed, significant and unexpected coupling exists between the lateral-directional and pitch axes at small angles of attack and sideslip. The influence of the coupling dynamics on longitudinal handling qualities appears to be only slightly less (about 3 db) than that of the short period dynamics.

The AFFTC is continuing to investigate and develop these new frequency domain handling qualities test and analysis techniques. While continuing to look at flight test data, we are also preparing to conduct an in-house simulation study. Our objectives are to reduce the quantity of data required for a good analysis, to investigate the suitability of additional test maneuvers, and to increase our experience in using these new handling qualities flight test tools.

#### REFERENCES

- Twisdale, Thomas R. and Franklin, David L., Captain, USAF, Air Force Flight Test Center, Edwards AFB, California, <u>Tracking Test Techniques for Handling Qualities</u> <u>Evaluation</u>, May 1975, FTC-TD-75-1.
- Otnes, Robert K. and Enochson, Loren D., <u>Digital Time Series Analysis</u>, New York, John Wiley & Sons, Inc., 1972.
- Bendat, Julius S. and Piersol, Allan G., Random Data: Analysis and Measurement Procedures, New York, John Wiley & Sons, Inc., 1971.
- Johnston, D. E., Ashkenas, I. L. and Hogge, J. R., Air Force Flight Dynamics Laboratory, Wright-Patterson AFB, Ohio, Investigation of Flying Qualities of Military Aircraft at High Angles of Attack, Volume 1, June 1974, FDL-TR-74-61.

## Acknowledgement

Mr B. Lyle Schofield, Chief, Flight Test Technology Branch (AFFTC/DOEST) was the first to recognize the potential value of a frequency domain analysis of precision tracking data. The authors wish to thank Mr Schofield for his conceptual and analytical insight and guidance. The authors also wish to thank Mr Schofield and Messrs David R. Mayhew (AFFDL/FGC), Jerry L. Lockenour (AFFDL/FGC), and William R. Turley (AFFTC/DOEST) for their help in evaluating the data presented in this paper.

Turn	Cooper-Harper rating	Feet on rudder pedals?	Pipper depression angle, mils
1	4.5	No	150
2	3	Yes	150
3	5	No	125
4	- 5	No	125
5	3.5	Yes	125

Table I. Summary of various data pertinent to the five precision tracking turns being analyzed (see also Figure 6)

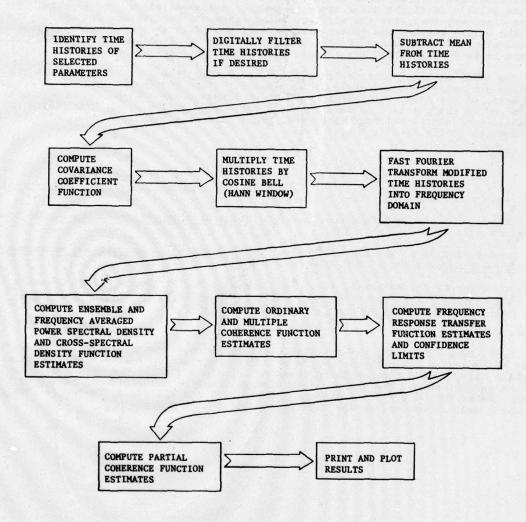


Figure 1. Simplified schematic outline of computations performed by Frequency Response Analysis computer program (FRA)

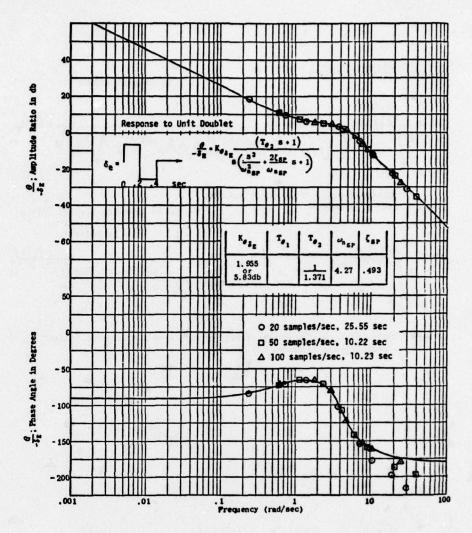


Figure 2. Results of check case to confirm analysis techniques implemented in Frequency Response Analysis computer program (FRA)

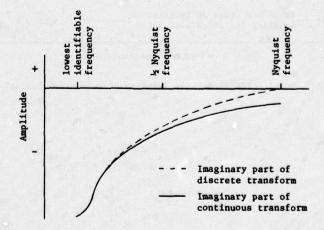


Figure 3. Comparison of the imaginary parts of discrete and continuous Fourier transforms

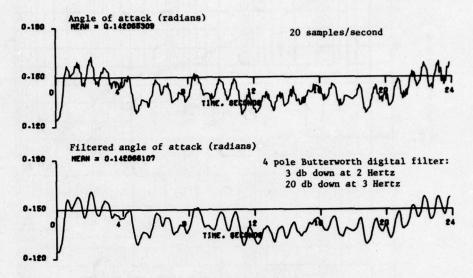


Figure 4. Time histories of angle of attack with resolution error "noise" included and filtered out.

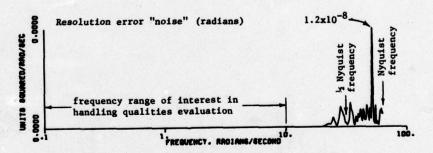


Figure 5. Power spectral density function of resolution "noise"

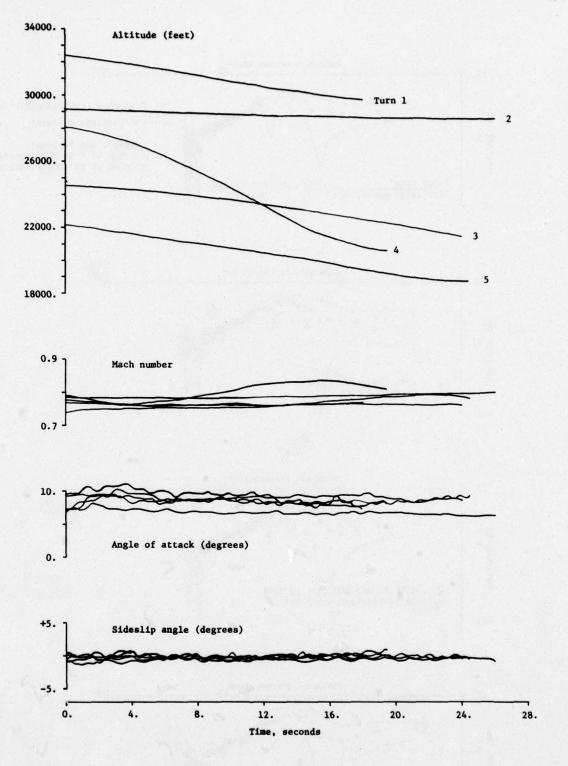
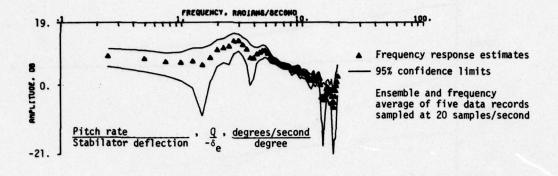
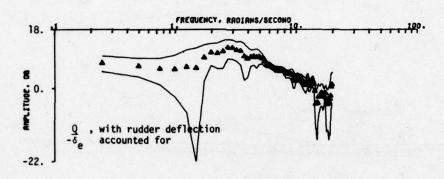
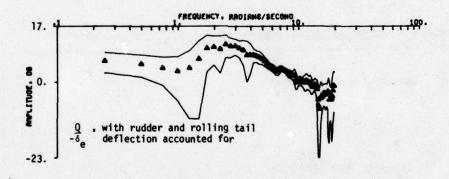


Figure 6. Flight conditions during precision air-to-air tracking turns being analyzed (see also Table I)







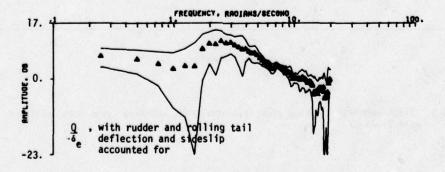


Figure 7. Bode amplitude plots of precision air-to-air tracking data, demonstrating sources of lateral-directional coupling into the pitch axis

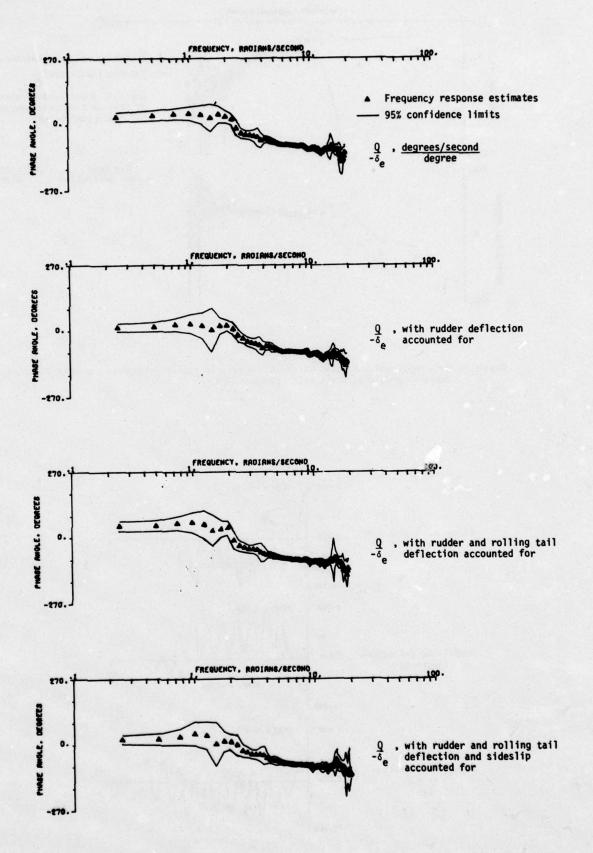


Figure 8. Phase angle plots corresponding to amplitude plots in Figure 7

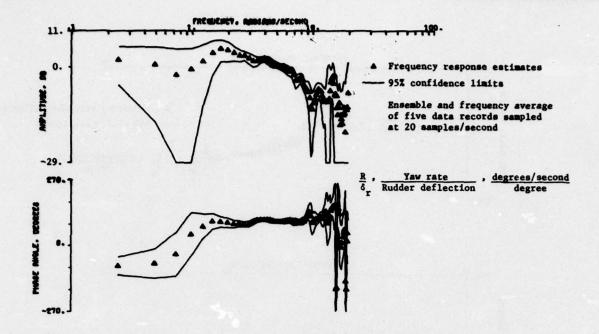


Figure 9. Bode amplitude and phase plots of yaw rate to rudder deflection transfer function, based on precision air-to-air tracking data

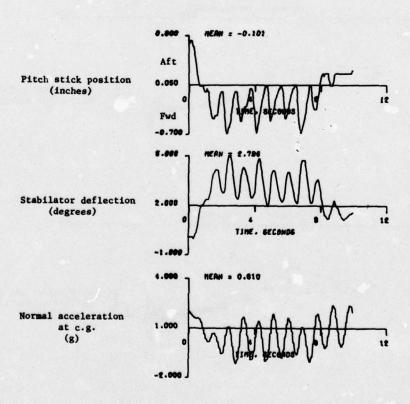


Figure 10. Time histories of pilot induced oscillation (PIO) data

A CONTRACTOR OF THE PARTY OF TH

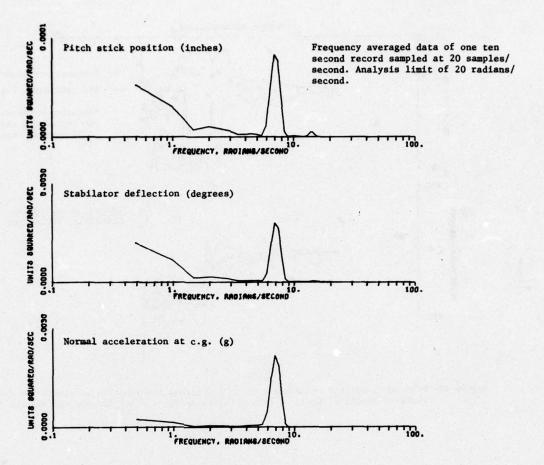


Figure 11. Power spectral density plots of three parameters recorded during a pilot induced oscillation (PIO)

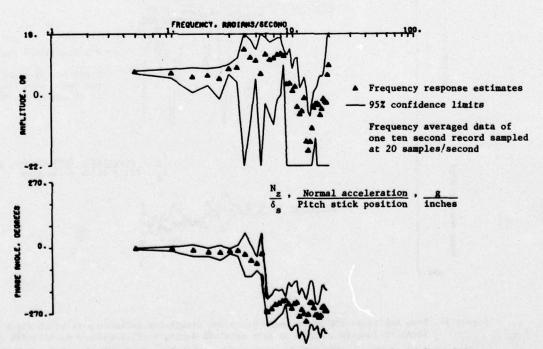


Figure 12. Bode amplitude and phase angle plots for normal acceleration to pitch stick position transfer function, based on data obtained during pilot induced oscillation (PIO)

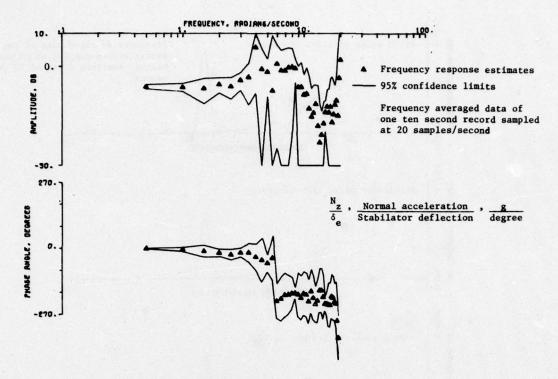


Figure 13. Bode amplitude and phase angle plots for normal acceleration to stabilator deflection transfer function, based on data obtained during a pilot induced oscillation (PIO)

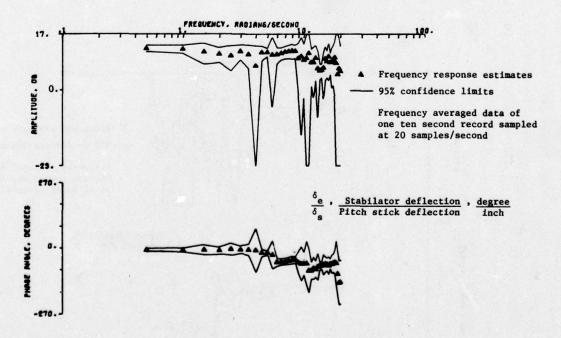


Figure 14. Bode amplitude and phase angle plots for stabilator deflection to pitch stick deflection transfer function, based on data obtained during a pilot induced oscillation (PIO)

OVERALL AIRCRAFT SYSTEMS EVALUATION

by
Frank N. Lucero
Charles E. Adolph
Systems Engineering Branch
Air Force Flight Test Center
Edwards AFB, California U.S.A. 93523

## SUMMARY

Today's military aircraft are extremely complex machines. The aircraft evaluation process and the organization required to accomplish the test have experienced a similar increase in complexity. Today's program managers must consider a multitude of technical specialties and test requirements simultaneously. This paper addresses the managerial and test procedures used by personnel at the Air Force Flight Test Center (AFFTC) to plan, conduct, and report on overall aircraft systems test programs.

## INTRODUCTION

The AFFTC evaluates all new United States Air Force manned aircraft, including advanced technology, prototype, and full-scale development airplanes as described in Air Force directives. These directives also prescribe the life cycle phases of a weapon system as shown in Figure 1. The AFFTC charter falls completely within the development, test, and evaluation (DT&E) area. However the AFFTC is not the only DT&E test agency; the combined efforts of personnel from the contractors and participating commands are also required. Further, the initial operational test and evaluation (IOT&E) is usually accomplished concurrently with DT&E.

Based on appropriate directives, DT&E is conducted to assess systems in terms of:

- 1. Development objectives identified in the Decision Coordinating Paper (published by the DOD), Program Management Directive (published by Hq USAF) and Program Management Plan (published by the AFSC Program Manager).
  - 2. Critical questions and areas of risk.
  - 3. Technical and contractual performance of the systems.
- 4. Engineering design relative to its practicality, safety, maintainability, reliability, logistics supportability, and suitability for operational use.

Using the above as a basis, AFFTC-conducted programs are oriented toward satisfying a variety of project requirements including determining compliance with applicable specifications, obtaining quantitative data for handbooks, obtaining procedural information for technical manuals, and identifying deficiencies which require corrective action. This paper addresses specific requirements and procedures used in the planning and conduct of USAF DT&E programs.

## TEST CHRONOLOGY

Most DT&E programs have a set pattern of evolution. Early participation of AFFTC personnel includes participating in program and design reviews, reviewing and commenting on all appropriate documents, such as specifications and hazard analyses, preparing detailed test plans, monitoring ground tests, and obtaining data for later use. Component qualification tests are not normally monitored at the vendors' facilities.

The overall evaluation begins as the first aircraft is assembled and the various subsystems are integrated for functional operation. During ground tests and the initial flight tests, the emphasis is on individual subsystem development and "debugging". This includes interface of the major subsystems. Flight tests begin with basic envelope expansion in the structures, flutter, and flying qualities areas. Initial functional systems checks are also performed. The contractor normally maintains the aircraft during this period. As the flight test activity progresses, the focus changes to an overall assessment of the total aircraft by subjecting the airplane to environmental extremes, allowable limits, and projected operational usage. Some of the subsystems are evaluated separately to obtain baseline information prior to evaluating the aircraft as a total weapon system. These tests are basically a continuation of the initial tests but the emphasis is testing against specification compliance and determining functional characteristics. The tests are designed to quantitatively and qualitatively assess the capability of the total weapon system to perform its design mission. Although not an integral part of the aircraft, support equipment must be evaluated as part of the total system. Reliability, maintainability, human factors, and other evaluations are accomplished to complete the test of support equipment and man-machine interfaces.

## PROGRAM MANAGEMENT

Test programs require a considerable amount of planning, defining objectives, organizing and staffing the test organization, identifying and obtaining required support, preparing detailed test plans and establishing reporting requirements. However, there are certain requirements that merit special attention. These include the following:

- l. Aircraft, systems and support equipment should be configured as closely as possible to a production version. (One of the problems in this area is that the test agency may be constrained to the use of preproduction aircraft and equipment which may not be updated in time to effectively evaluate the changes).
- 2. Instrumented aircraft and ranges must be available to provide quantitative analysis of test results.
- 3. Adequate calendar and flying time must be allocated to perform an effective evaluation.
- 4. The resources necessary to accomplish the program, including manning and facilities, must be provided.
- 5. The Air Force (customer) should maintain the test aircraft with adequate personnel, training, and skills to accomplish the test program effectively.
- Technical manuals that are adequate for use by maintenance, aircrew, and engineering personnel must be available.

## Organization

The test organization for a major program at the AFFTC is normally designated as a Joint Test Force (JTF). A JTF is organized and manned in a manner that will allow accomplishment of the program objectives, include all participating commands, and integrate all test and evaluation activities. A typical JTF is shown in Figure 2. To simplify the diagram, lines of communication within the JTF are not included. The number of personnel required is dependent upon the objectives, number of aircraft, complexity of the aircraft, and flying and calendar time required.

Present day major flight test programs focus on combined (AFFTC, contractor, and Air Force Test and Evaluation Center (AFTEC) and operating and support commands) DT&E/IOT&E (Initial Operational Test and Evaluation) programs. The AFFTC and the contractor are responsible for the DT&E portion of the program and AFTEC manages the IOT&E portion. One of the major areas of emphasis in working with personnel from the participating commands is to minimize duplication of testing and to insure that testing is oriented toward real-world requirements. The focal point for these operational command inputs is AFTEC. Although much of the testing has an operational flavor, critical parameters are rigorously controlled for an engineering assessment of test results.

A breakdown relative to the life cycle of a weapon system is shown in Figure 1. One of the key requirements in establishing a test organization is defining responsibilities. The concept used on the YF-16/YF-17 Lightweight Fighter Prototype Program, which met with considerable success and is being used as a model for other programs, included the following:

- 1. One Test Director (AFFTC) for DT&E. The test team was comprised of personnel from the AFFTC, AFTEC, participating command, and contractors.
- Combined detailed test plans. Preparation and coordination of specific plans were accomplished jointly by Air Force and contractor personnel. There was only one plan published for each area of test.
  - 3. Participation of Air Force pilots in all phases of testing.
- 4. Integration of Air Force and contractor engineers and pilots. The Air Force personnel were physically located with their contractor counterparts.
- 5. Availability of all data to all members of the joint test team. This concept facilitated independent analyses and reporting.
- 6. Combined Air Force (AFFTC, AFTEC, and participating commands) deficiency reporting. All deficiency reports were coordinated internally and therefore represented the total expertise and general consensus of the Air Force personnel.
- 7. Independent analyses and reporting. This allowed each organization to express its own views relative to its basic assumptions. This also gave the Air Force Management Agency (Program Office) added confidence in the test results on which all organizations agreed. In addition, it gave the Program Office more visibility and the opportunity to follow up on areas of disparity.

## Total Program Integration

There are numerous tests and evaluations that must be accomplished to adequately satisfy program objectives. One of the keys to overall systems testing is the inte-

gration of test planning and test activities.

Normally, all of the major systems and components are evaluated. Some are evaluated separately to obtain baseline data before evaluating the total system. As an example, accuracy of the ranging of a forward looking radar is assessed prior to determining air-to-air gunnery or weapon delivery accuracy.

Specific evaluations must also be integrated since many of them overlap. As an example, the human factors coverage must overlap into the pilots' evaluation of the cockpit and the maintenance evaluation. In turn, pilot's inputs are an important part of the stability and control evaluation.

## Instrumentation and Data Processing

Instrumentation and data processing systems are extremely important components of systems evaluation and require a significant amount of attention by program managers. The introduction of magnetic tape to airborne instrumentation systems approximately 20 years ago gave rise to the development of a variety of instrumentation hardware and software. Many airborne systems were developed in the United States by aircraft contractors to meet their own unique requirements. Compatibility with other facilities, such as the AFFTC, was not a design requirement since it was assumed that most of the data would be processed at the contractor's home plant. However, in many instances, the USAF eventually obtained the aircraft for testing. The AFFTC became involved with almost every type of aircraft and instrumentation system ever built in the U.S. This led to numerous support problems, such as incompatibility with data processing hardware and software, maintainability problems, and long data turnaround times because it was necessary to use nonproduction oriented operations to force data through the system. In addition, the system had little or no residual value to the USAF because of the proliferation of many unique, modified and often undocumented systems.

These problems, combined with the evolutionary changes in test philosophy towards joint testing, mandated standardization of data acquisition and processing systems. This led the AFFTC to develop, under contract, a modularized standard instrumentation system which could be easily maintained and supported as well as being compatible with AFFTC data processing facilities. This system is currently being used or is planned for use in a wide variety of future aircraft test programs. Its development and use has alleviated many of the past data acquisition system problems which confronted the AFFTC.

Similar problems were encountered with data processing hardware and software. Data acquisition system commonality solved some of the problems in these areas. In addition, action was taken at the AFFTC to develop and document a library of general purpose computer subroutines which can be combined with airplane unique subroutines such as engine thrust calculation procedures. This approach has alleviated many of the software development, checkout, control and documentation problems which occurred on past programs.

## Reporting

Written AFFTC reports on DT&E results typically include deficiency, management and final reports. (OT&E results are reported on separately and independently by AFTEC). A significant amount of effort is expended on deficiency reports since these are considered action documents. They are used to identify problems that should be corrected or studied for possible correction or refinement. The most effective method of preparing the deficiency reports is to have integrated inputs to each report from all interested organizations on the joint test team.

Management reports are submitted on a regular basis to the Program Office and other key organizations. Normally, they are submitted on a monthly basis and include program status and limited or summarized test results.

Final technical reports are published after the program is completed, or when significant portions of the test have been accomplished. Special emphasis is placed on including positive features as well as problem areas. Qualitative information and quantitative data are included. A compact test summary report is also published on some programs. The objective of this report is to present a concise overview of the entire test program in one document.

The AFFTC has also established a "corporate memory" data bank to feed back and compile problem areas with program management and major hardware problems. The intent is to have information available to aid personnel on new programs and thereby maximize utilization of past experience.

## SPECIFIC AREAS OF TEST AND EVALUATION

Certain tests are common to all aircraft programs. Included are functional tests of systems such as propulsion and avionics and integrated areas of evaluation, such as testing at various extremes. There are also evaluations such as the reliability and maintainability assessment which do not normally require dedicated flight time. Although not an integral part of the aircraft, support equipment must be evaluated as a

## Avionics Subsystems

The ultimate objective of avionics subsystem testing is to verify individual subsystem performance but at the same time evaluate the adequacy of the total integrated avionics package. One result of the sophistication of today's aircraft avionics systems is the difficulty in isolating systems for individual evaluation or trouble-shooting. The latest technological trend in integration of aircraft avionics systems is to employ digital data buses with internal time division multiplexing. This creates unique and challenging problems in the areas of instrumentation and software. Software is an integral part of the complete data acquisition system, and preparation for the evaluations begins with the initial software development and component fabrication. Early correlation of measured parameters with evaluation criteria is required as is a definition of the interface between airborne recording systems and ground processing of data. Subsystem components, instrumentation, and software are exercised and refined during preliminary development with dynamic simulation in an integration laboratory. Individual subsystem development dominates the initial flight tests. As the test activities progress, the focus changes to overall assessments of the total integrated avionics systems by subjecting the aircraft to allowable limits, projected operational usage, and environmental extremes.

There are a multitude of individual avionics subsystems and interfaces which may require evaluation. There are numerous ways of categorizing avionics equipment by functional elements. For discussion purposes, subsystems may be subdivided into the following major elements: navigation/guidance, fire control, penetration aids, communications, reconnaissance, automatic flight control, communications, central integrated checkout and auxiliary electronics equipment.

Rather than give a brief discussion of evaluation requirements for a number of the above subsystems, a system involving a number of interfaces will be treated in some depth. A terrain following system has been selected because it involves numerous avionics interfaces as well as with basic airframe subsystems such as the mechanical flight control system.

Terrain following radar (TFR) systems usually provide low altitude terrain following, terrain avoidance, and blind let-down capabilities. The TFR may consist of antenna-receivers, transmitters, computers and power supplies and a radar scope panel and a control panel. The TFR receives inputs from the radar altimeter, attack radar, bomb-nav system or auxiliary flight reference system and central air data computer.

With current TFR systems, the aircraft may be flown manually or automatically at a preselected terrain clearance. Climb and dive signals generated can be coupled into the attitude director indicator (ADI) and HUD. In the automatic mode, the climb and dive signals are coupled into the pitch channel of the flight control system. The TF mode can also be used to make blind let-downs to a preselected terrain clearance.

TFR test objectives typically include evaluation of manual and automatic terrain following modes, including an evaluation of performance against various terrain features such as sand dunes, trees, water, snow and sea-land transitions. The system must also be evaluated over terrain profiles which vary from gently rolling hills to abruptly changing mountainous terrain.

A TFR evaluation is a prime example of a type of test which blends an evaluation of integrated subsystem performance with an assessment of aerodynamic characteristics. Avionics subsystems evaluated during TFR runs include the radar, air data computer and cockpit displays, including the heads-up display. Airplane control characteristics and performance capabilities must be factored into the terrain following system to insure that terrain clearance profiles are compatible with the aerodynamic characteristics of the vehicle.

## Armament

The primary objective of armament testing is to determine if the aircraft/store combination can be employed to the criteria established by the technical specifications and user requirements. This includes testing for aircraft/munition compatibility and delivery accuracy. These are the final tests in a complex effort starting with the conception of a munition and an aircraft which demonstrate the ability of both to function as a weapon system.

Prior to beginning the certification process on a given aircraft, which is discussed herein, the weapon itself goes through a development cycle. To illustrate, a conventional bomb is designed to meet a given requirement which dictates shape, size, fin configuration, warhead arming and fuzing. The weapon is manufactured in prototype. Loading, fit checks and electrical compatibility tests are accomplished. The weapon is then tested for effectiveness against appropriate targets, arming/fuzing functions are evaluated and the ability to withstand airborne carriage environments is determined. If these tests prove satisfactory, the weapon is ready for certification on new and existing aircraft.

Initial tests are conducted in a wind tunnel using a wing model which simulates aeroelastic and structural characteristics of the aircraft wing. Weapon models are mounted on the wing and the critical airspeed for flutter is determined. Since the

store suspension and structural interfaces are extremely complex, ground vibration tests provide information on vibration frequency and damping characteristics. Flight tests are finally accomplished to validate the limit airspeed for the configuration.

The structural capability of a wing to carry external stores is first evaluated through laboratory stress-testing of critical load-carrying members. Flight tests are then conducted to validate structural integrity in positive/negative symmetrical and asymmetrical maneuvers. With flutter and structural limits established, the configuration is ready for validation of the separation envelope.

Separation characteristics are initially investigated in the wind tunnel. Model weapons may be separated from the wing in free-fall or in captive mode through sting balance measurements and computer positioning. Pitch, yaw, and roll rates are determined for varying airspeeds. The weapons are next separated from the aircraft with these parameters recorded by aircraft-mounted cameras. This data is compared with wind-tunnel results and a safe-separation envelope (airspeed-altitude) determined for the aircraft/store configuration.

The primary objective of store separation testing is to determine an airspeed/ altitude envelope within which a store may be safely separated from an aircraft. This may be a single store release or ripple (as used in weapon delivery) or jettison of a bomb rack with weapons attached.

In addition to analysis of single store separation, store/store collision after release and jettison of full/partially full racks and fuel tanks are also of interest. Ripple release of bombs is evaluated to determine the minimum release interval to obtain the tightest possible ground pattern without bomb collisions in flight. Determination of ejection velocity is also important for use in accuracy analysis and ballistic evaluation as discussed later. Clearance envelopes must also be determined for emergency jettison of loaded or partially loaded racks or pylone. Careful analysis of center of gravity locations must be accomplished prior to tests of this type. External fuel tanks may usually be jettisoned full with minimum difficulty. Empty tanks normally present problems at higher airspeeds as they tend to fly after release and may contact the aircraft. Partially full tanks may be difficult to jettison due to tumbling tendencies induced by center of gravity variations depending on the method of mounting jettison.

Weapon delivery accuracy evaluation is comprised of two major areas of endeavor: error analysis and a statistical presentation of weapon scoring. Error analysis is conducted to determine the reasons why the bomb missed the target. Errors may arise from two sources: (1) the aircraft was not at the planned release conditions when the bomb was separated, and/or (2) ejection/separation effects were such that the predicted ballistic trajectory was not obtained.

Aircraft dynamics at time of release are determined by range space positioning instrumentation and the recording of on-board parameters. If the bomb missed the target, the aircraft release conditions are reviewed to determine if planned release conditions were met. Errors on the ground are correlated with release errors. The analysis becomes more complex with computer bombing systems in automatic modes since the aircraft position at release is not preplanned. Here the aircraft conditions at release are compared with where the computer "thought" the aircraft was and the analysis conducted from this point. When aircraft release condition errors are identified, steps may then be taken to correct the problems which caused them.

If the aircraft was at the programmed release conditions and the bomb still missed the target, the problem lies in release dynamics; (i.e., delayed release, ejection velocity error) or basic weapon trajectory. Onboard cameras are used to study weapon separation and determine anomalies in the immediate vicinity of the aircraft. Phototheodolites are used to record weapon trajectory. The end result is an aircraft which can be positioned properly and a weapon which will hit the target (within the tolerances allowed in the weapon system specification).

A statistical analysis is prepared to present actual miss-distance data in a form which allows assessment of the system capability. Circular error probable (CEP) is perhaps the most common method utilized. In this analysis, the radius of a circle is defined which will contain 50 percent of all bomb impacts.

An important aspect of armament testing is the functional analysis of the weapon subsystem under all operating conditions including function in environmental extremes. A specific example might be a gunsight which vibrates from the set position due to a poor locking mechanism. These types of problems are evaluated throughout the test period and documented as they occur.

The instrumentation for armament system testing may be divided into three general categories: airborne systems to record aircraft parameters and photography, range instrumentation for external measurement of aircraft position/release conditions, and weather data for computation with range data. The armament engineer selects the airborne instrumentation parameters necessary to evaluate the armament test phase under consideration.

The physical properties of primary concern in armament testing are weight, center of gravity, and mass moments of inertia. Careful measurement and recording of these

properties is very critical for weapon separation characteristics. Stores must also be kept within these limits for accuracy testing due to effects on ballistic trajectory.

## Aerodynamic Characteristics

A typical US Air Force evaluation normally includes a significant amount of testing to define the aerodynamic characteristics of the aircraft. Aerodynamic tests are conducted to define performance, stability and control characteristics. Test objectives and procedures in these areas are generally well understood and are mentioned in this paper only for the sake of completeness. Airplane performance tests are accomplished to satisfy a number of objectives including data upon which to base any changes to flight manual performance curves which may be necessary. Other test objectives include obtaining data to determine compliance with performance guarantees, and data upon which to evaluate potential aerodynamic changes.

Stability and control test objectives include a definition of flight characteristics so that an adequate description of flying qualities can be included in the flight manual. Other major stability test objectives include obtaining data for comparison with specification requirements and for updating flight simulators.

## Climatic Testing

United States Air Force aircraft must be capable of worldwide operation and deployment on short notice. This commitment requires that the aircraft be capable of carrying out its assigned missions while withstanding climatic extremes throughout the world.

The overall goal of climatic flight test is to evaluate the aircraft, support equipment, maintenance procedures and related human factors while operating in the various environmental extremes. This is accomplished through four test phases: Climatic Laboratory tests at Eglin AFB, Florida, arctic tests at Eielson AFB, Alaska, tropic tests at Howard AFB, Panama Canal Zone, and desert tests at Yuma Marine Corps Air Station, Arizona, or El Centro Naval Air Station, California.

The primary goals of the Climatic Laboratory tests are to establish subsystem base-line data under controlled conditions and to identify any potentially hazardous climatic related deficiencies prior to flight tests. Any major deficiencies discovered in the laboratory are corrected and the modifications are evaluated at the remote test sites. The laboratory provides a full exposure of temperatures from -65 to 125 degrees F. All systems including the engine are operated in the laboratory. Normally, the tests begin at 70 degrees F and are then lowered to zero, -25, -45, and -65 degrees. Then they are raised to 70 and 125 degrees with the aircraft exposed to simulated rainfall and heat. Detailed aircraft inspections are accomplished after the cold and hot temperature exposure. Baseline data from the initial 70-degree runs and the 70-degree runs after cold soak and heat soak tests are compared.

The arctic test phase is conducted during January and February when the maximum number of cold days is normally encountered. The overall objective is the evaluation of aircraft operations in an extreme cold environment. The aircraft must be exposed (soaked) at or below -20 degrees F a sufficient length of time to allow internal stabilization of component temperatures at or near ambient conditions. Tests are then flown to simulate mission profiles while utilizing all of the systems.

The tropic test phase is normally conducted during October and November. The May-June time period may also be an acceptable alternative to the fall period. After periods of rainfall, the aircraft is inspected for entrapped moisture and initiation of corrosion. Special attention is also given to the environmental control system, due to the additional load required to remove humidity in the cooling period.

The desert test phase is conducted during July and August to expose the aircraft to maximum ambient temperature conditions, combined with high solar radiation levels. The aircraft is heat soaked for four hours prior to each mission and a 72-hour heat soak test is accomplished. Particular attention is given the environmental control system, hydraulic and engine lubrication system. Special attention is given the cockpit to exposure to solar radiation.

Instrumentation is a critical requirement for an adequate engineering evaluation. The time available for tests in the natural environments is brief and normally occurs only once each year. Systems deficiencies must be sufficiently well defined to identify casual factors and to allow for redesign as necessary to correct the problem. Airborne instrumentation may vary from 75 to over 300 parameters, depending on the complexity of the aircraft under test. Extensive temperature/pressure instrumentation is stressed. Engine oil temperatures and pressures, hydraulic system temperatures and pressures, and fuel temperatures and flow rates are typical examples. Selection of specific parameters is based on past climatic test experience and Air Force and contractor engineering requirements.

## Adverse Weather

The basic objectives of adverse weather testing are to evaluate the aircraft and its systems during all phases of operation in simulated and actual adverse weather and to establish operating procedures and techniques for inclusion in the flight manual.

This is accomplished by evaluating instrument flight characteristics during various phases of flight (descents, instrument approaches, etc.) and various simulated and natural climatological conditions (rain, turbulence, thunderstorm activities, etc.). Other general evaluations include evaluation of the cockpit, night operations, ground handling on runway surfaces covered with ice, snow, slush, and water, and effects on systems.

The simulation tests are conducted under stringently controlled conditions prior to conducting tests in natural conditions. Rain and icing conditions are simulated by the use of KC-135 and C-130 aircraft water spray tankers. Special emphasis is placed on analysis of ice formation and texture to verify icing severity, water droplet size, and ambient temperature conditions. In the case of the F-16 aircraft, very stringent lightning tests will be accomplished on the ground prior to flying near thunderstorm activities. After the simulation tests are completed, testing is accomplished in natural conditions.

Reliability and Maintainability (R&M)

The R&M evaluation results in qualitative and quantitative information. The latter includes data products such as mean-time-between failure and maintenance manhours per flying hour. The evaluation is heavily supported by maintenance personnel and must interface with the human factors efforts in a number of areas such as accessibility.

The basic procedure used to obtain, store, retrieve, and analyze all maintenance and operational data is called the Systems Effectiveness Data System (SEDS). This system is an Air Force Systems Command unique system and is designed specifically for use on weapon systems undergoing test.

The concept of building prototype aircraft to predict operational suitability and reduce risk had a resurgence in the U. S. in the early 1970's. The value of an R&M effort on a prototype program was the subject of considerable debate for a number of reasons. Normally, maintenance is performed by the contractor with very little (if any) USAF "hands on" maintenance activity. This limits the R&M evaluation to an overthe-shoulder observation exercise. Secondly, many features of prototype aircraft are not representative of a production article. As a consequence of these and other factors, objectives that have been developed as realistic expectations for protytype R&M evaluations are to: 1) identify system candidates for R&M improvement; 2) identify areas to retain prototype R&M; 3) identify system and component candidates for reliability verification testing; 4) compute achieved/forecast R&M parameters; and 5) update R&M analytical models. In addition, the maintainability evaluation will result in a qualitative assessment of operational suitability (access, skill level, inspection cycle, etc.), analyses of fault isolation equipment, logistics support requirements and maintenance technical data, determination of compatibility with USAF facilities, and assessment of training aids. In summary, the AFFTC believes the R&M evaluations are required to realize the full benefit of the prototype concept.

Human Factors Engineering (HFE)

The HFE evaluation is an integral part of the total weapon system evaluation and therefore is integrated with all aspects and elements of the Joint Test Force. It is concerned with determining whether USAF personnel can operate, maintain, and support the weapon system in its intended mission. The specific objectives are to determine if: 1) human engineering requirements and criteria (noise, temperature, access, comfort, visibility, performance and anthropometry) have been incorporated into the system design and are adequate; 2) biomedical and safety criteria lighting, toxic gas, acoustics, and ventilation) have been met; 3) the system provides for efficient human performance in its intended operational environment; 4) personnel (speciality codes, skills, and number) planning information is appropriate, complete, and adequate; 5) job performance aids are efficient and adequate; and 6) training and training equipment requirements have been addition there is participation in the technical publication verification effort.

The HFE evaluation is supported by the pilots and maintenance personnel. The methods of acquiring information include observations, interviews, debriefings, photography, and cockpit evaluations. In addition, a video tape is invaluable in documenting human tasks and verifying and extracting results. Flight test instrumentation is also used for obtaining cockpit toxic gas data and temperature.

Systems Safety

The Systems Safety evaluation consists of reviewing hazard analyses accomplished by the contractor, addressing systems safety during planning of hazardous tests, and classifying problem areas by hazard level. Although AFFTC personnel do not develop detailed hazard analyses, such as fault free analysis, reviewing the contractor analyses offers the opportunity of becoming familiar with areas of concern, providing feedback to the contractor and Program Office, and monitoring areas of concern throughout the program. A considerable amount of effort is expended in identifying hazards and hazard codes and effects of potential hazardous areas in deficiency reports. On some programs, safety related trends are determined by assigning hazard codes to inflight-discovered discrepancies.

# Technical Manual Verification

When new aircraft are evaluated, the technical manuals are preliminary documents that require verification by the Air Force. A team is organized within each Joint Test Force to verify their accuracy and format. After identification of problems, a board is convened to recommend appropriate changes. Interface between the participating commands is stressed; therefore board members include personnel from the contractor, Air Training Command, Air Force Logistics Command, using Command, and Air Force Systems Command. This provides feedback to allow the preliminary documents to be published as formal manuals for field use. The two major sets of documents include the maintenance and flight manuals.

# Support Equipment

The entire area of testing support equipment requires special attention. There is usually a multitude of support equipment which ranges from wrenches to very complex avionics equipment. This equipment should be evaluated individually and collectively for functional adequacy, human factors, reliability, and systems safety. Ideally, the equipment is evaluated for adequacy and against specification requirements during DT&E. However, many of the items are not available during DT&E or are not close enough to production configuration to allow effective testing. In addition, some items are not used within the course of the program and may not be evaluated unless the aircraft are specifically dedicated to evaluate them.

## Lead-the-Force Concept

A lead-the-force or high-flying-time test concept is addressed on some programs. This concept stresses the acceleration of flight time on selected aircraft so that these aircraft achieve a flying hour total that is 2-3 years ahead of the other aircraft. The intent is to identify problems that result from high flying time and to address these problems in an orderly fashion prior to achieving a comparable number of flying hours on many of the production aircraft. The overall concept requires a considerable amount of planning and resources. Priorities must be given in the areas of maintenance, logistics support, aircraft configuration and operations to keep the aircraft flying at the desired rate. Of special interest is flying typical missions with heavier than normal emphasis on operationally oriented tasks, such as air combat maneuvering with fighter aircraft. Periodic inspections or examinations are an integral part of the evaluation. The reliability and maintainability results from these aircraft are carefully documented and this in turn aids in evaluating the life cycle costs. After a thorough DT&E effort, the same aircraft could be transferred to an operational test status for continuation of lead-the-force flying.

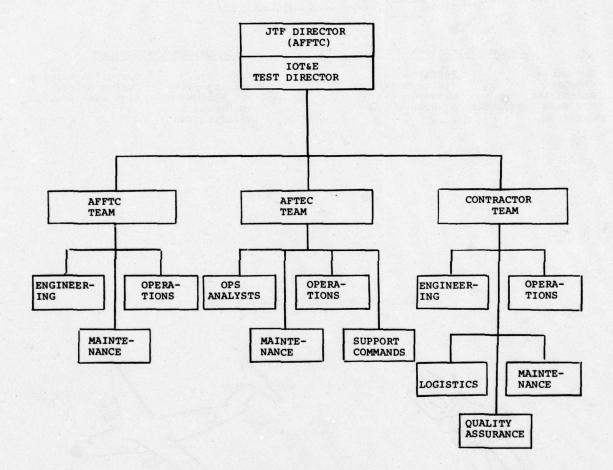
## CONCLUDING REMARKS

In conclusion, there are a number of salient points to be recapped. The systems evaluation of a manned aircraft begins as the first airplane is assembled and the various subsystems are integrated for functional operation. During ground tests and the initial flight tests, the emphasis is on individual subsystem developmental testing. As the flight test activity progresses, the focus changes to an overall assessment of the total aircraft by subjecting the airplane to environmental extremes, allowable limits, and projected operational usage. The overall evaluation is task-oriented in that emphasis is placed on evaluation during segments of typical operational mission profiles. Although certain operational tasks are duplicated, important parameters are rigorously controlled and there is an engineering assessment of test results. Although not an integral part of the aircraft, support equipment must be evaluated as part of the total system. Reliability, maintainability, and human factors assessment are accomplished to complete the evaluation of support and man-machine requirements. Development test and evaluation, as defined in United States Air Force directives, includes determining the technical and contractual performance of the system. Therefore, test results are used to satisfy a variety of requirements including determining compliance with applicable specifications, obtaining quantitative data for handbooks, obtaining procedural information for technical manuals, and identifying deficiencies which require correction. In addition, information is gathered for spares support planning, life cycle cost determination and for future subsystem design.

Figure 1
TEST AND EVALUATION ACTIVITIES
LIFE CYCLE PHASE

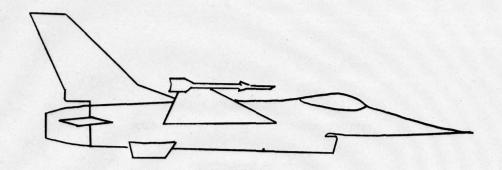
CONCEPTUA	L VALIDATION	FULL-SCALE DEVELOPMENT	PRODUCTION	DEPLOYMENT
5	DEVELOPMENT TEST & EVALUATION (DT&E)		FOLLOW-ON D	T&E {
overall T&E octivities				
	INITIAL OPERATIONAL TEST AND EVALUATION (IOT&E)		OT&E	
pecific JTF {	PLANNING & PARTICIPATING	COMBINED TESTS	FOLLOW-ON TES	TING
		INDEPENDENT ANALYSES		
		INDEPENDENT		

Figure 2
TYPICAL JOINT TEST FORCE ORGANIZATION



# Figure 3

#### GENERAL EVALUATIONS



# COMMON EVALUATIONS

Structure Cockpit Propulsion Airframe Subsystems Adverse Weather Avionics

Performance Flying Qualities Climatic

# CONCURRENT EVALUATIONS

Reliability Maintainability Human Factors Tech Manual Verification

Support Equipment System Safety High Time Concept

# Figure 4 SPECIALIZED AIRCRAFT EVALUATIONS



Weapons Delivery Gunnery Armament Air Combat Maneuvering
Integrated Fire Control System
Arresting Gear Compatibility
Photo-Recce



Ground Loading/Unloading Aerial Delivery Off-Runway Operation Rescue Operation

#### Table 1

# CRITICAL AREAS AND MAJOR SYSTEMS EVALUATIONS\*

# AI RFRAME

General Condition of Structure
Effects of Cumulative Loadings
Effects of Off-runway Operations
Effects of Aerial Delivery Operations
Airframe/Engine Compatibility
Airframe/Armament Compatibility
Airframe/Avionics Compatibility
Aircraft Radar Cross Section

# COCKPIT

Ground Ingress/Egress
General Arrangement
Display/Control Adequacy
Comfort/Workload
Canopy Operations
Field-of-View
Noise Levels
Toxicity
Cabin Conditioning
Anthropometry

# LANDING GEAR

Extension/Retraction Steering Characteristics Braking Characteristics Aircraft/Arresting Gear Compatibility Effects of Off-runway Operations

#### ENVIRONMENTAL SYSTEMS

Cockpit Temperature Survey
Cockpit Airflow
Pressurization Schedule
Ram/Dump Characteristics
Defog/De-ice Characteristics
Avionics Bay Cooling
Anti-g Suit Functional Adequacy
Oxygen System Functional Adequacy

# ELECTRICAL SYSTEM

Functional Characteristics Degraded Mode Characteristics Electromagnetic Interference Interface With Other Systems

#### HYDRAULIC SYSTEM

Functional Characteristics
Degraded Mode Characteristics
Operating Temperatures & Pressures
Interface With Other Systems

# FUEL SYSTEM

Ground Fueling/Defueling
Functional Characteristics
Degraded Mode Characteristics
Quantity Indication Accuracy
Dump Characteristics
Aerial Refueling
Fuel System/Airframe Compatibility
Interface With Other Systems

# FLIGHT CONTROLS

Functional Characteristics Flying Qualities Interface With Other Systems

#### ENGINE

Ground Start Characteristics
FOD Susceptibility
Trim Characteristics
Effects of Water Ingestion
General Operations
Engine/Airframe Compatibility
Engine/Armament Compatibility
Airstarts
Throttle Transients
Afterburner Relight Characteristics
Effects of Alternate Fuels
Exhaust Smoke Signature
External Noise Survey
Infrared Radiation Signature

# AUXILIARY POWER UNIT/JET FUEL STARTED/ EMERGENCY POWER UNIT

Ground Start Characteristics Manual/Auto Airstarts General Operations Effects of Alternate Fuels

# COMMUNICATIONS

Functional Characteristics Power Output Max Range Antenna Patterns

# NAVIGATION AIDS (TACAN, ADF, ILS, IFF, etc.)

Functional Characteristics Max Range Distance/Bearing Accuracies Attitude Limits

# FIRE CONTROL/NAVIGATION ACCURACIES (Radar, Inertial, Head-up Display, Radar Homing/Warning, etc.)

Functional Characteristics
Max Range
Accuracies
Attitude Limits
Effects of Terrain Surfaces
Interface With Other Surfaces

# ARMAMENT

Armament/Airframe/Engine Compatibility Gun System Accuracy Functional Characteristics (Stores Management, Launches, Racks, etc.) Carriage/Separation of Stores Interface With Other Systems

\*This is not intended to be a complete list but to show the magnitude of evaluating a major weapon system.

DETERMINATION OF ANTENNA RADIATION PATTERNS, RADAR CROSS SECTIONS AND JAM-TO-SIGNAL RATIOS

BY FLIGHT TESTS by

O.B.M. Pietersen G.J. Alders R.B.A. Wasch

National Aerospace Laboratory NLR Anthony Fokkerweg 2, Amsterdam, The Netherlands

#### SUMMARY

This paper contains information on a data acquisition and processing method, aimed at the determination of radiation patterns of airborne equipment. It describes the data acquisition procedure and, more specific, the data processing and presentation schemes used.

#### 1. INTRODUCTION

For evaluation and acceptance testing of newly installed airborne RF energy radiating or receiving equipment it is often necessary to measure antenna patterns or jam-to-signal ratios. Especially in the latter case it is not practical to obtain the required information by means of ground tests on scaled models or mock-ups of parts of the aircraft. Thus in-flight testing has to be carried out.

In the paper a flight test data acquisition and processing technique is described, which enables the measurement of jam-to-signal ratios, antenna patterns and radar cross sections as a function of aircraft aspect angle.

The method was developed in co-operation with the Royal Netherlands Air Force and the Laboratory for Electronic Developments for the Armed Forces for the evaluation of a prototype jammer installation.

#### 2. BASTCS

The method is described in its application to the measurement of jam-to-signal ratios of active radar jamming equipment, the purpose for which it was originally designed. Other applications, such as the determination of antenna patterns of radiating or receiving airborne antennas and the determination of the radar cross section of aircraft are within the capability of the method, since for the determination of the jam-to-signal ratio these parameters are measured separately.

The performance characteristics of aircraft antenna installations will be fixed with respect to an aircraft related co-ordinate system. The co-ordinate system used is shown in figure 1. The aspect angle is defined by  $\theta$  and  $\Phi$ .

When an active jammer is used, the RF signals flow as depicted in figure 2.

The power received by the ground element can be expressed in system properties as follows

$$\begin{split} \mathbf{S}_{\mathbf{J}} &= \mathbf{P}_{\mathbf{J}} \mathbf{G}_{\mathbf{J}} \mathbf{G}_{\mathbf{R}} (\frac{\lambda}{4\pi\mathbf{R}})^2 \\ \mathbf{S}_{\mathbf{T}} &= \mathbf{P}_{\mathbf{R}} \mathbf{G}_{\mathbf{R}}^2 (\frac{\lambda}{4\pi\mathbf{R}})^4 \; \frac{4\pi}{\lambda^2} \; \sigma \end{split}$$

where  $S_{J}$  = received power from the jammer (dependent on  $\theta$ ,  $\Phi$ )

 $S_{T}$  = received power reflected by the target (dependent on  $\theta$ ,  $\phi$ )

P<sub>J</sub> = power transmitted by the jammer (constant)

PR - power transmitted by the radar (constant)

 $G_J$  = gain of jammer antenna (dependent on  $\theta$ ,  $\Phi$ )

GR = gain of radar antenna (constant when tracking)

R - distance radar-target

 $\sigma$  = radar target cross section (dependent on  $\theta$ ,  $\Phi$ )

A = wavelength (constant)

At a certain moment, the aspect angles  $\theta$ ,  $\Phi$ , the received powers  $S_m$  and  $S_m$  and the distance R can be determined. The jammer antenna gain and the radar cross section then can be calculated.

$$G_{J} = \frac{s_{J}(4\pi)^{2} R^{2}}{P_{J}G_{R} \lambda^{2}} - K_{1}s_{J}R^{2}$$

$$\sigma = \frac{s_{T}(4\pi)^{3} R^{4}}{P_{P}G_{P}^{2} \lambda^{2}} - K_{2}s_{T}R^{4}$$

The jam-to-signal ratio can be obtained directly from the measured signal powers:

$$J/S = \frac{S_J}{S_m}$$

This J/S however, depends on the distance R:

$$J/S = \frac{S_J}{S_m} = \frac{4 \pi P_J}{P_R G_R} \frac{G_J}{\sigma} R^2 = K_3 \frac{G_J}{\sigma} R^2$$

To obtain a meaningful value the jam-to-signal ratio has to be normalized for a reference distance:

$$(^{J}/s)_{ref} = (^{J}/s)_{measured}(\frac{^{R}ref}{R})^{2}$$

To construct a  $(^J/S)_{ref}(\theta, \Phi)$  diagram it is thus required to determine  $S_J$ ,  $S_T$  and R, at a number of aspect angles  $\theta$  and  $\Phi$ .

#### 3. MFASUREMENT SYSTEM CONFIGURATIONS

The basic measurement system set-up (Figs. 3 and 4) consists of:

- a ground based tracking radar provided with a data acquisition system, serving as signal source as well as a measurement instrument.
- an airborne data acquisition system, primarily to measure the attitude of the aircraft.
- a synchronisation link between the airborne and ground based data acquisition unit.
- a communication link to enable information exchange between the airborne and ground-based personnel.

A number of alternative measurement configurations is possible: Once an instrumented tracking radar is available, other high frequency antennas can be slaved to this tracker as indicated in figure 5. This opens the possibility to measure the electromagnetic properties of aircraft installations at frequencies different from the tracker frequency or at several frequencies simultaneously.

Using the measurement system configurations as described above, the aspect angle is determined by combining radar range, azimuth and elevation information with the aircraft attitude data. Alternatively the aircraft navigation system can be used to determine aircraft position (TACAN, IME/VOR or an inertial navigation system). The data processing routine accepts these parameters as input. It should be noted that the position data obtained in this way provide less accurate aspect angles than the radar results when the measurements have to be taken at short distances (a few miles) from the radar. Such short ranges are usually necessary when testing ECM equipment.

In order to obtain information over the full hemisphere, the aircraft has to fly certain patterns. In a large number of locations in the Netherlands restrictions apply with respect to the utilisation of the airspace. Therefore no particular standard flight profile can be devised. Because in any aircraft attitude valid data is obtained, no significant limitations on the aircraft manoeuvres are imposed. Thus one can always define a pattern, tailored to the local situation that will yield the required data.

one can always define a pattern, tailored to the local situation that will yield the required data.

The data acquisition systems that have been used employ data loggers, that can accommodate 64 channels, sampled at a rate of one per second. Higher data rates were attained by using more channels for one parameter. Measured were the parameters listed below (between brackets the number of channels):

Recorded parameters in aircraft	Recorded parameters at the ground
Frame count (1)	Frame count (1)
Transmitted synchronization (1)	Received synchronization (1)
Received synchronization (1)	Transmitted synchronization (1)
Radio altimeter (4)	Radar distance (4)
Pressure altimeter (1)	Azimuth and elevation (8+8)
Angle of pitch (8)	Amplitude of received jammer signal (16)
Angle of roll (8)	Amplitude of received target echo signal (16)
Grid heading (1)	Radar "Lock-on" (1)
X and Y co-ordinates of inertial navigation system (1+1)	
Tacan range and Tacan bearing (1+1)	

Pictures of the data acquisition systems are shown in the figures 6 and 7.

The jammer in the aircraft was slightly modified such that jammer transmissions took place after a fixed delay following reception of the radar signal in the aircraft. This was necessary to facilitate the measurement of the power emitted by the jammer and the power reflected by the aircraft separately.

In the ground installation two time gates, separated by the same fixed time delay, were used for the measurement as illustrated in figure  $\theta$ .

# 4. DATA PROCESSING SCHEME

The two data tapes obtained with the ground-based and airborne data acquisition systems are fed into the computer, where the data is calibrated using standard routines. Than a series of three dedicated antenna pattern processing programmes is applied to the data. The general lay-out of the data processing for one particular test configuration is provided in figure 9.

The processing is divided into three parts, to facilitate debugging and to provide a sufficient flexibility in the creation of various types of output.

The first part is dedicated to the synchronisation of the flight— and the ground—data. The synchronisation signals are used to define in each data set the common points in time. These points are identified every second, with an accuracy of about 0.05 second. Since the common points in time will not coincide with the instants when the data samples were taken, an interpolation routine is used to determine the values of all parameters except the measured powers, at the common points in time, thus yielding one ordered synchronized data set each second. At this stage print—outs of the time histories can be obtained. The data is stored on tape.

The second part of the program converts the measured data into the required parameters. The attitude and position data of the aircraft are used to calculate the aspect angle. Further the applicable values of the target echo signal power and the jammer signal power are selected from the data set. From the 16 measurements in one second the one closest to the common point in time is selected to calculate the radar cross section, the jammer antenna gain and the normalized jam-to-signal ratio. The resulting data sets are stored on magnetic tape. Print out may be obtained.

The third part of the programme converts the data sets into graphic output. First a data-array is formed. Sphere elements are defined in terms of  $\theta$ ,  $\phi$ . The practical magnitude of these  $\theta$ ,  $\phi$  combinations has a lower limit, determined by the accuracy of the measurements. The smallest size that can be handled by the program is 2x2 degrees. This yields an array size of 16200 elements. In practice 5x5 degrees (2592 elements) is normally used. The data tapes are searched for data in these elements. For each sphere element the following information is determined:

i) number of observations.

 ii) average, maximum and minimum value of radar cross section, jammer antenna gain and normalized jam-to-signal ratio.

iii) standard deviation of these parameters.

With this array, plots can be made such as in figure 10, where the information is shown in numerical form (in this case for the radar cross section). Alternatively the data may be presented in graphical form for given conical cross sections of the sphere, see figure 11.

With this system set-up a high flying time efficiency can be obtained. The next table shows values that apply to a recent flight test programme.

measurement configuration	number of flights	total flight time (seconds)	number of valid data sets
A	5	23500	12400
В	5	17800	10400
С	2	5200	4100

# 5. CONCLUSION

The method described in this paper has proven to be a versatile tool in the determination of the properties of airborne RF radiating equipment and the determination of radar cross sections. Its main features are:

- no significant restrictions on the flight path to be flown by the aircraft.
- efficient utilization of flying time.
- data from individual flights can be combined to one result.
- the data sets can be used to construct diagrams in any required conical or planar cross section.

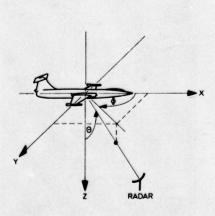


Figure 1 Co-ordinate system

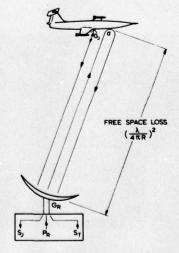


Figure 2 Signal power flow

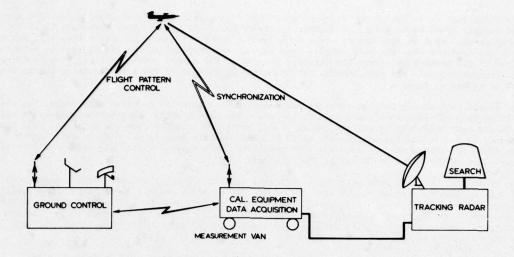


Figure 3 Basic measurement system set-up

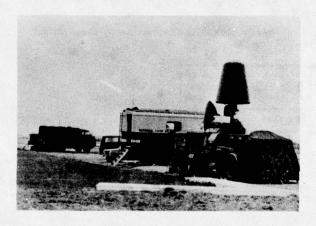


Figure 4 Measurement set-up at the ground

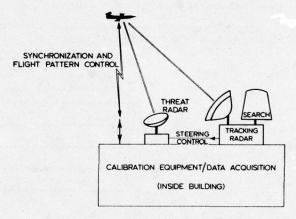


Figure 5 Measurement set-up in case of slaved antennas

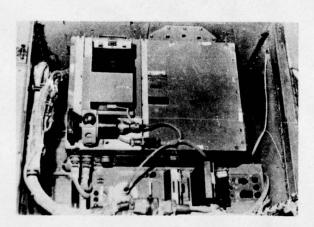


Figure 6 Airborne data acquisition system

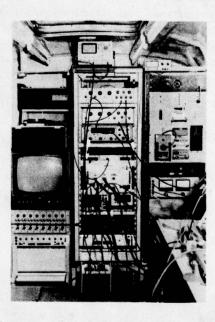


Figure 7 Ground-based data acquisition system

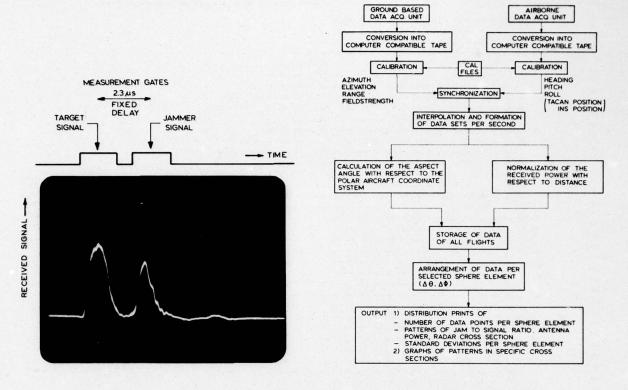


Figure 8 Measurement time gates in relation to the received signal

Figure 9 Data processing scheme

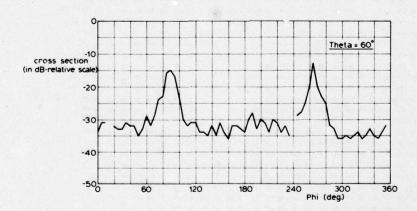


Figure 11 Radar target cross section at THETA =  $60^{\circ}$ 

```
THETAM 0 5 10 15 20 24 30 35 40 45 50 55 60 65 70 75 80 85 90 95 100 105 110 115 126 125 130 135 140 145 150 155 160 165 170 170 180
              -30 -24 -37 -37 -39 -35 -34 -35 -34 -33 -34 -32 -38 -38 -34 -27 -33
                 -23 -37 -41 -34 -35 -37 -34 -36 -31 -34 -29 -32 -32 -31 -33 -36
           -31 -27 -36 -39 -15 -35 -33 -34 -37 -34 -31 -29 -31 -31 -30 -32 -32 -34
                 -77 -37 -34 -34 -37 -34 -36 -36 -29 -32 -32 -31 -29 -32 -30
  20
                             -15 -31 -37 -37 -31 -34 -32 -32 -27 -28
                                                                       -33 -28 -30 -34 -29
  25
                           -35 -35 -36 -44 -30 -33
                                                          -37 -31
                                                                      -30 -28 -29 -28 -31
  30
                        -37 -34 -34 -37 -34 -37 -33 -29 -30 -31 -27 -29 -34 -32 -33 -35 -37
  34
                 -27 -14
                                  -36 -37 -34 -31 -31 -32 -31 -32 -30 -33 -33 -31 -29 -28 -27 -32 -28
  40
                                                                                                    -32
                     -28 -11 -32 -39 -36 -42 -35 -16 -32 -33 -36 -30 -31 -29 -36 -26 -30 -26 -30 -27 -32 -34 -33 -36 -32 -33 -32 -33 -32 -30 -34
  45
                                                                                                    -30 -34
                                                           -32 -32
                 -31 -37 -24 -35 -36 -31 -33 -33 -34 -35 -37 -30 -37 -37 -34 -31 -32 -32 -32 -31 -31
  55
                     -24 -24 -26 -29 -34 -37 -39 -33 -29 -33 -30 -33 -30
                                                                                    -34 -30 -29 -27
                        -24 -27 -29 -29 -31 -34 -29 -32 -32 -27 -31 -27 -33 -33
                                                                                 -26 -35 -35 -32 -26 -31 -27
  65
                    127 -24
                                  -2# -32 -33 -31 -32 -33 -31 -33 -31 -33 -35 -32 -34 -33 -35
                                                                                                 -31 -25
                                                                                                              -19
                                   -27 -33 -36 -29 -31 -30 -31 -32 -31 -34 -31 -36 -33 -35 -34 -36 -25 -28 -25
                       -22 -20
  75
                     -14 -19
                                       -24 -27 -24 -24 -27 -25 -30 -31 -32 -31 -31 -28 -26 -26 -30 -27 -29 -24 -23 -27 -20
  80
                  -17 -11 -17 -28 -19 -21 -25 -23 -23 -26 -26 -26 -25 -25 -25 -25 -25 -27 -25 -26 -26 -23 -25 -22 -22 -19
  .
                              -17 -21 -14 -18 -18 -16 -22 -21 -20 -27 -21 -21 -22 -19 -25 -10 -25 -19 -14 -20 -21 -21 -19 -28
                     -16
  90
                     -13 -27 -11 -15 -13 -15 -17 -15 -14 -14 -16 -19 -17 -21
                                                                                            -13 -19 -14 -14 -18 -16
                 -17 -14
                                   -16 -14 -15 -17 -17 -22 -20 -23 -25 -21 -24
 100
                                                                                          -19 -24 -21 -17 -16 -15 -12
                       -12 -20 -14 -10 -24 -23 -24 -27 -28 -31 -30 -25
                                                                                                -27 -21 -20 -19
 105
                 -29 -12 -19 -1H -2R -24 -26 -30 -30 -28 -32 -34 -34 -34
                                                                                 -37 -33 -32 -30 -27 -25 -22 -21 -19
 110
                 -17 -24 -27 -30 -28 -36 -37 -30 -34 -35 -34 -36 -37
                                                                                    -35 -35 -36 -35 -35 -27 -26 -16
 115
                        -22 -30 -29 -33 -29 -30 -33 -31 -30 -32 -33 -34 -33 -37
                                                                                     -34 -36 -37 -33 -35 -32 -30 -28 -23
 120
      -20
                                     -31 -31 -31 -31 -32 -33 -35 -34 -35 -37 -37 -38 -38 -35 -34 -40 -36 -35 -29 -32
                        -25 -32
 125
      -23
                 -27 -29 -40 -33
                                         -31 -33 -34 -32 -33 -34 -34 -34 -36 -35 -35 -36 -36 -38 -35 -36 -34 -38
 130
                   -32 -31 -29 -31 -35 -35 -35 -36 -32 -34 -36 -36 -33 -33 -36 -30 -35 -37 -38 -34 -35
 135
                 -2# -31 -32 -34 -30 =16 -34 -35 -33 -32 -34 -32 -31 -35 -29 -31 -30 -36 -37 -37 -35
          -23
 140
         -22
                                       -12 -31 -32 -33 -31 -31 -32 -33 -30 -32 -33 -36 -37 -37 -35
 145
                          -30 -35 -36
                                            -34 -35 -33 -34 -31 -31 -31 -32 -35 -36 -34 -34 -32
 150
                            -36 -37 -31 -32 -37 -31 -34 -33 -31 -29 -30 -33 -34 -32 -34 -32 -30 -28
 155
                                                                                                   -31
                    -34 -20 -32 -38 -24 -31 -36 -35 -34 -32 -31 -31 -32 -33 -32 -32 -32 -30 -27 -33
 160
                -33 -37 -37 -34 -35 -31 -35 -34 -32 -36 -33 -33 -37 -37 -31 -31 -29 -27 -28 -30 -30
 165
                 -37
                           -37 -34 -33 -35 -35 -33 -32 -31 -31 -31 -28 -28 -25 -27 -26 -29 -28 -30
 170
                 -35 -36 -34 -35 -36 -31 -32 -34 -35 -32 -31 -32 -29 -27 -27 -26 -27 -28 -32
 175
                        -34 -13 -35 -35 -36 -36 -35 -33 -30 -28 -29 -29 -25 -26 -27
 180
               -34 -17 -35 -35 -37 -36 -33 -34 -31 -28 -28 -26 -26 -26 -24 -27 -29 -31
 145
                    -32 -31 -31 -42 -34 -34 -35 -31 -39 -29 -28 -27 -26 -29 -28 -26 -27 -27 -31 -31
 190
                 -32 -36 -34 -38 -35 -37 -32 -28 -28 -31 -28 -29 -30 -28 -28 -28 -28 -28 -28 -28 -32
 195
             -34 -30 -38 -30 -37 -38 -37 -35 -35 -35 -37 -33 -28 -33 -31 -32 -27 -28 -29 -30 -30 -31 -30 -20
200
                          -34 -37 -35 -31 -39 -29 -30 -32 -33 -34 -34 -32 -29 -31 -30 -29 -30 -31 -30 -29 -30
205
          -33 -26 -37 -40 -34 -31 -30 -33 -37 -33 -33 -31 -31 -30 -34 -29 -30 -29 -30 -29 -30 -30 -30 -30 -30 -28 -37
210
         -24 -33 -36 -34 -31 -17 -39 -2# -31 -34 -34 -34 -30 -33 -30
                                                                       -26 -28 -31 -31 -31 -31 -31 -37
215
             -30 -34 -34 -37 -30 -34 -29 -34 -30 -32 -30
                                                                 -32
                                                                            -33 -32 -31 -29 -29 -32 -31
     -21 -26 -37 -35 -41 -37 -34 -47 -35 -32 -33 -31 -32 -32 -30 -33 -33
                                                                                   -27 -32 -33 -31 -34
225
        -32 -35 -35 -35 -36 -44 -20 -33 -33 -34 -31 -32 -20 -31 -34 -31 -27 -27 -33 -25 -33 -32 -31 -30 -32 -33 -31
230
         -27 -30 -28 -28 -13 -37 -32 -34 -33 -12 -32 -32 -33 -34 -32 -33 -29 -30 -37 -34 -31 -30 -32 -33
235
                      -11 -28 -34 -35 -29 -31 -35 -34 -31 -35 -36 -34 -31 -36 -35 -31 -36 -34 -31 -31 -31
240
                                         -33 -31 -33 -32 -31 -34 -35 -35 -33 -34
             -27 -25 -26 -24 -31 -29
                                                                                             -34 -32 -29 -26 -24 -23
245
                     -27 -29 -31 -17 -31 -30 -29 -33 -30 -33 -34 -34 -34 -34 -32 -33 -36 -33 -32 -27 -22 -22 -21 -26 -21
250
           -27 -19 -32 -20 -24 -22
                                         -28 -29 -28 -28 -32 -31 -32 -34 -34 -31 -40 -30 -35 -29 -25 -26 -26 -17 -23 -20 -13
755
            -23 -27 -21 -31 -24 -16 -20 -20 -25 -23 -25 -26 -26 -25 -29 -31 -30 -30
260
                                                                                       -30 -27 -24 -19 -17 -19 -14 -16 -18
            -17 -24 -10 -10 -14 -15 -23 -15 -20 -21 -19 -21 -25 -23 -22 -23 -22 -20 -22 -20 -19 -16 -15 -13 -14 -15 -14
245
              -21 -22 -17 -16 -15 -16 -17 -13 -15 -16 -16 -17 -17 -18 -17 -13 -16 -15 -16 -13 -15 -16 -12 -15 -16
270
         -21 -27 -21 -22 -23 -21 -18 -16 -10 -10 -15 -15 -20 -21 -20 -20 -10 -12 -17 -23 -22 -10 -17 -17 -18 -19 -18 -17 -17 -16 -16
275
     -31
               -27 -22 -25 -27 -21 -26 -21 -21 -26 -23 -26 -25 -23 -25 -21
                                                                                       -25 -22 -24 -23 -21 -21 -19 -20
280
            -76 -25 -24 -74 -22 -29 -26 -29 -26 -25 -28 -24 -28 -32 -24
                                                                                       -27 -26 -27 -25 -24 -23 -24 -20 -20
285
                  -28 -34 -31 -28 -24 -26 -32 -32 -31 -32 -31 -32 -33 -31
                                                                                       -35 -22 -28 -27 -25 -23 -20 -25
290
                -27 -28 -37 -30 -31 -33 -30 -33 -32 -32 -32 -33 -32 -33 -30
295
                                                                                   -31 -36 -35 -28 -28 -26 -28 -25
            -79 -28 -32 -31 -31 -32 -32 -42 -32 -31 -36 -30 -30 -37 -33 -35 -30
                                                                              -33 -34 -33 -32 -30 -31 -27 -26 -26 -27
         305
                                -36 -35 -37 -38 -15 -35 -32 -37 -33 -33 -31 -35 -31 -36 -32 -34 -31 -31 -29 -36 -28 -24
                  -33 -14 -32
310
            315
                                   -37 -37 -37 -35 -36 -38 -34 -33 -34 -38 -36 -33 -34 -31 -33 -32 -32 -31 -31 -25 -26
320
             -33 -34 -32 -35 -31 -37 -34 -35 -36 -33 -33 -34 -36 -35 -32 -32 -32 -32 -31 -31 -26 -28 -23
125
               -37
                        -19 -43
                                       -40 -36 -36 -35 -36 -30 -33 -30 -34 -34 -32 -33 -29 -30 -31 -31 -31
330
            -25 -35
                     -17 -44 -39 -34 -27 -35 -34 -34 -33 -35 -34 -34 -30 -31 -31 -30 -29 -29 -32
335
            -35 -31 -33 -37 -39 -41 -40 -38 -35 -33 -32 -32 -32 -31 -32 -33 -32 -31 -31 -28 -29 -27 -30 -28
340
                 -40 -30 -36 -38 -37 -36 -37 -36 -35 -32 -31 -37 -31 -31 -28 -28 -29 -30 -30 -30 -20
345
            -36 -47 -36 -30 -37 -34 -36 -37 -36 -33 -32 -32 -30 -27 -30 -30 -30 -20 -28 -26 -24
350
               -35 -28 -35 -35 -35 -35 -37 -37 -38 -34 -34 -31 -28 -31 -33 -29 -30 -31
395
                   -10 -47 -42 -37 -33 -34 -34 -32 -32 -37 -35 -30 -28
360
```

# REAL TIME DATA TRANSMISSION AND PROCESSING FOR THE DETERMINATION OF AIRCRAFT ANTENNA RADIATION PATTERNS

by

#### Helmut Bothe

Deutsche Forschungs- und Versuchsanstalt für Luft- und Raumfahrt e.V. (DFVLR)
Institut für Flugführung
3300 Braunschweig, Flughafen
Germany

#### SUMMARY

A measuring system determining aircraft antenna radiation patterns in flight has been developed.

The following paper describes the radiation pattern measurement technique. The measuring system requirements and configuration are outlined. Real time data processing and quick-look monitoring during flight tests are enabled by a telemetry system, the state of which is described in detail.

#### INTRODUCTION

On a modern civil or military aircraft a high number of antennas (sometimes up to 30 and more) are mounted at various locations to the aircraft. These antennas are serving numerous radio systems mainly associated with communications ground/air/ground and radio navigation. The antenna radiation patterns with their different requirements are frequently optimized by scale model measurements. But for official registration a required coverage has to be proven by in-flight measurements of radiation patterns from the actual aircraft due to inaccuracies in adapting the model measurements to the model laws.

It is well known, that flight tests are very expensive. Hence much cost can be saved by using an automatic measuring system with on-line data processing, that is able to keep the running time of the tests low. This can be done by real time quick-look monitoring the measurement results, which deliver a main decision element for the continuing flight test program. The following paper describes a system developed by the DFVLR, that fulfills these requirements.

#### RADIATION PATTERN MEASUREMENTS

The radiation pattern of an antenna is the sensitiveness of field-strength to direction in a constant distance. Measuring radiation patterns of aircraft antennas the instantaneous direction with respect to a field-strength measuring device (normally a ground station) must be determined. The instantaneous direction denoted by aspect angle can be computed if the aircrafts attitude and location are known. Normally the required constant distance between the antenna under test and the receiving station cannot be held due to imposed requirements on attitude. But the influence of a distance variation can be corrected when the distance is known.

Figure 1 shows the determination of the horizontal angle of aspect  $\phi$ . It can be seen, that  $\phi$  depends on heading angle  $\psi$  of the aircraft and the angle  $\beta$ , which is a function of the aircraft's location with respect to the receiving station M.

$$\phi = 180^{\circ} - \psi - \beta$$

A complete horizontal pattern can be caught by flying the aircraft on a horizontal circle. If the circle is flown with different angles of roll, radiation patterns in the corresponding inclined planes through the aircraft's roll axis are caught. If the antenna under test is acting as a transmitter, a receiving antenna has to be located in the plane of the circle flown. In flat country this requirement cannot exactly be met with a ground based receiving antenna. But a distance of 40 km between flight path and receiver results in a deviation of only a few degrees. The heading angle  $\psi$  and the location dependent angle  $\beta$  are expressed in a ground based coordinate system. Hence  $\phi$  in equation (1) is related to the same system. After Ref. [1]  $\phi$  can be transformed to  $\phi$  in an aircraft oriented system, if the roll angle  $\phi$  is known:

(2) 
$$\phi_{C} = \operatorname{arc} \cos \left( \left( \cos \phi / \sqrt{1 - \left( \sin \phi \sin \phi \right)^{2}} \right) \right)$$

Evaluating air/ground/air communication links and radio navigation systems the ground based coordinate system is most convenient and prefered.

Vertical patterns are achieved by flying across the receiving antenna M (Fig.2), where the aspect angle is denoted by  $\theta$ . This angle depends on pitch angle  $\delta$  and the

TOTAL THE STATE OF THE STATE OF

angle  $\zeta$ , which is a function of the aircraft's location with respect to the ground receiver M.

$$\Theta = 90^{\circ} + \delta - \zeta$$

These patterns are normally restricted to a range of  $180^{\circ}$  (below the fuselage of the aircraft) and may be slightly extended by the maximum allowable in-flight angle of pitch of the aircraft.

The necessary attitude parameters like angle of pitch, roll and heading are normally derived from gyro systems or a gyro platform.

Determining the position of the aircraft under test several systems with different accuracies like theodolite, radar, inertial navigation or radio navigation are usefull. The lowest system design effort can be achieved by using radio navigation systems like VOR/DME (Very High Frequency Omnidirectional Range System/Distance Measuring Equipment) and TACAN (TACtical Air Navigation System). Systems like VOR/DME or TACAN are installed in almost every well equipped civil and military aircraft. All necessary information determining the aspect angle is obtained on-board the aircraft. A telemetry system enables real time calculation in a ground computer. The inaccuracies in aspect angle caused by navigation errors are depending on the available radio navigation stations with respect to the flight area and the special systems used.

The different radio navigation systems are supplying distance (DME/TACAN) and/or bearing (VOR/TACAN) information. There are at least 4 possibilities to determine the position of an aircraft by radio navigation (Fig. 3). Which one is used depends on the available facilities in the flight area and on the required accuracies. The highest accuracy is achieved in version 3c while 3b and 3d are nearly equivalent. Due to its poor accuracy system 3a is unsuited for this kind of measurements. Using the possibility of Fig. 3b the position dependent angle  $\beta$  of equation (1) can be computed as shown in [2]:

(4) 
$$\beta = \arcsin \left[ \left( \sin(\alpha - \theta) \right) e / \sqrt{\rho^2 + e^2 - 2\rho e \cos(\alpha - \theta)} \right] - \theta$$

where  $\vartheta$  and  $\alpha$  are bearings of the aircraft and the field intensity measuring antenna.  $\rho$  and e are denoting the distances between the radio navigation ground facility and the aircraft respectively the ground measuring station.

The method of position finding pointed out in Fig. 3c is demonstrated in [3]. Here a Cartesian co-ordinate system with its origin at DME-station 1 has been chosen. Let the co-ordinates of station 2 be a and b and of the measuring antenna be m and 2n. The measured distances are  $\rho_1$  and  $\rho_2$  and the distance between DME 1 and DME 2 d. If  $\rho_1 - \rho_2 = \rho^2$ , then  $\beta$  is given by

(5) 
$$\beta = \arctan \frac{m - \frac{a}{2} \left(\frac{\rho^2}{d^2} - 1\right) \pm \sqrt{\frac{a^2}{4} \left(\frac{\rho^2}{d^2} + 1\right)^2 - \frac{(\rho^2 + d^2)^2/4 - r_1^2 b^2}{d^2}}}{\frac{\rho^2 + d^2}{2b} - \frac{a^2}{2b} \left(\frac{\rho^2}{d^2} - 1\right) \pm \frac{a}{b} \sqrt{\frac{a^2}{4} \left(\frac{\rho^2}{d^2} + 1\right)^2 - \frac{(\rho^2 + d^2)^2/4 - r_1^2 b^2}{d^2} - n}}$$

The configuration of Fig. 3d is described in [4] . Here the VOR (TACAN 1) radial intersects with a circle around the DME (TACAN 2) station. Again a Cartesian coordinate system with it's origin at station 1 is introduced. The coordinates of station 2 and the measuring antenna are a, b and m, n. The aircraft's bearing is measured by  $\vartheta$  and the distance to station 2 by  $\rho$ . Then the position dependent angle  $\beta$  of equation (1) becomes

(6) 
$$\beta = \arctan \frac{n - \cot \theta \left(\frac{b \cot \theta + a}{\cot^2 \theta + 1} - \sqrt{\left(\frac{b \cot \theta + a}{\cot^2 \theta + 1}\right)^2 + \frac{\rho^2 - a^2 - b^2}{\cot^2 \theta + 1}}\right)}{m - \frac{b \cot \theta + a}{\cot^2 \theta + 1} + \sqrt{\left(\frac{b \cot \theta + a}{\cot^2 \theta + 1}\right)^2 + \frac{\rho^2 - a^2 - b^2}{\cot^2 \theta + 1}}}$$

The determination of the position dependent angle  $\zeta$  in vertical diagrams (Eq. (2), Fig.2) is much less sophisticated. Here the location of the aircraft is determined by the method explained in Fig.3b while flying on a radial crossing the field strength measuring antenna. Under this condition  $\zeta$  becomes

(7) 
$$\zeta = \arctan \left[ \left( \sqrt{\rho^2 - h^2} - e \right) / h \right]$$

where  $\rho$  and e are the distances from the VOR/DME (TACAN) facility to the aircraft respectively ground measuring station and h is the altitude measured on-board the aircraft.

# MEASURING SYSTEM CONFIGURATION

The above mentioned radiation pattern measurements require a measuring system with onboard transducers, telemetry link and data processing facilities on ground. Designing the measuring system the number of data channels and the required accuracies are of great importance. They are listed in Table I.

Parameter	bandwidth Hz	max error %	data transmission error %
heading angle	1	.3	.1
pitch angle	5	2	1
roll angle	5	2	1
bearing (VOR/TACAN)	1	1	.3
distance (DME/TACAN)	2	.2 of range	< .1
altītude	< 1	2	1
6 house-keeping	< 1	_ 2	1

Table I

A number of 6 house-keeping data channels is added for

- checking radiated and/or reflected power of the telemetry antenna and the antenna under test
- monitoring 28 V DC and 110 V AC/400 Hz power supply of the system
- control of AGC voltages of one to two radio navigation receivers.

Tab. I shows, that a telemetry system with a few number of channels only is needed. Certainly all parameters have to be transmitted on one radio frequency carrier, thus a multiplexing system has to be chosen. The low bandwidth of the required channels and the high required accuracy in some channels of Tab. I normally would lead to a PCM-time division multiplex system. On the other hand Fig. 4 shows, that a PCM-system is not economical, if only a few channels are used. The reason is, that some expensive equipment like a bit and frame synchronizer is needed the price of which is independent of the number of channels. Compared to it the cost function of a frequency division multiplex with frequency modulated subcarriers starts at the O-point in Fig. 4. The economy of this system up to a number of 20 channels is obvious. The only problem is accuracy. The errors in an analog multiplex channel can hardly be kept below 1%. A way out can be found by splitting the high accuracy parameters into a coarse and fine signal. Especially in this antenna measuring system where only a few high accuracy parameters have to be transmitted, this solution is favourable.

Fig. 5 shows how the heading parameter is split up into two analog signals. The synchro output of the heading gyro is fed to a synchro to digital converter with a 12 bit binary parallel output. Starting at the most significant bit 4 binary outputs are connected to a 4 bit digital to analog converter the output of which forms the analog coarse signal with 16 distinct levels each one representing 22.5°. The remaining 8 output lines are forming the analog fine output in an 8 bit digital to analog converter. The full range of this output is 22.5° represented by 256 levels. That means a resolution of more than .1°. The error of a subcarrier channel can be kept at 1%. Therefore the total error in heading transmission will not be more than 0.23° = .1% as required in Tab.I. The 16-level coarse channel will not lead to any error if the individual level stays within at3% tolerance, which is well above the ±1% specification of a subcarrier channel. In this signal conditioning unit the only additional effort compared to a PCM-system are the two digital to analog converters.

A second example for an analog coarse-fine transmission is shown in Fig. 6. The DME-equipment used in this system has a binary coded decimal output. The four-line output of each digit is fed to a digital to analog converter where a ten-level signal for transmission in a subcarrier channel is shaped. This ten-level signal allows errors up to 15% in the analog channel without any degradation in accuracy. For a range up to 100 nautical miles 3 analog transmission channels are needed as the resolution is wanted to be .1 nautical mile.

In the data processing unit on ground the coarse and fine signals have to be combined again. The rise times of the transmission channels have to be smaller than the time between the sampling points of the two channels, which is 3ms in this system, if the channels are sampled right next to each other. Hence the required bandwidth of the coarse and fine channel is relatively large. Good experience has been gained with a ratio of 4 between sampling time and channel rise time. Then the lowest limit of bandwidth in the analog transmission channels is 470 Hz. That is about 100 times more than the required data bandwidth and a disadvantage of the coarse-fine transmission system. On the other hand in an IRIG-FM-multiplex with proportional-bandwidth channels this bandwidth is available in the upper channels anyhow.

#### INSTALLATION OF THE MEASURING SYSTEM

The complete airborne system is shown in Fig. 7. It consists of the necessary transducers and transducer systems, the coarse-fine splitting and signal-conditioning circuits matching the transducer outputs (a potentiometer for altitude, synchros for heading, pitch and roll angle and VOR bearing, voltages for TACAN bearing, distance and house-keeping parameters) to the inputs of the voltage controlled frequency modulated subcarrier oscillators (VCO). The VCO outputs are now mixed linearly and the composite signal frequency modulates the telemetry transmitter. Transmission is possible in the VHF and UHF telemetry bands. Small airborne transmitters exciting the antennas under test in question have been built. They are covering the frequency ranges of currently installed radio aids in civil and military aircraft.

Though the whole airborne system including VOR and DME is constructed as a black box (Size 0.25 m³, weight 75 kg, power consumption 300 VA) the aircraft's VOR and DME antennas are needed and a telemetry antenna must be installed. If the radiation pattern of the VOR antenna itself has to be measured, this antenna can be excited via diplex equipment at the same time. During pattern recording of the DME antenna the DME equipment can be connected to the secondary radar transponder antenna. By that the transponder is put out of operation.

If necessary the airborne equipment can be kept much smaller and lighter if it is possible to derive attitude and radio navigation parameters from the avionic system of the aircraft. But due to matching difficulties it is preferred to make use of the complete self-sufficient antenna measuring system.

In the ground station (Fig. 8) the received telemetry signal is heterodyned down to a low intermediate frequency. After demodulation of the radio frequency carrier the individual subcarriers in the composite signal are separated and demodulated by the subcarrier discriminators. The outputs of the discriminators as well as the output of the field-intensity meter are sampled and digitzed 10 times per second each. The composite subcarrier signal, and the field-intensity signal are recorded on magnetic tape (postdetection recording) for reproduction purposes of the measurement results. The field-intensity signal modulates a VCO (IRIG channel number 6) whose carrier is mixed linearly with the composite signal, in which this channel must be omitted on-board. Now all information including field-strength can be recorded on one track of the magnetic tape recorder.

All digitized data is transferred to a computer. First the coarse-fine channels are recombined. For this purpose the coarse channel levels are accurately replaced by predetermined values. Then the fine channel values are scaled down and added to the appropriate coarse channel information. After that the horizontal angle of aspect \$\phi\$ is computed 30 times per second according to equation (1) considering also one of the Eq. (4), (5) or (6) depending on the radio navigation system used. If the vertical angle of aspect 0 is wanted, Eq. (3) and (7) have to be used. Furthermore, corrections have to be made in accordance with Eq. (2), if an aircraft oriented coordinate system is preferred. Variations in the distance d between aircraft and field-strength measuring antenna have to be corrected by the link attenation factor D

$$p = 20 \log \left(\frac{d}{Km}\right)$$

Limit exceedances for instance in angle of roll or pitch, are checked and printed out. Finally flight-path information, derived from angle ß and distance d in Fig. 1, and radiation-pattern information which are present in polar coordinates are transformed to Cartesian coordinates by the computer. After digital to analog conversion real time recording of radiation pattern and flight path is done by two analog x-y-recorders. Each x- and y-output parameter is calculated 30 times per second.

Sometimes measurements have to be made externally for different reasons. Then the data processing part of the ground system is not available. In this case the system outlined in Fig. 9 will be used. The x-y-recorder writes field-strength with respect to heading angle for quick-look demonstration of the uncorrected radiation pattern in polar coordinates. To avoid a complex coarse-fine recombiner in the receiving station an additional subcarrier channel is used to transmit the total heading angle. The input signal of this channel is gained by an additional 8 bit digital to analog converter connected to the synchro to digital converter output in Fig. 5 starting at the most significant bit. In addition 8 important channels are monitored on a strip chart recorder and all information is stored on analog magnetic tape for data processing later on. To control the flight path the radio navigation parameters are indicated on panel meters.

## ERRORS OF THE SYSTEM

The measured radiation intensity is normalized to its maximum value. Recording of one pattern will last only a short period of time. Therefore the gain stability of the field intensity measuring device including exciter transmitter is not critical. The main errors are caused by the amplitude characteristic of the logarithmic amplifier, which is specified to ± 1.5 dB error over a full range of 70 dB.

In horizontal pattern recording angle of aspect errors are caused by different influences. Errors in angle of heading  $\Psi$  will fully enter into the aspect angle  $\Phi$ . They are

kept below 1° as an airline quality gyro is used. Radio navigation errors enter into the aspect angle ¢ to a degree, which depends on the position of the aircraft compared to the radio navigation station in question and to the location of the field-strength antenna. Another factor is the chosen radio navigation station itself. A computer program is prepared to calculate the expected errors when the radio navigation station and system parameters are put in. Some examples are given in Ref. [2], [3], and [4]. These examples show, that in most cases this error can be kept well below 1°.

When vertical patterns are recorded the error in angle of pitch fully enters into the angle of aspect  $\theta$ . It is caused by the vertical gyro and can be kept well below  $1^{\circ}$ . Errors in altitude h and distance  $\rho$  measured by DME are more severe. It has been shown in Ref. [2] , that errors in the order of  $2^{\circ}$  have to be expected.

#### EXAMPLES OF MEASUREMENT

In Fig. 10 the measured horizontal radiation pattern of a UHF blade type antenna installed on the upper side of the fuselage of a fighter aircraft is shown. This pattern has been measured at an exciting frequency of 395 MHz during a left 360 turn of the aircraft, while the roll angle has been 30°. Fig. 11 demonstrates the ability of the mobile quick-look system (Fig. 9) without on-line data processing. The shape of the two patterns is very similar. The corrected pattern (Fig. 11) shows small differences in agrect angle  $\phi$ . For instance the glitches at  $\phi=230^\circ$  and  $\phi=240^\circ$  are rotated by about 5°.

#### FURTHER DEVELOPMENTS

In the near future large transport aircraft may be equipped with antennas for air-to-satellite communication. These antennas will be installed on the upper side of the fuselage and the radiation pattern will be directed towards the sky. Due to manoeuvring restrictions the patterns will not be measurable by a ground station but by a second flying aircraft. Attitude and navigation parameters of both aircrafts are needed for aspect angle calculation. Real time data processing presumed two telemetry systems are needed. An uplink providing the pilots with path following information computed on ground is nearly mandatory. A system performing these requirements is under development.

In the data processing area additional programs will be prepared to allow statements about the performance of the antenna radiation patterns with respect to a required coverage.

Until now the measured patterns are providing the relative radiation intensity. For absolute measurements including antenna efficiency the isotropic radius (the radiation pattern of a fictitious isotropic radiator on board the aircraft) has to be added to each measured diagram. The determination of the isotropic radius requires standard gain antennas in the surroundings of the aircraft. Influences of the airframe and propagation irregularities like ground reflections have to be avoided carefully Ref. [5]. Work is going on on this subject too.

#### REFERENCES

- [1] MATTES, H., HINZPETER, U., "Ermittlung der Strahlungscharakteristiken von Flugzeugbordantennen im Fluge", Nachrichtentechnische Fachberichte Band 45, S. 180 185,
  Berlin: VDE-Verlag 1972
  and
  HINZPETER, U., MATTES, H., "Real-Time-Meßverfahren und -Meßanlage zur Flugvermessung
  der Strahlungsdiagramme von Flugzeugbordantennen", DLR-Forschungsbericht 73-97,
  505 Porz-Wahn: DFVLR, 1973
- [2] BOTHE, H., "In-Flight Measurement of Aircraft Antenna Radiation Patterns", AGARD-CP-139, Antennas for Avionics, 1974, p. 35-1 to 35-9
- [3] BOTHE, H., "Weiterentwicklung des DFVLR-Systems zur Antennenvermessung im Fluge durch Einsatz von zwei DME-Geräten", DFVLR-Institut für Flugführung, Interner Bericht 153-74/17, Braunschweig 1974
- [4] BOTHE, H., HAENSEL, H., "Flugvermessung der Strahlungsdiagramme von 12 Bordantennen des Alpha Jet", DFVLR-Institut für Flugführung, Interner Bericht 153-75/38, Braunschweig 1975
- [5] KLEIN, K., "Feldstärkeuntersuchungen zur Beseitigung von Bodenreflexionsstörungen bei der Antennenvermessung im Fluge", DFVLR-Institut für Flugführung, Interner Bericht 153-76/08, Braunschweig 1976

[6] "Telemetry Standards Document 106-71, Appendix A", Inter Range Instrumentation Group (IRIG), Range Commanders Council, White Sands Missile Range, New Mexico 88002

# ACKNOWLEDGEMENT

The author wishes to acknowledge the assistance of N. Döler, H. Haensel, H. Keese and K. Klein during the further development and test of this system.

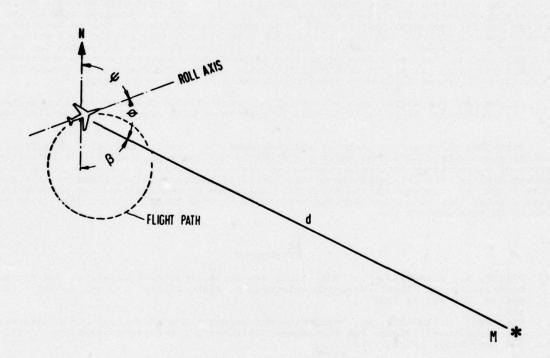


FIGURE 1: DETERMINATION OF HORIZONTAL ASPECT ANGLE

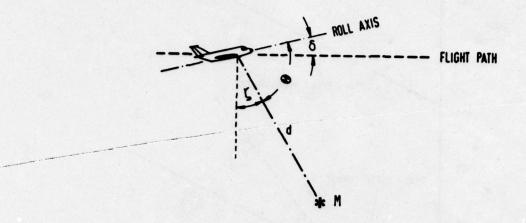


FIGURE 2: DETERMINATION OF VERTICAL ASPECT ANGLE

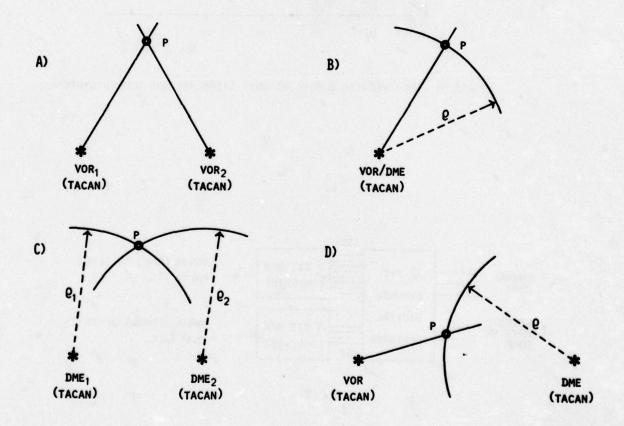


FIGURE 3: POSITION DETERMINATION BY RADIO NAVIGATION

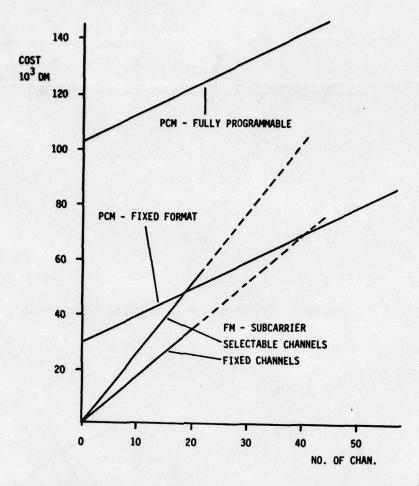


FIGURE 4: MULTIPLEXING EQUIPMENT COST (AIRBORNE AND GROUND SYSTEM)

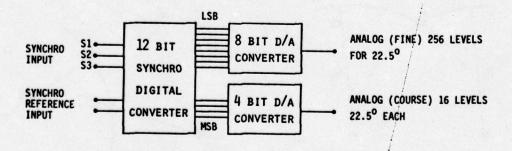


FIGURE 5: HEADING SIGNAL CONDITIONING UNIT

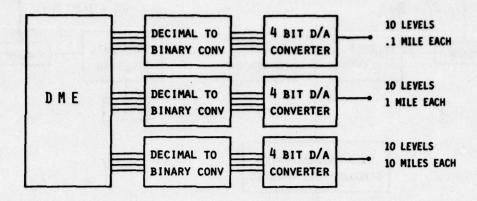


FIGURE 6: DISTANCE MEASURING EQUIPMENT SIGNAL CONDITIONING UNIT

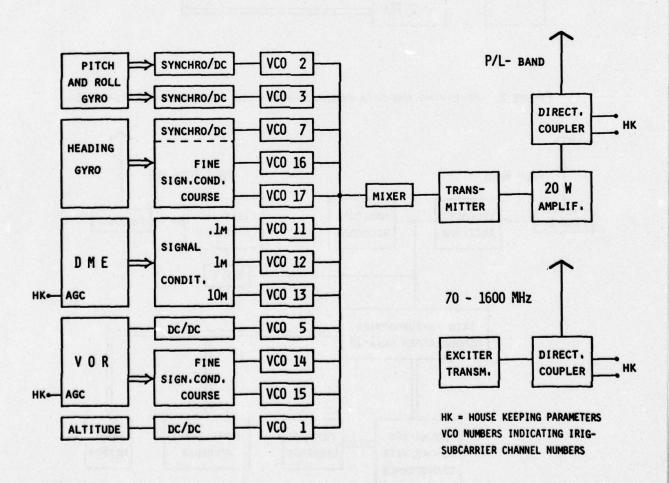


FIGURE 7: AIRBORNE SYSTEM FOR ANTENNA PATTERN MEASUREMENTS

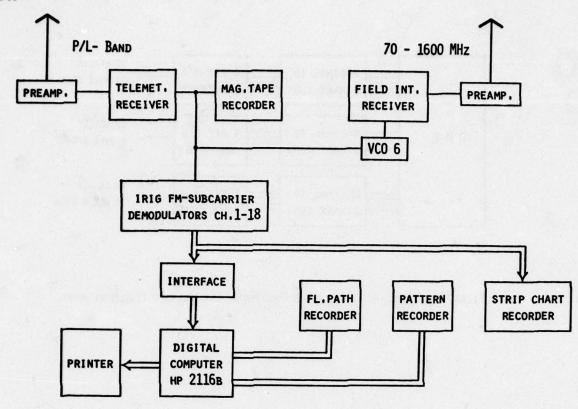


FIGURE 8: RECEIVING AND DATA PROCESSING STATION FOR ANTENNA MEASUREMENTS

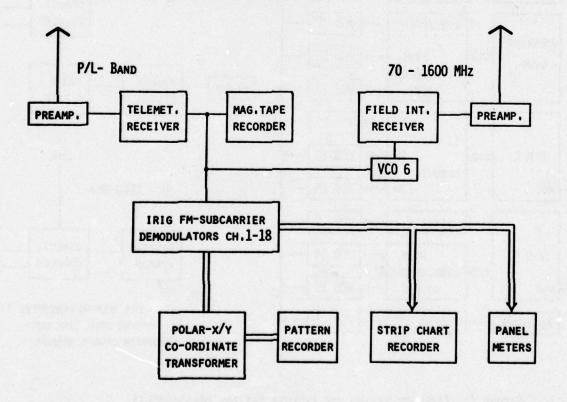


FIGURE 9: MOBILE RECEIVING STATION WITH QUICK-LOOK FACILITIES

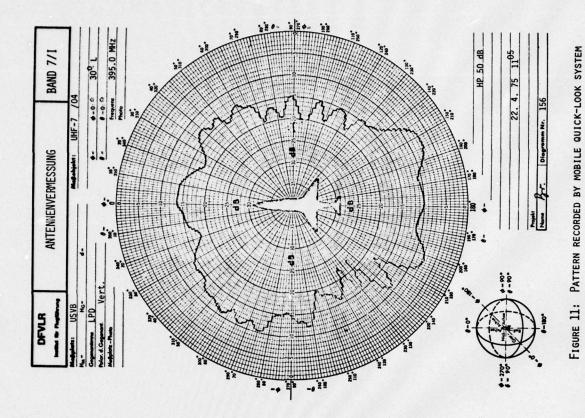


FIGURE 10: PATTERN RECORDED BY DATA PROCESSING SYSTEM (FIG. 8)

#### HYBRID REFERENCE SYSTEMS FOR FLIGHT TESTING

Heinz Winter and Ulrich Brokof Deutsche Forschungs- und Versuchsanstalt für Luft- und Raumfahrt e.V. (DFVLR) Institut für Flugführung 3300 Braunschweig, Germany

#### SUMMARY

Hybrid reference systems consisting of ground-based measuring equipment (tracking radar, long distance radar) and on-board sensors (Doppler or inertial navigation systems) have been analysed with respect to the accuracy of position, velocity and attitude measurement. Flight experiments have demonstrated that the high accuracies required for weapon guidance systems testing can be obtained with such systems.

#### 1. INTRODUCTION

For the evaluation of flight tests, high precision reference information is required for the aircraft trajectory, velocity, attitude and heading. In this paper hybrid combinations of ground-based equipment (tracking radar, long distance radar) and on-board sensors (Doppler or inertial navigation systems) are analysed with respect to the obtainable accuracies. The ground-based sensors provide low-frequency information about the aircraft flight path. These measurements are combined with those of the on-board sensors, which give the required high frequency information, in an optimal smoothing algorithm. The high accuracies of such hybrid systems have been varified in various flight tests for the accuracy calibration of hybrid navigation systems [1, 2] and during the flight testing of the german microwave landing system DLS [3].

# 2. TEST FLIGHT PROFILES AND SENSOR ERRORS

As typical examples of flight test profiles, a long range and a short range test flight, flown with the HFB 320 test aircraft of the DFVLR have been chosen for the demonstration. Figure 1 shows the long range test flight from Hannover airport, via Meppen, Norderney and Helgoland back to Hannover. This test flight lies partly within the coverage range of three tracking radars, which are located at Hannover (L4/3), Meppen (MPS-36), and Norderney (Fledermaus). Figure 2 shows the short range test flight in the vicinity of Hannover airport. This flight profile lies completely in the coverage range of the L4/3 tracking radar. Tracking radar measurements are taken every 10 seconds.

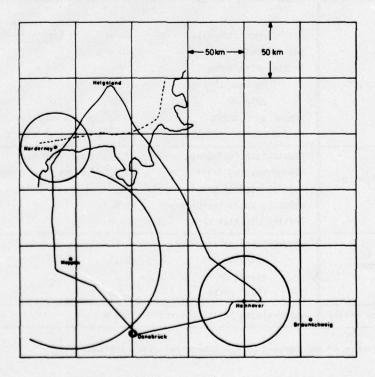


Fig. 1 Long range test flight. Tracking radars at Hannover, Meppen and Norderney.

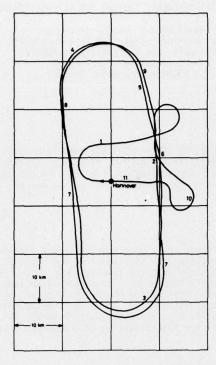


Fig. 2 Short range test flight. Tracking radar at Hannover.

For the analysis, as an alternative to the tracking radar, the case has been considered that both test flights have been completely measured with a long distance radar (measurements every 10 seconds). The assumptions about the measuring errors of this device (s. Table 1) are such, that they also correspond to range-range TACAN measurements.

	Errors (1σ)	
High accuracy INS	initial position error initial velocity error initial misalignment - horizontal axes - azimuth random gyro drift random accelerometer error	20 m in each axis 0 m/s  20" 3' 0.01° in one hour (random walk) 10 <sup>-4</sup> g (averaged over 0.2 s)
Doppler navigation system	fluctuation (velocity) error random heading drift initial heading misalignment velocity scale factor error initial position error	
Tracking radar	uncorrelated errors - azimuth - elevation - slant range	0.1° 0.1° 10 m
Long distance radar	uncorrelated position error	200 m

Table 1 Errors of the sensors of the hybrid reference systems.

As on-board sensors, the Litton LN3 inertial platform, the SYP-820 attitude and heading reference system and three different types of Doppler radars (stabilized and fixed antennas, pulse and CW Dopplers) have been used for the flight tests. The data of the ground-based and the on-board sensors have been written on magnetic tapes, and the evaluation of the flight tests has been made with the main computer of the DFVLR Braunschweig.

The error model for the LN3 inertial platform is given in Figure 3 for the three channels. This error model contains the Schuler loops, earth rate-, velocity- and acceleration-couplings. The vertical channel (both in the INS and in the Doppler) is independent of the horizontal channels. The vertical channel problem is not considered in this paper (s. [1] and [4]). The error model for the Doppler navigation system is given in Figure 4. The main error sources are: Velocity scale factor error, heading error and Doppler fluctuation. The numerical values of the sensor errors, which have been used for the analysis and the flight test evaluation are summarized in Table 1.

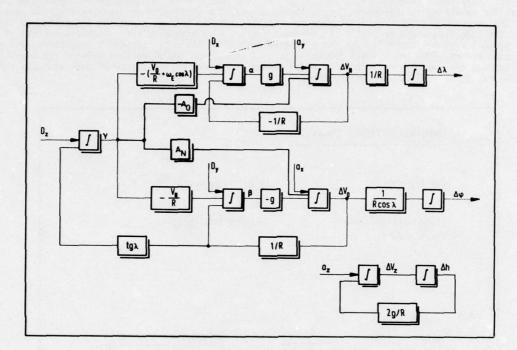


Fig. 3 Error model for the LN3 inertial platform

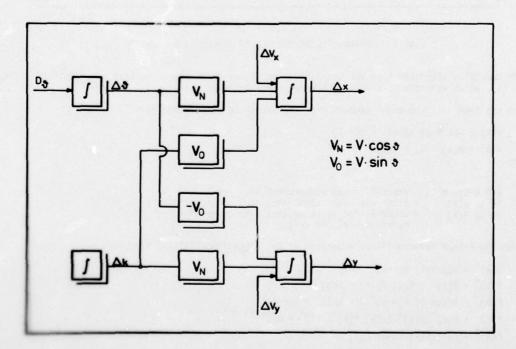


Fig. 4 Error model for the Doppler navigation system

#### 3. HYBRID REFERENCE SYSTEM PHILOSOPHY AND MECHANIZATION

In the hybrid reference systems discussed in this paper the high precision information about the aircraft trajectory, velocity, attitude and heading is obtained by smoothing the radar data with the help of an INS or Doppler system. Direct smoothing of radar data is very common in flight test evaluation, for example by least square curve fitting techniques. The disadvantage of direct smoothing is that not only the high frequency errors of the tracking radar out also the high frequency movements of the aircraft are smoothed out. This disadvantage is avoided, when the hybrid technique proposed in this paper is used.

Figure 5 summarizes the basic principles of the hybrid smoothing technique: The low frequency aircraft movements are measured with high precision by a tracking radar, long distance radar, TACAN or cinetheodolites. Sampling at low frequency only is required (e.g. once every 10 seconds). The high frequencies of the aircraft movement are measured with the on-board INS or Doppler navigation system. These sensors have the necessary short term stability to provide accurate measurements of the high frequency aircraft movements. The smoothing is applied in the following manner: The difference between the position measurements of the on-board and the ground-based sensors are fed into an optimal smoothing algorithm, which estimates the (low frequency) errors of the on-board sensors with high precision. The measurements of the on-board sensors are then corrected for the estimated errors to obtain the reference trajectory, velocity, attitude and heading. Thus the optimal smoothing is only applied on the difference between the measurements of two sensors and this difference is equal to the difference of the errors of both sensors, and the true trajectory is not affected by this method.

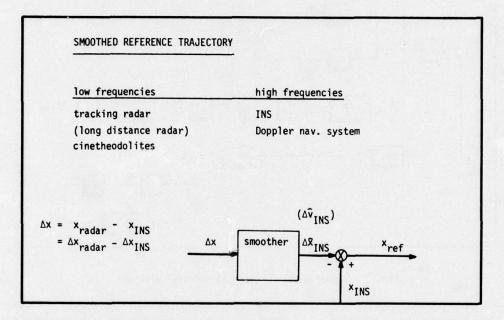


Fig. 5 Principles of the hybrid smoothing technique.

The smoothing algorithm used for the evaluation of our flight tests is that given by RAUCH/TUNG/STRIEBEL [5], which consists of a Kalman forward- and a backward-filter.

Let the time-discrete model equations of the system to be smoothed be

$$x(k) = \phi(k,k-1) x(k-1) + u(k-1)$$
  
 $y(k) = H(k) x(k) + v(k)$ 

where

 $\begin{array}{lll} \varphi(k,k-1),\; H(k) &= transition\; and\; measurement\; matrices\\ x(k),\; y(k) &= state\; and\; measurement\; vectors\\ u(k),\; v(k) &= uncorrelated\; noise\; vectors\; with\; covariance\\ &= matrices\; Q(k)\; and\; R(k). \end{array}$ 

Then the Kalman forward-filter equations of the RAUCH/TUNG/STRIEBEL algorithm are

$$\begin{split} \bar{x}(k)^{-} &= \phi(k_*k-1) \; \bar{x}(k-1)^{+} \\ \bar{x}(k)^{+} &= \bar{x}(k)^{-} + K(k) \; (y(k) - H(k) \; \bar{x}(k)^{-}) \\ P(k)^{-} &= \phi(k_*k-1) \; P(k-1)^{+} \; \phi(k_*k-1)^{T} + Q(k-1) \\ K(k) &= P(k)^{-} \; H(k)^{T} \; (H(k) \; P(k)^{-} \; H(k)^{T} + R(k))^{-1} \\ P(k)^{+} &= (I - K(k) \; H(k)) \; P(k) \end{split}$$

where

$$P(k)^{-}$$
,  $P(k)^{+}$  = covariance matrices of  $(\bar{x}(k)^{-} - x(k))$  and  $(\bar{x}(k)^{+} - x(k))$   
 $\bar{x}(k)^{-}$ ,  $\bar{x}(k)^{+}$  = filtered estimates of  $x(k)$  immediately before and after measurement  $k$   
 $K(k)$  = optimal gain of forward-filter.

The backward-filter equations of the RAUCH/TUNG/STRIEBEL algorithm are

$$\bar{x}(k,N) = \bar{x}(k)^{+} + C(k) (\bar{x}(k+1, N) - \phi(k+1, k) \bar{x}(k)^{+})$$
 $C(k) = P(k)^{+} \phi(k+1, k)^{T} (P(k+1)^{-})^{-1}$ 
 $P(k,N) = P(k) + C(k) (P(k+1, N) - P(k+1)^{-}) C(k)^{T}$ 

and are started with

$$\hat{x}(N,N) = \hat{x}(N)^{+}$$
  
 $P(N,N) = P(N)^{+}$ 

where

N = total number of measurements

 $\Re(k,N)$  = smoothed estimate

P(k,N) = error-covariance matrix of smoothed estimate

C(k) = optimal gain of backward-filter.

The smoothing process consists of two steps

# 1. Forward-filtering

The Kalman filter equations are solved for the flight time in consideration. The results are the estimates  $\bar{x}(k)^+$  and the corresponding covariance matrices  $P(k)^+$ .

# Backward-smoothing

The backward-smoother equations are solved backward in time, utilizing and improving the estimates  $\mathfrak{R}(k)^+$  of the forward-filter. The algorithm is initialized with the last estimate  $\mathfrak{R}(N)^+$  of the forward-filter and the corresponding covariance matrix  $P(N)^+$ .

The improved accuracy, which is obtained by smoothing the data, in comparison with Kalman filtering, can be explained with the help of Figure 6. This figure shows the optimal smoother in a somewhat different mathematical formulation, the two-filter-form. In this formulation the optimal estimate of the state vector at the time t is obtained by combining two Kalman filter estimates in an optimal manner: A Kalman forward-filter gives an optimal estimate  $\Re(t)$  of the state at the time t, based on all the measurements before the

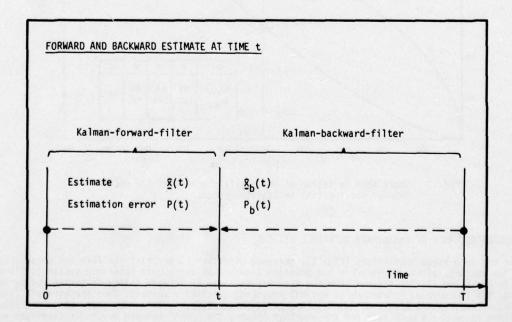


Fig. 6 The optimal smoother in the two-filter-form

time t. This estimate has the accuracy of ordinary Kalman filtering. The second estimate is obtained from a backward Kalman filter and gives an estimate  $\bar{x}_b(t)$  of the system state at the time t, based on all the measurements collected after the time t. The smoothed estimate is the weighted mean of these two estimates (the weighting factor is the inverse of the estimation error covariance matrix). It can be shown that the smoothed estimate is always at least as accurate as the Kalman filtered one. In most cases it is considerably more accurate.

The accuracy of the smoothed estimates of the position, velocity, attitude and heading errors depends strongly on the short term stability of the on-board sensors. For the calibrated INS, the short term position error is determined by the noise in the acceleration measurements. This noise is twice integrated, to give the INS position error (see Fig. 3). In the Doppler system the short term position error is determined by the fluctuation (velocity) error. This velocity noise is integrated, to give the Doppler position error (see Fig. 4). (These statements are only valid, if all the constant errors of the INS and the Doppler system given in table 1 are perfectly estimated and compensated.)

Figure 7 shows the time variation of these short term position errors for the Doppler and inertial navigation system:

- The Doppler position error (random walk) increases rapidly in the first hundred seconds (3 m in 2 s; 7 m in 10 s).
- The INS position error (integrated random walk) remains very small in the first hundred seconds (1 cm in 2 s; 8 cm in 10 s).

Figure 7 demonstrates that the INS has by far the better short term stability compared with the Doppler system, and that after 1000 seconds the position error of the INS is greater than that of the Doppler system. If the measurements of the radar are sampled once per 10 seconds, between the successive measurements the position error due to the INS can be neglected. But in the Doppler system between these measurements a random error of the order of 10 metres builds up, thus basically limiting the obtainable accuracy of the hybrid reference system. In the following text, the results of flight tests and theoretical analyses are presented, which illustrate these basic facts.

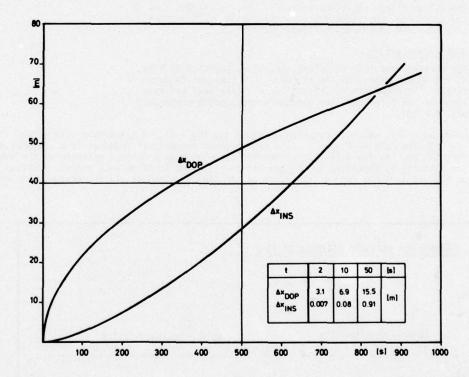


Fig. 7 Short term variation of the position errors of the calibrated Doppler and inertial navigation systems.

# 4. MEASURING ACCURACY OF THE HYBRID REFERENCE SYSTEMS

For the long range test flight (Fig. 1), measured with the LN3 inertial platform and three tracking radars, the heading, attitude, velocity and position accuracy of the hybrid reference system is illustrated in Fig. 8, 9, 10 and 11. The figures show the accuracy obtained by forward Kalman filtering and by backward smoothing. The improvement introduced by optimal smoothing is clearly visible. When the aircraft flies out of the radar coverage the errors of velocity and position increase, as it can be observed in the Figures 10 and 11. This increase is much less for the smoother because the "gaps" between two radar coverages are closed from both sides.

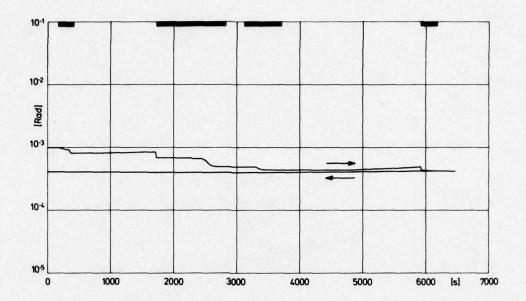


Fig. 8 Hybrid reference system with INS and tracking radar: Heading error ( $1\sigma$ ), forward-filter and backward-smoother. (Long range flight)

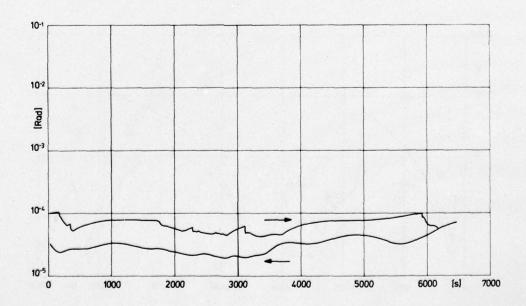


Fig. 9 Hybrid reference system with INS and tracking radar:
Attitude error (10), forward-filter and backward-smoother.
(Long range flight)

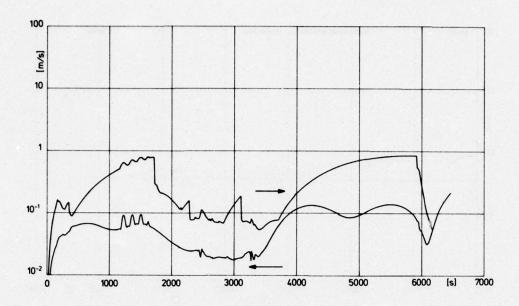


Fig. 10 Hybrid reference system with INS and tracking radar: Velocity error (1 $\sigma$ ), forward-filter and backward-smoother. (Long range flight)

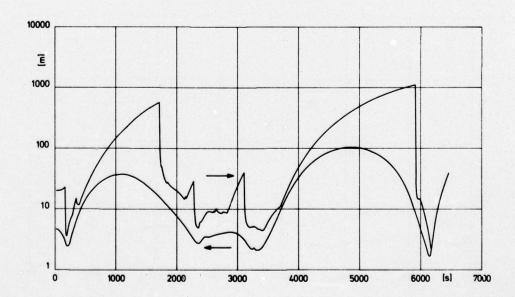


Fig. 11 Hybrid reference system with INS and tracking radar: Position error ( $1\sigma$ ), forward-filter and backward-smoother. (Long range flight)

Under tracking radar coverage the roll and pitch angles are measured with 10", the heading with 1.5', the velocity with 0.03 m/s and the position with 2 ~ 8 m accuracy ( $1\sigma$ ) by the hybrid reference system, consisting of an INS and a tracking radar.

Figures 12, 13, 14 and 15 display the same information as the Figures 8 - 11 for the short range test flight: Again the considerable improvement by optimal smoothing in comparison with forward Kalman filtering can be observed in these figures. This flight is almost completely in the coverage range of the L4/3 tracking radar so that the reference data are obtained with the above mentioned high accuracy for the whole flight.

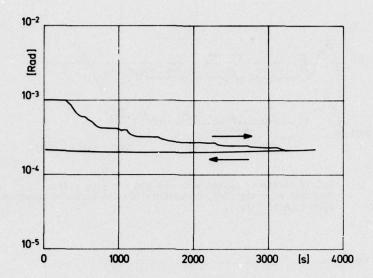


Fig. 12 Hybrid reference system with INS and tracking radar: Heading accuracy ( $1\sigma$ ), forward-filter and backward-smoother. (Short range flight)

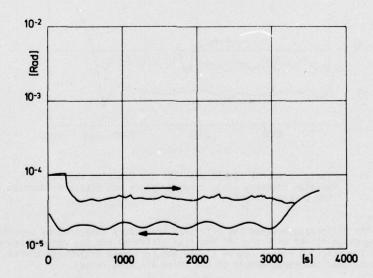


Fig. 13 Hybrid reference system with INS and tracking radar: Attitude accuracy ( $1\sigma$ ), forward-filter and backward-smoother. (Short range flight)

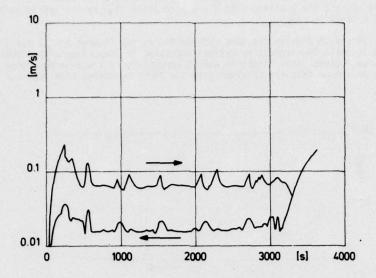


Fig. 14 Hybrid reference system with INS and tracking radar: Velocity accuracy ( $1\sigma$ ), forward-filter and backward-smoother. (Short range flight)

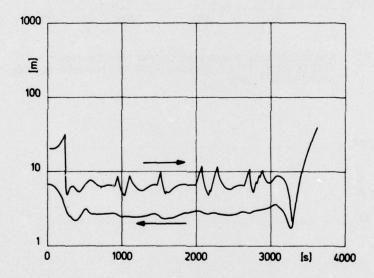


Fig. 15 Hybrid reference system with INS and tracking radar: Position accuracy ( $1\sigma$ ), forward-filter and backward-smoother. (Short range flight)

Figure 16 shows the difference between the reference trajectory (obtained by smoothing the tracking radar data for the long range flight with the LN3 inertial platform) and the radar measurements (curve 1). The accuracies ( $1\sigma$ ) of the tracking radars (curve 2) and the reference trajectory (curve 3) are also shown. This figure demonstrates, that the measurements of the three tracking radars

- L4/3 - MPS-36 - Fledermaus

have approximately the same error dynamics. This can be explained by the fact, that these errors are mainly caused by the radar fluctuations on the test aircraft HFB 320.

The Figures 17, 18 and 19 show the accuracy of the hybrid reference system, obtained by filtering and smoothing the tracking radar data with the Doppler system for the long range flight. Figure 17 gives the accuracy of the heading. Figure 18 shows the accuracy of the Doppler scale factor: by smoothing this scale factor can be estimated with 0.3  $^{\circ}$ /oo accuracy. The mean velocity of the aircraft is measured with this accuracy by the reference system. The high frequency velocity errors (Doppler fluctuation) can not be diminished. In Figure 19 it can be observed that smoothing does not very much improve the position accuracy

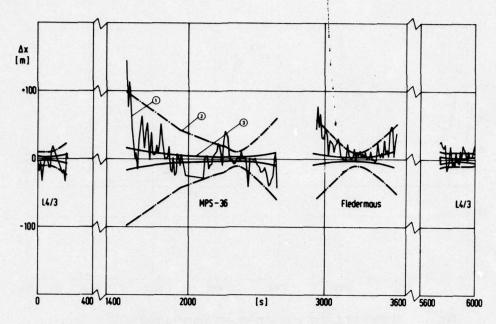


Fig. 16 Difference between reference and radar position (curve 1). Accuracy ( $1\sigma$ ) of the radars (curve 2) and of the reference (curve 3).

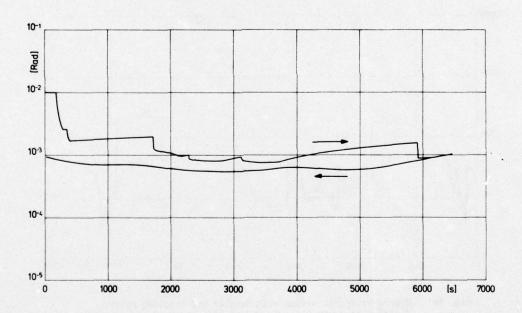


Fig. 17 Hybrid reference system with Doppler and tracking radar: Heading accuracy ( $1\sigma$ ), forward-filter and backward-smoother. (Long range flight)

compared with Kalman filtering under radar coverage. This is due to the less accurate short term behaviour of the Doppler system (see Fig. 7). The heading accuracy is 2', the mean velocity accuracy is 0.3  $^{\rm O}$ /oo and the position accuracy 3 - 10 m under radar coverage.

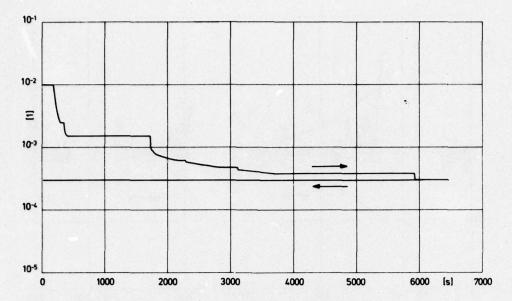


Fig. 18 Reference system with Doppler and tracking radar: Velocity scale factor accuracy ( $1\sigma$ ), forward-filter and backward-smoother. (Long range flight)

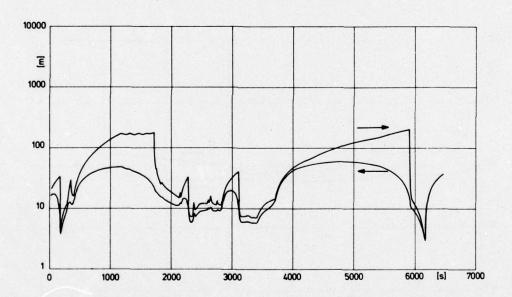


Fig. 19 Hybrid reference system with Doppler and tracking radar: Position accuracy ( $1\sigma$ ), forward-filter and backward-smoother. (Long range flight)

The Figures 20, 21 and 22 show the accuracy obtained by filtering and smoothing the long distance radar measurements with the Doppler navigation system for the long range flight. Heading and mean velocity accuracies are equal to those obtained under tracking radar coverage. The position accuracy is 30 m ( $1\sigma$ ).

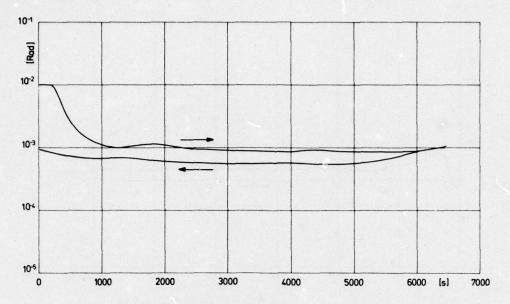


Fig. 20 Hybrid reference system with Doppler and long distance radar: Heading accuracy ( $1\sigma$ ), forward-filter and backward-smoother. (Long range flight)

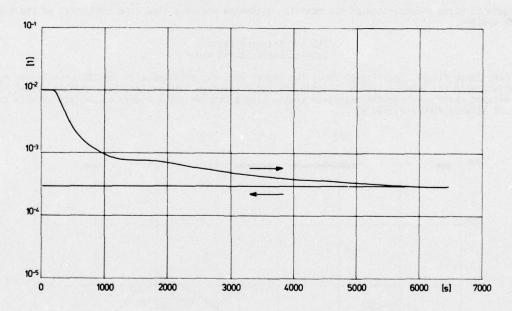


Fig. 21 Hybrid reference system with Doppler and long distance radar: Velocity scale factor accuracy ( $1\sigma$ ), forward-filter and backward-smoother. (Long range flight)

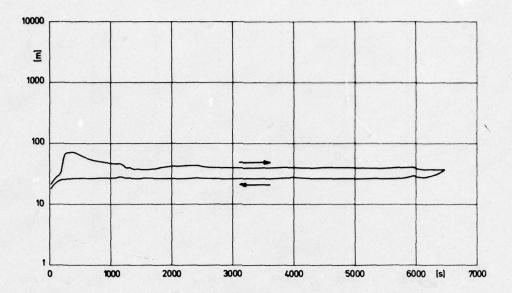


Fig. 22 Hybrid reference system with Doppler and long distance radar:
Position accuracy (lo), forward-filter and backward-smoother.
(Long range flight)

Figure 23 gives a comparison of the position measuring accuracy (smoothed estimates) of the two reference systems  ${\sf S}$ 

- INS and tracking radar

- Doppler and tracking radar

for the long range flight. This figure shows the higher accuracy obtained with the INS under radar coverage in comparison with the Doppler system. Outside the radar coverage both systems have similar errors. In long periods between radar coverage the reference system with a Doppler has a higher accuracy than with an INS (in Fig. 23 between 4500 and 5500 s).

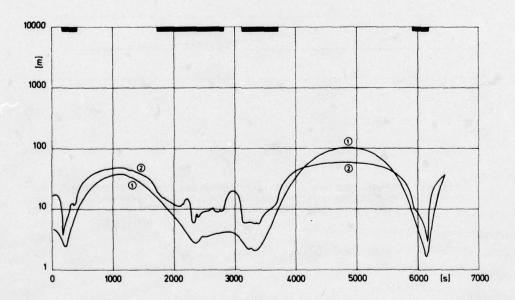


Fig. 23 Comparison of the hybrid reference system position errors (10, smoothed errors). (1) INS and (2) Doppler with tracking radar. (Long range flight)

Table 2 summarizes the measuring accuracies of the different hybrid reference systems.

Hybrid reference system	Accuracy o	
INS and tracking radar	roll and pitch azimuth velocity position	10" 1.5' 0.03 m/s 1.7 - 8 m
Doppler navigation system and tracking radar	heading mean velocity position	2' 0.3 <sup>0</sup> /oo 3 - 10 m
INS and long distance radar	roll and pitch azimuth velocity position	15" 1.8' 0.06 m/s 22 m
Doppler navigation system and long distance radar	heading mean velocity position	2' 0.3 <sup>0</sup> /00 30 m

Table 2 Accuracy of the hybrid reference systems.

### 5. CONCLUSIONS

Theoretical analysis and flight tests have shown, that a high precision measurement of the trajectory, velocity, attitude and heading of a test aircraft is possible with hybrid reference systems. For the highest desired accuracies a combination of INS and tracking radar gives the best results, due to the excellent short term stability of the INS. A combination of Doppler navigation system and tracking radar can be taken, if a position accuracy not better than 3 m is required.

The use of a long distance radar, or TACAN range-range measurements instead of tracking radars gives comparable results as far as attitude and velocity are concerned. The position measuring accuracy is worse than with a tracking radar.

### 6. REFERENCES

- [1] Winter, H., "Experiences in Flight Testing Hybrid Navigation Systems", AGARD-LS-82.
- [2] Hurraß, K., "Anwendung von optimaler Glättungstechnik bei der Erprobung von Navigationssystemen", DFVLR-Nachrichten, Heft 17.
- [3] Hurraß K., Stieler B., "Zum Einsatz des hybriden Flugmeßsystems bei der Vermessung eines Mikrowellenlandesystems", DGON-Symposium Kreiseltechnik, Braunschweig, 31. 3. 1. 4. 1976.
- [4] Winter, H., Zenz, H., Jenscheck, J., "Messung der Vertikalbewegungen eines Flugzeugs", Deutsche Luft- und Raumfahrt, Forschungsbericht 74-41, 1975.
- [5] Rauch, H.E., Tung, F., Striebel, C.T., "Maximum Likelihood Estimates of Linear Dynamic Systems", AIAA Journal, Vol. 3, No. 8, S. 1445, 1965.

### FLIGHT TESTING OF DISPLAYS IN A HELICOPTER

Dipl.-Ing. R. Beyer
Deutsche Forschungs- und Versuchsanstalt für Luft- und Raumfahrt e.V.
Institut für Flugführung
33 Braunschweig-Flughafen
Germany

#### SUMMARY

Electro-optical sensors and electronic displays for a future helicopter avionics system may extend the flexibility of helicopter operation at night and in bad weather. Flight tests were made with a simulated system which presented a combination of flight instruments and an image of the terrain to the pilot. Means were developed to assess flight performance and pilot strain in flights with the system and some of the measures and the results obtained are discussed.

#### LIST OF SYMBOLS

```
- mechanical work
       - barometric altitude
hG
hR
IAS
       - height of rising grounds with reference to the initial point of a course
       - radio altitude
       - indicated airspeed
IMC
       - instrument meteorological conditions
       - torque
       - product-moment-coefficient of correlation; distance
       - time
Ť
       - duration of test

    velocity

VMin
VG
VZB
VZR
       - minimum indicated airspeed
       - ground speed
       - vertical velocity derived from barometric altitude
       - vertical velocity derived from radio altitude
VMC
       - visual meteorological conditions
       angle of rotationslope of terrain
α
γG
φ
       - pitch angle
       - roll angle
       - moment of inertia
Θ
       - angular velocity
ω
       - roll rate
       - pitch rate
       - yaw rate
```

## 1. INTRODUCTION

For the design of a future helicopter avionics system electronic head-up and head-down displays and electro-optical sensors, as for example, low light level television cameras or forward looking infrared cameras are of increasing interest. With the present state of technology such systems are readily available though further technological advances are still desirable, of course. But it is felt that an appropriate balance between technology and application oriented studies should exist now to support advances in both fields. In particular, questions of the attainable flight performance, of a human engineered layout of the display and the control of the sensor, and the aspects of pilot training and flight safety need greater attention.

In order to give some answers in this respect a number of rather comprehensive flight tests has been made in a Bell UH-1D helicopter [1, 2]. Prior to these experiments means were developed to gather relevant subjective and objective data. Though both types of data are of equal interest and importance the scope of this paper had to be limited by giving particular emphasis to the objective data only.

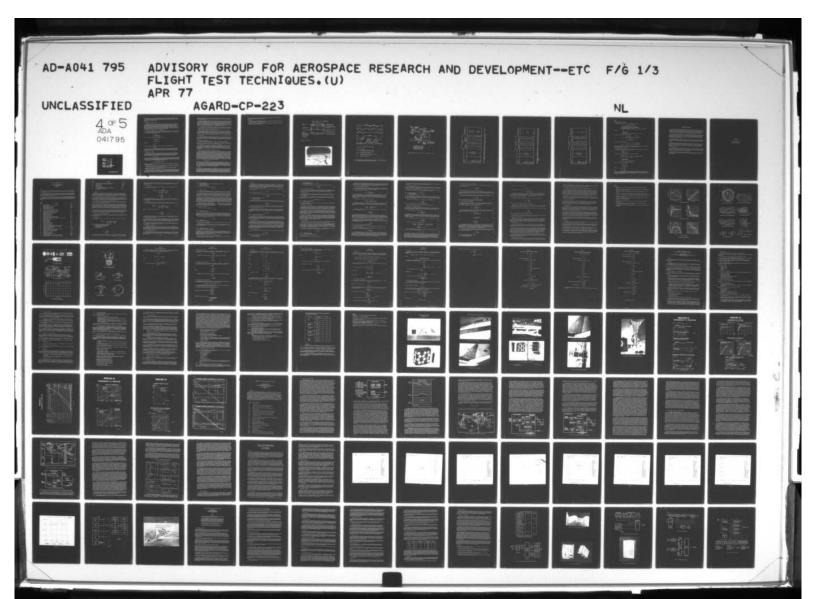
### 2. THE EXPERIMENT

In order to illustrate the experiences gathered from flight testing of advanced helicopter displays an experiment will be referred to which was designed to investigate the efficiency of a display presenting a superposition of an image of the outside world and instrument displays. If an adequate image of the terrain ahead of the helicopter can be obtained by an appropriate sensor at night or in bad weather such a display could be a major step forward to extend the flexibility of helicopter operations (fig. 1 and 2).

The main objective of this experiment was to investigate and to predict as quantitatively as possible how well the pilots are able to fly a helicopter at 150 ft height above ground and 80 knots IAS under IMC using the display in comparison to identical flights under VMC. Other variables were

flight over level and undulated terrain

flight over known and unknown courses
 flight with different control modes of the sensor, i.e. the sensor being fixed to the axes of the helicopter, being stabilized in pitch or looking ahead.



The flights had to be made without any external measurement aids like cinetheodolites, radar etc. and INS or a doppler radar was also not available. 13 parameters were recorded and some of them may be found in the tables to follow. But here only those measures shall be presented in more detail which are less well known from other comparable experiments.

### 3. MEASURES

# 3.1 THE MEASURE OF "COORDINATED FLYING"

Helicopter pilots are trained to fly coordinated with respect to bank and yaw, i.e. to keep the slip indicator centered. Less coordinated flying may be caused by turbulences but also by a detraction of pilot's attention from this task if other tasks are becoming more demanding. Therefore the squared productmoment coefficient of correlation between bank angle  $\phi$  and yaw rate  $\omega_Z$  was determined because it represents the proportion of coordinated flying, i.e. the proportion of the total variation of yaw rate  $\omega_Z$  which is correlated with a variation of bank angle  $\phi$ . The parameter  $r_0^{\phi}$  may serve as an indirect measure then to indicate a variation of pilot's attention in this respect,  $\omega_Z$  if other influencing factors as, for example, turbulences or a variation of torque are less appearing.

### 3.2 MEASURE FOR PILOT STRAIN PRODUCED BY THE STABILIZATION TASK

In an unstabilized helicopter pilot strain may be considered to be related directly to the mechanical work A which is controlled by the pilot in order to stabilize the helicopter in its axes. An elementary unit of work may be calculated as (see appendix)

$$dA = d \left(\frac{\Theta}{2} \omega^2\right)$$

 $\Theta$  - moment of inertia  $\omega$  - angular velocity

And for  $\Theta$  = const. the mean value of A with respect to time is

$$\bar{A} = \frac{\Theta}{2} \begin{bmatrix} \frac{1}{T} & \int_{0}^{T} \omega^{2} dt \end{bmatrix}$$

T - duration of test

But the term

$$\frac{1}{T} \int_{0}^{T} \omega^{2} dt$$

is equal to the squared rms-value of  $\omega$  which can be measured in flight and which leads to

$$A = \frac{\Theta}{2} \omega_{RMS}^2$$

Thus for  $\theta$  = const. and for nearly constant friction loads (which can be assumed for a nearly uniform progress of flights which in turn can be examined by means of the recorded flight parameters) and for  $\bar{\omega} = 0$ ,  $\omega_{RMS}^{2}$  may be considered a relative measure to assess pilot strain produced by the stabilization task.

## 3.3 ROUGHNESS OF THE TERRAIN

As it is somewhat unrealistic to compare helicopter low level flight test results irrespective of the type of the terrain a quantitative measure to indicate the roughness of the terrain the helicopter flew over is desirable. If  $\mathbf{v}_{zB}$  is the radio altitude derived vertical velocity and if  $\mathbf{v}_{zB}$  is the barometric altitude derived vertical velocity then it can be seen from  $\underline{\text{fig. 3}}$  that the difference

$$\Delta v_z = v_{zR} - v_{zB}$$

exists only in the presence of undulated terrain. If ground speed can be measured the slope of the terrain  $\gamma_G$  may be calculated continuously (see appendix). But if ground speed is not available the rate of descent of the terrain  $\Delta v_z$  is an adequate substitute to characterize the type of terrain if ground speed is nearly constant for the flights to be compared. Therefore the rms-value of  $\Delta v_z$ 

$$\Delta v_{z,RMS} = \sqrt{\frac{1}{T}} \int_{0}^{T} \left[v_{zR} - v_{zB}\right]^{2} dt$$

was considered a measure to indicate the effective rate of descent of the terrain which in turn reflects the roughness of the terrain.

The three measures discussed so far were recorded in the course of the experiments with the combined display and the following tables illustrate the results obtained.

Table 1 presents a comparison of parameters obtained from flights under VMC and simulated IMC irrespective of the type of the terrain (level or hilly).

Emphasizing the guidance of the helicopter it can be seen that under simulated IMC the pilots did not reduce average airspeed compared to VMC flights as it is anticipated sometimes but increased height above ground by 26 %. This may be due to safety requirements as well as to the fact that objects of the outside world are moving more slowly on the screen and therefore for a longer period of time are available for

identification and orientation. The increased safety requirements of the pilots flying under simulated IMC may be recognized also by an increase of minimum height above ground by 26 % and by a decrease of minimum indicated airspeed by 11 %.

An increase of  $\omega^2_{\rm RMS}$  by a factor of 29 and an increase of  $\omega^2_{\rm RMS}$  by 25 % indicate much higher pilot strain when flying under simulated IMC. This may be because a quantitative assessment of pitch and roll and their variation is much easier for the pilots under VMC than it is by means of the display. Increased pilot strain is also indicated by the measure of "coordinated flying" rg which drops from 52 % under VMC to 39 % under simulated IMC. A major cause may be the higher and more distribution in roll ( $\omega^2_{\rm RMS}$ ) under simulated IMC already mentioned. It is interesting to note that the pilots also allowed an increase of the average bank angle  $\phi$  by 80 % when flying under simulated IMC. The later addition of a slip indicator to the display, however, gave no significant improvement in this respect.

A significant difference of parameter means for  $\omega_Z^2$  RMS and for  $\Delta v_Z$  RMS (roughness of the terrain) could not be expected from this analysis because the data sets for level and hilly terrain were combined.

 $\underline{\text{Table 2}}$  presents a comparison of parameters obtained from flights over level and hilly terrain irrespective of the flight conditions, i.e. VMC or simulated IMC.

From this table it can be seen that for the flights over hilly terrain there is only a moderate increase of height above ground by 14 % which may be caused by the greater difficulty of the task and by greater safety demands as compared to flights over level terrain. An increase of  $\omega_z^2$ , RMS by 13 % reflects higher pilot strain caused by much more turns to be flown and by the varying stope of the terrain. The different types of terrain are marked by a significant difference of  $\Delta v_z$ , RMS.

Table 3 presents a comparison of parameters obtained from flights under simulated IMC over wellknown and unknown courses.

The pilots responded to the new task of flying over unknown courses in comparison to flights over a well-known course by a reduction of indicated airspeed by 14~% and by a major increase of height above ground which, however, was statistically not significant because of the relatively large variability of height. To a major degree this variability is caused by the somewhat conflicting demands to maintain a certain

Safety aspects (high altitude)

The need to discern relatively small objects on the ground for navigation (low altitude)
 The need for a general view and perspective in the case of a loss of orientation (high altitude)

The greater safety requirements of the pilots are reflected furthermore by an increase of minimum height above ground  $h_{R,Min}$  by 56 % and by the reduction of minimum airspeed  $v_{Min}$  by 33 %.

An increase of  $\omega^2_{z,RMS}$  by a factor of 2.6 marks higher pilot\_strain because of much more turns to be flown on the unknown z,RMS courses. But while the magnitude of  $\omega^2_{z,RMS}$  dropped by a factor of 43,r $\phi^2_{z,RMS}$  reached a maximum of 0.54 compared to all other flights. This demonstrates that the pilots flew coordinated with respect to roll and yaw but in gentle turns only because the danger to lose orientation on an unknown course is much greater than on a well-known course which in each case would have stopped the experiment.

## 3.4 LATERAL POSITION OF THE HELICOPTER WITH REFERENCE TO A GIVEN TRACK

In one of the experiments a "look-ahead" control mode of the sensor with respect to the flight path in a turn was investigated in comparison to the sensor being fixed to the longitudinal axis of the helicopter. A difference of performance was expected for low level flights when steep turns had to be flown. The deviation of the helicopter from a given track (road, river, railway track etc.) was considered to be one measure of performance in this respect. An additional fixed camera, therefore, was mounted vertically under the helicopter facing the ground. The image of the ground was presented on an observer's monitor. Two horizontal lines placed around the center of the monitor screen were margins to define a given area ahead and aft the helicopter ground position (see fig. 4). If, for example, the pilot tried to follow a road under simulated IMC the image of the road was tracked by the observer by moving a vertical line as a cursor horizontally over the monitor screen so that it coincided with the image of the road within the area defined by the two margins. The system was calibrated so that the deflection angle  $\beta$  of the apparent cursor line of sight was known and as radio altitude h and bank angle  $\phi$  were also available the lateral deviation d of the helicopter from the road could be calculated as

$$d = h_R \cdot \tan (\varphi + \beta)$$

Static tests in hover flight showed for  $h_{\rm B}$  = 150 ft that d could be determined with a tolerance of  $\pm$  5%. In cruise flight at  $h_{\rm B}$  = 150 ft and v = 80 kts IAS the tolerance of d was larger and in the order of  $\pm$  10 to  $\pm$  15% which, however, did not impair the test results: Following a river at 150 ft above water and 80 kn IAS under simulated IMC using the combined display produced average absolute deviations of 110 m from the desired track with the sensor being fixed to the axes of the helicopter. But when the sensor was in the look-ahead mode the average absolute deviations were reduced to 45 m. The difference of 65 m was statistically significant on the 1 o/oo level of error probability.

## 4. CONCLUSION

The availability of electro-optical sensors and electronic displays as part of a helicopter avionics system shows promise to extend the flexibility of helicopter operation. Flight tests have to be made in order to evaluate the efficiency of new displays in comparison to the conventional instrumentation and it has been shown that relevant and significant results can be obtained even by relatively simple means. Although particular emphasis was given to objective measures similar advances exist for the aquisition of corresponding subjective data. An unambiguous methodological design of the experiment, however, is the

most important prerequisite for an application of the measures presented and it is hoped that some experimenters may derive benefit from this presentation.

### 5. REFERENCES

- R. Beyer, Untersuchung einer kombinierten Darstellung von Umweltbild und Instrumentenanzeigen in einem Hubschrauber Bell UH-1D. 1976, DFVLR IB 153-76-11.
- 2. R. Beyer, E. Kohnen, F.V. Schick, U. Stolzke, Demonstration eines Head-up Displays in einem Hubschrauber Bell UH-1D. 1976, DFVLR IB 153-76-07.

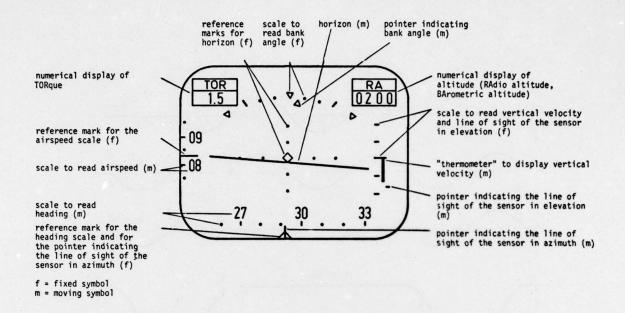
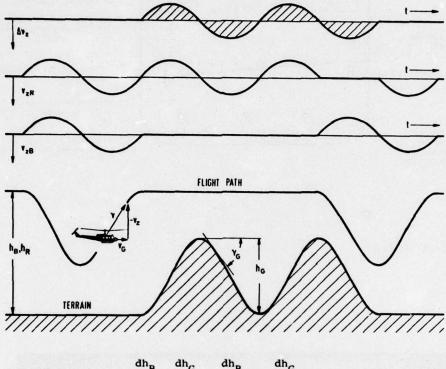


Figure 1: Instrument displays



Figure 2: Combined outside world/instrument displays



$$\Delta v_z = v_{zR} - v_{zB} = (\frac{dh_B}{dt} - \frac{dh_G}{dt}) - \frac{dh_B}{dt} = -\frac{dh_G}{dt}$$

$$\gamma_G = \arctan \left(\frac{\Delta v_z}{v_G}\right)$$

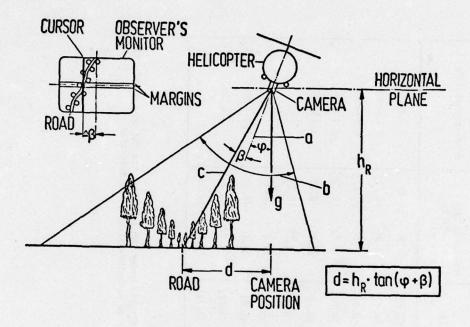
 $\begin{array}{ll} \gamma_G & = \mbox{ arc } \tan \ (\frac{\Delta v_z}{v_G}) \\ h_B, \ v_{zB} & - \mbox{ barometric altitude and barometric } \\ \end{array}$ 

 $\mathbf{h_{R'}}$   $\mathbf{v_{zR}}$  - radio altitude and radio altitude derived vertical velocity

 $\mathbf{h}_{\mathbf{G}}$ height of rising grounds with reference to the initial point of a course

- slope of the terrain YG

 $\frac{\textbf{Figure 3:}}{\textbf{measurement of the roughness of the terrain on the basis of the difference of barometric}}{\textbf{altitude and radio altitude derived vertical velocities}}$ 



- a) CAMERA LINE OF SIGHT
- b) CAMERA ANGLE OF VIEW
- c) CURSOR LINE OF SIGHT

 $\underline{\text{Figure 4:}}$  Measurement of the lateral deviation d of the helicopter from a road

			known course	urse		
parameter	dim.	VMC (level, hilly terrain)	yllı	Simulated IMC (level, hilly terrain)	IMC V[li	error probability
>	s/w	43.6	(2.6)	41.9	(1.8)	< 2 0/0
Ę	E	53.8	(5.4)	67.9	(12.7)	< 1 0/00
9	deg	- 1.5	(0.4)	- 2.7	(0.5)	< 1 0/00
", RMS	(deg/s) <sup>2</sup>	0.06	(0.05)	1.72	(1.7)	< 1 0/00
w, RMS	(deg/s) <sup>2</sup>	0.73	(0.2)	0.91	(0.1)	< 1 0/00
"Z,RMS	(deg/s) <sup>2</sup>	1.02	(0.49)	1.17	(0.29)	
, Min	s/m	35.0	(6.2)	31.3	(3.8)	< 1 0/00
h <sub>R,Min</sub>	E	24.7	(5.0)	31.1	(9.9)	< 1 0/00
2,5 3,	•	0.52	(0.0)	0.39	(0.0)	< 1 0/00
AVZ,RMS	m/s	2.76	(0.71)	2.62	(1.22)	

Table 1: Comparison of parameter means obtained from flights under VMC and simulated IMC on a known course regardless of the type of the terrain. Number in parantheses: standard deviation

r       dim.       level terrain (VMC, sim. IMC)       hilly terrain (VMC, sim. IMC)         m/s       43.0       (2.5)       42.5       (2.2)         m       56.9       (11.2)       64.7       (11.8)         deg       - 2.2       (0.7)       - 2.1       (0.8)         (deg/s) <sup>2</sup> 0.76       (1.2)       1.02       (1.6)         (deg/s) <sup>2</sup> 0.76       (0.19)       0.87       (0.16)         (deg/s) <sup>2</sup> 0.91       (0.3)       1.28       (0.41)         m/s       33.8       (4.2)       32.5       (3.4)         m/s       28.6       (5.4)       27.2       (7.7)         -       0.46       (0.12)       0.46       (0.11)         m/s       2.18       (0.74)       3.19       (0.96)				-			
m/s 43.0 (2.5) 42.5 (2.2) m/s 43.0 (2.5) 42.5 (2.2) m 56.9 (11.2) 64.7 (11.8) deg -2.2 (0.7) -2.1 (0.8) (deg/s) <sup>2</sup> 0.76 (1.2) 1.02 (1.6) (deg/s) <sup>2</sup> 0.91 (0.3) 1.28 (0.41) m/s 33.8 (4.2) 32.5 (3.4) m 28.6 (5.4) 27.2 (7.7) - 0.46 (0.12) 0.46 (0.11) m/s 2.18 (0.74) 3.19 (0.96)				known	course		
m 56.9 (2.5) 42.5  deg -2.2 (0.7) -2.1  (deg/s) <sup>2</sup> 0.76 (1.2) 1.02  (deg/s) <sup>2</sup> 0.91 (0.3) 1.28  m/s 33.8 (4.2) 32.5  m/s 28.6 (5.4) 27.2  - 0.46 (0.12) 0.46  m/s 2.18 (0.74) 3.19	parameter	dim.	level t (VMC, si	errain m. IMC)	hilly t (VMC, si	errain m. IMC)	error probability
deg - 2.2 (0.7) - 2.1 (deg/s) <sup>2</sup> 0.76 (1.2) 1.02 (deg/s) <sup>2</sup> 0.76 (0.19) 0.87 (deg/s) <sup>2</sup> 0.91 (0.3) 1.28 m/s 33.8 (4.2) 32.5 m m/s 28.6 (5.4) 27.2 - 0.46 (0.12) 0.46 m/s 2.18 (0.74) 3.19	>	s/w	43.0	(2.5)	42.5	(2.2)	
deg     - 2.2     (0.7)     - 2.1       (deg/s)²     0.76     (1.2)     1.02       (deg/s)²     0.76     (0.19)     0.87       (deg/s)²     0.91     (0.3)     1.28       m/s     33.8     (4.2)     32.5       m     28.6     (5.4)     27.2       -     0.46     (0.12)     0.46       m/s     2.18     (0.74)     3.19	ڇ	E	56.9	(11.2)	64.7	(11.8)	< 5 0/0
(deg/s) <sup>2</sup> 0.76     (1.2)     1.02       (deg/s) <sup>2</sup> 0.76     (0.19)     0.87       (deg/s) <sup>2</sup> 0.91     (0.3)     1.28       m/s     33.8     (4.2)     32.5       m     28.6     (5.4)     27.2       -     0.46     (0.12)     0.46       m/s     2.18     (0.74)     3.19	9	deg	- 2.2	(0.7)	- 2.1	(0.8)	
(deg/s) <sup>2</sup> 0.76     (0.19)     0.87       (deg/s) <sup>2</sup> 0.91     (0.3)     1.28       m/s     33.8     (4.2)     32.5       m     28.6     (5.4)     27.2       -     0.46     (0.12)     0.46       m/s     2.18     (0.74)     3.19	wx,RMS	(deg/s) <sup>2</sup>	0.76	(1.2)	1.02	(1.6)	
(deg/s) <sup>2</sup> m/s m/s 33.8 (4.2) 32.5 m 28.6 (5.4) 27.2 - 0.46 (0.12) 0.46 m/s 2.18 (0.74) 3.19	w, RMS	(deg/s) <sup>2</sup>	0.76	(0.19)	0.87	(0.16)	0/0 5 >
m 28.6 (5.4) 27.2 - 0.46 (0.12) 0.46 m/s 2.18 (0.74) 3.19	wz,RMS	(deg/s) <sup>2</sup>	0.91	(0.3)	1.28	(0.41)	< 2 0/00
m 28.6 (5.4) 27.2 - 0.46 (0.12) 0.46 m/s 2.18 (0.74) 3.19	VMin	s/w	33.8	(4.2)	32.5	(3.4)	
- 0.46 (0.12) 0.46 m/s 2.18 (0.74) 3.19	hR,Min	E	28.6	(5.4)	27.2	(7.7)	
m/s 2.18 (0.74) 3.19	6,6,6,	•	0.46	(0.12)	0.46	(0.11)	
	ΔVZ,RMS	s/w	2.18	(0.74)	3.19	(96.0)	< 1 0/00

Table 2: Comparison of parameter means obtained from flights over level and hilly terrain on a known course regardless of the conditions of flight, i.e. VMC or simulated IMC. Number in parentheses: standard deviation

			simulated IMC	DWI Pe		
parameter	dim.	known	known course	unknown course	course	error probability
>	s/w	41.9	(1.8)	36.0	(1.4)	۸ دن ۶۵
Ľ.	E	67.9	(12.7)	103.5	(41.0)	
9	deg	- 2.7	(0.55)	- 3.4	(0.7)	
"x, RMS	(deg/s) <sup>2</sup>	1.72	(1.7)	0.04	(0.01)	< 2 %
wy,RMS	(deg/s) <sup>2</sup>	0.91	(0.11)	1.06	(0.2)	
wz,RMS	(deg/s) <sup>2</sup>	1.17	(0.29)	3.10	(0.7)	< 2 %
Vmin	s/m	31.3	(3.85)	21.0	(3.8)	< 2 %
hR,Min	E	31.1	(9.9)	48.5	(15.6)	× 24
7.2 6,6	•	0.39	(0.0)	0.54	(0.08)	56 5 7
ΔVZ,RMS	s/w	2.62	(1.22)	2.26	(1.5)	

Table 3: Comparison of parameter means obtained from flights under simulated IMC over known and unknown courses.

Number in parentheses: standard deviation

#### 1. AVERAGE ROUGHNESS OF THE TERRAIN

The average roughness of the terrain may be determined by (see fig. 3)

$$\Delta v_z = v_{zR} - v_{zB} = (\frac{dh_B}{dt} - \frac{dh_G}{dt}) - \frac{dh_B}{dt} = -\frac{dh_G}{dt}$$

 $v_{ZR}$  - vertical velocity derived from radio altitude vzB - vertical velocity derived from barometric altitude hg - barometric altitude hG - height of rising grounds with reference to the initial point of course

**Furthermore** 

$$-\frac{dh_G}{dt} = v_G \cdot \tan \gamma_G$$

 $v_G^{\rm c}$  - ground speed - slope of the terrain with reference to the horizontal plane

An effective slope of the terrain may be defined as

$$(\tan \gamma_G)_{eff} = \sqrt{\frac{1}{T}} \int_0^T \left[ \frac{-dh_G/dt}{v_G} \right]^2 dt = \sqrt{\frac{1}{T}} \int_0^T \tan^2 \gamma_G dt$$

$$\gamma_{G,eff} = \arctan \sqrt{\frac{1}{T}} \int_0^T \tan^2 \gamma_G dt$$

or

As it was not possible to determine  $v_G$ 

$$\Delta v_{z,RMS} = \sqrt{\frac{1}{T}} \int_{0}^{T} \left[ v_{zR} - v_{zB} \right]^{2} dt = \sqrt{\frac{1}{T}} \int_{0}^{T} \left[ -\frac{dh_{G}}{dt} \right]^{2} dt$$

was calculated which represents the effective rate of descent of the terrain. If  $v_G$  is maintained almost constant  $\Delta v_{z,RMS}$  may serve as a measure for the average roughness of the terrain.

## 2. CONTROL OF THE HELICOPTER IN ITS AXES

In an unstabilized helicopter pilot strain may be regarded as directly related to the (mechanical) work A required for a rotation of the vehicle in its axes:

$$\begin{array}{lll} A &=& M_{\alpha} \\ M &=& torque \\ \alpha &=& angle \ of \ rotation \end{array}$$

The total amount of work may be calculated as the sum of units of work dA:

$$\begin{array}{lll} dA &=& M & d\alpha &=& m & \frac{dv}{dt} & r & d\alpha \\ m & -& mass & & & \end{array}$$

v - tangential velocity at distance r from the center of rotation

$$\frac{d\alpha}{dt} = \omega$$
  $dv = r \cdot d\omega$   $\Theta = mr^2$ 

 $_{\omega}$  - angular velocity  $_{\odot}$  - moment of inertia

$$dA = mdvr\omega = mr^2\omega d\omega = d (mr^2 \frac{\omega^2}{2}) = d (\frac{\Theta}{2} \omega^2)$$

For  $\Theta$  = const. the average value of A may be calculated:

$$\bar{A} = \frac{\theta}{2} \begin{bmatrix} \frac{1}{T} & \int_{0}^{T} \omega^2 dt \end{bmatrix}$$

T - duration of test

And for

$$\omega_{\text{RMS}}^2 = \frac{1}{T} \int_{0}^{T} \omega^2 dt$$

it is

For  $\Theta$  = const. and for nearly constant friction loads (to be assumed for a nearly uniform progress of flights which can be examined by means of the flight parameters) and for  $\bar{\omega} \simeq 0$  the value of  $\omega_{RMS}^{RMS}$  may be taken as a relative measure for pilot strain caused by the control of the work A required to control the believes  $\bar{\omega}_{RMS}^{RMS}$  to control the believes  $\bar{\omega}_{RMS}^{RMS}$ trol the helicopter in its axes.

## COMMENTS ON SESSION II

These 10 papers gave a broad but fairly coherent coverage of the techniques used in weapon system development and evaluation. There were several examples of different techniques being used for the same basic objective, and the presentations were deliberately arranged to emphasize these comparisons. Despite this, the discussions tended to concentrate on the results of the individual test programs, and only a few comments compared and contrasted the differing techniques. Where this was done, authors were able and willing to explain and justify their chosen procedures.

As a general rule, the techniques chosen seemed to fit naturally with the facilities available. If actual flight testing is judged to be very expensive, then effort is made to develop sophisticated data-gathering and processing techniques to minimize flying time. If flying costs can be borne, then ingenuity is shown in developing statistical procedures for arriving at credible results from relatively simple data. No author claimed that the techniques which he used would necessarily be best for a different application.

Several authors made the point — either in their papers or in the discussion — that the best accuracy is obtained by using more than one technique or procedure, and by combining the results to produce a weighted mean. Failing this, if a choice can or must be made, a careful sensitivity analysis needs to be done first to choose the method with the least uncertainty.

Although great progress is being made, handling qualities assessments still require a great deal of attention. A combination of objective comparison with specification requirements and pilot's subjective opinion of acceptability is still widely used. There is evidently still room for improved definition of handling qualities requirements. Several new techniques for more objective and informative test procedures were mentioned (e.g., the mission-oriented precision tracking tests in Paper No.13).

Three papers dealt with the vexed problem of engine thrust measurement in flight; but although one claimed high accuracy without dependence on ground calibration, in a rather special case, no universal panacea was offered. However, the importance of reaching agreement between engine and airframe specialists on the matter of definitions of thrust and drag, before the tests and analysis proceed too far, was strongly emphasized.

Overall, this Session presented an encouraging picture of the state of the art. There is wide recognition of the many problem areas still outstanding, and activity to devise new techniques to fill these gaps was reported from widely separated organizations.

SESSION III

DATA ACQUISITION AND HANDLING TECHNIQUES

### ANGULAR MOTION SENSING WITH GAS ROTORS

by
W. R. Macdonald
Instrumentation and Trials Department
Royal Aircraft Establishment
Farnborough

England

#### SUMMARY

In this paper, new angular motion transducers based on a gas rotor are discussed. These exploit the fact that when a coil of tube containing gas experiences angular acceleration, a pressure proportional to the acceleration is generated.

The pressure is measured by a capacitive membrane sensor and depending on the design characteristics, outputs representing angular acceleration, vibratory angular displacement or vibratory angular velocity may be obtained. The design and performance of these three types of transducer are discussed in detail and examples of practical instruments are given.

Gas rotor transducers display characteristics similar to those of rotary spring-mass systems, but they are effectively devoid of moving parts and in principle are perfectly balanced. They are therefore potentially cheap and very robust. Moreover, since the rotor can be of any convenient shape, optimum use can be made of available space and multi-axis instruments of similar size to their single-axis counterparts are feasible.

#### SYMBOLS

Symbol	Meaning	Unit
a A b	radius of membrane linear acceleration normal to plane of membrane radius of electrode	m m s-2
cc	damping coefficient of constriction	Nsm <sup>-1</sup>
cm	damping coefficient of membrane	N s m <sup>-1</sup>
Ct	damping coefficient of tube capacitance shunting bridge output	Nsm <sup>-1</sup>
CO AC		
ΔC C	fractional capacitance change of pressure sensor	-
d	initial gap between membrane and each electrode	m
foi	lowest secondary resonant frequency	Hz
Fα	performance factor of acceleration transducer performance factor of velocity transducer	
Få	effective stiffness of membrane	N m-1
k L	length of constriction	m
m	actual mass of gas in tube	kg
m <sub>e</sub>	effective mass of gas in tube	kg
n	number of turns of tubing	
P	pressure generated, pressure applied to sensor	Pa
	effective pressure due to linear acceleration	Pa m2
P <sub>A</sub>	area, in a plane normal to input axis, enclosed by one turn of tubing	m <sup>2</sup>
r	internal radius of tube	m
r <sub>c</sub>	internal radius of constriction	m
ri	radius of each inlet	m
R S	mean radius of helix tension in membrane	m N m <sup>-1</sup>
t	thickness of membrane	
u	velocity of sound in the gas	m s-1
v	mean velocity of gas in tube	m s-1
v <sub>0</sub>	output voltage of bridge	v
	source voltage of bridge	V
v <sub>s</sub>	mean velocity of gas in constriction	m s-1
x;	vibratory linear displacement normal to plane of membrane	m
*i *i	vibratory linear velocity normal to plane of membrane	m s-1
у	deflection of membrane at radius x	m
y <sub>m</sub>	deflection of membrane at centre	m
α	input angular acceleration	rad s 2
aA	linear acceleration error in terms of angular acceleration	rad s-2
β	additional mass factor due to flow profile	
Y	additional mass factor due to constriction	F m-1
6	dielectric constant of gas ≈8.85 × 10 <sup>-12</sup>	rm.
ζ n	damping ratio dynamic viscosity of the gas	N s m-2
θi	input angular displacement	rad
$\theta_m$	absolute angular displacement of mass	rad
ďi	input angular velocity	rad s-1
θ.	linear acceleration error in terms of angular displacement	rad
θx <sub>i</sub>	linear displacement error in terms of angular displacement	rad
~i		

Symbol	Meaning	Unit
<sup>θ</sup> Α <sup>θ</sup> * <sub>i</sub>	linear acceleration error in terms of angular velocity linear velocity error in terms of angular velocity	rad s-1 rad s-1
P	density of the gas	kg m <sup>-3</sup>
$\rho_{\mathbf{m}}$	density of membrane	$kg m^{-3}$
ф	phase error	rad
ω	2π × input frequency	s-1
ω1	2π × lower -3dB frequency limit of velocity transducer	s <sup>-1</sup>
ω2	2π × upper -3dB frequency limit of velocity transducer	s <sup>-1</sup>
ωn	2π × undamped natural frequency	s-1
Ω	flow parameter	

#### INTRODUCTION

Non-gyroscopic angular motion sensors traditionally employ a balanced mass, suspended in bearings, which generates a torque proportional to angular acceleration. If the mass is constrained by a spring, its angular displacement is hence a measure of the acceleration if the input frequency is significantly lower than the natural frequency of the rotary spring-mass system. Alternatively, the acceleration may be measured by a torque feedback system as in the modern servo accelerometer.

Such arrangements basically respond to acceleration, but they can also be used to measure vibratory displacement and velocity (section 2). Whatever the measurand however, there are practical problems associated with the rotary mass and these may become acute in instruments where the mass must have a large moment of inertia. In these cases, bearing friction may degrade the performance and moreover, the instrument is unlikely to be sufficiently robust for some aerospace applications.

This problem has been overcome in low-range accelerometers by using a liquid rotor , a circular column of liquid coupled to a relatively light mass. By these means, the load on the bearings is greatly reduced and this results in a more robust instrument.

In this paper, attention is devoted to a yet more robust and relatively simple arrangement which is effectively devoid of moving parts. It exploits the fact that when a coil of tubing, containing gas, is subjected to angular acceleration, a differential pressure proportional to the acceleration is generated 2-4. No pressure is generated by linear acceleration. In essence, the instrument consists of a coil of tubing, containing gas, whose ends are connected to a pressure sensor. Bearings, and the need to balance the mass, are therefore eliminated. Moreover, the arrangement is not sensitive to angular velocity about axes in a plane normal to the input axis, as is the case of a rotary mass lacking radial symmetry (e.g. a balanced bar).

The arrangement in effect constitutes a rotary spring-mass system with the mass being that of the gas in the tubing and the stiffness being provided by the pressure sensor. Damping is obtained by the viscous flow of the gas in the tubing, or by its flow through suitably dimensioned constrictions. The use of gas damping, in contrast to liquid damping, has the merit of being relatively unaffected by temperature.

### FREQUENCY RESPONSE OF ROTARY SPRING-MASS SYSTEMS

Before discussing the design and performance of transducers with gas rotors, the three modes of operation of rotary spring-mass systems with damping will be briefly reviewed. These are relevant to the instruments to be described later.

## Acceleration mode

For a system excited below its natural frequency, the stiffness force predominates and the response to acceleration is  $^{5}$ 

$$\frac{\theta_{m} - \theta_{i}}{\alpha} (j\omega) = \frac{1}{\omega_{n}^{2} \left\{ \left[ 1 - \left( \frac{\omega}{\omega_{n}} \right)^{2} \right]^{2} + 4\zeta^{2} \left( \frac{\omega}{\omega_{n}} \right)^{2} \right\}^{2}} \Delta^{\phi}$$
(1)

where  $\theta_m$  = instantaneous absolute angular displacement of mass

θi = instantaneous input angular displacement

α = instantaneous input angular acceleration

 $\omega = 2\pi \times input frequency$ 

 $\omega_n = 2\pi \times \text{undamped natural frequency}$   $\zeta = \text{damping ratio}$ 

$$\phi = \tan^{-1} \frac{2\zeta \frac{\omega}{\omega_n}}{\left(\frac{\omega}{\omega_n}\right)^2 - 1} \qquad -\pi < \phi < 0 .$$
 (1a)

THE RESERVE TO SERVE THE TAXABLE PROPERTY OF THE PARTY OF

These equations describe the well-known amplitude and phase response of a force-excited second-order system, and are plotted in Fig.la for ζ = 0.3, 0.65 and 1.0. A damping ratio of 0.65, so-called optimum

damping, gives an amplitude response essentially flat up to 70% of the natural frequency. It also gives a phase error which is a linear function of frequency, and hence complex waveforms are not distorted but merely shifted in time.

### 2.2 Displacement mode

For excitation at frequencies above the natural frequency, the inertia force predominates and the response to vibratory displacement is  $^{5}$ 

$$\frac{\theta_{m} - \theta_{i}}{\theta_{i}} (j\omega) = \frac{\left(\frac{\omega}{\omega_{n}}\right)^{2}}{\left\{\left[1 - \left(\frac{\omega}{\omega_{n}}\right)^{2}\right]^{2} + 4\zeta^{2} \left(\frac{\omega}{\omega_{n}}\right)^{2}\right\}^{\frac{1}{2}}} \Delta \Phi$$
(2)

where

$$\phi = \tan^{-1} \frac{2\zeta \frac{\omega}{\omega_n}}{\left(\frac{\omega}{\omega_n}\right)^2 - 1} \qquad 0 < \phi < \pi \qquad . \tag{2a}$$

These are plotted in Fig.1b for  $\zeta$  = 0.3, 0.5, 0.65 and 1.0. A damping ratio of 0.65 leads to an amplitude response which is sensibly flat down to 150% of the natural frequency, but the phase error is not linear with frequency and complex waveforms will be distorted.

### 2.3 Velocity mode

If the system is provided with a very large damping ratio, at excitation frequencies centred on the natural frequency the damping force predominates and the response to vibratory velocity is  $^5$ 

$$\frac{\theta_{m} - \theta_{i}}{\hat{\theta}_{i}} (j\omega) = \frac{\frac{\omega}{\omega_{n}}}{\omega_{n} \left\{ \left[ 1 - \left( \frac{\omega}{\omega_{n}} \right)^{2} \right]^{2} + 4\zeta^{2} \left( \frac{\omega}{\omega_{n}} \right)^{2} \right\}^{\frac{1}{2}}} \Delta^{\phi}$$
(3)

where  $\dot{\theta}_i$  = instantaneous input angular velocity

and

$$\phi = \tan^{-1} \frac{1 - \left(\frac{\omega}{\omega_n}\right)^2}{2\zeta \frac{\omega}{\omega_n}} \qquad -\frac{\pi}{2} < \phi < \frac{\pi}{2} \qquad (3a)$$

The response is plotted in Fig.1c for  $\zeta = 1$ , 5, 7.07 and 25. Eq.(3) shows that the ratio of the upper and lower -3dB cut-off frequencies is approximately equal to  $4\zeta^2$ , and high damping ratios give wide bandwidth at the expense of sensitivity.

Transducers operating in this mode must have a stable damping ratio since this controls the sensitivity. However, phase errors within the working frequency band are much smaller than those of the acceleration and displacement modes, and the response at the lower and upper frequency limits resembles that of first-order systems. In contrast, conventional rate sensors, such as rate gyros, have a response similar to that of Fig.1a.

The seismic vibratory velocity transducer has been a device of mainly academic interest on account of its low sensitivity and the need to furnish it with a stable damping ratio. It may, however, be a more viable proposition if it embodies a gas rotor (section 8).

# 3. CHARACTERISTICS OF THE GAS ROTOR

To establish the performance of angular motion transducers with gas rotors, the relationship between the pressure generated by the gas, and the input motion, must be derived. Values of the effective mass, stiffness and damping of the system must also be obtained. Inasmuch as the mass and damping are associated with the rotor, these are considered in this section, whilst the stiffness is discussed together with other aspects of the pressure sensor in section 4.

## 3.1 Pressure generated by the rotor

A typical arrangement of a gas rotor transducer is shown in Fig.2, where a helix of tubing containing gas is connected to a sensitive pressure sensor. There is no compelling reason to confine the rotor to a helix. The tubing may be coiled into any desired shape, and it is shown in Appendix Al that the pressure generated is given by

$$p = 2Qn\rho\alpha$$
 (4)

p = pressure generated where

Q = area, in a plane normal to input axis, enclosed by one turn of tubing

n = number of turns of tubing

p = density of the gas

and a = input angular acceleration.

In the special case of a helix, the pressure generated is

$$p = 2\pi R^2 n \rho \alpha \tag{4a}$$

where R = mean radius of helix.

For convenience, the discussion below relates to transducers with a helical rotor, but the methods used may be adapted to suit other shapes such as rectangular, which is useful for multi-axis transducers.

In all gas-rotor transducers, the problem is usually that of generating a pressure large enough to be measured with sufficient accuracy. In practice, this means generating pressures not lower than, say, 50Pa and inspection of Eq. (4a) shows that there is a distinct advantage in using a large diameter helix with many turns. These, however, will be limited by restrictions on size and the need to avoid secondary resonances in the gas column (section 3.4). It is thus necessary to use a gas of high density.

There is a wide choice of gases available, and the writer has successfully used the refrigerant gas 'Arcton 13'\*, which has a molecular weight of about five times that of nitrogen and is compatible with many engineering materials. Its density may be considerably increased by using it at high pressure, and densities of about 100kg m-3 may be achieved. Apart from problems of containing the gas, however, there are limitations imposed on the values of pressure and density schievable because at high pressure the gas will liquify more readily. The maximum usable density therefore depends on the lowest temperature at which the transducer must operate. Fig.3 shows the relationship between dendity and minimum operating temperature whilst Fig. 4 shows the pressure, at 15°C, required to produce " ( density.

To overcome the practical problem of sealing gas at W , I pressure into the tubing and pressure sensor, these components are enclosed in a sealed housing containing t as, and the gas is allowed to communicate with the interior of the tubing through a small bleed hole. A sealing, the density of the gas will remain substantially unaffected by temperature change.

#### Effective mass of the gas

The mass of gas in the helix of tubing is

$$m = 2\pi^2 \rho Rnr^2 \tag{5}$$

where m = actual mass of the gas in tube r = internal radius of tube. and

Under dynamic conditions the gas, when accelerated, moves against the constraints arising from the pressure sensor and the viscous forces generated by the flow. For laminar incompressible flow, it may be shown<sup>6,7</sup> that the velocity profile across the bore of the tube is parabolic at low frequencies and uniform at high frequencies (Fig.5). Parabolic flow leads to an effective mass\*\* of 4/3m. As the frequency is increased the flow profile gradually changes from parabolic to uniform and the effective mass reduces to m

The flow profile depends on a parameter defined by

$$\Omega = \frac{\rho r^2 \omega}{n} \tag{6}$$

where  $\Omega = flow parameter$ 

n = dynamic viscosity of the gas. and

Depending on the flow profile, the effective mass may exceed the actual mass by an amount  $\beta$ , which is plotted as a function of a in Fig.6.

When damper constrictions are used, the effective mass will be further increased by a factor  $\gamma$ , due to the large kinetic energy associated with the rapid flow of gas in the damper (section 3.3). The effective mass is therefore

$$m_{\alpha} = m(1 + \beta + \gamma) \tag{7}$$

where  $m_e$  = effective mass of the gas  $\beta$  = additional mass factor due to flow profile

y = additional mass factor due to constriction.

The quantity  $m(\beta + \gamma)$  represents the additional mass over and above that of the gas at rest. increases the inertia of the system but plays no part in the acceleration forces exciting it. Thus it may be regarded as a parasitic mass which lowers the natural frequency of the system. Moreover, since & is a function of frequency, it can have an adverse affect on the performance but this is only significant in transducers measuring vibratory displacement (section 7).

<sup>&#</sup>x27;Arcton 13' is the ICI registered trade name for triflourochloromethane.

<sup>\*\*</sup> The effective mass is that mass which, if moving at the average velocity of the gas in the tube, has the same kinetic energy as that of the actual gas.

#### 3.3 Damping

It is expedient to use the viscous forces generated by the flow of gas in the tube, or in one or more constrictions in series with the tube, to provide the required damping force. Damping in this manner is relatively constant over a useful temperature range because the viscosity of a gas is, to a fair approximation, proportional to the square root of absolute temperature. Thus the damping ratio remains within ±10% of its value at 20°C over the temperature range -30°C to +70°C. This is at least an order better than that normally achieved with oil damping.

If it is assumed that the flow of gas in the tube is parabolic, it is shown in Appendix A2 that the damping coefficient is

$$c_{r} = 16\pi^{2} nRn \tag{8}$$

where c = damping coefficient of tube.

And if a constriction is placed in series with the tube, the additional damping coefficient is

$$c_{c} = 8\pi \eta \ell \left(\frac{r}{r_{c}}\right)^{4} \tag{9}$$

where  $c_c$  = damping coefficient of constriction  $\ell$  = length of constriction

rc = radius of constriction.

As mentioned in section 3.2, the high flow velocity of gas in the constriction relative to that in the tube gives it a large kinetic energy. This leads to an additional mass factor, derived in Appendix A2,

$$\gamma = \frac{2}{3\pi} \frac{\ell}{Rn} \left( \frac{r}{r_c} \right)^2 . \tag{10}$$

Inspection of Eqs.(9) and (10) shows that if the effective mass of the system is not to be increased substantially by the damping constriction, the constriction must have a small bore and be kept short.

### Secondary resonances of gas in the tube

The assumption that the gas in the tube is incompressible is valid only when the excitation frequency is significantly lower than the lowest organ-pipe resonance. Resonances occur at frequencies where the tube length equals odd multiples of half the wavelength of sound in the gas. The lowest resonance is given by

$$f_{01} = \frac{\mu}{4\pi Rn} \tag{11}$$

where  $f_{01}$  = lowest secondary resonant frequency and  $\mu$  = velocity of sound in the gas.

At a frequency of  $f_{01}$ , a velocity node exists half way along the tube and an antiresonance is seen by the pressure sensor. The length of the tube must therefore be restricted so that  $f_{01}$  is greater than the upper cut-off frequency of the transducer. It is also advisable to split the damping constriction, if used, into two sections and position these close to the sensor inlets in order to damp secondary resonances.

### THE PRESSURE SENSOR

Because the pressure generated by the rotor is small, typically 10-100Pa, the pressure sensor must have a high sensitivity. At the same time, the stiffness which it imparts to the system must satisfy the required dynamic characteristics of the transducer. In angular accelerometers, for example, a large stiffness is usually required in order to achieve the necessary bandwidth. Since the sensitivity is an inverse function of stiffness, the characteristics of the pressure sensor must be carefully matched to requirements.

The pressure sensor considered in this paper is an electrically-conductive membrane situated between two circular electrodes. When pressure difference is applied across the membrane, its displacement causes a differential capacitance change between the membrane and the electrodes (Fig.7). In cases where this relatively simple arrangement cannot meet accuracy requirements, a more advanced sensor based on electrostatic pressure feedback may be used<sup>2</sup>.

## Sensitivity and stiffness

It is shown in Appendix A3 that the fractional differential capacitance change provided by a membrane

$$\frac{\Delta C}{C} = \frac{2a^2 - b^2}{8Sd} p \tag{12}$$

where  $\frac{\Delta C}{C}$  = fractional capacitance change of sensor

= radius of membrane

= radius of each electrode

S = tension in membrane

d = initial gap between membrane and each electrode

and p = applied pressure difference.

It is also shown that the stiffness which the membrane imparts to the gas in the tube is

$$k = 8\pi S \left(\frac{r}{a}\right)^4 \tag{13}$$

where k = effective stiffness of membrane.

Thus it is evident that the stiffness, apart from being a function of the characteristics of the sensor itself, is governed by the fourth power of the ratio of the radii of tube and membrane. This means that the stiffness may be controlled by choice of tube radius without affecting the sensitivity.

#### 4.2 Damping of membrane

When the membrane deflects, it displaces gas through the narrow gaps formed by the membrane and electrodes (Fig.7). The resulting viscous flow leads to a small, but sometimes significant, damping force on the membrane.

An approximate value of the damping coefficient arising from this cause, based on the simplifying assumption that the membrane remains flat and moves as a piston between the two electrodes with central pressure inlets, is  $^2$ 

$$c_m \approx 12\pi n r^4 [\log_e(a/r_i) - \frac{1}{2}]/d^3$$
 (14)

where  $c_m = damping$  coefficient of membrane and  $r_i = radius$  of each inlet.

Damping of the membrane can usually be ignored, except in angular displacement transducers where the required damping coefficient is small.

### 4.3 Construction of pressure sensor

The pressure sensor consists essentially of a tensioned membrane clamped between end pieces which carry the electrodes. Because its sensitivity must be high, the tension in the membrane is low. Moreover, the membrane should be very thin, and of low density, so that its mass will not cause a significant unbalance in the transducer system. At the same time, the characteristics of the membrane and the parts which clamp it must be such that the tension, and hence sensitivity, does not vary significantly with temperature.

These requirements are broadly satisfied by using metallised 'Melinex'\* which is available in films ranging in thickness from  $4\mu m$  upwards. In contrast to many plastics, the polyesters have a relatively low temperature coefficient of expansion which matches that of aluminium alloy, and experience has shown that a reasonable performance can be achieved up to a temperature of at least  $60^{\circ}$ C. Although there is some evidence that humidity can cause tension changes, these do not arise in the present application since the membrane is permanently operating in dry gas.

The end pieces, which clamp the membrane, and the electrodes are constructed from aluminium alloy for three reasons. First, the temperature coefficient of expansion of the alloy matches that of the membrane to within about 5ppm/OC. Second, it is easily machined and allows easy adjustment of the gaps by lapping. Third, and most important of all, it is ideally suited to sensors with capacitive output because insulation may be achieved by means of anodising. In this way, separate insulators are not required and the construction becomes very simple. This type of construction leads, however, to large values of stray capacitance between the earthed end pieces and the membrane and electrodes.

### 5 SIGNAL CONDITIONING

The design of the pressure sensor is such that the full scale capacitance change is small, typically 0.1pF, and strays within the sensor and its connecting cables may amount to 100pF or more.

The problem of measuring very small changes of capacitance in the presence of much larger strays was solved by Blumlein over 40 years ago<sup>8</sup>. His solution lay in the use of a bridge with inductively coupled ratio arms, where all the strays are led to the neutral terminal of the bridge, usually earthed (Fig.8). In this arrangement, the strays shunt the source and output terminals of the bridge but do not affect its balance. However, since strays shunting the output can affect the bridge sensitivity, these may be swamped by a fixed capacitor across the output of the bridge.

If the inductance of the ratio arm is large enough to ensure that the reactance appearing across the output terminals is essentially that of the capacitive shunt, it can be shown that

$$v_0 = \frac{v_s}{c_0} \frac{\Delta C}{C} \tag{15}$$

where v<sub>0</sub> = output voltage of bridge

vs = source voltage of bridge

and Co = capacitance shunting output of bridge.

<sup>\* &#</sup>x27;Melinex' is the ICI registered trade name for polyester film.

A block diagram of the conditioning circuit is shown in Fig.9. It consists of the capacitance bridge, energised from a sine or square wave source, whose output is amplified prior to demodulation by a phase sensitive rectifier. The demodulated signal is then fed to a low gain dc amplifier which may incorporate a filter to remove carrier ripple and shape the frequency response if required.

#### 6 DESIGN OF ANGULAR ACCELERATION TRANSDUCER

In the design of angular acceleration transducers the problem is usually that of achieving high sensitivity over a wide frequency range. As with other open loop accelerometers, the design must therefore involve trading sensitivity with the square of undamped natural frequency.

From Eqs.(4a) and (12), the sensitivity is

$$\frac{\Delta C}{C} = \frac{\pi}{4} \frac{R^2 n \rho (2a^2 - b^2)}{Sd} \alpha . \tag{16}$$

To achieve high sensitivity, it is clear that the helix radius R and gas density  $\rho$  should be as large as possible consistent with size and temperature requirements respectively (section 3.1). The number of turns of the tube n should also be large, but compatible with the need to avoid secondary resonances colouring the frequency response (section 3.4). On the other hand, small sensor gaps d enhance the sensitivity, but these must not be too small lest any foreign particles adversely affect the performance.

The undamped natural frequency, from Eqs. (5), (7) and (13) is

$$\omega_{\rm n} = \left(\frac{k}{m_{\rm e}}\right)^{\frac{1}{2}} = \frac{2r}{a^2} \left[\frac{S}{\pi \rho R n \left(1 + \beta + \gamma\right)}\right]^{\frac{1}{2}} . \tag{17}$$

In deriving the damping ratio, it is reasonable to neglect the damping of the membrane (section 4.2), and also the damping in the tube since the radius of this must be large to achieve a reasonably high natural frequency. Hence the damping ratio, governed by the constriction, is from Eqs.(5), (7), (9), (13) and (17)

$$\zeta = \frac{c_{c}}{2(km_{e})^{\frac{1}{2}}} = \frac{2}{\pi} \frac{\eta \ell r^{2}}{r_{c}^{4} \rho Rn \omega_{n} (1 + \beta + \gamma)} . \tag{18}$$

The additional mass factor  $\gamma$ , caused by the constriction, is a function of its radius and can be obtained from Eqs.(10) and (18) giving

$$\gamma = \frac{\zeta \rho \omega_n r_c^2 (1+\beta)}{3n - \zeta \rho \omega_n r_c^2} . \tag{19}$$

The value of the additional mass factor  $\beta$ , due to the flow profile of gas in the tube, may be obtained for any frequency from Eq.(6) and Fig.6 if the tube radius r is known. Being frequency dependent, it means that the parameters  $\omega_n$  and  $\zeta$  vary with frequency and thus the transducer response does not strictly conform with that of a second order system. However, this is of little practical significance and in order to calculate the parameters it is fair to take the value of  $\beta$  at the natural frequency, when  $\beta\approx 0$ . Very small errors arise in calculating  $\omega_n$  and  $\zeta$  in making this assumption.

Although the above relationships define the parameters of a transducer of known geometry and gas characteristics, they do not permit the geometry to be deduced from specified values of  $\omega_n$  and  $\zeta$ . It is therefore expedient to introduce a performance factor, equal to the product of sensitivity and the square of natural frequency, defined by

$$F_{\alpha} = \omega_{n}^{2} \frac{\Delta C}{\alpha C} \tag{20}$$

where  $F_{\alpha}$  = performance factor of acceleration transducer.

Transducers of high performance factor (those of high sensitivity and wide bandwidth) are clearly difficult to realise in practice.

Putting the values given by Eqs.(16) and (17) into (20), assuming  $\beta=0$  and b=a, gives the performance factor in terms of transducer geometry. Thus

$$F_{\alpha} = \frac{1}{1+\gamma} \frac{R}{d} \left(\frac{r}{a}\right)^2 . \tag{21}$$

From the already known values of R, d and  $\gamma$ , the ratio of tube to membrane radius necessary to meet the required performance factor may hence be obtained. It then remains to select a suitable value of membrane tension S when, from Eqs.(17) and (18), the absolute values of r and a, and the constriction length  $\ell$ , respectively, may be found. In choosing the value of tension, it is important that its value is such that the stress in the membrane (the quotient of tension and thickness) is well below the yield stress of the material, yet not too low lest accurate tensioning becomes difficult.

Since Eq.(21) assumes that the electrode radius equals that of the membrane (b = a), the sensitivity in practice, with b < a , will be slightly greater than that aimed for.

### Effect of linear acceleration

Linear acceleration does not generate pressure across the ends of the tube unless there are density gradients in the gas. Thus it is important to keep temperature gradients within the tube to a minimum by insulating the tube from the transducer housing.

However, linear acceleration produces a force on the membrane, and for acceleration along an axis normal to the plane of the membrane it is easily shown that the effective pressure is

$$p_{A} = \rho_{m} tA \tag{22}$$

where pA = effective pressure due to linear acceleration

ρ<sub>m</sub> = density of membrane t = thickness of membrane

A = linear acceleration normal to plane of membrane. and

Clearly, thin membranes of low density help to reduce errors caused by linear acceleration. Moreover, the linear motion errors discussed here and in sections 7.1 and 8.1 can be substantially reduced by using a pair of nominally identical pressure sensors arranged such that signals due to pressure add whilst those due to acceleration subtract.

From Eqs.(4a) and (22), assuming  $\rho \ll \rho_m$  , the error in terms of the measurand is

$$\alpha_{A} = \frac{\rho_{m}t}{2\pi R_{no}^{2}} A \tag{23}$$

where  $\alpha_A$  = linear acceleration error in terms of angular acceleration.

This shows yet a further reason for making the helix radius as large as possible.

#### DESIGN OF ANGULAR DISPLACEMENT TRANSDUCER

In contrast to accelerometers, vibratory displacement transducers must be used at frequencies above resonance. This means that the undamped natural frequency is low, and hence for damping ratios near the optimum the required damping coefficient is small. Thus a damping constriction is not used and  $\gamma = 0$ .

It is shown in Appendix A4 that the sensitivity is

$$\frac{\Delta C}{C} = \frac{Rr^2(2a^2 - b^2)}{a^4d(1+8)} \theta_i \qquad (24)$$

Although the sensitivity is independent of the membrane tension, the mass factor  $\beta$  affects it. Since in practice  $\beta \approx 1/3$  at resonance, and decreases with frequency, the sensitivity gradually increases with frequency to settle at a final value which is 4/3 that of the sensitivity at low frequency. This fundamental defect inherent in the transducer performance may, however, be outweighed by other advantages in practice (section 9.2).

At the natural frequency, it is fair to assume that  $\beta = 1/3$ . Thus, from Eqs.(5), (7) and (13)

$$\omega_{\rm n} = \frac{r}{a^2} \left( \frac{3S}{\pi \rho Rn} \right)^{\frac{1}{2}} \quad . \tag{25}$$

From Eqs. (5), (7), (8), (13) and (14) the damping ratio is

$$\zeta = \frac{c_t + c_m}{2(km_a)^{\frac{1}{2}}} = \left(\frac{3}{\pi}\right)^{\frac{1}{2}} \frac{\eta a^2}{4r^3(\rho RnS)^{\frac{1}{2}}} \left\{4\pi Rn + 3\frac{r^4}{a^3} \left[\log_e\left(\frac{a}{r_i}\right) - \frac{1}{2}\right]\right\}$$
(26)

$$\approx \frac{na^2}{3} \left( \frac{3\pi Rn}{\rho S} \right)^{\frac{1}{2}} \quad \text{if} \quad c_m \ll c_t \quad . \tag{26a}$$

Since the damping on the membrane is usually a small fraction of that in the tube, Eq. (26a) can be used with (25) in the initial design stage to give

$$\zeta \omega_{n} = 3 \frac{\eta}{\rho r^{2}} . \qquad (27)$$

This shows that for given values of gas characteristics  $\eta$  and  $\rho$ , the specified product  $\zeta \omega_n$  can only be achieved with a unique value of tube radius r. Small values of  $\zeta \omega_n$  are required if the transducer is to operate at low frequencies, and it is evident that the kinematic viscosity  $\eta/\rho$  should be small if the tube radius is to be kept down to a reasonable size. Having established the value of r, Eqs.(24), (25) and (26) can then be used to establish the other design values. In doing this, special care must be observed in keeping the lowest secondary resonance well above the specified maximum frequency since the damping of secondary resonances will be small (section 3.4).

### Effects of linear acceleration and displacement

From Eqs.(12), (22), (24) and (25), the sensitivity to steady linear acceleration acting normal to the plane of the membrane is

$$\theta_{\mathbf{A}} = \frac{1}{2\pi} \frac{\rho_{\mathbf{m}}^{\mathbf{t}}}{\omega_{\mathbf{n}}^{2} R^{2} \rho_{\mathbf{n}}} \mathbf{A}$$
 (28)

where  $\theta_A$  = linear acceleration error in terms of angular displacement.

Large static and quasistatic errors can be caused by linear acceleration, particularly with transducers of low natural frequency and small diameter. However, since the transducer is restricted to the measurement of vibratory displacement, static errors may be removed with an ac coupling in the conditioning circuit.

Errors within the frequency band of the transducer are very small. It is shown in Appendix A4 that for vibratory linear displacement acting normal to the plane of the membrane, the error is

$$\theta_{\mathbf{x}_{i}} = \frac{\rho_{\mathbf{m}}^{\mathbf{t}}}{2\pi\rho R^{2}_{\mathbf{n}}} \mathbf{x}_{i} \tag{29}$$

where  $\theta_{x_i}$  = linear displacement error in terms of angular displacement xi = vibratory linear displacement normal to plane of membrane.

#### DESIGN OF ANGULAR VELOCITY TRANSDUCER

Angular velocity transducers must have a very large damping ratio whose size is governed by the required bandwidth. Moreover, it may be shown from Eq.(3) that the undamped natural frequency should equal the geometric mean of the upper and lower cut-off frequencies.

It is shown in Appendix A5 that the mid-band sensitivity is

$$\frac{\Delta C}{C} = \frac{\pi}{4} \frac{R^2 r_c^4 \rho n (2a^2 - b^2)}{a^4 dn^2} \dot{\theta}_i \qquad (30)$$

Because of the high damping ratio, a damping constriction is essential and damping forces in the tube and on the membrane can be neglected. The relationships for natural frequency and damping ratio are therefore the same as those for the accelerometer, namely

$$\omega_{\rm n} = \frac{2r}{a^2} \left[ \frac{S}{\pi \rho Rn (1 + \beta + \gamma)} \right]^{\frac{1}{2}}$$
 (31)

and

$$\zeta = \frac{2}{\pi} \frac{\eta \ell r^2}{r_c^4 \rho R n \omega_n (1 + \beta + \gamma)}$$
 (32)

with

$$\gamma = \frac{\zeta_{\rho\omega_n} r_c^2 (1+\beta)}{3\eta - \zeta_{\rho\omega_n} r_c^2} . \tag{33}$$

Although the mass factors  $\beta$  and  $\gamma$  influence the natural frequency and damping ratio, they do not affect the sensitivity. Hence the change of  $\beta$  with frequency has no effect other than to slightly broaden the frequency band. Moreover, the sensitivity is independent of the membrane tension. However, since the viscosity  $\eta$  of the gas controls sensitivity, a variation of about  $\pm 10\%$  will occur over the temperature range -30 to  $\pm 70\%$ . Such a variation could be compensated by temperature sensitive capacitors controlling the source voltage and shunt capacitance of the bridge (section 5).

In order to achieve an optimum design, it is again useful to introduce a performance factor. In this case, it is convenient to define it as the product of sensitivity, natural frequency and the ratio of the upper and lower frequency limits. Thus

$$F_{\dot{\theta}} = \frac{\omega_2 \omega_n}{\omega_1} \frac{\Delta C}{\dot{\theta}_i C}$$
 (34)

where Fg = performance factor of velocity transducer

ω<sub>1</sub> = lower -3dB frequency limit

ω2 = upper -3dB frequency limit.

From Eq.(3), if  $\omega_n = (\omega_1 \omega_2)^{\frac{1}{2}}$  and  $\omega_2 \gg \omega_1$ ,

$$\frac{\omega_2}{\omega_1} = 4\zeta^2 \qquad . \tag{35}$$

Hence, from Eqs. (30), (32), (34) and (35), assuming b = a,

$$F_{\theta} = 2 \frac{\zeta R}{d(1+\beta+\gamma)} \left(\frac{r}{a}\right)^2 . \qquad (36)$$

For reasons similar to those raised in section 6, the quantities R,  $\rho$  and n should be made as large as the constraints imposed on them allow, whilst d should be kept small. Then, knowing the values of  $\beta$  at frequency  $\omega_n$  from Eq.(6) and Fig.6, and the value of  $\gamma$  from Eq.(33), the required ratio r/a can be obtained from Eq.(36). Absolute values of r and a can then be determined from Eq.(31) for a suitable value of S, and the constriction length  $\ell$  obtained from Eq.(32).

### 8.1 Effects of linear acceleration and velocity

From Eqs.(12), (22), and (30) to (32), the sensitivity to steady linear acceleration is

$$\dot{\theta}_{A} = \frac{1}{\pi} \frac{\zeta_{\rho_{m}} t}{\omega_{n} R^{2} \rho_{n}} A \tag{37}$$

where  $\dot{\theta}_{A}$  = linear acceleration error in terms of angular velocity.

This again points to the advantage of having a large value of R .

A large value of  $\zeta$  (wide bandwidth) increases the acceleration sensitivity but the natural frequency is not important since in practice  $n\omega_n$  tends to be constant (section 3.4). As with displacement transducers, static errors may be removed by ac coupling.

Within the frequency band, it is shown in Appendix A5 that the sensitivity to vibratory linear velocity is

$$\dot{\theta}_{\dot{x}_{i}} = \frac{\rho_{m}^{t}}{2\pi R^{2} n_{0}} \dot{x}_{i} \tag{38}$$

where  $\dot{\theta}_{\dot{x}_i}$  = linear velocity error in terms of angular velocity and  $\dot{x}_i$  = vibratory linear velocity normal to plane of membrane.

Errors generated within the frequency range are much smaller than those caused by steady acceleration. But should they be too large, a pair of back-to-back pressure sensors must be used.

### 9 EXAMPLES OF PRACTICAL TRANSDUCERS

Prototype angular acceleration and displacement transducers have been constructed, and were found to successfully meet the requirements of the applications for which they were designed. These are briefly described in this section together with an angular velocity transducer of arbitrary, but perhaps realistic, specification. Since the prototypes constructed behaved substantially as predicted, there is good reason to believe that the purely theoretical data derived for the velocity transducer would be confirmed in a practical instrument.

### 9.1 Angular acceleration transducer

A number of accelerometers of range  $\pm 10$  rad s<sup>-2</sup>, undamped natural frequency 10Hz and damping ratio 0.65, have been made and successfully used for aerodynamic and other trials of weapons and models<sup>10</sup>. Of length 85mm and diameter 40mm, they require a supply of  $\pm 14$  volts nominal and provide a full-scale ouput of  $\pm 3$  volts.

The transducer is illustrated in Fig.10, from which it can be seen that the signal conditioning unit, built on a circular printed circuit board, is housed in a compartment outside the sealed section of the container. The circuit (Fig.11) is unusual in that the source of the capacitance bridge is a 9 volt 100kHz square wave generated by NI and stabilised by back-to-back zener diodes DZ1 and DZ2. The bridge, whose inductive ratio arms are formed from a bifilar coil wound on a toroidal ferrite core, is followed by a carrier amplifier N2 of gain 450. The output of N2 is demodulated by TR1 and the demodulated signal is amplified and filtered by N3 to provide a full-scale output of ±3 volts at low impedance. Use of square waves greatly simplifies the source generator with little adverse effect on performance 11.

The major design characteristics of the transducer are listed in Appendix A6 and Ref.10 describes the results of tests performed on it. Although it has only been tested to steady linear accelerations of  $100g_{\rm n}$  and shocks of  $500g_{\rm n}$  the basic construction is such that with suitable design transducers of this type should survive very much harsher environments.

### 9.2 Angular displacement transducer

An angular displacement transducer having the same dimensions, supply voltage and full-scale output as the accelerometer, has also been constructed and successfully used. With an undamped natural frequency

of 0.64Hz and damping ratio of 0.5, its range is ±5 degrees and it is designed to operate over the frequency range 2-15Hz. This transducer has a conditioning unit whose circuit is broadly similar to that shown in Fig.11, and details of the mechanical construction are listed in Appendix A7.

The frequency response is similar to that of Fig. 1b for  $\zeta = 0.5$  but, for the reason discussed in section 7, the amplitude slowly rises within the frequency band by about 10% (Fig. 12).

These transducers have been successfully used to measure angular vibrations about two perpendicular axes of an Isocon TV camera for image motion compensation. In this system, the transducer outputs are scaled to produce electronic deflections in an image intensifier which cancel the effects of camera motion. To keep the compensation error acceptably small down to 2Hz, a damping ratio of 0.5 has been chosen and a lag-lead network incorporated in N3 (not shown in Fig. II) to reduce phase error. Because the angular motion of the camera tends to be small at the higher frequencies, the imperfection of amplitude response inherent in the transducer is of little practical significance. Moreover, the errors arising from this cause are smaller than those resulting from the use of rate gyros with integration, where large phase lags at high frequencies (Fig. Ia) lead to significant errors in the vector subtraction process.

The gas rotor transducer seems to be ideally suited to this type of application because of its low power consumption, low noise threshold and long maintenance-free working life. If manufactured in reasonably large quantities it should be much cheaper than a rate gyro, yet tests suggest that for this application it is, if anything, technically superior.

### 9.3 Angular velocity transducer

Although an angular velocity transducer incorporating a gas rotor has not been constructed, the design and calculated performance details of such a transducer are given in Appendix A8. With a range of ±60deg s<sup>-1</sup>, covering the frequency band 0.1 to 2CHz, it is housed in the same size of container as the accelerometer and employs a similar electronic circuit. The errors quoted for linear acceleration and velocity could be substantially reduced by using paired pressure sensors (section 6.1).

## 10 FUTURE DEVELOPMENTS

As discussed in section 3.1, the pressure generated by unit angular acceleration (i.e. the effective moment of inertia) of a gas rotor is proportional to the area enclosed by each turn of tubing and the number of turns. Because the rotor can be of any shape, it should be possible to design transducers to fit into irregular spaces. Although in the designs discussed in this paper, the rotor tube is enclosed in the transducer housing, there is no reason why this should be so. One can visualise many situations where external 'plumbing' would permit very large effective moments of inertia to be realised and yet allow the space within the rotor to be used for housing other equipment.

Flexibility of rotor shape should also mean that compact three-axis motion sensors are feasible. Fig.13 shows the layout of such an instrument where the three coils of tubing, mutually orthogonal, overlap each other and occupy the same space<sup>4</sup>. With careful design, a three-component pressure sensor, sharing a common membrane, can be used to achieve a substantial saving in components and assembly work. Development of such an instrument is taking place. With a range of  $\pm 50 \, \mathrm{rad} \, \mathrm{s}^{-2}$  in roll and  $\pm 250 \, \mathrm{rad} \, \mathrm{s}^{-2}$  in pitch and yaw, its size is less than that of the single-axis accelerometer described in section 9.1. The possibility of using transducers of this nature in small diameter projectiles is thus a reality.

It seems reasonable to assume that if further development of the vibration transducer, successfully applied to image motion compensation, takes place this will include the provision of a two-axis unit. Besides being cheaper than two individual instruments, it would simplify the installation of such a facility on TV cameras.

## 11 CONCLUSIONS

In this paper the writer has endeavoured to outline the salient features of angular motion transducers with gas rotors, and to present a detailed approach to their design.

Gas rotor transducers are basically simple and their construction is relatively straightforward. Their inherent balance and the absence of delicate mechanical components mean that they are very robust. With no parts to wear out, they offer the prospect of long operational life even in conditions of exceptionally severe shock and vibration.

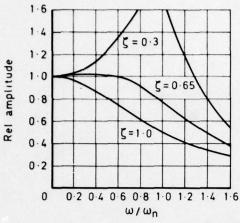
Because the rotor can be of almost any shape, it should be possible to design transducers to fit most available spaces be they long and narrow, short and wide, or irregular. For the same reason, multi-axis transducers of similar size and cost to their single-axis counterparts should be feasible.

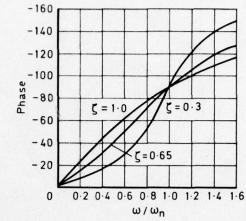
Gas rotors seem to make the seismic angular velocity transducer, hitherto a somewhat academic device, a practical proposition. Although it cannot do all that a rate gyro can do, it merits careful consideration for certain applications. For example, low cost and long life might outweigh its limitations in performance.

In general, it may be concluded that angular motion transducers based on the gas rotor could find application in several spheres of aerospace trials and service.

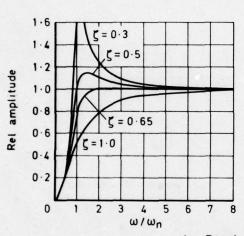
#### REFERENCES

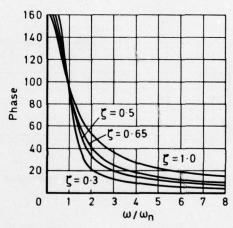
- 1 Leigh, P.G., "Use of the angular accelerometer for stabilisation and control", Systron-Donner Corporation
- Macdonald, W.R., "A guide to the design and performance of angular acceleration transducers with gas rotors", RAE Technical Report 74146 (1974)
- 3 Macdonald, W.R., "Angular accelerometers and torsional vibration transducers", UK Patent 1323702 (1973)
- 4 Macdonald, W.R., "Three-axis angular accelerometers", UK Patent application No.9436/76 (1976)
- 5 Doebelin, E.O., "Measurement systems: application and design", McGraw-Hill Book Company 1966 pp.291-296
- 6 Knight, J., "The flow of gas in an oscillating tube with a fluctuating axial pressure gradient", RAE Technical Report 74030 (1974)
- 7 Knight, J., "The frequency response of angular vibration and acceleration transducers having gas rotors", RAE Technical Report 74038 (1974)
- 8 Blumlein, A.D., British Patent 323037
- 9 Macdonald, W.R., "The transformer ratio arm bridge as a transducer input network", RAE Technical Note IR 19 (1962)
- 10 Cole, P.W., Whitall, J.S., "A gas rotor acceleration transducer for measuring low angular accelerations", RAE Technical Memorandum IT 160 (1976)
- Macdonald, W.R., "A miniature conditioning unit for inductive transducers. RAE Technical Memorandum IR 134 (1973)



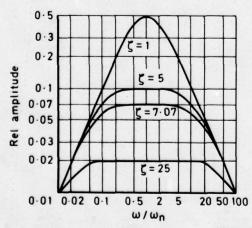


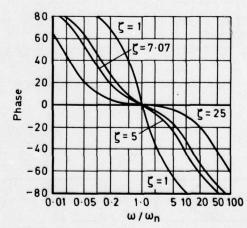
a Acceleration response





b Displacement response





c Velocity response

Fig.1 Response of spring-mass systems

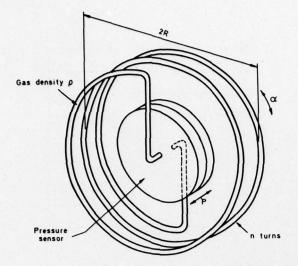


Fig.2 Typical arrangement of transducer

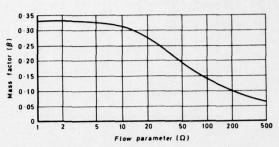


Fig.6 Variation of mass factor with flow parameter

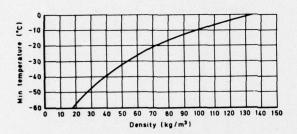


Fig.3 Variation of minimum temperature with density

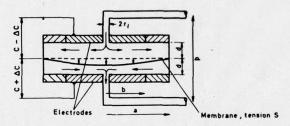


Fig.7 Schematic of pressure sensor

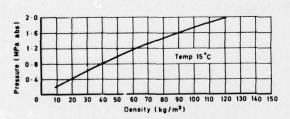


Fig.4 Variation of filling pressure with density

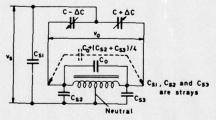


Fig.8 Capacitance bridge

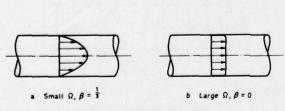


Fig.5 Profiles of flow in tube

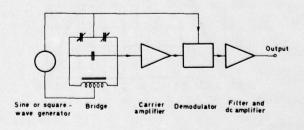


Fig.9 Signal conditioning method

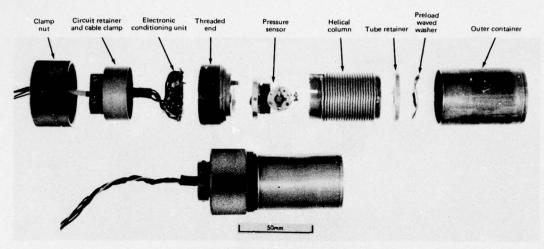


Fig.10 Construction of accelerometer

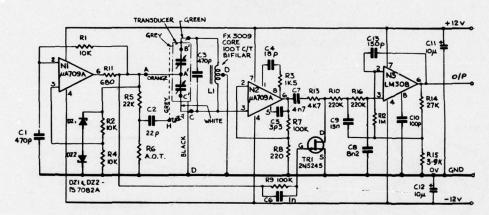


Fig.11 Circuit of conditioning unit

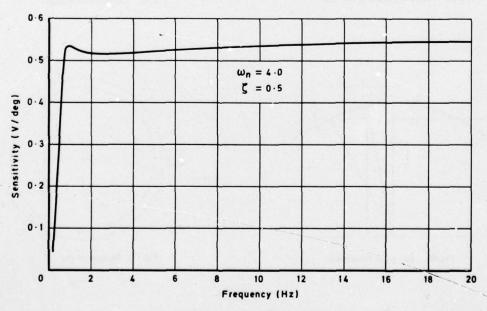


Fig.12 Response of displacement transducer

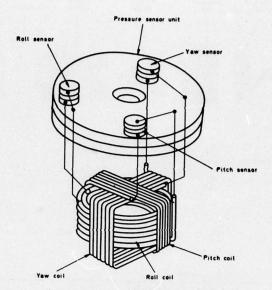


Fig.13 Three-axis angular accelerometer

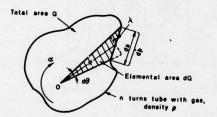


Fig. 14 Pressure generation in rotor

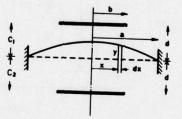


Fig.16 Capacitance change

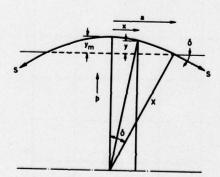


Fig.15 Action of membrane

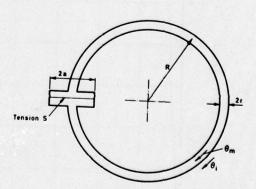


Fig.17 Motion of gas

## Appendix Al

## PRESSURE GENERATED BY THE ROTOR

Let the rotor consist of n turns of the tube enclosing an area Q (Fig.14). If the tube contains gas of density  $\rho$  and angular acceleration  $\alpha$  is applied about an axis normal to the plane of Q at point 0, then the pressure generated across an element of tube length ds is

$$dp = R\rho\alpha \cos \lambda ds$$
$$= R^2\rho\alpha d\theta .$$

Now

$$\frac{R^2}{2} d\theta = dQ = \text{area of segment}$$

therefore

$$dp = 2\rho\alpha dQ$$

and

$$p = 2Q\rho\alpha$$
 for one complete turn .

Hence the pressure generated by n complete turns of tube is

$$p = 2Qn\rho\alpha$$
.

## Appendix A2

#### CHARACTERISTICS OF ROTOR

### (a) Damping coefficient of tube

Consider a tube of internal radius r and length L . If gas, of viscosity  $\eta$ , flows in a laminar manner with mean velocity  $\overline{\nu}$ , the well-known Poiseuille law will apply and the pressure drop is

$$\Delta p = \frac{8\eta L \overline{v}}{r^2} .$$

The damping coefficient, being the force on the gas per unit mean velocity, is therefore

$$c_{t} = \frac{\Delta p \pi r^{2}}{\bar{v}}$$

$$= 8\pi n L$$

$$= 16\pi^{2} \eta Rn .$$

## (b) Damping coefficient of constriction

If Poiseuille flow takes place in a constriction, of length  $\ell$ , and radius  $r_c$ , connected in series with the tube, gas will flow with mean velocity  $\bar{w}$  in the constriction causing a pressure drop of

$$\Delta p = \frac{8n\ell \bar{w}}{r_c^2}$$

$$\bar{w} = \bar{v} \left(\frac{r}{r_c}\right)^2$$

$$\Delta p = \frac{8n\ell r^2}{r_c^4} \bar{v} .$$

but

hence

The damping coefficient experienced by the gas in the tube, due to the constriction, is therefore

$$c_{c} = \frac{\Delta p \pi r^{2}}{\bar{v}}$$

$$= 8\pi \eta \ell \left(\frac{r}{r_{c}}\right)^{4} .$$

### (c) Additional mass factor due to constriction

Since the radius of the constriction is very small, it is assumed that the flow is parabolic which leads to an effective mass of 4/3 that of the actual mass (section 3.2). Hence

effective mass of gas in constriction = 
$$\frac{4}{3} \pi r_c^2 k\rho$$
.

In order to determine the effect which this mass will have on the inertia of the whole system, its kinetic energy must be compared with that of the gas in the tube.

The kinetic energy of the gas in the tube, assuming uniform flow, is

$$\pi^2 \rho Rnr^2 \overline{v}^2$$

whilst the kinetic energy of the gas in the constriction is

$$\frac{2}{3} \pi r_{c}^{2} t_{\rho} \bar{w}^{2}$$

$$= \frac{2}{3} \pi \frac{r^{4} t_{\rho}}{r_{c}^{2}} \bar{v}^{2}$$

the additional mass factor is therefore

$$\gamma = \frac{\text{KE of gas in constriction}}{\text{KE of gas in tube}}$$
$$= \frac{2}{3\pi} \frac{t}{\text{Rn}} \left(\frac{r}{r_c}\right)^2 .$$

### CHARACTERISTICS OF PRESSURE SENSOR

## (a) Sensitivity

With reference to Fig.15, let a pressure difference p act on a membrane of radius a and tension S . If it is assumed that the tension is large enough to remain effectively unaltered when the pressure is applied, then

 $2\pi a S \sin \delta = \pi a^2 p$ 

therefore

 $\sin \delta = \frac{ap}{2S}$ 

but

 $\sin \delta = \frac{a}{X}$ 

whence

 $X = \frac{2S}{P}$ 

also

 $x^2 = a^2 + (x - y_m)^2$ 

therefore

 $2Xy_{m} = a^{2} + y_{m}^{2}$   $\approx a^{2} \text{ if } y_{m} \ll a$ 

therefore

 $y_{m} = \frac{a^2}{2X} = \frac{a^2p}{4S} .$ 

Now

 $x^2 = x^2 + (y - y_m + x)^2$ .

Hence, since  $y < y_m < X$ 

 $y - y_m = -\frac{x^2}{2X}$ 

and

$$y = \frac{a^2 - x^2}{4S} p .$$

With reference to Fig.16, consider now the difference of capacitance between the deflected membrane and each electrode of radius b. For initial gaps d and dielectric constant  $\epsilon$ , the difference in capacitance of an elemental ring of width dx at radius x is

$$d(C_1 - C_2) = 2\pi \varepsilon x dx \left(\frac{1}{d - y} - \frac{1}{d + y}\right)$$
$$= \frac{4\pi \varepsilon y x}{d^2} dx \text{ if } y < y_m < d$$
$$= \frac{\pi \varepsilon p}{s d^2} x (a^2 - x^2) dx$$

therefore

$$c_1 - c_2 = \frac{\pi \epsilon p}{Sd^2} \int_0^b x(a^2 - x^2) dx$$
  
=  $\frac{\pi}{4} \frac{\epsilon p b^2}{Sd^2} (2a^2 - b^2)$ 

now the initial capacitance is

$$C = \frac{\pi \varepsilon b^2}{d}$$

hence

$$\frac{\Delta C}{C} = \frac{C_1 - C_2}{2C}$$
$$= \frac{2a^2 - b^2}{8Sd} p .$$

### (b) Effective stiffness of membrane

Consider the volume displacement of the membrane when pressure  $\, p \,$  is applied (Fig. 16). For an elemental ring of width  $\, dx \,$  at radius  $\, x \,$ , the volume displaced is

$$dV = 2\pi y x dx$$
$$= \frac{\pi p}{2S} x(a^2 - x^2) dx$$

therefore

$$V = \frac{\pi p}{2S} \int_{0}^{a} x(a^{2} - x^{2}) dx$$
$$= \frac{\pi a^{4} p}{8S} .$$

If the gas in the tube is displaced through unit distance, the volume displacement is

$$V = \pi r^2$$
.

This gives rise to a pressure of

$$p = \frac{8SV}{\pi a^4}$$
$$= \frac{8Sr^2}{a^4} .$$

The force on the gas in the tube, per unit displacement is therefore

$$k = \pi r^2 p$$

$$= 8\pi S \left(\frac{r}{a}\right)^4 .$$

#### Appendix A4

#### DISPLACEMENT TRANSDUCER

#### (a) Sensitivity

With reference to Fig.17, let the input angular displacement be  $\theta_i$  and the absolute angular displacement of the gas in the tube be  $\theta_m$ . By analogy with a spring-mass system, for sinusoidal inputs, the equation of motion describing the behaviour of the gas, treated in Refs.6 and 7, may be written

$$R\left\{\left(j\omega\right)^{2}m\theta_{m}+\left(j\omega\right)^{2}m\beta\left(\theta_{m}-\theta_{i}\right)+j\omega c_{t}\left(\theta_{m}-\theta_{i}\right)+k\left(\theta_{m}-\theta_{i}\right)\right\}=0.$$

The second term in the curly brackets describes the inertia of the parasitic mass (section 3.2).

The angular displacement of the gas relative to the tube is therefore

$$\theta_{m} - \theta_{i} = \frac{\omega_{m}^{2}}{-\omega_{m}^{2}(1+\beta) + j\omega_{r} + k}\theta_{i} .$$

For vibratory inputs well above the natural frequency the damping and stiffness forces become small compared with the inertia force, hence

$$\theta_{m} - \theta_{i} = -\frac{\theta_{i}}{1+\beta}$$
.

The linear displacement of the gas is, neglecting the sign

$$(\theta_{m} - \theta_{i})R = \frac{R\theta_{i}}{1 + \beta} \tag{A4-1}$$

and the pressure is

$$\frac{R\theta_{i}}{1+\beta} \frac{k}{\pi r^{2}} = \frac{8Sr^{2}\theta_{i}}{a^{4}(1+\beta)}$$
 (see Eq.(13)).

Hence from Eq. (12)

$$\frac{\Delta C}{C} = \frac{Rr^2(2a^2 - b^2)}{a^4d(1+\beta)} \theta_i .$$

#### (b) Error caused by linear displacement

If a sinusoidal linear displacement of amplitude  $x_i$  be applied along an axis normal to the plane of the membrane, the equivalent pressure acting on the membrane is, from Eq. (22)

$$\rho_{m} tx_{i} (j\omega)^{2}$$

and the force on the gas in the tube is

$$\pi r^2 \rho_m t x_i (j\omega)^2$$
.

Above the natural frequency, this force is balanced by the inertia of the gas, the stiffness and damping forces being negligible. Hence the acceleration of the gas in the tube is the quotient of the force and mass, namely

$$\frac{\pi r^2 \rho_m t x_i (j\omega)^2}{m(1+\beta)}$$

and the displacement of the gas in the tube is

$$\frac{\pi r^2 \rho_m t x_i}{m(1+\beta)}$$

$$= \frac{\rho_m t x_i}{2\pi \rho Rn(1+\beta)} \qquad \text{(see Eq.(5))}.$$

But the gas displacement due to an input of  $\theta_i$  is, from Eq.(A4-1)

$$\frac{R\theta_{i}}{1+\beta}$$

Hence the angular displacement equivalent to the linear displacement is

$$\theta_{x_i} = \frac{\rho_m t}{2\pi \rho R^2 n} x_i .$$

#### VELOCITY TRANSDUCER

#### (a) Sensitivity

With reference to Fig.17, let the input angular displacement be  $\theta_i$  and the absolute angular displacement of the gas in the tube be  $\theta_m$ . The equation of motion is, for reasons similar to those stated in Appendix A4,

$$R\left\{ \left(j\omega\right)^{2}m\theta_{m} + \left(j\omega\right)^{2}m(\beta + \gamma)\left(\theta_{m} - \theta_{i}\right) + j\omega_{c}^{c}(\theta_{m} - \theta_{i}) + k(\theta_{m} - \theta_{i}) \right\} = 0$$

therefore

$$\theta_{m} - \theta_{i} = \frac{\omega_{m}^{2}}{-\omega_{m}^{2}(1+\beta+\gamma)+j\omega_{c}+k}\theta_{i}$$

Because of the very high damping ratio, at input frequencies close to the natural frequency the damping term predominates and, neglecting the sign

$$\theta_{m} - \theta_{i} = \frac{m}{c_{c}} j\omega\theta_{i}$$

$$= \frac{m}{c_{c}} \dot{\theta}_{i}$$

$$= \frac{\pi \rho Rnr_{c}^{4}}{4n\epsilon r^{2}} \dot{\theta}_{i} \quad (\text{see Eqs.}(5) \text{ and } (9)). \quad (A5-1)$$

The linear displacement of gas in the tube is

$$R(\theta_m - \theta_i)$$

and the pressure is

$$R(\theta_m - \theta_i) \frac{k}{\pi r^2} = \frac{2\pi R^2 r_c^4 onS}{n\ell a^4} \dot{\theta}_i$$
 (see Eq.(13)).

The fractional capacitance change is therefore, from Eq.(12)

$$\frac{\Delta C}{C} = \frac{R^2 r_c^4 \rho n (2a^2 - b^2)}{a^4 dn \ell} \dot{\theta}_i .$$

#### (b) Error caused by linear velocity

If a sinusoidal linear velocity  $j\omega x_i$  be applied along an axis normal to the plane of the membrane, the equivalent pressure acting on the membrane is, from Eq.(22)

and the force on the gas in the tube is

$$\pi r^2 \rho_{\mathbf{m}} t x_{\mathbf{i}} (j\omega)^2$$

This force, if it is within the frequency range of the transducer, is balanced by the damping force. Hence, from the equation of motion, neglecting inertia and stiffness forces

$$\pi r^2 \rho_m t x_i (j\omega)^2 = R(\theta_m - \theta_i) j\omega c_c$$

where  $R(\theta_m - \theta_i)$  denotes the displacement of the gas relative to the tube, hence

$$R(\theta_{m} - \theta_{i}) = \frac{\pi r^{2} \rho_{m} t j \omega x_{i}}{c_{c}}$$
$$= \frac{\pi r^{2} \rho_{m} t \dot{x}_{i}}{c_{c}}.$$

But from Eq. (A5-1),

$$R(\theta_m - \theta_i) = \frac{mR}{c_c} \dot{\theta}_i$$
.

Hence the angular velocity equivalent to the linear velocity  $\dot{\mathbf{x}}_{i}$  is

$$\dot{\theta}_{\dot{x}_{\dot{1}}} = \frac{\pi r^2 \rho_{m} t}{mR} \dot{x}_{\dot{1}}$$

$$= \frac{\rho_{m} t}{2\pi R^2 n \rho} \dot{x}_{\dot{1}} \quad \text{(see Eq.(5))}.$$

Appendix A6

#### SALIENT FEATURES OF ANGULAR ACCELERATION TRANSDUCER

$$\omega_n = 63s^{-1}$$

ζ = 0.65

minimum working temperature = - 4°C

full scale 
$$\frac{\Delta C}{C}$$
 = 0.03 with C = 2.8pF

R = 15mm

r = 0.61mm

a = 3.3mm

b = 2.25mm

l = 5.2mm (in two lengths of 2.6mm)

 $r_c = 50 \mu m$ 

 $s = 92N m^{-1}$ 

n = 40

 $d = 50 \mu m$ 

 $\eta = 1.8 \times 10^{-5} \text{N s m}^{-2}$ 

 $\rho = 120 \text{kg m}^{-3}$ 

gas pressure = 2.0MPa absolute at 15°C

 $t = 4\mu m$ 

 $\rho_{\rm m} = 1.4 \times 10^3 {\rm kg m}^{-3}$ 

stress in membrane = 2.3 × 10<sup>7</sup>Pa (0.24 × yield stress)

linear acceleration error =  $8.1 \times 10^{-3} \text{rad s}^{-2}/\text{g}_{\text{n}}$ 

- 0.04% FS/gn

Appendix A7

#### SALIENT FEATURES OF ANGULAR DISPLACEMENT TRANSDUCER

Range = 
$$\pm 5^{\circ}$$
 ( $\pm 0.087$  rad)

$$\omega_{\rm n} = 4.0 {\rm s}^{-1}$$

4 - 0.5

minimum working temperature = - 18°C

full scale 
$$\frac{\Delta C}{C}$$
 = 0.048 with C = 13.6pF

R = 15mm

r = 0.61mm

a = 9.0mm

b = 7.0mm

 $s = 10N m^{-1}$ 

n = 30

 $d = 100 \mu m$ 

 $n = 1.8 \times 10^{-5} \text{N s m}^{-2}$ 

 $\rho = 75 \text{kg m}^{-3}$ 

gas pressure = 1.4MPa absolute at 15°C

 $t = 4\mu m$ 

 $\rho_{\rm m} = 1.4 \times 10^3 {\rm kg \ m}^{-3}$ 

steady-state linear acceleration error =  $0.062^{\circ}/g_{n}$ 

= 0.62%FS/gn

linear displacement error = 0.1°/m

= 1.0%FS/m

Hence the membrane mass has a negligible effect for linear vibration within the frequency band of the transducer.

#### Appendix A8

#### SALIENT FEATURES OF ANGULAR VELOCITY TRANSDUCER

Range =  $\pm 50^{\circ}/s (\pm 0.87 \text{rad s}^{-1})$ 

lower -3dB cut-off frequency = 0.1Hz

upper -3dB cut-off frequency = 20Hz

 $\omega_{\rm n} = 8.89 \rm s^{-1}$ 

 $\zeta = 7.07$ 

minimum working temperature = - 10°C

full scale  $\frac{\Delta C}{C}$  = 0.015 with C = 10.0pF

R = 15mm

r = 1.25mm

a = 8.3mm

b = 6.0mm

l = 3.6mm (in two lengths of 1.8mm)

 $r_c = 63.5 \mu m$ 

 $S = 12N m^{-1}$ 

n = 18

d = 100um

 $\eta = 1.8 \times 10^{-5} \text{N s m}^{-2}$ 

 $\rho = 100 \text{kg m}^{-3}$ 

gas pressure = 1.65MPa absolute at 15°C

c = 4um

 $\rho_{\rm m} = 1.4 \times 10^3 {\rm kg m}^{-3}$ 

steady-state linear acceleration error = 1.97°/s/gn

= 1.97%FS/gn

linear velocity error = 0.13°s-1/ms-1

= 0.13%FS/ms<sup>-1</sup>

## EXEMPLES D'UTILISATION DU LASER POUR LES ESSAIS DE CERTIFICATION D'AVIONS CIVILS

Nicolas LAPCHINE Ingénieur au Centre d'Essais en Vol d'Istres Instructeur à l'Ecole du Personnel Navigant d'Essais et de Réception 13800 ISTRES FRANCE

#### 1. RESUME

Cet exposé est consacré à la présentation de deux exemples d'utilisation d'une station de trajectographie par laser, pour la mise au point et la certification de deux avions civils.

#### 2. INTRODUCTION

Le système STRADA de trajectographie par laser installé au CENTRE D'ESSAIS EN VOL de BRETIGNY depuis fin 1973 est utilisé couramment pour la mise au point et la qualification d'équipements aussi bien civils que militaires.

Le but de cette note est de montrer comment ce moyen d'essai a été utilisé avec succès, au cours de la certification de deux avions civils, le MERCURE 100 et le CONCORDE

Notre exposé comprend d'abord une présentation sommaire du système STRADA, puis une description partielle avec quelques résultats significatifs des essais de certification des performances au décollage du MERCURE 100 et d'atterrissage automatique catégorie 3A du CONCORDE.

#### 3. DESCRIPTION SOMMAIRE DU SYSTEME STRADA

La description succincte de ce système est volontairement limitée aux connaissances que doit avoir tout ingénieur d'essais, client de la station, pour pouvoir l'utiliser avec profit.

- 3.1 Tous les éléments constitutifs de STRADA énumérés ci-après sont disposés dans un bâtiment autonome implanté en bordure de piste de façon à restituer la meilleure précision de localisation.
- 3.2 La partie maîtresse est un radar optique, le LIDAR (LIGHT DETECTION AND RANGING), montée sur une tourelle asservie et consistant en un émetteur laser. Ce dernier est un laser YAG (cristal de grenat d'YTRIUM-ALUMINIUM) émettant dans l'infrarouge (1,06 p) à une fréquence de 3200 impulsions par seconde.
- 3.3 L'énergie lumineuse recueillie par un rétroréflecteur passif monté sur l'avion est reçue dans un système optique de réception relié à deux récepteurs :
  - . un récepteur de telemetrie pour la mesure de distance.
  - . un récepteur d'écartométrie pour la mesure des écarts angulaires, en site et en gisement, entre l'axe de visée laser et la direction qu'il devrait occuper. Ces informations permettent la commande des servomécanismes de la tourelle et la poursuite automatique de l'avion.
- 3.4 L'ensemble de traitement des informations est composé d'un calculateur, qui assure le calcul en temps réel de la trajectoire du réflecteur monté sur l'avion, et en assure l'édition, sous forme de courbes, de tableaux de chiffres et d'une bande magnétique.

Les paramètres ci-après sont enregistrés sur la bande magnétique au format 0,5 pouce, 9 pistes, 800 b.p.i :

- . temps en seconde et 0,1 seconde
- . coordonnées X,Y,Z lissées ou brutes
- . vitesses lissées VX,VY,VZ
- . tops de synchronisation
- . éventuellement site, gisement, écarts en site et en gisement.
- 3.5 Des équipements de visualisation des résultats composés en particulier d'un traceur de courbe imprimante et d'un tableau de chiffres, permettent à l'ingénieur d'essai de diriger et de surveiller le déroulement de l'essai.
- 3.6 Un pupître ou se tient l'opérateur, rassemble les moyens de commande et de contrôle contenus dans la salle d'opérations du bâtiment. Ce pupître permet notamment les commandes de l'émetteur laser et de la tourelle en poursuite automatique ou manuelle. En outre, un système de télévision comprenant une caméra installée sur l'arbre en site de la tourelle et d'un moniteur de télévision situé sur le pupître d'exploitation, permet de visualiser l'objectif afin de faciliter l'acquisition et le contrôle

de la poursuite.

#### 4. CERTIFICATION DES PERFORMANCES AU DECOLLAGE DE L'AVION MERCURE 100

Les essais ont été exécutés en Novembre 1973 à BRETIGNY en équipage mixte OFFICIELS/ CONSTRUCTEURS.

#### But des Essais et Paragraphes Concernés de la Réglementation FAR 25

Le but des essais a été l'établissement des performances de l'avion au décollage, du lâcher des freins au passage à 35 pieds, avec ou sans panne moteur.

Les résultats de ces essais doivent satisfaire aux paragraphes suivants de la réglementation américaine FAR 25 : 25-105, 25-107, 25-111, 25-113 amendement 23.

#### Mesures et Enregistrements

L'avion a été équipé d'une installation anémométrique de série permettant l'enregistrement des paramètres suivants.

#### 4.2.1 Paramètres Avion

- . pression statique
- . pression totale
- . température totale
- . incidence

#### 4.2.2 Restitution de la poussée

La poussée a été déterminée à partir de l'enregistrement des paramètres suivants :

- . vitesse de rotation HP
- . vitesse de rotation BP
- . température du carburant
- . débit volumétrique instantané de carburant
- . pression totale primaire plan 7
- . pression totale fan plan 7

#### 4.2.3 Calcul de l'Assiette Longitudinale

L'assiette a été restituée à partir des informations provenant d'un des équipements suivants :

- . centrale à inertie SAGEM
- . gyroscope d'assiette longitudinale
- . laser, par la fourniture de la pente que l'on associe à l'incidence enregistrée par ailleurs

#### 4.2.4 Paramètres Délivrés par la Centrale à Inertie SAGEM

- . assiette longitudinale
- . assiette latérale
- . cap géographique
- . composantes de la vitesse sol VX, VY, VZ
- . composantes de la position de l'avion X, Y, Z

#### 4.2.5 Restitution de la Trajectoire de décollage.

- . On a utilisé le laser, moyen le plus rapide et le plus précis, chaque fois que cela était possible.
- . Mais dans le cas d'un mauvais fonctionnement de la station STRADA, la reconstitution de la trajectoire de l'avion a pu être effectuée à partir de l'ensemble centrale à inertie - radio sonde.
- . Les cinéthéodolites, ont été mis en oeuvre systématiquement, à titre de précaution, pendant toute cette tranche d'essais qui correspondait en fait au début de l'utilisation opérationnelle de la station STRADA. Ils pouvaient donc servir en cas de pannes du laser ou de la centrale à inertie.

#### 4.2.5.1 Utilisation du Laser

Le système STRADA permet l'obtention directe de la trajectoire du réflecteur laser, qui a été monté pour tous ces vols destinés à la restitution du décollage, sur le dixième hublot du côté droit de l'avion (fg n $^\circ$  3)

En utilisant l'assiette longitudinale, on a corrigé la trajectoire du réflecteur laser pour en déterminer celle du centre de gravité de l'avion. La hauteur de l'avion par rapport à la piste, est obtenue en retranchant de l'altitude du centre de gravité de l'avion l'altitude du point de la piste correspondant.

#### 4.2.5.2 Utilisation de l'Ensemble Centrale à Inertie SAGEM et de la Radio Sonde

Cet ensemble a été utilisé avec profit, pour restituer la trajectoire, dans le cas d'un mauvais fonctionnement de la station STRADA ou d'une interruption momentanée de la poursuite automatique du laser.

Au préalable, le constructeur DASSAULT-BREGUET, s'est assuré de la qualité des informations issues de la radio sonde et de la centrale à inertie par comparaison avec les informations laser.

. Pour la radio sonde il a été déterminé fg n° 10 les écarts altitude laser/altitude radio sonde, en fonction de la distance X de l'avion à l'extrêmité ouest de la piste de BRETIGNY qui correspond à l'origine zéro des distances pour les décollages monomoteur et bimoteur. Les résultats permettent de constater que l'erreur maximale ne dépasse pas + 1 mètre, quand on restitue la hauteur à partir de la radio sonde, et ceci sur toute la longueur de la piste.

- De la même façon, il a été comparé, pour la centrale à inertie SAGEM la distance X, délivrée par la centrale à inertie avec le même X donné par le laser STRADA.Les résultats des écarts X CENTRALE A INERTIE/ X STRADA sont présentés sur la figure n° 11 On peut constater que l'écart de distance, dû principalement à une synchronisation imparfaite des moyens de mesure, reste tolérable et ne dépasse pas 10 mètres à l'extrêmité de la piste.

#### 4.2.5.3 Utilisation des Cinéthéodolites

L'exploitation classique des films cinéthéodolites pour la restitution de quelques trajectoires au décollage a été prévue en cas de pannes du laser ou de la centrale à inertie. L'inconvénient majeur de cette méthode, est la durée de dépouillement des images cinéthéodolites ainsi qu'une synchronisation médiocre avec les autres moyens de mesures.

A cet effet, il a été effectué à titre de contrôle, au cours de 3 vols, la comparaison des distances et des altitudes d'un même point de l'avion, déterminé, soit à partir des cinéthéodolites soit de la station STRADA.

Les écarts en X qui apparaissent sont essentiellement dus aux erreurs de synchronisation. (fg.  $n^{\circ}$  12)

#### 4.2.6 Détermination de V LOF

Cette vitesse a été obtenue à partir de l'enregistrement des vitesse de roue

#### 4.2.7 Détermination de la Vitesse du Vent

La vitesse du vent a été calculée aisément à partir des projections horizontales des vitesses aérodynamique et laser.

#### 4.3 Résultats

#### 4.3.1 Généralités

La présentation détaillée des résultats des performances de l'avion MERCURE 100 au décollage sort du cadre de notre exposé. Aussi, il ne sera présenté, à titre d'information, que quelques résultats jugés significatifs en insistant sur les deux avantages fondamentaux présentés par la station laser STRADA pour la détermination des trajectoires:

- possibilité pour l'ingénieur d'essai responsable, de suivre, en temps réel, le déroulement de l'essai avec jugement immédiat de la qualité de la trajectoire obtenue.
- rentabilité de l'essai, par la faculté de décider, quasi instantanément, de la reprise d'un essai en cas de nécessité.

#### 4.3.2 Historique des Essais

7 vols concernant les essais de décollage normaux, avec et sans panne moteur, ont été exécutés entre le 7 et le 9 Novembre 1973. Ces vols ont été suivis, le 20 Novembre par 4 autres, comprenant des décollages au cours desquels on a effectué des écarts à partir des procédures normales d'utilisation, pour démontrer que de tels décollages, ne conduisent ni à des situations dangereuses, ni à une augmentation de la longueur de piste nécessaire.

#### 4.3.3. Calcul des Performances

Les performances de décollage sont obtenues par le calcul à partir de la simulation des décollages effectués.

#### 4.3.3.1 Données Nécessaires aux Calculs

Ces calculs ont nécessité un certain nombre de données :

- la modélisation mathématique et aérodynamique simulant les conditions du décollage effectué
- la poussée minimale installée déterminée à partir des abaques de PRATT AND WHITHNEY en utilisant les paramètres moteurs enregistrés
- la loi de pilotage moyenne, qui tient compte de l'évolution de la poussée et de la loi d'assiette.
- . La variation de l'EPR pendant l'établissement de la poussée est donnée sur la figure n° 13 Il est admis qu'au moment de la panne, à V1, la poussée devient instantanément nulle.
  - . L'assiette au cours du roulement est en moyenne de 0,2 degré.
- . La prise d'assiette, à l'instant du décollage, est différente selon qu'on décolle avec un ou deux moteurs. Les différentes prises d'assiette pour les décollages, considérés par les services officiels comme le maximum acceptable pour une procédure normale, sont représentés sur la figure numéro 14 . Dans les deux cas de décollage monomoteur et bimoteur, la croissance de l'assiette est limitée pour que le facteur de charge longitudinal ne dépasse pas 1,2 g.
- . La loi de rentrée du train, représentée par sur la figure n° 15 est fonction de la vitesse de l'avion. Le début de rentrée s'effectue 3 secondes après V LOF.

#### 4.3.3.2 Comparaison des Résultats de Calcul et des Evolutions en Vol

Pour tous les vols ont été tracés les évolutions comparées des paramètres du vol avec ceux de la simulation.

L'ensemble des résultats, qui ne sera pas commenté dans ce rapport, a montré que le recoupement est bon et que la méthode de simulation choisie est conservative. La figure n° 16 montrant l'évolution comparée, des paramètres de vol et de simulation, a été reproduite à titre d'exemple. Les instants caractéristiques du décollage y sont représentés :

- le lächer des freins LDF
- la vitesse de rotation VR correspondant au début du mouvement à cabrer de la profondeur.
- la vitesse d'envol V LOF correspond à la cassure de la courbe d'enregistrement des vitesses de roue
- la rentrée du train, intervalle de temps s'écoulant entre les instants d'ouverture et de fermeture des trappes.

Les notations suivantes ont été utilisées par le constructeur DASSAULT - BREGUET

#### Paramètres de vol mesurés par le laser

- vitesse sol en m/s : V DAEL
- hauteur en mètres : Z DAEL
- distance longitudinale parcourue, l'origine étant l'extrêmité ouest de la piste, en mètres : X DAEL
- assiette longitudinale (déterminée à partir de l'incidence et de la pente déduite des mesures laser) en degrés : TETEL
- assiette longitudinale gyroscopique : TETEV

#### Paramètres de vol obtenus à partir des enregistrements et des abaques

- poussée du moteur droit FPW DEL en daN
- poussée du moteur gauche FPW GEL en daN

#### Paramètres de simulation et de calculs

- poussée du moteur droit FRE 1 AR en daN
- poussée du moteur gauche FRE 2 AR en daN
- assiette de l'avion en degrès : ASSAR
- vitesse par rapport au sol en m/s : VISAR
- hauteur en mètres : HAUAR
- distance parcourue en mètres : DISAR

Sur la figure n° 16 , les paramètres tracés en trait continu sont les paramètres d'essais en vol, alors que les paramètres tracés point par point, sont ceux calculés par la simulation.

#### 4.3.4 Longueur de Décollage

- La longueur de décollage d'après la FAR 25, 25-111 d, est la distance parcourue par le centre de gravité depuis le lâcher des freins jusqu'à ce que ce point se soit élevé de 35 ft.
- Avec les données nécessaires aux calculs, précisées en 4.3.3, a été déterminé le mouvement du centre de gravité, en négligeant, au cours du roulement, le déjaugeage du train. Par contre, il a été tenu compte de l'allégement pendant le décollage. Sur les figure n° 17 et n° 18 ont été représentées l'évolution de la hauteur pour divers points de l'avion, soit au cours d'un décollage monomoteur, soit au cours d'un décollage bimoteur.
- La figure n° 19 présente l'évolution de la longueur de piste nécessaire en fonction de la vitesse de panne d'un moteur pour une masse au lâcher des freins de 54 tonnes et dans les conditions z=0, ISA +  $14^{\circ}C$ .
- La figure n° 20 représente l'évolution de la loi d'assiette au cours d'un décollage réalisé avec écart de procédure. L'essai correspond à une rotation exagérée de l'avion et à une VR trop faible de 8 KTS. En se ramenant aux conditions de référence Z = 0, ISA + 14°C et à la masse maximale de 54 tonnes, cet écart de procédure a conduit à une distance de décollage (1755 mètres) inférieure à la distance normale (1875 mètres), pour une vitesse à la fin du premier segment pratiquement égale à la vitesse V2 nominale.
- 5. CERTIFICATION DE L'ATTERRISSAGE AUTOMATIQUE CATEGORIE IIIA DE L'AVION CONCORDE

#### 5.1 Généralités - Programme d'essais

Le programme défini par le constructeur SNIAS en accord avec les Services Officiels franco-britanniques comporte l'ensemble des essais nécessaires à l'obtention de la certification de l'atterrissage automatique catégorie 3A. Ces essais incluent un certain nombre d'approches et d'atterrissages qui ont été effectués au titre de la certification catégorie 2.

Ce programme d'essais définit deux parties distinctes :

- la première intitulée NAVIGABILITE précise les essais qui permettent de démontrer les performances du système. Les conditions suivantes y sont précisées : piste utilisée, force et direction du vent, utilisation du pilote automatique en place pilote ou copilote.

Son exécution réussie permet l'obtention de la certification de l'atterrissage automatique à l'exclusion des conditions météorologiques catégorie 3A et des turbulences thermiques. Le programme précise en outre l'obligation de restituer toutes les trajectoires d'approche et d'atterrissage.

- la deuxième partie de ces essais doit permettre, par la démonstration du fonctionnement en conditions réelles catégorie 3A, par turbulence thermique, ou sans installation d'essai à bord de l'avion (mais avec restitution de la trajectoire) d'obtenir la certification de l'atterrissage automatique en conditions météorologiques catégorie 3A et en turbulence thermique.

Seuls les essais correspondant à la première partie ont été réalisés à la date de rédaction de cet exposé. Un quart environ des approches et atterrissages prévus dans le programme d'essais général, s'est déroulé à BRETIGNY où la station laser STRADA a systématiquement été utilisée pour la restitution de la trajectoire.

Avant de décrire de façon plus détaillée les paramètres permettant de juger les performances en catégorie 3A, nous donnerons une brève description du système d'atterrissage automatique de l'avion CONCORDE et rappelerons les définitions de visibilité correspondantes aux catégories 2 et 3A évoquées dans cette présentation.

- 5.2 Description Sommaire du Système d'Atterrissage Automatique
- 5.2.1 Principes de Conception du Système

Le système a été conçu de façon à satisfaire à la fois les niveaux de sécurité et de disponibilité requis par la réglementation de l'avion de transport supersonique TSS 1.2 et TSS 9.2.1.

#### 5.2.2 Description du Système

Le système se compose essentiellement de deux ensembles indépendants, de pilotes automatiques et d'automanettes, autosurveillées, associés à deux centrales anémométriques. La procédure d'utilisation mise au point, demande l'action directe du pilote, par une suite logique de sélection des modes du pilote automatique, et une surveillance des indications ou alarmes, permettant la poursuite ou l'interruption de l'atterrissage.

A une altitude d'approche (1500 à 2000 pieds) et après avoir testé les diverses alarmes et l'indicateur d'écarts excessifs, le pilote enclanche la fonction de maintien d'altitude (ALTITUDE HOLD). Ensuite, il sélectionne un cap d'interception, par rapport au QFU, et conserve le cap par le mode maintien de route (TRACK HEADING). Le pilote affiche alors sur l'automanette, la vitesse d'interception, et engage l'automanette en acquisition de vitesse (I A S ACQUIRE). Le pilote présélectionne enfin les modes de capture des faisceaux directionnels longitudinal (GLIDE), latéral (VOR - LOC), et le mode d'atterrissage (LAND) par action directe sur le bouton poussoir LAND.La suite de l'atterrissage s'effectue automatiquement. Le pilote automatique efface le mode maintien de cap et active la fonction capture localizer, puis efface le mode maintien d'altitude et active la fonction capture glide.L'avion commence à descendre vers la piste le pilote affiche sur l'automanette la vitesse d'approche fonction de la masse, V référence, qui permet de maintenir, pratiquement constante, l'assiette longitudinale malgré le changement de trajectoire. Quand les captures sont effectuées, le pilote automatique passe en mode atterrissage (LAND) après avoir testé le mode arrondi. Le pilote est informé d'un éventuel écart excessif par rapport aux faisceaux directionnels, et l'allumage des voyants, au dessous de 200 pieds, doit entraîner de la part du pilote une action directe : soit l'enclanchement sur le pilote automatique du mode remise des gaz (GO AROUND), soit une reprise en main. Si l'atterrissage n'a pas été interrompu, la fonction arrondi (FLARE) est activée au dessous de Z = 50 pieds, puis à 15 pieds l'automanette réduit progressivement la poussée. Quand le toucher des roues du train principal a été réalisé, le pilote reprend l'avion en main, pose le train avant, freine et guide l'avion sur la piste,soit à vue, soit au moyen de l'indicateur du directeur de roulage au sol.

#### 5.2.3 Définition des Conditions Minimales de Visibilité.

#### Pour l'atterrissage automatique catégorie 2

- . Plafond : 100 pieds
- . Portée visuelle de piste : 400 mètres
- . Hauteur de décision : 100 pieds

#### Pour l'atterrissage automatique catégorie 3

- . Hauteur minimale d'interruption d'approche : 10 pieds
- . Portée visuelle de piste : 150 m
- . Hauteur de décision : supérieure ou égale à 10 pieds (la 2e partie des essais évoquée ci-dessus en 5.1 n'a pas été exécutée à la date de rédaction de cet exposé. Les résultats de cette prochaine tranche d'essais doivent fixer la valeur de cette hauteur).

#### 5.2.4 Historique des Essais

60 atterrissages de performances, nécessitant la restitution de la trajectoire avion ont été exécutés depuis le dernier trimestre 1975 en équipage constructeurs ou équipage mixte constructeurs/services officiels. Respectant les conditions du programme d'essais, l'intensité du vent imposé a bien été comprise entre - 5 kts (vent arrière) et 10 kts. Le réflecteur laser a été monté au bas du train avant (fg n° 9). Toutes les trajectoires d'approche et d'atterrissage exécutées à BRETIGNY (13 au total) ont été réalisées avec la station laser STRADA. Toutes les autres trajectoires ont été effectuées à TOULOUSE, et restituées à partir de cinéthéodolites qui ont filmé, en particulier, une mire située au sommet de la dérive de l'avion.

#### 5.2.5 Installation d'Essais à Bord de l'Avion

Les principaux paramètres suivants, nécessaires pour qualifier l'atterrissage automatique ont été enregistrés à bord de l'avion :

- . Assiette longitudinale TETA
- . Assiette transversale PHI
- . Cap géographique PSI
- . Angle de dérapage
- . Angle d'incidence
- . Vitesse Vc
- . Ecart glide GLID
- . Ecart localizer LOC
- . Altitude radio sonde TRT1

Un certain nombre de signaux permettant de restituer entièrement les diverses phases de l'approche et de l'atterrissage avec les alarmes éventuelles.

#### 5.2.6 Résultats

#### 5.2.6.1 Simulation des Trajectoires et Validation de la Simulation

Nous ne développerons pas cette partie qui sort largement du cadre de notre exposé. Soulignons toutefois que le constructeur a eu en permanence le souci de valider sa simulation et de la rendre conforme aux résultats des vols d'essais.

En particulier, le traitement combiné des paramètres délivrés par l'installation d'essais de l'avion et ceux en provenance des systèmes au sol (STRADA ou cinéthéodolites) lui ont permis de restituer le vent et les turbulences sur les 3 axes.

Pour valider la simulation, trois niveaux de validation ont été utilisés :

- un premier niveau, par recalages successifs des coefficients aérodynamiques dans tout le domaine de vol et en tenant compte de l'effet de sol.
- un deuxième niveau de validation de la simulation, par utilisation en simulation des vents réels obtenus au cours des atterrissages réels.
- un troisième niveau de validation de la simulation a été obtenu, en comparant statistiquement, les résultats de simulation avec les résultats obtenus en vol.

#### 5.2.6.2 Résultats des Essais en Vol

A titre d'exemple, nous présentons les figures  $n^\circ$  21 et  $n^\circ$  22 caractérisant une approche automatique, effectuée à Brétigny, et qui comporte, des paramètres fournis par l'installation de bord et par la station laser STRADA.

De telles planches permettent l'analyse, des performances des approches et atterrissages automatiques, selon schéma suivant :

#### Performances jusqu'à 100 pieds

La performance de maintien de l'axe (LOC et GLIDE) est déterminée par l'écart des faisceaux aux altitudes radioaltimètre de 500, 200 et 100 pieds respectivement.

#### Présentation au seuil de piste

Le paramètre qui caractérise la performance au seuil de piste est la hauteur de passage des roues ZG. L'inconvénient est d'être tributaire de la courbure des faisceaux Afin d'obtenir des résultats comparables d'une piste à l'autre, on fait un recalage qui amène le faisceau glide à passer à 50 pieds au seuil piste.

#### Impact

Les paramètres caractéristiques de la performance à l'impact sont :

- . le point d'impact défini par sa distance longitudinale au seuil de piste et son écart latéral par rapport à l'axe de la piste
- . la vitesse verticale au toucher des roues
- . la vitesse latérale de l'impact
- . le temps d'arrondi entre 50 pieds et l'impact.

<u>Tableau résumé des résultats d'atterrissage automatique des 60 atterrissages de performances.</u>

Paramètre	Moyennes et écarts type	Résultats
ZG pieds	moyenne	32,7
	écart type	3,7
Distance longitudinale d'impact (m)	moyenne	527
	écart type	78
Ecart latéral à l'impact (m)	moyenne	0,7
	écart type	2,6
Vitesse verticale à l'impact pieds/sec	moyenne	- 1,9
	écart type	0,9
Vitesse latérale à l'impact m/s	moyenne	0,1
	écart type	0,5
Temps d'arrondi (sec)	moyenne	7,9
	écart type	1,1

#### 6. CONCLUSIONS

Le système STRADA de trajectographie par laser, s'est avéré, au cours de ces essais de certification d'avions civils comme un moyen d'essai efficace et sûr.

Son avantage essentiel, est la possibilité offerte à l'ingénieur d'essais, de contrôler en permanence l'éxécution de la trajectoire effectuée par l'avion, et d'intervenir immédiatement pour poursuivre, ou modifier le cas échéant, le programme initial.

Il est évident, qu'un tel moyen d'essai, comparé au système classique de trajectographie par cinéthéodolites, permet, en plus d'une meilleure précision et des facilités de synchronisation des moyens en mesure, de réaliser un gain de temps, substantiel, pour l'obtention des résultats.

Insistons à nouveau sur les vols de MERCURE pour constater que 11 vols réussis ont été effectués en 3 jours ouvrables seulement. Cette forte cadence n'aurait jamais pu être soutenue si la trajectographie avait été restituée par des moyens internes ou par cinéthéodolites.

#### REFERENCES

- RAPPORT AGARD CP 198 FLIGHT SIMULATION/GUIDANCE SYSTEMS SIMULATION.
- RAPPORT AGARD CP 160 TAKE-OFF AND LANDING.
- RAPPORT AGARD-AG-195 EVALUATION OF THE POTENTIAL BENEFIT TO THE AERONAUTICAL FIELD FROM LASER TECHNOLOGY.
- T.S.S. CONCORDE D.E.V. SNIAS RAPPORT D'ESSAIS EN VOL DE CERTIFICATION ATTERRISSAGE AUTOMATIQUE CATEGORIE 3 A DE JUILLET 1976.
- MERCURE D.E.V. AVIONS MARCEL DASSAULT BREGUET AVIATION.
  RAPPORT D'ESSAIS EN VOL DE CERTIFICATION CONCERNANT LES METHODES ET MOYENS DE CALCUL DES PERFORMANCES ET LES DISTANCES DE DECOLLAGE DECEMBRE 1973 ET MARS 1974.
- SYSTEME STRADA NOTICE DE SYNTHESE SERVICE DES EQUIPEMENTS DE CHAMPS DE TIR.
- STRADA PANNEAUX RETROREFLECTEURS POUR TRAJECTOGRAPHIE PAR LASER U 9100 CENTRE D'ESSAIS EN VOL DE BRETIGNY.

#### PANNEAU RETROREFLECTEUR Divers exemples de montage FIGURES n° 1 à 9

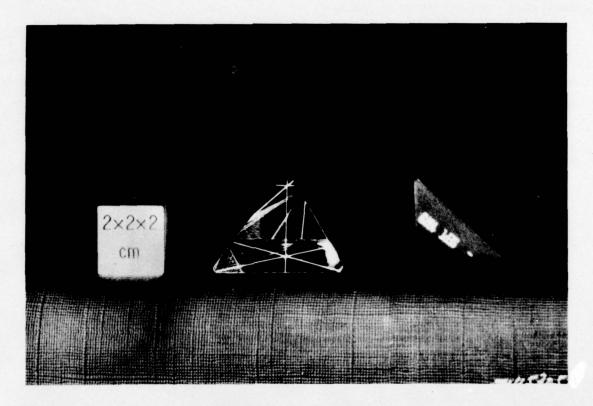


Fig.1 Trièdres de silice montés sur le panneau

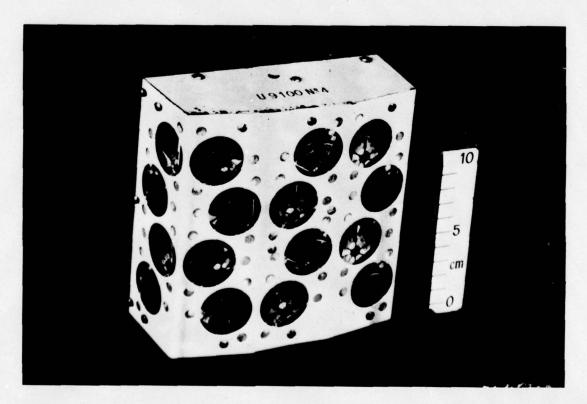


Fig. 2 Panneau rétroréflecteur - vue de 3/4 avant

#### DIFFERENTES TYPES DE MONTAGE DE PANNEAUX

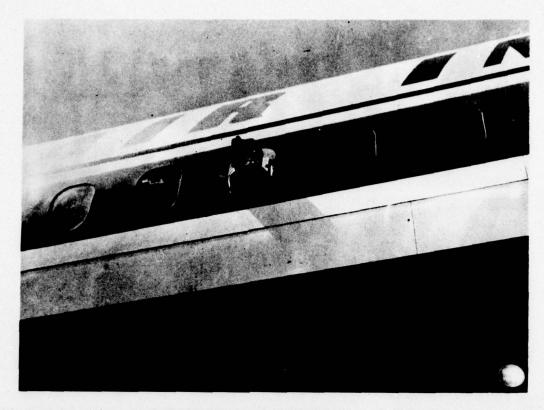


Fig.3 Montage sur hublot: MERCURE



Fig.4 Montage sur la dérive: MERCURE



Fig.5 Montage sous le bord d'attaque de l'aile MYSTERE 20

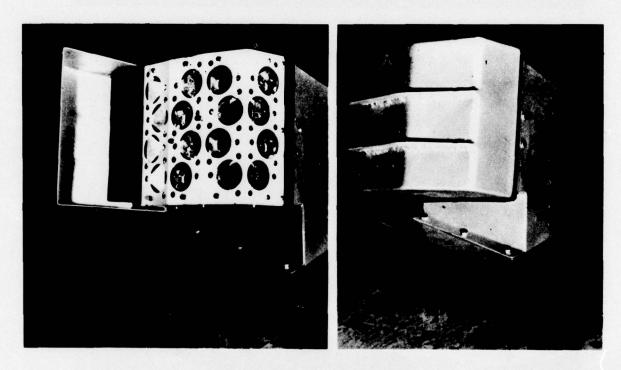


Fig.6 Sur le MYSTERE 20, vue du panneau

En éloignement, panneau protégé par un capot protecteur, dans ce cas fermé

En approche, capot ouvert



Fig.7 Montage tête bêche des panneaux MERCURE

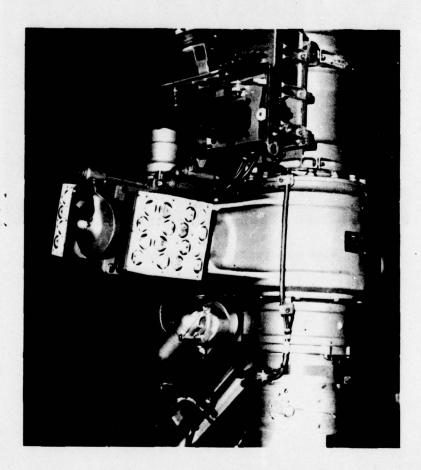


Fig.8 Même type de montage sur CONCORDE

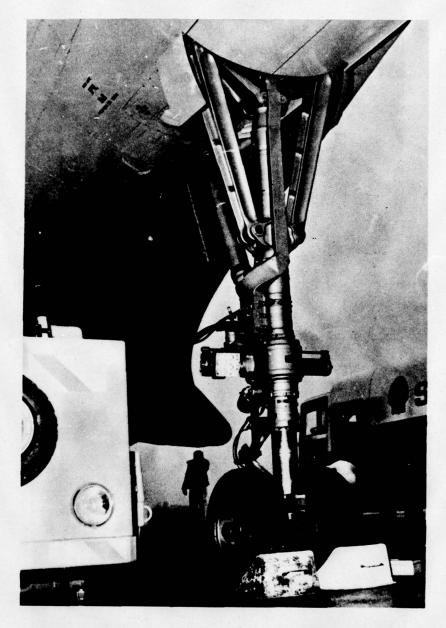
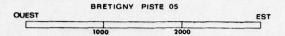
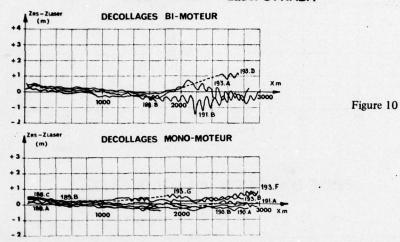


Fig.9 Montage sur la jambe de train d'atterrissage CONCORDE

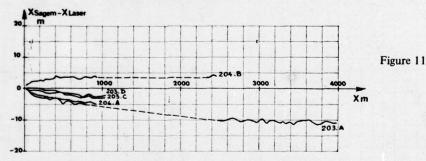
## MERCURE 02 PERFORMANCES AU DECOLLAGE



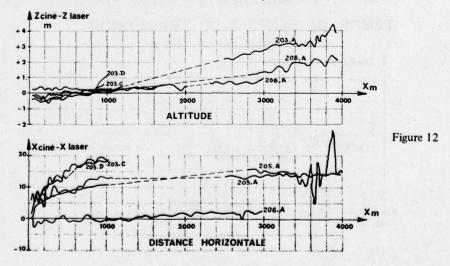
## ECARTS Z<sub>Radio</sub> Sonde /Z<sub>Laser</sub> STRADA



ECARTS Z Centrale à inertie /Z Laser STRADA



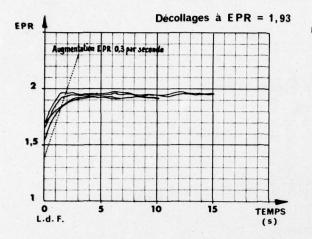
### COMPARAISON CINETHEODOLITES/LASER STRADA



## **MERCURE 02**

#### ETABLISSEMENT DE LA POUSSEE

EVOLUTION DE L'E.P.R. EN FONCTION DU TEMPS



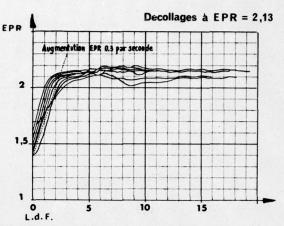
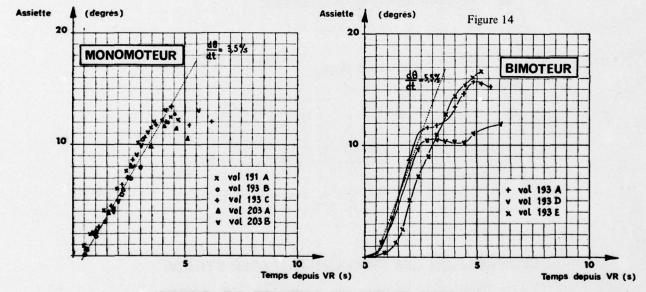


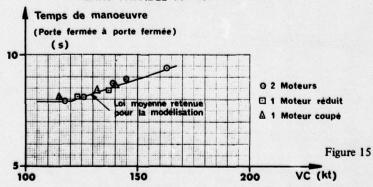
#### Figure 13

#### PRISE D'ASSIETTE AU DECOLLAGE

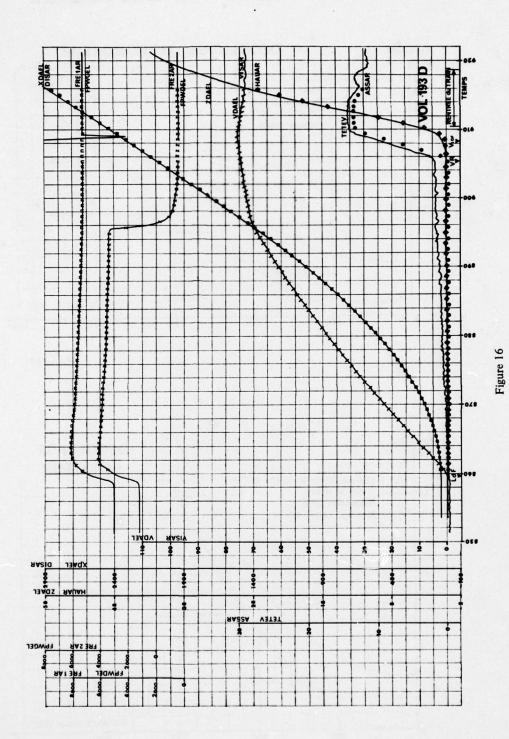


#### TEMPS DE RENTREE DU TRAIN DROIT

VERIN CAPABLE de VLOF = 200 kt-



MERCURE 02
PERFORMANCES AU DECOLLAGE



# MERCURE 02 PERFORMANCES AU DECOLLAGE

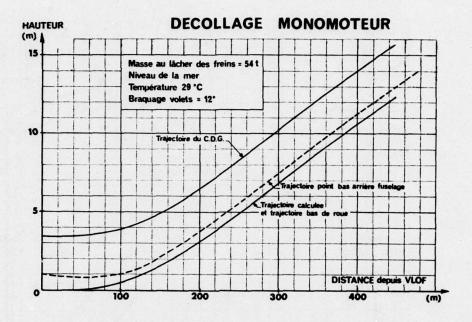


Figure 17

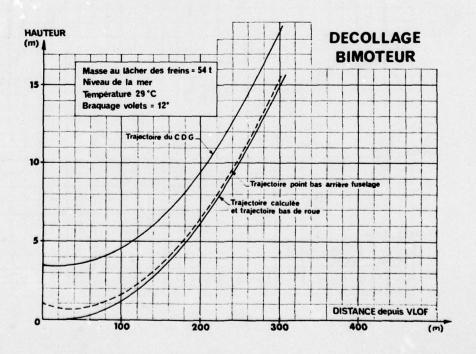


Figure 18

## **MERCURE 02**

#### LONGUEUR DE DECOLLAGE FAR 25

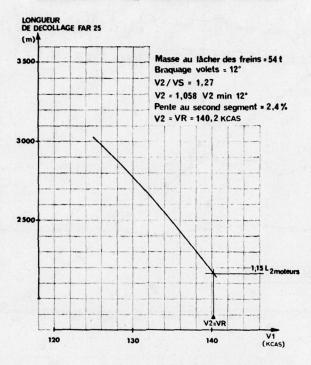


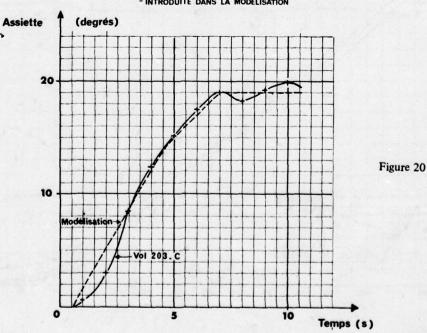
Figure 19

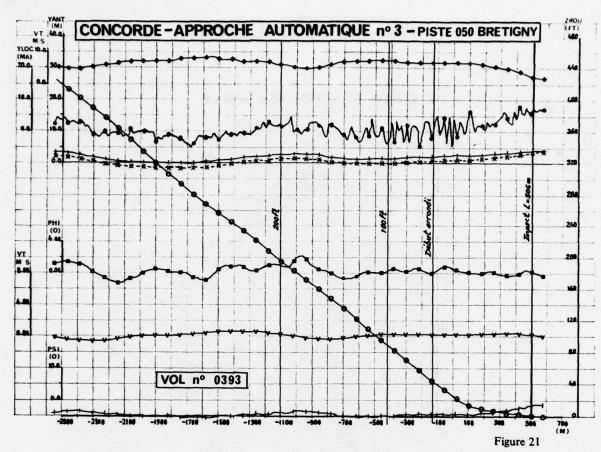
#### DECOLLAGES AVEC ECART DE PROCEDURE

CAS DU VOL 203 C : VR - 8 M ET ROTATION EXAGEREE DE L'AVION COMPARAISON DES LOIS D'ASSIETTE :

- REALISEE EN VOL

- INTRODUITE DANS LA MODELISATION





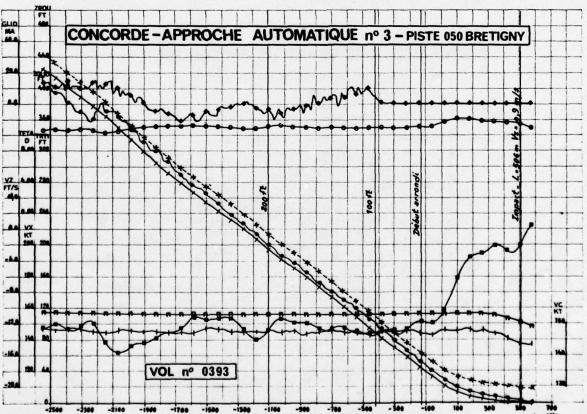


Figure 22

#### TELEMETRY AND DATA RELAY FOR MANNED SPACE PROGRAMS

by

Mr. Kim W. Anson
Aerospace Technologist
National Aeronautics and Space Administration
Lyndon B. Johnson Space Center
Code CF3
Houston, Texas 77058
U.S.A.

#### I. SUMMARY

Previously and currently planned methods of transferring or relaying telemetered information from a remote receiving station to the Mission Control Center, at the National Aeronautics and Space Administration Lyndon B. Johnson Space Center, are discussed in this paper. The data flow techniques of the Apollo Program (fixed formats), the Skylab Program (data compression), and the Space Shuttle Program (data throughput) are defined and analyzed according to their advantages and deficiencies from an operations viewpoint. Excluded from the data flow technique discussions are command data, tracking data, television data, and Teletype and Datafax messages. Voice transmissions are addressed in the Space Shuttle Program discussion because they form a part of the telemetry data stream. The trade-offs between actual data flow requirements and existing communications limitations are addressed for each of these programs. Finally, a short discussion of current problem areas in the planned ground data transmission system for the Space Shuttle Program is presented.

#### II. ACRONYMS AND ABBREVIATIONS

ACRONYMS	AND ABBREVIATIONS
ABS	absolute value
ALT	approach and landing test, Space Shuttle Program
AM	airlock module, part of the Skylab spacecraft
ATM	Apollo telescope mount, part of the Skylab spacecraft
bps	bits per second
CSM	command and service module, Apollo and Skylab spacecraft
DFI	developmental flight instrumentation, Orbiter telemetry
GSFC	NASA Goddard Space Flight Center, Greenbelt, Maryland
JSC	NASA Lyndon B. Johnson Space Center, Houston, Texas
kbps	kilobits per second
KSC	NASA John F. Kennedy Space Center, Kennedy Space Center, Florida
LM	lunar module, Apollo spacecraft
Mbps	megabits per second
MCC	Mission Control Center, at JSC
MSFN	Manned Space Flight Network
OD	operational downlink, Orbiter telemetry
OFT	Orbital Flight Test, Space Shuttle Program
Orbiter	Space Shuttle Orbiter
POCC	Payload Operations Control Center
RF	radiofrequency
SCA	Shuttle Carrier Aircraft
STDN	Spaceflight Tracking and Data Network, formerly MSFN
TDRSS	Tracking and Data Relay Satellite System, part of STDN

#### III. PREVIOUS DATA FLOW TECHNIQUES

A. Apollo Program - Telemetry data retrieval from ground stations of the Manned Space Flight Network (MSFN) was vital to the successful execution of each Apollo mission. In addition to routine monitoring of spacecraft systems, Flight Controllers in the Mission Control Center (MCC) utilized vehicle telemetry to interpret the seriousness of anomalous conditions and to precisely follow the astronauts' activities with a minimum of time-consuming conversation. It was not mandatory to retrieve all significant samples of all measurements during the mission but, rather, to retrieve a cross section of the available measurements which provided flight controllers with sufficient information to perform their monitoring and control functions. Detailed engineering and scientific analyses of mission performance were conducted after a mission ended; that is, after the ground-station wideband tapes, which contained all the raw telemetry data, had been shipped to a data reduction complex located at the NASA Lyndon B. Johnson Space Center (JSC). Apollo telemetry was composed of independent radiofrequency (RF) data links from the command and service module (CSM) and the lunar module (LM). The Saturn launch vehicle, which boosted the CSM and LM into Earth orbit, provided two additional real-time data links during its short lifetime. One link was active for only the initial portion of the ascent phase. The other was active for several hours after orbit insertion. The MSFN ground stations could not simultaneously track the LM and the Saturn launch vehicle instrument unit, since both vehicles used the same transmission carrier frequency. However, the LM was not activated until after the instrument unit batteries were depleted. Consequently, the ground stations were configured to support either the CSM and instrument unit or the CSM and LM.

All telemetry consisted of digitized analog and bilevel measurements in a serial output, which was available from each vehicle both as live data and as an accelerated-rate playback of onboard recorded data. The amount of telemetry increased with each new series of missions, as greater emphasis was placed on the return of meaningful scientific data. However, the total capacity of the data transmission circuits available for each mission was always less than the size of the combined data link telemetry. With the exception of a few hours at the beginning and end of each mission, the CSM spacecraft was in semicontinuous acquisition and the LM was in constant acquisition over one, two, or three MSFN stations. The in-flight telemetry data retrieval requirements were satisfied by applying the technique of fixed format telemetry transmission and by taking advantage of this simultaneous MSFN acquisition coverage.

A telemetry format was defined as a subset of the total number of measurements available in a data link. These telemetry subsets were called fixed formats since inflight measurement substitutions were not allowed. Some fixed formats contained selected measurements from more than one vehicle or data link. It became evident that one standard format could not contain enough measurements at the required sample rates to adequately satisfy the spacecraft systems monitoring task while at the same time containing all of the required experiment systems and scientific telemetry data. The solution was to define a set of standard formats, each of which was designed to provide a large number of system and experiment measurements at low sample rates, and to define a set of special-purpose formats which contained a limited number of high-sample-rate measurements for precise monitoring of critical spacecraft functions. The biomedical special-purpose format was built by collecting every other measurement sample. At the MCC, this format was input to a third-order-polynomial digital-to-analog converter which reconstructed the smooth waveform of the original heartbeat signal.

The size of these fixed formats was constrained to 2400 information bits such that any ground station could output one standard format on one 2400-bps-capacity data circuit and one special-purpose format on another 2400-bps-capacity data circuit. At first, two 2400-bps circuits were used. Then, near the middle of the Apollo Program, two 4800-bps circuits were used for fixed format transmission. This expansion enabled the simultaneous output of two standard formats on one circuit and one special-purpose format on the other circuit. Near the end of this program, when the Skylab Program data flow requirements were known, NASA decided to increase the single-circuit capacity to 7200 bps (necessary for Skylab data flow) but to retain both the 2400-bit fixed format size and the limit of two standard formats and one special-purpose format already established for Apollo data flow. The additional 2400 bits of circuit capacity were not used during the Apollo Program.

An exception to the 2400-bit fixed format limitation was the direct routing of launch vehicle telemetry data from the NASA John F. Kennedy Space Center (KSC) Apollo launch data system to the MCC. A 40 800-bps data circuit was used for this direct interface and, each second, one 40 800-bit fixed format (the only source of launch vehicle data) was output on this circuit. This format also contained CSM and LM telemetry and provided a redundant source of telemetry during the critical launch-through-ascent phase of each Apollo mission.

In a typical configuration (Fig. 21-1), one ground station could simultaneously output one standard format with CSM and LM spacecraft system measurements, another standard format with CSM and LM onboard computer measurements, and one special-purpose format with astronaut biomedical measurements. Other standard fixed formats contained specific system parameters (the attitude control system, for example) of just one spacecraft and were selected when several stations were in simultaneous view of both spacecraft. A nominal ground-station fixed format output sequence was developed for each flight to satisfy the phase-dependent monitoring requirements, which were implicitly determined by the astronaut flight plan. A choice of alternate formats was identified

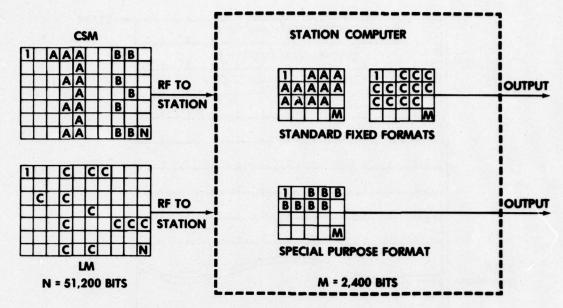


Figure 21-1.- Apollo fixed-format technique.

for critical mission phases, events, or unexpected system anomalies. This nominal format selection plan also required the output of more than three telemetry formats when overlapping coverage was provided by the ground-station network.

The MCC was designed to accept various combinations of the standard formats from as many as three stations simultaneously. There was an understandable constraint that the same measurement could not be input to the MCC telemetry computer as a real-time parameter from more than one station at a time, because a processing ambiguity would have resulted. This situation was avoided by identifying the illegal format combinations and procedurally selecting only the valid format combinations. Only one special-purpose format could be input to the MCC from one station at any one time. This limitation forced the Flight Controllers to accept a format priority plan, in which only the highest priority special-purpose format was selected during an Apollo acquisition period.

An additional ground-station capability was that of recording all live and dump data received during acquisition and of replaying selected data intervals in fixed formats during a postpass interval, as long as the playback was completed before the next acquisition period of that station. This capability provided an excellent means of viewing real-time telemetry data in a high-priority telemetry format during acquisition, then replaying it in a secondary format possibly desired during acquisition but not allowable because of the measurement-overlap prohibition or the unavailability of another ground station. This capability was especially advantageous for the special-purpose telemetry formats because of the single-input limitation. A playback of data in a special-purpose format, if required, necessitated the interruption of any other currently selected special-purpose format. It was also possible to schedule a playback from one station, either of real-time data or of delayed-time data which had previously been recorded onboard, to occur at the same time real-time data were being received from the current acquisition station. In this situation, the MCC telemetry computer was partitioned such that two identical combinations of standard telemetry formats could be dynamically and asynchronously processed without ambiguity. This capability to play back CSM dump data enabled Flight Controllers to monitor vehicle system performance measurements for all periods when the CSM passed behind the Moon and out of direct view from Earth. This knowledge was used as a guide in maximizing the attainment of mission goals without exceeding the capabilities of the CSM or depleting its performance

A block data scheme was chosen to facilitate complete visibility into, and to maintain both quality control and data destination control over, the data transmission system. The ground-station telemetry computer would load all required measurement samples for the currently selected fixed formats into output buffers. Each buffer received only measurements for one fixed format. When a buffer was full, a block of fixed format data had been collected. Header and trailer information were added to this block, and the combination (containing exactly 2400 information bits) was output serially as one entity, starting with the header (Fig. 21-2). The header contained information such as block destination, data type, vehicle identification, time of block generation, and a station identifier. The trailer contained a sequential block number, a block parity bit, and the polynomial error protection code that was applied to the data to provide a data transfer error detection capability at the destination. The block output rate on the data circuits initially was 1 block/sec, or 2400 bps; then, 2 blocks/sec, or 4800 bps; and, finally, 3 blocks/sec, or 7200 bps, to match the available circuits.

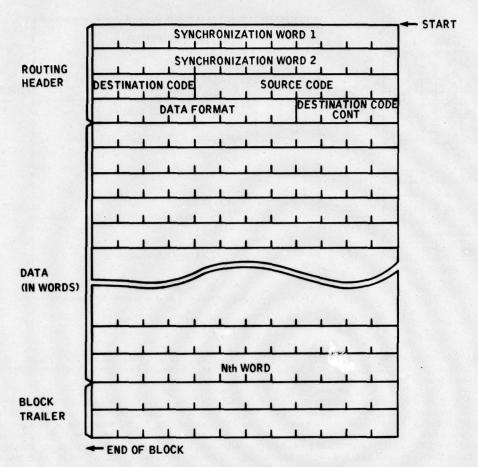


Figure 21-2.- Typical block data format structure.

A message switching center had been established at the NASA Goddard Space Flight Center (GSFC), located at Greenbelt, Maryland, which controlled the communications interfaces between the MSFN and the MCC. The GSFC-to-MCC data interface was initially a 40 800-bps-capacity data circuit, which later was replaced by a 50 000-bps-capacity circuit. Both allowed for simultaneous output to the MCC of data from several stations. In each case, a backup data circuit of identical size was available to allow transfer of mandatory telemetry to the MCC if the primary circuit had failed. A GSFC communications processor identified the destination of all incoming telemetry data blocks and routed blocks for the MCC accordingly. Thus, GSFC was effectively transparent to the MSFN/MCC telemetry flow while providing a necessary network control service. If the MCC detected an abnormal block statistic (for example, a skipped block number), an error message was generated. Thus, it was an easy task to determine whether the data transmission system was functioning properly and, if not, to know the probable cause of the data flow interruption.

The block data scheme was not limited to transfer of fixed format telemetry data. Other data generated by the ground stations, such as spacecraft tracking data, received radiofrequency signal statistics, and uplink command receipt messages, were also digitized, buffered, and output to the MCC in identically sized block formats. By use of a common destination code, each block was routed to the MCC, and, by use of a unique datatype code, each block was then routed to the telemetry, command, or tracking data processor as required.

The capability to transfer a small number of measurements to the MCC in analog format also existed during the Apollo Program but was seldom used. The ground station would convert all samples of the required measurement to analog form and output the resultant analog signal on an analog data circuit. This technique effectually bypassed the normal digital data processing system, was time consuming to set up, but did provide all available samples for precise monitoring of some measurements.

B. Skylab Program - A primary goal of the Skylab Program was the collection and in-flight processing of empirical data generated by experiments in several scientific disciplines. The basic telemetry requirement was for the MCC to collect all significant measurement samples on a routine basis from the ground-based stations of the Spaceflight Tracking and Data Network (STDN). Skylab telemetry was composed of independent data links from the CSM, the airlock module (AM), and the Apollo telescope mount (ATM). The two Saturn launch vehicle real-time data links used in the Apollo Program were also available during the early phases of Skylab missions. Of the four data links (CSM, AM, ATM, instrument unit) available during these phases, the STDN ground stations could

receive any three. This constraint prompted the development of a data link priority table which specified a phase-dependent station configuration for receiving the three highest priority data links.

All telemetry consisted of digitized analog and bilevel measurements in a serial output that was available from each vehicle both as live data and as a playback of onboard recorded data. The importance of the onboard recorded data, which were dumped later during an acquisition period, should not be overlooked. The geographic location of the ground stations had been limited to lie within the latitude extremes of the lunar subsatellite point (Fig. 21-3). Consequently, the high inclination of the Skylab orbit caused many long nonacquisition periods, during which the vehicle systems recorder and experiment recorders collected valuable information. If the astronauts or the real-time telemetry indicated that a problem had developed, the dump data became singularly important in the analysis and resolution of the anomaly. Long before the first Skylab mission began, it was determined that the Apollo data flow technique would not meet the basic Skylab data collection requirement. Also, it was known that the Skylab downlink telemetry would exceed the data circuit bandwidth of the three 7200-bps-capacity circuits planned for Skylab usage. To correct this deficiency, the technique of data compression and the concepts of data link priority, measurement (or parameter) priority, and processing level were adopted.

Each telemetry measurement was given a priority according to its relative importance and acceptable retrieval delays. Thus, a priority 4 measurement would never be input to the ground-station telemetry computer for in-flight transmission to the MCC; instead, it was stored on a wideband analog recorder at the ground station and retained for later shipment after completion of that particular Skylab mission. Priority 3 measurements were primarily experiment-oriented information. Although in-flight processing was necessary, these measurements were stored on a digital data recorder at the ground station (after data compression processing), then transmitted to the MCC soon after the end of each Skylab acquisition period. Priority 1 and 2 measurements were important enough for spacecraft or experiment control that they were mandatory for output during all Skylab acquisition periods.

The data compression technique enabled the network tracking stations to filter all nonsignificant telemetered measurement samples and to output only significant samples to the MCC. The algorithm used for data compression is expressed mathematically in Eq. (21-1).

ABS 
$$\begin{vmatrix} X & -X \\ t & t+1 \end{vmatrix} \le K$$
 (21-1)

The current value of a telemetered measurement X was assumed to be significant if t+1 its absolute difference from a reference value X exceeded the predefined tolerance K.

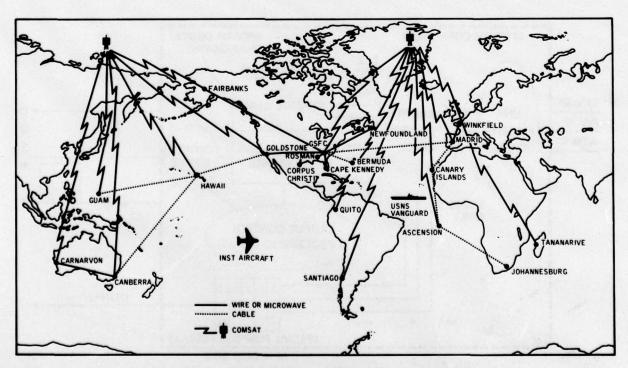


Figure 21-3.- Spaceflight Tracking and Data Network.

An initial measurement list of reference values contained the first-received sample of each measurement in the repeating data cycle. This initial measurement list was stored in the station telemetry computer and was also transferred to the MCC telemetry computer. When a measurement sample satisfied Eq. (21-1) for output, an appropriate identifier was also output with the measurement sample. The capability to reinitialize all reference values simultaneously and to change the tolerance on a measurement basis was necessary to overcome the possible instabilities of measurement sensors. The MCC reconstructed the significant telemetry downlink by retaining the most current value for processing until another significant sample was received from the network. The measurement identifiers provided sufficient information for the MCC telemetry computers to match the received samples to the correct processing logic. If no sample was received, the reference value was assumed to be the most current value.

During Skylab acquisition periods (Fig. 21-4), even after limiting transmission of telemetry to only priority 1 and 2 measurements, the total number of telemetered samples exceeded the available data circuit capacity (21 600 bps), and data compression was necessary. The effect of reducing the total number of measurement samples actually transmitted from the network to the MCC was achieved primarily through this data compression technique. However, when the Skylab astronauts performed simultaneous experiment operations in addition to normal spacecraft systems operations, the resultant increased telemetry activity nearly canceled the data compression effect. The effectiveness of this scheme was measured as the ratio of input-to-output bit rates, also called compression ratio. Typical compression ratios achieved were 20:1 during quiescent, inactive periods and were variable from 10:1 to approximately 18:1 during periods of high activity.

When the real-time output of significant measurement samples exceeded the data circuit bit-rate capacity, the ground-station telemetry computer sensed the overload condition and automatically attempted to reduce the number of output samples by sequentially selecting one of six predefined processing levels. Each level restricted the amount of telemetry actually output to a subset of that in the previous level. In level 0, all significant samples, determined by Eq. (21-1) with the tolerance set at a normal value, of all measurements were output from the ground station. Level 1 was identical to level 0 except that the tolerance in Eq. (21-1) was set at the maximum acceptable value for each measurement. In level 2, all priority 1 and 2 measurements were handled as in level 1; in addition, all priority 2 measurements were rate reduced to no more than 1 sample/sec/measurement. In level 3, all measurements were compressed with the maximum acceptable tolerance and were rate reduced to no more than 1 sample/sec. Level 4 was identical to level 3 except that all priority 2 measurements were inhibited from being output. If the telemetry activity required processing in levels 1 to 4 and then returned to a lower activity state, the telemetry computer would also return to the appropriate processing level. If level 5 was reached, a state of computer saturation had occurred and all telemetry output was completely interrupted. Recovery from processing level 5 required manual deselection of telemetry on an entire data link basis; that is, only the highest priority data link was allowed to enter the telemetry computer for output processing until the high-activity period had ended. Regardless of the amount of measurement activity, if a data circuit temporarily failed such that data

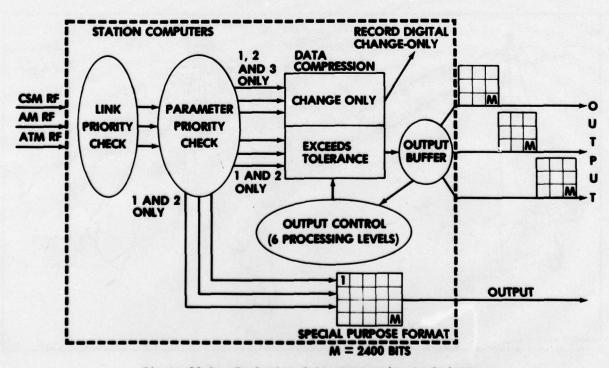


Figure 21-4.- Real-time data compression technique.

transmission on that circuit was inhibited, the ground-station computer would adjust the processing level to match the remaining circuit bit-rate capacity.

During the postpass data transmission periods (Fig. 21-5), the data compression tolerance was set to zero so that all samples of a measurement different from the reference value would be retrieved. All measurements with a priority of one, two, or three were eligible for this postpass change-only transmission, which caused a slight increase in the amount of data available for output. The output rate was limited to the data circuit capacity, so the postpass change-only transmission time was somewhat longer than the real-time pass; for example, up to twice as long for postpass transmission of real-time data. For dump data, the actual change-only transmission time was about half (worst case) of the total record time. For example, 40 minutes of AM dump data required as much as 18 minutes of change-only transmission time. These postpass playbacks of dump data often involved several short-duration transmissions, caused by short recording intervals on one hand and by dissimilar characteristics between the CSM, AM, and ATM recorders on the other hand. The CSM and ATM recorders always played back data in a forward, time-increasing direction, whereas the AM recorders output data in a reverse direction. Consequently, the AM dump data had to be transmitted separately from the CSM and ATM dump data.

The block data transmission scheme chosen for the Apollo ground system was modified for application to the Skylab ground system. Each telemetry data block was the same size (2400 information bits) as the standard Apollo fixed format data blocks. The block data output rate was 9 blocks/sec, or 21 600 bps. These were metered out in such a way that each data circuit received only 3 blocks/sec. The same capabilities for system visibility and control were retained, and were even more important since the goal was to maximize the amount of high-quality telemetry transferred to the MCC during the flight, rather than to wait for postflight tape shipment. The feature of transmission error detection and correction was added to enhance the probability of successful data transfer to the MCC. Approximately 13 percent of the information bits per data block were used as error correction parameters.

As in the Apollo Program, the network coordination and control function was assigned to the GSFC. The communications processor provided the necessary message switching capability for data blocks destined for the MCC. The expected data loading due to simultaneous input of data from several stations resulted in a requirement for two of the 50-kbps-capacity data circuits between the GSFC and the MCC. Experience gained during the Apollo Program indicated the reliability of these circuits was such that only one 50-kbps data circuit would be necessary for circuit redundancy.

It must be stated that the MCC utilized four separate computers to process incoming telemetry. One was dedicated to the dynamic processing of live telemetry transmitted during Skylab acquisition, such that Flight Controllers could monitor the current activities of the astronauts and the status of the spacecraft and experiment systems. The others performed all of the near-real-time data storage and processing, and generated reports upon request both for detailed spacecraft systems analysis and for in-flight scientific investigations.

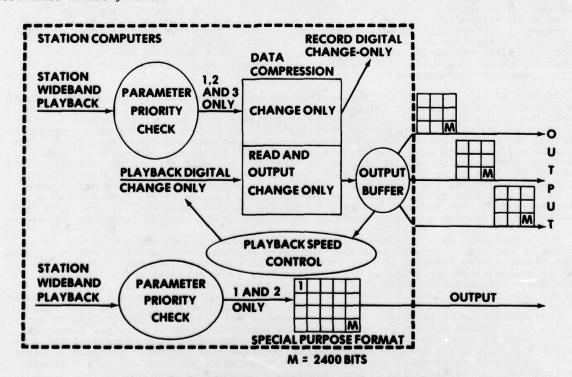


Figure 21-5 .- Postpass data compression technique.

Certain measurements provided high-sample-rate information, such as an astronaut's heartbeat waveform or the buildup of main engine thrust chamber internal pressure. The biomedical measurements were rate reduced by selecting every other sample for output similar to the Apollo Program technique. Since all samples of the vehicle systems measurements were occasionally required for correct problem analysis, and since the data compression technique did not guarantee output of all samples, a special-purpose format technique similar to that used in the Apollo Program was adopted, and a nominal format output sequence was determined before each mission. These formats, one at a time, were transmitted to the MCC on a separate data circuit than those used for the data compression output, and were formatted into block data formats similar to the compressed output blocks to simplify the means of transfer to the MCC. (See Figs. 21-4 and 21-5.)

The capability to transfer a small number of measurements to the MCC in analog format existed during the Skylab Program as in the Apollo Program. The ground station would convert all samples of the required measurements to analog form and output the resultant analog signal on an analog data circuit. This technique effectually bypassed the data compression processing system, was time consuming to set up, and was limited to only a few measurements. Several Skylab measurements were important enough to require a redundant measurement which could be downlinked in the event of a primary measurement sensor failure; but, since the data compression technique was designed only to handle the primary measurements, it was easier to set up this type of bypass than to modify the station computer programs. A special display in the MCC was available for monitoring these redundant measurements, since they were not a part of the standard data flow. The need for this analog transfer did occasionally arise during the Skylab Program.

C. Lessons Learned - The Apollo experience indicated that short-duration missions could be monitored extremely well without the in-flight availability of all samples of all measurements. Yet it was still necessary to occasionally obtain all samples for such mission events as a system anomaly or failure or during a mission-critical maneuver sequence. One conclusion is that the entire telemetry stream could not have been transmitted to the MCC during acquisition, even if the ground system designers had known from the start of the Apollo Program the full CSM and LM capabilities. The rationale for this statement lies in the fact that the data circuit transmission technology required to handle the full Apollo telemetry link was known at the start of the Apollo Program, but the prohibitive cost of providing several 50-kbps data circuits to each station in the ground network and maintaining them for the 5-year active duration of the program precluded the purchase of these circuits. As the cost of these circuits gradually decreased, the throughput transmission method again was addressed; but the immediate efforts to adapt the existing MSFN/MCC fixed format telemetry interface to the requirements of the next mission far outweighed the desire and the cost involved to completely redesign the ground system. A second conclusion is that the method of fixed format selection does indeed provide a most flexible capability to transmit those measurements of immediate interest to the Flight Controllers. However, it is limited to situations typical of the Apollo Program; that is, for flights having a large data link, a much smaller ground transmission capacity, and a fairly stable flight plan which does not require in-flight feedback from scientific data analysis. A third point concerns the operational impact caused by format selection limitations. The fixed format but one had to be delayed and played back later because of either limited station coverage or processing incompatibility between the two formats. Thus, the determination

Because of the length of the Skylab missions and the flexibility in onboard experiment scheduling, the astronaut flight plan was written during flight on a daily basis. Much of the returned scientific data had to be analyzed in a quick-look fashion so that any impact to the flight plan for the next day could be determined. The data compression technique for data retrieval satisfied this daily Skylab data analysis requirement. The technique was proven to have a definite advantage over the Apollo technique of format selection, especially in the Skylab mission, in which the emphasis was on scientific data return in addition to constant spacecraft systems monitoring. As in the latter flights of the Apollo Program, the technology existed for throughput of the entire Skylab telemetry stream from STDN ground stations to the MCC; but, because of its high initial cost of implementation, the decision was made to use the smaller, more readily available data circuits and to develop a data compression capability in the station telemetry computers.

Two significant data flow anomalies were encountered through the use of the data compression technique, and, fortunately, they were corrected by exercising certain ground system flexibilities inherent in this technique. In one case, the predicted standard level of Skylab telemetry activity was significantly lower than the actual in-flight conditions. The unexpected high activity, which turned out to be normal, caused near-constant processing in level 1 through level 4 and thus reduced the number of measurement samples of real-time data available at the MCC. Also, during the MCC process of reconstructing the telemetry link, the telemetry computer was frequently overloaded; consequently, it inhibited all but the mandatory data processing functions. This situation was alleviated by changing the priority of several measurements from priority 1 and 2 to priority 3 status, which enabled processing of the real-time telemetry normally in level 0 and occasionally in levels 1 and 2. The high measurement activity had only a slight effect on postpass transmission of the change-only measurement samples, but the large number of input measurement samples and the associated processing required overloaded

the MCC playback telemetry computer. This overloading was the primary cause of data retrieval and processing delays and of temporary data backlogging at the ground stations. A data playback priority scheme, which inhibited the simultaneous retrieval of certain telemetry links that required significant computer time for processing, was implemented to ease this problem. Because of the cyclic nature of the Skylab ground-track, a predictable backlog pattern developed such that, during periods of dense network coverage, a backlog was created; when the groundtrack again shifted to the area of sparse network coverage, the backlogged data were finally retrieved. However, the typical delay in retrieving backlogged data was approximately 8 hours, which enabled performance of sufficient quick-look processing for verification of experiment operations, with enough time remaining to modify the crew activity plan for the next day if necessary. The lesson to be learned was that more precise knowledge of the nominal telemetry activity level is required during the ground system design stage to preclude this problem.

The second problem was related to the separate processing of real-time telemetry in one MCC computer system and playback telemetry in another MCC computer system. Initially, the data products of the two computer systems were not identical. This inconsistency raised the question of the validity of all quick-look processing logic in the playback telemetry computer. The source of the problem was traced to the method of tagging each playback measurement sample with the proper time of occurrence, a function which was performed differently in each computer. This experience reinforced the need for total compatibility, from the flight vehicle to the control center data display devices, in the final ground system design. Once these problems were identified and resolved, the data flow and processing system performed well and demonstrated the capability of the data compression system to adequately satisfy all data retrieval requirements.

When the Skylab missions began, there was a sizable performance uncertainty in the data compression software routines at the MCC and STDN tracking stations. This uncertainty should not imply a lack of detailed verification and checkout testing of each component and of the whole data system. The actual testing was rather sophisticated. However, because of such factors as the high level of complexity of the compression technique, the unavailability of a realistic telemetry source or a high-fidelity data generator before the actual flight, and a very limited testing interval between system delivery and the first Skylab Program launch, there were several response characteristics of the whole system that were either untested or unknown at the start of the first mission. The two problems stated previously attest to this situation. It was because of the success-oriented problem-solving techniques employed by the ground system operators during the initial days of the first mission that the Skylab data compression technique withstood the test of critical mission support and became a viable data retrieval tool.

#### IV. SPACE SHUTTLE PROGRAM DATA FLOW TECHNIQUES

A. Approach and Landing Test Phase - Prior to actual orbital flight tests, the Space Shuttle Orbiter will be tested to demonstrate its capability to successfully approach and land at a preselected airfield. For these tests, the Orbiter will be carried to a specific altitude and downrange position by the Shuttle Carrier Aircraft (SCA), then released to simulate the gliding flight profile which will be characteristic of typical Orbiter atmospheric entry profiles. Since continuous communications coverage can be provided in the vicinity of the landing field, only one STDN ground station will be required. Digitized analog and bilevel measurements, as well as several raw analog measurements, will be transmitted in telemetry data links from the SCA and from the Orbiter. Because of the short duration of each approach and landing test (ALT) flight, there will be no dumps of onboard recorded telemetry data during flight. In the interest of reducing the number of ground system design changes, NASA has decided to use an identical data flow technique for each of the Space Shuttle Program phases. The chosen technique is that of data throughput. The rationale for that decision and a description of the throughput technique are stated in the Orbital Flight Test (OFT) phase paragraphs below. However, some ALT-unique configurations for data flow deserve further discussion here.

A block data scheme similar to that developed for the Apollo Program will be used to transfer telemetry from the ALT ground station to the MCC. The same block data size (2400 information bits) will be retained, and the block output rate will guarantee throughput of the entire 128-kbps Orbiter telemetry link plus 1 sample/sec of selected SCA measurements and station-generated measurements. To stay ahead of the Orbiter downlink bit rate and to allow the insertion of an extra block per second containing SCA and station status measurements, each block will be output at a rate equivalent to 168 kbps. The resultant output will be approximately 58 blocks/sec. The burst mode will be the method of block output. Thus, there will be a few milliseconds of dead space between each output block.

A point-to-point domestic satellite channel will be leased for telemetry flow from the ALT ground station to a satellite station in the vicinity of the MCC. A direct microwave RF link will provide the remaining data interface to the MCC. This routing bypasses the GSFC communications processing facilities and relieves the GSFC of the short-term, but quite large, ALT data routing task.

The capability of separately transmitting special digital fixed formats, or of stripping measurements from the digital downlinks for separate analog transmission, will not be necessary since all samples of all Orbiter digital measurements are output just as they are received. The SCA measurements will remain in digital form to facilitate output in the digital block data messages. For the case of the raw analog measurements, only a handful of these are required for in-flight monitoring at the MCC. They will be detected at the ground station and routed directly to the MCC on a standard analog data circuit independent of the satellite data link.

B. Orbital Flight Test Phase - The second phase of Space Shuttle Orbiter verification and demonstration testing will consist of six low Earth-orbit flights of as long as 7 days. The OFT data return requirements are to a great degree identical with those of the Apollo Program, and are based on the need to verify Orbiter performance of flight test objectives. The basic telemetry system will provide visibility into the Orbiter systems to enable Flight Controllers to accurately monitor the progress of each flight. All Orbiter operational downlink (OD) telemetry data are transmitted in a digital format. These real-time data will be simultaneously transmitted from the Orbiter together with playbacks of onboard recorded OD telemetry. All voice conversations between the astronauts and the MCC, whether live or recorded, will be digitized and multiplexed into the telemetry link before being downlinked. The combined downlink bit rate will be 192 kbps (real-time OD plus voice) and 5:1 or 8:1 multiples of that rate (recorder dumps). The current Orbiter communications systems delivery schedule indicates that a significant flow increase in the telemetry flow rate will be available on the fourth flight. This data flow increase is necessary to allow simultaneous transmission of the standard Orbiter telemetry links and a large amount of payload telemetry data.

The Orbiter will have an additional real-time data link known as developmental flight instrumentation (DFI) telemetry, which will be removed at the completion of the OFT phase of the Space Shuttle Program. The DFI telemetry contains both analog and digital measurements which supplement the OD telemetry but which are not mandatory for in-flight monitoring of the spacecraft. The digital DFI downlink bit rate will be 128 kbps (real time only) with no associated voice. Since the DFI measurements will only be used for postflight engineering analysis, they will not be electronically transferred to the MCC but will be recorded for later tape shipment.

The early OFT Spaceflight Tracking and Data Network will be composed of several Earth-based stations, each capable of supporting one spacecraft at a time. For low Earth-orbit flights, characteristic of the Orbiter flights, the ground stations provide approximately 17 percent coverage per day. The ground-station network is also planning to provide a major increase in data flow capacity, which currently coincides with the Orbiter telemetry modification schedule. The network modification involves deactivating most of these stations and replacing them with two Tracking and Data Relay Satellites at Earth-synchronous altitude. A benefit of the Tracking and Data Relay Satellite System (TDRSS) network is that only one ground station is required; thus, the data flow interface to the MCC is simplified. Each satellite will be capable of simultaneous communications relay with several spacecraft in addition to the Orbiter. The satellite network is expected to provide 30 to 85 percent orbital coverage for the typical Orbiter flights, depending on altitude, orbit inclination, and communications attitude (Fig. 21-6).

Several goals prompted the selection of the OFT data flow technique: to minimize the number of flight-to-flight ground-station modifications during the early OFT Orbiter flights; to develop a technique which could be directly applied to the simultaneous user concept of the satellite network; and to eliminate the built-in reliance on ground-station raw data tape shipment for accurate data transfer to each user's data center. The Apollo format selection technique was quite dependent on the composition of the CSM and LM telemetry data links, the contents of which were modified between each flight. The Skylab data compression technique had been tailored to handle only the telemetry link for the Skylab Program, and it was radically different from those techniques being used for all other STDN-supported spacecraft projects. Since neither of these methods would satisfy the OFT goals, NASA decided to adopt the technique of telemetry data throughput.

The telemetry data throughput technique can be applied to any digital telemetry link, and basically allows all samples of all measurements to be transferred to the correct destination during the time of data acquisition (Fig. 21-7). The ground-station telemetry computer will collect a predetermined number of telemetry information bits into an output buffer, which operates independent of the spacecraft telemetry link but requires that all telemetry to be throughput must be in a recognizable digital format. Recognizable, in this sense, applies only to characteristics of the data bits being transmitted and not to the intricate downlink structure or measurement channelization. The rather large logistics problem of providing all STDN stations with the latest vehicle-unique decommutation and telemetry preprocessing software programs will be eliminated in the throughput technique. The burden of measurement identification will rest upon the MCC, as will the task of synchronizing the basic Orbiter systems telemetry with the subcommutated but possibly asynchronous Orbiter flight computer telemetry.

When the buffer is full, the contents are automatically output to the data circuit as a serial bit stream, but inside an envelope of header and trailer information similar to the block data formats of previous programs. The rate at which these data blocks are output must be great enough to preclude an overload at the input to the buffer while handling the full telemetry bit rate. The size of the block data messages has been set

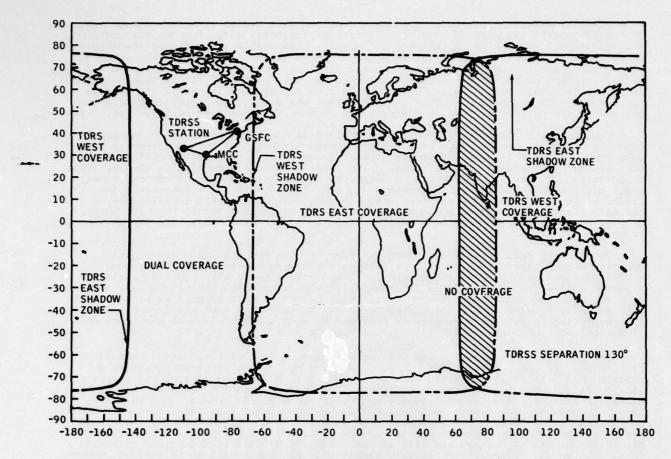


Figure 21-6.- TDRSS coverage at typical Orbiter altitude.

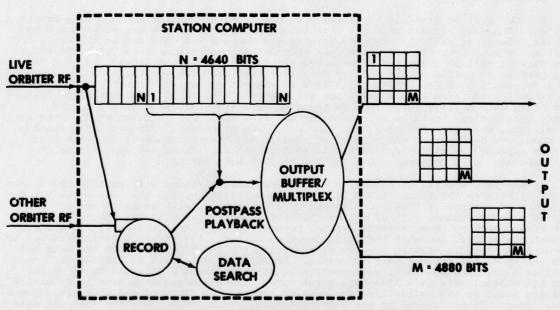


Figure 21-7.- Data throughput technique.

at 4800 information bits, or double the ALT block size. The block data burst output mode will also be retained, with the output rate per block approximating 168 kbps.

A limiting factor for this throughput technique is the total data circuit capacity, which must exceed the total downlink telemetry size. The data circuit capacity between the ground stations and the GSFC will be 168 kbps as in the ALT phase. This early OFT capability will be obtained by using three 56-kbps-capacity data circuits in parallel, rather than the single channel of the ALT satellite interface described previously. The

data circuits will be capable of handling the output data blocks at a fast enough rate to throughput the 128 kbps of Orbiter real-time OD telemetry data, but not the combination of digital voice plus OD telemetry. To solve this problem, the ground stations will be required to separate the digital voice from the 192-kbps link, convert the voice to analog form, and throughput the voice on separate analog voice circuits at the same time as the 128-kbps OD telemetry is being output on the data circuits. It is interesting to note that the real-time OD telemetry data rate from the Orbiter is nearly the same as the composite Skylab real-time data rate, and that the data transmission technology has matured to the point of full-link telemetry throughput as opposed to partial-link output.

The real-time telemetry does not completely fill the total available data circuit capacity. However, the 40-kbps excess circuit capacity will not be sufficient to allow throughput of the DFI telemetry or any onboard recorder dump telemetry received during acquisition. These data must be recorded for later electronic transfer to the MCC (tape shipment for DFI data). The dumped OD telemetry will be transmitted to the MCC immediately after an Orbiter pass, since those data are also mandatory for spacecraft inflight monitoring. The postpass dump playback must again be limited to telemetry on the data circuits and analog voice on separate voice circuits. Recall that the philosophy of postpass retrieval of dump data was also applied in the Apollo and Skylab Programs.

The primary data interface between the GSFC and the MCC will be a 1544-kbps-capacity single circuit, which will support data throughput from a maximum of four ground stations simultaneously for early OFT, and will support the larger data flow expected during later OFT. It is interesting to note that this GSFC-to-MCC data interface for only one OFT support station will be of the same order of magnitude as the bit rate actually handled during the Skylab Program simultaneously from six ground stations. A backup 224-kbps data circuit will be provided to enable restoration of mandatory data flow should the primary circuit fail during support.

For the later OFT flights, the Orbiter will communicate directly with ground stations during periods of prelaunch, ascent, and landing, and will communicate with a Tracking and Data Relay Satellite during all on-orbit periods and part of the ascent and landing flight phases. To enhance the probability of complete data relay by way of the satellite link, the Orbiter will employ a convolution encoding scheme. The telemetry rate is increased by a factor of three, but two-thirds of the total bits transmitted can be lost without affecting the amount of data output from the ground station convolution decoder. The satellite network and its ground station are known as the Tracking and Data Relay Satellite System, and will accept a variety of digital data links with data rates as high as 300 Mbps. The primary function of the TDRSS will be to receive, recognize, and throughput all detected telemetry information. Data storage at the TDRSS ground station will cover short-term problems associated with circuit outages or MCC data system faults.

The MCC will be directly connected with the TDRSS ground station for data transmission. The data circuit used for this interface will be a 1544-kbps-capacity data circuit, identical with the one used between the MCC and the GSFC during the early OFT flights. The GSFC-to-MCC 1544-kbps data service will be retained. A third 1544-kbps data circuit will be installed between the satellite ground station and the GSFC for the dual purpose of providing the primary data flow path for GSFC-controlled space vehicles and a secondary path for Orbiter data flow to the MCC by way of the GSFC. This three-way network path forms a data bus which will use the concept of port addressing, rather than block data message switching, to transfer data from the TDRSS ground station to the proper destination. Message switching, in use from the Apollo Program through the early OFT flights, was performed by a GSFC communications processor. Each incoming message was read, its destination was recognized, and it was then reformatted into the block pattern expected by processors at the final destination. Thus, any one termination point received only data messages required at that destination.

In the port addressing scheme, a multiplexer/demultiplexer will provide the direct interface between the TDRSS ground station, the destination, and the data circuit. The TDRSS ground station will output all data of a given type, such as real-time OD telemetry to a predetermined port of its multiplexer. Data types will be assigned to port addresses according to agreements reached between GSFC, which coordinates and controls network operations, and each participating data center. All demultiplexers attached to the data bus network will be capable of receiving any incoming data from the data bus when set up to the correct port addresses. Transfer of data will be handled with the familiar block data messages, each containing 4880 information bits and being output from the multiplexers at a 1544-kbps burst rate. The 80 information bits in excess of 4800 are added by the multiplexer for routing control and for data transfer error detection. They will be removed by the demultiplexers, which output only the 4800-bit data blocks to the destination processors. The MCC and a Payload Operations Control Center (POCC) at GSFC will be the only data destination centers during the OFT phase.

For the OFT flights, the total required data rate from the Orbiter does not exceed the 1544-kbps data bus limitation, although the Orbiter data system will be capable of a 50 000-kbps scientific data output. Payloads requiring such data rates will not be flown until the Orbiter is ready for mature operations flights.

C. Mature Operations Phase - The end of the OFT phase will mark the beginning of several years of continuous Space Shuttle operations. The unique characteristics of the

operations phase are the emphasis on scientific and technological return; the decreasing emphasis on vehicle testing and continuous monitoring; and the flight schedule, which will require as many as three Orbiters in flight simultaneously. The TDRSS, the data throughput technique, and the 1544-kbps data bus network established in the OFT phase will form the backbone for data flow in the initial years of Orbiter operations, when only one or two Orbiter flights will be concurrent.

The ground system is currently being designed to accommodate a future data capacity expansion from 1544 kbps to approximately 6300 kbps on the data bus network while requiring only a minimum number of engineering modifications. The actual need for this implementation is dependent on the future cost effectiveness of using the Earth-based data bus network or a point-to-point satellite channel. It also depends on when in the program the third Orbiter will be required and when the payload average data rate will exceed 1544 kbps on a regular basis.

A point-to-point domestic satellite channel interface between the TDRSS ground station and the MCC and any of several POCC's may eventually become the standard data flow path. Current ideas on this configuration imply that the actual data flow network will utilize elements of the domestic satellite system and the data bus network in parallel. However, the currently planned data bus network is expected to be sufficient at least for the first several years of Space Shuttle operations (OPS). Table 21-I shows a comparison of vehicle, MSFN/STDN station, and GSFC data output capabilities for the Apollo, Skylab, and Space Shuttle Programs.

TABLE 21-I.- REAL-TIME DATA RATE COMPARISON
[Values in kilobits per second]

Program		Data source	RF output	Station output	GSFC output
A P O L L		CSM	51.2	Fixed format blocks	Capacity
		LM	51.2	2 at 2.4 = 4.8	50 std.
		Launch vehicle	72	1 at 2.4 or 4.8	100 max.
		venicie	72	1 at 40.8 (launch)	
S K Y L		CSM	51.2	Compressed data blocks	Capacity
		AM	51.2	9 at 2.4 = 21.6	100 std.
		ATM	72	1 at 2.4 or 4.8	150 max.
A B		Launch vehicle	72 72		
SPACE SHUTTLE		Orbiter OD	128	Throughput data blocks	Not applicable
	L	SCA	144	∿57 at 2.4 = 128 OD	
				1 at 2.4 = 2.4 (SCA measurements)	
		Orbiter OD	128	Throughput data blocks	Capacity
	0	Air-to-ground (A/G) voice	64	~28 at 4.8 = 128 OD	1544 std.
	F	Orbiter DFI	128	To be determined (TBD) at 4.8 = TBD PL	224 backup
		Payload (PL) telemetry (TLM)	5000 max.		
		Orbiter OD	128	Throughput data blocks	Same as for OFT
	OP	A/G voice	64	√41 at 4.8 = 192 OD	
	S	Payload TLM	2000 max.	TBD at 4.8 = ∿1000 PL	
		Payload TLM	50 000 max.	TBD at TBD = 50 000 PL (via satellite)	

D. <u>Issues and Operations Constraints</u> - During the period in which material for this paper was obtained and compiled, most of the system design issues and problems had been resolved. The two remaining significant data flow issues are identified in the next two paragraphs. Also included are the significant operations constraints imposed by those issues already resolved.

The TDRSS is in the design stage and currently is planned to be operational for the fourth OFT flight. This system will not be owned by NASA, although it will be required to meet NASA specifications, and it will be a leased service. Consequently, until the TDRSS contractor is selected and begins detailed design reviews with NASA, many details of the TDRSS design and their impact on the MCC will not be available. The bit-rate change constraint described later will also be a major concern for TDRSS support, especially because of a design decision to record only the station output (1544 kbps) rather than the downlink input. The port address logic to be used for TDRSS output to the MCC is another area of concern. Since the GSFC-to-MCC port addressing scheme will be defined first (for early OFT), it is desired that the TDRSS-to-MCC scheme be identical to facilitate a simple changeover from early OFT station support to TDRSS station support. However, because the MCC is only one of several network users, an alternate scheme may be selected to better serve all participants even though a change to the MCC would be required.

A potential data handling problem exists for multimegabit payload telemetry down-links. The Orbiter can throughput 50 Mbps from a payload to the Tracking and Data Relay Satellite, which will be capable of relaying as many as 300 Mbps to its ground station. Subsequent point-to-point relay by way of domestic satellite seems to be the only feasible routing technique for these data links. The TDRSS ground station will not record this data link. A noisy satellite interface could compromise the payload data quality or quantity. A more important problem is that of data storage, since data input at these rates for more than a few minutes will saturate current state-of-the-art storage devices. The immediate necessity to resolve other Orbiter and TDRSS design issues, and to proceed toward detailed ALT and OFT data flow interface agreements, has temporarily superseded the active resolution of this data flow and storage issue.

The Orbiter will have the capability to output real-time OD telemetry and voice either at the 192-kbps rate described previously (called high bit rate) or at a 96-kbps rate (called low bit rate). Each occurrence of a bit-rate change will cause the ground station in acquisition to temporarily lose bit synchronization, which must be regained before data output to the MCC can resume. The agreed solution to this situation is a standard procedure of verbal coordination preceding all bit-rate changes, with the intent of minimizing the data flow interruption. An automatic method to enable detection of either rate would require the purchase of additional bit synchronizers. The cost of this equipment for the 12 ground stations supporting early OFT does not warrant this purchase.

The second constraint concerns the temporary failure of one or more of the 56-kbps data circuits during early OFT flights. A quick calculation reveals that, if one circuit fails, the remaining capacity is insufficient for 128 kbps OD throughput. Although different methods such as data truncation and fixed formats were considered, the approved concept will mean loss of data transfer capability to the MCC until the disabled circuit is again restored. The station will continue to record all current telemetry for later playback to the MCC. There is also the possibility of selecting the low-bit-rate OD telemetry if one circuit has failed, since only two circuits are required for low-bit-rate throughput. However, this selection reduces the amount of data downlinked and may not be acceptable under flight conditions. This situation will not exist for the GSFC-to-MCC and TDRSS-to-MCC interfaces because each will have a backup data path available.

The question of Orbiter dump data quality during early OFT flights raised another issue. Since most of the Orbiter flight time will be during nonacquisition periods, a majority of the downlinked telemetry will be from onboard recorder playbacks. However, these data will not be throughput but will be recorded for later playback. To provide an indication of dump quality during the initial receipt of the data, the ground stations will be able to recognize certain bit patterns in addition to the normal bit synchronization process. In the approved method, the station telemetry computer will be used to detect dump quality and generate statistics for transfer to the MCC. Fortunately, the existing computers will be capable of handling the real-time OD telemetry throughput processing while simultaneously performing this dump quality analysis.

The method of OD dump data retrieval (separating the data and voice prior to transmission from the station) had raised a concern over loss of information about the time of occurrence of the voice, since the telemetry contains the vehicle time measurement. A detailed study revealed that the maximum skew (delay between data transfer time and voice transfer time) will not exceed the stated correlation requirement. The MCC will detect the time measurement during station dump playbacks and will record the time with the voice to preserve the time-to-voice correlation. This is not a concern for dumps made through the TDRSS since they will be immediately throughput intact with no need for separating data from voice.

#### V. CONCLUDING REMARKS

The need for data transfer will not diminish as knowledge increases. The technique chosen for a particular project should, as a minimum, provide a faithful representation of the actual flight events. In each program described, a technique was selected to best match the vehicle and crew activity monitoring philosophy, the flight vehicle data characteristics, the current communications technology, and the allowable budget for ground system development, purchase, and maintenance.

## RESORS - A SYSTEM FOR ON-LINE, ON-BOARD DATA REDUCTION AND PERFORMANCE ANALYSIS DEVELOPED ESPECIALLY FOR E-3A FLIGHT TESTS

H. A. WILLIAMS BOEING AEROSPACE COMPANY SEATTLE, WASHINGTON

#### ABSTRACT

RESORS - (REport SORting Test Set) is a system of computer programs to analyze radar report data using an interactive graphics terminal. Developed for E-3A test flights, RESORS permits on-board, on-line engineering judgemental decisions in data reduction and analysis. With RESORS, complex multi-dimensioned data can be displayed and sorted in any pair of twenty or so dimensions assiting in immediate decisions affecting test conduct and control. Primary functions include a "quick look" at flight results, isolation of identifiable radar reports such as tracks, detection of radar anomalies and determination of false alarm rates. The program flexibility provides both detailed analysis capability, and a "big picture" overview of flight test data.

#### 1. DIMENSIONAL ANALYSIS

In what set of coordinates does a set of data display a smooth curve? The answer to the question segregates data from different sources. In the case of a new surveillance radar capable of generating hundreds of target reports per antenna revolution and six revolutions per minute, the data sorting problem is rather significant. Target reports come from a number of sources: flying airplanes, moving cars, ground clutter, thermal noise, and internal instabilities are the major sources (until such time as the maritime modification is implemented). The E-3A surveillance is supposed to detect flying airplanes and reject the rest. The task, therefore, is to sort through all the target reports and categorize the sources accurately enough to evaluate performance and identify and solve problems.

To size the task in numbers, a typical exercise sequence will last about thirty minutes with six scans per minute with an average of two hundred reports per scan to yield a total of thirty-six thousand target reports. Each target report must be individually examined to identify its source. Since there is no individual unique characteristic to identify a report as coming from one source or another (if there were, it would be incorporated into the radar), the reports must be examined in their relationship to one another, i.e., dimensional analysis.

Dimensional analysis is a powerful tool but traditionally very laborious. The large digital computer in combination with a fast display (cathode ray tube) and rapid means of operator input (light pen) provide the means by which a large volume of data can be dimensionally analyzed very quickly. The program is set up so that the operator (by use of an on-screen menu) can select the data he wants displayed in the particular dimensions he thinks are the most useful. The light pen is used to sort data into different bins by virtue of the inter-relationship of the points, one to another.

The predecessor to RESORS was RAPID, used on a large corporate computer. With RAPID, it was possible to sort through twenty minutes of radar reports in about two hours. If RAPID could be improved to the point where data could be sorted as fast or nearly as fast as it was generated, then such a data reduction system would be very useful in flight.

The primary usefulness is that with the ability to evaluate performance in real time, test plans can be changed to accommodate the outcome or progress of a test. Real time data analysis is also a very powerful educational aid. Since RESORS permits an operator to sort data based on obvious patterns (even to the uninitiated), the performance of the radar can be confirmed during and immediately following a demonstration.

Observers, particularly government officials, are usually very skeptical about what is seen on a situation display for fear that the display may have been somehow pre-recorded and pre-sorted. RESORS has proven to be very useful in developing the credibility of demonstrations to various otherwise uninitiated observers. For example, after observing a track and intercept on the situation display, one can go to RESORS and sort through all the reports and actually see paths that the two airplanes followed. The demonstration is made all the more credible because the observer, if he desires, can participate in the sorting by instructing or questioning the RESORS operator.

#### II. USE OF RESORS

To illustrate the use of RESORS, a series of photographs were taken of the RESORS display during a typical analysis of radar performance. Figure 1 is normally the first display format used. It shows all reports both radar (dots) and IFF (c's) on a geographical map background with range rings from the center of the map. The location of E3A would normally be shown by a special symbol, but is deleted in this series of charts to satisfy military classification requirements. Note the text around the periphery of the display map. The text is a combination of information and light pen menu.

With only three scans displayed, Figure 1 is very dense and difficult to interpret.

In Figure 2, the IFF reports have been deleted, leaving only radar reports. Six scans are now displayed and trails or tracks begin to be visible. Further examination requires a scale magnification. In Figure 3, a 100 by 100 nautical mile sector is displayed. The range scales are referenced to the original geographical center in Figure 1. Figure 3 displays 20 scans, and data trails are very obvious.

At this point in the analysis, the operator is ready to select a particular data trail for detail analysis. Figure 4 shows one data trail in asterisks. By use of the light pen, one data trail was selected and the asterisks indicate the particular points that have been selected. In Figure 5, the display has been cleared of all data except that data selected for detail analysis.

The operator now selects certain crossplots and Figure 6 shows a crossplot of range versus scan number (or time). Note how some reports follow a smooth curve and others do not. The reports along the smooth curve obviously have some common source and the reports away from the curve have some other source. Figure 7 illustrates another crossplot of azimuth relative to E3A versus time with the reports still falling along a smooth curve. Figure 8 is a crossplot of R dot, or radial component of target ground speed versus AZ-A or azimuth relative to E3A. The curve in this case is not quite so smooth, indicating that the R dot parameter is not quite so useful as a sorting parameter. After all identifiable tracks have been removed, the residue is displayed as reports versus scan number in Figure 9. The number of scans are very large in this example because only one track has been removed.

#### III. RESORS MECHANIZATION

RESORS was a piece of special instrumentation aboard the E3A System Integration Development test airplane and was, therefore, not in line with the total avionics system. RESORS was used primarily for radar analysis but in addition to radar data, RESORS used a few other inputs. The additional inputs were navigation data to first space stabilize then, as needed, to ground stabilize all radar and identification transponder reports. Since most airplanes of interest carry identification transponders, RESORS used inputs from the identification system. IRIG time is used to provide a standard time base.

Conceptually, RESORS requires three basic components - a display with light pen, a very large random access bulk storage and a central computer. In operation, all of the data is recorded in the bulk storage. The operator using the light pen then calls up for display whatever data he desires. The data can be selected based on whatever criteria the operator may choose. For example, only radar, or transponder data, or data between certain IRIG times may be displayed.

The objective, of course, is to sort data and sorting is accomplished by crossplotting. Once sorted, the sorted data is identified by "bin tags" which are written into the bulk storage along with the sorted data. The final result then is that all radar reports are each identified with a bin tag indicating, in the opinion of the operator, the most probable source of the report.

RESORS is configured so that the only information the operator can add to the reports in the bulk storage is bin tags. The data cannot be modified or changed in any other way. This restriction is very important and is carefully controlled because the results of RESORS analysis are used to measure contractual compliance.

The results of RESORS analysis are permanently preserved in different ways. There is an immediate hard copy used to make immediate records of particularly significant displays. This is very useful during a demonstration flight so that the visitor can be given an immediate copy of what he observed in flight. A document quality hard copy is also provided so that significant crossplots can be preserved in document form. The third form of permanent record is the line printer, where all reports can be listed by bin tag number.

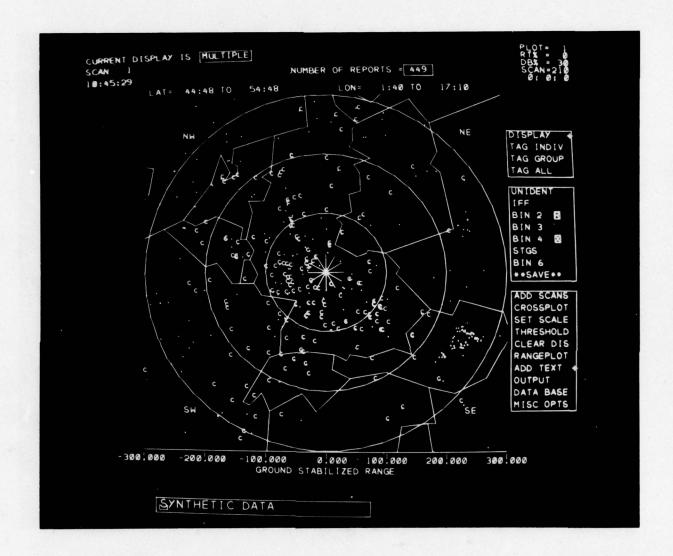
#### IV. RESORS HARDWARE

The display is a random location stroke write cathode ray oscilloscope with a pressure or touch sensitive light pen. The central computer was selected for its high speed and memory capacity. It has a two (2) microsecond add time and 184,000 bytes of memory with one (1.0) microsecond access time and 64,000 three tenths with (0.3) microsecond access time. The bulk storage is a 7,200,000 byte magnetic disc.

#### V. SUMMARY AND CONCLUSION

RESORS has proven to be a useful adjunct to the E3A complement of situation displays. By observing and analyzing radar data in dimensions and coordinates not normally associated with a situation display and by using more than some fixed number (say 5 or 10) of scans for analysis, it is possible to credibly identify the sources for essentially all radar reports in near real time. In addition, by data sorting, it is possible to individually record the activities and paths of targets of particular interest.

RESORS is also useful for analyses that require a combination of data sorting followed by bulk calculation. A particular instance is data sorting to select reports from a certain target followed by completion of detection range.



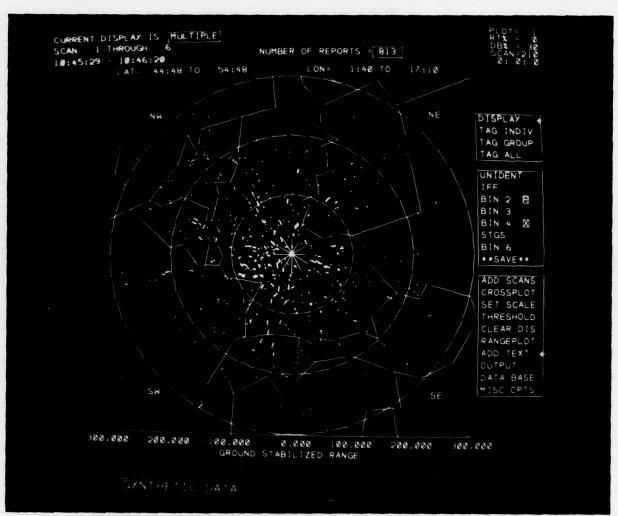


FIGURE 2

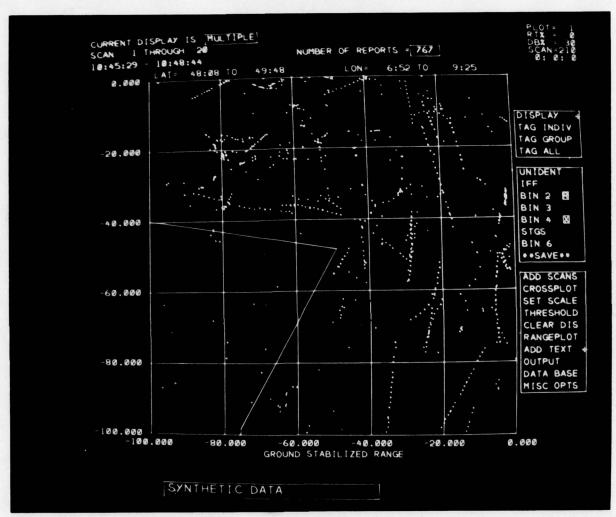


FIGURE 3

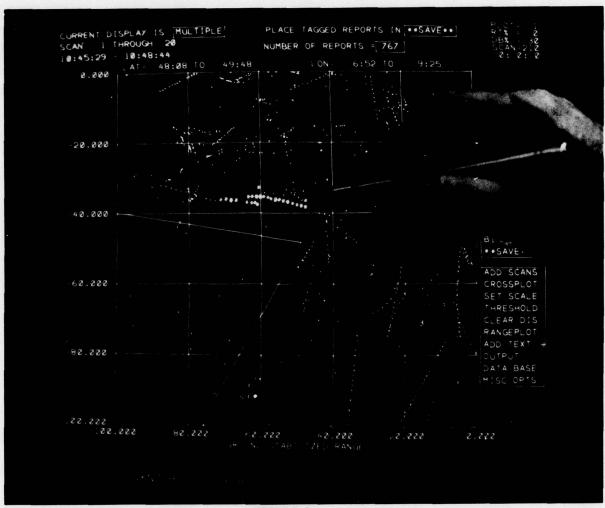


FIGURE 4

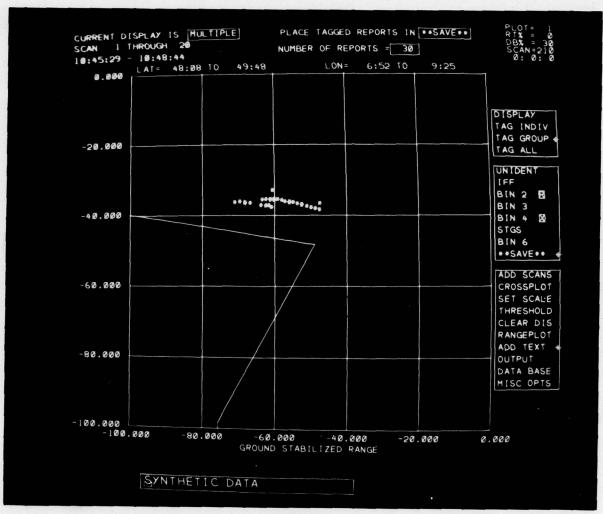


FIGURE 5

TOTAL TOTAL

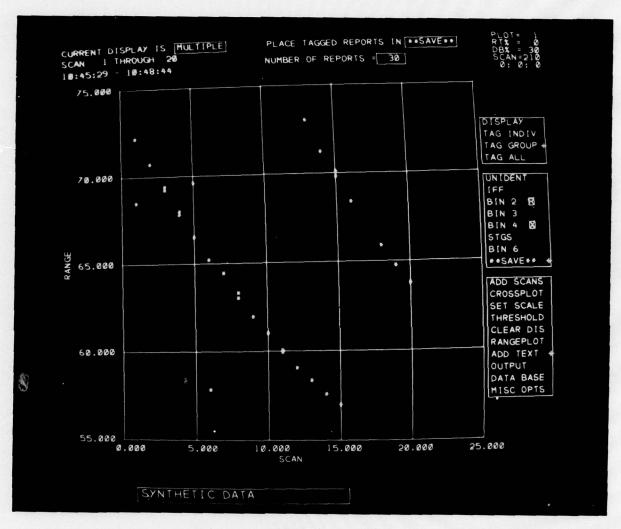


FIGURE 6

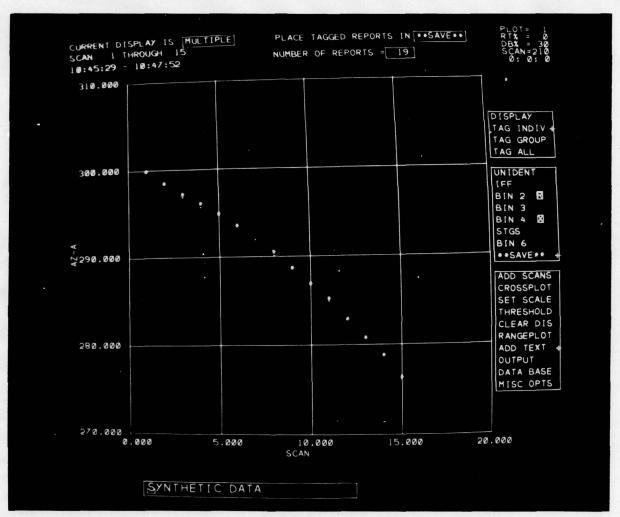


FIGURE 7

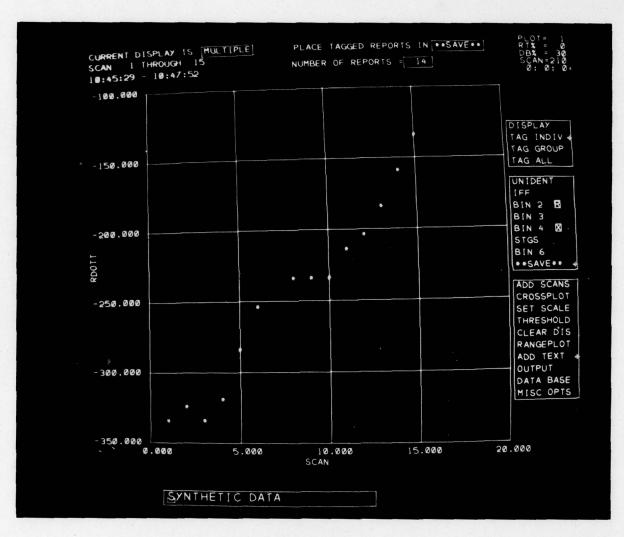


FIGURE 8

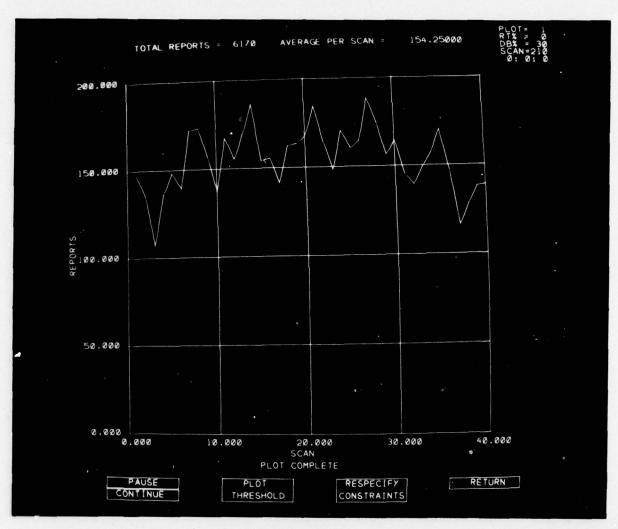
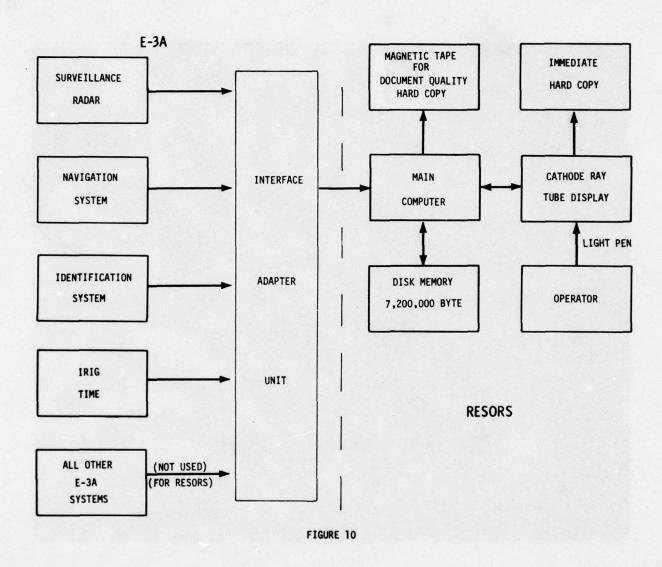


FIGURE 9



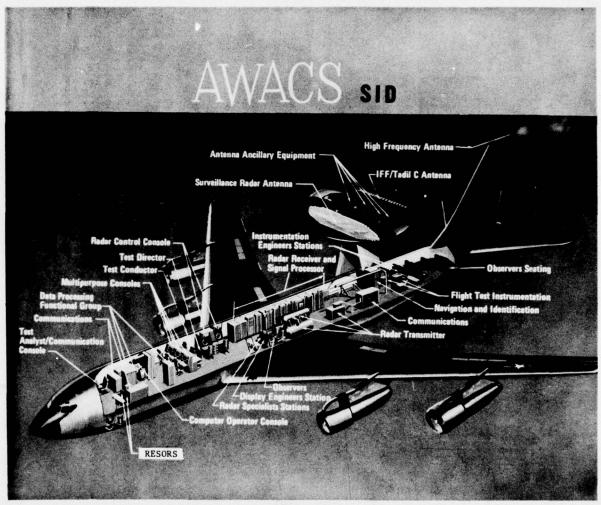


FIGURE 11

#### AN ADVANCED AIRBORNE DATA ACQUISITION SYSTEM

Febo Bartoli Aerospace Technologist NASA Dryden Flight Research Center Edwards, California 93523 U.S.A.

#### SUMMARY

This paper describes the development and features of and user experience with an advanced airborne data acquisition system.

The new system consists of as many as 16 high speed pulse code modulation data acquisition units which are integrated with an airborne computer and a cockpit display unit. The data acquisition units may be operated without the computer. Operation without the computer is termed standalone operation. Computer-integrated operation is intended for large-scale projects, and stand-alone operation is designed for small-scale projects.

The cockpit display unit, which is part of the computer-operated system, displays computed real-time data in engineering units.

An example of the cost reduction experienced by a major aircraft company by using the advanced data acquisition system is given.

#### 1.0 HISTORICAL BACKGROUND

Since its establishment, the NASA Dryden Flight Research Center has played a major role in the investigation of transonic and supersonic flight. The X-15 program, begun in 1954 with a memo of understanding between the National Advisory Committee for Aeronautics (NACA), the U.S. Air Force, and the U.S. Navy, was the last in a series of distinguished rocket-powered research airplane programs.

In the early planning stages for the X-15 program, an all-electronic flight data acquisition system was considered. The planning committee rejected an all-electronic flight data acquisition system for two main reasons. First, they doubted that the state of the art of electronics permitted the development of a suitable system. Secondly, the X-15 data measurement requirements (0-Hz to 10-Hz frequency response) were within the capability of existing oscillographic flight data acquisition systems. As a result, the committee decided to use a flight data acquisition system consisting of NACA film-recording oscillographs and NACA precision photorecording instruments.

The successful use of this flight data acquisition system during the X-15 program can be attributed mainly to the efforts of a large dedicated supporting organization.

The flight data acquisition system was limited in a number of ways. When measurement requirements changed, the film data did not always provide the resolution, frequency response, and accuracy required by the researchers. Changes in program direction required major instrumentation changes and therefore long aircraft down times. Maintaining reasonable maintenance and operation schedules required great manpower and facility resources. Finally, the processing of film data to a form compatible with electronic data processing resulted in long end-to-end data reduction cycles.

#### 2.0 DEVELOPMENT OF AIRBORNE INTEGRATED FLIGHT TEST DATA SYSTEM

Because of the limitations of the oscillographic flight data acquisition system, it was decided in 1962 to develop an all-electronic flight data acquisition system with an output that was directly compatible with electronic data processing. Propitiously, by 1962 major advances had been made in electronic technology. On the basis of the X-15 program experience, a general specification was written for the development of an all-electronic pulse code modulation (PCM) flight data acquisition system. A state-of-the-art PCM flight data acquisition system resulted from this effort. Designated model CT-77, the system had 80 channels, fixed frame length, fixed word length, and 144,000-bit-per-second operation. The CT-77 system was first used in 1964 in the lunar lander research vehicle program. This unit, with updated electronics, remains the principal flight data acquisition system for the Center's projects.

As experience with the CT-77 system was acquired, it became apparent that its fixed characteristics limited its capacity to meet user requirements. It was during this period that airborne computers were successfully demonstrated as control elements in inertial guidance and flight control systems.

Using an airborne computer seemed a logical way to provide control inputs to a PCM system to vary word size, word rate, and sampling format and to permit real time computation. The possibility of using the computer to provide the pilot or crew with impending failure warning made its use even more attractive.

In 1965 a study was undertaken to investigate the feasibility of implementing a computer with a PCM system. The study indicated that using a computer in such a way was indeed practical. In 1970 the development of a computer-oriented PCM flight data acquisition system began. The general system design was based on the results of the 1965 feasibility study, the requirements of new research projects (e.g., the need to acquire dynamic data and the need to make a greater number of data measurements), and the suggestions of the users of the CT-77 system.

#### 3.0 AIRBORNE INTEGRATED FLIGHT TEST DATA SYSTEM DESCRIPTION

The resulting data acquisition system, called the airborne integrated flight test data system (AIFTDS, pronounced  $\bar{a}'$ -fids), has many advantages. Briefly, they are as follows:

It is small, light, inexpensive, quick to install, and easy to modify. This is the result of integrating different functions, which minimizes the number of auxiliary support units, by using remote multiplexing and digitizing and by using automatic system checkout and troubleshooting.

It has the capacity to digitize all flight research data from a variety of aircraft. The sampling rate is sufficiently high to accommodate dynamic data requirements without auxiliary flight data acquisition systems. To handle different size programs efficiently, the data acquisition units can operate as stand-alone units (without a computer) during small flight research programs or with a computer and in conjunction with as many as 16 data acquisition units for larger flight research programs.

It provides flexibility in channel capacity, word rate, and word size. This was accomplished by storing the sampling format in memory and by having software control of word rate and word size. Having several sampling formats stored in memory corresponding to several flight research programs permits several flight research objectives to be conducted during one flight using the same system.

It performs airborne real time computations for display to the flight crew in engineering units. The sampled data can be directed to the computer for processing to provide the flight crew with information on flight progress.

It provides simultaneous sampling and adaptive gain. Data sampling is a time-sequential procedure, making exact time correlation between two data channels difficult. However, requirements for exact time correlation between two or more data channels do occasionally arise. To meet this requirement, the capability was provided to sample as many as four data channels simultaneously. If for one reason or another the anticipated full-scale range of the data measurement is exceeded, the PCM data system saturates at the maximum digital count regardless of the amount the measurement exceeds full scale. To cope with such contingencies and to continue the acquisition of useful data, a capability is provided that automatically reduces the gain by half before a channel goes into saturation.

A complete AIFTDS system consists of an airborne computer system, 16 remote multiplexer/digitizer units (RMDU's), and a cockpit control and display unit. A block diagram of a typical AIFTDS system is shown in figure 1.

#### 4.0 AIRBORNE COMPUTER SYSTEM

The airborne computer system consists of a processor unit and a memory unit (fig. 2). Each of these components is 19.3 centimeters (7.6 inches) high, 15.2 centimeters (6.0 inches) wide, and 49.6 centimeters (19.5 inches) long. Together, the processor and memory units weigh 22.2 kilograms (49 pounds).

The cover of each unit has a finned heat exchanger containing corrugated ribbing for cooling the unit during operation. The cover allows natural convection cooling through the fins and forced air cooling through the corrugated ribbing under adverse temperature and pressure conditions.

Each unit may be operated from either 115 Vac (plus or minus 10 Vac) at 400 hertz or 28 Vdc (plus or minus 4 Vdc) with a power consumption of 149 watts. With cooling air at 38° C (101° F), the unit can be operated in a temperature environment of 71° C (160° F). Without cooling air it can be operated in temperatures up to  $60^{\circ}$  C (140° F). It operates from sea level to 30,480 meters (100,000 feet) and withstands vibration of 10 g's from 55 hertz to 2000 hertz.

#### 4.1 Processor Unit

The processor unit is a high speed, general purpose, stored program digital computer containing a central processor unit, a PCM controller, and a time code generator.

#### 4.1.1 Central processor unit

The central processor unit is organized around nine registers consisting of accumulators, index registers, buffers, and address pointers. The word length is 16 bits for both operands and instructions. Data is in fixed-point fractional form, with negative numbers represented in two's complement.

Duplicate sets of working registers are provided in the central processor unit. One set of registers, referred to as prime, is used for general program usage. The second set of registers, referred to as input, is reserved for the processing of PCM data words. Selection of either register set can be hardware forced or software controlled. Hardware-forced selection of the prime register set occurs at power on. Hardware-forced selection of the input register set is controlled by a signal from the PCM controller upon selection of the PCM data processing mode. Transfer from one register set to the other under software control is accomplished through a discrete command instruction. The duplicate register set allows two independent computer programs to be interleaved without reloading any register. The dual register feature was provided to allow sufficient time for the processing of PCM data in the airborne computer system at the highest PCM word rate.

A relatively powerful complement of 70 instructions is provided in the airborne computer system. Categorized functionally, there are 17 arithmetic, seven shift, 27 data transfer, three logical, 12 branch, and four input-output instructions. Capability for interregister operations, byte processing, and bit testing are provided.

The addressing modes provided are common, direct, indirect, immediate, relative to the program counter, and relative to the index registers.

In addition to the primary input-output dedicated to the PCM functions, the airborne computer system has a general-purpose input-output with an input capability for both serial and parallel transfer of data and an output capability for parallel transfer of data. The general purpose input-output permits the interfacing of other devices with the airborne computer system. The cockpit control and display unit is an example of a device interfaced to the airborne computer system using the general purpose input-output.

#### 4.1.2 PCM controller

The PCM controller has five primary functions. It accepts instructions from the central processor unit; automatically reads the sampling format memory, decoding the control word and transmitting the address words to the RMDU's; accepts and assembles the data returned from the RMDU's into serial and parallel PCM bit streams; routes data to the central processor unit for processing and accepts data from the central processor unit for insertion into the serial PCM bit stream; and transfers the serial PCM bit stream to a telemetry transmitter or a magnetic tape recorder, or both. The operation of the PCM controller is described in more detail in the appendix.

#### 4.1.3 Time code generator

The processor unit contains an integral time code generator that produces binary coded decimal format time-of-day in hours, minutes, and seconds and an IRIG B format. The IRIG B format is a standardized time format developed by the telecommunications working group of the Inter-Range Instrumentation Group (IRIG) for use by the various test ranges, contractors, universities, and government laboratories. The IRIG B format output is used for recording the time on the tape recorder for data correlation.

The time code generator is driven from the main processor clock, which has a stability of two parts in  $10^7$  per minute and two parts in  $10^6$  per day. The binary coded decimal output of the time code generator drives the time display on the cockpit control and display unit, which also has start/stop and counter preset controls. In addition, the means has been provided to synchronize the time code generator to a signal received from radio station WWV, which broadcasts the time standard. To synchronize, the operator presets the time display counters from the cockpit control and display unit and arms the time code generator so that it detects the start of any minute automatically, except the first minute in the hour.

#### 4.2 Memory Unit

The memory unit houses the semiconductor random access memory, the memory timing, the interface logic, and a battery pack. Nonvolatility is provided by a replaceable, rechargeable battery pack capable of supporting 16,384 words of memory for 100 hours without the application of external power.

The memory is divided into two segments, each of which has independent electronics. Having a two-port memory and independent electronics permits a program to be executed in the main memory at the same time that direct memory accesses are made in the auxiliary memory by the PCM controller. Without this provision, little time would be available to do any meaningful processing of selected PCM data.

#### 5.0 REMOTE MULTIPLEXER/DIGITIZER UNIT

The RMDU (fig. 3) is 10.2 centimeters (4.0 inches) high, 18.8 centimeters (7.4 inches) wide, and varies in length from 15.2 centimeters (6.0 inches) to 24.1 centimeters (9.5 inches). The length varies according to the number of signal processing cards accommodated (four to 11 cards). The shorter unit is designed for mounting in extremely limited space. To date, limited space has not been a problem, and only the maximum capacity unit has been manufactured. The power supply for the RMDU is contained in a detachable module. A block diagram of the RMDU is shown in figure 4.

The RMDU can be operated in two modes, slaved or stand-alone. The slaved operation mode has the RMDU's under the control of a computer, whereas in the stand-alone mode local generation of timing, sampling format, and output formatting permit the RMDU to be used as an autonomous PCM system.

The circuit board modules of the RMDU are divided into two categories—overhead modules and input-output modules.

#### 5.1 Overhead Modules

The overhead modules are concerned with the processing and digitizing of analog signals, system timing, sampling and output format generation, and system power generation. There are four overhead modules: the stand-alone timing module, the digital data processor module, the analog data processor module, and the power supply module.

#### 5.1.1 Stand-alone timing module

The stand-alone timing module permits operation of the RMDU as an autonomous PCM system. The principal functions of the module are clock generation, sampling format control, and PCM data output formatting.

The clock generator produces two sets of timing signals. One set of timing signals, referred to as internal or RMDU timing, is used to generate all of the timing associated with the internal operation of the RMDU. The second set of timing signals, referred to as external or PCM timing, determines the word rate of the PCM output serial data stream. The second set of timing signals is hardwire programmable through an external connector to select any one of 256 word rates. The relationship between each word rate is a factor of 1/n times the highest word rate, where n varies from 2 to 256. Since a crystal frequency determines the highest word rate, additional word rate selection may be achieved by changing the plug-in crystal of the crystal oscillator assembly. With this method for determining word rate, no problems are anticipated in meeting the word rate requirements of virtually all users.

The sampling format address generator features four erasable programmable read-only memories to store the format. The format consists of sequence of main frame and subframe addresses. The addresses contain data channel selection, amplifier gain selection, and control information. The main frame and subframe counters increment through the sampling format memory, generating the desired data channel sampling sequence.

The PCM output data formatter generates the serial PCM data output bit stream. The binary bit representations provided by the formatter are nonreturn to zero, both level and mark; biphase, both level and mark; and delay modulation mark (also known as Miller code). Any two of the binary bit representations can be selected to provide two independent serial PCM output bit streams for radio frequency transmission or magnetic tape recording. In addition to the two serial PCM outputs, bit clock, word clock, frame sync, and data cycle sync outputs are provided for test purposes.

#### 5.1.2 Digital data processor module

The digital data processor module interfaces the RMDU with a computer system. The module accepts clock and address information and returns data to the computer. It also decodes the address word to provide control signals for card and channel selection, gain programmable amplifier gain selection, and special function selection.

The RMDU will accept either a stand-alone timing module or a digital data processor module. The conversion of an RMDU from one mode of operation to the other is a matter of interchanging the modules.

#### 5.1.3 Analog data processor module

The analog data processor module is composed of a gain programmable amplifier, an autoranging amplifier, and an 11-bit analog-to-digital converter. The analog data processor module amplifies the pulse amplitude-modulated signals from all analog input-output modules and converts the signals to an 11-bit digital word.

The gain programmable amplifier can be set up for any eight gains, ranging from 1 to 1024. The eight gains are program selectable through the format address word. If the output of the gain programmable amplifier exceeds 90 percent of full scale, the condition is sensed by the autoranging amplifier and the gain is reduced by half. A gain tag which is generated by the autoranging amplifier is appended to the digital word as the most significant bit, indicating that a data word value was obtained at half the programmed gain.

The high level calibrate is an addressable calibrate function which applies a precise voltage to the input of the analog-to-digital converter for the dual purpose of calibration and fault isolation. An additional addressable calibrate function in the analog data processor module applies a short circuit as the input signal to the gain programmable amplifier to provide an indication of amplifier malfunction for fault isolation purposes.

#### 5.1.4 RMDU power supply

The RMDU power supply is a pluggable module which provides the regulated voltages for the operation of the overhead modules and sensor excitation voltages for the input-output modules. The sensor excitation voltages available for the input-output modules are 5 Vdc, 10 Vdc, 15 Vdc, 28 Vdc, and 6 Vac at 2000 hertz. The input power to the module is 115 Vac at 400 hertz. Module operation complies with the characteristics of the military aircraft environmental standard MIL-STD-704B.

All of the power supply output voltages are applied to a bipolar comparator which produces a fault status digital word. This word is addressable as the power supply built-in test equipment (BITE) and indicates the deviation of any output voltage greater than  $\pm 10$  percent from the nominal value.

#### 5.2 Input-Output Modules

The input-output modules include all of the signal conditioning and multiplexing modules necessary to accommodate many types of sensors. A representative input-output module complement is shown in table 1.

#### 6.0 COCKPIT CONTROL AND DISPLAY UNIT

The cockpit control and display unit (fig. 5) is designed to operate with the airborne computer system. It features light-emitting-diode alphanumeric displays in addition to a numerical keyboard and various control switches.

Four lines of 10 characters each make up the data display. The remaining displays consist of a three-character magnetic tape elapsed-time indicator, a one-character PCM format select display, and a six-character time-of-day display, two each for the hours, minutes, and seconds.

The cockpit control and display unit provides system power control, remote control operation of a magnetic tape recorder, synchronization of the time code generation in the airborne computer system with the radio station WWV time standard, selection of as many as five of the PCM formats stored in the sampling format memory of the airborne computer system, display of computed data in engineering units on a real time basis, display and change of the contents of the sampling format memory, and insertion of documentary data into the data stream.

### 7.0 DRYDEN FLIGHT RESEARCH CENTER EXPERIENCE WITH AIRBORNE INTEGRATED FLIGHT TEST DATA SYSTEM

#### 7.1 Flight Tests

After the normal learning period and laboratory evaluation of the AIFTDS, plans were made to flight test the AIFTDS. The flight testing was to take place in two phases. In the first, an RMDU would be flown in the standalone mode to gain some experience. In the second, the complete AIFTDS, consisting of the RMDU's, the computer, and the cockpit control and display unit would be flown.

The decision to conduct the flight tests in two phases was prompted by some overriding considerations. First, to make full use of the capabilities of the AIFTDS, a software package known as an operating system was required, and this software package had not yet been procured. Second, in order to accommodate the full capability of the AIFTDS some revisions of both the existing telemetry ground station software and the ground-based flight data processing software would be required.

At about the same time that the AIFTDS requirements became known, a study of the existing ground-based flight data processing system was being conducted. The study concluded that for efficiency a new flight data processing system was needed.

The software development for the new flight data processing system has been in progress for the past 2 years. It is being designed about a general framework so that it accommodates not only the AIFTDS and the existing PCM systems but has sufficient flexibility to cope with future PCM systems.

In an established flight testing facility, the introduction of a flight data acquisition system similar to AIFTDS probably necessitates some revision of the ground-based data processing software. In view of the experience with this system, a thorough and detailed analysis of the needed software revision is recommended. The effort involved in the revision may be minor or major, depending on the nature of the existing software.

The first test flight of the AIFTDS with the stand-alone RMDU was made in June of 1976. The phase one flight test program is continuing as airplane availability and scheduling permit.

The first flight of the phase two part of the program was scheduled for May 1977, but will probably be delayed because of the lack of funding necessary for the procurement of an operating system software package for the computer.

The high cost of implementing this computer has prompted a search for less costly alternatives. One promising alternative uses a data management unit in conjunction with an airborne version of a commercially available minicomputer. This unit has a well developed software library, including one or more operating systems. The data management unit houses a PCM controller, the sampling format memory, the interface for the cockpit control and display unit, and the interface for the computer used.

#### 7.2 Environmental and Accuracy Study

A comprehensive environmental and accuracy study was performed on an early production RMDU. The environmental tests covered altitudes of up to 30,480 meters (100,000 feet) in 7620-meter (25,000-foot) increments, temperatures ranging from a cold soak temperature of  $^{-54^{\circ}}$  C ( $^{-65^{\circ}}$  F) to a hot soak temperature of  $^{71^{\circ}}$  C ( $^{160^{\circ}}$  F), and vibration levels of 10 g's. The vibration tests were sinusoidal accelerations in three orthogonal axes. Throughout the tests, the RMDU was operational and data were recorded. The RMDU operated well within its specifications, even withstanding an inadvertent vibration in excess of 80 g's.

The accuracy study was performed at five temperatures in the operating temperature range. These temperatures were -54° C (-65° F), -34.5° C (-30° F), -18° C (0° F), 26.5° C (80° F) and 71° C (160° F). The tests were performed at all gain programmable amplifier gains. However, only gains of 1000, 400, and 100 resulted in significant error and are reported here. A least-squares analysis was performed on the data obtained. The results for the uncorrected raw data are summarized in the following table:

Gain	Temperature, °C (°F)	Theoretical slope, counts/mV	Measured slope, counts/mV	Offset, counts
1000	-54 (-65)	200	200.74	19
1000	71 (160)	200	199.41	9
400	-54 (-65)	80	80.79	13
400	71 (160)	80	79.75	10
100	-54 (-65)	20	20.00	-2
100	71 (160)	20	20.00	5

The slope change and offset were attributed principally to the gain programmable amplifier. As one would expect, higher gains magnified the effects, causing slope and offset changes, and the higher the gain the greater the magnification. The slope and offset changes exceeded the manufacturer's specifications. The manufacturer is attempting to resolve the discrepancies, which appear to be due to an anomaly unique to this RMDU. In the course of the study, it was discovered that RMDU data are amenable to correction. The analysis of the data resulted in the development of procedures for correcting the data to 0.3 percent (±3 counts in 2047 counts). The details of the accuracy study and the correction procedures have been documented, but the most suitable form of publication has not been decided.

#### 7.3 Cost Effectiveness

The cost effectiveness of the RMDU's is best illustrated by a major commercial aircraft company installation of several RMDU's. Compared with their standard data acquisition system, the RMDU system reduced wiring from 62,484 meters (205,000 feet) to 7620 meters (25,000 feet), wiring costs by \$55,000, installation time by 3900 man-hours, and weight by 3182 kilograms (7000 pounds).

The money saved on the installation was estimated to have paid for all of the RMDU system hardware.

#### 7.4 Impact of RMDU Use

At a gain of 1000, the RMDU's input sensitivity becomes 5 microvolts per bit. At this sensitivity, noise due to such effects as improper signal cable shielding and grounding, common mode voltage, source impedance, and crosstalk is not negligible. These noise problems are common to all measurement systems involving high amplification, and the first flight tests of the system indicated that they were indeed significant. As a result, in future flights greater emphasis will be placed on determining ways to reduce these effects.

#### 8.0 APPENDIX - PCM CONTROLLER

A unique feature of the AIFTDS is the PCM controller contained within the airborne computer system. Once initialized, the PCM controller operates autonomously under the control of the stored sampling format. As many as 16 RMDU's can be accommodated by the PCM controller. The addressing capability of the RMDU's is completely random in that any channel of any RMDU can be addressed in any sequence. The RMDU's are connected to the PCM controller through three twisted pair shielded wires for clock, address, and data return.

Initialization of the PCM controller by the computer requires the loading of three registers. The first is the word size and word rate register shown in figure 6, which selects one of 11 word rates ranging from 125,000 words per second to 122 words per second and one of three word sizes—9, 10, or 11 bits plus the gain tag bit. The remaining two registers are the main frame address register and the subframe address register (fig. 7). These registers are loaded by the computer to provide the starting addresses of the main frame and subframe PCM format in the sampling format memory. Selection of different PCM formats is simply a matter of reloading these three registers to provide new main frame or subframe start addresses and operationally new word size or word rate information. The AIFTDS is presently mechanized to select as many as five different sampling formats from the front panel of the cockpit control and display unit.

The PCM controller communicates with the sampling format memory through a direct memory access channel. At the beginning of every second PCM word time, a control sequence is initiated by the PCM controller, causing three locations in the sampling format memory to be loaded into three control registers, as shown in figure 8. Words 1 and 2 are address words, and word 3 is the control word pertaining to both address words. The address words are loaded into the address register for subsequent transmission to the RMDU's. The control word is loaded into various control registers, where it is decoded to initiate the mode of operation specified by the content of the control word.

The modes of operation are called the normal mode, the monitor mode, and the simultaneous mode. In the normal mode, addresses are transmitted to the RMDU's serially and the data are returned serially. The data returned from the RMDU's are assembled into two serial PCM bit streams and one parallel PCM bit stream (figs. 9 and 10). When the monitor mode is selected for either one or both of the address words, the data returned from the RMDU are earmarked for central processor unit processing. The monitor mode causes a sequence of operations to be initiated. The RMDU address of the word to be monitored is stored in a dedicated memory location as an identifier (fig. 8). The returning RMDU data are diverted to the monitor data input register as indicated in figure 10. Replacement data previously loaded into the monitor data output register by the central processor unit are shifted from the register into the serial PCM bit stream as shown in figure 10. A signal is generated to automatically transfer the central processor unit to the input working register set. Two sets of monitor data registers are provided so that either or both of the address words associated with a control word may be monitored.

The simultaneous mode causes two, three, or four address words to be transmitted to the RMDU's simultaneously from the four address registers shown in figure 8. Data from these address words are returned from the RMDU's to the PCM controller simultaneously and are shifted into the serial PCM bit stream in their usual non-simultaneous sequence. This mode of operation permits the simultaneous sampling of as many as four selected data measurements where time correlation is essential. Obviously, the data measurements must be located in four different RMDU's if four channels are to be sampled simultaneously.

#### 9.0 REFERENCES

- Robert W. Borek, NASA, Development of AIFTDS-4000, a Flight-Qualified, Flexible, High-Speed Data Acquisition System, 1973, NASA TM X-56018.
- William F. Trover, A High Speed Airborne Data Acquisition and Control System With an Integrated Digital Computer, International Telemetering Conference Proceedings, Volume IX, c.1973, pp.88-105.
- L. D. Crowley, Evolution of the Douglas Flight-Test Data System, International Telemetering Conference Proceedings, Volume X, c.1974, pp. 182-195.
- William F. Trover, Firmware Controlled, High Speed, Random Data Acquisition Unit, International Telemetering Conference Proceedings, Volume X, c.1974, pp. 312-336.
- K. C. Sanderson, A New Flight Test Data System for NASA Aeronautical Flight Research, Proceedings of the 8th International Aerospace Instrumentation Symposium, 1975.

TABLE 1. RMDU PROCESSING CAPABILITIES

Aircraft sensor/load (digital conditioning)	Number of channels per card	Type of card	
Differential dc (±10 mV to ±10 V full scale)	32		
Variable reluctance (LVDT) or ac bridge (phase sensitive demodulator)	4		
Strain gages, resistance thermometers, potentiometers	12		
Thermocouples 1	30	Analog input	
Dual purpose presample filters (low level signals)	4		
Three-wire synchros	3		
Three-input selectable programmable knee presample filters	4 or 2		
Flowmeters, tachometer generators (pulse generators 0 to 11,000 pulses per sec)	4		
Scanivalve driver and position indicator	2		
Differential bilevel sources	24		
Pulse totalizer (flow sensors)	4	Digital input	
20-bit serial digital pressure transducers	4		
ARINC 561 inertial navigation system interface	16		
Discretes/parallel digital (with switch excitation)	36/24		
Relay/contacts <sup>2</sup> (500 mA loads)	24		
Cockpit indicators <sup>2</sup> (analog meters)	3	Output	

<sup>&</sup>lt;sup>1</sup>Each card can be configured to process 30 thermocouples.

Thermocouple can only be used in card slots 1, 2, 3, and 4.

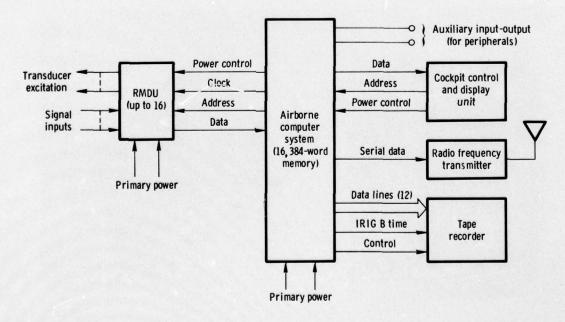


Figure 1. Airborne integrated flight test data system (simplified).

 $<sup>^2\</sup>mbox{These cards}$  are not intended for use in the stand-alone RMDU .

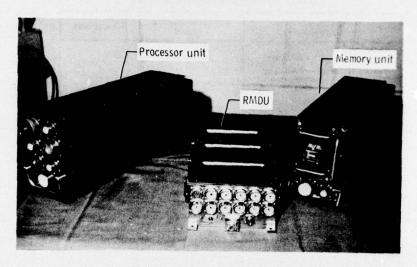


Figure 2. Airborne integrated flight test data system.

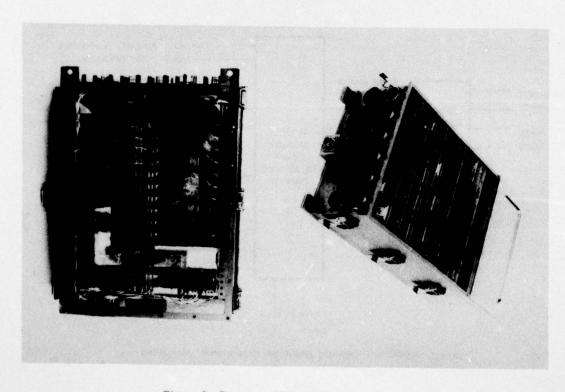


Figure 3. Remote multiplexer/digitizer unit.

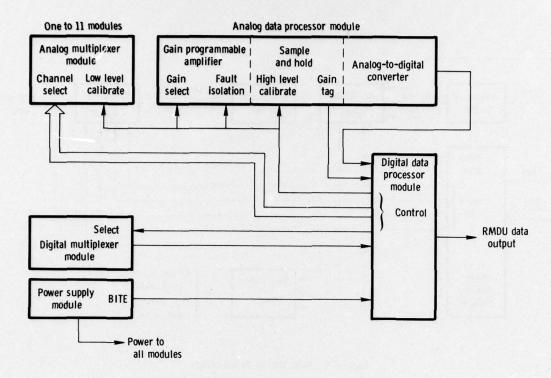


Figure 4. Remote multiplexer/digitizer unit (simplified).

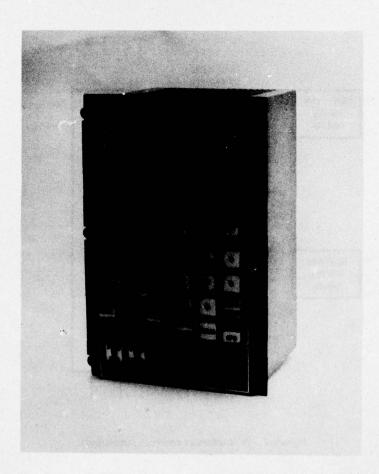


Figure 5. Cockpit control and display unit.

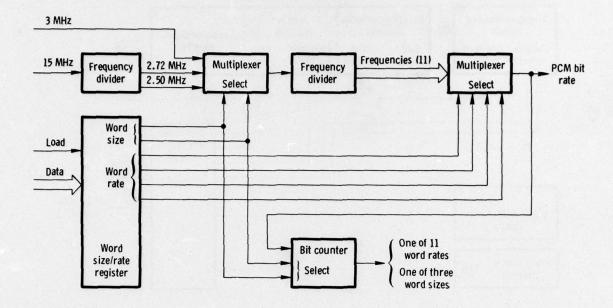


Figure 6. PCM timing (simplified).

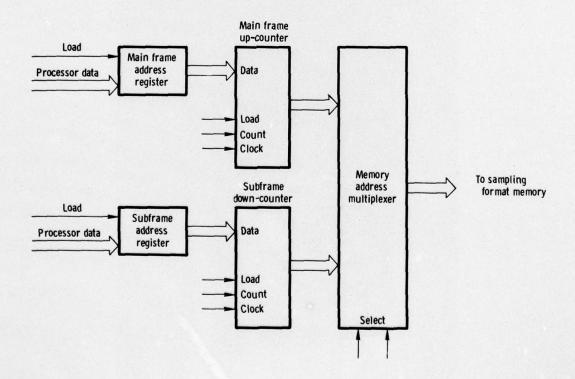


Figure 7. PCM address control (simplified).

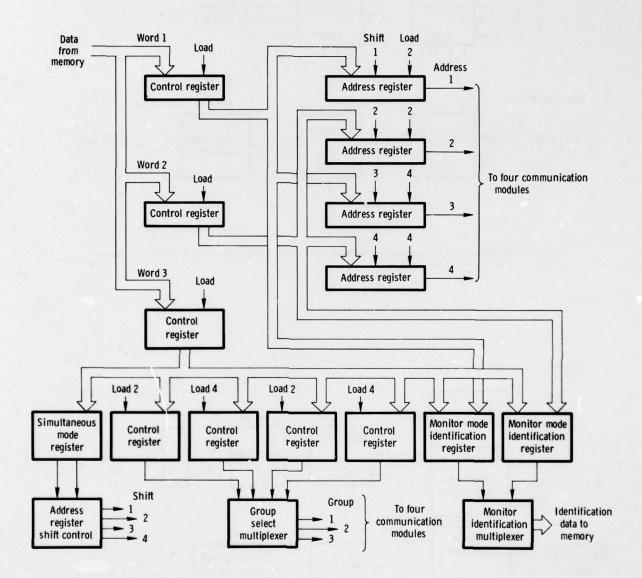
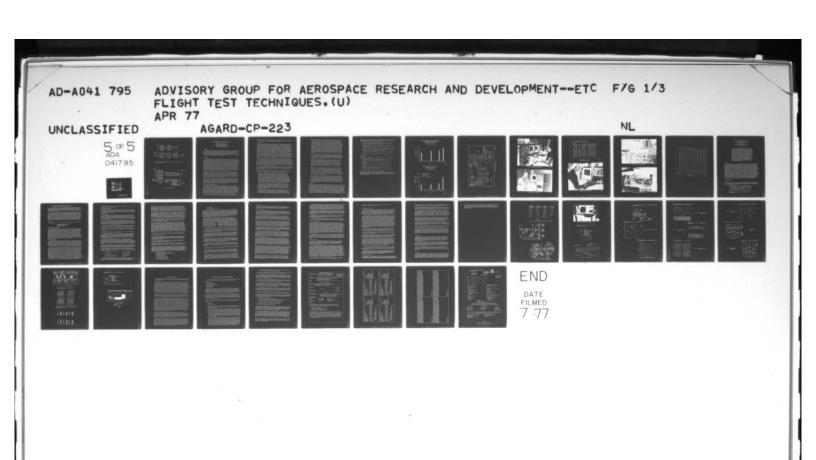


Figure 8. PCM address (simplified).



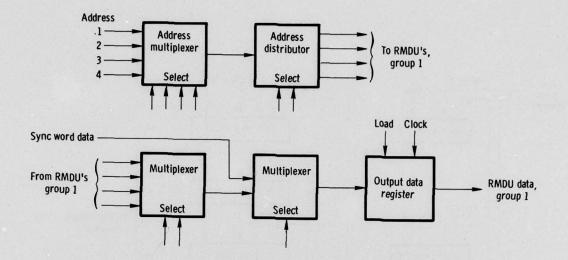


Figure 9. PCM communication module (simplified). Four identical communication modules are used in PCM controller.

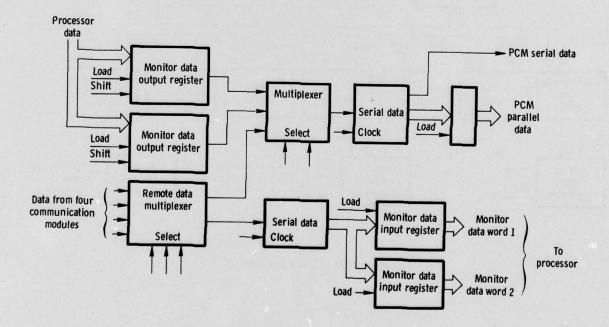


Figure 10. PCM data (simplified).

#### USE OF ONBOARD REAL-TIME FLIGHT TEST ANALYSIS & MONITOR SYSTEMS - A PROGRESS REPORT

William S. Lieberman
Project Flight Test Engineer,
Technology & Planning
The Boeing Commercial Airplane Company
P. O. Box 3707 (Orgn. B-7990, M/S 24-74)
Seattle, Washington 98124

#### SUMMARY

The objective of this paper will be to report on the actual usage of onboard real-time computer controlled data analysis systems during the recent flight test programs for two different Boeing model aircraft, and the plans for use in future application. The results of such usage have been the shortening in schedule flow time and cost of the programs, as well as the increased accuracy of results and reduction in post-flight batch data processing. They have also reduced the dependency on geographical location of the test area since down link telemetry systems are not required. A short motion picture of the system in operation during a test will be shown.

#### INTRODUCTION

With the development of modern high technology aircraft equipped with sophisticated primary control systems a myriad of electronic and mechanical devices are being used to optimize the full performance potential of these vehicles. The cost of flight testing in terms of flight time has risen dramatically. No longer are we able to evaluate the safety and performance characteristics of a particular flight mode with a single flight condition at nominal settings. Instead, we are forced into the position of accounting for each possible combination of the interfacing systems. In some cases we must resort to repetitive statistical sampling procedures. Additional regulatory requirements which have developed over the years have also increased the conditions for flight demonstration relative to evaluation of a new aircraft. Some examples of the additions are the Noise Demonstrations, per Federal Air Regulation Part 36, and the adoption of FAR 25. These additional flight tests also increase the flow time for a developmental or evaluation test program. On Figure 1 we see a vivid graphical representation of this escalation during the past era of the turbine powered commercial aircraft family from the days of the original 707 and DC8s to the present day of the wide body jumbo jets. The cost of a typical FAA certification in terms of test program flight hours has increased by a factor of 50%. As aircraft increase in complexity we can predict a continued increase in the flight conditions required to complete a program and a subsequent increase in flow time.

In addition to the flight hour and flow time, we face the additional increase in the actual dollar cost of testing. The effects of the higher value of the advanced vehicles, the greater direct operating costs in terms of fuel, oil, spares, insurance premiums, instrumentation and data processing (all influenced by inflation), contribute to this increase. In Figure 2 we see a chronological cost picture of the Boeing jet family with an escalation of two to three times in dollars per flight hour over the same period of time. If this trend continues, we will soon be out of business. With this picture in mind, it is evident that the task ahead of the responsible flight test manager is to find some way to reduce the cost of experimental testing.

Since the flight test engineer is not the airframe designer, he has no control over the operating cost or hull value of the aircraft which are the main contributors to the cost per flight hour. He seldom has direct control over the test requirements as established by the designers or by the regulatory, certification, or customer agencies, therefore, his working area is constrained. He must get more test results for each hour flown and reduce the total hours necessary to complete the fixed requirements. This will in turn reduce total flow time which will be a significant contribution to reduced costs. The problem for him now becomes one of increasing productivity.

#### THE CHALLENGE - Greater Productivity

If one makes a detailed study of a normal experimental test flight, he concludes that a large percentage of the flight time consists of "boring holes in sky" type activities, i.e., climbing to altitude, finding stable air, bracketing conditions, repeating conditions, making calculations, etc. If this lost time could be minimized, then the productivity would be increased. One other area where a payoff would be evident is in the increase of concurrent test conditions; that is, simultaneous accomplishment of two or more tests that require the same ambient conditions and test configuration. This gets to be a problem for flight crews, since keeping track of all events is difficult and the monitor tasks become unmanageable. Resolving this problem would result in reducing flight and flow time. In the area of reducing dollar costs, the possibilities are somewhat limited. However, final data processing which is controlled by the flight test engineer is very expensive, and minimizing the amount requested for reduction is a step in the right direction.

An approach used at the Boeing Commercial Airplane Company in Seattle to increase productivity of test flying is to use Real Time On-Board Monitoring of test information. This,

of course, is not a new technique; however, we have developed some unique features that have proven themselves in increasing productivity. A description of these features and a progress report on their use is the purpose of this paper.

#### THE SOLUTION

With instrumentation requirements for the new aircraft ever expanding, the concepts of multiplexing of intelligence channels and the high speed serial PCM schemes for data acquisition developed by the space and missile industry became popular with the aircraft manufacturers. Mr. Bartoli's paper has described one such system as developed by the NASA Dryden Flight Research Center at Edwards, California. Using these systems, we are able to reduce weight and volume of the on-board data system; while at the same time increasing recording capacity, frequency response, and accuracy. Many airframe manufacturers and government testing agencies down link the PCM bit stream by telemetry to a fixed base ground station. On the ground various methods of monitoring are used including display of raw digital words, digital to analog conversion, and display of calibrated data. Some systems play the signals into a ground based computer where it is manipulated and presented as calculated engineering parameters. We at the Boeing Commercial Airplane Company, however, do not use this scheme except for the high risk, minimum crew type testing such as flutter where we have no other choice. Our experience over the years has proven that the natural geographical and climatic conditions prevailing around the Seattle area would cause schedule delays for tests based on a telemetry monitor system. Since we cannot afford schedule delays in a program, our approach is to use onboard monitoring. This allows us complete flexibility in that the testing can be accomplished wherever conditions are proper. Even when high risk type flights using telemetry are scheduled at Seattle, an alternate plan can be executed if telemetry conditions are unsuitable. Test monitor equipment is always on the aircraft, and made ready for the alternate plan dispatch.

The heart of the airborne monitor system is a mini-computer that has been ruggedized for flight. Our scheme is to use this processor for all pre-flight set up functions as well as use during the flight. We then use its generous capacity to monitor and manipulate the incoming data stream onboard in real time. With the appropriate display presentations to the test crew, test conduct is much more efficient and productive. The computer, of course, does not differentiate between a signal taken from a hard wire and one taken from a telemetry transmission. Anything that can be done on the ground can be done on-board and the geographical restrictions are lifted. If the appropriate data base in terms of calibration information, scientific equations, data identification, bit stream location, etc. are loaded into the processor before flight, it has all the tools necessary for real time presentation of the results of the test in engineering terms.

Figure 3 shows a schematic of a typical monitor system used by Boeing Flight Test to accomplish these functions. Figure 4 shows the actual Monitor System as installed on a test aircraft. A ROLM 1602 processor with 32K words of memory and a Cartrifile tape cassett loading device, Figure 5, are used to control the system, store the data base and feed in the application software.

The test engineers use a standard keyboard device for interactive command and a Cathode Ray Tube (CRT) for primary display. Auxiliary display devices are also provided. The software so far developed allow the following functions to be accomplished:

- 1. Engineering Unit Display: Any data channel activated can be displayed to the observer in engineering units updated 1 time per second on the visual display devices (CRT and Digital meters) and up to ten times per second on the digital printer and as a continuous sampled analog display at the data sampling rate on the strip chart recorder. These values in engineering units are of the same accuracy as the final data as long as their calibration can be expressed in reasonably simple equations (up to a 9th degree polynomial). The limit, of course, is the memory capacity of the computer for table look-up for the extreme multi-segment curve fits. The CRT display which the test engineer uses as his primary monitor has a format as shown in Figure 6. The measurement identification and its present value are shown with a set of predetermined upper and lower limits by which he can determine the quality of the data he is observing. A simple command on the keyboard allows him to make a permanent copy of the CRT on the electrostatic printer shown in Figure 7. If he has called up the right data this copy could suffice for the final data without further processing.
- 2. Limit Checking: A software program has been written which checks the output of each transducer signal against the predetermined set of limits. This occurs in a background mode in the computer. If any signal is out of limits, the measurement number is presented on the CRT whether or not that particular measurement is being monitored directly on the display at the time. In this way the test engineer can reserve his attention to those critical items for the specific test being conducted but be cognizant of anomalies on other measurements not being watched.
- 3. Application Programs: In most cases the engineer is interested in a parameter of performance of an airplane or system rather than a measured data value. Airspeed rather than static and impact pressure drag coefficients rather than engine parameters and ambient pressure data. A number of scientific application programs have been written to give the direct result of these calculations to the observer on the CRT where they are updated once each second and are a key factor

in increasing productivity of flight time. The final results of the test are presented in real time. Is the drag of this configuration as predicted? If not, should we continue the test? What was the stall entry rate? Is there a need to repeat the stall in order to bracket the entry rate? Was the gross weight and airplane center of gravity during the condition correct or should we repeat to make sure? Figure 7 shows the test engineers monitor station in a 747 aircraft during a test flight. Two separate monitor stations are in use; one by an instrumentation engineer who is watching the critical instrumentation for the test in progress, and the other by a test engineer who you see comparing results of a computed value shown on the CRT with a predicted value so that he can make the decision whether to continue with the test or proceed along a different tack. Prior to the use of real time monitoring most of these questions could not be answered until after final data processing. This occurred many hours after the flight and the prudent test engineer had to make sure he had enough data from the flight to complete the test if indeed the test was satisfactory. He therefore used more flight time to insure completion. After the data was processed and if it did not agree with predictions, the test would be re-run when appropriate action had been completed. The guessing process would be repeated. Real time monitoring provides the information to make the go, no go decision on the spot without completing all the test points or reducing all the data.

The application programs that were used during the recent 747SP certification included calculation of Basic Airplane Parameters, Gross Weight and Center of Gravity, Airplane Performance, Engine Performance, Stall Speed and Air Loads. An additional function was accomplished on-board by programming the computer to inject signals into the control system for oscillatory frequency sweeps during flutter testing. This forcing function generator software greatly reduced the time for this type of testing.

- 4. Instrumentation preflighting and trouble shooting: The computer has been programmed to step through the entire activated instrumentation installation, limit checking to ground preflight values. When a variable does not fall within the required limits it is indicated on the CRT. In this manner a very quick automatic step through of all transducers can be made, stopping to adjust only those indicated as out of limit. Since the instrumentation engineer making the check is aboard the aircraft instead of in a remote telemetry room his reaction time and effort are much reduced. Manual switching and reading of each output are eliminated and concentration on only those variables indicated as out of limits can be given. Here again, reduced flow time.
- 5. Remote Display: The computer has been programmed to allow the display of any variable or calculation at remote devices throughout the aircraft. The pilot may want to fly the condition by computed result rather than indication of raw parameters. Remote digital displays with one second updating are used for this capability. Figure 8 shows these displays located on the pilots' panel. In cases where the test crew would prefer an analog display as more convenient for decision making the computer organizes the display by digital to analog conversion and presents it as a sampled analog on a direct write oscillograph and/or an X-Y plotter, as shown in Figure 9. The electrostatic printer can also be used to sample several measurements at frequency of up to ten times per second with a format as shown in Figure 10.
- 6. Post Flight Analysis: The monitor system is configured in such a way as to be able to interrogate the data stream either before or after the record heads of the acquisition system. It is possible therefore to play back the flight tape and take a look at any data desired using the system as if in real time. Events that occurred during flight which were not being directly monitored can be called up. Data processing using application programs can be accomplished. Trouble shooting and investigations can be performed immediately after the flight and and final data requests can be minimized. This capability has a great payoff potential, especially when operating at a remote base without final data processing capability. In addition, interrogation after the record head gives monitor proof of good data recording.

#### THE RESULT

The On-Board Monitor System described has been used on two recent major flight test programs by the Boeing Company; the 747SP certification, and for a military derivative of the 707. In each program the monitor system was credited with expediting the testing and saving flight hours. Since the system was a new development, there were growing pains and problems with both hardware and software. The problems were mainly caused by insufficient lead time and underestimation of the time required to write and debug the software. Historically, development of new test techniques and equipment occur concurrently with the requirements. This reduces the lead time available, and vendors of the various pieces of equipment used had difficulty meeting schedules. The software for the limited mini-computer memory must be written in efficient assembly language rather than the simple higher order languages such as Fortran or Basic that most engineers can master, and this endeavor was late. To do all the tasks outlined, computer instructions must be minimized; resulting in difficult software development. The test engineer users of the system were very suspicious at first and

insisted on verification of real time results with final data. After a little operating experience, however, they began to rely on the monitor and many additional features were requested for incorporation the next time around. Specific examples of increased productivity which were obtained during these programs are:

- Flight Load Survey flying was cut by approximately 20% since the decision to proceed to the next critical condition was contingent on the results of the last condition, which were available in real time.
- Airplane Performance testing was reduced approximately 15 20% since conditions could be shortened by observing air mass stability and by recognition of instrument malfunctions.
- Remote base operations were reduced considerably since there was no wait for data turn around. The monitor system was used as a post flight quick look ground station.
- Flutter testing set up for frequency sweeps was accomplished in half the time required with previously used manual or mechanical methods.
- 5. Quick look data processing volume was reduced considerably during structural testing.
- Final Data processing was materially reduced in volume, saving processing dollars and flow time.

#### CONCLUSIONS

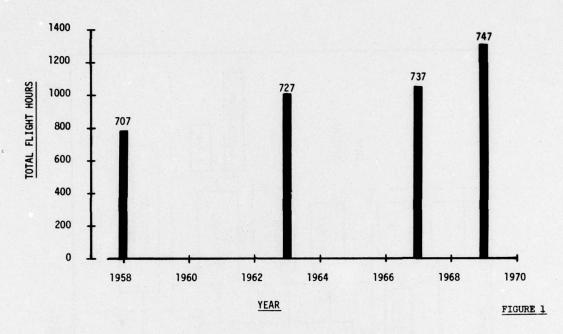
A real time on-board monitor system allows more efficient test conduct and greater productivity. Its use provides:

- Determination of out-of-limit test data so testing can be terminated and instrumentation malfunctions corrected before continuation.
- Determination of "goodness of condition" by monitor of calculated test parameters.
- More rapid stepping to next condition by observation of computed results of last condition.
- Elimination of redundant test conditions by observation of these computed results.
- Reduction of final data batch processing through the large computers by aiding the editing of final data requests.
- 6. Elimination of re-flights due to non-detection of instrumentation malfunctions.
- 7. More rapid preflight activities and quicker turn around.

The list of advantages will grow with time and experience with the system. We have established our point that the cost effectiveness necessary to justify a technical advance has been obtained. Each of the above items contribute to a reduction in flight time and calendar flow which reduces significantly the cost of the experimental flight testing of an airframe.

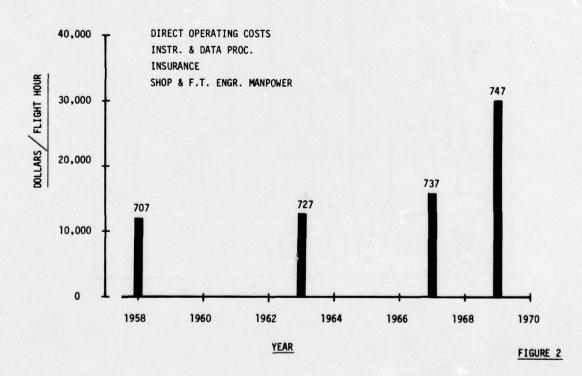
### TOTAL EXPERIMENTAL FLIGHT HOUR REQUIREMENTS FOR COMMERCIAL CERTIFICATION

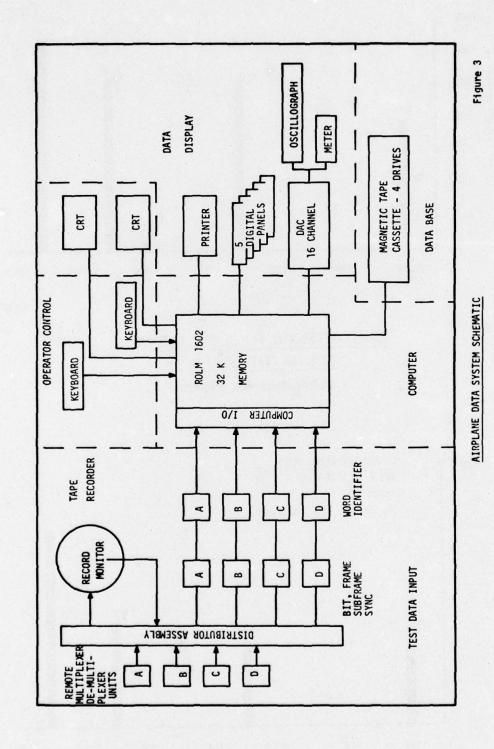
(INCLUDES DEVELOPMENT TESTING)



# TOTAL EXPERIMENTAL FLIGHT TEST PROGRAM COST FOR CERTIFICATION

(INCLUDES DEVELOPMENT TESTING)







TYPICAL ON BOARD MONITOR SYSTEM INSTALLATION

FIGURE 4



ROLM 1602 PROCESSOR & CARTRIFILE

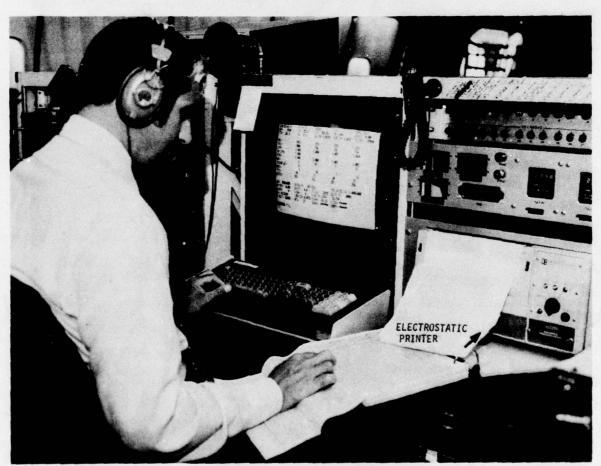
FIGURE 5

R0801 103-03 02/06/75 747-100 SP JNM CERT. R0801 103-03 02/06/75/ 747-100 SP JNM CERT.

11:13:11.6				
MEAS UL	LL	VALUE		TITLE LIST# 100
2145 12 499	. 00022	1. 5612		QI COPT-PI (AWACS)
2415 1, 9995	. 00001	. 55139	INHG	E1 PBLD DUCTPT-PS(AUACS)
105 280, 90	. 19999	296. 97 k	CNOTS	GND SPD INS COMP CHIACS)
400 535, 99	.0	71, 337 0	JAL.	AFU FUEL TOT (AMACS)
401 10222	. 0	1733. 8 0	GHL.	ENG 1 FUEL TOTAL CAMACS
402 10270.	.0	6840, 5 0	iat_	ENG 2 FUEL TOTAL CAUSES
403 10257.	. 0	1685.5 0	GAL.	ENG 3-FUEL TOTAL (AMACS
* 5089 . 72297	- 04978	8, 4230 (	arm .	FUEL FLOW E1 (AMACS)
* 5090 . 79797	03439	11 701 0	SPM .	FUEL FLOW 62 (GMGCS)
* 5091 . 71871	- 04829	10.981 0	SPM	FUEL FLOW E3 (AMBOS)
* 5092 . 72605	- 03099	5, 9899 (		FUEL FLOW E4 (RMRCS)
2408 17, 956	-23.961	-1. 5695 C		ELEV POS RH INSD (BURCS)
2409 17, 927	-23. 979	1. 4649 [		ELEV POS RH OTED (ALACS)
2410 20 993	-28, 995	-24. 833 D		HIL POS FIH INED (RUNCS)
	4, 5011	24, 879		COPILOTS PI (RMACS)
2144 30 999	50895	732, 50	1077/Att (0.00 Tr)	PS4 ENG 1. (AMACS)
2403 749, 99		53. 737		PS4 ENG 1 HIRESP (ANACS)
2437 949 36	4, 5492			PT2.5 ENG 1 (AMACS)
* 5001 64.998	4. 0007	17752		
★ 5073 64,998	4, 6397			PTZ ENG 1 GHARCS)
105 280 90	. 19999	206, 97 k	CNU12	GND SPD INS COMP (RUACS)

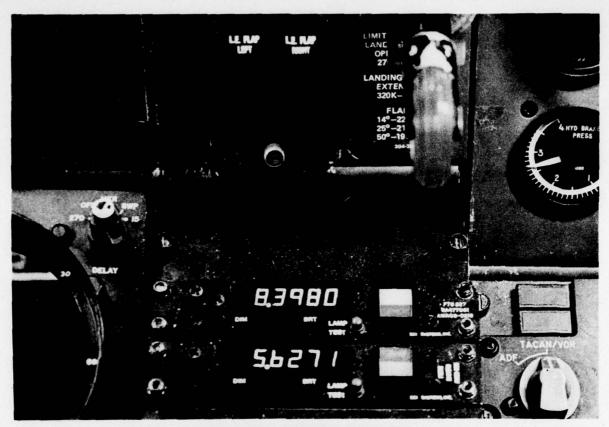
# ENGINEERING UNIT DISPLAY ON CRT

FIGURE 6



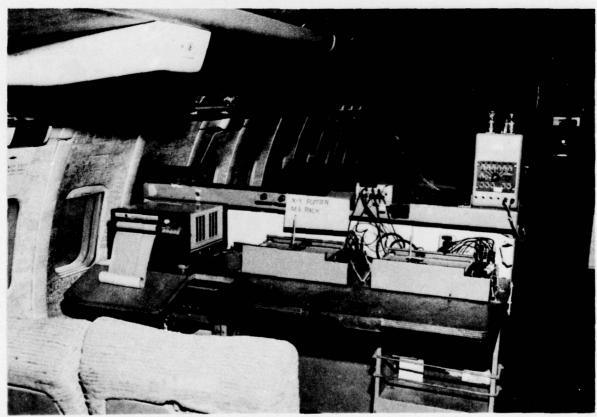
ON BOARD TEST ENGINEERS MONITOR STATION

FIGURE 7



REMOTE DIGITAL DISPLAYS ON PILOT'S PANEL

FIGURE 8



DIRECT WRITE OSCILLOGRAPH AND X-Y PLOTTER

FIGURE 9

L15T#	400	401	402	403	5089	5090	5091
11:18:00.8	213, 72	71. 372	1815. 3	6917. 6	1.759. 2	9, 8160	16. 134
11:18:00.9	213, 72	71 372	1815. 4	6917. 7	1.759. 2	9, 8160	16. 134
11:18:00.9	213, 72	71. 372	1815. 4	6917. 7	1.759. 2	9. 8160	16, 134
11:18:01.0	213, 72	71. 372	1.815. 4	6917, 7	1.759. 2	9, 8169	16, 309
11:18:01.1	213, 72	71. 372	1815. 4	6917, 7	1.759. 3	9, 8160	16, 309
11:18:01. 2	213. 72	71. 372	1815. 4	6917, 7	1759. 3	9, 8160	16, 309
11:18:61.3	213, 60	71, 372	1815. 5	6917, 8	1.759, 3	9, 8160	16, 309
11:18:01.3	213, 60	71, 372	1915. 3	6917, 8	1.759, 4	9, 8160	16, 309
11:18:01. 4	213, 60	71, 372	1915. 5	6917. 8	1.759. 4	9, 8160	16, 309
11:18:01.5	213, 60	71, 372	1915. 6	6917. 9	1.759, 4	9, 8160	16: 309
11:13:01.6	213, 60	71, 372	1815. 6	6917, 9	1.759. 4	9, 81.50	16, 309
11:18:01. 6	21.3, 60	71, 372	1815. 6	6917, 9	1.759. 4	9, 8160	16, 324
11:18:91.7	213, 69	71, 372	1915. 6	6917, 9	1.759, 5	9, 8169	16, 324
11:18:01. 8	213, 60	71, 372	1,815, 6	6917, 9	1,759, 5	9, 8160	16, 148
11:18:01.9	213, 47	71, 372	1815. 7	6918, 8	1.759. 5	9, 8160	16, 148
11:18:01.9	213, 47	71, 372	1915. 7	691.8. 8	1.759. 5	9, 8160	16, 148
11:18:02.0	213. 47	71, 372	1815. 7	6918. 0	1.759. 5	9, 81,60	16, 134

TIME HISTORY DATA

Figure 10

THE AUTOMATED FLIGHT TEST DATA SYSTEM

by Charles O. Johnson

Chief, Operations Management Branch Air Force Flight Test Center

and Paul J. Sehnert

Chief, Technical Development Branch Air Force Flight Test Center

#### SUMMARY

The United States Air Force, Air Force Flight Test Center Automated Flight Test Data System (AFTDS), a derivative of the Grumman real-time system, has been extensively used by the B-1 development test program, was used to a lesser degree for the F-5E spin evaluation, and has considerable use planned during the F-16 full scale development tests. The applications range from simple real-time validation of instrumentation system health to presentation of engineering data such as drag polars, load analysis, and terrain following/ terrain avoidance system information. Included is a brief description of a system that employs on-line computation to generate real-time engineering data. Interfaces with the onboard instrumentation system, the planning activity required to effectively apply this data system, description and presentation of typical data analyses packages, consideration of the limitations, benefits, and indication of future plans are covered in greater detail.

#### INTRODUCTION

Historically, the Air Force Flight Test Center (AFFTC) has performed its flight test missions with only minimal use of real time data except for tests conducted in connection with vehicles such as the X-15 and the lifting bodies. It became increasingly apparent during these missions that real-time data for flight safety, mission control, and test conduct was a necessary tool. As the Center became more involved in joint programs with the National Aeronautics and Space Administration (NASA) and in joint programs with Department of Defense contractors, it also became evident that real-time data would be required if we were to develop sophisticated systems within a minimum time at the least possible expense. The increasing effort required to prepare complex systems for test missions dictated that available test time and resources must be better utilized. The advent to the B-l test program further emphasized that the AFFTC must evaluate the use of real-time data such that tests could be accelerated to provide data in support of a production decision. Two major United States airframe manufacturers had developed and previously made extensive use of real-time data processing and analysis through scientific computers and displayed in alpha numeric digital or plotted form on cathode ray tubes in real-time to flight test personnel; Grumman on the F-14 and McDonnell-Douglas on the DC-10 certification program. Evaluation on each of these systems revealed that the Grumman system closer met the AFFTC requirements with a minimum of development and as such was procured from the Grumman Data Systems Corporation in 1973. The system was called the Automated Flight Test Data System (AFTDS). Since then, the system has been used for the B-1 and F-5E flight test programs, and will play a major role during the F-16 Full Scale Development tests.

# SYSTEM DESCRIPTION

#### General

The AFTDS consists of both hardware and software which provides the integrated system capability required to perform real-time on-line flight test data analysis. The system is designed and employed to increase the probability of safe and timely completion of a flight test program by:

- o providing quality control of each maneuver and allowing the test conductor to direct repeats of invalid maneuvers,
- o monitoring selected instrumentation for safety purposes and for instrumentation system health,
- displaying engineering data in a readily understandable form,
- o reducing data turnaround time for post flight batch processing, and

o providing preliminary data plots or tabulations which in some cases may replace batch processing.

Figure 1 illustrates the four basic hardware subsystems of the AFTDS and the functional responsibilities of each. The AFTDS integrates the Telemetry Formatting, Preprocessor, Central Computer, and Display Subssytems into a real-time flight test analyses capability. From the flight analysis station, flight test personnel can direct the system to acquire, condition, format, and display data parameters in pre-described formats for real-time analysis.

Initially, as shown in Figure 2, the AFTDS which one input telemetry stream provided two data stream output utilizing the TeleSCOPE 340TM operating system. (The TeleSCOPE operating system, a superset of the standard Control Data Corporation SCOPE operating system, was developed by the Grumman Data System Corporation and remains proprietary to that corporation. For simplicity throughout this paper, the trademark, TM, notation will be deleted.) The displays included two master cathode ray tube control consoles called Flight Analysis Stations (FAS), three repeater cathode ray tubes, and three analog strip chart recorders. Concurrent with real-time, the Central Computer Subsystem supports batch processing, INTERCOM, EMR 6135 precomputer processor input, and space positioning system data processing and operation. TeleSCOPE 340 possesses the ability to support an expanded system (Figure 3) of three individual telemetry input streams, three data stream output, plus the concurrent operations detailed above.

#### Hardware

AFTDS hardware can be grouped into four basic subsystems according to functional responsibilities:

Telemetry Formatting Subsystem (TFS) Preprocessor Subsystem Central Computer Subsystem Display Subsystem

#### Telemetry Formatting Subsystem

The Telemetry Formatting Subsystem operates basically as a special purpose peripheral device for the Preprocessor Subsystem. It receives serial pulse code modulation (PCM), frequency modulated (FM), time and audio inputs from the AFFTC range complex. Serial PCM data containing noise and other perturbations is conditioned to generate reconstructed and coherent PCM data and timing signals. FM data is digitized in the Analog-to-Digital Conversion Section (ADC) and placed in the Analog-to-Digital and Digital-to-Analog Interface (ADI and DAI) unit when directed by the Analog Data Formatter of the Preprocessor. Thereby, serial PCM data is formatted to parallel PCM information and FM data is digitized and synchronized with the PCM stream. The TFS also accepts logic commands from the Preprocessor to switch from the forward data flow and allow digital data to return from the Preprocessor, be converted to analog form in the digital-to-analog converter and pass to the analog presentations (presently three 8-channel strip charts) which are part of the Display Subsystem. Finally, all raw data inputs are recorded on two 14-track wide bank (2 mHz) analog tape transports and can be made available to be processed through AFTDS at a later time.

#### Preprocessor Subsystem

The Preprocessor Subsystem is structured around a CDC 1700 computer with certain tasks assigned to special software and peripheral devices. The basic task of the Preprocessor is to effect real-time transfer of data between the Telemetry Formatting Subsystem and the Central Computer Subsystem. PCM data is decommutated and reformatted, digitized FM data is converted, and both types of data are made available for engineering unit conversion within the Preprocessor. The subsystem can process up to 50,000, 12-bit PCM data words per second; however, if FM data is being processed simultaneously the PCM processing rate is reduced. At maximum input rate, only thirty percent of the processed data may be transferred to the Central Computer (15,000 words per second).

One section of the Preprocessor Subsystem normalizes, linearizes, and limit checks data. Normalizing adjusts FM data from any shift in the zero or full scale calibration points. Linearizing data converts from a voltage into usable engineering units. However, these two processes are carried out in one algorithm in the preprocessor, utilizing adjusted coefficients in a polynomial (up to fifth order for PCM data an linear for FM data) generation method. Limit checking either compares the magnitude of the sample to specified high and low limit values or compares the difference between the present sample and previous sample to a specified maximum rate of change. Whenever a parameter fails either of these checks, it is immediately sent to the Central Computer Subsystem for alarm display on the FAS. The preprocessor also selects data for strip chart display, and provides for digital recording on seven-track magnetic tape for further processing in the Central Computer. At the command from the Flight Analysis Station operator, the magnetic tape in the Preprocessor subsystem (called the 100-percent pseudo engineering units tape) records all of the data input to the preprocessor. This option allows the engineer to record all data that is input to the preprocessor, not just the maximum of 15,000 words per second which can be directed to the Central Computer by the preprocessor. Further, the 100-percent tape can be later processed through a special program to produce a formatted tape for batch processing. This feature is

TO ME

A THE NAME OF THE PARTY OF THE

designed to reduce data turnaround time by producing engineering unit data tapes which are available immediately after the test.

## Central Computer Subsystem

Currently, the AFFTC CDC 6500 is the Central Computer Subsystem. It has 24 input/output channels, 20 peripheral processor units, two central processors, central memory, disc storage, and extended core storage. This system architecture provides considerable multiprocessing capability and allows simultaneous processing of real-time data along with INTERCOM terminal and batch inputs.

#### Display Subsystem

The Display Subsystem is the flight test team's communications link with the AFTDS. It currently consists of a display controller, two master control consoles, three repeater cathode ray tubes, a hard copy/microfilm section, and three strip chart recorders. The controller performs all Display Subsystem logical operations: accepting digital data from the computer, routing it to the selected output devices, buffering data for the hard copy/microfilm section and accepting display control logic instructions from application software.

The Flight Analysis Station operator (a flight test engineer for real-time test mission) uses the CDC 252-2 Graphics Display Console (Figure 4) to initialize packages, make last minute revisions to displays, initiate maneuvers and events, select displays, select time for recording 100-percent pseudo engineering units tape, and recall selected portions of data for post-maneuver analysis. The operator also selects images of special interest and chooses the type of permanent record (photo sensitive hard copy or 35mm microfilm) to fit the requirement of the test team.

The graphic Display repeaters provide duplicate images of whatever is displayed at the Flight Analysis Station console. These repeaters provide the test conductor and engineering discipline monitors ready access to data as it appears on the screen.

Finally, the strip chart recorders provide supplemental analog time histories. These displays are used to complement the data displayed on the Flight Analysis Station.

#### System Software

AFTDS software consists of four categories based on the functional usage: preprocessor, system, real-time applications, and interface.

The preprocessor software is created by processing the instrumentation definitions for a test through the TELIN compiler in a batch mode. Any change to the instrumentation definitions result in a different preprocessor program (called a preprocessor configuration file). Under real-time operation the program is loaded, by command of the engineer, from the FAS into the preprocessor by the Central Computer. For non-real-time operations, the program can be loaded into the preprocessor in a stand-alone mode by the preprocessor operator.

In stand-alone operations, the preprocessor can create a 100-percent pseudo engineering units tape and operate the strip charts. In real-time operations, it additionally passes three different data buffers to the Central Computer system: out-of-limits, critical parameters, and real-time data. The software includes a time smoothing routine which assures that time (PCM and FM source) updates correctly. It extrapolates over drop outs and assures time integrity through losses of synchronization. The time smoothing routine also distributes time to the various data buffers for data/time correlation.

Within the Central Computer Subsystem software, the Grumman TeleSCOPE 340 operating system is the element that makes the AFTDS such a powerful tool. It was developed for the Grumman Automated Telemetry Station by Grumman, and was modified to accommodate the AFFTC computer configuration, software requirements, and concept of operation.

The modifications made to SCOPE were a software interrupt system, priority disk accesses for the writing of recall and plot files and a change of the job priority scheduler to assure proper allocation of resources for real-time execution. In addition, TeleSCOPE 340 includes:

o Real-Time Control Point Director o Common I/O Processor

o Plot Executive o Real-Time Scheduler

o Loader Executive o Testlog Executive

o Extended Core Storage Manager o Error Processing

o Real-Time Communication o SIGNON

The Real-Time Control Point Director (RTCPD) is the executive routine which controls all activities required for real-time operation. It loads and controls the real-time operation through requests from the FAS. In addition, RTCPD initiates and

controls the selection and recording of data on disk, the processing of selected data and the storing of calibrated data which is accessible to user derived application programs. RTCPD is capable of servicing up to three real-time output data streams on a time-sharing basis. The central memory of the real-time control point is divided into two distinct areas, one containing system routines which are always resident in central memory; the other containing real-time application routines for the data stream currently executing. The contents of the second area are periodically transferred in and out of central memory and extended core storage by RTCPD as each data stream is serviced.

The loading of any program into the swap area is the function of the Loader Executive Subprogram. Upon request from RTCPD, it will search program Library files for the requested program and accomplish the loading task. All communication between the Display Subsystem and RTCPD is the responsibility of Plot Executive Subprogram. RTCPD makes periodic calls to Plot Executive checking for FAS activity; once activity begins, RTCPD continues calling Plot Executive for FAS servicing of the displays, type-ins, light pen, and function keys. Extended Core Storage Manager handles all memory transfers to or from extended core. Involved in these transfers are data to and from central memory or disk, and the swapping of the application programs to and from central memory.

The Real-Time Communication Subprogram interfaces the Preprocessor and Central Computer. It has the ability to control the transfer of real-time data, out-of-limit data, and critical parameter data; or to control the preprocessor in writing the 100-percent pseudo engineering units tape.

Common I/O (input/output) Processor handles all the input/output requests from programs in the swap area. Whenever the swap area requests I/O, the swap area is exchanged from Central Memory (CM) to Extended Core Storage (ECS) and the I/O occurs from the ECS to disk rather than CM to disk. Once I/O is completed, the program is allowed to be swapped into CM again. Real-Time Scheduler allocates central processor resources to real-time background batch and/or INTERCOM. The scheduler also distributes the central processor time availablefor real-time among the applications software. Testlog Executive provides an interface between the Testlog program and system software or real-time applications software which sends messages to various files. Such files may be the display on the central computer console, accounting files, engineering files, etc. Several different error processing routines exist, each being used depending upon the class of error. Errors occurring within the swap area will not cause RTCPD aborts, hence one stream can abort without affecting the other streams. Hardware or system software errors are generally catastrophic and will normally cause all streams to abort.

Once signaled by the Flight Analysis Station Operator, RTCPD loads SIGNON into the swap area, allowing the engineer to enter his project unique statement and files.

Real-Time Applications Software

The real-time applications programs do not manage core, load routines, or schedule time. Rather, they interface with the user, calibrate data, or perfrm engineering analysis. They are data stream oriented and are swapped in and out of central memory to extended core as each data stream is serviced. The applications programs are generally written in FORTRAN.

Of all of the applications software, generally only those known as HEADING and the Data Analysis Package (DAP) are aircraft or project unique. The remainer is generally not accessible for modification by users.

MASTER is the main program in the swap area. It is the interface between the Flight Analysis Station operator and RTCPD, as it services all latch keys, function keys, light pen, and keyboard inputs from the FAS. It loads and executes all major subprograms.

Once the FAS operator has completed the SIGNON operation, RTCPD loads MASTER into the swap area. Immediately, MASTER MENU appears on the CRT (Figure 5) and allows the operator to attach files, configure the preprocessor, initialize data analysis packages, enter maneuver mode, enter intermaneuver plot mode, enter utility, deconfigure the preprocessor, and logout. Basic to the operating software is Telemetry Input Language (TELIN). TELIN language permits the user to "write" the preprocessor program, to define preprocessor output requirements, and to define DAP display requirements. Functions of the TELIN language are to specify:

- o telemetry instrumentation and formats
- o measurands and corresponding locations (track and channel assignments, etc)
- o EU conversion coefficients
- o limit parameters and limits
- o real-time (Recall) parameters
- o critical parameter parameters
- o DAC and Discrete Board parameters

- o DAP parameters
- o DAP displays and configuration
- o DAP initialization

Three separate input files are required for TELIN operation. The TELIN instrumentation descriptive subset of language permits the user to describe the format and attributes of data entering the telemetry system. The instrumentation file can be created either by software called the Format Conversion Program or produced by hand as a punched card deck. This file contains descriptive parameters for telemetered PCM frames and subframes and FM multiplexers. Additional parameters name the sources of data and provide their type. TELIN provides a file that contains predefined plot and tab specifications and annotations, and maneuver definition file that identifies the Plot/Tab File to be used and the latch key combinations for the plot/tabs. Also specified are the initialization constants and parameters to be used from the real time data buffer.

Two separate output files are a product of TELIN. One TELIN output file is essentially the Preprocessor Configuration File (PCF) which has several sections. The instrumentation section consists of all the active PCM and FM measurements in the telemetry stream. All the active measurements will have the latest calibration information (i.e., information obtained from the instrumentation file). The recall section consists of all the measurements required by the maneuver packages which are to be run on a particular real-time stream. The Central Computer generates a disk file of recall data which can be used to processive all-time DAPs between maneuvers. The Digital-to-Analog Converter (DAC) section if fies which measurements should be routed through the DACs to the strip chart recorders. The parameters are automatically routed to the DAC section by relating an eighteen character designator unique to a parameter to a physical DAC via the DAC statement. The Cr. all Parameter section defines up to thirty measurements for continuous, once per seconomercal processing for input to the HEADING subroutine.

The other TELIN output file, the Run File, is the result of processing the Plot/Tab file and Maneuver Definition file. There exists a separate Run File for each DAP.

Two types of programs are generally written for each different aircraft. The first is the HEADING package, of which there is generally only one written for each aircraft. The second is the Data Analysis Package (DAP), of which there are generally one or more written for each test discipline to use AFTDS.

HEADING is loaded into AFTDS as a subroutine of MASTER. Once the preprocessor has been configured, HEADING will begin executing and continue to execute until LOGOUT or loss of telemetry. Generally there is only one HEADING package for each aircraft; therefore, all flight test disciplines must agree on what should be placed in the first two lines of the HEADING display. The HEADING package is executed once per second and the display values are normally updated at the same rate, although a slower rate is possible.

The HEADING display (Figure 6) is composed of information from the system, from SIGNON, from HEADING, and from the executing DAP. HEADING has control of the first fifty characters (including blanks) on the first and second line of the HEADING display. The remainder of the first and second line are fixed in format and are controlled by the system. The first 50 characters of the third line of HEADING are controlled by the executing DAP. This line is called the Free Format Line.

The Data Analysis Package (DAP) specifications are prepared by the discipline engineer and are coded by project mathematicians. Several constraints exist that dictate the size of the DAP and its execution time; however, those are beyond the scope of this paper. It suffices to discuss only briefly the characteristics of the FAS presentations.

A maximum of ten plot and/or tabs may be selected for each DAP (Figure 7). Because of this strict limitation, the designer must be judicious in assessing the objective of the DAP in question.

Only 200 points per plot are allowed. Plots may be of time history form or x-y form. The latter may be based on criteria such as to plot parameters at given delta time, to plot parameters at given delta in x or in y, or both, or to plot parameter at given delta in third parameter. Scaling notation may be fixed point or exponential. Although normally only one trace is made on a plot, more than one trace can be accomplished.

Of the ten slots for plot and/or tabs, the remainder of the ten slots that are not used for plot selection can be used for tabs. In tabs, a maximum of ten columns of a data with a limit of 120 characters (including blanks) exists. The time-history tab generally has time in column one and the corresponding data in the other columns. If the tab is being displayed full screen forty lines (or rows) will be displayed before it is refreshed. If the tab is displayed half screen, the twenty lines will be shown before it is refreshed. The matrix tab is used to display a set of data at a given time slice.

#### APPLICATIONS

The AFTDS has become one of the elements of the AFFTC's integrated data system concept; the other two elements being a standardized airborne instrumentation system called ATIS (Airborne Test Instrumentation System) and a set of standardize data analysis subroutines called UFTAS (Uniform Flight Test Analysis System).

#### B-1 Joint Test Program

Since the B-l test program planning had progress substantially before the advent of ATIS, it was highly impractical and financially prohibitive to change to ATIS from the Rockwell International designed instrumentation system. UFTAS was implemented, however, and has proven to be a valuable asset. The real-time monitoring of B-l test information has been originally planned using analog strip chart recorders, the method commonly used by Rockwell on previous aircraft tests.

AFTDS presented a challenge to management and engineers. The cost and time to implement would be significant and the operating philosophy would have to change. These same factors were prevalent in other applications: The F-5E spin tests and the F-16 Full Scale Development program (the later tests to begin in January 1977). Since there are additional costs incurred both for preparation and for use of the system one must attempt to balance those financial and human resource costs versus the benefits incurred.

In the case of the B-1, to accelerate the time to implement AFTDS for aircraft number one, several of the Grumman F-14 data analysis packages were modified to accommodate the B-1 data requirements. The disciplines affected were aerodynamic performance, flying qualities, and propulsion. It became evident shortly after the packages were received at Edwards AFB that it would have likely been more appropriate to develop new packages rather than modify those of the F-14. In that group of packages, there were additionally several that were designed and programmed specifically for the B-1. Those were ready for operation approximately the same time as the modified F-14 items.

Since development of the original group of packages, there have been approximately ten additional packages developed; additionally, many of the packages have been modified to accommodate B-l test aircraft numbers two and three. Applications software are now available for the flying qualities, flight controls, performance, propulsion, fuel system, engine inlet, structural loads, and avionics disciplines.

The inertia of the engineering community is interesting to observe. Although the AFTDS presents data in a for more usable and accurate form, the strip chart recorder continues to be the preferred display for many engineers. I would be remiss not to point out that there is some foundation for their reluctance to accept the AFTDS as a sole source of real-time data. By the nature of the system, it is much less tolerant of telemetry drop out and out of synchronization conditions than are systems that provide analog data on strip charts. Further, we have had both software and hardware anomalies that cause loss of AFTDS data displays when less sophisticated systems continue to operate in an acceptable manner.

The acceptance of AFTDS implementation for the B-l is also affected by the interface of the Rockwell airborne instrumentation system and the AFTDS hardware. The B-l airborne instrumentation is a relatively complex system that receives information from several standard aircraft systems, all of which are in their own distinctive formats. Since the Grumman system was developed in an environment where control over both the instrumentation and real-time system was possible, the system design became rather channeled and considerable difficulty was (and still is) experienced when instrumentation techniques and formats other than those used by Grumman, or very similar thereto, are used. Fortunately, ATIS generally presents a standardized format, and it is expected that the F-16 will experience considerably less difficulty in implementing the system.

On flights representative of those for flight envelope expansion, the AFTDS is used from engine start, throughout the mission and post flight ground tests. With changing of displays within an analysis package (generally applicable to a single discipline) possible in about five seconds, one can easily monitor start of the auxiliary power units and the engines in either time history plots or tabs (Figure 8). The flight control system preflight checks are controlled from the mission control area using x-y plots to show surface and cockpit control travels (Figure 9) and to assure that instrumentation parameters are functioning normally. Takeoff and climb performance are monitored through a general performance package, which is also used to assess stabilization of test points for drag determination. Simplified calculation of lift and drag coefficients are performed as are specific range ad engine parametric information. Figure 10 presents a typical format, but for security purposes the data has been removed from the presentation.

Monitoring of the fuel and center of gravity management system is accomplished throughout the flight on displays such as shown in Figure 11. This is particularly applicable during inflight refueling. (The use of the AFTDS to take maximum advantage of inflight refueling will be addressed in discussions on the F-16.) The structural loads will be closely monitored through several applications packages, typical displays are shown in Figures 12 and 13.

A rather unique application of the system accommodates the number three B-l aircraft in the terrain following environment. Figures 14 and 15 present displays showing the terrain profile of a test course at Edwards AFB and the aircraft flight profile above that course, as well as deviation from predictions. The flight test range radar and/or Contraves phototheodolite digital data are merged in the Central Computer to provide real-time data. With the requirement to rapidly expand the terrain following/avoidance envelope, this analysis package has received considerable attention. Real-time decisions are truly made and the envelope expansion has progressed in an outstanding manner.

Figure 16 depicts how the AFTDS may be used for a single input stream with a two Flight Analysis Station output. There may be two different analysis packages displayed simultaneously; each may then recall the data between maneuvers and process it through another package. Hence, within about twice the event time, four disciplines may evaluate the data from any one event. The recall file permits as many replays of the data as the user may require.

In the case of the B-l terrain following tests, extensive use is made of the plot file information to acquire test data suitable for further analysis by the avionics subsystem integration contractor. These data are available on computer listings, in most cases, before the aircraft lands.

The AFTDS has been used on all flights of the B-l test program and is projected to be used for most remaining flights of aircrafts one and two. Aircraft three applications may be limited primarily to those terrain following tests over the Edwards range.

## F-16 Full Scale Development

The advantages of the AFTDS resulted in additional funds being awarded General Dynamics to implement the system on the F-16. Additional funding was required since the full scale development contract had been awarded before the AFTDS was an operational entity. There have been approximately twenty-five data analysis packages identified for the test program. There has been a concerted effort by both the contractor and the Air Force to use the system to the maximum extent possible. In fact some of the innovative uses of the system devised by this test program have taxed the systems capability and growth to the ultimate. With the time between first flight and production decision spanning only ten months, it becomes necessary to make maximum use of every flight hour. With a powerful tool like AFTDS, one can make maximum use of the inflight refueling ability of modern aircraft and can successfully accomplish a myriad of tests on one flight. To do this there is a concerted effort to develop data analysis packages to investigate and assure the integrity of the onboard instrumentation system. Once one can assure that the instrumentation is functioning properly and that the test conditions are being satisfied, through inflight refueling the duration of a test flight can be substantially extended.

The ultimate goal of the F-16 test program is to reduce the data turnaround time so as to accelerate progression of tests. To do this, maximum practical use of the 100-percent engineering units tape will be made. With that information being placed on the tape in real-time, it is possible that high priority batch processing can be accomplished during a flight or only shortly thereafter rather than having to wait for post test processing through the pre-computer processor and the engineering units conversion program.

# F-5E Spin Test Program

The B-l is a successful application of the system and the F-l6 is an ambitious program that will tax the system to its limits. The F-5E spin test program was an application that was possibly premature and while the applications packages met the using engineer specifications, it was decided that use of the system should be discontinued and real-time monitor should revert to strip chart recorders and a few special purpose digital displays.

This test program was the first application of the system that was undertaken by the AFFTC using primarily all AFFTC personnel. The application package preparation was completed on schedule; however, interpretation of instrumentation system formats and operational difficulties in maintaining instrumentation configuration and calibration files initially led to several fairly severe errors in data presentation. Although these were overcome, there were other factors that led to the decision to terminate use of the system. Probably the most significant was the scheduling of use of the facility. Not only were we experiencing system instability and instrumentation file definition difficulties, B-1 operations out prioritized the F-5E to the point that the Northrop backup facility was used more often than was the AFTDS. Probably the most significant factor that contributed to dropping use of the system was the reaction of pilot and management personnel to the system. In this case, unfamiliarity bred lack of confidence for a very useful tool. The engineers were enthusiastic about the use of the system, but the pilots acting as control room safety officers were not due to the lack of interest, and therefore knowledge of the System's capability, characteristics, and displays. Evaluation of the displays by a management official on his first exposure to the system led to his recommendation that use of the system be terminated.

Although there were only three data analysis packages prepared, all of the data required to evaluate the spin entry, spin characteristics and recovery, as well as

the status of emergency systems was presented to test personnel in a readily readable format (Figures 18 and 18).

#### INSTRUMENTATION INTERFACES

The success of the AFTDS is not only directly related to the ingenuity of the user, but also to the integrity and complexity (or lack thereof) of his instrumentation system. Whereas Grumman operated in a cooperative environment, the AFFTC operates in about as uncooperative environment as may exist. The Grumman instrumentation system and the Automated Telemetry Station were virtually controlled by the same agency, hence assuring a maximum of compatibility and adherence to system restrictions. The AFFTC must accommodate a variety of airborne instrumentation systems some which may be extremely incompatible with the AFTDS.

In the case of the B-1, Rockwell designed instrumentation by the nature of being a very comprehensive system is very complex. As previously mentioned, it receives data from several standard aircraft subsystems, most of which have their own peculiar format. The PCM word from those sources may take the form of between twelve and sixteen bits and may be either least or most significant bit first, or the data may be inbedded within a word. Since the Preprocessor Subsystem is structured around a twelve bit word, the incompatibilities become a formidable problem. Since those words that are greater than twelve bit cannot be converted to engineering units by the Preprocessor, they must be disassembled into smaller words, passed to the Central Computer, reassembled, converted to engineering units, and then made available to the applications packages. This condition not only causes inefficient use of the preprocessor (limits the number of parameters transferred from the preprocessor to the central computer) it also requires that additional calibration files must be maintained; now data are engineering units converted within two sources. Further, the digital-to-analog section that directs data to the strip chart recorders and the out-of-limits feature is unusable. In addition to requiring more effort for mission preparation, the test program is unable to take advantage of all of the system capabilities.

The F-5E PCM instrumentation system with a few minor exceptions was totally compatible until the AFTDS. Double precision words such as airspeed and altitude had to be engineering units converted by the Central Computer. All of the AFTDS system capabilities were successfully exercised for that application.

The F-16 instrumentation system (the Edwards AFB Airborne Test Instrumentation System) with a few exceptions, will be totally compatible. The exceptions again being a few double precision words.

Compatibility in word format and size is not the only criteria, there are some known Preprocessor limitations that must be honored. Therefore, the instrumentation engineer must assure that data to be processed via the AFTDS are located in the proper positions in the telemetred data stream. The limitations are not severe and can be easily accommodated by conscientious instrumentation personnel.

Instrumentation calibration and system format files preparation and maintenance can become a virtual nightmare. We have exercised systems ranging from annual record keeping to a fully automated system with varying degrees of unsuccess. The files require the immediate care and attention of both instrumentation and data handling personnel. The luxury of updating files during or after the flight does not exist. All of the system information should be available not later than four hours before station ready time. Although last minute changes may be accommodated by typewriter keyboard inputs from the Flight Analysis Station (Figure 19), the possibility of error becomes so large that their use is discouraged.

Furthermore, there are limitations on the types of items that may be changed by the Flight Analysis Station operation just prior to flight.

The relatively infrequent B-l flights (two flights per week) should provide ample time to prepare all of the necessary files, but as may be expected, instrumentation changes necessitated for a myriad of reasons still result in last minute panic situations.

The AFFTC has recognized that our operational philosophy must change, and we are currently staffing to support an around-the-clock files preparation and files maintenance operation. The success or failure of the system ultimately rests in this one area, and depends on the close coordination and cooperative spirit of engineers, instrumentation personnel, and data handlers.

# PREPARATION TO USE AFTDS

Commensurate with the complexity of the AFTDS is the lead time required to implement the system. All disciplines are affected. The flight test engineer must plan far enough ahead to establish his data analysis criteria and to design analysis packages to provide the maximum of data presentations. Once the packages are developed, it is

incumbent on the engineer to plan the overall test program and the test sequences to take advantage of the new tool now at his disposal. This requirement for very distinctive advance planning may in itself lead to significant program savings.

Applications programming is time consuming and requires a significant lead time. Figure 20 presents the total manpower estimated required to provide for ten application packages. The estimated sixty man-month effort are in addition to the effort required from the analysis engineer to prepare his data analysis package specifications.

As previously indicated, the instrumentation engineer becomes a very important element of the AFTDS team. He must make every effort to not only provide an airborne system compatible with the ground based system, but must also assure that his preflight techniques and calibration file preparation information are geared toward a real-time environment rather than post test processing. He must maintain constant liaison with using engineers and data handling personnel. It is also extremely important that the instrumentation engineer becomes an integral part of the test team so that he may make real-time advisories to the test engineer relative to the status of the airborne system.

Training of Flight Analysis Station Operators and Test Conductors is of utmost importance. The FAS operator must be so intimately familiar with each and every analysis package, that he can respond to test engineer requests with minimum delay. The test conductor must, likewise, be familiar with system characteristics and FAS displays so he may not only correctly interpret the data presented to him, but will understand what displays he may want to request to investigate problem areas.

Even the mission-by-mission planning becomes more involved. The test cards must be appropriately annotated to assure that the proper display is presented at the required time. Where standard blocks of test maneuvers are used, the process becomes rather simple; however, where multi-discipline test maneuvers are performed, the coordination of all elements is vital.

Even the piloting personnel must have familiarity with the AFTDS, if they are to be able to interpret direction, requests, and comments from the ground controllers. Somehow control of the test must transfer from the cockpit to the ground.

Use of the system is not inexpensive. Now one has the added use of the Central Computer, the use of the preprocessor (and the labor associated therewith), and the costs associated with having to feed this seemingly hungry monster. One can easily rationalize the use if one looks at some rather realistic cost projections. Assuming that telemetry and strip charts would be used whether or not AFTDS was used, it would be necessary to reduce the number of flights by only one-percent (for a program the magnitude of the F-16 program) to recover the incremental costs of using the AFTDS.

#### FUTURE PLANS

Currently the Air Force Flight Test Center is in the process of testing and accepting the second increment of AFTDS to provide a two-in-three-out capability. I believe that the ultimate goal of three-in-three-out capability will not be required in the immediate future, and probably will not be realized until a second generation system is available. The Preprocessor Subsystem is a ten year old design that is fairly inflexible; more recent techniques and equipment will greatly improve the Preprocessor capabilities.

The AFFTC is also currently installing two Control Data Corporation CYBER 74 computers to replace our one CDC 6500. The Center will then basically dedicate one computer to real-time processing while batch and INTERCOM processing is accomplished by the other. Workload forecasts indicate that the "real-time" Central Computer will be processing data either during actual missions or in a post flight mode for two eight hour work periods per day.

It is the Air Force Flight Test Center's goal to apply the AFTDS as universally as possible. I hasten to indicate, however that the system is no panacea. It may enjoy wide use on some tests and may have little to no application for others. It suffices to say that hand recorded notes from the pilot may still be adequate for some test programs.

## CONCLUSIONS

The AFFTC Automated Flight Test Data System represents a significant improvement in the Center's data processing and analysis capability. It is a powerful tool that, when managed and utilized properly, can effect cost savings to test programs heretofore not realized. Implementation of the system requires a considerable volume of advance planning, coordination between engineering disciplines, and changing of operations philosophy by the user. It is imperative that the maximum compatibility between the airborne system and the AFTDS be realized if its features and capabilities are to be

fully utilized. The requirement for effective communication between the instrumentation and data handling disciplines is amplified when one considers now that all instrumentation status and variables must be known and loaded into the AFTDS before the test mission begins. The entire test team must gear itself toward implementation and maximum utilization if their investment in the AFTDS is to pay the potentially high dividends available.

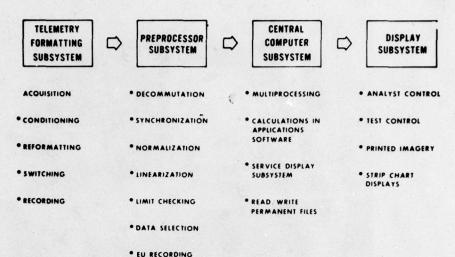


FIGURE 1 - HARDWARE SUBSYSTEM FUNCTIONAL RESPONSIBILITIES

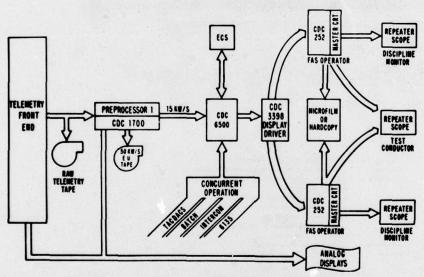


FIGURE 2 - FIRST INCREMENT AFTDS CONFIGURATION

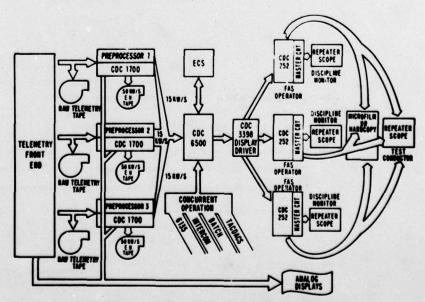


FIGURE 3 - FINAL DESIRED AFTDS CONFIGURATION

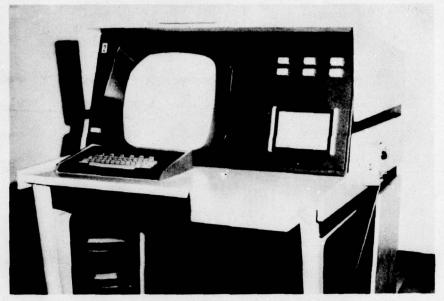


FIGURE 4 - FLIGHT ANALYSIS STATION CONSOLE

H 0.10E H 5912E VC 661 6W 691266 TA 17 HZ 0.05 g1 90/09/76 ET 00.22.47.0 FLT 000 E09 H 0.072 H 1-8717 VC 645 CG 60.6760.6 ADA 15.6 2 90.22.47 FK 11 ST 00.26.24.0 HH 000 FS1 V 9570F26220478971TA-, 101+, 20+, 745A82414- SUECPS -ALARMS DISABLED

# - MASTER MENU -

A, XXXXXX, YYY ATTACH TELIN FILE MHHHH CYCLE YYY CONFIGURE PREPROCETSOR WITH MANEUVER MINNER C. XXXXXX INITIALIZE MANRUVER PACKAGE KHEKEK 1. XXXXXX ENTER MANEUVER HODE ENTER RECALL PROCESSING HODE ENTER INTERHANGUYER PLOT PACKAGE ENTER UTILITY PACKAGE DECONFIGURE PREPROCESSOR - RELEASE EQUIPMENT DECON ENTER LOGOUT MEQUENCE L060UT AUTO-LOAD FROM FILE MENERS RETURN PLOT FILE AND OPEN A NEW ONE RETURN ATTACHED TELIN FILE -

CYCLE NO. -

FIGURE 5 - MASTER MENU

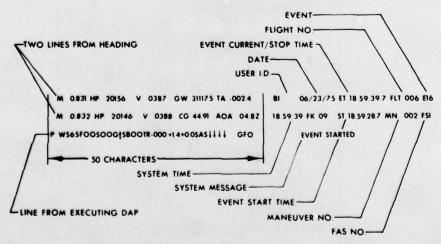


FIGURE 6 - SAMPLE HEADING

```
H 0.102 H 05122 VC 061 GW 051200 TA 17 NZ 0.05 91 09/09/76 ET 00.20.25.0 FLT 005 E05 H 0.072 H 03717 VC 045 CG 08.0/08.0 AOA 19.0 Z 00.20.25 FK 09 ST 00.20.24.0 HII 008 F51 V WS15F00500GFS800TR+.3904.29-.035A51414- SWEEPS - EVENT STARTED
```

```
SELECT SIZE AND POSITION FOR DISPLAY

SIZE

OR HX HY WH TL TR BL BR

S S S S S S S S

SELECT ONE PLOT FOR DISPLAY

0. COCKPIT FORCE V3 COCKPIT POS B090 S
1. SURFACE POS V3 COCKPIT POS B091 S
2. INBOARD SPOIL POS V3 LATERAL STICK POS B092 S
4. LOWER RUDDER POS V3 LATERAL STICK POS B093 S
4. LOWER RUDDER POS V3 LATERAL STICK POS B093 S
5. LAT STK POS V3 NEG LONG STK POS B094 S
5. LAT STK POS V3 NEG LONG STK POS B096 S
7. COCKPIT CONTROL POSITION V3 TIME B097 S
6. CONTROL SURFACE POS V3 TIME B097 S
6. CONTROL SURFACE POS V3 TIME B097 S
7. COCKPIT CONTROL POSITION V5 TIME B097 S
7. COCKPIT CONTROL POS TIME B097 S
7. COCKPIT CONTROL POS
```

FIGURE 7 - PLOT SELECTION MENU

```
H 0.161 H 07682 VC 002 6W 076800 TA 34 NZ 5.08 B1 09/09/76 ET 00.10.34.3 FLT 005 E02 H 0.161 H 07682 VC 002 CG 12.0/12.0 AOA 5-02.6 Z 00.15.34 FK 08 3T 00.10.10.17.4 H// 005 FS! 2 PTO/11.2 TTO/035 NA/018/018/018/018 STARTS READY FOR NEXT EVENT ALARMS DISABLED.
```

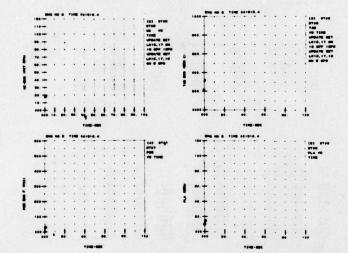


FIGURE 8 - SAMPLE START DAP DISPLAY



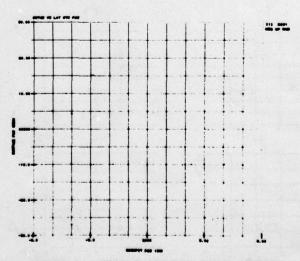


FIGURE 9 - SAMPLE CONTROL SWEEP DISPLAY

#### H 8.181 H 87888 VC 888 OF 878800 TA B4 NZ 8.00 D1 88/88/76 ET 85.16.84.0 FLT 888 ES1 H 8.188 H 88188 VC 881 CA 18.8/18.0 AGA 8-08.0 Z 20.16.04 FK 80 ST 85.16.59.0 PM 898 FS1 UNTO FR7 B81 61 SB72 UD414 TY 800F GRADY FOR MEXT EVENT

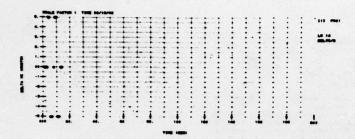


FIGURE 10 - SAMPLE PERFORMANCE DAP DISPLAY

				-						
* ****	•		-	-		-	9.46	-	-	
PAINEC				-	-		-	••		
1040.000		-0. 10476	-0. 19007			0.100007	10000.00		0.000047	
1641.		-0. 10476	-0. 10007	0.000000		4.100007	10000.00	9160.004		
1048. Pto	-1.10000	-0. 40000	-0. DI 700	0.000000	0.010070	0. 107184	10000.00	7000.000	1. 10100	
1040. Fbs	-1.19900	-1.00000	-1.00700	0. 000000		0.100004	10000.00	7000.000	1.414004	
1044. 900	. 701044	-0.07000	1.000000	0.000000			7000.000	7000.000		
1040.000			8. 9000444	0. 000000	0.000007		7460,000	8717.401	-0.10004	
1046. 440		-0.01000	-11.4070	0.000000	4. 410000		10000.00	9100.004		
1047.417		-0. 10070	-0. 19007	0.00000		4. 100007	10000.00	9188. 884	0.000047	
1040.000	-1.10000	-1. 00000	-1.00700		4. 119000	0.100004	10000.00	7000.000	1.414000	
1040.000	-1.10000	-1	-1.00700			0.100004	19900.00	7000.000	1.41400	
1004.047			8. 998444	0.000000			7450.000	8717.001	-0.10004	
1001.000		-0. 00001	-0. 10000		4. 410400		10040.00	9717.401		
1000.000		-0.10470	-0.19007			0.100007	10040.00	9100.004	1.000047	
1000.014	-1.18010	-8. 99007	-0. 50070		1.110000	0.100007	10000.00	9100. Des	1.10100	

H 8.161 H 97600 VC 800 GW 976000 TA 34 HZ 8.80 B1 80/98/76 ET 88.14.36.2 FLT 898 ESB H 8.872 H 93713 VC 848 CG 12.8/12.8 AGA 8-82.6 Z 89.14.36 FK 88 ST 89.14.21.2 IN 994 FS1 TPS/ 38605 GMZ/461200 CGR/88.8 FUELS MEADY FOR MEXT EVENT ALARMS DIRABLED

							103
				100			
PARMETER	-	- Desired	-	-		010H7	
-					9100	*100	
-	7001.71	6007.00		1944.74			
•	W1. 700	000.710	600.070		1.0000	0.0000	
10 7	-94.010	-84.010	-04.010	-04.010	0.0000	0.0000	
10 0	81.4071	10.0004	9. 60471	0.00070	0.0000	0.0000	
1M 100	0.10001	0,10001	0.10001	0.10001	0.0000	0.0000	
and and	0.00000	0.00000	0.00000	0.00000	84. 001	84.001	
-	0.00000	0.00000	0.00000	0.00000	CO0. D1	004.00	

FIGURE 11 - SAMFLE FUEL SYSTEMS DAP DISPLAY



H 5.672 H 65717 VC 645 GW 656666 TA 66 N2 -2.72 ATV 69/08/76 ET 31.02.49.9 FLT 1 ED3 H 5.161 H 67662 VC 655-CC 65.7/05.6 AGA 51.3 Z 61.02.45 FK 69 ST 61.02.25.0 M; 903 FS1 WS 61.6 FLY 14.0 LSP 26 RSP 11.0 GARA DOWN

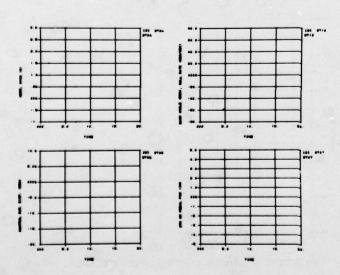


FIGURE 12 - SAMPLE LANDING GEAR DAP DISPLAY

# H 0.67E H 09717 VC 948 GW 036680 YA 08 NZ 12.72 ATY 09/09/76 ET 01.08.28.7 FLT 1 E01 H 0.161 H 07682 VC 682 GG 08,7/667 ADA 2 51.9 Z 01.68.28 FK 09 ET 01.08.29.7 FM 004 FFT W 01.0 FLT-14.0 LLSP 84.7 FMP 10.0 ED VERTICAL Z 01.68.28 FK 09 ET 01.08.29.7 FM 004 FFT M 01.0 FLT-14.0 LLSP 84.7 FMP 10.0 ED VERTICAL

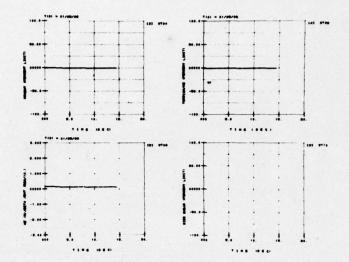


FIGURE 13 - SAMPLE TAIL LOADS DAP DISPLAY

H 8. MP V1 84 64 TA 600.1-01 162/20/76 ET 17.18.88.8 F." 10- E14 H 8. MP V 84 GA ANAHOL E 2 17.18.88 FX 88 ET 17.18.88.2 m. 214 FZ MEADOGAMENTAL OITETERS (EACH COLLEGE STATES) EVENT ATAMES.

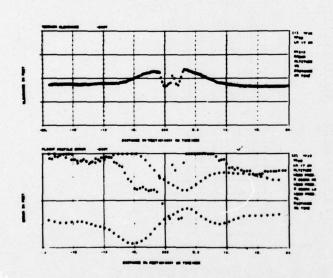
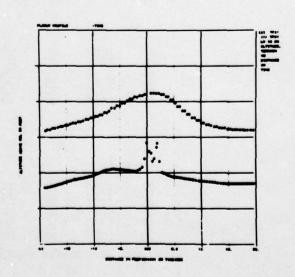


FIGURE 14 - SAMPLE TERRAIN FOLLOWING DAP DISPLAY

R 8. 00 VI 64 60 TA 600.0 D1 56/20/76 ET 17: (8.87.2 FLT 22: E14 R 2 V 64 CA ADA1-67: 9 2 17: 19: 27 PK 19 37: 17: 18: 80.2 PK 19: 484 R 2 V 64 CA ADA1-67: 9 2 17: 19: 27 PK 19 37: 17: 18: 80.2 PK 19: 484 R 2 V 64 R 2 V

FIGURE 15 - SAMPLE TERRAIN FOLLOWING DAP DISPLAY



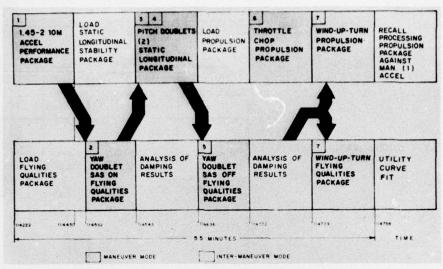


FIGURE 16 - DUAL FAS OPERATION

VI 0848 MP 68266 VT 0884 M2 +1.02 ADA +04.8/+10.5 FBE 08/08/76 ET 20.08.84.8 FLT 080 E07 VI 0824 MP 08169 M8.00 GW 18620 CG 18.8 L01 AM62.02 20.09.84 FK 09 ST 20.08.22.4 MI 015 FBS P 1917/7/188PH100/1007RT780/2279 8801 ES 700 444444 EVENT STARTED 4 T0408 MYD PRESS-R 00000000

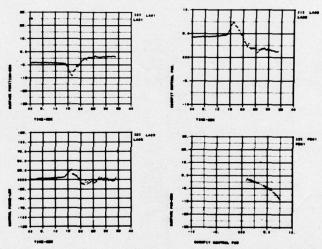


FIGURE 17 - SAMPLE F-5E FLIGHT CONTROL SYSTEM DISPLAY

VI 0315 MP 08640 VT 0368 NZ +0.84 AOA +03.4/+03.1 PBE 09/09/76 ET 20.07.29.6 PLT 080 R0: VI 0315 MP 08620 M0.84 6W 18417 C6 10.9 L01 AM62.0Z 20.07.20 PK 09 ST 20.07.29.7 MN 015 PBS P ++F00/00RPM099/100FR1603/2235 SB00 ES 764 444444 EVENT STARTED ALARMS DISABLED

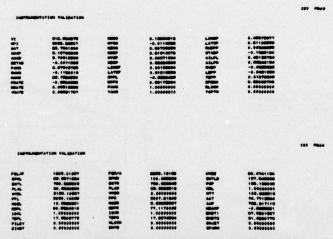
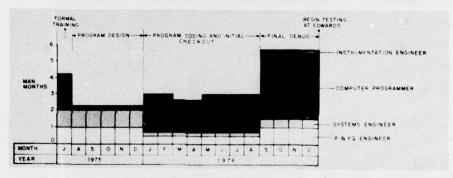


FIGURE 18 - SAMPLE F-5E EMERGENCY SYSTEMS TAB

```
N 0.072 H 02717 VC 048 GW 036000 TA 00 HZ -2.72 B1 09/99/76 ET 00.22.06.5 FLT 000 E06
N 0.072 H 02717 VC 048 CC 09.7/05.8 AGA 5 31.3 Z 00.22.06 FK 11 ST 00.20.24.0 HG 000 FE1
V WSTOTESZEGOFEDITET..1010.201.745A81444 SWEEPS -
ALARMS DISABLED
```

FIGURE 19 - LIMIT/COEFFICIENT MODIFICATION DISPLAY

# **APPLICATIONS PROGRAMMING RESOURCE ESTIMATES**



TOTALS (10 PACKAGES)

FIGURE 20

#### COMMENTS ON SESSION III

The seven papers in this session provided a broad coverage of advanced state-of-the-art of instrumentation sensors and instrumentation systems, and airborne and ground-based data processing and display techniques which assist in safe and efficient flight tests.

There were two examples of new devices — a gas rotor accelerometer and a laser tracker — that were discussed and indicated promising applications. The gas rotor accelerometer, a device for the measurement of angular motions, is extremely robust and very simple, although somewhat lacking in accuracy. It was noted that while at first sight liquids seem appropriate, they are too viscous for low frequency applications, they require an expansion chamber, density and dielectric constant change with temperature, and there may be cavitation problems in the rough flight environment. The absolute damping coefficient must be very low; therefore low kinematic viscosity is required. It was indicated that the accelerometer could be used as a rate and angle sensor by electronically integrating the output; the damping ratio was linear and better than ½% of full-scale for quasi-static conditions with no noticeable distortion under dynamic conditions. The paper on the laser tracker prompted a discussion of operational aspects from both reliability and safety aspects. The station, declared operational in September 1973 and in use since that time, has reached the point where the laser system reliability is considered acceptable but a cinetheodolite system is always on "stand-by". Adjustments must be made to the laser for humidity effects if droplet size approaches wave length; fog is a problem, but to a lesser extent than for the cinetheodolite system. On the safety side, there have been no eye accidents and the laser will not damage the unprotected eye beyond 200–250 meters. There is a possible risk to unprotected eyes of cinetheodolite operators.

One paper was presented on the techniques used to acquire and relay data from manned space flights. The discussion centered on the need to retransmit data when an error was uncovered. In general, the answer was no. During Apollo, errors were detected and data replays were made to attempt to retrieve more valid data. During Skylab, an error correction scheme was developed and used at Mission Control Center which eliminated most replays.

The presentations on the development of an advanced airborne data acquisition system and its integration into an on-board, real-time flight test analysis and monitor system demonstrated an interesting approach to the need for real-time data. It was noted that data lost during processing could be replayed from the airborne tape and reprocessed. Approximately 1200/1400 parameters were measured during the flight loads surveys using the Boeing system. The normal sampling rate is 5-10 per second and for dynamic measurements at least 10 samples per cycle, after which it depends on the frequency. Two hundred Hz can be handled; however, at higher frequencies the data becomes questionable. To establish cruise performance and end up with a drag estimate requires 200 to 300 parameters. Special decommutation equipment is used. In the case of the NASA system, it is a computer controlled part of the ground station. The on-board programs are written so that the flight test engineer can utilize them without a knowledge of programming. The keyboard utilized by the flight test engineers was reported to be easy to learn and could be operated in a timely fashion by the two-finger "hunt and peck" system. There is not a separate power system for the airborne system. The power drain has not been significant in US testing, although there had been problems reported in Concorde testing. No effects of lightning or static discharge were experienced by Boeing and NASA did not investigate the effect of lightning. There were some problems in bringing the systems on line. The initial flight phases required some extra flight hours. However, once the initial problems which were in software were solved, the Boeing system worked well. The NASA system has experienced problems because of the high gains used.

Another interesting approach to on-line, on-board data reduction was the system developed for AWACS. The system which was described, RESOURCE, is separate from the planned AWACS system. It is more powerful than AWACS, but the additional capability provided does not appear warranted at this time; thus, Boeing has not been able to sell it. The equipment is different from AWACS, which is a Hazeltine display, IBM computer and Westinghouse radar—all elements being airworthy. RESOURCE is based on available parts and disk recorders and the system is not airworthy for production at this stage. The system is totally dependent on the human operator, but a trained operator can beat AWACS' 20-minute resolution by handling the problem in 3-4 minutes.

The final paper presented a ground-based, real-time data system that is part of an overall data system consisting of airborne instrumentation (Airborne Test Instrumentation System — ATIS), batch software (Uniform Flight Test Analysis System — UFTAS), and the real-time data system (Automated Flight Test Data System — AFTDS). The AFTDS capability must be examined on the basis of the relationship between batch and real-time processing techniques in order to select the most effective use of the system. The minimum time for a completely new AFTDS system software analysis package is of the order of six months, but small changes are possible in a much shorter period of time. Instrument drift cannot be accommodated at present but software to handle this is being developed for the F-16 program. Calibration data must be available in time for last minute changes; this puts a limitation on real time as compared with batch processing. However, all data are retained on magnetic tape for future use.

#### SUMMARY OF ROUND TABLE DISCUSSION AND FLOOR COMMENTS

(No attempt is made to ascribe either questions or comments to specific individuals. The objective here is to provide a summary of the round table discussion and the comments that were provided by Symposium attendees.)

## **Round Table Participants:**

Prof. Dr.-Ing. K.H.Doetsch, FRG Prof. Ir. T. van Oosterom, Netherlands Mr D.Lean, Great Britain Mr J.Renaudie, France Mr F.N.Stoliker, USA

The Chairman opened the discussion with a short appraisal of the Symposium, pointing out the difficulties of predicting how well the selected papers would cover all the subjects that required discussion. The fundamental issue, pertaining to all flight test applications, came out quite well; i.e., striving for the best final results either for certification or for R&D purposes, always bearing in mind test economy. The achievement of best final results is not synonymous with elaborate and expensive test instrumentation. A better contact between the test designer and instrument man could still achieve great savings without sacrificing accuracy of final results, as demonstrated in paper No.17.

It was noted that there were many areas and/or techniques which were not covered during the Symposium primarily because of the lack of time. Some of the specific areas not covered were: terrain following/terrain avoidance radar testing; adverse weather tests and the associated special ground and airborne facilities and instrumentation; weapons compatibility, separation and accuracy testing; dynamic test techniques for performance determination; and engine-inlet matching. It was suggested that a specialists meeting on subsystem/system testing which would include adverse weather and climatic testing would be appropriate.

All the authors agreed that flight tests should be conducted with extensive preparation on the ground, by testing the whole aircraft on the ground or in the simulator. But three subjects have not been extensively covered by the speakers.

- the role of the pilot
- the safety aspect
- the cost/effectiveness ratio
- (a) Regarding the role of the pilot, only one speaker proposed a test method for flying qualities, putting the pilot in "the loop". This method was based on the idea of optimizing the aircraft for its primary purpose, air combat maneuvering in this case.
- (b) Safety was not emphasized except in one paper that showed that it was possible to have a "safety pilot" on the ground, ready to assist the pilot in flight, and this without involving expensive and sophisticated equipment. This speaker was also the only one to mention the use of special features on the instrument panel, added to the basic aircraft to lower the workload of the pilot, and thereby increasing safety. It was surprising that we did not hear more from, or about, test pilots in this Symposium. We claim to consider their safety by better pre-flight prediction of behaviour, on-line data processing for critical parameters, etc. Perhaps we do not make enough use of their skills in devising assessment tests better related to actual missions. Again, in many tests the pilot can recognize when poor data has been collected, without waiting for the data read-out, if he is well informed as to what test conditions are required. This aspect, the role of the test pilot, was one of the main gaps in the coverage of the Symposium.
- (c) The descriptions we were given of the performance and capability of modern data acquisition and processing systems were most impressive. No doubt their initial investment (financial and manpower) was justified in these cases because of the time saved on expensive development programs, but a warning should be sounded that what matters is the total cost of achieving the desired end result. The costs of setting up and verifying a new automatic data system (where one does not exist already) have to be weighed against the saving in flight test time. No one suggests going back to the old knee-pad, pencil, and stop-watch; but there are circumstances where the simpler data-gathering methods are still good enough, and at least force the flight test engineer to restrict his data collection to what is really needed. There is no justification for filling up 100 or more data channels if only 10 are ever going to be properly analyzed and digested. Data reduction in real or near real time is an efficient method to prevent the proliferation of data and documents. It makes it possible to

concentrate the efforts on selecting the points which are the most important or the points where the greatest accuracy is needed. It also enables one to refly bad points immediately.

A method used by Avions Marcel Dassault which consist of replaying, in the simulator, the magnetic tape of a flight in order for the specialists to make a more efficient analysis was also noted as a cost savings/avoidance.

One of the problems of all the government flight test agencies is how to work with raw data from the contractors. These data come from measuring systems based on a variety of principles and need a variety of interfaces to go into the computer. It is regrettable that a standardization of the inputs and outputs of these systems has not been undertaken, as the ARINC committee did for equipment. This lack of standardization leads to high costs because of the continuing requirement for hardware and software modification.

The importance of a well balanced man-machine relationship has long been recognized in many areas of technology. However, when considering the many complicated flight data acquisition and handling systems that are presently available, it appears doubtful whether the system designer has been well aware of this principle.

Sometimes sophisticated data processing techniques primarily developed for on-line application are used in systems where on-line functioning seems to be not strictly required. In such cases, the inclusion of a human interpretation link might result in a simpler and less expensive system with higher flexibility. In on-line systems, sometimes the need for access of a human operator to the various stages of the automatic data handling process (e.g., by special displays or other means for checking proper functioning of the system) seems to be neglected.

The remedy for controlling the immense data stream produced by present data acquisition systems is not necessarily only automation of data processing. Often a more effective method might be reducing the data amount to a selection of really meaningful data only through human interference. In the just mentioned situations optimal effectiveness will not be attained and the costs of hardware and especially those of software may be excessive.

The system designer, therefore, should always be aware of the potential of the human being and not be tempted to blindly apply advanced automatic handling techniques mainly for their technological or mathematical elegance!

Transducers are at the foundation of any data acquisition system. We might have expected more positive statements on the adequacy of available equipment than emerged in the papers or the discussion. One or two papers in Session III mentioned new ideas, but mostly the users seemed satisfied with what they could get. Examples of where one would expect further development to be welcomed are:

- (a) the traversing (swinging) probe for thrust measurement;
- (b) airflow direction sensors, particularly in terms of reliability and robustness for free-stream direction, and in miniaturized versions for boundary layer studies, perhaps using radioactive particles;
- (c) a simple, reliable and credible device for determining vertical velocity at touchdown;
- (d) motion sensing utilizing the ring laser or advanced gyroscopic developments;
- (e) measuring airspeed or exhaust gas velocity by means of a doppler radar; and
- (f) magnetic recorders utilizing solid state (bubble memory).

Despite the abundance of off-the-shelf transducers for the majority of applications with well documented claims for high performance in manufacturers' brochures, it might nevertheless be useful to establish either a forum for exchange of users' experience or some central independent testing/assessment agency as already exists; for example, for domestic and household equipment, automobiles, hi-fi equipment, etc. What is required is not only the results of bench or environmental tests, but actual in-service experience with real practical installations.

Several questions were raised regarding the instrumentation accuracies that were quoted during the presentation on non-steady performance testing. The claimed accuracies were restated, but it was noted that these accuracies are acquired only by rather sophisticated instrumentation and by exercising great care in the instrumentation calibration. Another question concerned thrust and drag evaluation. It was suggested that for the time being at least three different methods for thrust evaluation could and should be used simultaneously to achieve reasonable reliability of results. It was also suggested that it might be worthwhile for the relevant AGARD Panels to fix the border between drag (responsibility of the aerodynamicist) and thrust (responsibility of the engine manufacturer) if necessary in an arbitrary but acceptable way.

Instrumentation specialists should receive more stimuli from flight test people. This can be promoted by disseminating more basic knowledge in physics, electronics, and in areas specifically related to design and development of airborne instrumentation. The AGARD Flight Test Instrumentation Series is one of the tools to serve this purpose by bridging the gap between both categories of specialists.

	REPORT DOCU	MENTATION PAGE	
1. Recipient's Reference	2.Originator's Reference AGARD-CP-223	3. Further Reference ISBN 92-835-0194-2	4. Security Classification of Document UNCLASSIFIED
ľ	Advisory Group for Aero North Atlantic Treaty Or True Ancelle, 92200 Ner		ppment
6. Title			
	FLIGHT TEST TEC	CHNIQUES	
	nt Mechanics Panel Sympon, Germany, 11–14 Oc	posium held at DFVLR, tober 1976.	
8. Author(s)			9. Date
	Various		April 1977
10. Author's Address			11. Pages
	Vari	ous	434
12. Distribution Statement	policies and regul	distributed in accordance lations, which are outlined wers of all AGARD publications.	on the
13. Keywords/Descriptors			
Flight tests	Data processing	Flight control	
Tests	Display devices	Certificate of airworth	niness
Weapon systems	Test facilities	Military aircraft	
14. Abstract			

This Fluid Mechanics Panel Symposium on Flight Test Techniques held at DFVLR, Porz Wahn, Germany, 11-14 October 1976 was organized around three subject areas and concentrated on techniques rather than results:

Weapons System Clearance,

Weapon System Development and Evaluation; and Data Acquisition and Handling Techniques.

The first session was devoted to techniques used in flight clearance of the basic air vehicle, including flight control systems, engines, engine-inlet systems, etc., and the externally carried weapons. Session II papers gave a broad but fairly coherent coverage of the techniques used in weapon system development. Papers in the third session covered advances in the state-ofthe-art of instrumentation systems and components, data transmission, data processing, and airborne displays required for safe and efficient flight tests. The Symposium was concluded with a Round Table Discussion.

AGARD Conference Proceedings No.223 Advisory Group for Aerospace Research and	AGARD-CP-223	AGARD Conference Proceedings No.223 Advisory Group for Aerospace Research and	AGARD-CP-223
Development, NATO FLIGHT TEST TECHNIQUES Published April 1977	Flight tests Tests	Development, NATO FLIGHT TEST TECHNIQUES Published April 1977	Flight tests Tests
434 pages	Weapon systems	434 pages ','	Weapon systems
This Fluid Mechanics Panel Symposium on Flight Test	Data processing Display devices	This Fluid Mechanics Panel Symposium on Flight Test	Data processing Display devices
Techniques, held at DFVLR, Porz Wahn, Germany, 11-14 October 1976 was organized around three	Test facilities Flight control	Techniques, held at DFVLR, Porz Wahn, Germany, 11-14 October 1976 was organized around three	Test facilities Flight control
subject areas and concentrated on techniques rather than results:	Certificate of airworthiness Military aircraft	subject areas and concentrated on techniques rather than results:	Certificate of airworthiness Military aircraft
<ul> <li>Weapons System Clearance,</li> <li>Weapon System Development and Evaluation,</li> <li>Data Acquisition and Handling Techniques.</li> </ul>		<ul> <li>Weapons System Clearance,</li> <li>Weapon System Development and Evaluation,</li> <li>Data Acquisition and Handling Techniques.</li> </ul>	
P.T.O.	2 d	P.T.O.	
AGARD Conference Proceedings No.223 Advisory Group for Aerospace Research and	AGARD-CP-223	AGARD Conference Proceedings No.223 Advisory Group for Aerospace Research and	AGARD-CP223
Development, NATO FLIGHT TEST TECHNIQUES Published April 1977 434 pages	Flight tests Tests Weapon systems	Development, NATO FLIGHT TEST TECHNIQUES Published April 1977 434 pages	Flight tests Tests Weapon systems
This Fluid Mechanics Panel Symposium on Flight Test Techniques, held at DFVLR, Porz Wahn, Germany, 11-14 October 1976 was organized around three subject areas and concentrated on techniques rather than results:	Data processing Display devices Test facilities Flight control Certificate of airworthiness Military aircraft	This Fluid Mechanics Panel Symposium on Flight Test Techniques, held at DFVLR, Porz Wahn, Germany, 11-14 October 1976 was organized around three subject areas and concentrated on techniques rather than results:	Data processing Display devices Test facilities Flight control Certificate of airworthiness Military aircraft
Weapons System Clearance,     Weapon System Development and Evaluation,     Data Acquisition and Handling Techniques.		<ul> <li>Weapons System Clearance,</li> <li>Weapon System Development and Evaluation,</li> <li>Data Acquisition and Handling Techniques.</li> </ul>	
P.T.O.		P.T.O.	

\*\*\*\*

- The transfer of the second

The first session was devoted to techniques used in flight clearance of the basic air vehicle, including flight control systems, engines, engine-inlet systems, etc., and the externally carried weapons. Session II papers gave a broad but fairly coherent coverage of the techniques used in weapon system development. Papers in the third session covered advances in the state-of-the-art of instrumentation systems and components, data transmission, data processing, and airborne displays required for safe and efficient flight tests. The Symposium was concluded with a Round Table Discussion.	The first session was devoted to techniques used in flight clearance of the basic air vehicle, including flight control systems, engines, engine-inlet systems, etc., and the externally carried weapons. Session II papers gave a broad but fairly coherent coverage of the techniques used in weapon system development. Papers in the third session covered advances in the state-of-the-art of instrumentation systems and components, data transmission, data processing, and airborne displays required for safe and efficient flight tests. The Symposium was concluded with a Round Table Discussion.
ISBN 92-835-0194-2	ISBN 92-835-0194-2
The first session was devoted to techniques used in flight clearance of the basic air vehicle, including flight control systems, engines, engine-inlet systems, etc., and the externally carried weapons. Session II papers gave a broad but fairly coherent coverage of the techniques used in weapon system development. Papers in the third session covered advances in the state-of-the-art of instrumentation systems and components, data transmission, data processing, and airborne displays required for safe and efficient flight tests. The Symposium was concluded with a Round Table Discussion.	The first session was devoted to techniques used in flight clearance of the basic air vehicle, including flight control systems, engines, engine-inlet systems, etc., and the externally carried weapons. Session II papers gave a broad but fairly coherent coverage of the techniques used in weapon system development. Papers in the third session covered advances in the state-of-the-art of instrumentation systems and components, data transmission, data processing, and airborne displays required for safe and efficient flight tests. The Symposium was concluded with a Round Table Discussion.
ISBN 92-835-0194-2	ISBN 92-835-0194-2

# National Aeronautics and Space Administration

WASHINGTON, D. C. 20546

POSTAGE AND FEES PAID NATIONAL AERONAUTICS AND SPACE ADMINISTRATION **NASA-451** 



SSIFIED NS

'AGARD

stribution of AGARD

copies are sometimes

Agencies listed below.

7 RI

available

BELGIU!

OFFICIAL BUSINESS Penalty For Private Use, \$300.00

SPECIAL FOURTH CLASS MAIL BOOK

Dept. of Defense **AGARD** publicati

Defence Documentation Center Scientific - Technical Info. Atn DDC-TC

Coc Cameron Station Bldg. 5 Eta Cas Plac

Alexandria, Va. 22314 CANADA Def

Depa Ottawa, Ontario K1A OZ2

DENMARK Danish Defence Research Board Østerbrogades Kaserne Copenhagen Ø

FRANCE O.N.E.R.A. (Direction)
29 Avenue de la Division Leclerc 92 Châtillon sous Bagneux

GERMANY Zentralstelle für Luft- und Raumfahrtdokumentation und -information Postfach 860880 D-8 München 86

Hellenic Armed Forces Command D Branch, Athens

**ICELAND** Director of Aviation c/o Flugrad Reykjavik

Netherlands Delegation to AGARD National Aerospace Laboratory, NLR P.O. Box 126 Delft

NORWAY Norwegian Defence Research Establishment Main Library P.O. Box 25 N-2007 Kjeller

PORTUGAL Direcção do Servico de Material da Forca Aerea Rua de Escola Politecnica 42 Lisboa Attn: AGARD National Delegate

TURKEY Department of Research and Development (ARGE) Ministry of National Defence, Ankara UNITED KINGDOM

Defence Research Information Centre Station Square House St. Mary Cray Orpington, Kent BR5 3RE

**UNITED STATES** National Aeronautics and Space Administration (NASA), Langley Field, Virginia 23365 Attn: Report Distribution and Storage Unit

THE UNITED STATES NATIONAL DISTRIBUTION CENTRE (NASA) DOES NOT HOLD STOCKS OF AGARD PUBLICATIONS, AND APPLICATIONS FOR COPIES SHOULD BE MADE DIRECT TO THE NATIONAL TECHNICAL INFORMATION SERVICE (NTIS) AT THE ADDRESS BELOW.

# **PURCHASE AGENCIES**

Microfiche or Photocopy National Technical Information Service (NTIS) 5285 Port Royal Road Springfield Virginia 22151, USA

Microfiche Space Documentation Service European Space Agency 10, rue Mario Nikis 75015 Paris, France

Microfiche Technology Reports Centre (DTI) Station Square House St. Mary Cray Orpington, Kent BR5 3RF England

Requests for microfiche or photocopies of AGARD documents should include the AGARD serial number, title, author or editor, and publication date. Requests to NTIS should include the NASA accession report number. Full bibliographical references and abstracts of AGARD publications are given in the following journals:

Scientific and Technical Aerospace Reports (STAR), published by NASA Scientific and Technical Information Facility Post Office Box 8757
Baltimore/Washington International Airport
Maryland 21240, USA

Government Reports Announcements (GRA), published by the National Technical Information Services, Springfield Virginia 22151, USA

